NUREG/CR-3986
SAND84-1219
AN
Printed August 1984

Thermal-Hydraulic Process Modeling in Risk Analysis: An Assessment of the Relevant Systems, Structures, and Phenomena

G. G. Weigand, Project Leader

Prepared by
Sandia National Laboratories
Albuquerque, New Mexico 87185 and Livermore, California 94550
for the United States Department of Energy
under Contract DE-AC04-76DP00789

Prepared for
U. S. NUCLEAR REGULATORY COMMISSION

Available from

GPO Sales Program
Division of Technical Information and Document Control
U.S. Nuclear Regulatory Commission
Washington, D.C. 20555

and

National Technical Information Service
Springfield, Virginia 22161

NUREG/CR-3986
SAND84-1219
AN

THERMAL-HYDRAULIC PROCESS MODELING IN RISK ANALYSIS: AN ASSESSMENT OF THE RELEVANT SYSTEMS, STRUCTURES, AND PHENOMENA

Sandia National Laboratories

August 1984

G. G. Weigand, Project Leader

Sandia National Laboratories
Albuquerque, NM 87185
Operated by
Sandia Corporation
for the
U. S. Department of Energy

Prepared for
Division of Risk Analysis and Operations
Office of Nuclear Regulatory Research
U. S. Nuclear Regulatory Commission
Washington, DC 20555
Under Memorandum of Understanding DOE 40-550-75
NRC FIN No. A1339

LIST OF CONTRIBUTORS

K. D. Bergeron (SNL)
T. E. Blejwas (SNL)
A. L. Camp (SNL)
M. J. Clauser (SNL)
R. K. Cole, Jr. (SNL)
M. L. Corradini (U of Wisconsin)
P. N. Demmie (SNL)
S. E. Dingman (SNL)
F. E. Haskin (SNL)
S. N. Kempka (SNL)
R. Knight (Applied Physics, Inc.)
R. J. Lipinski (SNL)
K. K. Murata (SNL)
M. Pilch (SNL)
A. C. Raczel (SNL)
R. T. Reese (SNL)
P. E. Rexroth (SNL)
J. B. Rivard (SNL)
C. J. Shaffer (Risk Management Associates)

ABSTRACT

The MELCOR project is developing a new generation of risk assessment computer programs for analysis of severe accidents at nuclear power plants. As a part of this project, a three-part study was conducted to identify the relevant phenomena and models required for performing these PRA studies. Evaluations were performed in (1) thermal-hydraulics, (2) fission product behavior and (3) health and environmental consequences areas. This document details the findings in the thermal-hydraulic areas for PWRs and areas common to both PWRs and BWRs. A separate BWR specific report has been published by Oak Ridge National Laboratory. Reports are being prepared for the other two topics.

The study was performed by specialists from each of the various nuclear plant design or analysis areas where thermal-hydraulics is important; these specialists conducted a review of the modeling requirements of each area and contributed a section to this report detailing their findings. The general guidance as to scope for each section provided each author was: (a) identify the systems, structures, and phenomena that must be modeled, (b) review available models, (c) assess models for uncertainties, (d) identify numerical solution strategies and (e) make recommendations for the first version of MELCOR.

The study found that the current level of thermal-hydraulic modeling that exists for performing risk assessments is typified by the modeling in the MARCH code. This level of modeling was found to be inadequate for MELCOR because of inconsistent or nonexistent modeling of important phenomena, particularly invessel phenomena, systems, and structures. Pressurized water reactor modeling was found to be more complete than modeling for boiling water reactor designs, particularly in containment. Finally, although reactor cavity modeling was considered essential for risk assessments, the lack of adequate modeling found for the cavity was identified as a serious impediment to the development of second generation risk codes.

CONTENTS

ACKNOWLEDGMENTS

This report was written in support of the MELCOR program being conducted by Sandia National Laboratories for the Nuclear Regulatory Commission (NRC). We are particularly indebted to Mark Cunningham, Tim Margulies, and Roger Blond, NRC, for their support and review.

The sections in this report are the work of a large number of Sandia staff and contractors. The contributions of their management and NRC project managers are gratefully acknowledged for allowing the diversion of effort to this project.

Review and assistance in defining boiling water reactor issues was provided by the SASA Program, particularly Bob Curtis, NRC, Steve Hodge, ORNL, and Sherrell Greene, ORNL.

Significant peer review of the first draft of this compendium of papers was provided by experts in the various fields. Considerable information was added as a result of the reviews from

P. Cybulskis, Battelle Columbus Laboratory
R. Denning, Battelle Columbus Laboratory
S. Greene, Oak Ridge National Laboratory
M. Hayns, United Kingdom Atomic Energy Authority
M. McGlaun, Sandia National Laboratories
J. Sprung, Sandia National Laboratories
D. Walker, Offshore Power

We are grateful for the comments received at the peer review meetings organized by NRC's Division of Risk Analysis and attended by specialists from: Battelle Columbus Laboratory, Brookhaven National Laboratory; EG&G-Idaho; Electric Power Research Institute; Industry's Degraded Core Project (IDCOR); Oak Ridge National Laboratory; Offshore Power; Pickard, Lowe, and Garrick; Sandia National Laboratories; Tennessee Valley Authority; United Kingdom Atomic Energy Authority; University of California at Los Angeles; and Westinghouse Electric Corporation.

INTRODUCTION

The MELCOR program, conducted by Sandia National Laboratories for the Nuclear Regulatory Commission (NRC), is developing a second generation of risk assessment codes to replace the MARCH [1], MATADOR [2], and CRAC [3] system of risk analysis codes. User experience and peer review have identified major deficiencies in this set of codes, including:

- models that are inadequate or employ inconsistent treatments of important phenomena or plant features.
- code architectures that do not easily permit the uncertainties associated with calculated results to be estimated.
- code architectures that do not facilitate the incorporation of alternative or improved phenomenological modeling.
- interfaces that are not well matched.
- documentation that is inadequate.

To overcome these deficiencies, the MELCOR program is developing a new integrated system of risk assessment codes, the MELCOR system of codes. The key features of this system of codes are:

- accommodation of sensitivity and uncertainty analyses
- portability (ANSI FORTRAN 77 Standard Code)
- ease of modification and development
- modularity and structured format
- user friendliness
- appropriate execution speed
- self-documenting coding

A series of phenomena assessments were performed to identify the modeling requirements for the MELCOR code system. The scope of the assessment was broad and included the identification of the systems, structures, and phenomena in power reactors that can significantly influence the progression and consequences of severe accidents. The assessments were not limited to systems, structures, or phenomena that are treated in existing risk analysis tools or that could reasonably be expected to be included in the first version of MELCOR. Future research areas were also considered.

The assessment effort was divided into four parts: (1) pressurized water reactor (PWR) thermal-hydraulic issues, (2) boiling water reactor (BWR) thermal-hydraulic issues, (3) fission product issues, and (4) health and environmental consequence issues. This report contains the results of the

assessments of PWR thermal-hydraulic issues and issues common to both PWRs and BWRs. The latter three studies are documented in separate reports [4,5,6,7,8,9].

This assessment was conducted by technical specialists with expertise in reactor safety from Sandia National Laboratories and their contractors. It is a compendium of topical papers covering:

- PWR Plant Accident Scope and Systems
- Reactor Coolant Systems
- Containment Systems
- Auxiliary Systems

The authors of these topical papers are acknowledged in Table 1. The format, whereby the authors were independently responsible for the contents of their papers, allowed each of the specialists to conduct the assessment with relatively little constraint. General guidance as to the scope for each paper was provided as follows:

- Identify The Systems and Structures Involved
- Identify The Phenomena That Must Be Modeled
- Review Available Models
- Assess Models For Uncertainties
- Make Recommendations For First Version of MELCOR
- Identify Numerical Solution Strategies.

Furthermore, organizational meetings with the participants in the assessment resulted in the following additional general guidelines and constraints on modeling recommendations:

> The MELCOR code's principal use will be for performing severe accident risk analysis, e.g., probabilistic risk assessments (PRAs), and for evaluating the risk-reduction benefit or impact of design alternatives or plant operation changes. Risk analysis, which is currently characterized by large uncertainties, does not necessarily require thermal-hydraulic models that have a high degree of detail and accuracy. Instead, risk-code models need to characterize the key physical behavior of the more detailed mechanistic treatments and must be thoroughly exercised to document the parameter sensitivities and modeling uncertainties.
>
> Since the fundamental goal of severe accident analysis is to determine the timing, mode and magnitude of releases of fission products to the environment, any reactor system, structure, thermal-hydraulic phenomenon, or fission-product phenomenon that has a capacity to significantly influence the fission product release should be represented in MELCOR, irrespective of the modeling uncertainty that may exist.

The relationship between MELCOR and existing, developing, or planned codes that utilize a mechanistic approach is shown in Figure 1. Table 2 lists the required features for new risk assessment codes and lists, ranked in rough order of importance for MELCOR, the desirable features of models for systems, structures, or thermal-hydraulic phenomena. Each element is self explanatory; however, several are worth discussing. An integrated system of codes approach is essential for MELCOR; without it modeling approximations are inconsistent, interfaces between modeled physics are incomplete, and code interfacing costs are large when compared to execution costs. A broad spectrum of phenomena and systems models for both PWR and BWR reactors is also essential; a lack of modeling capabilities is one of the major shortcomings of the current generation of risk-assessment codes. Finally, unless the codes can demonstrate mass and energy conservation, the technical community will remain skeptical of the risk assessment code's computational capabilities.

The compendium of papers in this report contains detailed discussions about reactor systems, structures, and thermal-hydraulic phenomena required for risk analysis. Details of the available models are provided along with the identification of the gaps that exist in the modeling of the required systems, structures, and thermal-hydraulic phenomena. The thoroughness, level of detail provided, and level of modeling sophistication recommended vary widely between the papers. This variation in modeling recommendations will require synthesizing to arrive at a consistent modeling approach for MELCOR.

This assessment does not, nor was ever intended to, describe the MELCOR code or develop models for the MELCOR code. It attempted to gather the information from the experts in the various fields that will be needed by the MELCOR code developers to define a consistent set of models to be used in the MELCOR system of codes.

The papers are arranged in three major sections: papers 1.1 and 1.2, PWR Plant Accident Scope And Systems; papers 2.1 and 2.2, Reactor Coolant Systems (Primarily PWR); papers 3.1 through 3.8, Containment and Auxiliary Systems.

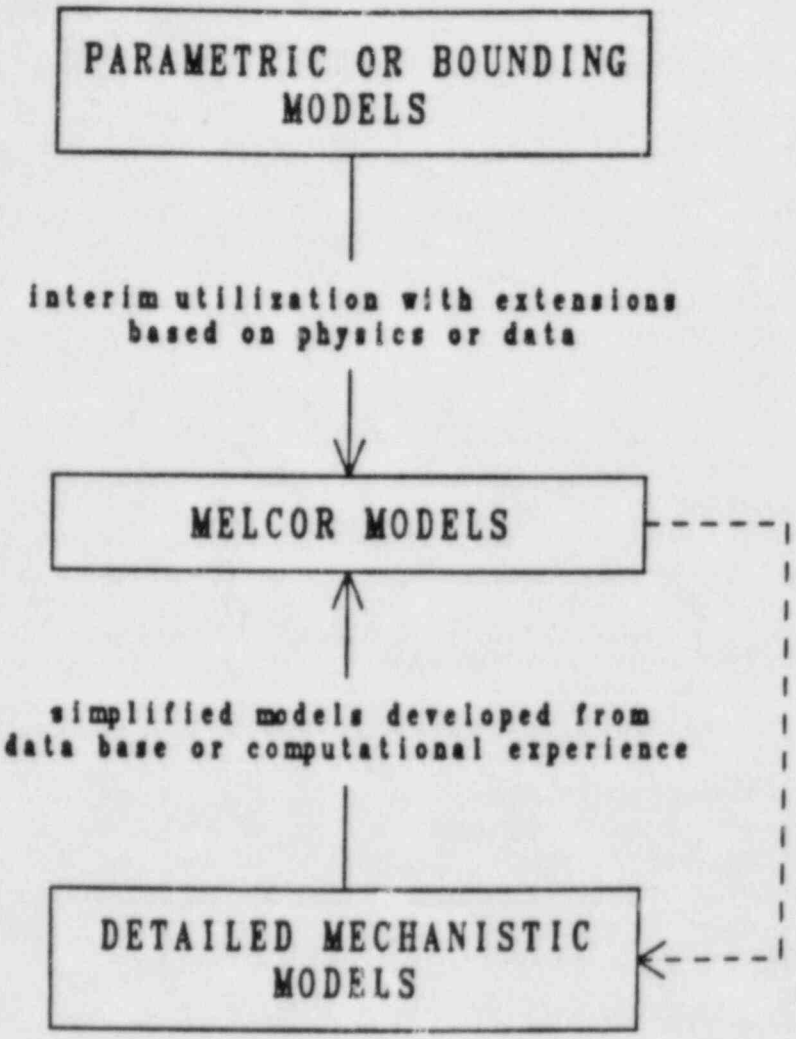

Figure 1. Illustration showing the role of a risk code in thermal-hydraulics modeling

TABLE 1

ASSESSMENT STAFF

PROJECT LEADER -- G. G. Weigand (SNL)

PWR PLANT ACCIDENT SCOPE AND PWR SYSTEMS --
F. E. Haskin (SNL)
C. J. Shaffer (Risk Management Associates)

REACTOR COOLANT SYSTEMS (PRIMARILY PWR) --
J. B. Rivard (SNL)
C. J. Shaffer (Risk Management Associates)

CONTAINMENT SYSTEMS MODELING REQUIREMENTS --
K. D. Bergeron (SNL)
T. E. Blejwas (SNL)
A. L. Camp (SNL)
M. J. Clauser (SNL)
R. K. Cole, Jr. (SNL)
M. L. Corradini (U of Wisconsin)
P. N. Demmie (SNL)
S. E. Dingman (SNL)
F. E. Haskin (SNL)
S. N. Kempka (SNL)
R. Knight (Applied Physics, Inc.)
R. J. Lipinski (SNL)
K. K. Murata (SNL)
M. Pilch (SNL)
A. C. Ratzel (SNL)
R. T. Reese (SNL)
P. E. Rexroth (SNL)
J. B. Rivard (SNL)

EDITOR -- W. Schmidt (SNL)

TABLE 2

SECOND GENERATION RISK-CODE MODELING CONSTRAINTS

Required Features

Run Times Consistent With PRA Requirements
Clear Modular Interfaces With Well Defined Data Base
Model For Each Essential Phenomenon, An Interim Model
Broad Spectrum Of Accidents Predicted
Operator Interventions And Mitigative Features Modeled
Integrated System Of Thermal-Hydraulic, Fission-Product Behavior, And Health and Economic Consequence Codes Having Well Defined, Robust Interfaces
Mass And Energy Conservation
PWR And BWR Modeling Capabilities
Friendly Interface With Users
Uncertainty/Sensitivity Analysis Accesses Via Input
Maximized Machine Independent Codes

Desirable Features*

Models And Methods Are Code Proven And Do Not Encounter Numerical Or Stability Problems
Realistic Phenomenological Models (acceptability of models to the scientific community)
Immediately Available Models
Fast Executing Models
Models With Alternative Bounding Options For Poorly Understood Phenomena
Models Having Some Degree Of Validation With Experiment
Accurate Models
Simple Models That Are Easy To Code

*The desirable features list became a mechanism to narrow the assessment effort and maintain a focus on the current state of the art in risk code modeling.

REFERENCES

1. R. W. Wooten and H. I. Avci, MARCH (Meltdown Accident Response Characteristics) Code Description And Users Manual, USNRC NUREG/CR-1711, 1980.

2. P. Baybutt, S. Raghuram, and H. I. Avci, MATADOR: A Computer Code for the Analysis of Radionuclide Behavior During Degraded Core Accidents in Light Water Reactors, draft under Sandia Order 68-9148, prepared by Battelle Columbus Laboratory, 1982.

3. L. T. Ritchie et al., CRAC2 Model Description, SAND82-0342, (NUREG/CR-2552), Sandia National Laboratories, Albuquerque, NM, March 1984.

4. Sherrell R. Greene, Realistic Simulation of Severe Accidents in BWRs -- Computer Modeling Requirements, Oak Ridge National Laboratory, USNRC NUREG/CR-2940, April 1984.

5. J. L. Sprung et al., An Assessment of Fission Product Behavior During Severe LWR Accident Sequences: Modeling Recommendations for the MELCOR Code System, Sandia National Laboratories, Albuquerque, NM, to be published.

6. R. M. Ostmeyer and J. C. Helton, Exposure Pathways Models for Accidental Radiological Releases, Sandia National Laboratories, Albuquerque, NM, to be published.

7. D. W. Cooper et al., Critical Review of the Reactor Safety Study Radiological Health Effects Model, SAND82-7081, (NUREG/CR-3185), Sandia National Laboratories, Albuquerque, NM, March 1983.

8. D. W. Moeller et al., Improved Radiological Health Effect Model, Sandia National Laboratories, Albuquerque, NM, to be published.

9. R. P. Burke, D. C. Aldrich and N. C. Rasmussen, Economic Risks of Nuclear Power Reactor Accidents, SAND84-0178, (NUREG/CR-3673), Sandia National Laboratories, Albuquerque, NM, April 1984.

1.0 PWR PLANT-ACCIDENT SCOPE AND PWR SYSTEMS

1.1 PWR PLANT-ACCIDENT SCOPE

by

F. E. Haskin

CONTENTS

LIST OF FIGURES

LIST OF TABLES

1.1.1 INTRODUCTION

In PRAs the continuum of possible occurrences is grouped into a finite number of "events." An "event" constitutes a set of possible occurrences any of which would have a similar impact on plant safety. There are three basic types of events: accident initiating events, failures of plant systems, and failures of containment. The continuum of possible accidents is approximated by event trees which start with the various initiating events and proceed through the various failure events to define a finite number of sequences of events. These accident sequences, their estimated probabilities, and their estimated consequences collectively constitute the risk estimate for the plant. Sequences with the largest probability-consequence products dominate the risk.

Customarily events are denoted by alphanumeric symbols and accident sequences by strings of such symbols. A standard event nomenclature does not exist for either PWRs or BWRs. Different symbols are used in the various PRAs due to plant differences, differences in event definitions, and preferences of the analysts. In Section 1.1.2 we introduce representative PWR event nomenclature. In Section 1.1.3 we use this representative nomenclature to summarize the dominant accident sequences which have been identified in existing PRAs.

We should emphasize that there is no standard definition of dominance. Different PRAs have employed different criteria for dominance. Insights which have been gained since the PRAs were performed tend to alter the perceived dominance of particular sequences. Also, uncertainties regarding the thermal hydraulic progression of some sequences are large. Future reductions of such uncertainties may further alter perceptions of dominance.

In Subsections 1.1.3.1 through 1.1.3.6 we discuss the dominant accident sequences from existing PRAs and the insights and uncertainties which tend to alter their perceived dominance. Based on these considerations we make some recommendations regarding the PWR systems, components, parameters, and modes of operation which MELCOR should model. Ideally MELCOR would be capable of treating any accident sequence which is currently or could in the future be perceived as dominant. However, we point out some areas in which the scope of MELCOR may have to be compromised due to practical considerations.

The material in this part of the assessment draws heavily upon results from existing PRAs and upon research currently being conducted at Sandia National Laboratories in the Accident Sequence Evaluation Program. The ASEP research

is sponsored by the U.S. Nuclear Regulatory Commission. ASEP results will be documented in much greater detail in forthcoming reports.

1.1.2 REPRESENTATIVE EVENT NOMENCLATURE

Figure 1.1.2-1 is a very simplified event tree which illustrates the failures which can lead to PWR core damage. The event headings in Figure 1.1.2-1 are safety functions which, if failed, may lead to core damage. More specific PWR failure event symbols are indicated on the failure branches of Figure 1.1.2-1. These alphanumeric failure event symbols are based primarily on the nomenclature used in the Reactor Safety Study [1] and are defined in Table 1.1.2-1.

The first function on the general event tree is reactor scram, the achievement of reactor subcriticality by control rod insertion. As indicated by Outcome 4 on Figure 1.1.2-1, failure to scram (Event K) does not necessarily lead to core damage. For example, given a large LOCA, injection of borated water is sufficient to maintain subcriticality and control rod insertion is not required. Also, it should be noted that many of the physical processes governing core meltdown and associated threats to containment integrity are the same for accidents involving failure to scram as for accidents in which reactor scram occurs.

Outcomes 1, 2, and 3 in Figure 1.1.2-1 result from accident sequences in which reactor scram occurs. Core damage is avoided in sequences leading to Outcomes 1 and 2 but occurs in sequences leading to Outcome 3.

Outcome 1 is reached when adequate cooling of the primary system is provided via the steam generators. This requires that the primary system pressure boundary (PSPB) be substantially intact. Primary coolant can then flow through the steam generators by natural circulation or be forced through the steam generators if the reactor coolant pumps are available.* Steam from the secondary side of the steam generators would either be relieved to the outside atmosphere or, as long as condenser vacuum and cooling can be maintained, dumped to the condenser. Feedwater to the steam generators would usually be pumped by the auxiliary feedwater system which would take suction from the condensate storage tank or from backup sources, if required. The main feedwater pumps (used intermittently) could provide backup pumping capability. The plant could be maintained in hot shutdown as long as feedwater could be supplied to the steam generators or until primary system makeup was required to compensate for primary system leakage (e.g., through pump

---

* At later stages of accidents when primary water inventory is low, steam produced in-vessel could condense on cold steam generator tubes. It is uncertain whether heat removed in this manner would be adequate to prevent core melting.

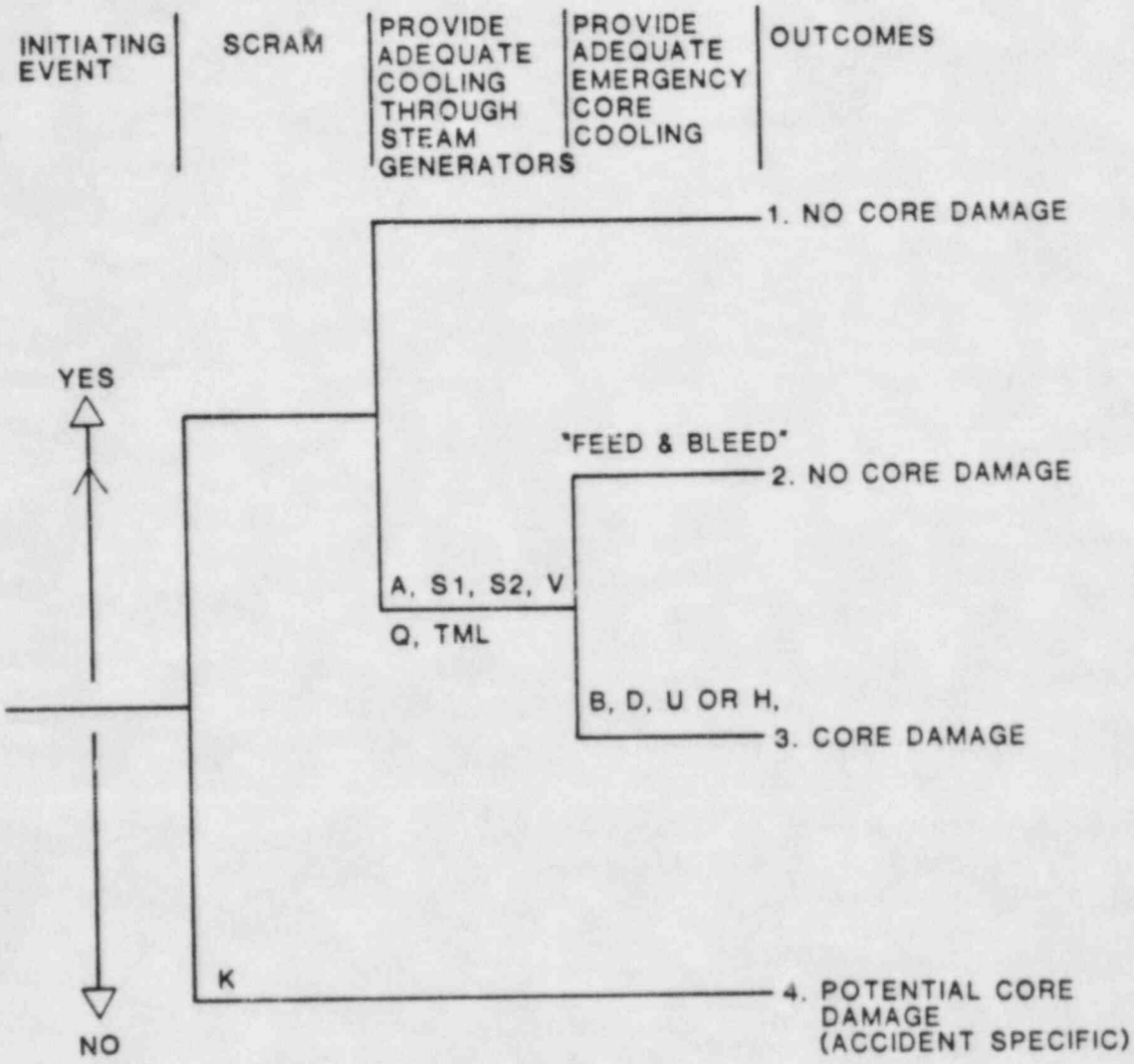

Figure 1.1.2-1. PWR Early Sequence Event Tree

Table 1.1.2-1

PWR Event Symbols

A - Breach of reactor coolant pressure boundary with an equivalent diameter of greater than 6 inches.
B - Failure of electric power to ESF's.
B'- Failure to recover either onsite of offsite electric power within about 1 to 3 hours following an initiating transient which is a loss of offsite AC power.
C - Failure of the containment spray injection system.
D - Failure of the emergency coolant injection system.
F - Failure of the containment spray recirculation system.
G - Failure of the containment heat removal systems.
H - Failure of the emergency coolant recirculation system.
K - Failure of the reactor protection system.
L - Failure to provide steam generator cooling by use of the auxiliary feedwater system.
M - Failure to provide steam generator cooling by use of the power conversion system.
O - Failure of the containment fan coolers to prevent containment overpressure failure.
P - Failure of the reactor coolant system safety relief valves to open.
Q - Failure of reactor coolant system relief valves to close after opening.
R - Reactor pressure vessel rupture.
S1 - Breach of the reactor coolant pressure boundary with an equivalent diameter of 2 to 6 inches.
S2 - Breach of the reactor coolant pressure boundary with an equivalent diameter of 0.5 to 2 inches.
T - Transient event.
U - Failure to establish adequate flow from the borated water storage tank to the reactor coolant system using the high pressure injection pumps for the purpose of core cooling via a "feed and bleed" operation.
V - Failure of the valves which isolate the reactor coolant system from the low pressure systems outside containment.
W - Failure of the residual heat removal system.
α - Containment breach due to an in-vessel steam explosion.
β - Containment isolation failure.
σ - Containment failure due to combustion.
δ - Containment failure due to gas overpressure.
ϵ - Containment failure due to basemat melt-through.

seals) or thermal contraction upon cooldown. The residual heat removal system would be required to cool the plant to cold shutdown after initial cooling via the steam generators.

For some accident initiators, adequate cooling via the steam generators is not possible. In particular, for LOCAs (initiating events A, S1, S2, and V in Table 1.1.2-1) failure of forced and natural circulation would occur. The time required for such failure obviously decreases with increasing break size. Also, for transient-initiated accidents involving total loss of feedwater (TML-initiated sequences per Table 1.1.2-1), cooling via the steam generators would become ineffective when all the secondary side liquid boiled away.

If scram occurs, but cooling via the steam generators is not possible, the core can still be cooled if adequate coolant can be pumped into the reactor vessel in a "feed" and "bleed" mode of operation. This is true both for LOCAs and TML-initiated accidents. The high-pressure injection system must be capable of delivering sufficient "feed" flow and there must be sufficient area for "bleed" out of the break or, for transients, the relief valves. If adequate coolant is provided, Outcome 2 is reached and there is no core damage. Inadequate cooling leads to core damage, as indicated by Outcome 3.

For very small openings in the primary pressure boundary, the pumps which provide reactor coolant makeup during normal operation will suffice for inventory maintenance. For larger openings, higher capacity emergency core cooling (ECC) pumps would be required in a feed and bleed mode of operation. The ECC pumps are automatically actuated if the primary system pressure falls below a specified level (usually from 1600 to 1700 psig).

Given a safety injection signal, emergency coolant injection (ECI) of water from the borated water storage tank (BWST) is attempted. If ECI fails (Event U or D, Table 1.1.2-1) or the BWST inventory is depleted, switchover to emergency coolant recirculation (ECR) from the containment sump is required. Failure of ECR is Event H in Table 1.1.2-1.

ECI failure (Event D) does not necessarily imply ECR failure (Event H); however, this is a likely result because the two functions are accomplished with the same pumps and much of the same piping--differing only in the source of water (BWST for ECI and containment sump for ECR). Even if the cause of the ECI failure (Event D) were blocked flow from the BWST and the ECC pumps were operable, recirculation failure (Event H) might still result. Blockage of flow from the BWST would also result in containment spray injection

(CSI) failure (Event C) in plants using common lines for ECI and CSI flow from the BWST. If such blockage occurred early, water in the containment sump would be from primary system blowdown alone and could be insufficient to permit sustained ECR.

The loss of electrical power to engineered safeguard features (Event B or B' in Table 1.1.2-1) implies failure of AC-dependent systems including both ECI and ECR. A power outage of limited duration may or may not lead to core damage depending on the accident initiator and the time at which power is restored.

Failure of ECR alone can result due to a failure to automatically or manually align suction to the containment sump, due to failures of valves required for such alignment, due to failures of the low-pressure injection pumps if they are required for recirculation but not for injection, or physical blockage of water flow to or from the containment sump. A failure of ECR could also result from a failure of containment heat removal (containment spray recirculation heat exchangers and fan coolers if installed, Event G). In this case, the containment sump water could heat up sufficiently to cause recirculation failure due to pump or pump-motor overheating.

1.1.3 DOMINANT ACCIDENT SEQUENCES

Table 1.1.3-1 identifies the PWR accident sequences which have been indicated as dominant in existing PRAs. The event nomenclature and functional acronyms are found in Table 1.1.2-1. For each sequence, Table 1.1.3-1 indicates the functional failures associated with the reactor protection system (RPS), main feedwater (MFW), and auxiliary feedwater (AFW) to the secondary side of the steam generators, the primary coolant pressure boundary (PCPB) and safety relief valves (SRVs), emergency coolant injection (ECI), emergency coolant recirculation (ECR), containment spray injection (CSI), containment spray recirculation (CSR), and containment heat removal (CHR). Table 1.1.3-1 also indicates the core criticality state (yes or no), the relative primary system pressure at the time of fission product release (high, medium, or low), and the relative timing of core melting (early, intermediate, or late).

In Table 1.1.3-1 and the subsections which follow, the dominant PWR accident sequences are divided into six groups:

a. ATWS Sequences (Subsection 1.1.3.1)
b. Loss of Feedwater Sequences (Subsection 1.1.3.2)
c. ECI-Failure Sequences (Subsection 1.1.3.3)
d. ECR-Failure Sequences (Subsection 1.1.3.4)
e. V-Sequence LOCA (Subsection 1.1.3.5)
f. Other PWR Events and Sequences (Subsection 1.1.3.6).

In the indicated subsections we discuss the sequences and identify insights and uncertainties which may alter future perceptions of dominance. We also discuss implications with respect to MELCOR modeling. Section 1.1.4 provides a list of key PWR systems and components and their control actions, failures, and key parameters to be modeled in MELCOR.

1.1.3.1 ATWS Sequences

Sequences of this type are initiated by transients and involve failure to insert the reactor control rods (scram) sufficiently to achieve subcriticality. Such sequences are commonly referred to as anticipated transients without scram (ATWS). Dominant ATWS sequences include TKML, TKMU, TKMQ, and TKQ. LOCAs involving failure to scram have not been found to be dominant in existing PRAs.

In accidents, reactor subcriticality is normally accomplished by the rapid insertion (scram) of the reactor control rods. In a PWR, the control rods are released, by an interruption of electrical power, to drop by gravity into the core. Following a failure to scram, the ECC systems may or may not be able to render the reactor subcritical via injection of borated water. This depends on the degree of control

Table 1.1.3-1

Dominant PWR Accident Sequence Types Based on Existing PRAs

Accident Sequence	Init. Event	RPS	MFW	AFW	SRV PSFB	F&B ECI	ECR	CSI	CRS	CHR	Crit.	Press	Timing
ATWS SEQUENCES													
TKML	T	K	M	L							y	hi	e
TKMQ	T	K	M		Q						y	hi	e
TKMU	T	K	M			U	dU				y	hi	e
TKQ	T	K			Q						y	hi	e
LOSS OF FEEDWATER SEQUENCES													
TMLU	T		M	L		U	dU				n	hi	e
TMLUC	T		M	L		U	dU	C	dC	pC	n	hi	e
TMLUO	T		M	L		U	dU			pO	n	hi	e
TMLB'	T		M	L	pB'	B'	B'	B'	B'	B'	n	hi	e
ECI-FAILURE SEQUENCES													
TMLQ-D	T		M	L	Q	D	dD				n	hi	e
TMQ-D	T		M		Q	D	dD				n	hi	e
AD	A				A	D	dD				n	lo	e
S1D	S1				S1	D	dD				n	m	e
S2D	S2				S2	D	dD				n	hi	e
ADC	A				A	D	dD	C	dC	pC	n	lo	e
S1DC	S1				S1	D	dD	C	dC	pC	n	m	e
S2DC	S2				S	D	dD	C	dC	pC	n	hi	e
ECR-FAILURE SEQUENCES													
TMQ-H	T		M		Q		H				n	hi	l
TMQ-HP	T		M		Q		H		P	pP	n	hi	l
TM-H	T		M		T		H				n	hi	l
AH	A				A		H				n	lo	e
S1H	S1				S1		H				n	m	e
S2H	S2				S2		H				n	hi	l
S1HP	S1				S1		H		P	P/pP	n	m	e
S2HP	S2				S2		H		P	P/pP	n	hi	l
S2C	S2				S2		dC		C	C	n	hi	l
V-SEQUENCE													
V	V				V	dV	V	dV	dV	dV	n	m	l

Key: E : failure due to event E
dE : may fail, depends on nature of event E
pE : partial failure due to event E

c : critical
s : subcritical

hi : (> 1000 psig)
m : medium (300 1000 psig)
lo : low (< 300 psig)

e : early (< 4 h)
l : intermediate (4-20 h)
l : late (> 20 h)

rod insertion and the rate and nature of the subsequent neutronic and thermal hydraulic response of the system.

If the ECC systems operate but the buildup of the boron concentration in the core is too slow, continued generation of a substantial fraction (up to 30 percent or more) of normal reactor power could result. The ECC systems are designed to remove decay heat but do not ensure flow rates high enough to remove substantial fractions of normal core power. Therefore, relatively early core melting could occur in ATWS accidents. Recent ATWS work [2] suggests that, in the TKQ and TKMQ sequences in which auxiliary feedwater (AFW) and high-pressure injection (HPI) function normally, the primary system could survive an initial pressure spike with adequate boration to achieve subcriticality. Also, there exists the possibility of accident termination after partial core melting in ATWS sequences in which HPI functions [2.1]. There is considerable uncertainty regarding these possibilities; however, if true, TKMU would tend to become the dominant ATWS sequence with TKQ, TKMQ, and possibly TKML becoming less important.

Variations in ATWS sequence probabilities in existing PRAs are not large compared to variations in other sequence classes. The sequence probabilities range from 6×10^{-5} to 1×10^{-6} or even nondominant. A consensus on the RPS failure probability has not yet been obtained based on the various studies performed. Assumptions regarding relative weighting of electrical versus mechanical failures and definition of scram failure differ. RPS failure values near the WASH-1400 value of 3×10^{-5} have been used in most PRAs. Depending on the resolution of the uncertainties mentioned above, plant differences in feedwater systems, primary system relief capability, and HPI systems could determine the significance of TKQ, TKML, and TKMQ sequences.

The role MELCOR should play in modeling ATWS sequences deserves careful consideration.

Based on preliminary ASEP work, the probabilities of some ATWS sequences may have been overestimated in existing PWR PRAs; however, this is true for some non-ATWS sequences as well--see discussion of ECR Failure and V-sequences below. Thus, there is no clearcut reason to believe that ATWS sequences will be totally removed from PWR dominant sequence lists. Conversely, there is no reason to doubt that sequences involving successful scram will continue to vastly outnumber the ATWS sequences on such lists.

The challenges involved in modeling core degradation are formidable even with successful scram [2.1]. For ATWS accidents significant additional challenges would be encountered. A consistent treatment of reactor kinetics would have to be coupled with the thermal hydraulic models of core

degradation. Clearly, MELCOR is not intended to be developed as a primary tool for resolving uncertainties in the Nuclear Steam Supply System (NSSS) response in ATWS accidents. Other codes such as TRAC, RELAP5, SCDAP, and MELPROG will be applied to resolve such uncertainties. We therefore adopt the position that the appropriate level of modeling for MELCOR should be established by careful assessment of phenomenological modeling for severe accidents involving successful scram.

Once this appropriate level of modeling is established for MELCOR, a consistent level of reactor-kinetics modeling can be adopted. Time constraints may preclude incorporating reactor kinetics in the initial version of MELCOR. All versions of MELCOR should, however, be designed so that calculations for ATWS sequences can be initiated after criticality is precluded using initial conditions based on calculations with other, more sophisticated codes.

1.1.3.2 Loss of Feedwater Sequences

The TMLU, TMLUC, TMLUO, and TMLB' sequences are all transient-initiated sequences involving total loss of feedwater and no "feed and bleed" cooling. Variations exist regarding the operability of containment systems. These include:

a. All containment systems operable,
b. No containment systems operable,
c. Containment sprays operable but fan coolers failed,
d. Fan coolers operable but containment spray failed.

Many PRAs suggest there is little difference among these sequences since the containment failure modes, their probabilities, and release category assignments are similar. However, the Zion PRA suggest that "b" above is potentially very significant. That is, for containments with high-failure pressures, the loss of all containment cooling may be required before above-ground containment integrity is threatened. All containment failure modes except melt through appear to be potentially important for loss of feedwater sequences.

Since the probabilities of dominant loss of feedwater sequences range from 1×10^{-3} to 1×10^{-7}, it would seem that plant-specific differences, particularly in AFW reliability and "feed and bleed" capability affect the probabilities of such sequences to a large degree.

Pre-TMI-2 estimates of AFW failure probabilities were probably too low based on pre-TMI-2 licensing event reports (LERs). However, post-TMI-2 fixes have improved AFW reliability by improving and automating AFW initiation circuitry,

eliminating AC dependencies in steam-driven AFW trains, and locking open certain flow isolation valves. The degree of redundancy and diversit' in AFW pumps and flow paths can be important. Some plants are adding cross-connects between adjacent units to improve AFW reliability.

The use of HPI in a "feed and bleed" cooling mode is generally believed possible in most of the B&W units and in roughly half of the Westinghouse units. The ability to "feed and bleed" depends primarily on:

a. Whether PORV's are installed, and, if installed their number and capacity,
b. Electrical and compressed air needs for PORV operation,
c. Probability of PORV block valve closure,
d. Ability of operators to manually open PORVs,
e. PORV and safety valve setpoints,
f. Flow versus head curve for HPI pumps, and
g. Whether "feed and bleed" would be interrupted on eventual safety injection (for example by containment isolation of instrument air which could close the PORVs) and the associated recovery potential.

For some of the Westinghouse units the ability to feed and bleed is uncertain. None of the CE units have the capability to "feed and bleed" at high pressure due to relatively low-head pumps or insufficient to no PORV capacity. Such units must be depressurized in order to utilize HPI flow for decay heat removal. If the operator can depressurize sufficiently, the residual heat removal system could be used to bring the plant to safe shutdown. Depressurization would have to be accomplished using some combination of pressurizer sprays, PORVs, turbine bypass valves, or steam generator atmospheric dump valves.

Generic considerations of offsite power recovery suggest that recovery potential does not increase at as rapid a rate beyond 1-2 hours as previously thought. This would tend to increase the relative significance of the TMLB' sequence. In addition, the A-44 Station Blackout work has suggested the potential importance of TMB'-L sequence which involves early success of AFW (the steam-driven train) with later failure due to battery depletion or condensate storage tank depletion. The ability to provide backup source of AFW without AC power would be important for such sequences. Also, the possibility of initiating a LOCA via RCP seal failure should be considered in both TMLB' and TMB'-L sequences.

Early ASEP work suggests relatively high probabilities for loss of feedwater sequences in which core cooling and makeup is restored in time to arrest core damage. For such

sequences, hydrogen burns may be particularly important if they induce failure of restored core cooling and makeup. It should be recognized that restoration of both secondary cooling and "feed and bleed" may differ from restoration of "feed and bleed" alone in terms of the amount of hydrogen released to containment.

The above considerations imply that MELCOR should be capable of modeling features which affect "feed and bleed" and primary system depressurization. This implies modeling of ECC system flow curves including pump performance curves and system resistances, flow from PORVs or primary system safety relief valves, pressurizer sprays, and turbine bypass or steam generator atmospheric dump valves. MELCOR should be able to treat intermittent operation or throttling of ECC and containment spray systems. RCP operation, trip, coast-down, restart, and seal failure may also be involved in loss of feedwater sequences. Late RCP restart could result in quenching a partially uncovered core as could late ECI. Such quenching should be modeled to the extent feasible.

Primary to secondary coupling is very important in loss of feedwater accidents. In general, voiding in the primary system would not occur until steam generator dryout unless the operator failed to maintain subcooling in a depressurization attempt. Restoration of feedwater before or after steam generator dryout may have a significant impact on accident progression. MELCOR should allow the user to postulate steam generator tube ruptures upon feedwater restoration. In addition, some attention should be devoted to modeling of condensing heat transfer within steam generator tubes in the case of feedwater restoration after voiding has occurred in the primary. Finally, RELAP4 and TRAC calculations indicate that at the time of initial core uncovery in loss of feedwater sequences, the pressurizer may be full or nearly full. Careful attention should be paid to the disposition of this pressurizer liquid since flow back into the reactor vessel could significantly alter accident progression. An assessment of core uncovering and core-damage modeling is provided in [2.1].

Containment ESF's in most loss of feedwater sequences are fully operational. However, in the station blackout (TMLB' or TMB'-L) sequences, failure of containment ESFs could lead to early overpressure failure or inerting of the containment atmosphere due to high steam concentrations which would permit the buildup of combustible gas concentrations in containment. Hydrogen burns are possible in loss of feedwater sequences with containment ESFs operating or upon restoration of containment ESFs. In either case the effects of combustion on subsequent ESF operation should be considered.

1.1.3.3 ECI-Failure Sequences

Sequences in this group are all loss of coolant accidents (LOCAs) either induced by transients or the result of small to large pipe breaks. The sequences include TMLQ-D, TMQ-D, AD, S1D, S2D, ADC, S1DC, and S2DC, all of which involve Event D, failure of emergency coolant injection (ECI).

Event C, failure of containment spray injection (CSI) also occurs in sequences ADC, S1DC, and S2DC. Only two of the existing PWR PRAs list corresponding D and DC sequences as dominant. Both of these plants have fan coolers as well as containment sprays, so that the operation of containment sprays does not appear to be particularly significant when containment failure modes are compared for D and DC sequences. However, for some plants with containment sprays but without fan coolers or ice condensers, this conclusion could prove incorrect.

Considering the dominant PWR sequences, it is clear that MELCOR should be capable of modeling all size LOCA sequences with failure of ECI. The capability to model any feasible break location should be included. For large LOCAs, accumulator success seems highly probable even though active ECI systems fail. Thus accumulator injection should be modeled in MELCOR. Based on existing PRAs, combustion and steam explosions are important causes of containment failure for ECI-failure sequences. For containments with low failure pressures, the buildup of noncondensible gases from core-concrete interactions could also be significant.

The probabilities of ECI-failure sequences range from approximately 7×10^{-5} to less than 5×10^{-7}. While some of this variation is due to the range of LOCA sizes, variations in criteria for success in preventing core damage and relevant system failure probabilities also contribute to the wide range.

Preliminary ASEP work suggests that for the small-break and transient-induced LOCAs, the probability of restoring some core cooling and makeup before full melting may be large enough to warrant consideration for MELCOR modeling. Hydrogen burns could prove important in such sequences if they compromise the restored functions.

1.1.3.4 ECR-Failure Sequences

As for the ECI-failure sequences, the ECR-failure sequences are all loss of coolant accidents either initiated by transients or small to large breaks in the primary system pressure boundary. Dominant ECR-failure sequences include TQM-H, TQM-HF, TM-H, AH, S1H, S2H, AHF, S1HF, S2HF. Event

H, ECR failure, is explicit in all these sequences. The S2C sequence for Surry is also included in this group because it involves ECR-failure induced by CSI failure.

Event F, CSR failure, also occurs in some of the dominant ECR-failure sequences. In reviewing the containment failure mode probabilities for ECR-failure sequences from existing PRAs, Event F does not appear to be particularly significant for plants with fan coolers or ice condensers as well as containment sprays. For plants with containment sprays but no other containment heat removal systems, Event F could prove more significant.

PRAs have identified dominant sequences involving recirculation failure for all LOCA sizes. However, preliminary ASEP work indicates that for small-break or transient-induced LOCAs, recirculation failure may not be as important as indicated in existing PRAs. For such initiators, sufficient time is available to depressurize the primary system and bring the plant to shutdown using the AFW, feed and bleed with HPI, the PORVs and pressurizer sprays, or combinations of these. The operator would have many indications of the need to depressurize. He would have to be careful to keep the primary system subcooled so as to prevent voiding and associated complications, but with post-TMI procedures and training, successful depressurization seems likely. Early ASEP estimates indicate that core-melt probabilities associated with TMQ-H, TMQ-HF, S2H, S2HF, and the Surry S2C sequences should be reduced by at least an order of magnitude from their values in existing PRAs.

In addition to the MELCOR modeling requirements identified for loss of feedwater and ECI-failure sequences, the ECR-failure sequences require modeling of BWST level, ECR-pump net positive suction head available (NPSHA), ECR-pump inlet temperature, debris dispersed to the containment sump, and possibly ECR-pump room temperatures. Limits based on any of these parameters could initiate ECR-failure.

1.1.3.5 V-Sequence

The V-sequence interfacing system LOCA is caused by failure of the valves (in series) which isolate the low-pressure systems in the auxiliary building from the high-pressure reactor coolant system inside containment. The postulated isolation valve failures would result in flow from the reactor coolant system into the low-pressure systems (LPS), initially through the LPS relief valves.* Should the backflow through the failed valves exceed the capacity of the LPS relief valves, breach of the LPS pressure boundary due to overpressure or dynamic loading beyond the design basis could occur. Thus, a V-sequence LOCA could

result in the discharge of primary coolant directly to the auxiliary building.*

Core damage in a V-sequence LOCA could, in general, only be prevented if the operators act promptly to isolate the discharge flow path by closing the appropriate motor-operated valve. If this valve were not closed promptly, the motor for the valve operator could overheat since it would be located in the vicinity of the postulated break in the auxiliary building. The ECC pump motors could also fail due to steam flooding unless prompt action were taken. An astute operator might diagnose the V-sequence LOCA by its distinct signature--no initial change in containment parameters but sharp increases in auxiliary building pressure, temperature, and radiation levels. Obviously, the larger the flow area, the less time would be available for the operator to isolate the break.

The probability for a V-sequence LOCA and the details of its progression are very plant specific, depending on the design and testing and maintenance procedures.

The Reactor Safety Study [1] assumed that a V-sequence LOCA would "almost surely" lead to total ECC failure. The Reactor Safety Study postulated a 15.24-cm (6-inch) diameter break in the LPS pressure boundary. Even if ECC injection from the refueling water storage tank were to function properly, switchover to ECC recirculation would not be possible because the containment sump would be empty.

Depending on the nature of the LPS isolation valve failures and the details of the ECCS design and layout, it is conceivable that backflow through the LPS isolation valves could be accommodated by the LPS relief valves. If not, small breaks in interconnecting process or instrument lines could well occur before a larger (e.g., 6-inch diameter as per RSS) process line break. It is also conceivable that only one ECC train, the one in which the break occurred, would fail. To test such hypotheses would require detailed design information and analyses. Although break-size analyses are clearly beyond the scope of MELCOR, MELCOR should be capable of analyzing steam flooding which could affect the operability of ECCS pump motors and valve operators in the auxiliary building.

MELCOR should also be able to treat the holdup and plateout of fission products in the auxiliary building. Of course, at some point in a severe V-sequence LOCA, certainly by the time of vessel breach, materials would be discharged

---

* In some plants flow from the LPS relief valves is returned via a collection header to containment.

to the containment atmosphere. The size of the opening into the auxiliary building would then influence the degree of holdup and plate out of radionuclides in the containment atmosphere.

1.1.3.6 Other PWR Events and Sequences

There are at least two events which have not been treated in sufficient detail in existing PRA and which could prove significant based on future analyses.

First, steam generator tube ruptures (SGTR) constitute relatively likely initiating events which, if compounded by ECC failure, could lead to core damage. An important distinction between SGTRs and other small-break LOCA initiators (Events S1 and S2 in Table 1.1.2-1) is that the operator can effectively isolate a SGTR by depressurizing the primary system to less than the secondary system pressure. In doing so, the operator must be careful to maintain subcooling in the primary system. SGTRs also introduce the potential for steam generator overfill and liquid in the main steam lines such as occurred at Ginna. This introduces the potential for a stuck open main steam safety valve or even a main steam line break inside containment since the main steam lines are not designed to be liquid filled. Also, SGTRs could occur during the course of other severe accidents, particularly accident involving significant secondary system occurrences such as dumping feedwater into a dry steam generator.

Second, in accidents involving overcooling of the primary coolant system, pressurized thermal shock (PTS) could result in breach of the reactor pressure vessel where it has become embrittled due to neutron irradiation. In general, PTS would be most likely in high-pressure, low-temperature sequences. Post-TMI-2 operator training to avoid loss of primary subcooling should work to reduce the potential for high-pressure, low-temperature scenarios.

Uncertainties regarding SGTR and PTS are large. Considerable research is underway to resolve these uncertainties; however, decisions regarding the treatment of SGTR and PTS in MELCOR will have to be made before significant research results become available. We feel that MELCOR should permit the user to treat SGTRs as initiating events or postulate their occurrence during other sequences perhaps based on primary-to-secondary differential pressure and temperature criteria. Similarly, MELCOR should permit the user to postulate PTS based on primary-pressure and vessel-temperature criteria.

1.1.4 PWR FUNCTIONS TO BE MODELED

Table 1.1.4-1 summarizes the PWR systems and components to be modeled in MELCOR to permit analyses of potentially dominant PWR accident sequences identified in the preceding section. The systems and components are listed in Table 1.1.4-1 in roughly the same order as the functions are listed across the top of Table 1.1.3-1. Table 1.1.4-1 also indicates automatic and manual control actions, component failures, and system parameters to be modeled.

For the most part, the automatic functions listed in Table 1.1.4-1 are fairly straightforward, involving isolation or actuation of systems or components triggered by plant parameter responses with sensing and control system delays. The manual control functions and functional failures present more significant modeling challenges as indicated in the notes. In particular, as indicated elsewhere in this report, modeling of ATWS sequences, multiple SGTRs, "feed and bleed" capability, depressurization in transient-initiated or small-break initiated LOCAs with no "feed and bleed," late ECI onto a partially damaged core, and determination of success criteria in general are areas involving substantial thermal hydraulic uncertainties.

It should be recognized that MELCOR is not intended to be designed as a tool for the resolution of such uncertainties. Existing best-estimate codes such as TRAC and RELAP5 as well as future detailed phenomenological codes such as SCDAP and MELPROG are more appropriate tools for resolving such uncertainties. In fact, the detailed neutronic and thermal hydraulic capabilities associated with such codes would conflict with the objective that MELCOR be a fast running code with proven models. It is recognized that less detailed modeling may impose certain limitations on MELCOR.

The mitigation functions to be modeled in MELCOR as listed in Table 1.1.4-1 are those which we perceive could have a significant impact on the potential for above-ground containment failure or radionuclide releases to the environment.

Table 1.1.4-1

PWR System/Component Modeling Requirements for MELCOR

System, Function, or Component	Automatic Control	Manual Control	Failures	Parameters(1)
Reactor Protection	scram	yes(a)	Event K(a)	reactivity
Main Stream				
Safety Valves	open/close	---	fail open	x,F,T,P
Atmospheric Dump Valves	open/close	open/close(g)	fail open	x,F,T,P
Isolation Valves	no(b)	no	see note C	
Turbine-Bypass Valves	no(b)	no		
Main Turbine	no(b)	no		
Condensate	no(b)	yes		F,T,P
Main Feedwater	no(b)	yes(d)	Event M	F,T,P
Auxiliary Feedwater	init., flow control	yes(d,g)	Event L, parital to total on demand or delayed, CST depletion.	F,T,P, L-CST
Reactor Coolant System				
Pressure Boundary	---	---	Events A, S1, S2, R(f), V, SGTR(d), RCP Seal Failure	x,F,T,P
Safety Relief Valves	open/close	---	Event Q (stuck open)	x,F,T,P
PORVs	open/close	yes(g)	Event Q (stuck open), lack of power or block valve shut.	x,F,T,P
High Point Vent Valves	---	open/close	stuck open	x,F,T,P
Pressurizer Sprays	no(b)	yes(g)		
Pressurizer Heaters	no(b)	no		
RCP forced flow	trip	yes		x,F,P,T,J-RCP

Chemical & Volume Control	no(b)	yes		x,P,P,T for makeup, letdown, seal flows
Residual Heal Removal	no(b)	no		
Accumulator Injection	dump	---		
High-Pressure Injection	actuate, switch to recirculation	yes	inadv. actuation, Event D (partial to total, on demand or delayed).	T,P,P to RCS & Cont., RWST L, pump-room T
Emergency Boration	actuate	yes		
High Pressure Recirculation	switch from injection	yes	See Low Pressure Recirc.	See Low Pressure Recirc.
Low Pressure Injection	actuate,	yes	See High Pressure Injection	See High Pressure
Low Pressure Recirculation	switch from from ECI	yes	Event H (partial to total, on demand or delayed), due to inadequate NPSHA, high pump-inlet T, high pump-room T, debris in sump	T,P,P to RCS and Cont., J, sump L, NPSHA, pump-inlet T, pump-room debris in sump
Containment Spray Injection	actuate	yes	Event C (see Event D above)	F,T, others per High Pressure Injection above x-spray additives
Spray Chemical Injection	injection	---	Event I	
Containment Spray Recirculation	switchover	yes	Event H (see Event H above)	F,T, others per Low Pressure Recirculation above.
Containment HVAC				
Fan Coolers	actuate or switch speed	yes	Event O (partial to total,	heat removal rate, condensation rate.
Cont. Vent	isol.	yes	fail to close	P
Pre-inerting	---	---		Init. Cont. Gas Comp.
CO2 inerting	no	yes		dCO2/dt
H2 recombines	no	yes		dH2dt
Igniters	no	yes	loss of power	

Containment Flooding	no	yes		L-cont.
Circulating Water	no	no		
Service Water	actuate	no	total failure	P,T,J
Component Cooling Water	no	no	total failure	P,T,J
Ultimate Heat Sink	no	no	failure	J

NOTES:

a. Scram failure or delayed scram will require modeling of reactor kinetics, may not be feasible for MELCOR and may not be required.
b. For MELCOR can assume system or component is isolated. Manual control should be modeled if indicated. Subsequent versions of MELCOR may simulate automatic control for normal and off-normal modes of operation.
c. Inadvertent MSIV closure and failure of MSIV to close on demand do not contribute to dominant PWR sequences.
d. Delay of MFW or AFW until SG dryout could induce SGTRs.
e. Event P, stuck closed safety relief valves does not appear in dominant PWR accident sequences.
f. Event R could result from PTS in overcooling sequences.
g. Use of AFW, pressurizer sprays, ADVs, and PORVs to depressurize when feed and bleed is not available involves significant thermal hydraulic uncertainties.
h. Inadvertent spray actuation does not appear in dominant PWR accident sequences.
i. Parameter Key: F - Flow
J - Power or heat transfer rate
L - Level
NPSHA - Available net positive suction head
P - Pressure
T - Temperature
x - Composition or concentration

1.1.5 REFERENCES

1. Reactor Safety Study, WASH-1400 (NUREG-75/014), U.S. Nuclear Regulatory Commission, 1975.

2. Kolaczkowski, A.M. et al., "Interim Report on Accident Sequence Likelihood Reassessment (Accident Sequence Evaluation Program)," Sandia National Laboratories, February 1983.

1.2 PWR SUMMARY DESCRIPTION

by

C. J. Shaffer

CONTENTS

CONTENTS (Continued)

List of Figures

List of Tables

1.2.1 INTRODUCTION

Pressurized water reactors (PWR) are the energy source as shown in Figure 1.2-1 for the Nuclear Steam Supply Systems provided by three major manufacturers: Westinghouse, Combustion Engineering, and Babcock and Wilcox. A steam supply system consists of the reactor coolant system (RCS) known as the primary loop and a power conversion system known as the secondary loop. The primary loop is a closed cycle design located completely within the containment building and includes the reactor vessel, steam generator, circulation pump, and associated piping. The secondary loop includes the steam generator inside the containment building and the turbine generator, condenser, and feedwater pump outside the containment building.

This section will include descriptions of the reactor coolant system, the nuclear core, the RCS safeguards systems, the containment, the secondary loop, and the auxiliary cooling systems.

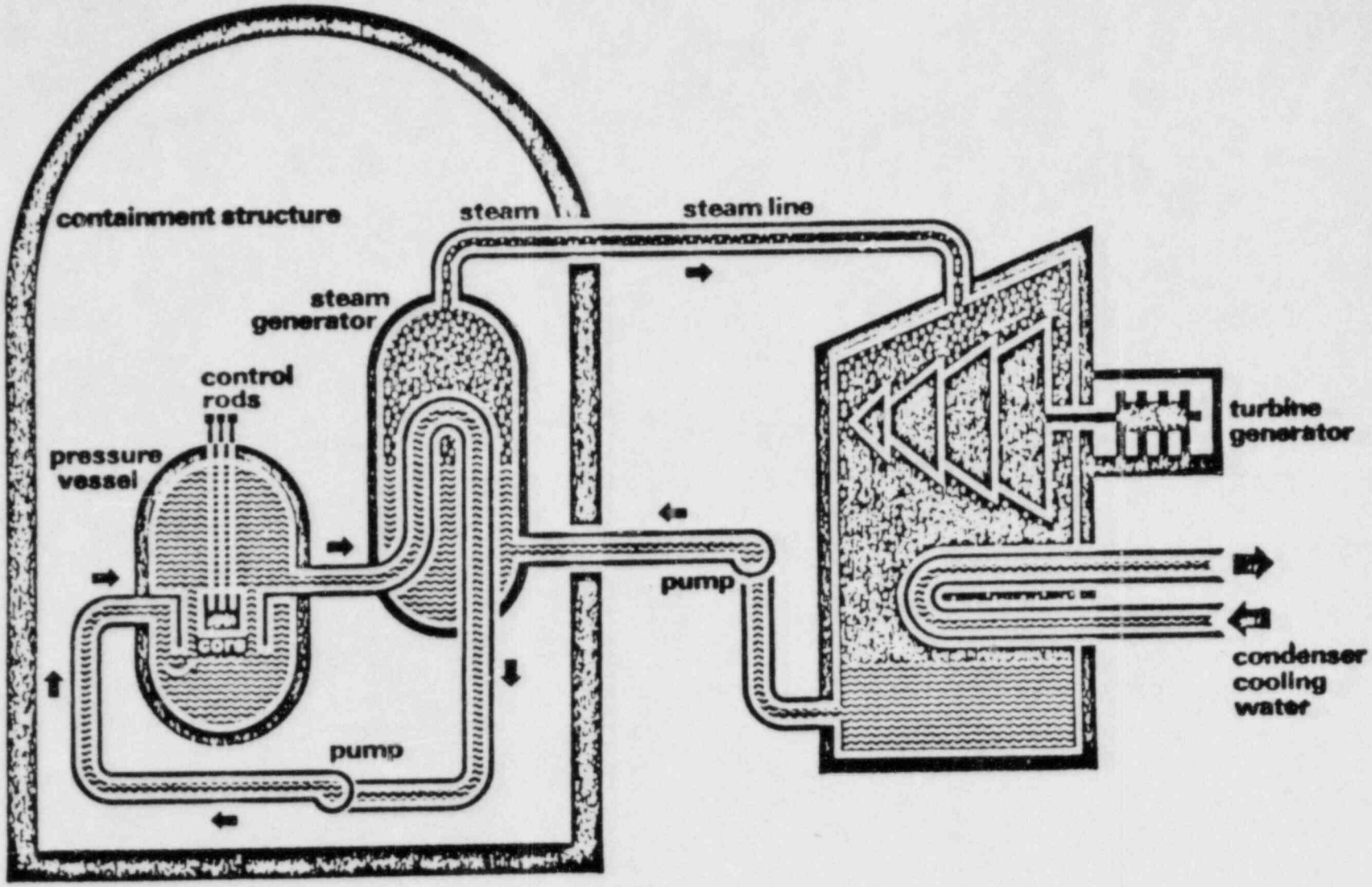

Figure 1.2-1. Pressurized Water Reactor

1.2.2 REACTOR COOLANT SYSTEM

The functions of the reactor coolant system are to:

A. Transfer energy from the reactor core to the steam generator where steam is produced for use in a turbine generator.

B. Serve as the primary barrier to the release of fission products from the reactor core to the environment (see Figure 1.2-2).

The major components of the system are the reactor vessel, two or more parallel heat transfer loops each containing a steam generator, reactor coolant pump, and a pressurizer connected to one of the reactor vessel outlet pipes. All components in contact with the reactor coolant are stainless steel, or carbon steel lined with stainless steel. All components that form part of the reactor coolant system pressure boundary meet the code requirements of ASME Section III Class I components.

During normal operation, the reactor coolant is circulated through the reactor vessel and steam generators by the reactor coolant pumps. The coolant is heated by the fissioning fuel in the core as it passes through the reactor vessel, and is cooled in the steam generators as it gives up heat to the secondary system to form steam. The coolant also serves as a neutron moderator in the core and contains a soluble neutron absorber (boric acid) for reactivity control. The coolant is maintained in a subcooled condition by maintaining a high-system pressure.

The reactor coolant system pressure is maintained and controlled through the use of a pressurizer in which steam and water are maintained in thermal equilibrium. During full-load operation, the pressurizer volume is almost evenly divided between saturated water and saturated steam. Steam is either formed by energizing immersion heaters in the pressurizer, or condensed by a subcooled pressurizer spray, as necessary to maintain operating pressure and limit pressure variations due to plant-load transients.

Overpressure protection for the system is provided by power-operated relief valves and/or spring-loaded ASME Code safety valves. These valves discharge to the quench tank where the steam is released under water to be condensed and cooled.

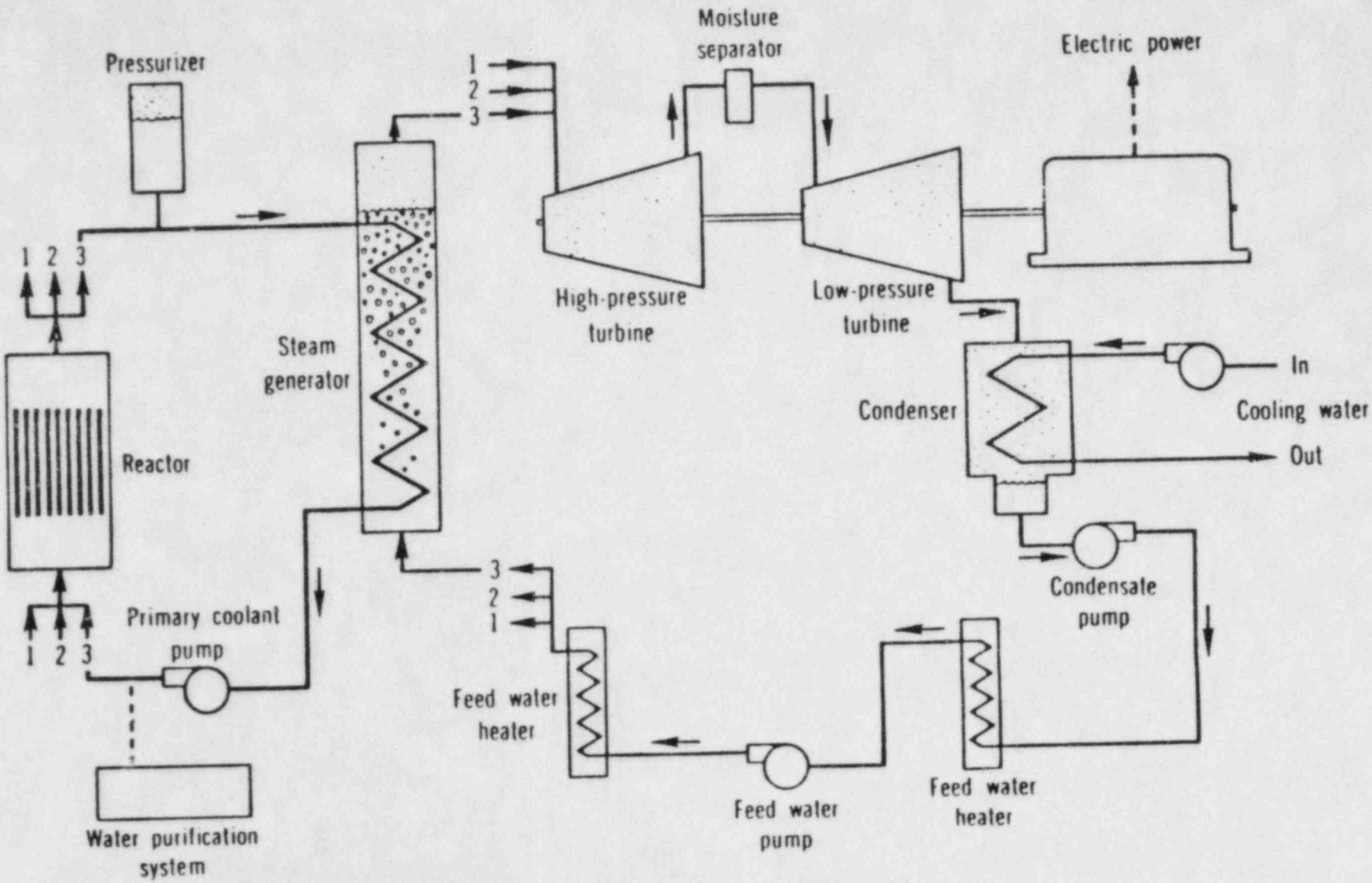

Figure 1.2-2. A Complete Nuclear Power Plant Based on A Pressurized Water Reactor

The system also includes the interconnecting piping to auxiliary systems and the instrumentation necessary for operation and control.

The functions of the systems and components provided by the three major manufacturers are nearly identical with major differences as summarized in Table 1.2.2-1 and is shown in Figures 1.2-3, 1.2-4, and 1.2-5.

Table 1.2.2-1

MAJOR DESIGN DIFFERENCES

Features	Westinghouse	Combustion Engineering	Babcock & Wilcox
Number of loops	4	2	2
Pumps per loop	1	2	2
Type of steam generator	U-tube	U-tube	Once-through

The components of the reactor coolant system are arranged with the reactor vessel located in the approximate center of the reactor building and the steam generators and the reactor coolant pumps located symmetrically on opposite sides of the reactor vessel. The steam generators are located at a higher elevation than the reactor vessel so that sufficient natural circulation in the RCS may exist to remove core-decay heat following coast down of all reactor coolant pumps in the event of loss of normal station power.

1.2.2.1 Reactor Vessel

The reactor vessel shown in Figure 1.2-6 for a typical reactor contains the fuel bundles, the control rods, and other internals necessary for support and flow direction. A PWR vessel is a large thick-walled right-circular steel cylinder approximately 4.0 m in diameter, 15.0 m in height, and 0.2 m thick. The vessel is closed at the bottom with an integral hemispherical head and closed at the top by an approximately hemispherical head held in place by about 50 bolts. The top head is removed for refueling. The vessel is designed to operate at about 15.0 MPa internal pressure. There are penetrations in the vessel for coolant flow, control mechanisms, and instrumentation. Major internal regions in the vessel are the reactor core, the lower plenum, the upper plenum, and the down comer.

During normal operation, the reactor coolant enters the vessel through four inlet nozzles, turns and flows downward through the down comer between the reactor vessel shell and the core support barrel, and enters the lower plenum through

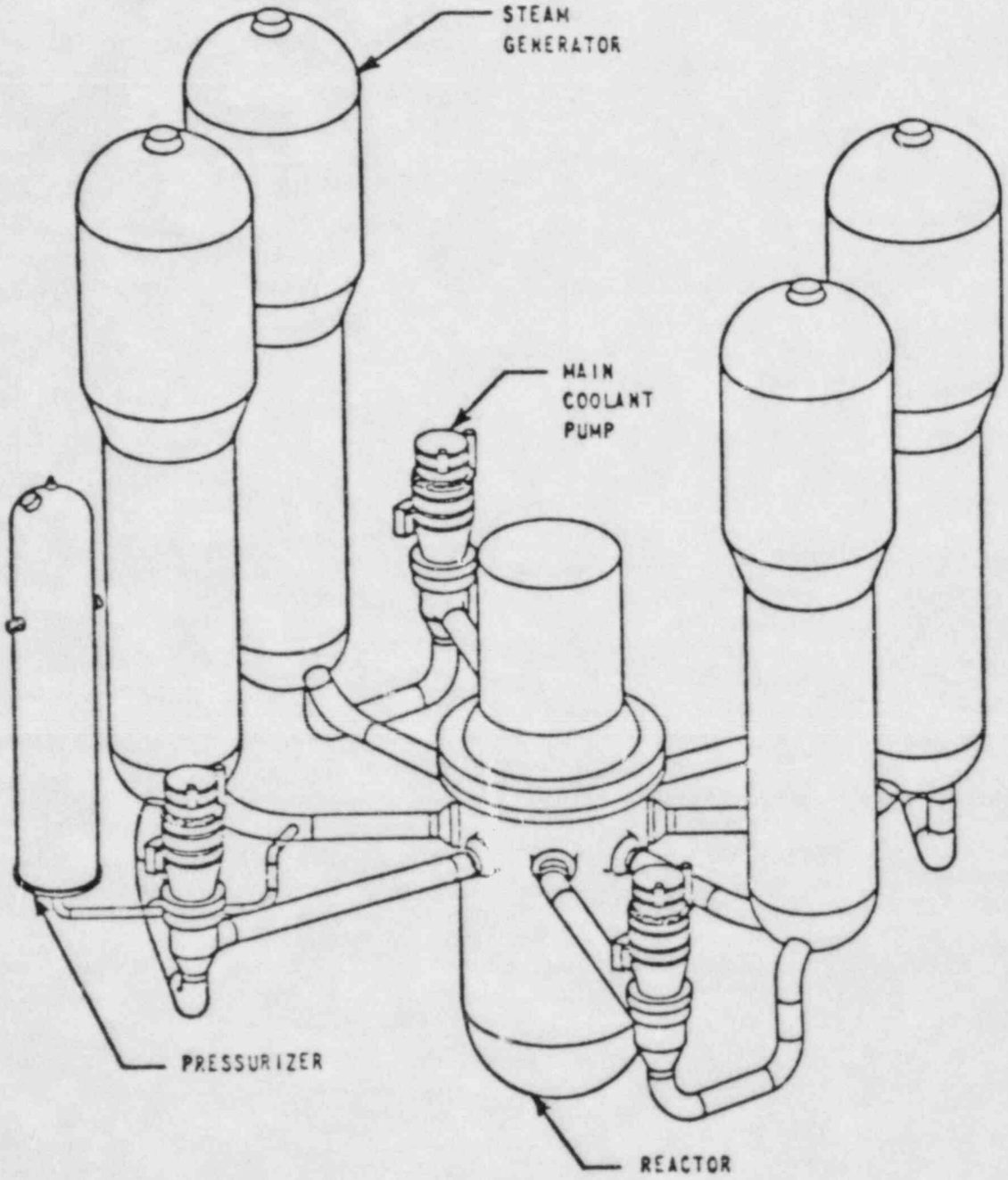

Figure 1.2-3. Westinghouse Four-Loop Reactor Coolant System

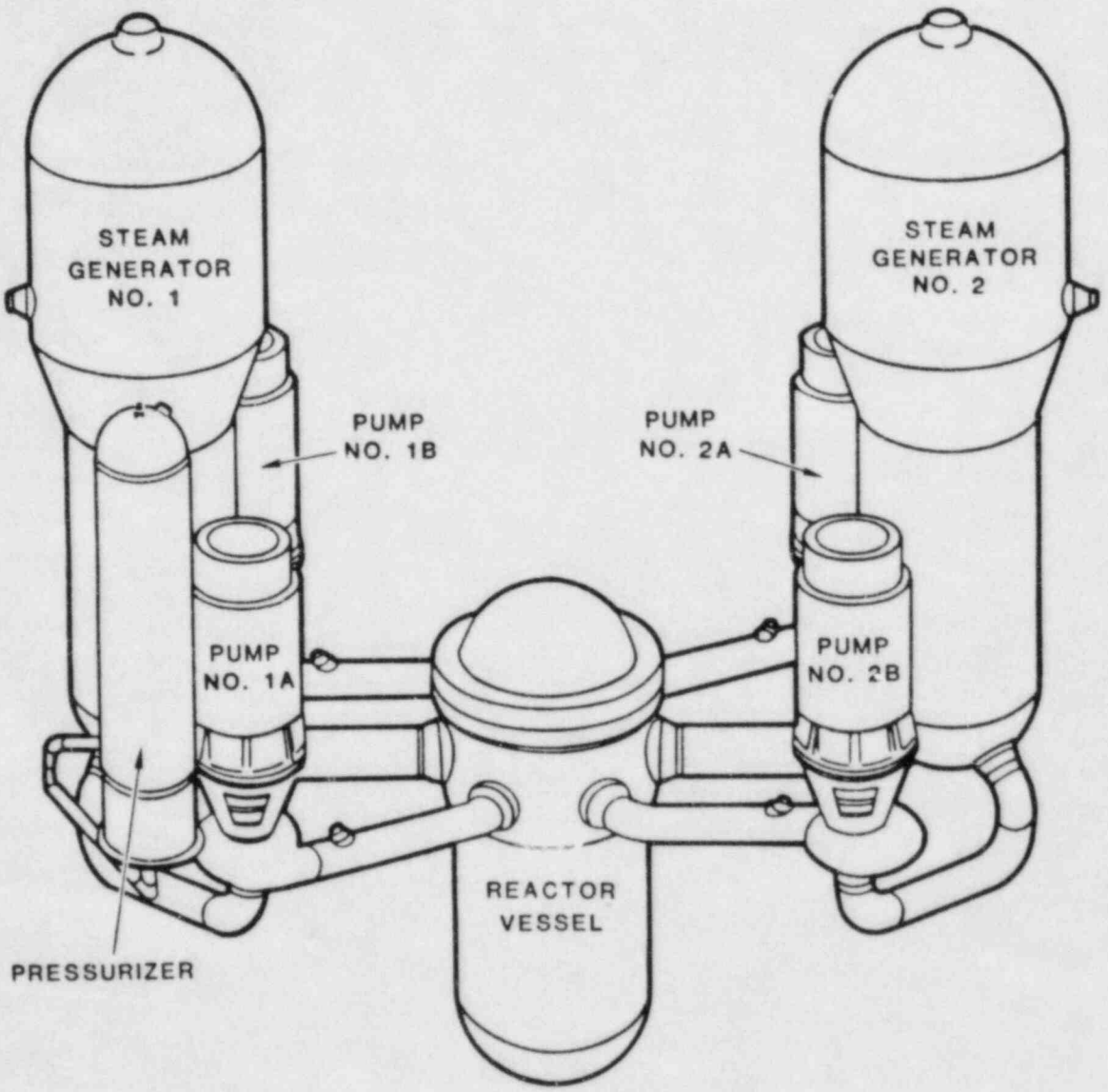

Figure 1.2-4. Combustion Engineering Two-Loop Reactor Coolant System

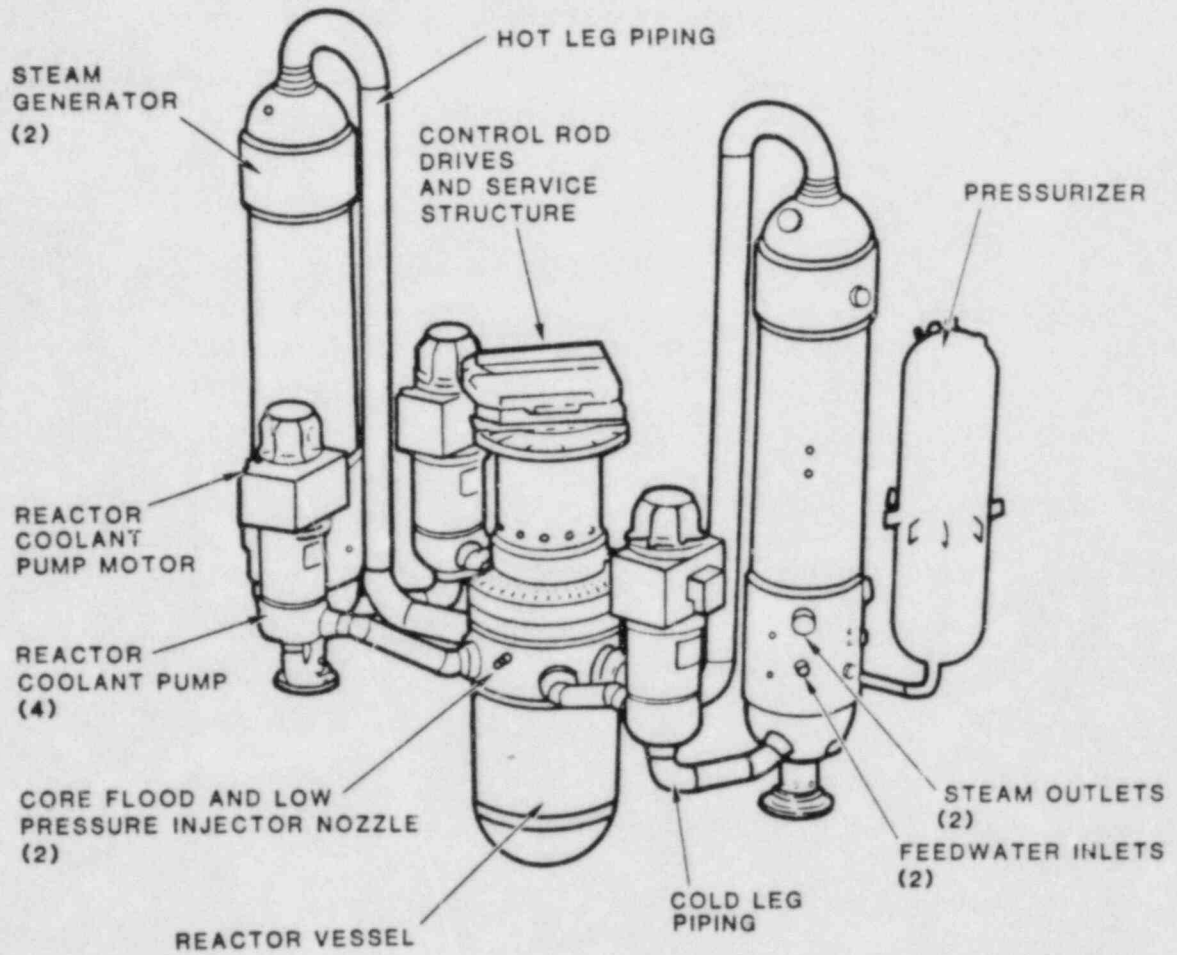

Figure 1.2-5. Babcock and Wilcox Two-Loop Reactor Coolant System

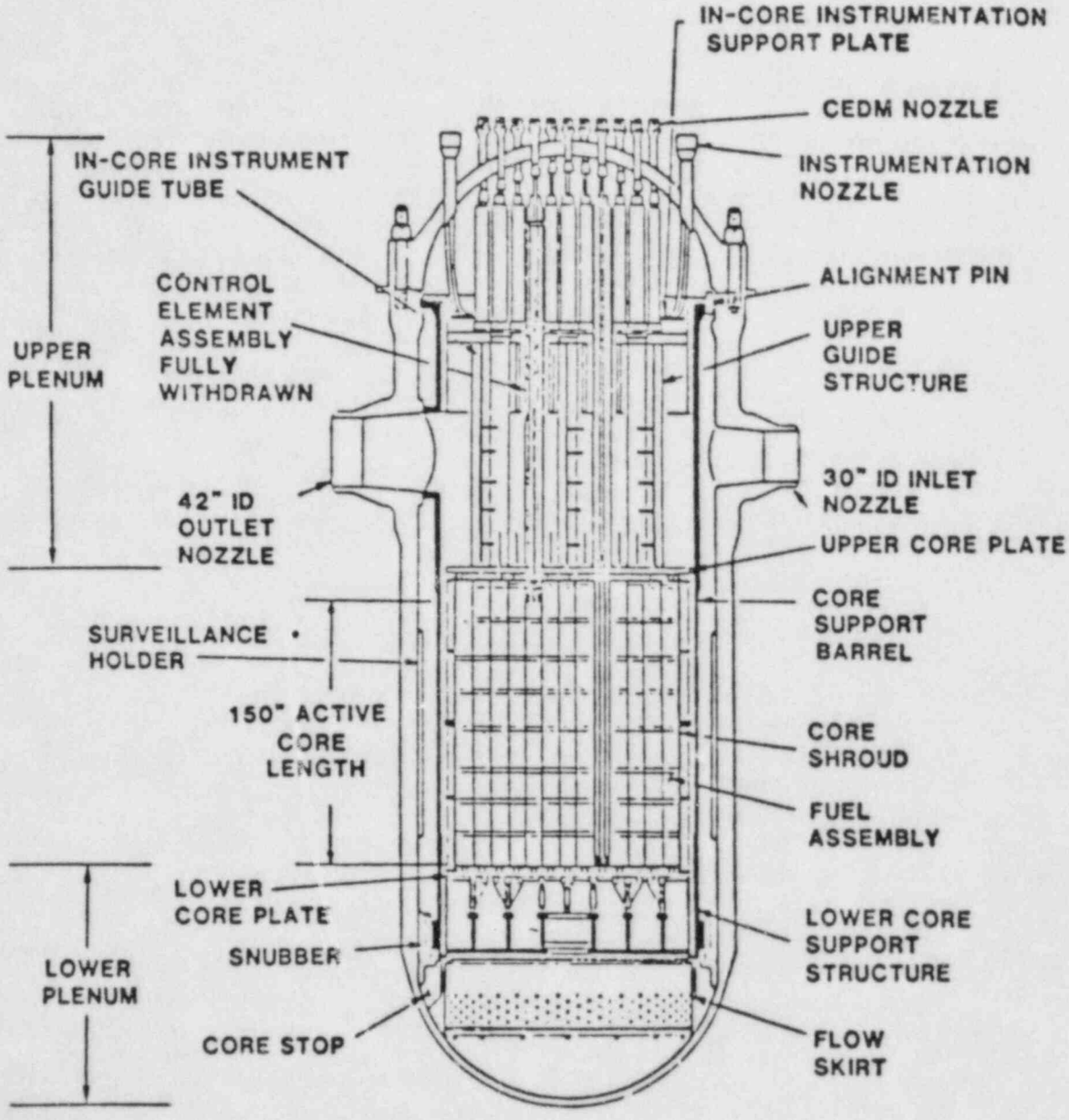

Figure 1.2-6. PWR Pressure Vessel and Generalized Arrangement of Its Contents

the flow skirt. Here the reactor coolant turns and flows upward through the core barrel lower support structure. The coolant then flows up through the core support plate holes and parallel to the axis of the fuel bundles, removing the heat generated within the fuel as it passes. The coolant continues its upward flow through the upper guide structure, then turns and leaves the reactor vessel through two or more outlet nozzles.

1.2.2.2 Reactor Core Assembly

The reactor core assembly is made up of fuel assemblies and control assemblies as shown in Figure 1.2-7. The core assembly is surrounded by the core baffle, the core support barrel, the thermal shield, and finally, the reactor vessel.

The fuel assemblies rest on a lower core plate which is perforated to allow the flow of coolant from the lower plenum to the reactor core. This plate is supported from the lower end of the core barrel by a lower core support structure. The core barrel which is the flow boundary between downward and upward flowing coolant is supported at the lower flange where the top head is bolted onto the vessel. Thus, the whole weight of the core hangs by the core barrel from the inside of the lower flange.

The thermal shield is a radiation and heat shield for the reactor vessel. Flow through the down comer between the core barrel and reactor vessel provides cooling for the thermal shield.

The lower plenum may contain a perforated diffuser plate between the lower core support structure and the lower core plate. The diffuser plate is designed to make the coolant flow suitably mixed and uniform. In addition, a support system between the lower end of the core barrel and the vessel bottom head is usually provided to take care of a design-basis accident in which the core barrel fails. In that event, this auxiliary support system permits the core to fall only a limited distance into the lower plenum and allows the core to retain its geometry.

1.2.2.2.1 Fuel Assemblies

The fuel rods and control rod guide tubes within a fuel assembly are structurally bound together in a square array of typically 15 x 15 or 17 x 17 rods. Typical PWR fuel rods (see Figure 1.2-8) consist of enriched uranium dioxide pellets inserted into zircaloy tubes and each end of the tube is welded shut. Reflector pellets are located above and below the fuel section in each rod. Above the upper reflector pellets in each rod there is a fission gas plenum, i.e., a space in which gases can accumulate. Recently, the PWR fuel rods are prepressurized to reduce the extent of

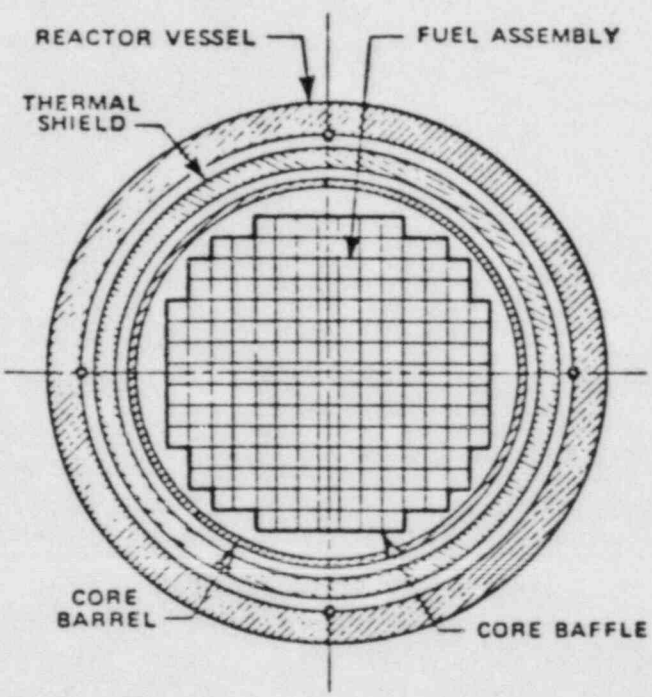

Figure 1.2-7. Cross Section of Typical Four-Loop Core (193 Fuel Assemblies)

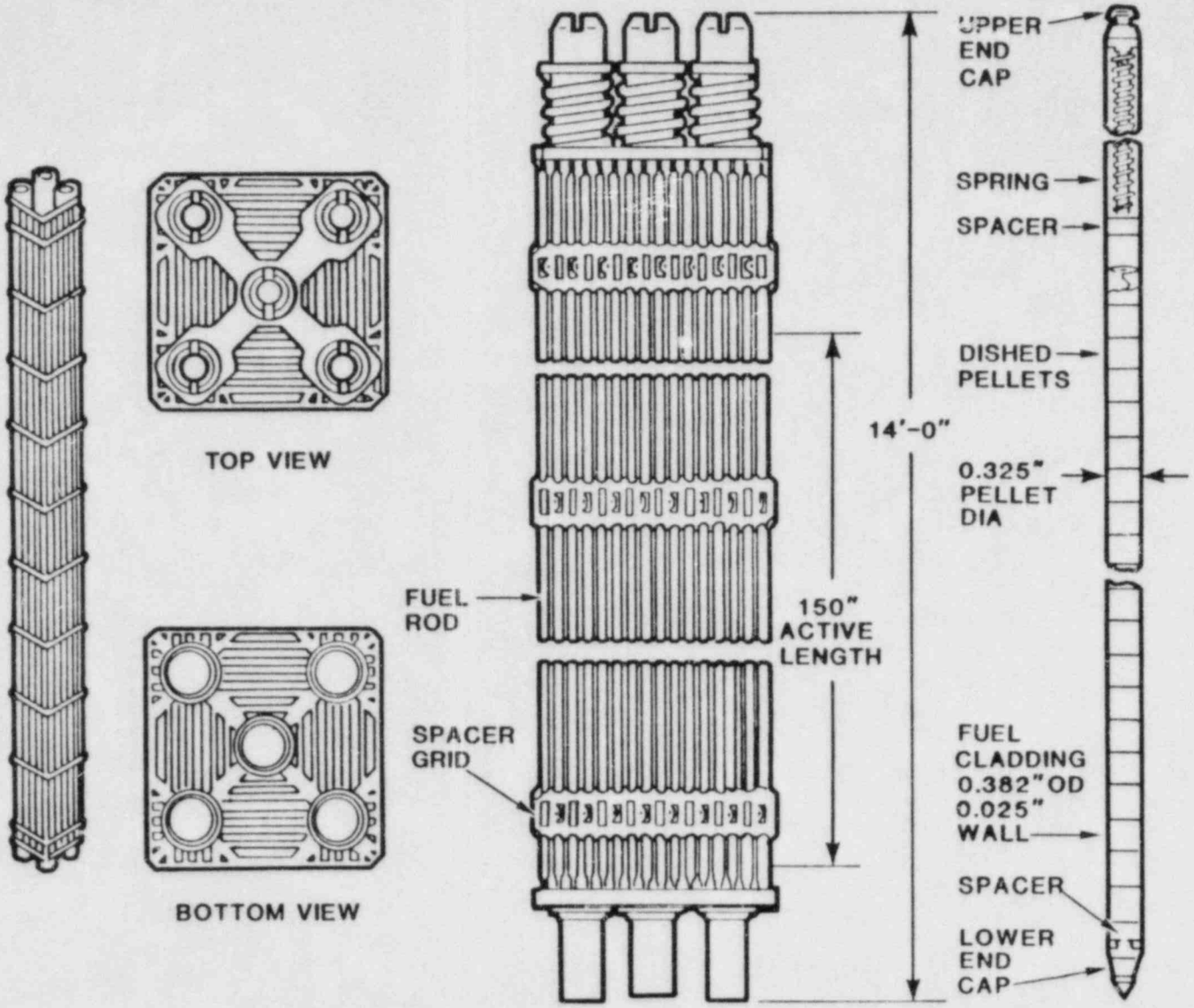

Figure 1.2-8. Fuel Assembly

cyclic stresses that the cladding undergoes. The fuel rod spacing is maintained by spring-loaded guide grid assemblies usually made of zircaloy located along the length of the assembly.

1.2.2.2.2 Control Assemblies

Control assemblies are used, along with chemical control (boric acid) for reactor start-up, shutdown, load following and compensation for small-power transients. The control assemblies as shown in Figure 1.2-9 consist of cylindrical neutron absorber rods, each having approximately the same dimensions as a fuel rod. Several rods are connected together at the top by a spider-like bracket to form a control assembly. Each absorber rod in a control rod assembly moves vertically in its own tubular guide tube.

The control rods typically occupy 12 to 20 fuel rod locations in each of about half of the fuel assemblies. A typical PWR reactor core will have 190 to 220 fuel assemblies and about 1400 to 1700 burnable poison rods.

The burnable poisons commonly used in control rods are boron carbide (B_4C) and an alloy of silver, indium, and cadmium (AgInCd). The control rod guide tubes and cladding are made of either stainless steel or zircaloy. Nonpoison sections of control rods might be filled with aluminum oxide.

Each control assembly is connected through a drive rod which passes through a penetration in the vessel top head to a drive mechanism. When withdrawn, the control rod assemblies occupy space in the upper plenum between the upper core plate and the upper core support.

Westinghouse and Combustion Engineering designs use a magnetic-jack type of drive mechanism as shown in Figure 1.2-10 in which the rod is moved in discrete steps by sequentially energizing coils located outside the pressure housing containing the drive shaft. The pressure housing is a welded extension of the reactor vessel head, made of stainless steel, has a design pressure of 2500 psia and, in effect, constitutes an integral part of the vessel.

The Babcock and Wilcox design used a motor-driven roller nut drive mechanism as shown in Figure 1.2-11. In this arrangement a threaded lead screw is rotated within a roller nut assembly, raising or lowering the control assembly.

1.2.2.3 Steam Generators

The steam generator is a tube and shell heat exchanger which transfers the heat generated in the reactor coolant system to the secondary system, forming steam for use in the plant turbine generator. Two basic steam generator designs

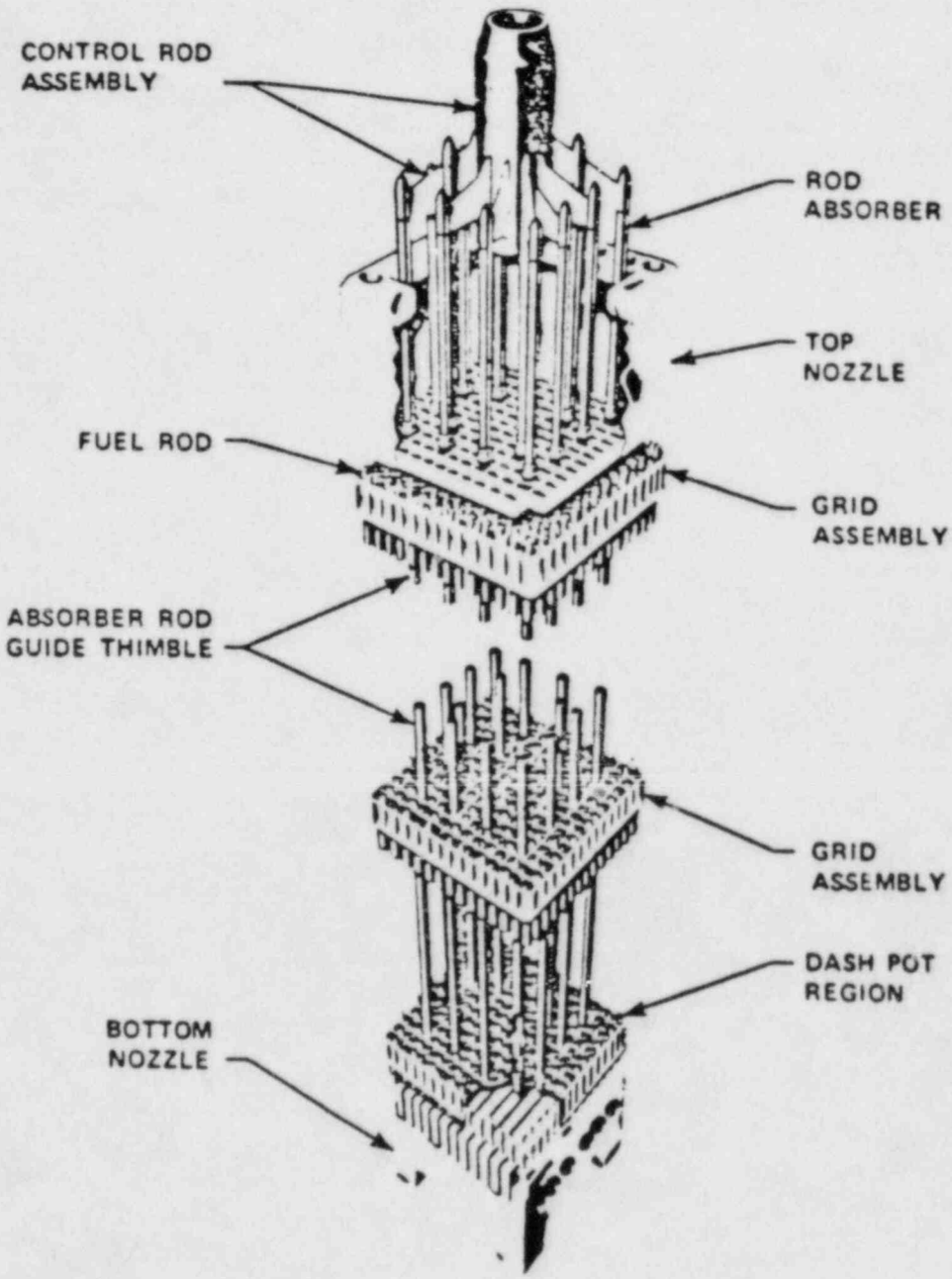

Figure 1.2-9. Cutaway of Typical Rod Cluster Assembly

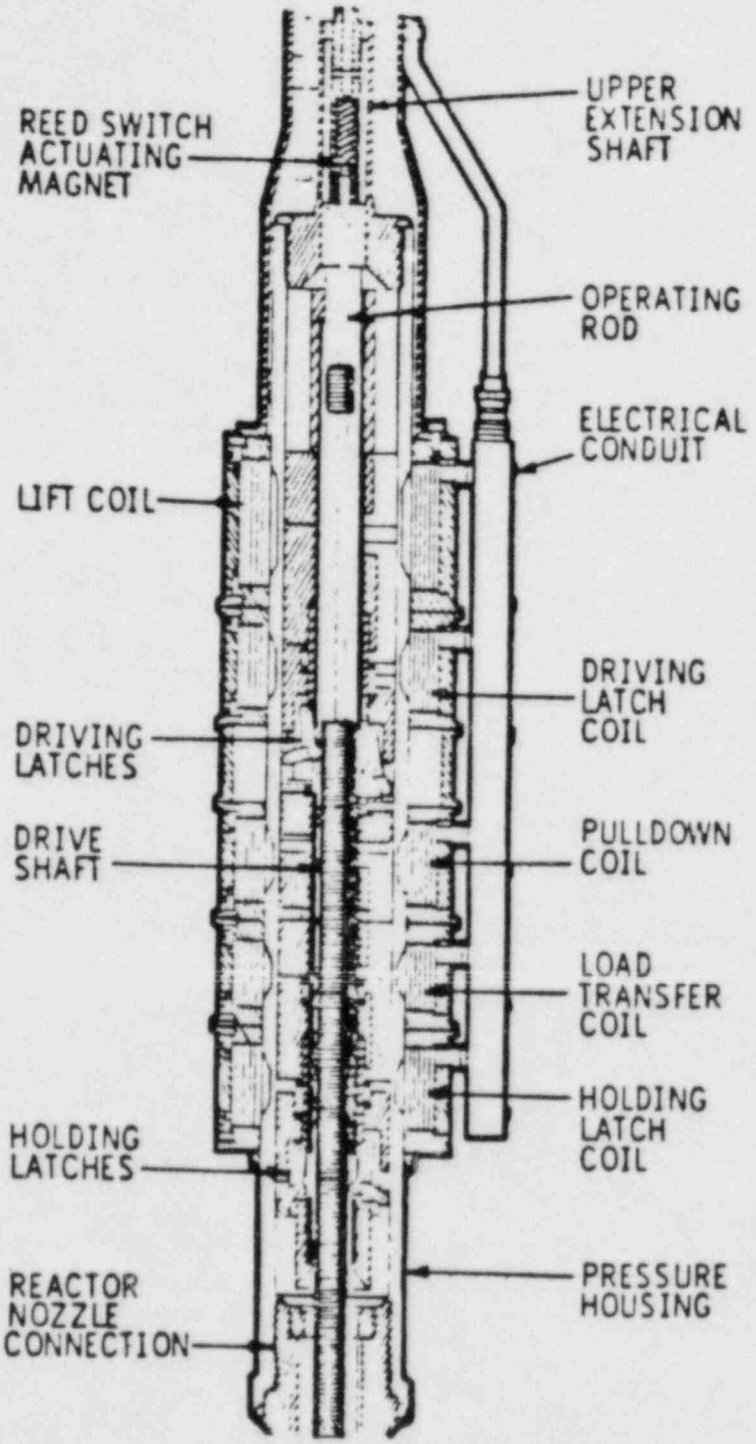

Figure 1.2-10. Control Element Drive Mechanism (Magnetic Jack)

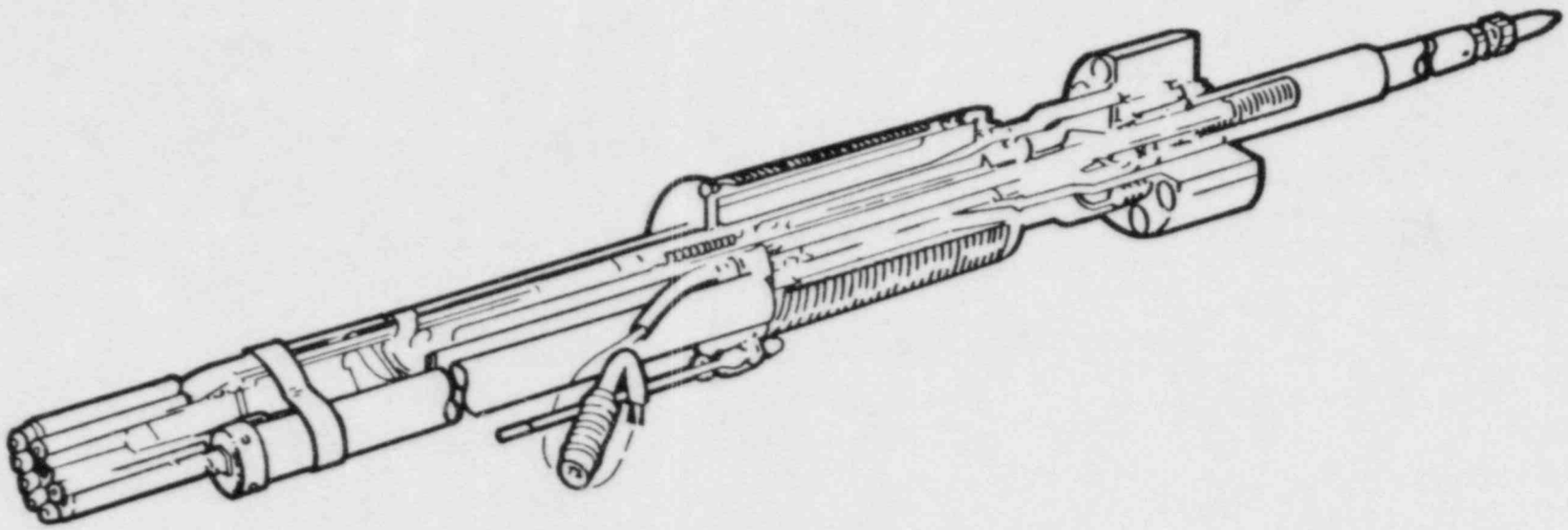

Figure 1.2-11. Canned Rotor Control Rod Drive, Cutaway Diagram

are used in PWR power plants. Both the Westinghouse and Combustion Engineering designs use a recirculation type (see Figures 1.2-12 and 1.2-13) and the Babcock and Wilcox design uses the once-through type (see Figure 1.2-14).

1.2.2.3.1 Recirculation-Type Steam Generator

Each recirculation-type steam generator is a vertical U-tube heat exchanger which operates with the reactor coolant on the tube side and the secondary coolant on the shell side.

Hot reactor coolant from the reactor vessel enters the steam generator through the inlet nozzle in the primary head. From here it flows through the U-tubes, where it gives up heat to the secondary coolant, to the outlet side of the primary head, and leaves through the outlet nozzles. A vertical divider plate separates the inlet and outlet plenums of the primary head. Secondary system feedwater enters the steam generator through the feed nozzle passing into a preheater section where it is heated by the cold leg reactor coolant. The preheater, or economizer, is designed to heat the feedwater almost to the saturation temperature before it mixes with the water in the boiling section.

The wet steam passes through sets of moisture separators and steam driers in the upper portion of the steam generator, and leaves as dry steam through the outlet nozzle at the top.

1.2.2.3.2 Once-Through Type Steam Generator

The once-through type steam generator is a vertical, straight-tube, shell-and-tube heat exchanger, which produces superheated steam at constant pressure over the power range. Reactor coolant flows downward through the tubes and transfers heat to generate steam on the shell side. The high-pressure (reactor coolant pressure) parts of the unit are the hemispherical heads, the tube sheets, and the tubes between the tube sheets. Tube support plates maintain the tubes in a uniform pattern along their length. The unit is supported by a skirt attached to the bottom head.

The shell, the outside of the tubes, and the tube sheets form the boundaries of the steam-producing section of the vessel. Within the shell, the tube bundle is surrounded by a cylindrical baffle. The upper part of the annulus, formed by the baffle plate and the shell, is the superheated steam outlet, while the lower part is the feedwater inlet heating zone.

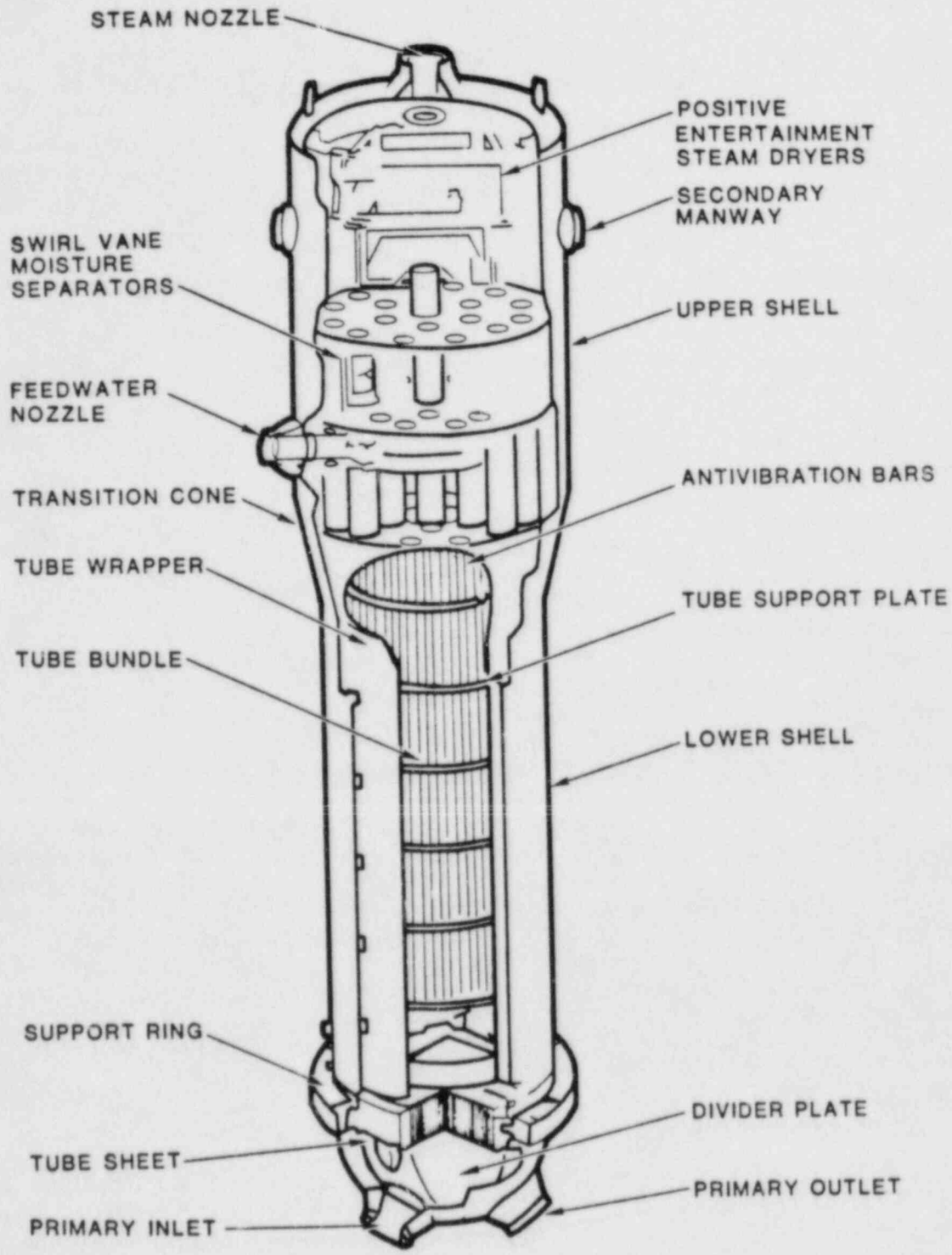

Figure 1.2-12. Westinghouse Steam Generator

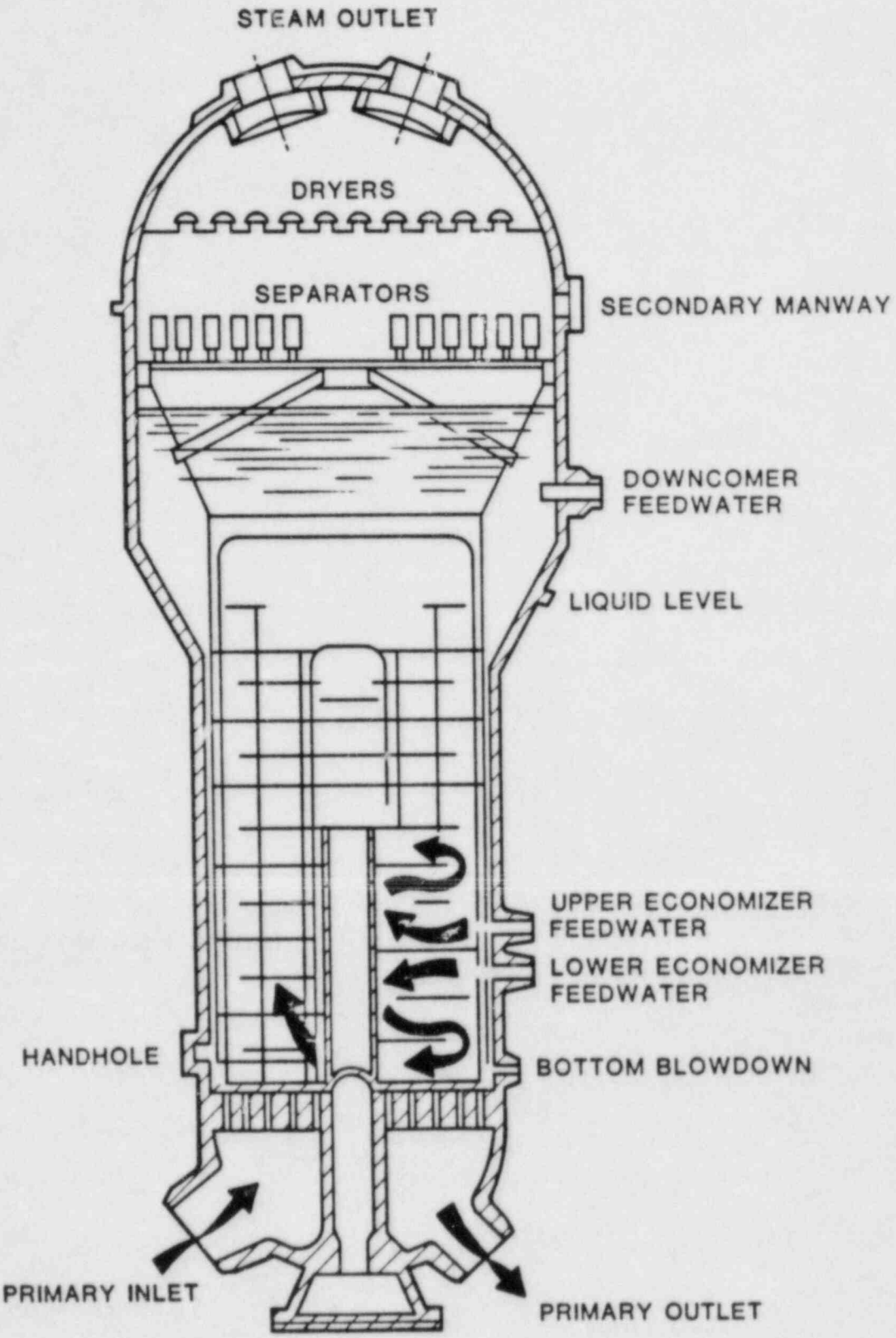

Figure 1.2-13. Combustion Engineering Steam Generator

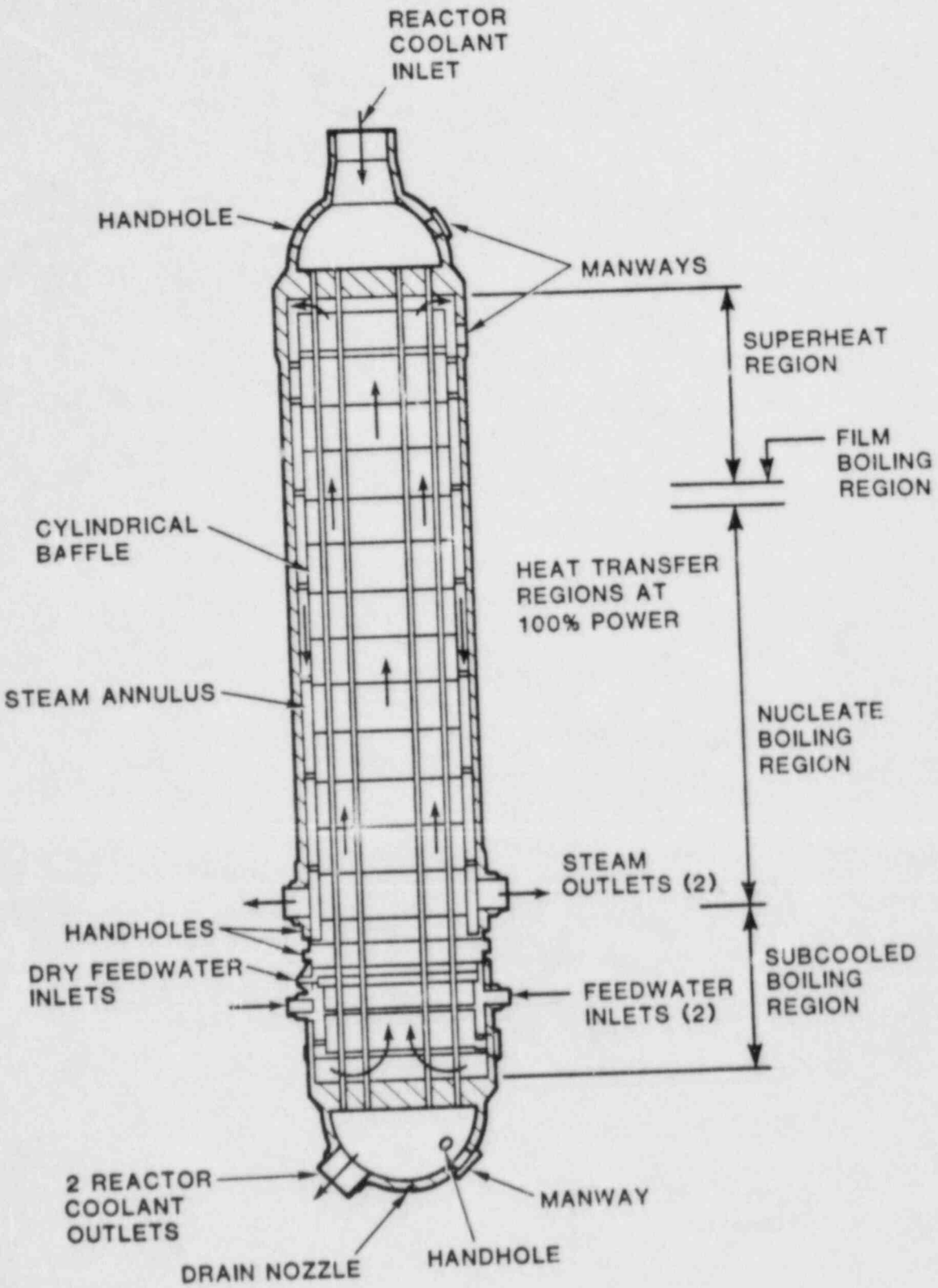

Figure 1.2-14. Babcock and Wilcox Once-Through Steam Generator

1.2.2.4 Coolant Pumps

The reactor coolant pumps (see Figure 1.2-15) are of single-speed vertical-shaft, single-stage, and shaft-sealed centrifugal type designed to pump large volumes of coolant at high pressure and high temperatures through the reactor coolant system. Reactor coolant is pumped by an impeller attached to the bottom of the rotor shaft. The coolant is drawn up through the bottom of the pump casing, through the impeller, and discharged through the diffuser and an exit nozzle in the side of the casing. The diffuser converts velocity head from the impeller to pressure head, and the circular casing collects the flow and discharges it to the single discharge nozzle.

Each pump motor is provided with a flywheel to increase the rotating inertia of the pump which increases the pump coast down time. Nonreverse rotation devices are provided on the pump motors to prevent pump windmilling in the reverse direction and to limit backflow through a stopped pump.

Typically, two cooling systems are provided for the pumps. Water is injected below the seal assembly where part of the injected water flows downward along the shaft, cooling the shaft and providing water for the lower bearing. The remainder of the injected water flows upward through and around the seal assembly. In the event that seal-injection water flow is lost, the lower bearing seal assembly can be cooled by a coil-type water heat exchanger located inside the pump casing and below the lower pump radial bearing and seal.

The shaft seal arrangement for a typical Westinghouse pump consists of three face-type seals operating in a series arrangement. The primary seal is located above the lower radial bearing and is basically a film-riding face seal designed for a normal leakage rate of 3 gal/min at system operating pressure. The second seal is a rubbing face-type seal of conventional design employing a rotating runner and a stationary carbon member designed to normally accept the 3 gal/min leakage of the primary seal at a pressure of approximately 50 psi with a leakage of 3 gal/hr. The second seal is also designed to handle for a short period of time, the full system pressure across its face during an emergency. A third seal, similar to the second seal is a smaller, low pressure, rubbing face-type seal designed to limit leakage into the containment to 100 cc/hr.

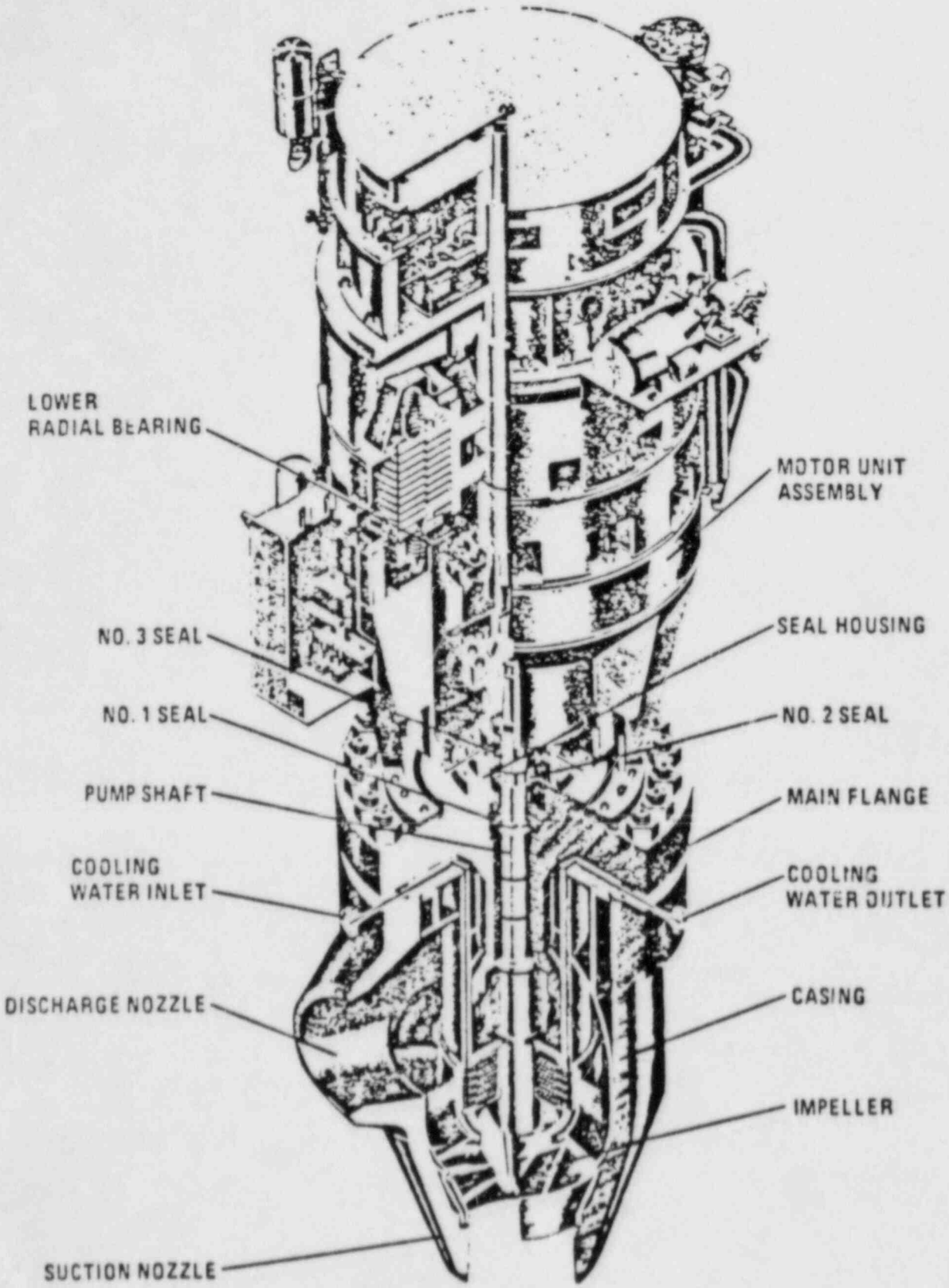

Figure 1.2-15. Cutaway of a Typical Reactor Coolant Pump

1.2.2.5 Pressurizer

The pressurizer attached to the hot leg of one loop maintains reactor coolant system operating pressure during steady state operation, and limits pressure changes during system transients. A sketch of the pressurizer is shown in Figure 1.2-16.

During steady state operating conditions, approximately 60 percent of the pressurizer volume is occupied by water and 40 percent by steam. Electrical immersion heaters, located in the lower section of the vessel, keep the water at saturation temperature and maintain a constant system operating pressure.

A reduction in plant electrical load causes a temporary increase in average reactor coolant temperature with an attendant increase in coolant volume. The expansion of the reactor coolant raises the water level in the pressurizer. This increase in water level compresses the steam, raising the pressure and actuating valves in the spray lines. Reactor coolant from the cold legs of the coolant loops sprays into the steam space and condenses a portion of the steam. This quenching action reduces pressure and limits the pressure increases.

An increase in plant electrical load results in a temporary decrease in average coolant temperature and a contraction of coolant volume. Coolant then flows from the pressurizer into the loops, thus reducing the pressurizer level and pressure. Water in the pressurizer flashes to steam to limit the pressure reduction. This reduction in pressure also closes immersion heater contacts, heating the remaining water in the pressurizer to further limit the pressure reduction.

1.2.2.6 Safety/Relief Valves, Relief Line, and Quench Tank

A typical pressurizer has both relief and safety valves located at the top. The Westinghouse design, for instance, has two power-operated relief valves and three self-actuating safety valves.

Reductions in plant electrical load, with resultant pressure increases beyond the pressure-limiting capability of the pressurizer steam system, cause the motor relief valves to open. The relief valves are automatically opened at a pressure below system design pressure and can also be opened manually from the control console. If the system pressure continues to rise, self-actuating ASME-code safety valves will open. The safety valves are spring load and self-actuating, with back pressure compensation.

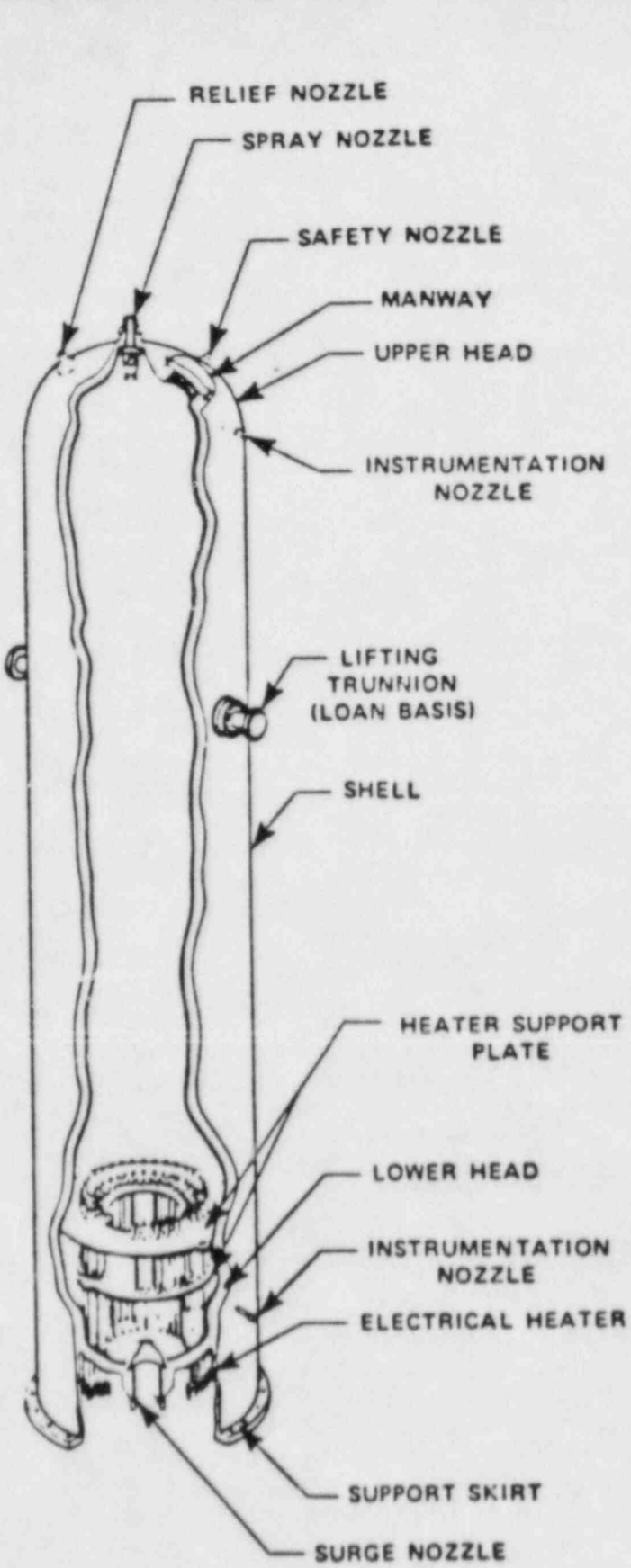

Figure 1.2-16. Cutaway of a Typical Pressurizer

Steam from the relief valves is piped to the pressurizer relief tank, which contains sufficient water to condense the steam. Cold water can be sprayed into the pressurizer relief tank to increase the heat sink capacity. If design pressure is exceeded, a rupture disc vents the tank to the containment. Carbon steel is used for the pressurizer relief line.

1.2.2.7 Reactor Coolant Piping

Reactor coolant piping and fittings are made either of stainless steel or carbon steel clad with stainless steel. Hot and cold leg pipe diameters for a typical 1000 MW(e) Combustion Engineering plant are 42 and 30 inches, respectively.

1.2.3 RCS SAFEGUARD SYSTEMS

Engineered safety features (ESF) are systems designed to minimize the severity and to mitigate the consequences of a loss of coolant accident (LOCA). Engineered safety features are not the only safety-related systems provided for PWR's; the term usually refers to just those systems required to protect against a LOCA. Many of the systems designated as safety features perform other safety-related functions, such as long-term cooldown, or perform normal operational functions, such as maintaining the RCS chemistry.

1.2.3.1 Chemical and Volume Control System

The Chemical and Volume Control System (CVCS) provides the equipment, piping, and instrumentation to maintain the:

- Purity of the reactor coolant
- Required volume of water in the reactor coolant system
- Chemistry of the reactor coolant
- Desired boric acid concentration in the reactor coolant
- Provides high pressure seal water for the reactor coolant pump seals.

During power operation, a continuous feed-and-bleed stream is maintained to and from the RCS (see Figure 1.2-17). Figure 1.2-17 is for a Westinghouse plant but is similar in function for all three PWR manufacturers. Let down water leaves the RCS and flows through the shell side of the regenerative heat exchanger where it gives up its heat to makeup water being returned to the RCS. The let down water then flows through the orifices where its pressure is reduced, then through the let down heat exchanger, followed by a second pressure reduction by a low-pressure let down valve. After passing through a mixed-bed demineralizer, where ionic impurities are removed, the water flows either through the thermal regeneration resins or directly through the reactor coolant filter, and into the volume control tank via a spray nozzle. The vapor space in the volume control tank contains hydrogen which dissolves in the coolant. Any fission gases present are removed from the system by continuous venting of the volume control tank.

The charging pumps take the coolant from the volume control tank and send it along two parallel paths: (1) to the RCS through the tube side of the regenerative heat exchanger; and (2) to the seals of the reactor coolant pumps. The streams divide with some water flowing into the RCS and the remainder leaving the pumps as seal leakage.

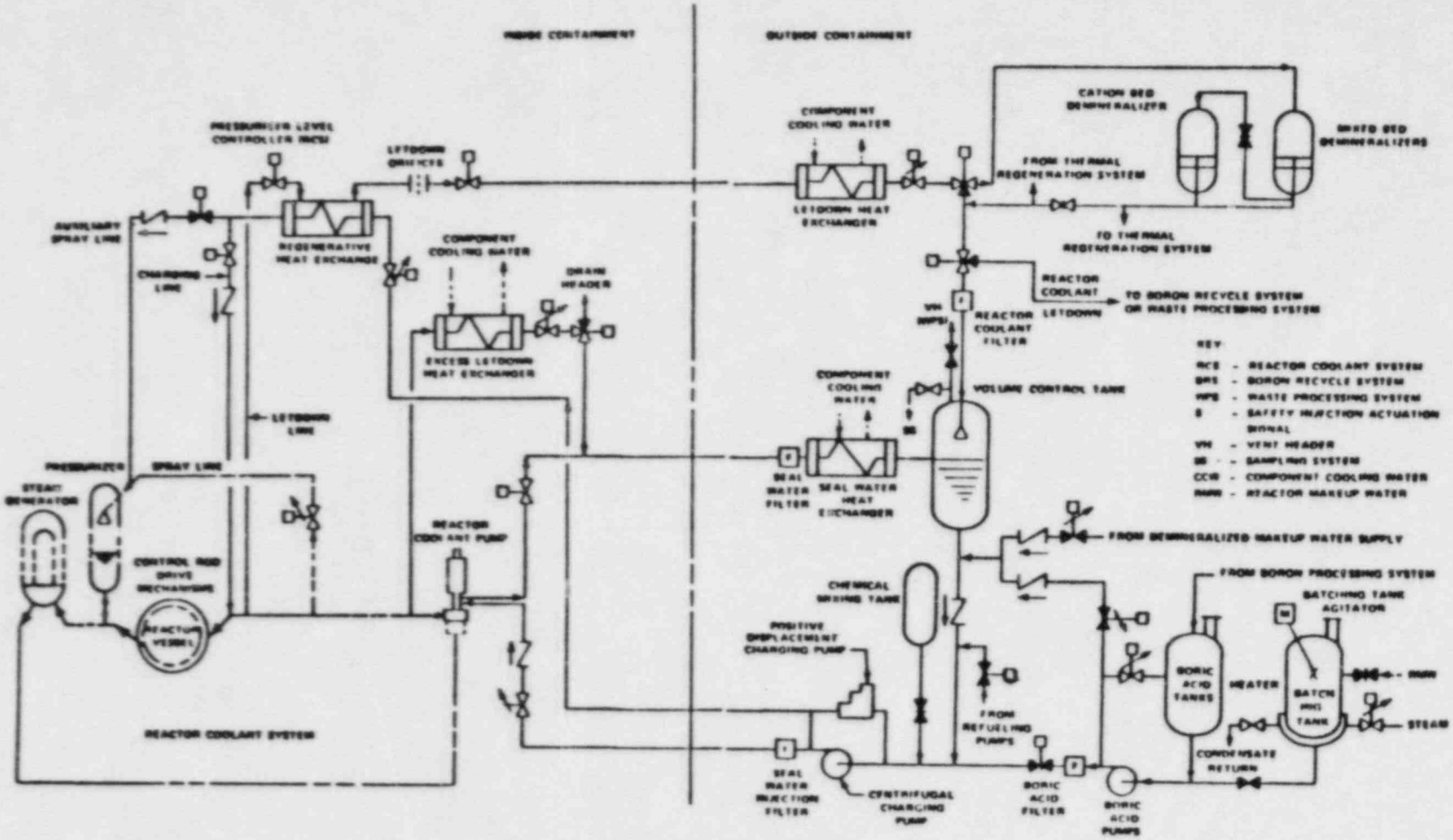

Figure 1.2-17. Chemical and Volume Control System, Flow Diagram

1.2.3.2 Residual Heat Removal System

The residual heat removal system (RHRS) has several functions, but will be used most frequently for removing fission product decay heat from the reactor core during the latter stages of cooldown. During cooldown, the reactor coolant temperature is reduced from the normal operating temperature to a temperature of about 300°F by the steam generators, and then it is further reduced by the RHRS to a temperature that permits refueling. The RHRS also provides cooling water flow to the pressurizer for normal cooldown, maintains the reactor coolant temperature at a suitable level for refueling, provides a means for recirculating the coolant in the fuel transfer canal during refueling, drains the fuel transfer canal following refueling, and provides an engineered safeguard action. The safeguard function of the RHRS is to provide reactor core with borated water and core cooling for the entire spectrum of rupture sizes in the Reactor Coolant System (RCS).

Operation of the system is basically identical for all three reactor manufacturers, with the only significant differences being the point of connection of the RHRS to the reactor coolant system. The following description is for the Westinghouse RHRS as shown in Figure 1.2-18.

To operate the RHRS, circulation of component cooling water through the shells of the residual heat exchangers is established. The block valves in the lines to the RCS are opened and the residual heat removal pumps are started. At this point the reactor cooling function has been taken over by the RHRS, and the turbine bypass system is shut down. One reactor coolant pump is kept running to ensure uniform cooldown of all loops until the coolant temperature is below 160°F.

When the RHRS is first placed in operation, a manual throttle valve is opened slightly to limit reactor coolant flow through the heat exchangers to minimize thermal shock. The valve is then adjusted for the desired flow to remove reactor core residual heat and cool the RCS at the desired rate.

A modulating valve is located in a bypass around the residual heat exchangers. This valve is automatically positioned by a flow controller that measures flow in the main return line to the RCS. Operation of the controller and bypass valve maintains constant return flow to the RCS. As the reactor coolant temperature decreases, the flow through the heat exchangers is increased to compensate for reduced temperature differences across the exchanger tubes.

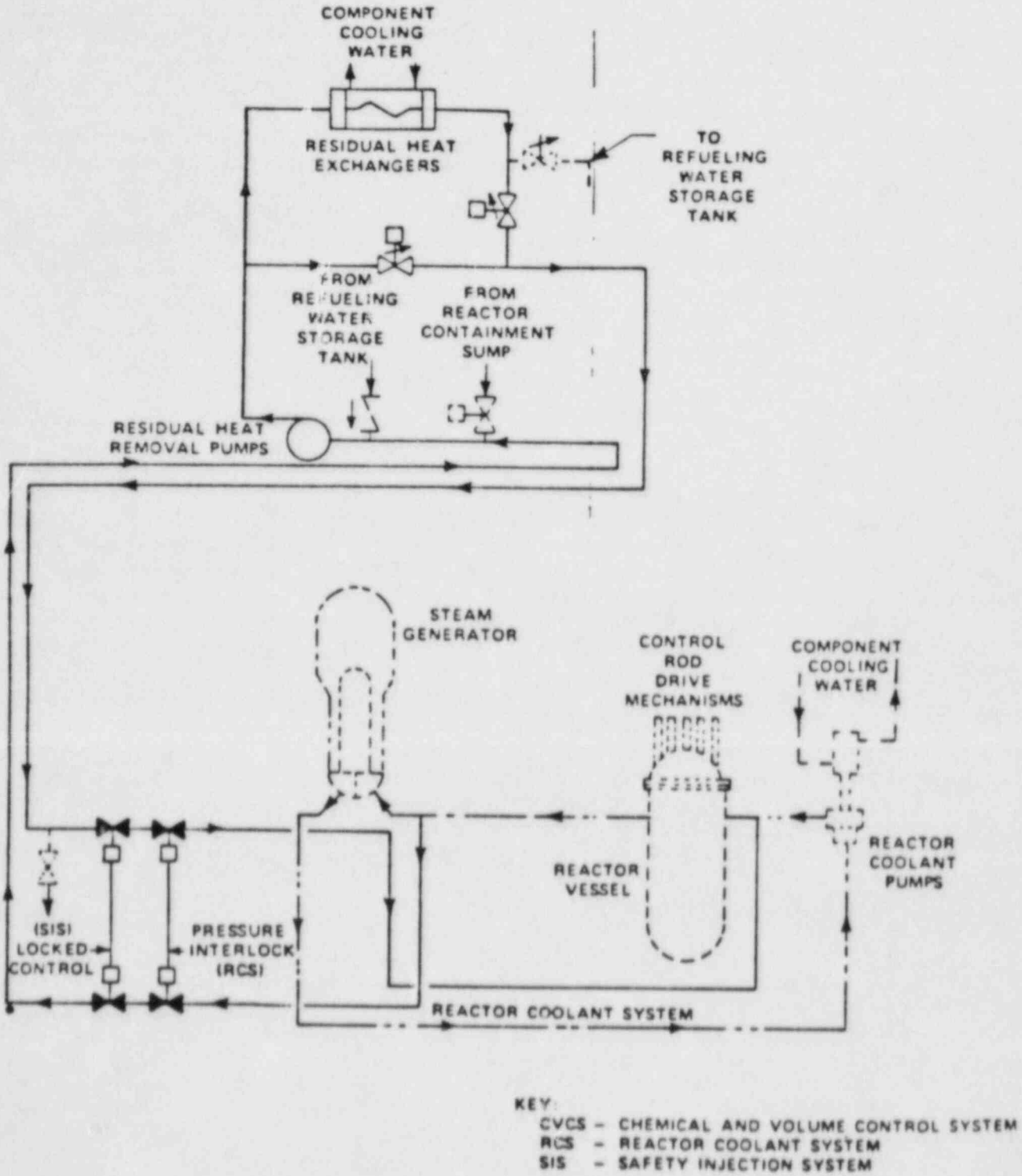

Figure 1.2-18. Residual Heat Removal System, Flow Diagram

Bypass flow is then automatically reduced. When the reactor coolant temperature is reduced to approximately 160°F, the reactor coolant pump is shut down.

With time, the residual heat produced by the reactor core declines until it is only necessary to operate one heat exchanger and one residual heat removal pump. The second heat exchanger and pump may then be taken out of service. The residual heat removal equipment continues to operate after the reactor vessel is opened and refueling operations proceed.

Until appropriate checkout of the RCS is complete, the system continues to remove heat or is in standby to do so. When the reactor coolant pumps are started, the residual heat removal equipment is shut down.

1.2.3.3 Safety Injection System

The primary function of the Safety Injection System shown in Figure 1.2-19 is to supply borated water to the reactor coolant system to limit fuel rod cladding temperature in the unlikely event of a loss of coolant accident. Short-term core cooling consists of injecting a large volume of borated water into the reactor cooling system from storage tanks. Long-term core cooling is provided by recirculating the borated water which has spilled out of the reactor coolant system through the pipe break into the containment sump, back to the reactor coolant system.

The effectiveness of the safety injection systems depend somewhat upon the location of injection which varies from plant to plant. Possible locations for safety injection into the RCS include injection into the hot leg piping, injection into the cold leg piping (on either side of the main pump), injection into the upper head (UHI) and injection directly into the upper plenum (UPI).

1.2.3.3.1 Accumulators

This system consists of tanks partially filled with borated water and pressurized with nitrogen gas which are isolated from the reactor coolant system by check valves. As the reactor coolant pressure falls below the flooding tank pressure (about 600 psig) after a LOCA, the check valves open and borated water is forced into the reactor coolant system.

1.2.3.3.2 High-Pressure Safety Injection System

The high-pressure injection system (HPIS) prevents uncovering of the core during small coolant piping leaks, where high reactor pressure is maintained, and delays uncovering of the core during intermediate-sized leaks.

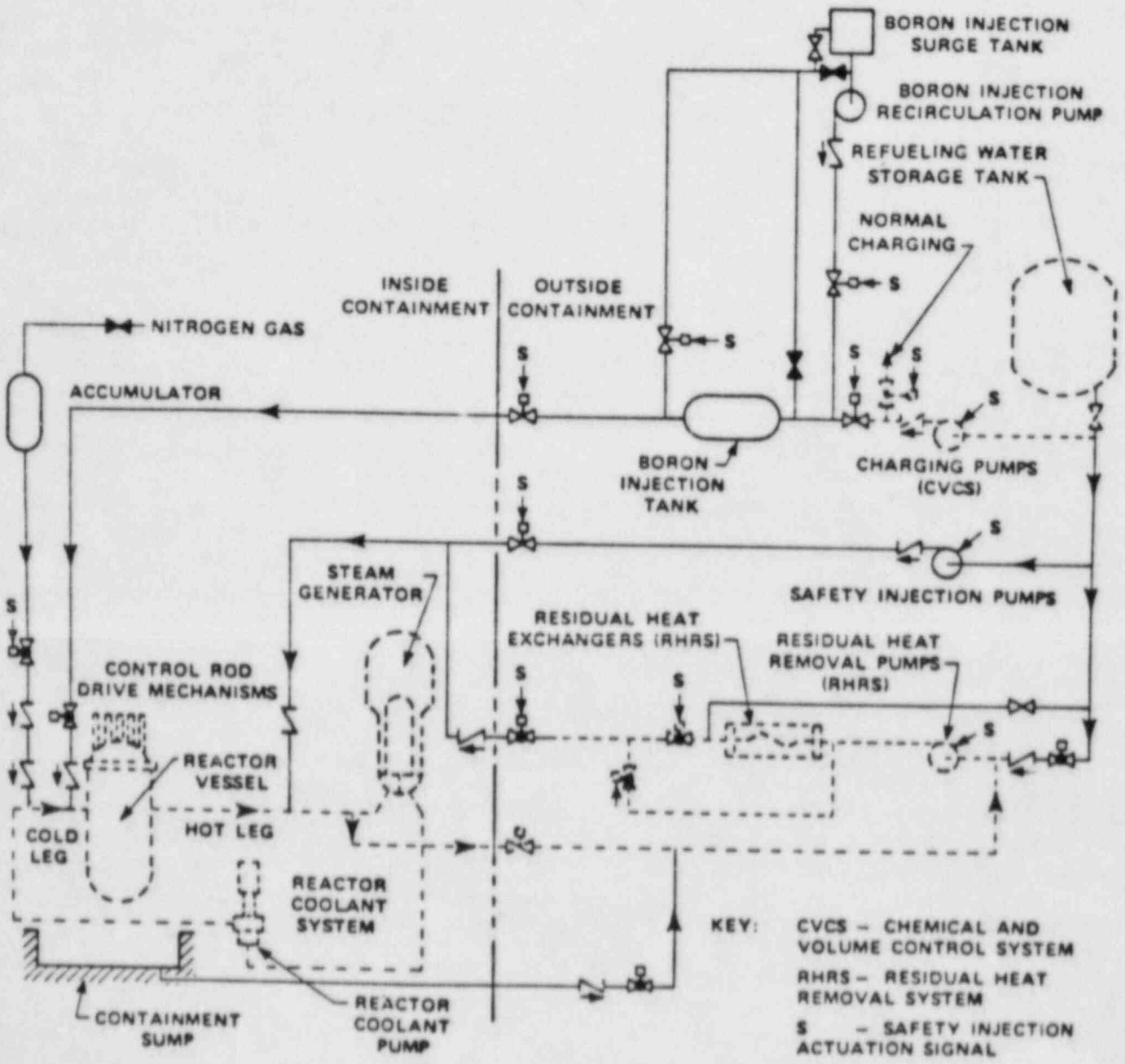

Figure 1.2-19. Safety Injection System, Flow Diagram

High-head centrifugal pumps valved to take suction from the refueling water storage tank delivers borated water to the core through the injection nozzles on each of the RCS hot legs. Some PWR's also have reciprocating charging pumps which provide with a rapid response a small amount of high-head flow into the cold-legs of each loop from a boron injection tank located upstream of the cold-leg injection header.

1.2.3.3.3 Low-Pressure Safety Injection System

The low-pressure injection system (LPIS) is available to inject borated water into the RCS for large breaks which would result in rapid blowdown and depressurization. The low-head system uses two residual heat removal centrifugal pumps which take suction from the same large refueling water storage tank as the high-head pumps and pumps a relatively high flow rate compared to the high-pressure safety injection pumps.

Borated refueling water is pumped through one of the two residual heat exchangers, and through an injection header, and injection lines to the hot-leg piping of each of the reactor coolant loops. The accumulators and low-pressure injection system are designed to recover the core at intermediate-to-low reactor coolant system pressures, and to ensure adequate core cooling for reactor coolant system break sizes ranging from intermediate breaks to the double-ended rupture of the largest pipe.

1.2.3.3.4 Recirculation

Long-term emergency core cooling is accomplished by recirculation of injection water from the containment sump back to the core by the high-pressure recirculation system (HPRS) or the low-pressure recirculation system (LPRS). Switchover from the injection phase to recirculation phase occurs after the large volume tank of injection water is nearly empty about 20 to 30 minutes, depending on the accident, after the initiation of safety injection. The water is cooled by heat exchangers as it recirculates back to the reactor coolant system. The high-head pumps take suction from the discharge of the low-head pumps.

1.2.4 PWR CONTAINMENTS

As the final barrier to the release of fission products from the reactor core to the environment, the PWR containment building houses the reactor and reactor coolant system including the steam generators, reactor coolant pumps, pressurizer, piping, and the safety injection equipment. The functional requirements of a containment structure which recognize every hazard that could conceivably occur as a criterion for the design of a nuclear generating station are indicated by the following criteria:

1. Containments must be as leak-tight as practicable to confine any escape of radioactive materials within reasonable limits.

2. Containments must withstand the peak pressure and time-varying thermal gradient resulting from a loss of coolant accident.

3. Containments must survive dynamic loadings due to earthquake, missile impact, tornado or other cyclonic wind, blast, "small compartment" pressurization, aircraft impact, pipe whip, etc.

4. Containments must provide for the necessary access for maintenance and for periodic refueling.

5. Containments must provide penetrations for steam and feedwater lines, electrical wiring, cabling, instrumentation, and control lines as well as personnel and equipment hatches.

6. Containments must provide for control and monitoring of leakage and surveillance of structural systems.

7. Containments provide shielding in case of major accident.

1.2.4.1 Containment Structural Design

The first containments for nuclear power plants, constructed prior to 1961, were steel spheres and usually single containments. The next step in containment development was to a steel cylinder with a hemispheric top and bottom, then some containment geometry with an outer reinforced concrete shield building making a double containment.

These have largely been supplemented by the various versions of the domed concrete cylinders with foundation slabs reinforced with high-strength reinforcing steel. The most widely used containment for the past several years has been the single containment or reinforced concrete with an integral steel liner plate. Used mostly for PWRs, the reinforced concrete is usually posttensioned by prestressing tendons. The containment is buttressed at three or six points to carry tendon anchorage loads. In its original concept, a flat-type dome of semi-elliptical, or torospheroidal shape was used with a ring girder for dome-tendon anchorage. This has since evolved to a hemispheric dome without ring girder since dome tendons are extended continuously down the side walls and anchored in the tendon galleries. The use of three buttresses rather than six for anchorage of hoop tendons has become standard.

There is an increasing trend toward double containment among the more recent nuclear power plant projects. The most significant advantage for double containment plants is in the postaccident conditions where the radiation dose to the public at large from released activity is reduced by a factor as much as 100, depending on the specific plant design. It may be noted that in double containment plants, the primary containment is either a self-supporting steel cylinder or sphere within the secondary concrete shield building, or, the primary containment is a concrete shell within a secondary concrete or steel building.

The approximate dimensions of a typical containment are: 124 feet inside diameter, 203 feet inside height, 3-1/2 feet wall thickness, and 2-1/2 feet dome thickness. The internal net-free volume is about 2,000,000 cubic feet.

Containment penetrations include equipment and personnel access hatches, a fuel transfer penetration, and ventilation system purge ducts. An equipment hatch 19 feet in diameter fabricated from welded steel and furnished with a double-gasketed flange and bolted disked door is provided. Two personnel locks are provided with a welded steel double door air-lock assembly. A 20-inch fuel transfer penetration is provided for fuel movement between the refueling transfer canal in the containment and the spent-fuel pool outside.

1.2.4.2 Containment System Layout

All components of the reactor coolant system are arranged inside the reactor building as shown in Figures 1.2-20 and 1.2-21. The reactor vessel is located in approximately the center of the reactor building. The steam generators and the reactor coolant pumps are symmetrically located on opposite sides of the reactor vessel and at a higher elevation. The symmetrical arrangement equalizes the friction pressure losses in each heat transfer loop.

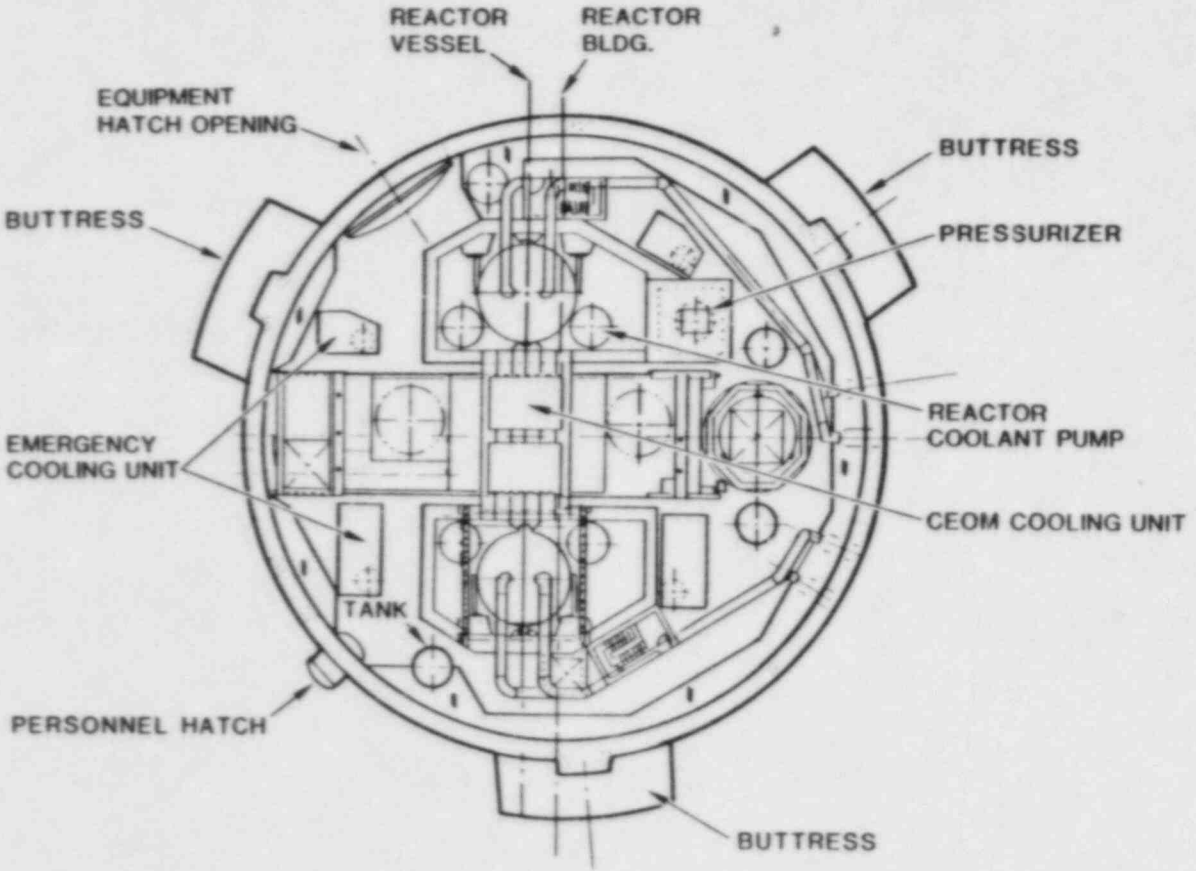

Figure 1.2-20. Arizona Nuclear Power Project Reactor Building Layout Plan at Operating Level, Elevation 140'-0"

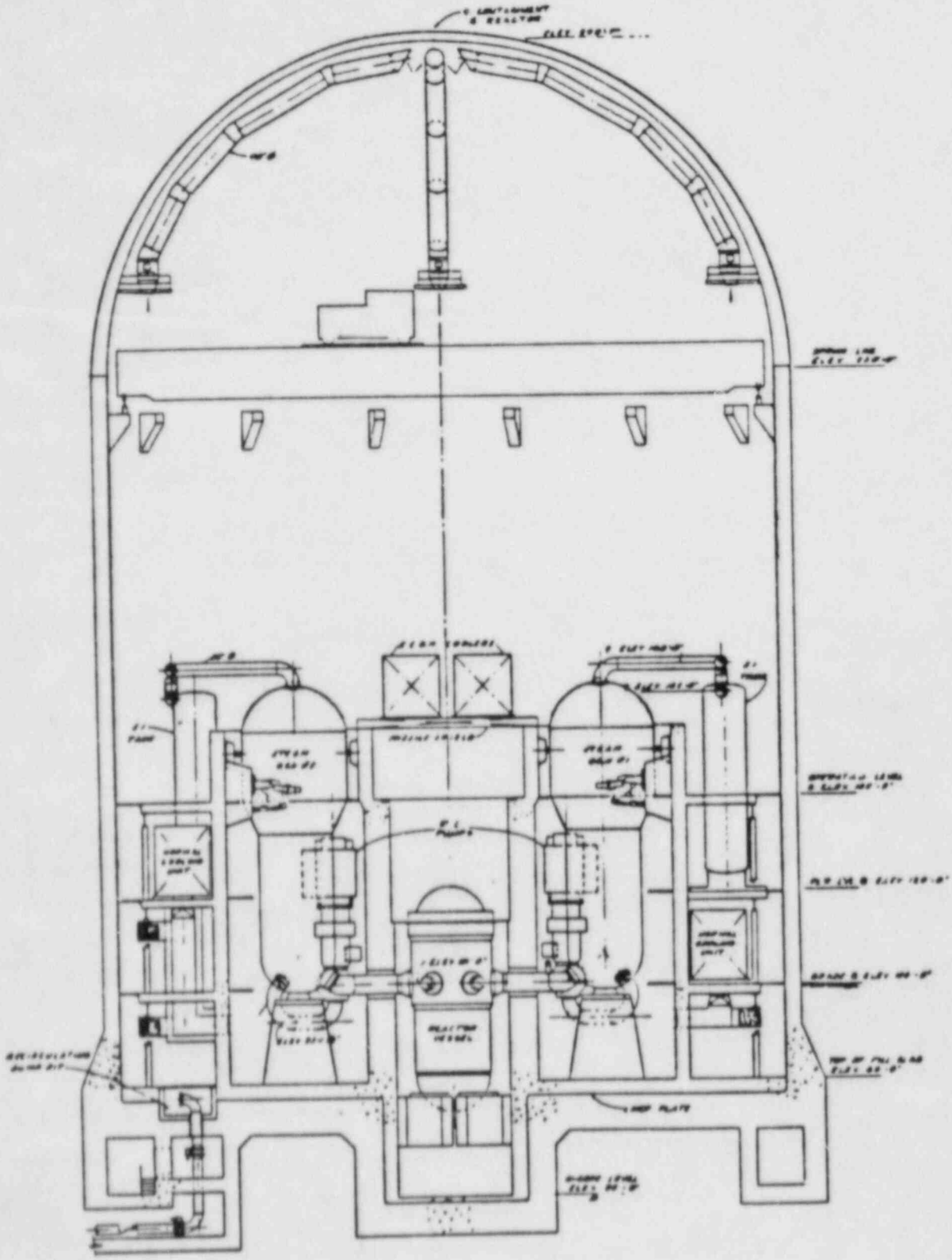

Figure 1.2-21. Arizona Nuclear Power Project Reactor Building Layout Section A-A

To permit personnel access to the reactor building during power operation, the reactor coolant system is surrounded, within the reactor building, by concrete shield walls. These walls around the steam generators are referred to as the secondary shield walls. In addition to this shield, the reactor vessel is installed in a thick concrete shield wall referred to as the reactor cavity or primary shield. The primary shield wall reduces the radiation level in the steam generator compartments, to maintain the activation of the loop components within acceptable limits to permit maintenance on these components during plant shutdown. The secondary shielding, in conjunction with the primary shield, limits the radiation levels in the reactor building so that, depending on the design criteria, it may be possible to have access to areas of the containment outside the secondary shielding for maintenance.

Spent fuel is handled underwater from the time it leaves the reactor vessel until it is placed in a cask for shipment from the site. The fuel handling facilities shown in Figure 1.2-22 are generally divided into two areas: the refueling cavity and fuel transfer canal, which are flooded only during plant shutdown for refueling; and the spent fuel pit, which is kept full of water and is always accessible to operating personnel. These two areas are connected by the fuel transfer tube through which an underwater conveyor carries the new fuel into the plant containment. In the refueling cavity, fuel is removed from the reactor vessel, transferred through the water and placed in the fuel transfer system.

The reactor cavity is a reinforced concrete structure; when filled with borated water for refueling, it forms a pool above the reactor. The cavity is filled to a depth that limits radiation at the surface of the water to acceptable levels during those brief periods when a fuel assembly is being transferred over the reactor vessel flange. The reactor vessel flange is sealed to the bottom of the reactor cavity by a clamped, gasketed seal ring that prevents leakage of refueling water from the cavity. This seal is clamped closed during the flooding of the cavity for refueling operations. The cavity is large enough to provide storage space for the reactor upper and lower internals, and for miscellaneous refueling tools.

The refueling canal is a passageway that extends from the reactor cavity to the inside surface of the reactor containment. The canal is formed by concrete shielding walls extending upward to the same elevation as the reactor cavity. The floor of the canal is at a lower elevation than the reactor cavity, thus providing the greater depth required for the fuel transfer system tilting device and the rod cluster control changing fixture located in the canal.

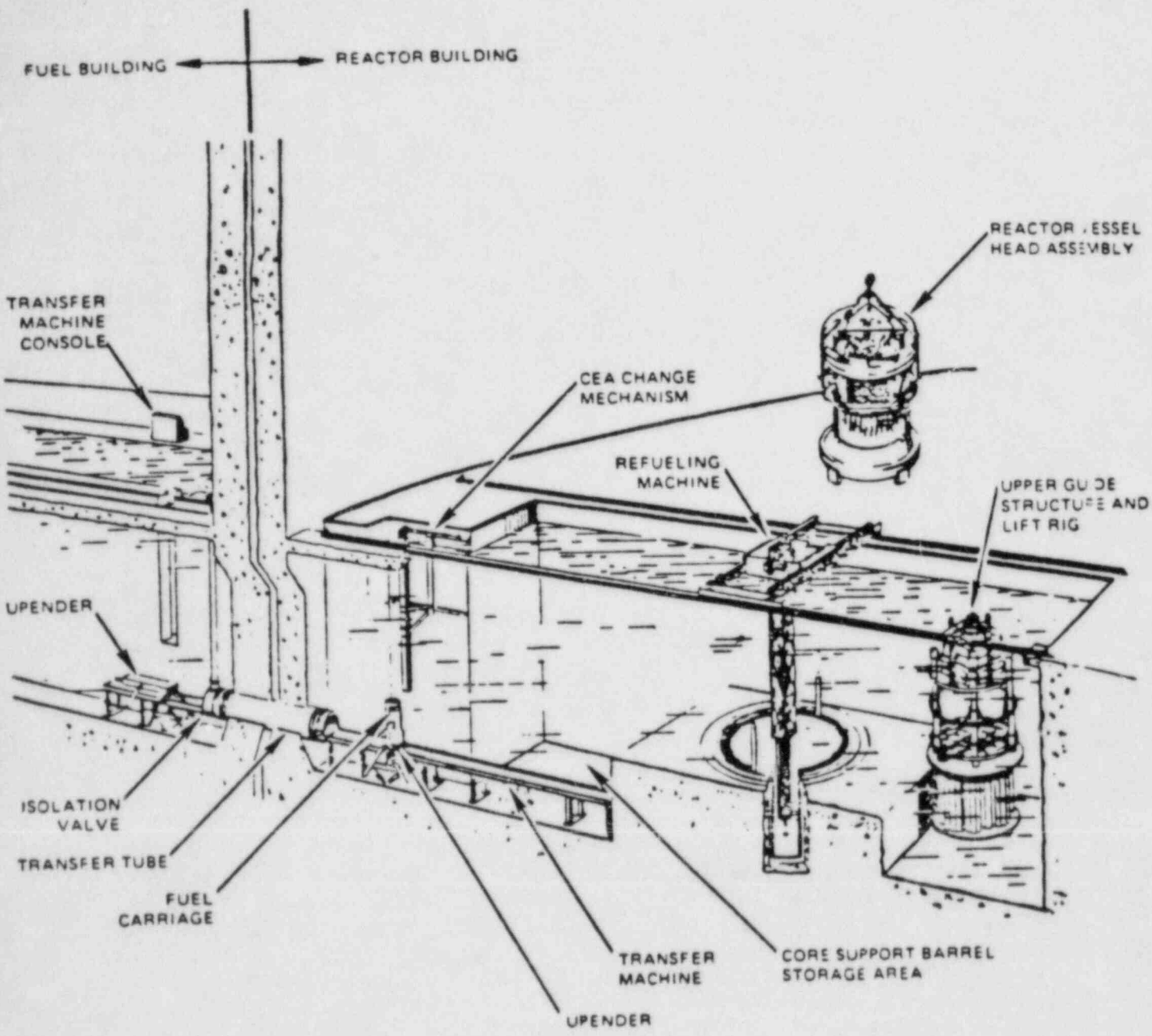

Figure 1.2-22. Combustion Engineering Fuel Handling Equipment Arrangement

The transfer tube enters the reactor containment and protrudes through the end of the canal.

1.2.4.3 Containment Isolation System

The Containment Isolation System is an engineered safety feature which provides the means of isolating the various fluid systems passing through the containment walls as required to prevent the release of radioactivity to the outside environment.

Subsequent to an accident which may release radionuclides within the containment, there must be a barrier in all fluid lines between the atmosphere outside the containment and (1) the containment atmosphere, (2) the RCS, or (3) closed systems inside the containment which are assumed vulnerable to accident forces. Leakage from the containment through all fluid lines which penetrate the containment and are not part of an engineered safeguards system is minimized by a double barrier. Use of a double barrier ensures that failure of a single active component along a leakage path will not result in loss of ability to isolate the containment.

A barrier may be a valve, a blind flange (two barriers by use of a double gasket), or a closed piping system or vessel, each of which must be missile protected, and designed for a pressure equal to or greater than the design pressure of the containment.

1.2.4.4 Containment Spray System

The containment spray system sprays borated water into the containment atmosphere. The spray cools the atmosphere and reduces the postaccident temperature and pressure within the building. Simultaneously, the spray reduces, by chemical reaction, the postaccident level of fission products in the containment atmosphere. Borated water is pumped into containment spray headers, located high in the containment. A chemical additive, such as NaOH, is sometimes added to the spray water to allow control of spray pH. The spray system operates in two phases similar to the emergency core cooling system: an injection phase, and a recirculation phase. During the injection phase, the containment spray pumps take suction from the same, large, borated water supply tank that supplies the highand low-pressure injection systems. Once this source is depleted, the spray pump suction is transferred to the containment sump, and recirculation occurs. Heat exchangers are sometimes provided to cool the spray during recirculation.

1.2.4.5 Containment Fan Cooler System

The containment fan cooler units, an engineered safeguard system, are designed to remove heat from the containment building during both normal operation and in the event of a severe accident. There are a total of about five units per containment located outside of the missile shields.

During normal operation, air is drawn from the upper part of the containment through the return air ductwork. The flow is routed through the normal flow inlet damper into the roughing filter plenum. The air is then drawn through the cooling coils and discharged by the fan into the ventilation system distribution ductwork.

During the post-LOCA operating mode, the air flow is routed from the return air ductwork through the accident flow inlet damper and then into the filtration package plenum. The air then flows through moisture separators, HEPA filters, and discharges through the accident flow outlet dampers into the roughing filter plenum and into the coils. When a LOCA is sensed, the fan motors are automatically switched to low speed to provide proper flow of the steam-air mixture. Space is provided in the filter package between the HEPA filters and the outlet dampers for possible future installation of charcoal filters and racks.

A gravity-actuated backdraft damper is provided for installation into the ventilation system discharge ductwork from each fan. These dampers serve to isolate units from the ventilation system when the fan is not in use and to protect each unit from damage due to a reverse flow during a LOCA pressure transient.

The cooling coils remove heat from the air with the fan providing the required air flow rates. Cooling water is supplied by the service water system. Drain troughs and piping are provided to remove condensate from the cooling coils. The drain piping is routed to the containment sump.

1.2.4.6 Containment Ice Condenser

The ice condenser system provides a large volume of ice within the containment to condense steam and absorb energy released during a severe accident. The heat sink capacity of the ice bed reduces the peak temperatures and pressures in the containment during an accident and allows the containment to be designed with a smaller volume.

The peak pressure in an ice-condenser reactor containment following a loss of coolant accident is one-quarter or less than that which could occur in an earlier type containment structure. Furthermore, the containment pressure is reduced to a few pounds per square inch within minutes after

an accident. Because of the reduced containment pressure, the probability of significant leakage of radioactive vapor or gases to the environment is greatly decreased. In addition, much of the radioactivity released within the containment is condensed with the steam. Finally, because the ice condenser is a static heat sink that is not dependent upon any external power source for its operation, its reliability as an engineered safe- guard is maximized.

The ice condenser system is an inherently passive (static) safeguard system. No external source of power is needed for operation of the ice condenser during the blow-down period. The chemical composition of the ice inventory allows the melted ice to be used for reactor cooling, and has the further capability of removing fission products from the containment atmosphere both during and after blowdown.

The ice condenser is a completely enclosed refrigerated annular compartment formed between the crane wall and the containment shell (see Figures 1.2-23 and 1.2-24). In elevation the ice condenser is generally above the operating deck.

In the event of a loss of coolant accident, door panels located below the operating deck to the bottom of the ice condenser open immediately due to the pressure rise in the lower compartment, thereby allowing the air and steam to flow from the lower compartment into the ice condenser. In turn, the door panels at the top of the ice condenser open and allow the air which was initially in the lower compartment to flow into the upper compartment. Steam contacting the ice is immediately condensed limiting the pressure in the containment. Condensation of steam within the ice condenser also promotes flow of steam from the lower compartment to the condensing surface of the ice, thus substantially reducing the time that the containment is at an elevated pressure.

1.2.4.7 Containment Air Purification and Cleanup Systems

The containment spray system, in addition to its depressurization function, serves as a medium for the removal of certain fission products, particularly iodine. Some PWR's have charcoal filters installed in the emergency air cooling system, as well, for the removal of fission products. Again, the fission product of primary interest is iodine, which is absorbed in the activated charcoal filters. In order to further reduce the amount of radioactivity released to the atmosphere after a LOCA, some projects have incorporated penetration-building charcoal filter systems. The Vogtle project has taken one further step with a containment enclosure building.

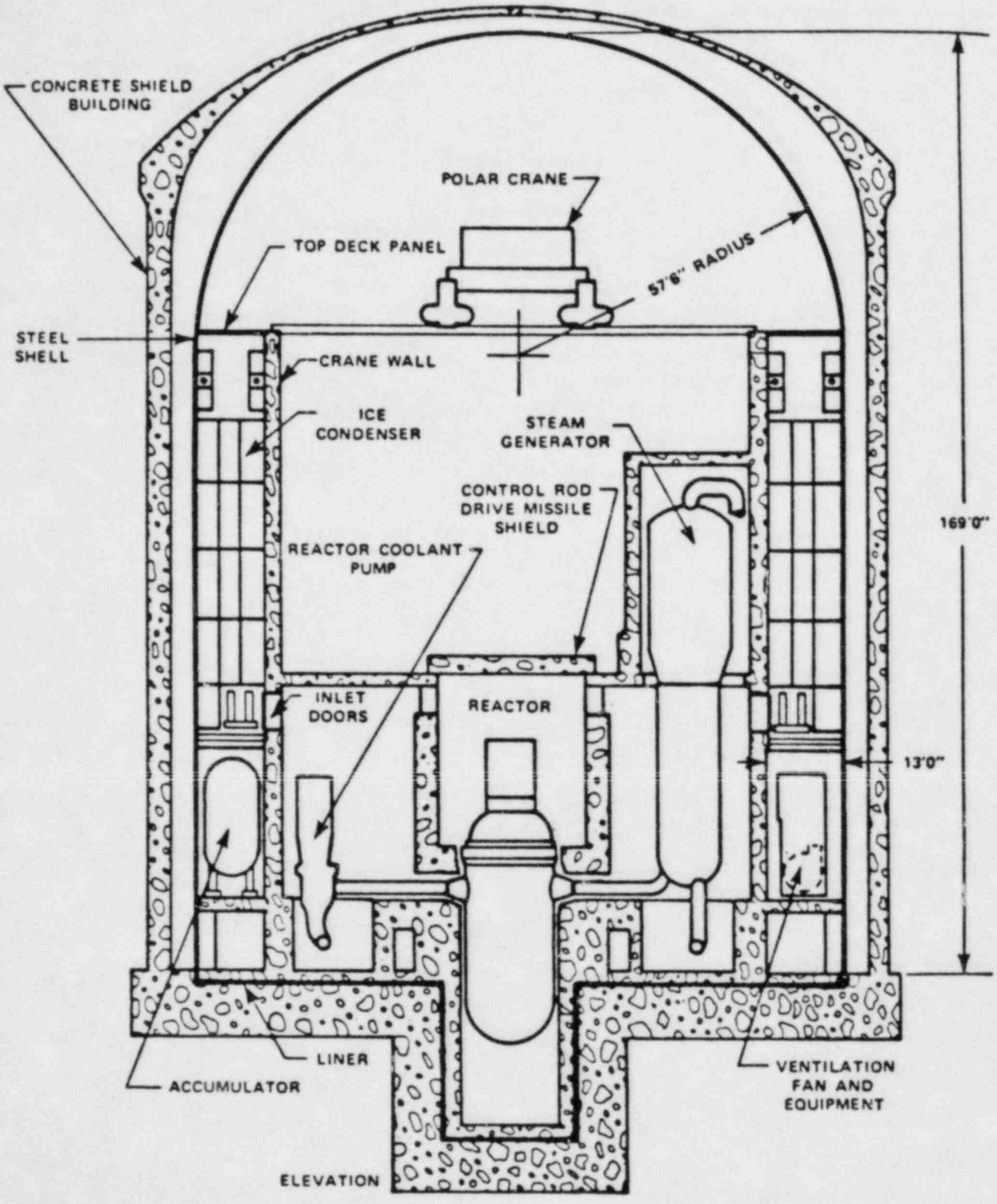

Figure 1.2-23. Cross Section of Ice Condenser Containment

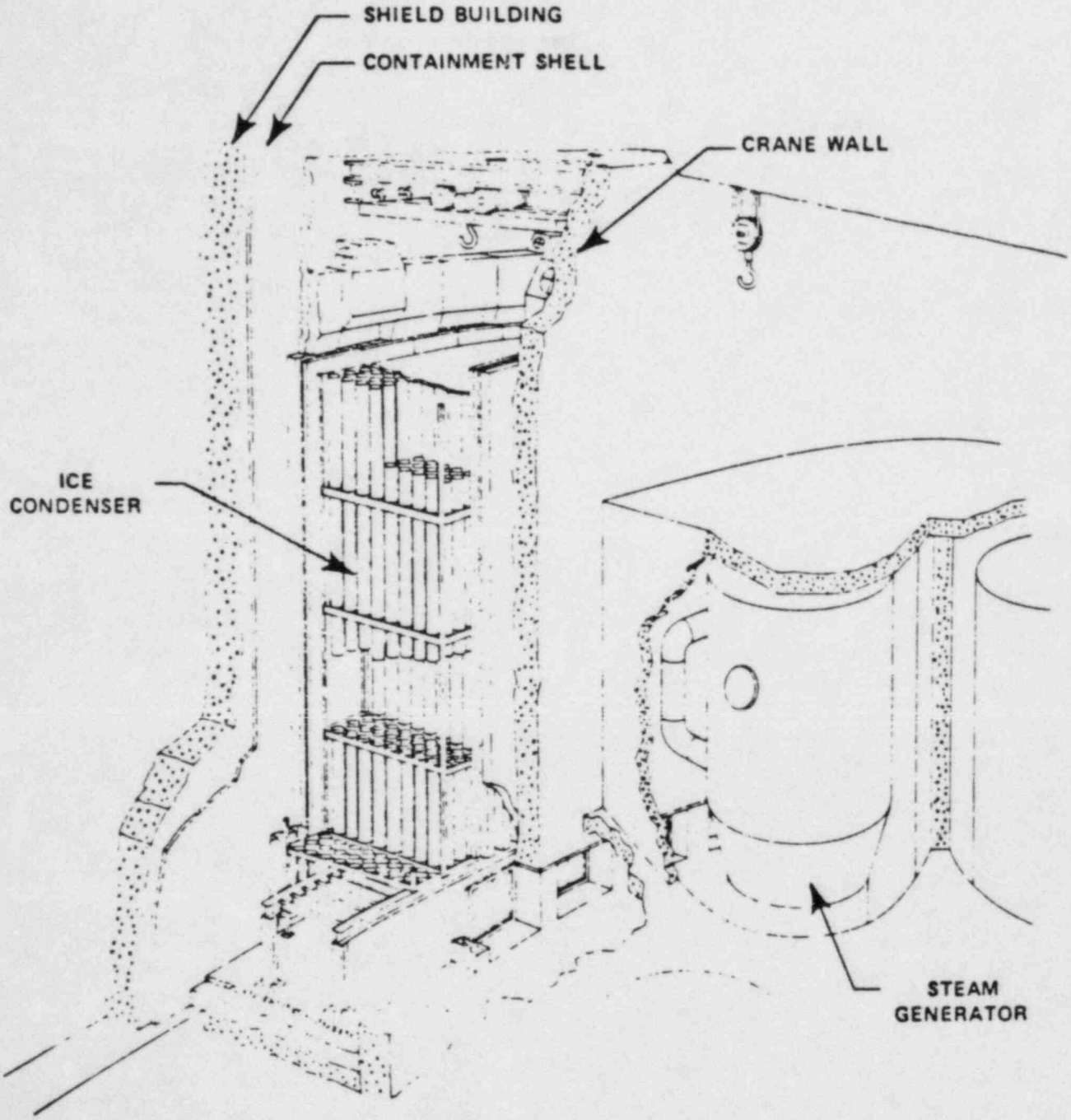

Figure 1.2-24. Ice Condenser Compartment

1.2.4.8 Combustible Gas Control Systems

Following a LOCA, hydrogen gas may be generated inside the containment by reactions such as zirconium metal with water, corrosion, and radiolysis of water in the core and containment sump. To ensure that the hydrogen concentration is maintained at a safe level, i.e., less than 4 percent, it is necessary that combustible gas control systems be provided. On earlier plants, the system simply consisted of a purge system which vented the containment to atmosphere, thereby reducing the hydrogen concentration of the containment air. More recently, hydrogen recombiners are being provided, with the hydrogen-purge system acting as a backup system. The hydrogen recombiners process containment air containing hydrogen, recombining the hydrogen with oxygen, to produce water. The recombiners being proposed on the Vogtle project are electrical recombiners, with recombination taking place in an electric heater device at temperatures around 1150 to 1400°F. Catalytic recombiner units are also available.

1.2.5 SECONDARY LOOP AND POWER CONVERSION SYSTEM

The secondary loop of a PWR nuclear steam power system includes the secondary side of the steam generator, the power conversion system (turbine generator, condenser, and feedwater pump) and associated piping, pumps, reheaters, etc. The secondary loop for a typical Westinghouse design will be described in this section and will be typical of other designs as well.

1.2.5.1 Turbine-Generator Set

The typical turbine (see Figure 1.2-25) is a four-casing 1800 rpm unit with tandem-compound six-flow exhaust and 44-inch last row blades. The turbine consists of one double-flow high-pressure element in tandem with three double-flow low-pressure elements. Combination moisture-separator steam reheater assemblies are provided between the high- and low-pressure elements to dry and superheat the steam.

The high-pressure turbine is a double-flow element with an impulse control stage followed by reaction blading in each end of the element. The steam enters the high-pressure element through two steam chests, one located on each side of the high-pressure casing. Each steam chest contains two throttle-stop valves and two governing valves. The governing valve outlets are connected to the high-pressure casing through four inlet pipes, each of which connects to a nozzle chamber enclosed within the high-pressure casing. Two of these inlet connections are in the base and two are in the cover. The steam flows axially in both directions from the nozzle chambers, through the control stage and reaction blading to the four exhaust openings (two at each end) in the casing base, then through the cross-under piping to the moisture-separator reheaters. Cross-over pipes return the steam through the reheat stop and interceptor valves to the three low-pressure turbines.

The cross-under and cross-over pipes are provided with diaphragm-link, hinge-type expansion joints. These joints absorb the differential pipe movements, utilizing axial pressure load, carrying links in conjunction with flat plate diaphragms.

Each low-pressure turbine is a double-flow element employing reaction blading. Steam enters at the center of the blade path, flows through the blading to an exhaust opening at each end, then downward to the condenser. Openings are provided in the casings through which steam may be extracted for feedwater heating.

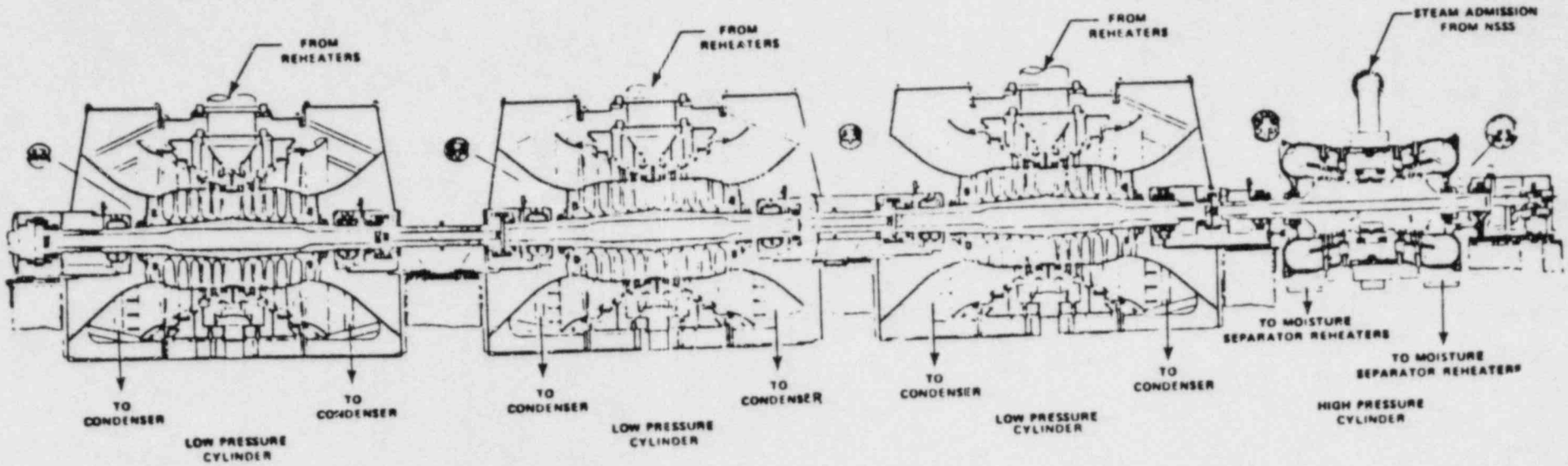

Figure 1.2-25. Main Turbine

A typical main generator for a large nuclear station is of the hydrogen inner-cooled synchronous type with a water-cooled stator. Cooling for a generator of this size is provided by circulating hydrogen, at a pressure of about 75 psig, through the generator by fans attached to the generator shaft. The hydrogen passes through the hydrogen coolers where the heat is transferred to the Service Water System. Cooling is provided for the stator by a closed-circuit cooling water system. The stator cooling water system uses demineralized water which passes through the stator coils and picks up heat to be transferred to the Service Water System at the stator cooling system heat exchangers.

1.2.5.2 Main Steam Lines

During operation the steam generators deliver saturated steam through an equal number of steam lines to the main turbine. These lines are crosstied near the turbine to ensure that the pressure difference between any of the steam generators does not exceed 10 psi thus maintaining system balance and ensuring uniform heat removal from the Reactor Coolant System.

Each steam line is routed from its steam generator to one of the feedwater-steam line containment tunnels by the shortest possible route. A flow limiter is located in each steam line inside the containment to limit the cool down rate of the Reactor Coolant System in maintaining an adequate shutdown reactivity margin after trip at end of core life if a steam line break occurs upstream of the main steam stop valves.

The main steam lines are provided with a stop valve and a check valve in each line just outside the containment. The main steam stop valves automatically close on high steam flow coincident with either low average temperature or low steam line pressure, or on a high-high containment pressure signal, and can be operated manually from the main control room or local panels. The swing check valves protect against back flow of steam in the event of a steam line break inside the containment.

1.2.5.3 Reheaters

A portion of the steam in the high-pressure turbine is extracted to the highest pressure feedwater heaters; the remainder is exhausted to six moisture-separator reheaters (see Figure 1.2-26) and the fifth-stage feedwater heaters. In the moisture-separator reheaters, moisture is mechanically separated from the turbine steam and the steam is then superheated before entering three low-pressure turbines. Part of it is extracted to the four lowest stage feedwater heaters and the remainder exhausted to the condenser.

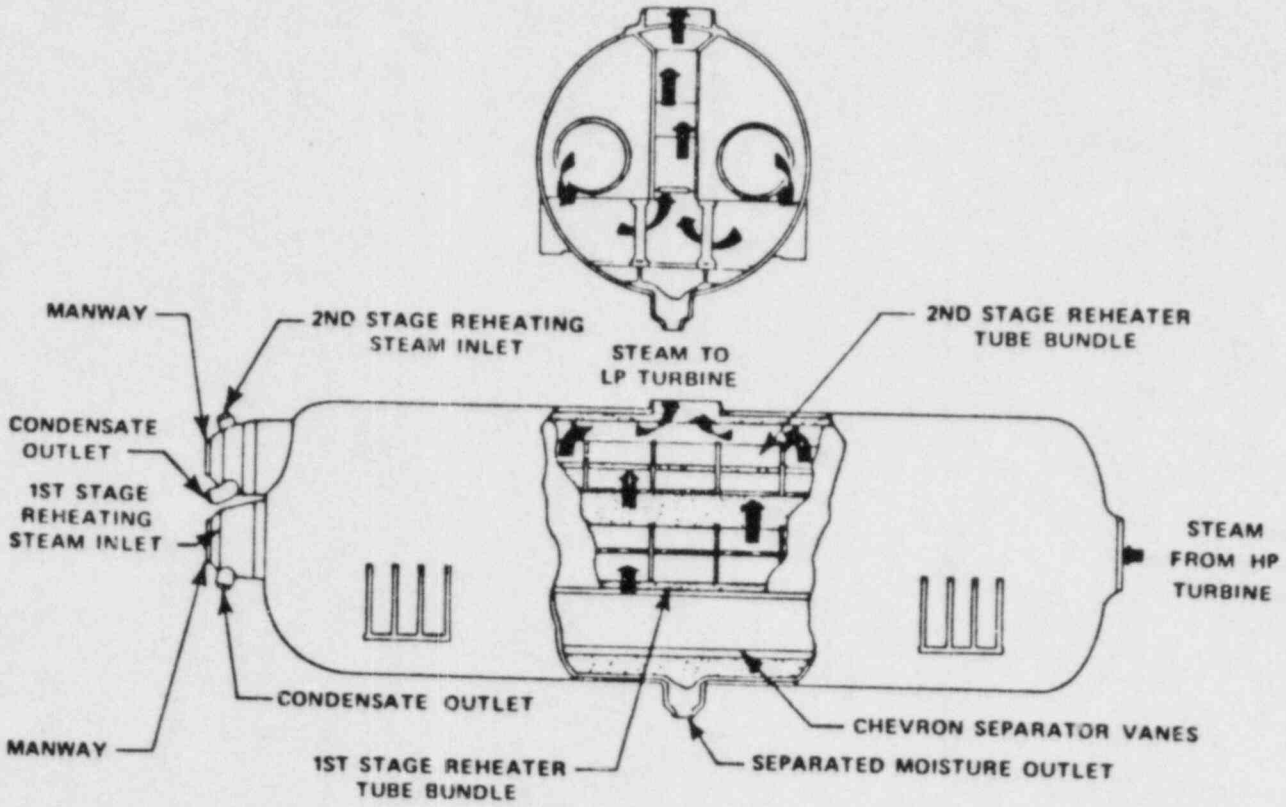

Figure 1.2-26. Moisture Separator Reheater, Two Stage

Typical combined moisture separator-steam reheaters between the high-pressure and low-pressure turbine elements remove the moisture in the wet steam coming from the high-pressure element exhaust and reheat the steam to over 100°F superheat. The wet steam enters the moisture removal section and rises through chevron-type moisture-separators where the water is removed and drained to the feedwater heater system. The dried steam then passes through the reheater section where it is reheated by a portion of the main steam which is withdrawn before the throttle valves, and passed through the tube bundles where it condenses in the tubes and is drained to the feedwater heater. The reheated steam goes to the low-pressure turbines and to the two main feedwater-pump turbines.

1.2.5.4 Main Steam Condenser

The main condenser condenses the exhaust from the main turbine and the two feedwater pump turbines. There is also sufficient surface to condense steam from the steam-dump system. The condenser is usually a single-pass deaerating type with admiralty tubes. Under normal operation the air is removed by steam jet-air ejectors.

The steam dump system is provided to accommodate the inertial heat from the primary cycle. Inertial heat, in the form of steam generated in excess of turbine demand, is present at times of sudden load reduction. This heat is rejected to the condenser through the steam-dump valves.

1.2.5.5 Feedwater Heating System

The Feedwater Heating System (see Figure 1.2-27) is of the closed type with deareration accomplished to the condenser hotwell. The condensate pumps take suction from the condenser hotwell and pump condensate through the air ejector condensers and the gland steam condensers to the suction of the condesate booster pumps. These pump the condensate through five stages of low-pressure feedwater heaters to the main feedwater pumps. The water discharge from the feedwater pumps flows through one stage of high-pressure heaters into the steam generators. All feedwater heaters are one-third-size units arranged in three parallel strings. Each string of low-pressure feedwater heaters is provided with motor-operated shut off valves. There is usually a single bypass sized to handle the flow of one low-pressure feedwater heater string. Each high-pressure feedwater heater is also provided with motor-operated isolating valves and a high single bypass sized to handle the flow through one feedwater heater.

There are four one-third capacity centrifugal condensate pumps with motor drives and common suction and discharge

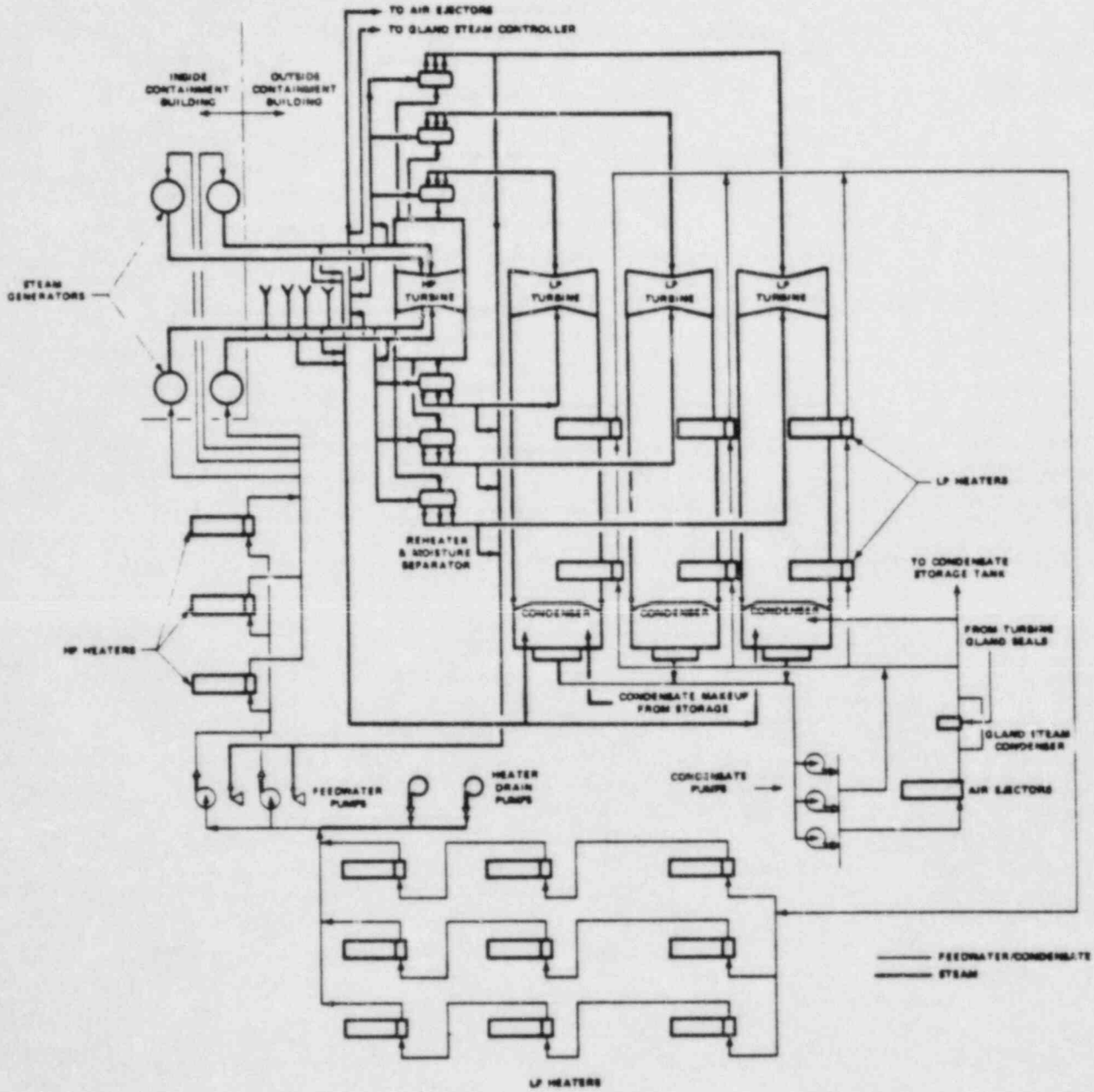

Figure 1.2-27. Main Steam and Feedwater System, One-Line Diagram

headers, and four one-third capacity condensate booster pumps with common suction and discharge headers.

There are three one-half capacity feedwater pumps with common suction and discharge headers. Two pumps are turbine driven with hot reheat steam and in this case the third pump is motor driven. The motor-driven pump may be used for start-up and as a reserve or standby pump. The discharge from the pumps is automatically recirculated back to the condenser whenever the flow to the high-pressure feedwater falls below minimum.

Feedwater flow to each steam generator is controlled by a feedwater regulator in each feedwater line. The regulator is controlled by steam generator level, steam flow, and feedwater flow.

Drains from the reheaters, the highest pressure feedwater heaters, and the moisture separators are cascaded to the fifth low-pressure feedwater heater and then to a single heater drain tank. An emergency overflow from the heater drain tank back to the condenser and an emergency makeup to the heater drain tank from the condensate booster header are provided. Drains from the four lowest pressure feedwater heaters are cascaded back to the condenser. Heater drain pumps take their suction from the single common heater drain tank and discharge into a common header which then splits up into three lines, one going to each condensate heater string.

1.2.5.6 Auxiliary Feedwater System

The function of the Auxiliary Feedwater System is to provide adequate cooling water to the steam generators in the event of a unit trip coupled with a loss of offsite power. One of the two motor-driven auxiliary feedwater pumps supplying two of the four steam generators will provide enough feedwater to safely cool the unit down to the temperature at which the Residual Heat Removal System can be utilized. The single turbine-driven auxiliary feedwater pump has twice the capacity of either motor-driven pump and can supply all four steam generators.

The Auxiliary Feedwater System consists of two subsystems, one of which utilizes a single turbine-driven pump, the other consisting of two motor-driven pumps. Each of the two subsystems can deliver feedwater to all four steam generators. The system is designed to meet single failure criteria which could be main feedwater line rupture coupled with a single active failure in the Auxiliary Feedwater System.

1.2.6 AUXILIARY COOLING SYSTEMS

The auxiliary cooling systems include the circulating and service-water systems, and the component and spent fuel pit-cooling systems. These systems will be described briefly for a typical Westinghouse design.

1.2.6.1 Circulating Water System

The Circulating Water System serves as the major heat sink for the station by providing large amounts of screened cooling water for the main condensers, the Service Water System, the Fire Protection System, and Screen Wash System.

Water entering the forebay of the crib house from the intake lines must pass through the bar grills mounted across the inlet. The crib house is divided into intake bays with each bay equipped with bar grills, traveling water screens, and circulating and service-water pumps.

Circulating water for each main condenser is supplied by vertical, mixed flow, volute-circulating water pumps taking suction from the intake bays and discharging water through individual discharge lines into a common discharge line for the main condensers.

1.2.6.2 Service-Water System

The Service-Water System (see Figures 1.2-28 and 1.2-29) supplies all the equipment cooling water for the plant, including the emergency shutdown requirements. The essential coolers are provided with two cooling water supplies by loop headers coming from the main supply header. The non-essential equipment coolers are fed from separate branch headers that can be isolated from the main headers under accident conditions to conserve water.

The pumps are located in the crib house forebay and discharge through strainers to a common header. Double isolation valves are provided in the loops and single isolation valves in each of the feeds to individual coolers so that the failure of the valve on a single line break will not jeopardize any essential cooling.

The service-water system typically supplies water to the component cooling heat exchangers, containment ventilation coolers, diesel generator coolers, auxiliary feedwater pumps, auxiliary building room coolers, containment-spray pump diesel engine coolers, penetration pressurization air-compressor coolers, auxiliary building ventilation system cooling coils, and control and computer room air conditioning system condensers.

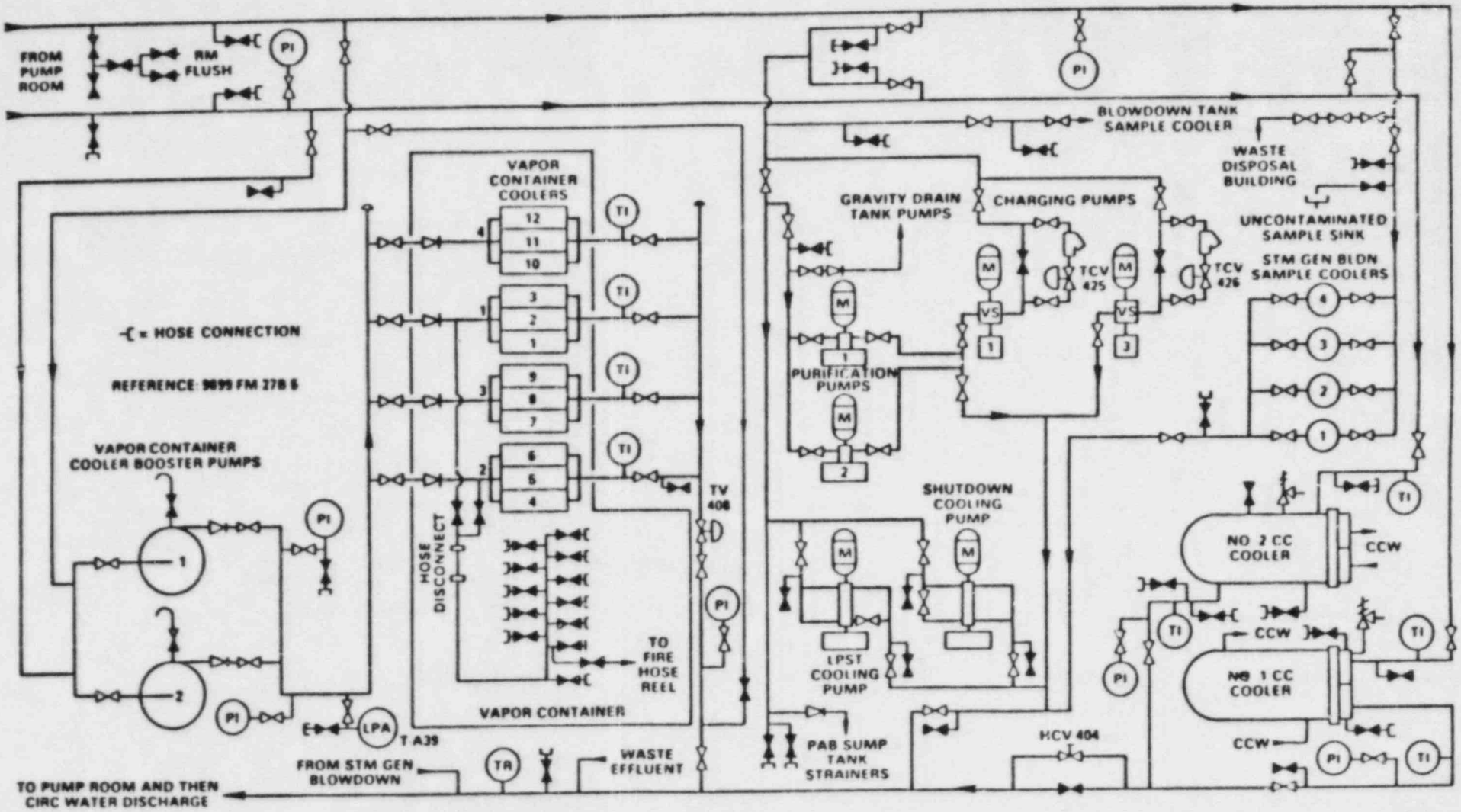

Figure 1.2-28. Service Water System Primary Plant

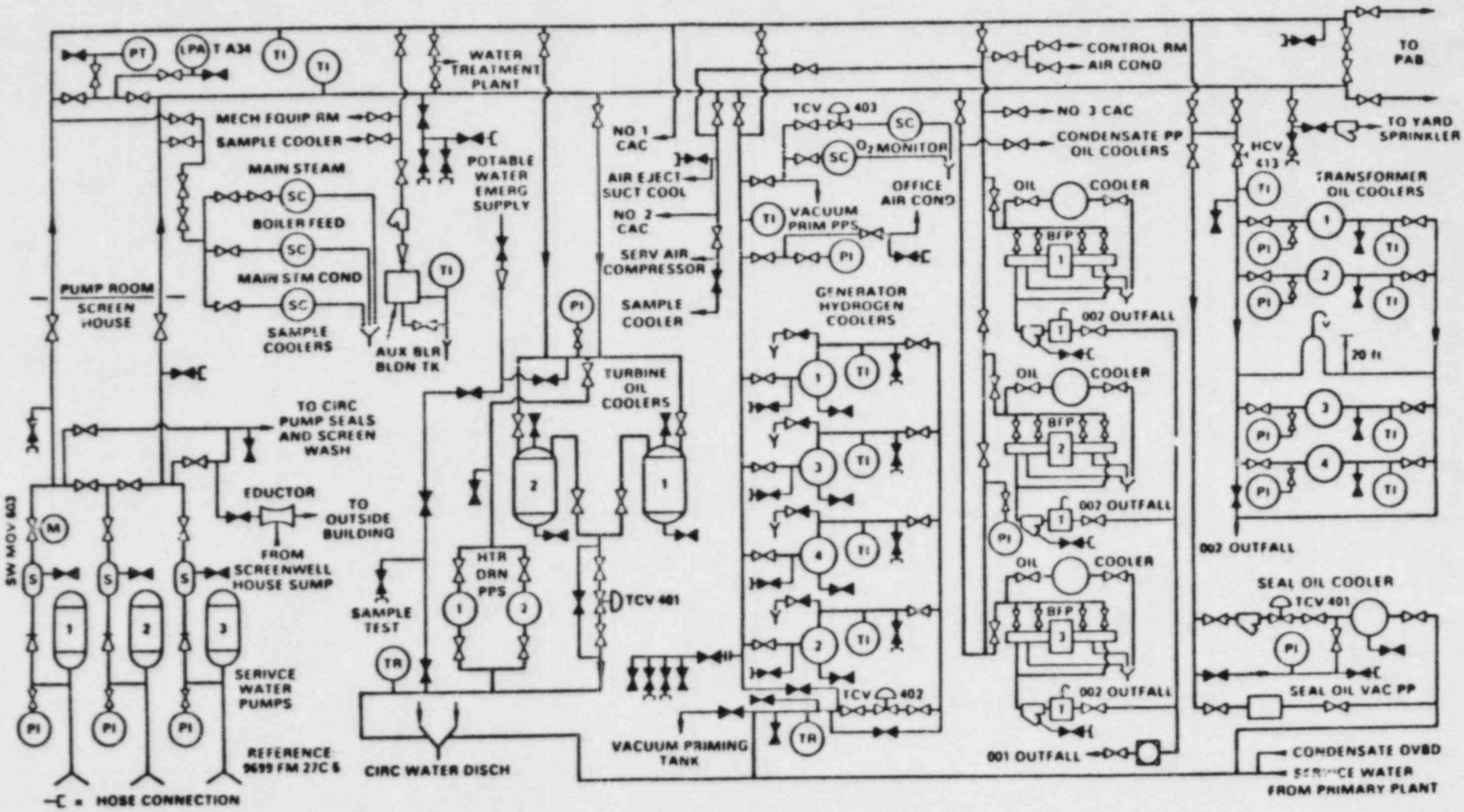

Figure 1.2-29. Service Water System Secondary Plant

1.2.6.3 Component Cooling System

The Component Cooling System (see Figure 1.2-30) is designed to remove heat from heat exchangers, pumps and waste disposal systems. Component cooling water flows through these units in parallel flow circuits, picks up heat from the various components, and flows to the component cooling heat exchangers which are cooled by the Service-Water System. The component-cooling loop thus serves as an intermediate system between the Reactor Coolant System and the Service-Water System.

The Component Cooling System consists of pumps, heat exchangers, a surge tank, and associated piping and valves. All components are arranged in parallel flow circuits so that individual components may be isolated. Component cooling is provided for the residual heat exchangers, reactor coolant pump-motor bearings, and thermal barriers, let down heat exchanger, seal-water heat exchangers, spent fuel-pit heat exchangers, boric and evaporator condenser, reactor vessel support cooling, residual heat removal pumps, safety injection pumps, charging pumps, waste gas compressors, and boric acid evaporator vent condenser and distillate cooler.

1.2.6.4 Spent-Fuel Pit Cooling System

The Spent-Fuel Pit Cooling System is designed to remove from the spent-fuel pit the heat generated by stored spent-fuel elements. The cooling loop in the Spent-Fuel Pit Cooling System consists of a pump, heat exchanger, filter, demineralizer, piping, and associated valves and instrumentation. The pump draws water from the pit, circulates it through the heat exchanger and returns it to the pit. Component cooling water cools the heat exchanger.

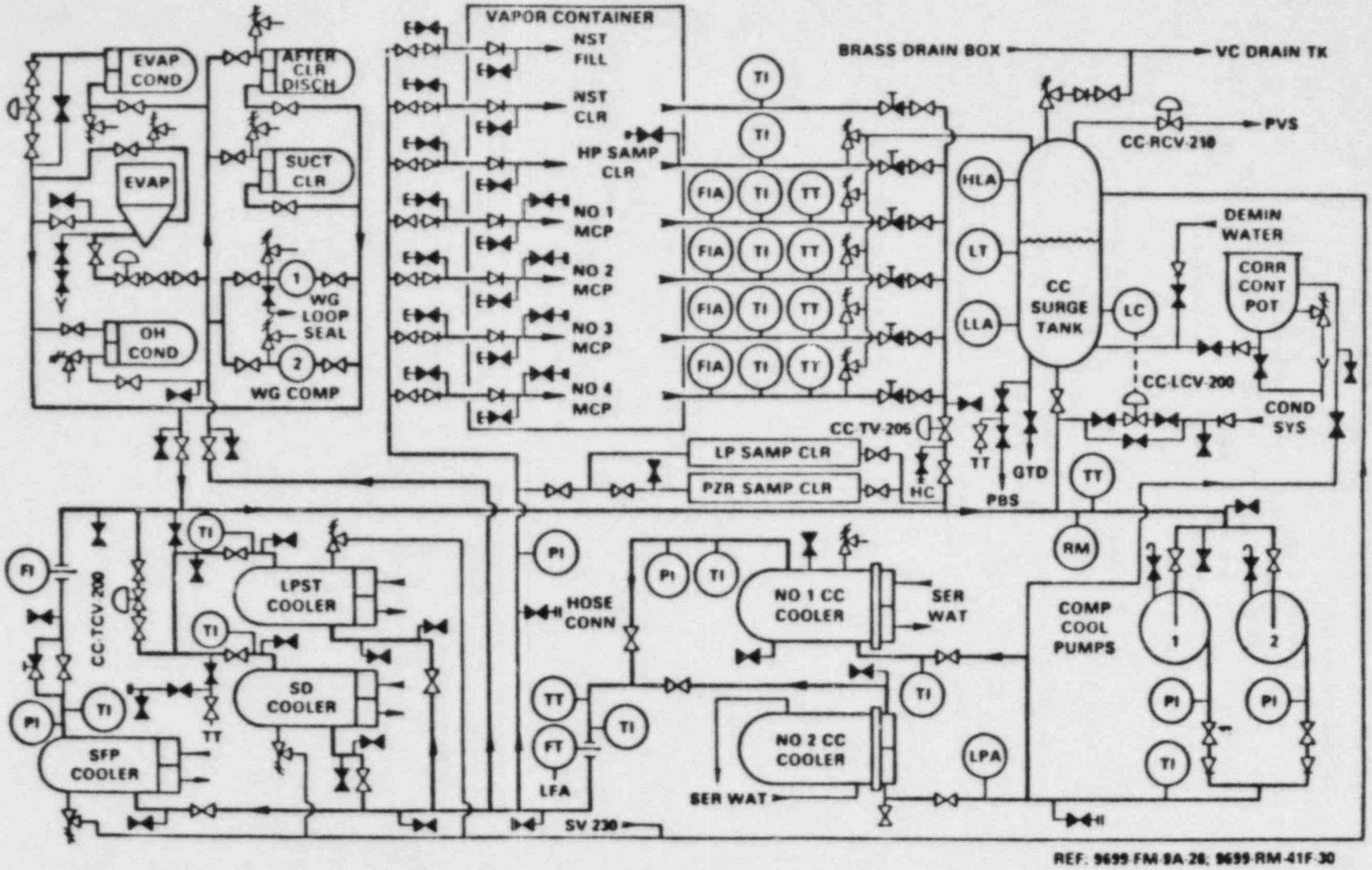

Figure 1.2-30. Component Cooling System

2. REACTOR COOLANT SYSTEMS

2.1 RCS ASSESSMENT FOR MELCOR

by

J. B. Rivard

CONTENTS

LIST OF FIGURES

LIST OF TABLES

2.1.1 GENERAL SYSTEM MODELS

2.1.1.1 Accident Time Regimes

For the purpose of organizing discussion of reactor coolant system (RCS) processes, it is convenient to divide the accident progression into six time regimes. The six are given in Table 2.1.1-1, together with their characteristics. Because the time regimes are not intended to be accident sequence-specific, detailed correspondence in the description to that for specific sequences cannot be expected. Also, it should be recognized that the coverage denoted by time regime 1 can be quite broad and may, for some sequences, overlap with time regime 2. Overlap between other time regimes is also possible.

Table 2.1.1-1

In-vessel Accident Time Regimes

Time Regime	Initial Event	Characteristics
1	Initiation	Large reduction in RCS coolant inventory; high, transient flows for larger LOCAs; RCS may depressurize
2	Core Uncovering	Gradual uncovering of core for many sequences; heat generation exceeds heat loss from core in uncovered region
3	Zr Oxidation	Fuel temperatures exceed 1300 K; energy addition from oxidation greatly exceeds local decay heat; core "melts"
4	Melt-H_2O Interactions	"Molten" core materials discharge from core region into lower plenum; steam explosion(s) may occur
5	Quasistatic RPV Attack	Evaporation of residual coolant; core debris heats reactor vessel; stress fields develop
6	Breach of RPV	Vessel is breached by stress failure and/or thermal weakening; core material is discharged to containment environment

The time regimes have been devised in an attempt to isolate thermal hydraulic regimes with similar characteristics from one another. Thus, it is intended that time regime 1 represent all the highly dynamic, two-phase flow which characterizes the initial stages of LOCAs (see Section 2.1.1.3 below), while time regime 2 represents the much less dynamic regime during the core uncovering process. When significant oxidation of the core begins, local heat generation at oxidation sites strongly accelerates local core heat up, and the bulk of the steam generated is reduced to hydrogen within the core. This marks the onset of time regime 3, during which sufficient energy is developed within the core matrix to produce distortion, liquefaction, and significant change in the geometry of the core components (i.e., "meltdown").

Unless arrested, the degradation of the core continues until sufficient liquefied core materials are formed to allow gravity-driven discharge of the materials from the core zone into the lower plenum of the RPV. This discharge marks the start of time regime 4, which represents the highly transient thermal hydraulic phenomena resulting from the mixing of very hot core materials with the coolant remaining in the lower plenum. Following the vaporization of all remaining coolant, a quasi-steady regime is again entered in which the reheating core debris in the plenum heats the RPV wall, which denotes the start of time regime 5. Time regime 5 continues until the breach of the RPV, which marks the start of time regime 6 which treats the discharge of core material and coolant through the breach into the containment, and continues until the impact of RCS conditions and events on containment or environment conditions becomes negligible.

The above-described time regimes do not specifically address the conditions arising from ECC injection of coolant into very hot (perhaps molten) regions of the uncovered reactor core, nor full or partial fission power conditions characterizing anticipated transients without scram (ATWS). In the first case, it is recognized that operator/system actions to stem-core degradation by injecting coolant into/onto an uncovered core (during a non-ATWS sequence) may occur at any time during the sequence. When this occurs early in the sequence before gross changes in core geometry and large-scale fuel liquefaction, termination of the accident sequence and long-term cooling of the core are quite likely if continued flow and necessary decay-heat removal (heat sink) conditions are satisfied (as at TMI-2). However, if coolant injection occurs late, when a significant fraction

of the core has undergone deformation at high temperature, an imbalance between the heat removed by vaporization of coolant and the heat generated by the enhanced oxidation of remaining core Zircaloy may result in acceleration, rather than termination, of the accident progression.

An assessment of conditions necessary and sufficient to cause termination of the accident due to coolant injection requires determination of the rate of cooling afforded by vaporization of the injected coolant relative to the rate of heating resulting from the exothermic oxidation of Zr.

To a first approximation, the cooling rate Q'_B is given by the surface integral

$$Q'_B = \iint_{S_B} q_B dS \qquad (2.1.1\text{-}1)$$

where q_B is the boiling heat flux over the surface S_B. This will be strongly affected by the boiling regime(s) (nucleate, film, etc.) present over S_B. S_B is, in general, time dependent.

The heating rate Q_X is approximately

$$Q'_X = \text{MIN}\left[\iint_{S_X} q_X dS, \frac{Q'_B}{h_{fg}} R_X\right] \qquad (2.1.1\text{-}2)$$

where q_X is the heat flux due to the oxidation reaction over the oxidation surface S_X. h_{fg} is the enthalpy of vaporization for water, and R_X is the heat of reaction referenced to water (16.5 MJ/kg). The rate of hydrogen evolution differs by only a constant from Equation (2.1.1-2). The latter approximation is introduced by assuming, in the term containing Q_B, no delay time for transport of steam from the boiling site to the site of the chemical reaction.

The magnitude of q_X depends upon the local oxide barrier thickness, and strongly (see Section 2.1.1.4.1) upon the local surface temperature. The enthalpy of vaporization h_{fg} decreases strongly at high pressure. It should be

noted that the surface being cooled by injected coolant, S_B, is not necessarily identical with the surface undergoing oxidation, S_X, so that questions of net energy increase or decrease must be posed over suitable volumes of the reactor core.

Instantaneously, termination of the accident is favored when $Q_B >> Q_X$; integration over time with consideration for the contribution due to decay heating and various loss terms considered here to be small relative to Q_B, is necessary to determine the actual outcome.

Examination of Equation (2.1.1-2) shows that, if all the steam generated by the boiling is reacted,

$$\iint_{S_X} q_X dS = \frac{R_X}{h_{fg}} \iint_{S_B} q_B dS \quad , \qquad (2.1.1\text{-}3)$$

where R_X/h_{fg} varies between 7.3 at 0.1 MPa and about 19 at 17.0 MPa. Equation (2.1.1-3) illustrates the difficulty of terminating the accident in the presence of substantial oxidation.

For MELCOR, the modeling difficulties are summarized by consideration of the need to evaluate the surface integrals in Equations (2.1.1-1) and (2.1.1-2). This requires not only knowledge of the respective configurations, but surface temperature information throughout S_B and S_X, as functions of time. Obtaining such information for a deforming core is obviously very difficult, and certainly not within the capabilities envisioned for MELCOR.

Yet, to model operator/system termination attempts using MELCOR, it will be necessary to provide a scheme for allowing the sequence branching described above. Such a scheme, which is a specific example of a more general requirement for treating poorly understood or difficult-to-model phenomena, is discussed in the next section.

Treatment of ATWS requires special attention because of the potential for uncovering part of the reactor core while at high (fission) power levels.

Standard, zero-dimensional neutron kinetics require

$$\frac{d\Phi}{dt} = \frac{\beta}{\xi}(\rho-1)\Phi + \sum_{i=1}^{N} \lambda_i C_i \qquad (2.1.1\text{-}4)$$

$$\frac{dC_i}{dt} = \frac{\beta_i}{\xi}\Phi - \lambda_i C_i, \quad i=1,\ldots,N \quad , \qquad (2.1.1\text{-}5)$$

where

$\Phi(t)$ = neutron density
t = time
β = delayed neutron fraction ($\Sigma\beta_i$)
ξ = neutron generation time
$\rho(t)$ = reactivity in dollars (subprompt critical)
λ_i = group i delayed neutron decay constant
$C_i(t)$ = group i delayed neutron precursor concentration
β_i = group i delayed neutron fraction
N = number of delayed neutron groups.

The effectiveness of such a formulation in modeling the temporal behavior of reactor power during ATWS depends upon two key requirements:

1. Ability to overcome the numerical limitations imposed by the small ξ, and

2. Ability to adequately model the reactivity feedback terms which determine $\rho(t)$.

Techniques for overcoming the numerical (timestep limitation) handicap are available - the several asymptotic approximations [1], including the well known "prompt jump" approximation, for example.

Calculating the time-dependent reactivity $\rho(t)$ is a multifaceted problem which can include the following factors:

1. Reactivity ramps due to control rod motion,

2. Doppler feedback due to fuel temperature,

3. Moderator feedback due to both homogeneous (continuous phase) and heterogeneous (bubble) density variations caused by temperature and heat flux variation within the mixed phase, and coolant voidage above the upper surface of the mixture,

4. Feedback due to motion of the fissile species when damage levels exceed those which permit the core to remain undeformed,

5. Feedback due to injection of boron solution.

This approach using point kinetics is approximate, yields no information on the spatial power distribution, and is difficult to implement with adequate accuracy because of the spatially heterogeneous nature of $\rho(t)$. A recent analysis of a LOFT ATWS [2] using point kinetics appears to be successful. However, the particular transient modeled led to benign termination, core uncovering apparently did not occur, and no reactivity modeling of the uncovering, boron injection, or fissile material motion processes was involved. Modeling of ATWS with more serious outcomes is, of course, essential for PRA applications.

A reasonably accurate treatment of ATWS fission power probably requires a one-dimensional (axial) kinetics model, but treatment using a two-region point kinetics hybrid may suffice. Considerable experimentation with various approaches* is needed to determine what scheme, if any, is consistent with the objectives of MELCOR. To the extent that MELCOR is unable to provide ATWS modeling, the generic treatment accorded MELCOR uncertainties is applicable, and is described next.

2.1.1.2 RCS Model Uncertainties

RCS model uncertainties will arise in MELCOR because of two basic modeling limitations:

1. The model is inadequate because the phenomenon is inadequately understood.

2. The model is inadequate because code-imposed constraints do not permit adequate modeling of the phenomena.

To some extent, all code models suffer from both limitations, and it is not necessarily useful to distinguish between the two causes of uncertainty. However, a few examples are given to attempt to clarify the intent here, which emphasizes severe limitations rather than the more routine, but less important, limitations which afflict code models generally.

---

* See for example the several approaches to space-dependent kinetics in D. L. Hetrick (loc. cit.).

As was mentioned above, current knowledge is insufficient to define some of the core conditions under which coolant injection becomes ineffective in cooling a deformed core and thus terminating the accident. The MARCH code handles these processes in a totally unrealistic manner [3]. Nevertheless, because of the great difference in outcomes, it is necessary to provide MELCOR with a mechanism for the branching in the sequence which can result, e.g., from termination of the accident sequence to an accelerated meltdown sequence.

In instances of this kind, where the progression of the accident is dominated by uncertainty, it is desirable that the uncertainty be made obvious to the code user, as well as to those applying the results of the calculation (e.g., NRC).

One method which emphasizes the uncertainty consists in requiring user input to control the outcome directly. In this instance, this would mean requiring the code user to select a value, for example, for an input temperature TECCFAIL such that, if the core-averaged fuel temperature is greater than TECCFAIL at the time of ECC actuation, meltdown is accelerated, whereas if the core-averaged temperature is less than, or equal to, TECCFAIL, benign termination of the accident is initiated. (A more complicated model with more parameters could, of course, be implemented with the same final result.)

An adjunct to this approach consists of assigning messages to output whenever a very uncertain branching decision is implemented. Such a message might consist of the following,

```
BRANCHING PHENOMENA UNCERTAIN.
CALCULATED RESULTS DEPEND
STRONGLY ON USER INPUT.  CONSULT
CODE DESCRIPTION FOR DETAILED
EXPLANATION.
```

which would serve to alert both the user and others of the uncertainty.

Other examples of RCS phenomena requiring this type of treatment include the occurrence and magnitude of steam explosions, transition from intact core geometry to highly damaged relocated geometry, the initial size and type of RPV breach for most scenarios, and some aspects of ATWS sequences. It is expected that other phenomena will be added to this classification as MELCOR development proceeds.

2.1.1.3 Mass, Momentum and Energy Transport, and Conservation

Before discussing the MELCOR RCS fluid flow modeling concept, it is useful to attempt a broad evaluation of the thermal hydraulic regimes which are operative in the RCS during the six accident time regimes given in Section 1.1 above.

Time regime 1 is intended to represent the highly dynamic, primarily two-phase flow which characterizes the initial stages of LOCAs, and, to a lesser extent, parts of transients (T sequences).

A large-break LOCA (LBLOCA) is caused by a broken large pipe in the reactor cooling system, and initiates a fast blowdown during which the reactor is shut down by excessive void. The licensing Design Basis LOCA is defined as a sudden severence of a large diameter cold leg pipe in a pressurized water reactor (PWR) or a recirculation jet-pump inlet pipe in a boiling water reactor (BWR). In the large LOCA accident, the reactor core is cooled by emergency core cooling systems (ECCS), which are automatically activated during a fast depressurization in a matter of tens of seconds. After the core is quenched, low-pressure long-term core cooling relies on the Decay Heat Removal system for any size break in either a PWR or a BWR. Failure of the ECC or Decay Heat Removal systems to perform may result in a severe accident.

A small-break LOCA (SBLOCA) is caused by a broken small pipe or a stuck-open safety relief valve in the RCS, and initiates a slow blowdown during which the heat initially stored in the core will be readily transferred to the coolant; however, the core decay heat may not be entirely removed by the break flow, such as during the Three Mile Island accident. The primary system pressures in SBLOCAs of various break areas are calculated to last for hours, as shown in Figure 2.1.1-1. During this period of sustained pressure, if ECCS does not work properly or if the accident results from a transient, such as loss of all feedwater or station blackout, a SBLOCA may result in prolonged uncovering of the core. This situation makes operator action crucial to the course of the accident, and timing during the transient important to the potential for plant recovery.

Table 2.1.1-2 [4] compares several characteristics of SBLOCAs and LBLOCAs. Important features to be modeled during a LBLOCA include

1. Subcooled blowdown (PWR) - propagation of pressure waves throughout the RCS at sonic velocities until the vapor pressure of the coolant is reached;

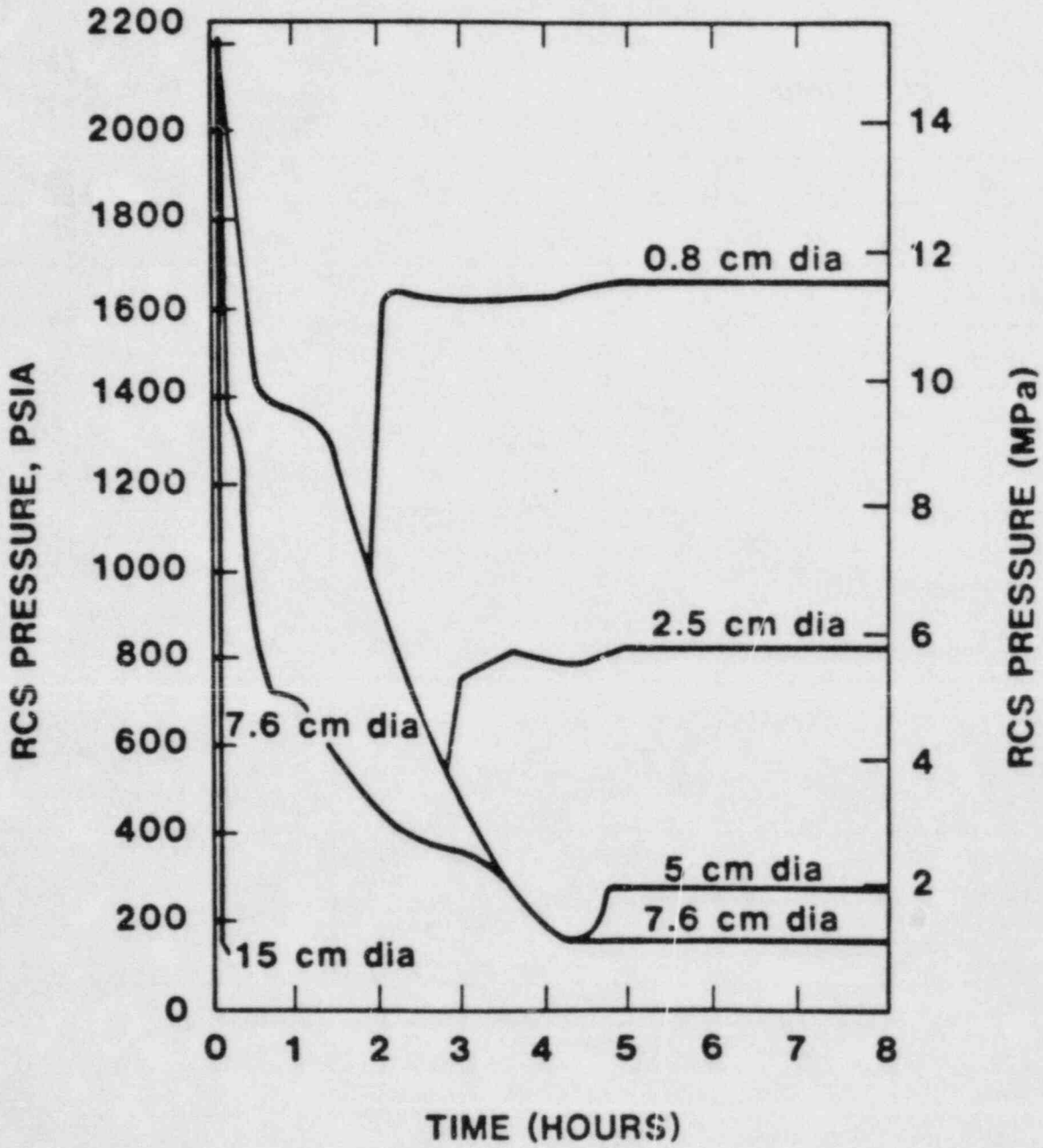

Figure 2.1.1-1. Coordinates and Velocities for Boundary Layer Flow, Equation (13)

Table 2.1.1-2

COMPARISON OF SMALL BREAK AND LARGE BREAK LOCA CHARACTERISTICS IN A PWR

	Small Break LOCA	Large Break LOCA
Sample break size	0.02 ft^2	2 x 4.0 ft^2
Significant Heat Source	Decay heat (Stored heat only in early stage)	Stored and decay heat
Significant Heat Sink	Break Flow, Heat Transfer thru S. G. to Secondary side, and ECC water	Break flow and ECC water
Heat Transfer in Steam Generator (S. G.)	$P_{pri} \geq P_{sec}$ Auxiliary Feed Water (AFW) Significant	$P_{sec} > P_{pri}$ Auxiliary Feed Water (AFW) Insignificant
Primary Side Pressure	High pressure maintained because of slow draining	Fast depressurization by blowdown
Flow Behavior in Primary Side	1. Stratified flow 2. Separation of non-condensibles at high spot 3. Gravitational force control 4. Core may uncover by flushing and draining 5. Pressurizer effect significant	1. Bubbly or droplets dispersed flow 2. Homogeneous flow during blowdown 3. Momentum control 4. Core emptied and recovered quickly 5. Pressurizer has small effect
ECCS	1. Charging pump and HPSI 2. Effectiveness depends on the pressure for initiation of injection 3. In cold leg break LOCA, core may have to be partially uncovered to vent steam thru loop seal.	1. Accumulator most effective 2. Effectiveness depends on the initiation pressure and location of injection 3. In cold leg break LOCA, there may be steam binding and ECC bypass which slows down reflooding.
Plant recovery	1. AFW and natural circulation for wet S.G 2. Manual opening of PORVs to lower the pressure for HPSI, Accumulator, LPSI and RHR when steam dump is not available	1. Accumulator and Reflooding 2. Continuous LPSI or RHR

2. Saturated blowdown - formation of steam "voids," damping of pressure waves, and choked flow at the break;

3. Accumulator injection - downcomer flooding (penetration) phenomena, steam venting, core frothing, and initial core uncovering;

4. Vessel reflood - refill thermal hydraulics, core quenching, and reflood.

Initial behavior during a SBLOCA has some of the characteristics of LBLOCA; transients (T sequences) may share some of these.

Modeling of LOCA phenomena is typified by that contained in codes such as RELAP [5], RETRAN [6], and TRAC [7]. They basically solve a one-dimensional transient version of the field equations for a one component, two-phase system. For example, the RELAP5/MOD 1 formulation includes two mass conservation equations, two momentum equations, (one for each phase), and a mixture energy equation. At least one phase is assumed to be at saturation, and interphase energy transfer is implicitly lumped into the vapor mass generation model. Auxiliary equations treat noncondensible gas as a component of the vapor phase and dissolved solids as a component of the liquid phase.

In TRAC, the field equations are augmented to a total of six by an additional energy equation. They are:

Mixture Mass Equation:

$$\frac{\partial \rho_m}{\partial t} + \frac{\partial}{\partial x} (\alpha_g \rho_g v_g + \alpha_l \rho_l v_l) = 0 \quad . \qquad (2.1.1\text{-}6)$$

Vapor Mass Equation:

$$\frac{\partial}{\partial t} (\alpha_g \rho_g) + \frac{\partial}{\partial x} (\alpha_g \rho_g v_g) = \Gamma_g \quad . \qquad (2.1.1\text{-}7)$$

Vapor Momentum Equation:

$$\frac{\partial v_g}{\partial t} + v_g \frac{\partial v_g}{\partial x} = - \frac{C_i}{\alpha_g \rho_g} (v_g - v_l) \left| (v_g - v_l) \right| - \frac{1}{\rho_g} \frac{\partial p}{\partial x}$$

$$- \frac{\Gamma_g}{\alpha_g \rho_g} (v_g - v_{ig}) - \frac{C_{wg}}{\alpha_g \rho_g} v_g \left| v_g \right| + g \quad . \qquad (2.1.1\text{-}8)$$

Liquid Momentum Equation:

$$\frac{\partial v_l}{\partial t} + v_l \frac{\partial v_l}{\partial x} = \frac{C_i}{\alpha_l \rho_l} (v_g - v_l) \left| (v_g - v_l) \right|$$

$$- \frac{1}{\rho_l} \frac{\partial p}{\partial x} + \frac{\Gamma_g}{\alpha_l \rho_l} (v_g - v_{il}) - \frac{C_{wl}}{\alpha_l \rho_l} v_l \left| v_l \right| + g \quad . \qquad (2.1.1\text{-}9)$$

Mixture Energy Equation:

$$\frac{\partial}{\partial t} (\alpha_l \rho_l u_l + \alpha_g \rho_g u_g) + \frac{\partial}{\partial_x} (\alpha_l \rho_l u_l v_l + \alpha_g \rho_g u_g v_g)$$

$$= - p \frac{\partial}{\partial x} (\alpha_l v_l + \alpha_g v_g) + Q_{wg} + Q_{wl} \qquad (2.1.1\text{-}10)$$

Vapor Energy Equation:

$$\frac{\partial}{\partial t} (\alpha_g \rho_g u_g) + \frac{\partial}{\partial x} (\alpha_g \rho_g u_g v_g) = - p \left[\frac{\partial \alpha}{\partial t} + \frac{\partial}{\partial x} (a v_g) \right]$$

$$+ Q_{wg} + Q_{ig} + \Gamma_g h_{sg} \qquad (2.1.1\text{-}11)$$

where

C_i = interfacial shear coefficient
C_{wg} and C_{wl} = wall shear coefficients
g = acceleration of gravity
h_{sg} = saturated vapor enthalpy
p = pressure
Q = volumetric heat transfer rate
t = time
u = specific internal energy

v = velocity
α = volume fraction
Γ = interphase mass transfer rate
ρ = density.

Subscripts

g = vapor
i = interface
ig = interface to gas
il = interface to liquid
l = liquid
m = mixture
wg = wall to gas
wl = wall to liquid.

Requiring the closure of the two-phase mass, momentum, and energy field equations in one dimension is essential but not necessarily adequate for a general representation of fluid flow in the RCS. This is especially true for the highly dynamic stages of (for example) the LBLOCA described above. It is recommended that tabular input (from RELAP, TRAC, etc.) be the preferred method for implementing LBLOCA dynamics into MELCOR (as is allowed in MARCH). The frequent availability of RELAP, etc. blowdown data makes this an especially attractive option. Ultimately, it may also be desirable to allow tabular input for the highly dynamic flow during time regimes 4 and 6 (Tables 2.1.1-1 and 2.1.1-3).

The computational effort required for full closure of the field equations is often considerable, especially when all constitutive relations are considered and when an extensive (multivolume) representation of the RCS is required. The treatment of hydrogen, fission product and aerosol components in the flow adds complexity. Current opinion holds that a one-dimensional, fully conservative treatment is inconsistent with the MELCOR requirement for rapid problem execution, and that a more simplified treatment is feasible and needed. Developing a modified treatment with adequate characteristics for MELCOR is clearly (as will be seen) a significant task.

2.1.1.3.1 Flow and Heat Transfer Regimes

Table 2.1.1-3 gives a few selected thermal hydraulic parameters (with very approximate values) arranged by sequence time regimes as discussed in Section 2.1.1.1. The Froude Number ($Fr = v^2/lg$), where v is the velocity, l is a characteristic length, and g is the acceleration of gravity, is a measure of the importance of the velocity terms in the momentum equation relative to the gravitational body-force term, such that for $Fr >> 1$, gravitational body force may generally be neglected in comparison with the remaining terms. Conversely, small Fr ($<< 1$) imply the dominance of fluid flow phenomena driven by gravity, i.e., natural

Table 2.1.1-3

TIME PERIOD	FrH.L.	RePl	ReH.L.	RAd/WTPl	RAH/WTPl	Grd/Re>50Pl	Uncover During Blow down	Flow Regimes
Normal Oper.	200(V) 6(I)	$>10^7$	N3x104	---	---	N.A.	---	---
1a. LBLOCA (>6")	3.5	$3x10^5$	$>10^6$	---	---	N.A.	Yes	2φ Bubbly/ Dispersed
1b. SBLOCA (2")	>0.05	$4x10^4$	$\sim10^6$	$\sim10^9K^{-1}$	$\sim5x10^{12}K^{-1}$	N.A.	No	Stratified
1c. SBLOCA (1")	>0.001	10^4	$\sim10^5$			No	Stratified	
2. Core Uncovering Until Zr-Ox Start	$\sim10^{-5}$	~3000	$\sim3x10^4$	$>10^9K^{-1}$	$>5x10^{12}K^{-1}$	N.A.	N.A.	Turbulent, 2φ Annular Stratified
3. Start of Zr-Ox Until Melt Dischg to Lower Plenum	$\sim10^{-5}$ (H_2)	~300 (H_2)	~3000 (H_2)	$\sim5x10^6K^{-1}$ (H_2)	$\sim2x10^{10}K^{-1}$ (H_2)	Yes	N.A.	Laminar/Turbulent Nat.Conv., 2φ Annular, Stratified
4. Melt-H_2O Interactions	>0.02 (CHF) <3x104 (Sonic)	$>7x10^4$ (CHF) <5x108 (Sonic)	$>10^6$ (CHF)	$>10^9K^{-1}$	$>5x10^{12}K^{-1}$	N.A.	N.A.	?
5. Quasistatic RPV Attack	0	0	0	$>10^9K^{-1}$	$>5x10^{12}K^{-1}$	Yes	N.A.	Laminar/ Turbulent Nat. Conv.
6. Breach of RPV Until no Impact	---	---	---	$\sim5x10^8K^{-1}$	$\sim10^{12}K^{-1}$	N.A.	N.A.	?

Abbreviations:
Fr = Froude Number
Re = Reynolds Number
Ra = Rayleigh Number
Gr = Grashoff Number
DT = Temperature Difference between bulk fluid and wall
2φ = Two-phase
CHF = Critical Heat Flux
N.A. = Not Applicable
H_2 = Hydrogen
H.L. = Hot Leg
d = Diametral
H = Height
Pl = Upper Plenum

circulation and free convection. The Reynolds numbers ($Re = vd/\nu$ where d is the diameter or hydraulic diameter and ν is the kinematic viscosity) given are based upon the length normal to the nominal flow direction, that is, the effective (hydraulic) diameter for the upper plenum and the actual diameter for the hot leg pipes. For $Re > 3 \times 10^3$, the flow may be considered turbulent.

For either laminar or turbulent forced convection flow, the heat transfer is conventionally described by an equation of the form

$$Nu = f(Re,Pr) \qquad (2.1.1\text{-}12)$$

where Re is the Reynolds number based upon the free stream velocity, and Pr is the fluid Prandtl number.

A flow regime is called free- or natural-convection flow when it is created by body forces. In this case, no prescribed velocity is available which might be used to define a Reynolds number. Under these conditions, the boundary layer momentum equation is

$$\rho\left(u\frac{\partial u}{\partial x} + v\frac{\partial u}{\partial y}\right) = \frac{\partial}{\partial y}\mu\frac{\partial u}{\partial y} + \rho u_\infty \frac{du_\infty}{dx} - \beta\rho g(T-T_\infty) \qquad (2.1.1\text{-}13)$$

where the velocities and coordinates are given in Figure 2.1.1-2, ρ is density, μ is viscosity, g is gravity, β is the temperature coefficient of expansion, and T the temperature. The last term on the right of Equation (2.1.1-13) is the body force, with which it is now coupled to the energy equation. In the case of pure forced convection, this last term may be neglected, which permits solving for the velocity distribution in the hydrodynamic boundary layer without consideration of the thermal boundary layer because of the absence of any term containing fluid temperatures.

Because of the lack of an <u>explicit</u> velocity, manipulation of the dimensionless boundary layer equations proceeds in such a manner so as to define the heat transfer behavior with parameters which do not contain velocity. When this is accomplished, it is found that the heat transfer is described by an equation of the form

$$Nu = f(Ra,Pr) \quad , \qquad (2.1.1\text{-}14)$$

where Ra is the Rayleigh number.

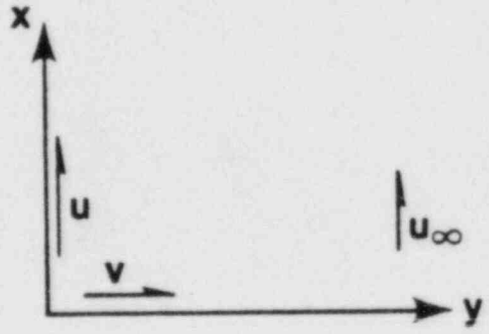

Figure 2.1.1-2. Coordinates and velocities for boundary layer

The Rayleigh numbers ($R_a = \beta L^3 \Delta T/\nu\alpha$ where β is the temperature coefficient of expansion, and α is the thermal diffusivity) given in Table 2.1.1-3 are for the upper plenum and are based upon lengths L either normal (d) or parallel (H) to the nominal (upward) flow direction, where d is the hydraulic diameter, with the ΔT representing the temperature difference between the bulk of the fluid and the wall. Dividing the Ra by the Prandtl number for the fluid yields the Grashof (Gr) number. Both the Ra and Gr are important measures of the magnitude of free convection effects on both fluid flow and heat transfer since they derive from the body force term which drives the convective flow under nonisothermal conditions. The flow situation is dominated by free or natural convection flow for large Ra and Gr and small Re.

In Table 2.1.1-3, the dimensionless Ra has been divided by ΔT to yield a number with dimensions K^{-1} because, in general, the temperature difference between the bulk fluid and the wall a priori is unknown. However, it can be noted that the values quoted in the table are generally such that, even in the existence of small ΔTs, the Ra would be very large, indicating the general importance of natural-convection flow and heat transfer during the latter stages of an accident.

For $Ra > 10^9$, the resulting flow regime generally is characterized by turbulence of sufficient irregularity and magnitude to be described statistically, while for $10^4 < Ra < 10^9$ the forces are smaller, and laminar flow dominates.

In mixed forced- and free-convection, velocities determined by both the conventional and body forces are comparable. The situation is complicated by the necessity for coupling the velocities induced by the thermal field with those induced by nonthermal forces.

For mixed free- and forced-convection in which the flow is parallel to the gravity vector (such as in the upper plenum and the hot leg of BW PWRs), the flow regime is affected by whether the body force aids (heat transfer to an upflowing stream) or counters (heat transfer from an upflowing stream) the forced flow. The situation, which is uniquely determined by the velocity profile normal to the flow vector, can be characterized by the Gr/Re ratio for a given condition (heated or cooled upflow, for example).

For cooled upflow and Re that would otherwise yield laminar flow, the velocity at the center of the flow stream increases, and the velocity at the wall decreases, as the heat flux increases. For Gr/Re~50 [8], flow reversal (i.e., down flow) occurs at the boundary of the flow stream

(Figure 2.1.1-3). An increase in the ratio of heat flux to flow rate increases the magnitude of this reversal and results in separation and a sudden transition to unsteady flow.

Figure 2.1.1-4 shows a visualization of a section through a possible flow field within the upper plenum of a PWR. Such a flow field is obviously three-dimensional, but incorporates features of the two-dimensional field illustrated in Figure 2.1.1-3.

Metais and Eckert [9] offered a flow regime map (Figure 2.1.1-5) for mixed free and forced convection in vertical flow which extends over a large range of Ra and Re, treats both heat-flux aided and heat-flux retarded flows, and contains both uniform heat flux (UHF) and uniform wall temperature (UWT) experimental results.

2.1.1.3.2 Flow Development

All of the information discussed up to this point about the flow and heat transfer regimes has been restricted to fully developed flow. A typically used criterion for determining the flow stream length required to achieve a fully developed flow condition is

$$L > .05ReD \quad , \qquad (2.1.1\text{-}15)$$

where L is the required length and D is the diameter (or hydraulic diameter). Thus, for the upper plenum in a PWR with a hydraulic diameter of 0.26 m, the required length is always greater than the physical length (height) for Re > 300. For hot legs, the required length for Re > 3000 is more than 100 m, and thus greater than any physical length. Only in steam generator tubes are developed flows attained. This means that the flow regimes of interest are most often of the developing type, Figure 2.1.1-6, in which the thermal and hydraulic boundary layers are always thinner than those posited by analyses and experiment (such as those discussed above). Correspondingly, the developing flows are characterized by generally higher heat transfer and less stable flows than the developed flow of equal Re.

Because of the often strong coupling of fluid flow and heat transfer regimes represented in Table 2.1.1-3, the absence of developed flow regimes in the RCS (except in steam generator tubes), and the central role of mass transfer-heat transfer analogies in the treatment of fission product and aerosol processes during time regimes 3, 4, 5, and 6 (Table 2.1.1-1), the appearance of widely varying values for Ra and Re for those time regimes implies:

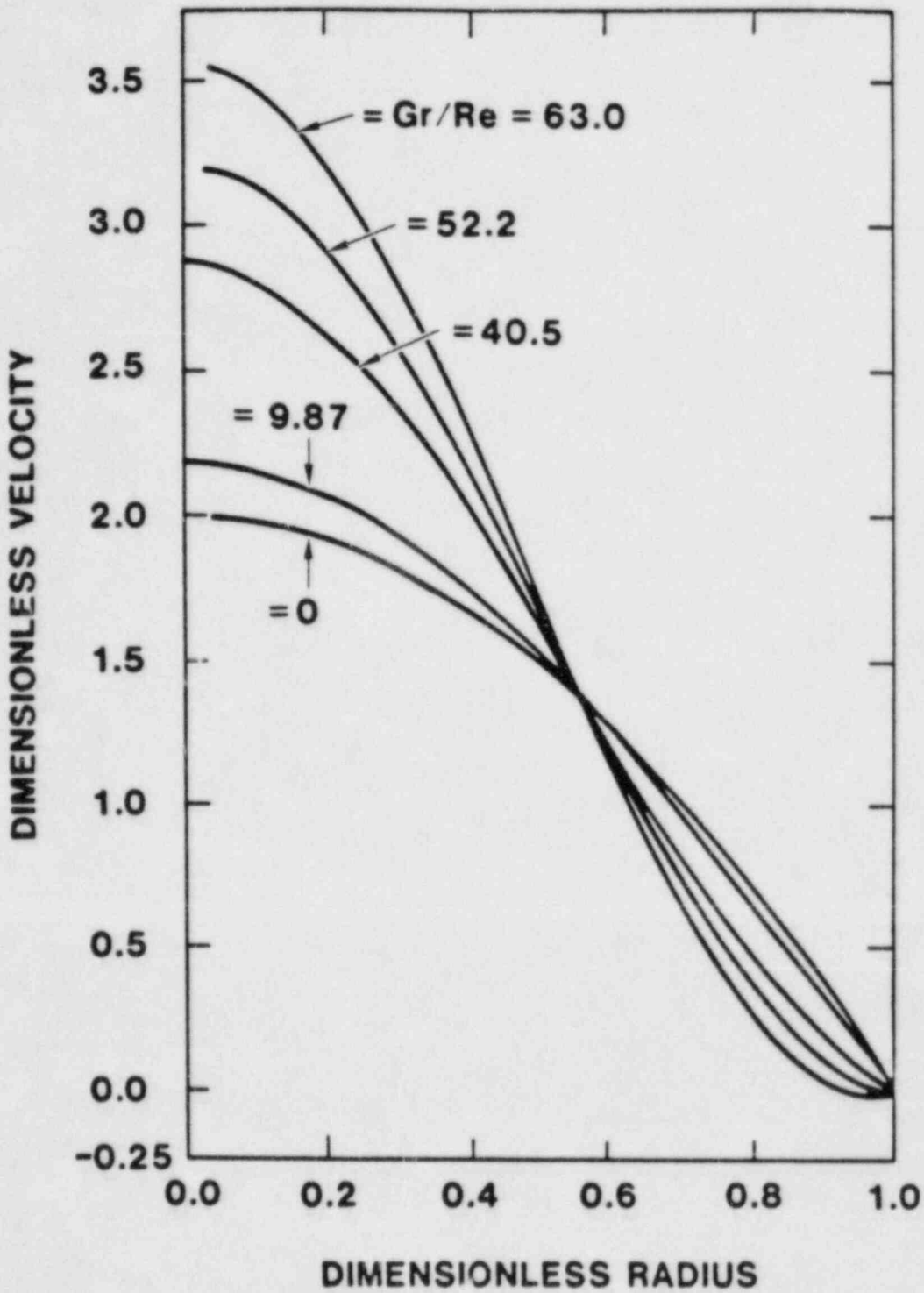

Figure 2.1.1-3. Velocity profiles for laminar down flow with uniform heat flux heating (from [8]). Note point of inflection near pipe wall for larger Gr/Re.

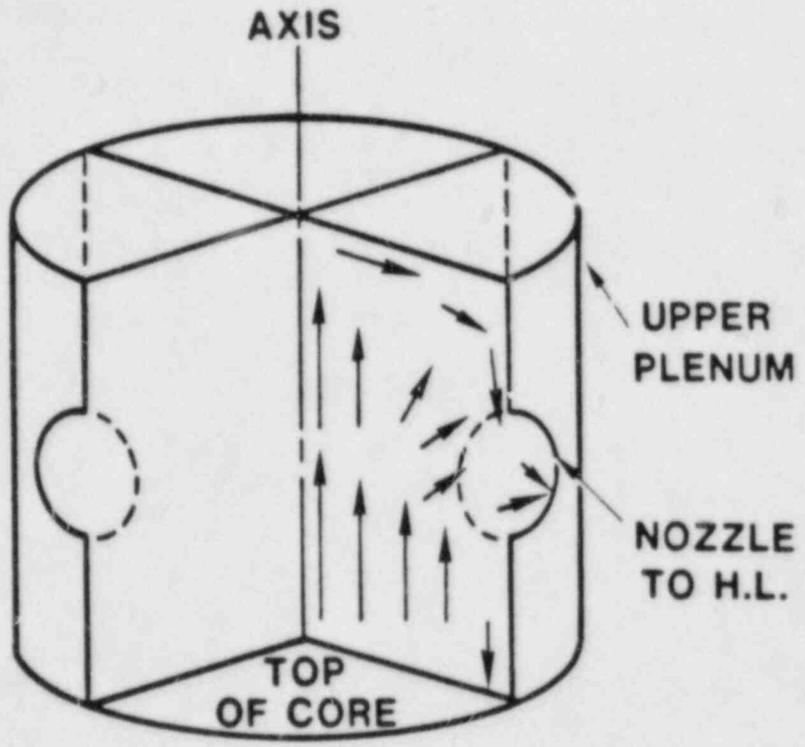

Figure 2.1.1-4. Visualization of a possible flow pattern on a nozzle bisector plane in an upper plenum quadrant, showing down flow at the outer periphery and suggesting the three-dimensional character of the flow field. (The represented velocities are proportional to the length of the vectors.)

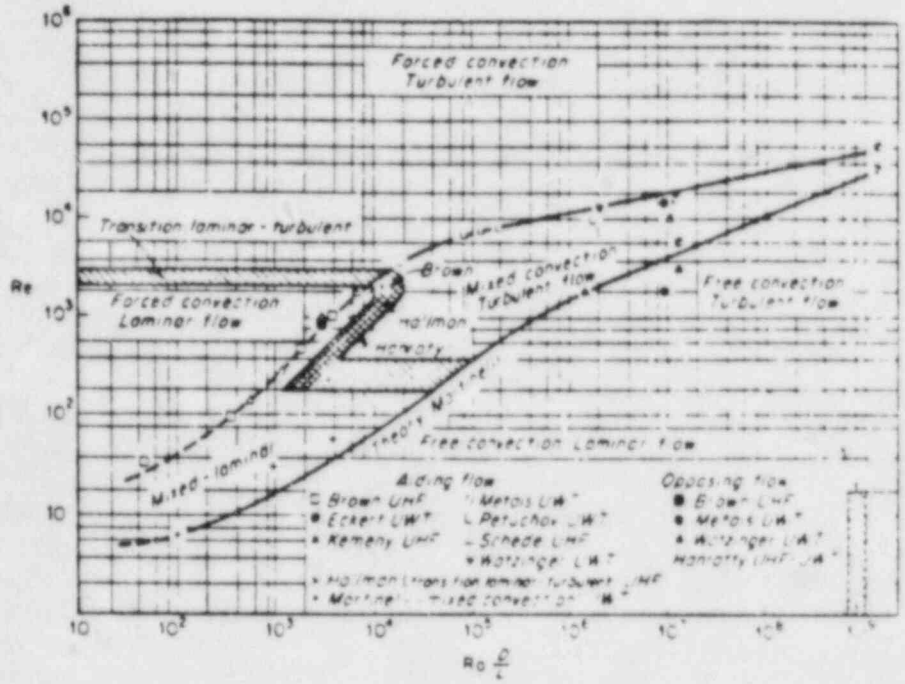

Figure 2.1.1-5. Regimes of free, forced, and mixed convection for flow through vertical tubes.[9]

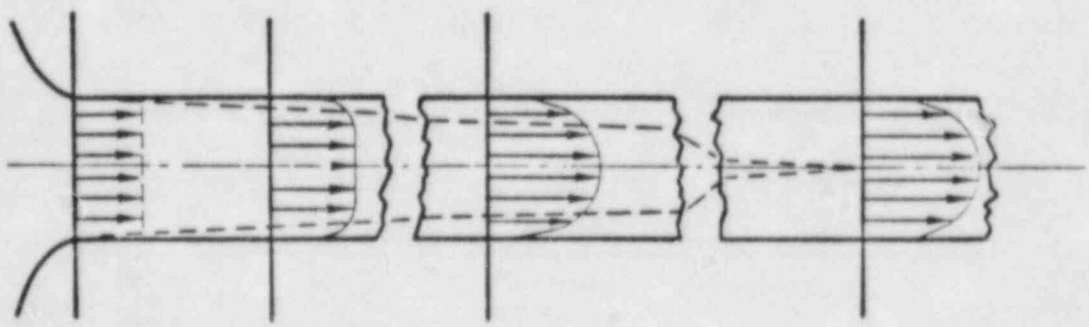

Figure 2.1.1-6. Development of Turbulent Velocity Profile in a Pipe

1. The need for choosing the thermal hydraulic treatment to conform to the flow and heat transfer regimes present during each time regime;

2. The requirement for treating free-convection as the dominant driving process in the upper plenum during time regimes 3 and 5; and

3. The need to develop improved modeling techniques applicable to mixed and free convection flow in regions of developing flow.

The situation confronting the thermal hydraulic MELCOR modeler is exemplified by consideration of the modeling requirements for a PWR upper plenum during time regime 3, say during a TMLB' sequence. Because steam flow during this time regime is driven mainly by core boiloff with the bulk of the core exposed, the net steam flow rates are quite low (on the order of a few kg/s). High fuel temperatures somewhat above the vertical center of the core result in vigorous Zr oxidation such that the reaction reduces virtually all of the steam in the flow stream. The resulting hydrogen, fission product, and aerosol flow at temperatures of 1000-1500 K exits the core at velocities on the order of 1 cm/s and enters the environment of the upper plenum, which, in a W reactor, resembles a high-ceilinged circular room nearly four meters across, with many columns spanning the distance between the floor and the ceiling. Several fractional-m openings (hot leg nozzles) pierce the walls. The walls and columns are at temperatures typically several hundred degrees below that of the entering flow stream. Because of the small Fr and Re, and the high Gr/Re, the flow regime is dominated by unstable free-convective flow (Figure 2.1.1-4). Because of the short length (height) of the plenum, the flow is developing, the boundary layers are thin (relative to developed thicknesses) and the flow is highly disturbed (and possibly unsteady) throughout the plenum. The net flow of gas out of the plenum into the hot leg nozzles is small, and has only a weak influence on the flow field. Based on the height Rayleigh number, the boundary layer on vertical surfaces is turbulent for all reasonable ΔTs. A mechanistic treatment of this three-dimensional, turbulent, and possibly unsteady flow field is probably beyond current modeling capabilities, and is obviously beyond the simplified one-dimensional fluids treatment scope of MELCOR.

A stylized, conventional treatment of the thermal hydraulics situation outlined above might (based on the small Re alone) result in the assumption of laminar, developed flow with a resultant Nusselt number of 3 or 4. Such a clearly incorrect result strongly underpredicts the heat loss from the flow, the mass transfer of vaporized

fission products to the wall, and the aerosol transport to surfaces via several of the operative mechanisms (see Radionuclide Transport and Deposition in LWR Coolant Systems).

A more correct treatment, consistent with MELCOR, calls for the use of Ra, Re flow regime maps somewhat along the lines of Figure 2.1.1-2, with the possible addition of auxiliary information relative to the local dimensionless flow distance x/L^*, where L^* is the developed length. One of the subroutines designated on the Ra, Re flow regime map could then be accessed for appropriate heat, mass, and aerosol transfer and transport correlations. Use of the x/L^* parameter would allow the development of pertinent spatially dependent information. This use of a flow and heat transfer regime map is distinct from the use of flow regime maps in codes like RELAP and TRAC in which the maps classify two-phase flow regimes as a function of mass flux and void fraction; interfacial areas and various coefficients are then determined in accordance with relations chosen on the basis of the appropriate flow regime.

Updating of the surface conditions at each time step may be necessary to the calculation of fission product and aerosol processes which depend strongly on wall conditions; updating is essential if, and when, deposition of fission products on surfaces is sufficiently dense to produce significant temperature increases at these surfaces due to the liberation of decay energy [10]. Preliminary calculations prior to the development of MELCOR would provide invaluable guidance in the development process. It may also be noted that the latter consideration implies the need (if it is not already required) to treat thermal conduction parallel and normal to the flow stream direction in surfaces adjacent to the flow (Section 2.1.1.6 below).

Implementation of the above-suggested approaches is not straightforward, however, when combined with the need for various degrees of spatial discretization within control volumes. Again for example, consider the upper plenum problem. Large parallel-to-flow temperature gradients in the walls, and rapid temperature reductions in the flow stream, due to enhanced heat transfer, combine to reduce severely the numerical solution accuracy with a coarse nodalization. Thus it may be necessary to employ a number of computational subvolumes within the upper plenum volume. However, such subvolumes must be meshed with the main volume in such a way that determination of the overall flow regime (which is determined partly by the physical plenum volume) is not compromised by introduction of subvolumes. In other words, the subvolumes must serve only to provide reduced parallel-to-flow wall temperature differences and a reduced

span of fluid temperatures within the subvolume for the calculation of local transfer and transport quantities, while not offering artificial restrictions to flow or introducing spurious flow regime considerations. The design of MELCOR will benefit from the use of control volume and subvolume selection techniques which insure conformance to these principles. This is discussed further in 2.1.1.3.5.

2.1.1.3.3 Flow Regime Framework

Table 2.1.1-3 is meant to suggest (though it is just a sample) that flow and heat transfer regimes varying with both space (location in the RCS) and time, and differing with sequence, can occur during severe accidents (variation with reactor type and manufacturer has been alluded to previously). For example, in time regime 3, during some PWR-SBLOCAs, the flow regime in the upper plenum will be developing turbulent free convection of mostly hydrogen species, while the regime in the hot leg of a W broken loop will experience developing turbulent forced flow of mostly hydrogen species. During time regime 6, the RCS high pressure will be relieved in a blowdown through the vessel breach into containment, inducing a highly transient decaying high-speed flow regime, reversing previous flow directions in some parts of the circuit with an attendant discharge of accumulator water into the cold leg(s) when the pressure reaches the discharge set point. Such regimes are important both because they determine the progress of thermal hydraulic events and because they provide the environment for the transport, chemistry, deposition, and possible resuspension of fission products and aerosols from time regime 3 onwards. These facts suggest a framework within which the modeling implications for MELCOR can be developed. A possible framework is illustrated in chart form in Table 2.1.1-4, which is intended to illustrate how the flow and heat transfer regimes vary with time and space for a given sequence, using the time periods from Table 2.1.1-3 and a set of PWR control volumes truncated from Figure 2.1.1-3 (Section 2.1.1.3.5). The letters A,B,...,F symbolically represent examples of applicable thermal hydraulic regimes during time regime 3.

A set of completed charts like Table 2.1.1-4 for dominant accident sequences would provide guidance for the selection of appropriate modeling approaches for MELCOR because it would indicate

1. What regime models are needed for thermal hydraulic event modeling,

2. What regime models are needed for fission product and aerosol process modeling,

3. What combination of parameters (input as well as calculated) best represents the flow regime (e.g., Re, Ra, Gr/Re, etc.),

4. Possible changes in models or model tradeoffs which could reduce MELCOR execution time without sacrificing overall accuracy.

Table 2.1.1-4

Flow and Heat Transfer Regime Framework

PWR Sequence TMLB' Location of Break __ Size __
AFW? N

Time Regime

RCS Volume	1	2	3	4	5	6
Core			A			
Upper Plenum			B			
H.L. (Break)			C			
St. Gen. (Break)			D			
C. L. (Break)			--			
Lower Plenum			--			
Pressurizer			E			
Dump Tank			F			
H. L. (Intact)			--			
St. Gen. (Intact)			--			
C. L. (Intact)			--			

Possible model changes or model tradeoffs include the following:

1. Truncation in the number of flow (and heat/mass transfer) calculations performed for a given control volume by recognition of the dominant regime (species/phase) in that volume (during a given time period).

2. Reduction of the number of control volumes utilized in the calculation during times that either fission product/aerosol processes can be neglected or when the calculation of thermal hydraulic events is relatively independent of processes in certain control volumes.

2.1.1.3.4 Mass and Energy Balance Verification

One of the chief criticisms [3] leveled at the MARCH 1.1 code is the lack of any explicit scheme which allows verification that mass and energy are conserved during code execution. It is therefore essential that such a scheme be included in MELCOR. For the RCS model, it is proposed that the method consist of two code modules which, when called at user-determined frequency, evaluate the energy or mass balance information and transfer the information to the output.

For the energy balance, this requires that a reference energy level be established for all masses initially in the system at the beginning of the problem, and that all energy additions to the system (fission product decay, exothermic chemical reactions, etc.) and energy losses from the system (steam vented to containment, etc.) be summed and accumulated in a systematic manner. At the time step at which balance information was requested, the module would reevaluate the energy level for all masses in the system and perform the balance

$$\Delta E_j = E_a - E_l + E_j - E_0 \qquad (2.1.1\text{-}16)$$

where

E_a = Energy added to RCS
E_l = Energy lost from RCS
E_0 = Reference energy for the RCS
E_j = Energy for the RCS at timestep j
ΔE_j = Energy imbalance at timestep j.

For this information to be useful, it is necessary that the same routines be used for evaluating energies as were used during code execution. An analogous procedure is used for determining the mass balance.

It should be emphasized that these procedures provide global information only and provide no information on the accuracy or appropriateness of the energy or mass partitioning within the system.

2.1.1.3.5 RCS Nodalization

Figure 2.1.1-7 shows a possible MELCOR control volume (CV) nodalization for a Westinghouse four-loop PWR with the break (if existing) in the pressurizer loop. If a break exists in a different loop, a rearrangement of Figure 2.1.1-7 would be necessary. (The flow directions shown are only the nominal ones, of course.) For other reactors, and for certain sequences, and/or certain conditions, it may be possible

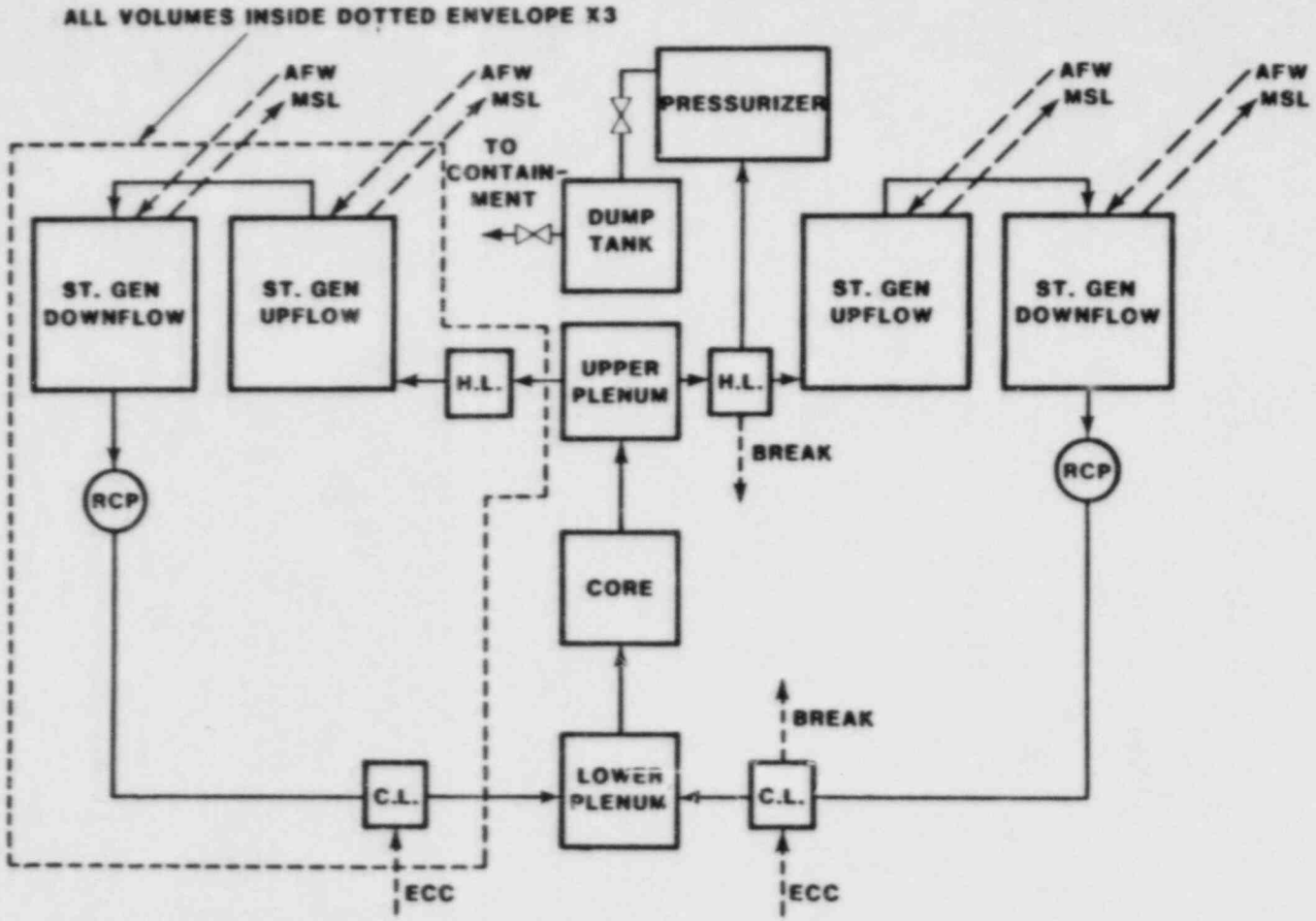

Figure 2.1.1-7. Possible MELCOR Control Volume Nodalization for Westinghouse 4-Loop PWR RCS

to reduce the number of CVs. For example, RCPs and C.L.s may be omitted if they have negligible deposition of fission products and are not thermal hydraulically significant. For BW reactors, the upflow CV in the steam generators would be omitted. For BWRs, a completely different nodalization is, of course, required.

Each CV must have specifications which match its functions during the accident sequence, and which are sufficiently flexible to allow treatment of the various vendors' designs. The BW hot leg, for example, is long and aligned vertically; this is important for any gravity-driven flow regime, such as condensate down flow or gaseous upflow with large Gr/Re, or for assessing the effects of noncondensible "pocketing" near steam generators. On the other hand, the Westinghouse and CE H.L.s are short and aligned horizontally, which have implications for both condensate flow and aerosol deposition in the leg.

For MELCOR, the division of CVs into subvolumes must be done in such a manner as to reduce the degree of subdivision to the requirements of the numerics such that acceptable accuracy is attained. Generally, it is assumed that subdivision occurs only in the flow direction (subdivision of the core volume is an exception - Section 2.1.2.1). The subdivision requirements will, in general, not be the same for all time regimes of the problem, so compromises between changing the subvolume nodalization during problem execution on the one hand, and performing the calculation with the subvolume nodalization required by the most stringent part of the calculation on the other hand, may need to be struck.

Subvolume nodalization will be determined by several needs:

1. Need to treat significant changes in geometry within CVs (pipe size transitions, etc.)

2. Need to treat liquid inventories in well-separated geometries (liquid level in pressurizer, loop seals, etc),

3. Need to obtain acceptable accuracy in CVs with high rates of heat transfer from fluid to surfaces (upper plenum during late times, etc.),

4. Need to treat distributed energy sources within CVs (due to fission product deposition) in the presence of distribution gradients,

5. Need to treat nonuniform concentrations in CVs (such as aerosols or coolant voids) to obtain acceptable accuracy in process calculations.

Subvolume nodalization requirements which minimize execution time and preserve a desired level of accuracy can only be established in an iterative manner, since establishment of optimum nodalization requires knowledge of the problem solution.

As mentioned above in connection with upper plenum modeling, the method of subvolume nodalization must not introduce artificial flow restrictions or spurious flow/heat transfer regimes.

2.1.1.4 Chemistry and Phase Change

2.1.1.4.1 Oxidation

Several models are available for treating the oxidation of solid Zircaloy cladding in a hot steam environment (e.g., Cathcart, Baker-Just, and Urbanic-Heidrick). These models make use of the so-called "parabolic" rate equation for the reduction of steam to hydrogen and the oxidation of Zircaloy

$$\frac{dx^2}{dt} = A \exp(-\frac{B}{T}) \qquad (2.1.1\text{-}17)$$

where

x = oxide layer thickness,
t = time
T = absolute temperature

and A and B are parameters with different values in the several models.

The models take account of the thickness of the oxide layer and are strongly dependent on temperature. None of these models is defined above the melting point of Zircaloy. Parabolic rate equations may also be used to describe the oxidation of steel. Associated with each reaction is the energy released (or absorbed). For the oxidation of Zr, this release has the value of 6.5 MJ per kg of Zr reacted.

The adequacy of these treatments depends very strongly on the ability to predict accurately the temperatures and the surface area available for interaction and to extrapolate beyond the applicable temperature range - where that is required. Because of large uncertainties in the surface area of liquefied species and the necessity to extrapolate the kinetics, recourse to the methods of Section 2.1.1.2 above are presently required to address the oxidation of molten Zircaloy and/or molten steel, or molten metals in an oxide matrix (i.e., the analyses are highly uncertain).

2.1.1.4.2 Phase Changes and Liquefaction

2.1.1.4.2.1 Core Materials

Zircaloy melting begins at the peak damage location as it attains a nominal 2000 K (Zircaloy-4 melts at 1993 K). There is a strong coupling (more forward than reverse) between fuel damage processes and the associated processes governing the release, chemistry, and transport of fission products.

When the local temperature of the fuel reaches the Zircaloy melting temperature, flow of metallic cladding beneath the oxidized layer will occur, which should provide significant contact between the melted metal and the UO_2 fuel. Recent experiments have provided dramatic evidence of the interaction of molten Zircaloy-4 and solid UO_2 which can subsequently occur. In one series of laboratory experiments [11], UO_2 crucibles holding molten Zircaloy at temperatures between 2073 K and 2273 K (in argon atmospheres) were rapidly destroyed by the dissolution of solid UO_2 in molten Zircaloy. In another laboratory experiment, [12] electrically-heated fuel rod (9-rod bundle) simulations in steam were massively liquefied and relocated when the oxidation-driven temperature approached (a measured) 2300 K.

This process, in which Zircaloy reduces UO_2 to form a homogeneous (U, Zr, O) melt at low oxygen concentrations or a heterogeneous (U, Zr, O) melt containing UO_2 particles at high oxygen concentrations, provides a powerful mechanism promoting the destruction of fuel rod geometry at temperatures slightly above the Zircaloy melting temperature but far below the melting point of UO_2.

Apparently, the rapid disintegration of the solid UO_2 is due initially to the formation of liquid uranium preferentially along UO_2 grain boundaries near the UO_2/Zircaloy interface, causing a loss of cohesion. (The uranium results from reduction of the UO_2 by the Zircaloy). In addition to destroying the UO_2 matrix, these processes will apparently also accelerate the release of fission products from the fuel.

It is thus presumed that significant liquefaction of fuel can occur at local temperatures between 2000 and 2300 K, resulting in downward flow of the liquid. Because of the much lower temperatures existing at lower levels in the core, freezing of the liquid will tend to be promoted. However, a countering tendency is the possibility of accelerated oxidation as high-temperature liquefied metal flows downward into a steam-rich region, Figure 2.1.1-8. The balance

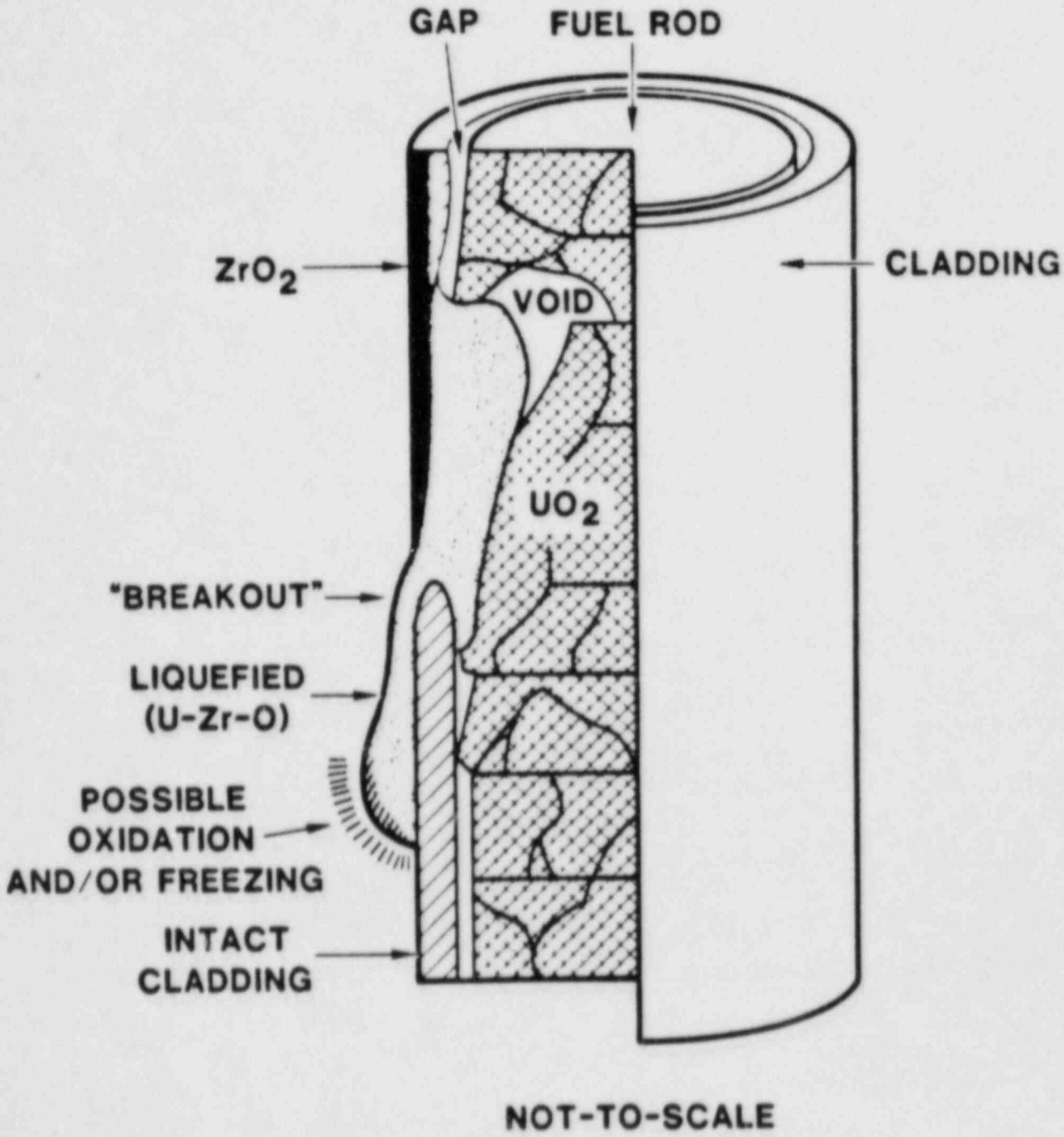

Figure 2.1.1-8. Schematic Representation of Possible Mode of Initial Fuel Liquefaction and Downward Flow (Scale Distorted for Illustrative Purposes).

between these countering tendencies will determine the extent to which material solidifies above the bottom of the core, and is currently very uncertain. Both the SCDAP [13] and ANCHAR [14] codes, which treat downward relocation of fuel rod materials, consider the freezing phenomena, but neither considers the oxidation of the downward flowing liquid. Such treatments may overemphasize blockage formation in LWR cores.

The equilibrium solubility of UO_2 in oxygen-saturated α-Zr (at ~2300 K) is uncertain, but lies between 8 and 20 mol percent, according to Hofmann et al. [11] At ~2700 K and high oxygen concentrations, an equilibrium 85 mol percent UO_2 is dissolved. Equilibrium conditions are not expected, in any case. Also, the extent of destruction of the UO_2 matrix may be only qualitatively related to the fraction dissolved in the melting Zr. Thus the degradation from rod geometry to a relocated, partially liquefied mass as temperatures increase involves complex chemical and physical processes.

In general, models that treat phase changes, e.g., ablation, melting and freezing, and vaporization and condensation, need to be formulated within the framework imposed by mass and energy conservation. Moreover, for mechanistic treatment of phase changes in the presence of fluid flow, additional constraints imposed by momentum conservation may need to be included. For multicomponent fluids, however, the models needed to treat vaporization and condensation in the presence of noncondensibles are very complicated, and formulation of such models is probably beyond the scope of MELCOR. The necessarily simplified treatment adopted for MELCOR should attempt to provide reasonable comparisons with existing data.

The phase change or liquefaction models in MARCH are too unrealistic [3] to be adopted for MELCOR, since they generally require a set of single property values (specific heat, melting point, etc.) for a "mixture" of core materials [(U-Zr-O) ternary plus steel, its oxides, etc.] Development of improved modeling capability for homogeneous and heterogeneous mixtures in MELCOR is considered absolutely necessary to provide reasonable estimates of the behavior of reactor materials and fission products/aerosols following significant core degradation.

2.1.1.5 Convective and Radiative Heat Transfer

2.1.1.5.1 Convective Heat Transfer

Parametric or correlational models are recommended for convective heat-transfer coefficients. Where available, correlations based on empirical results should be used. The

number of convective heat-transfer correlations (coefficients) needed depends on the fluid model chosen, on the number of fluid components, and on the specific flow and heat transfer regimes considered (see for example Figure 2.1.1-5). Table 2.1.1-5 lists the majority of the convective heat-transfer regimes that may be needed.

Table 2.1.1-5

Convective Heat Transfer Regimes

Water, Steam and Hydrogen

- Bubbly flow
- Slug Flow
- Annular Flow
- Dispersed Droplet
- Countercurrent flow
- Nucleate boiling
- Film boiling
- Transition (nucleate-film) boiling
- Dry steam
- Natural convection
- Water
- Particulates in steam
- Steam and hydrogen
- Rubble Bed Flow
- Debris

Core Materials Flow

- Liquid Zr
- Liquid (U, Zr, O)
- Liquid steel
- Liquid ZrO_2
- Liquid control materials (Cd, In, Ag)

Geometrical Considerations

- Axial flow through rod bundles
- Flow through porous media
- Stratified 2ϕ Flow

For fluid-surface heat transfer, single-, two-phase, and boiling (water) relations may be adapted from TRAC [7] or RELAP [5] formulations for fully developed flow. For single-phase, forced convection, developing flow, the laminar Nusselt number may be based on

$$Nu(d) = 0.036\ Re^{0.8} Pr^{0.33} (\mu/\mu_s)^{0.14} (d/x)^{0.055} \quad (2.1.1\text{-}18)$$

where d is the hydraulic diameter, (μ/μ_s) is the ratio of the fluid viscosities evaluated at the bulk and wall temperatures, and x is the length in the developing direction. For single-phase, forced convection, developing flow, the turbulent Nusselt number may be taken as

$$Nu(x) = 0.029\ Re(x)^{0.8} Pr^{0.33} \quad (2.1.1\text{-}19)$$

where the Nusselt and Reynolds numbers are now based on the length x. This equation is useful for all large diameter (> 10cm) pipes.

For free convection from single-phase fluids to vertical surfaces, the laminar Nusselt number is

$$Nu(L) = 0.59\ Ra^{0.25} \qquad (10^4 < Ra \leq 10^9) \quad (2.1.1\text{-}20)$$

and the turbulent Nusselt number is

$$Nu(L) = 0.13\ Ra^{0.33} \qquad (10^9 < RA). \quad (2.1.1\text{-}21)$$

In these equations, the Nusselt and Rayleigh numbers are based on the vertical height L, and thus the Nusselt number is the effective value over the full height. For Equation (2.1.1-21), the 1/3 power to which the Rayleigh number is raised results in cancellation of the characteristic dimension in the Nusselt number, so that the heat-transfer coefficient calculated is independent of the dimension used. However, it is known that local heat-transfer coefficients are larger near the entrance for developing flows.

Additional relationships as required may be derived from the appropriate literature.

2.1.1.5.2 Radiative Heat Transfer

Three models are considered for radiative heat transfer. All of the models require view factors between surfaces and emissivities for each surface. The first model treats the direct radiative exchange between two surfaces. The model is described by

$$Q_{12} = \sigma F_{12} A_1 (\epsilon_1 T_1^4 - \epsilon_2 T_2^4) \quad . \quad (2.1.1\text{-}22)$$

where

Q_{12} = net energy transfer from surface 1 to surface 2,
σ = Stefan-Boltzman constant,
F_{12} = view factor from surface 1 to surface 2,
A_1 = area of surface 1
ϵ_1, ϵ_2 = emissivities of surfaces 1 and 2, and
T_1, T_2 = temperatures of surfaces 1 and 2.

The second model is more complicated because it includes diffuse reflection. This model requires the simultaneous solution of a set of equations for the total flux leaving a surface. [15, 16] This model is called a net enclosure model.

The third model includes diffuse emission and absorption by intervening media. This model also requires the simultaneous solution of a set of equations for the total flux leaving a surface. [16] This model is a net enclosure model with intervening media.

Geometry is very important in radiative heat transfer, a. view factors are difficult to calculate for real (i.e., complex) geometries. The difficulty can be reduced somewhat by dividing the volume of interest into regions each of which is treated as a net enclosure. The artificial surfaces (defined numerically by cell boundaries) are treated as black bodies, and view factors between the surfaces (including cell boundaries) are calculated within each cell. [17] This procedure also applies to the calculation of the transmission coefficients [16] that are needed in the third model.

Because of the complexity of the geometrical aspects of the radiation problem, a clear choice of radiation model for MELCOR is not obvious at this time. However, because of the significant absorption of energy in steam at high pressures which is expected, the choice of model should include capability for treating absorbing and emitting intervening media.

2.1.1.6 Conductive Heat Transfer

Lumped-parameter or finite difference models can be used to model conductive heat transfer. An example of a lumped-parameter model is a model that uses an analytical solution for a steady state temperature distribution and treats the time-dependent solution as a perturbation. Depending on the geometry of the region being modeled, different steady state

solutions will be required for the different boundary conditions. Because of the limitations of lumped-parameter models, they cannot be used to treat transient phenomena.

A finite difference model divides the region to be modeled into a finite mesh. Although the accuracy of the treatment is a function of both the mesh size and the temperature gradient, finite difference models can be used to treat a wide variety of boundary conditions and rapid transients. [18] These models can also be formulated so that they are implicit in space and time.

Both types of models can be used to treat multiple dimensions, variations in material properties, and melting, freezing, and ablation. Crust formation, liquid-solid conduction, and time-dependent volumetric heat sources can also be handled through the use of these two types of models.

As has been implied above (Section 2.1.1.3), some parts of some sequences may be characterized by conditions which call for a two-dimensional, finite difference treatment of thermal conduction in RCS structures. An example of such a situation is a thick pipe wall upon which significant fission products have deposited with a strong gradient in density in the flow direction. Under these conditions, the wall temperature of the pipe is strongly affected by conduction through the wall thickness as well as parallel to the pipe axis.

Because such calculations are inherently time consuming, external calculations should be performed prior to implementation in MELCOR to determine the need, and the discretization and time step requirements, for such calculations. Only in this manner can the approach finally adopted for MELCOR be justified.

2.1.2 REACTOR VESSEL

2.1.2.1 Incore Models

The assumption of a one-dimensional fluid treatment implies uniformity of radial fluid conditions within the core region and requires that fluid conditions be based on averages over the core radii. Thus, for example, fluid enthalpies and void fractions (in two-phase mixtures) will be overestimated at the periphery of the core and underestimated in the highest power core zones. If radial variation in core power is modeled in the core fuel, the uniformity of radial fluid conditions leads to errors in local fuel rod-to-fluid heat transfer. Correction of the introduced error can be accomplished partially by modification of the fluid conditions (for heat transfer calculations alone) to yield more nearly correct local heat transfer, but only at the expense of additional computation. The error is particularly difficult to evaluate and correct when two flow regimes (e.g., turbulent and laminar) are simultaneously present in different radial zones of the core. Crossflow in a PWR core tends to decrease the magnitude of the errors by increasing the radial mixing. Fuel assembly shrouds in BWRs prevent crossflow, and enhance the radial nonuniformity of fluid conditions. This BWR feature may require incorporation in MELCOR of several one-dimensional fluid channel models in parallel to provide an adequate treatment of local fluid and heat-transfer conditions (such as the three channels used in TRAC-BD1). Such a scheme, while remaining within the context of a one-dimensional fluids treatment, requires calculation of branching flows in the core, and implementation of solution algorithms capable of satisfying the uniform pressure drop boundary condition for all such channels.

For MELCOR, it is assumed that the intact reactor core will be geometrically represented as a right cylinder comprised of a number of annular cylinders representing radial regions of uniform power. As the number of cylinders is increased, the radial power distribution approaches a smooth but otherwise arbitrary distribution. Each annulus is divided into a number of axial segments representing regions of uniform power. As the number of axial segments is increased, the axial power distribution approaches a smooth, but otherwise arbitrary distribution. For proper normalization, the core power fractions in each radial/axial segment, when summed over all segments, must equal 1.

It is also assumed that a single fuel rod and associated flow channel (Section 2.1.2.1.1 below) represents all fuel rods and channels within a constant radial power annulus such that if there are n_r radial segments, n_r rod and flow channel combinations represent the core. Each flow channel model is subject to the constraints imposed by the one-dimensional fluid treatment assumption, including errors introduced by radial averaging as discussed above. The goal in the design of these models is to achieve reasonably accurate calculated local heat transfer without incurring unacceptably complex fluid or correction calculations.

Within each annular cylinder, an auxiliary annular cylinder representing the control rods/blades within that region can be formulated. Again, all rods/blades in the annular cylinder would be represented by a single rod/blade calculation (Section 2.1.2.1.2 below).

The complexity introduced by the occurrence of a wide spectrum of core damage states is not easily accommodated in a simplified code like MELCOR. In particular, mechanistic modeling of the relocation of solid and liquid core materials appears to be infeasible.

One-dimensional relocation of fuel/control rod materials by gravity following severe damage can be represented within the assumed cylindrical geometry framework. However, upon the accretion of significant amounts of damaged materials, modification of the representational framework (example given below) is probably necessary to allow a crudely realistic treatment while maintaining simplified computational approaches. A modified framework may allow for subsequent conditions during which liquefied core material may flow from the core zone into the lower plenum of the reactor vessel. Such a framework should provide for at least a crude representation of the damaged states of the core materials and their location during the core damage process. Current attempts to treat these phenomena are represented by the SCDAP [13], ANCHAR [14], RPI [19], and MELPROG [20] code developments. In each, a small set of discrete damage states has been chosen to represent the continuum of damaged and relocated core components.

A parallel consideration is the necessity to model the release of fission products and the generation of aerosols during the progression of core damage. The loss of fission products from the fuel matrix significantly reduces the heating rate of the overall core and thus must be accounted for. As is discussed in detail in (D. Powers' section), the release rates for fission products and aerosols depend on melt and gas temperatures, core configuration, gas pressure, composition and flow rates, and vaporization chemistry.

Generally, these conditions will have a strong spatial dependence as well as time dependence. Especially at the higher temperatures, large quantities of aerosols are likely to be produced by vaporization of both fission products and structural/control materials, followed by nucleation and condensation of these vapors during transport from hot surfaces into cooler gas. Thus the framework, however crude, must allow estimation of these conditions and processes. None of the above-mentioned codes presently contain realistic models of fission product/aerosol processes.

An example of a possible framework is illustrated in Figure 2.1.2-1 and described below. The concept relies on dividing the continuous spectrum of damage states into a few discrete, less specific states. In the example, a crude division into 3 states (Table 2.1.2-1) is proposed. The core zone is subdivided into subzones within which a single state (or void) is allowed, based on energy, temperature and/or relocation criteria.

Table 2.1.2-1

Damage State Subzones

Damage State Subzone	Type	Fluid (not including melt) Vol Frac
1	Rod and Channel	0.56
2	Permeable Rubble	0.40
3	Melt w/Crust	0.10

The radial boundaries of the subzones coincide with the earlier-defined radial boundaries, but the upper and lower axial boundaries of the subzones would be relocated consistent with the mass, density, fluid volume fraction, and type of damage represented. Thus the calculation would allow a crude representation of downward relocation, coincident compaction, and the formation of blockages as core damage progressed.

Mass and energy fluxes across damage state subzone boundaries would be governed by rules which account for the adjacent discrete state pairs, the subzone conditions, and the orientation of the boundaries. Such rules would govern (for example) transformations from state 2 to state 3 (and the reverse), and from state 1 to state 2 (but prohibit the reverse).

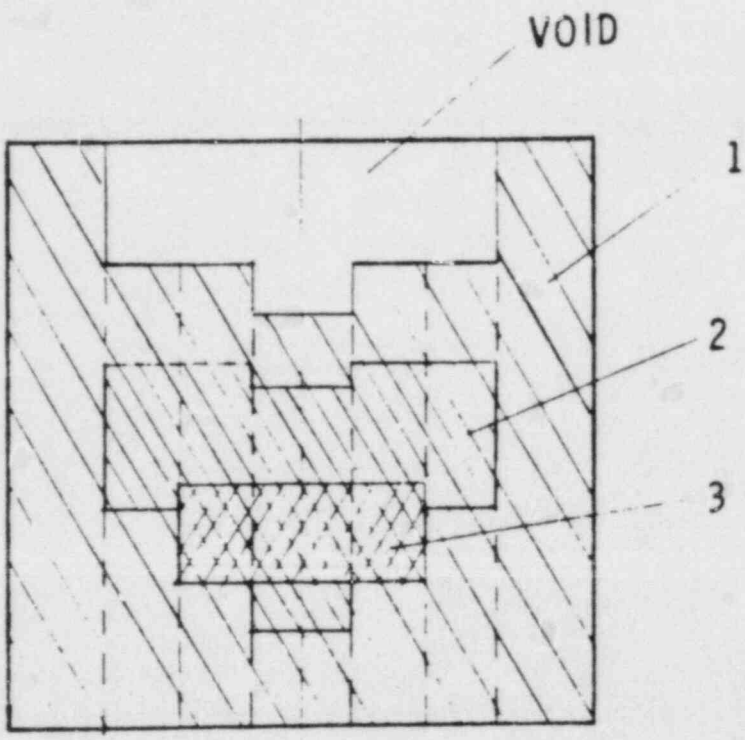

Figure 2.1.2-1. Coarse Representation of Core into Three Discrete Damage State Subzones

2.1.2.1.1 Fuel Rods

As described in Section 2.1.2.1 above, it is assumed that the intact core will be geometrically represented in MELCOR as a right cylinder comprised of a number of annular cylinders representing radial regions of different power, and that a single fuel rod and associated flow channel will represent the fuel rods in a given annular cylinder.

Modeling of intact fuel rods and associated flow channel is one of the more straightforward tasks in the development of MELCOR. A wide choice of models of varying levels of detail are available. The major considerations in such a model are the coupling of energy evolution/absorption processes (isotope decay, phase change, chemical reaction) with energy transfer and transport processes (heat transfer and fluid flow).

Evidence developed in recent years indicates that fairly simple rod/channel models suffice to treat nearly all the phenomena of importance during time regimes 1, 2, and 3 of Table 2.1.1-1. For example, it has been found that modeling of the radial temperature dependence within fuel rods and cladding is unnecessary during decay heat-driven sequences--a lumped model consisting of a fuel node and a cladding node connected by a simple gap conductance is adequate. Calculations have also confirmed that axial thermal conduction (even in the metallic phase of the cladding) is unimportant unless fidelity in the fuel/cladding temperatures in the vicinity of a quench front are required.

It is also likely that processes in the fuel and cladding such as cladding ballooning/embrittlement can probably be neglected as having only temporary importance in the progression of core damage. This is, of course, not true if modeling of the coupling of core damage with ECC injection processes assumes great importance (witness the core condition of TMI-2).

On the other hand, modeling of the cladding oxidation process must be done carefully because of the strong temperature dependence of the reaction and the positive feedback of relatively large quantities of energy evolved by Zr oxidation. It has been found, for example, that a small axial mesh size is needed to model the very localized deposition of cladding oxidation energy during time regime 3 (Table 2.1.1-1). Typically, this requires an axial mesh size (in the zone of oxidation) ~10 cm; a larger mesh size will artificially reduce the concentration of deposited energy and result in underprediction of the reaction rate. This mesh size constraint, if allowed to govern the choice of uniform core mesh, could result in several thousand core meshes, an unacceptable number for MELCOR. Thus, a system

allowing more than one axial mesh size in the core is essential for MELCOR. This is most easily accomplished by an automatic subdivision of the larger mesh into small meshes in core zones attaining temperatures above a threshold value.

Considerable uncertainty in the modeling of the core damage progression is introduced when fuel temperatures exceed ~2000 K, the approximate melting temperature of Zircaloy-4. This uncertainty is due to the very complex (U-Zr-O) interactions possible, which is discussed above in Section 2.1.1.4.2. For MELCOR, the method outlined in Section 2.1.1.2 above will be necessary to treat the transition of intact core zones at temperatures > 2000 K to a relocated core configuration--for example, the 3 damage-state zone model outlined above in Section 2.1.2.1.

2.1.2.1.2 Control Rods/Blades

Control rods/blades for LWRs consist of either boron carbide (B_4C) or an alloy of silver, indium, and cadmium (AgInCd), encapsulated in either stainless steel or Zircaloy. B_4C melts at about 2750 K, while the AgInCd alloy liquefies at temperatures between 900 and 1200 K. Control rods/blades clad with Zircaloy will be subject to exothermic oxidation at temperatures above 1300 K, while those clad with steel will oxidize relatively more slowly below 1700 K (and with less specific energy evolution).

Despite the fact that little energy is generated in the control materials during an accident sequence, surface temperatures of the control rods/blades will lag fuel rod temperatures by relatively small amounts due to convective and radiative heat transfer from the fueled rods. Thus it is expected the degradation of the control rods/blades will occur on roughly the same time scale as the remainder of the core. Models of control rod/blade degradation are not available--they will need to be developed for MELCOR.

2.1.2.2 Excore Models

Although the lower plenum participates to a limited extent in the accident progression prior to time regime 4, it is the source volume for evaluation during time regimes 4, 5, and 6. Time regime 4 begins with discharge of core materials into the lower plenum. The progression treated here assumes that water exists in the plenum although this will not be true for some sequences. Upon melt-water contact the conditions and nature of the contact are unknown. Based upon currently available knowledge, the melt might issue from the core region in three possible modes:

1. In a narrow continuous stream over a period of fractions of minutes to several minutes,

2. In a narrow discontinuous stream distributed over a longer period of time,

3. In a relatively massive, coherent discharge occupying a few seconds or less.

The temporal distribution of the discharge is related to the three modes listed and the timing of the discharge relative to the level of damage achieved (fraction of core liquefied). This is true because the rate of formation of liquefied fuel is slow compared to all but the very slowest discharge rates. Thus, if a large fraction of the core is liquefied at the onset of discharge, a larger amount might be discharged; conversely, if only a small fraction is liquefied at the onset of discharge, a smaller amount might be discharged (corresponding to mode 1 or 2 above).

Experiments have shown that, under certain conditions, high temperature melts explode upon water contact. Such a "steam explosion" results from transfer of thermal energy from the molten mass to water on a time scale so short (~1 ms) as to produce effects associated with chemical explosions. Industrial experience with thermal explosions has shown them to be often powerfully destructive.

The four major stages of such an explosion have been identified as

1. Initial coarse premixing without large heat transfer, generally implying stable film boiling,

2. Destabilization of film boiling either spontaneously or from an external pressure pulse (triggering), leading to small-scale mixing and rapid heat transfer in a local region,

3. Propagation of a zone of rapid heat transfer through the coarse mixture, which may develop into a propagating detonation.

4. Highly dynamic expansion driven by steam at high pressure.

Four major scenarios are possible:

1. A series of relatively low-yield steam explosions continuing until the whole of the molten mass of fuel has been fragmented or all the water evaporated,

2. A low-yield steam explosion which stimulates a large steam explosion involving a significant fraction of the melt,

3. A single large steam explosion,

4. No steam explosion but violent boiling which may or may not quench the debris depending on the quantity of water available and the agglomeration of the debris. Hot debris may collect at the vessel bottom and thermally attack it immediately.

Because of the resultant disruption (and possible dispersal) of internal structures and residual core materials, the occurrence of even a relatively low-yield steam explosion will qualitatively alter the subsequent progression of damage.

Outcomes 2 or 3 (above) could cause breach of the reactor vessel and possibly generation of containment-failing missiles. Either possibility would completely alter the course of the accident, particularly the second which would involve breach of the reactor vessel, ejection of fuel and fission products, and venting the containment, all nearly simultaneously.

Because of major uncertainties in all the processes discussed here and consequent lack of models, MELCOR will have to depend primarily on the methods outlined in Section 2.1.1.2 for treating these processes.

2.1.2.2.1 Core Support Structures Failure (PWR and BWR) and Core Discharge

The first criterion which should be met by this structural failure model is that it be consistent with the core deformation model discussed in Section 2.1.2.1, above.

Useful, but nonmechanistic, failure threshold criteria can be constructed for the discharge modes discussed at the beginning of the previous section by combining temperature or energy criteria, damage state subzone criteria (Table 2.1.2-1), and user input. An outline of a possible set of criteria is given in Table 2.1.2-2.

2.1.2.2.2 Steam Explosion

Occurrence of a steam explosion, and its magnitude, would be, as the table indicates, dependent on user choice, but would be constrained to correlate with the selected discharge mode, as indicated. The actual magnitude of the steam explosion would depend on the amount of melt available for discharge at the time of the structures failure and the efficiency for the explosion selected by the user as input.

Selections of options governing the branching during this time regime are highly uncertain, and the approach of Section 2.1.1.2 of making these obvious to the user is highly recommended.

Table 2.1.2-2

Structures Failure Threshold Criteria

Discharge Mode	Energy Transferred to Structures Prior to Failure	Adjacent Damage State	Selected Hole Size	Correlated Magnitude of Steam Explosion*
1. Narrow Continuous Stream	Medium	2 or 3	One to Several Fuel Assembly Areas	Small-Medium (multiple?)
2. Discontinuous Narrow Stream	Low	2 or 3	One Fuel Assembly	Small (Multiple?)
3. Massive	High	3	> 10 fuel Assembly Areas	Small-Large (single)

* If a steam explosion is selected by the user

2.1.2.2.3 Quenching and Debris Bed Formation

In the event that the vessel is not breached by a steam explosion, a fraction of the core melt (Table 2.1.2-3) may be quenched. For core fractions equaling or exceeding the values in Table 2.1.2-3 (or smaller fractions for less water), the quenching will vaporize all of the water in the plenum.

If excess melt over that which can be quenched is deposited in the plenum, it will begin heating the reactor vessel wall immediately. The fraction quenched by the vaporization of the residual water will subsequently begin reheating, but will require 20 to 40 minutes to attain temperatures which augment the attack of the pressure vessel.

The table indicates the limited capacity for the formation of quenched debris in the lower plenum. (The capacity is further reduced if the inventory of residual water has been reduced below $29m^3$). [3] The implication for debris cooling and vessel attack is discussed below.

Table 2.1.2-3

Fractions of Core Mixture* Which
Can Be Quenched in Below-Core Water**

	Atmos	800 psia	1600 psia	2500 psia
	0.1 MPa	5.5 MPa	11. MPa	17. MPa
ΔT = 1500 K				
NO FREEZE	0.79	0.44	0.31	0.17
ΔT = 2000 K				
NO FREEZE	0.59	0.33	0.23	0.13
ΔT = 2500 K				
FREEZE	0.37	0.21	0.14	0.08

* 10^5 kg UO_2 + 2(10^4) kg Zr + 10^4 kg Steel

** in 29 m^3 of Water

To this description must be added the contribution from accompanying chemical reaction. As is noted above, substantial quantities of unoxidized zirconium are likely to be involved in the core liquefaction processes. Mixing of this metallic phase at high temperatures with the water (and steam) in the lower plenum will promote rapid oxidation of the zirconium, depending primarily upon the degree to which fragmentation of the melt provides large increases in the interfacial area for interaction. Certainly in the case of a steam explosion, the resulting fine fragmentation in the presence of a steam environment should promote oxidation, and there is some experimental evidence of this occurring. Regardless of the exact outcome, the addition of substantial reaction energy and liberation of a quantity of hydrogen by the oxidation of zirconium during the melt-water interaction phase seems likely.

2.1.2.2.4 Vessel Breach

Treatment of the attack of the RPV by the high-temperature core materials is complicated by a wide range of initial conditions which may precede vessel breach, including:

1. RPV internal pressure excesses (over containment pressure) ranging from 0 to 17 MPa,

2. Quantities of core materials in the lower vessel head ranging from a few tons to a hundred tons at temperatures ranging from coolant saturation temperatures to 3000°K+,

3. Failure modes ranging from hoop stress-induced tears to failure of local features such as instrument tube penetrations in the vessel.

Once a breach has occurred, the rate of discharge of materials through the opening, and possible accompanying enlargement of the opening, also depend upon the above parameters.

In sequences in which accumulator (flood tank) discharge occurs during the blowdown following breach (as the RCS pressure falls below the discharge set point), the breach/discharge process will be complicated by melt-water interactions (Section 2.1.2.2) as the coolant flows toward the opening and meets the hot core materials discharging from the vessel.

Models for the formation of the RPV breach do not currently exist (the model contained in the MARCH code is quite unrealistic). Study is needed to

1. Develop a systematic classification of initial conditions and possible breach modes,

2. Develop a program of source characterization (pressures, loads, heat fluxes, etc.) and corresponding stress and strain field characterizations for representative RPV types.

Such studies could utilize existing large deformation-finite element structural analysis tools. Correlation of the results could yield formula or look-up tables applicable to MELCOR.

The implications of the breach characteristics for the treatment of fission products are several, including the possibilities of resuspension and of the formation of significant aerosols during core materials discharge [10].

2.1.3 CONCLUSIONS, MELCOR RCS MODELING ASSESSMENT

1. A very wide range of thermal hydraulic (flow and heat transfer) regimes occurs in the RCS during severe accidents. The regimes vary generally with time and space (RCS component), and are functions of accident sequence, reactor type, and (sometimes) manufacturer and RCS configuration (Section 2.1.1.3).

2. Some important flow regimes are difficult to characterize (and model) because of a strong influence of natural convection and the dominance of developing flow (as contrasted with fully-developed flow). Conventional, "stylized" treatment of these regimes can be shown to produce large errors in results (Sections 2.1.1.3.1.3).

3. Approximate treatment of the flow and heat transfer regimes is a necessary (but not sufficient) condition for meaningful treatment of the deposition of fission products/aerosols within the RCS because of the broad application of heat-transfer mass-transfer analogies, and the use of thermal hydraulic parameters in the analyses. Approaches have been recommended (Section 2.1.1.3). While this assessment has not defined the acceptable minimum treatment to be accorded the thermal hydraulic phenomena in the RCS, the assessment does show that meaningful fission product/aerosol deposition treatment requires a higher level of thermal hydraulic modeling than would otherwise be necessary. The assessment has not developed technical assurance that meaningful treatment of fission product aerosol processes is possible within current technical and code constraints; neither has the opposite proposition been confirmed. Considerable additional work, including numerical experimentation, is required to provide definitive resolution of this issue.

4. Nodalization of the RCS into control volumes (CVs), and discretization into subvolumes consistent with obtaining reasonable accuracy in the treatment of thermal hydraulic and fission product/aerosol phenomena, is sometimes restrictive (Section 2.1.1.3.5). Uniform, time-independent, discretization appears to be particularly restrictive, and could easily yield very impractical execution times for MELCOR (see also 6., below).

5. Sequencing and branching of MELCOR RCS models in the presence of certain phenomena is highly uncertain (Section 2.1.1.2). This is true because of limitations arising from code-imposed constraints and an inadequate understanding of phenomena (e.g., the treatment of the transition from intact core geometry to a highly distorted geometry, core support and RPV structure

breaching, steam explosions, etc.). MELCOR will therefore not generally provide a unique accident pathway even for the most carefully defined accident sequence. In this regard, MELCOR RCS treatment can represent only a modest advance over the currently available treatment (e.g., MARCH) in reducing the base uncertainty, although it can clearly offer broader and improved coverage of the phenomena.

User-selected options for controlling code sequencing and branching, and code output which emphasizes the nature of these selections, appear to be the best methods for treating these base uncertainties.

6. Depending somewhat upon the local nodalization which is finally found to be necessary for "adequate" thermal hydraulic and fission product/aerosol treatment, extensive application of regime-specific model selection techniques (Table 2.1.1-4) and selective nodalization and discretization approaches (in both time and space, see Sections 2.1.1.3.5 and 2.1.2.1.1) may be essential to achieving acceptable execution times with MELCOR.

2.1.4 NOMENCLATURE

AFW	Auxiliary Feedwater
ATWS	Anticipated Transients Without SCRAM
BW	Babcock and Wilcox
BWR	Boiling Water Reactor
CE	Combustion Engineering
C.L.	Cold Leg
CV	Control Volume
ECC	Emergency Core Cooling
H.L.	Hot Leg
LOCA	Loss of Coolant Accident
LOFT	Loss of Flow Test
MSL	Main Steam Line
NRC	Nuclear Regulatory Commission
PRA	Probabilistic Risk Assessment
PWR	Pressurized Water Reactor
RCP	Reactor Coolant Pump
RCS	Reactor Coolant System
RPV	Reactor Pressure Vessel
St.Gen.	Steam Generator
TMI-2	Three Mile Island (plant), Unit 2
W	Westinghouse

2.1.5 REFERENCES

1. MacMillan, D. B., "Asymptotic Formulas for Approximate Numerical Solution of the Reactor Kinetics Equations", p. 265-276 in Dynamics of Nuclear Systems, D. L. Hetrick, Ed, Univ. of Ariz. Press (1972).

2. Tylee, J. L. "Simple Reactor Model Simulation of a LOFT ATWS Event," Nuc.Tech, 61, April 1983, p. 25-32 (1983).

3. Rivard, J. B. et al., "Interim Technical Assessment of the MARCH Code," Sandia National Laboratories, SAND81-1672, NUREG/CR-2285 (1981).

4. Tong, L. S., "USNRC LOCA Research Program," IAEA-CN-39/99 (1980).

5. Ranson, V. H. et al., "RELAP5/MOD1 Code Manual, V.1: System Models and Numerical Methods," EG&G Idaho, Inc., EGG-2070, NUREG/CR-1826 (1982).

6. McFadden, J. H. et al., "RETRAN-01-A Program for Transient Thermal-Hydraulic Analysis of Complex Fluid Flow Systems, V.1: Equations and Numerics," EPRI, Palo Alto, CA, NP-1850 (1981).

7. Safety Code Development Group, "TRAC-PF1: An Advanced Best Estimate Computer Program for Pressurized Water Reactor Analysis," LANL Report Draft (1981).

8. Scheele, G. F., and Hanratty, T. J., "Effect of Natural Convection on Stability of Flow in a Vertical Pipe," J. Fluid Mechs, 14, 2, p. 244-246 (1962).

9. Metais, B. and Eckert, E. R. G., J. Heat Trans, 86, 295 (1964).

10. Sprung, J. L., et al., "Assessment of Fission Product Behavior During Severe LWR Accident Sequences: Modeling Recommendation for the MELCOR Code System," Sandia National Laboratories, Albuquerque, NM (to be published).

11. Hofmann, P., Kerwin-Peck, D., and Nikolopoulos, P., "Physical and Chemical Phenomena Associated with the Dissolution of Solid UO_2 by Molten Zircaloy-4," Kernforschungszentrum Karlsruhe GmbH, Report 06.01.16 p. 10c (PNS-Nr.675/82)(1982).

12. Hagen, S. J., (Kernforschungszentrum Karlsruhe GmbH, IT), private communication regarding experiment ESBU-1, July 1982.

13. Marino, G. P., Allison C. M., and Majumdar D., "SCDAP: A Light Water Reactor Computer Code for Severe Core Damage Analysis," Proceedings, Int'l Mtg. on Thermal Reactor Safety, NUREG/CP-0027, p. 1145-1157 (1982).

14. Bowers, C. H., Hosteny, R. P., and Thomas, G. R., "Status of Major Modeling Phenomena in the ANL/NSAC Core Heatup And Redistribution (ANCHAR) Code," Proceedings, Int'l Mtg. on Thermal Reactor Safety, NUREG/CP-0027 p. 1209-1221 (1982).

15. Hottel, H. C., and Sarofin, Radiative Transfer, McGraw-Hill (1967).

16. Siegel, R., and Howell, J. R., Thermal Radiation Heat Transfer, 2nd Ed, McGraw Hill (1981).

17. Maudlin, P. J. et al., "Light-Water Reactor Degraded-Core Cooling Program Technical Note: A Damage Assessment of TMI-2," LA-UR-83-737 (1983).

18. Carnahan, B., Luther, H. A., and Wilkes, J. O., Applied Numerical Methods, John Wiley and Sons (1969).

19. Ikeda, T., Podowski, M., Koh, B., Lahey, R. T., Jr., "A Heat Transfer Model for LWR Fuel Rods During Hypothetical Core Meltdown Accidents" (1982).

20. Rivard, J. B. et al., "Modeling of LWR Reactor Coolant Systems During Severe Accidents: MELPROG Perspective" Draft SAND Report, Sandia National Labs (1983).

2.2 RCS COMPONENT MODELS

by

C. J. Shaffer

CONTENTS

LIST OF FIGURES

LIST OF TABLES

2.2.1 INTRODUCTION

In a meltdown accident, the escape of radionuclides to the environment requires successive release from three physical barriers: (1) the reactor fuel rods, (2) the reactor coolant system, and (3) the containment system boundary. Section 2 discussed fission-product release from the fuel, and this section briefly discusses the phenomena and models that must be considered to determine the release of fission products from the reactor coolant system.

The radionuclide release to the environment depends strongly upon the release from the reactor coolant system. In past analyses, (e.g., MARCH analyses), fission-product release from the coolant system was assumed to be instantaneous and complete for all species released from the fuel. In a real accident, however, it is reasonable to expect that the fission products released from the melt will undergo chemical and physical changes and will deposit on various surfaces as they are transported through the reactor coolant system to the containment.

This section discusses the RCS and components, the RCS macrophenomena, and the alternative and recommended models.

2.2.2 RCS AND COMPONENT DESCRIPTIONS

A description of the PWR and BWR plant designs and steam supply systems is found in Section 1 of part 1 "Plant/Accident Scope." This section will review and summarize those aspects which are important in understanding the reactor cooling systems and component models.

2.2.2.1 PWR

The three PWR plant designs, Westinghouse (W), Combustion Engineering (CE), and Babcock and Wilcox (BW), are shown in Figures 2.2.2-1, 2.2.2-2, and 2.2.2-3, respectively and a comparison is shown in Table 2.2.2-1. One major distinguishing feature of the three designs in regards to the RCS is that the W design has four loops and CE and BW have two loops. However, the two-loop designs still have four cold legs and four coolant pumps. Another major distinguishing feature is the steam generator designs which are shown in Figures 2.2.2-4, 2.2.2-5, and 2.2.2-6. The W and CE designs are both vertical U-tube types (W has four and CE has two) and the BW design uses a once-through vertical type. Each PWR has a pressurizer connected to the hot leg of one RCS loop. A typical pressurizer is shown in Figure 2.2.2-7. Pressure relief valves are located on the top of the pressurizer.

2.2.2.2 BWR

The General Electric (GE) BWR reactor and RCS is shown in Figures 2.2.2-8, 2.2.2-9, and 2.2.2-10. The BWR generates steam directly within the reactor core which becomes the working fluid for the associated power cycle. The reactor coolant flow in the core is the sum of the feedwater flow and the recirculation flow. The feedwater flow, as shown in Figure 2.2.2-8, is the cold leg, or return, water flow from the condenser of the power-cycle loop. The reactor water recirculation system shown in Figures 2.2.2-9 and 2.2.2-10 consist of two loops external to the reactor vessel each of which contains a recirculation pump, a flow control valve, and two shutoff valves. High-performance jet pumps, located within the reactor vessel, are used in the recirculation system.

Table 2.2.2-1

PWR Plant Design Comparison

Parameter	Westinghouse	Combustion Engineering	Babcock and Wilcox
Number of RCS Loops	4	2	2
Reactor Coolant Pumps/ Loop	1	2	2
Steam Generator/Loop	1	1	1
Steam Generator Type	Vertical, U-tube	Vertical U-tube	Vertical once-through
Total RCS Water Volume, ft^3	~11,720	~12,540	~12,800

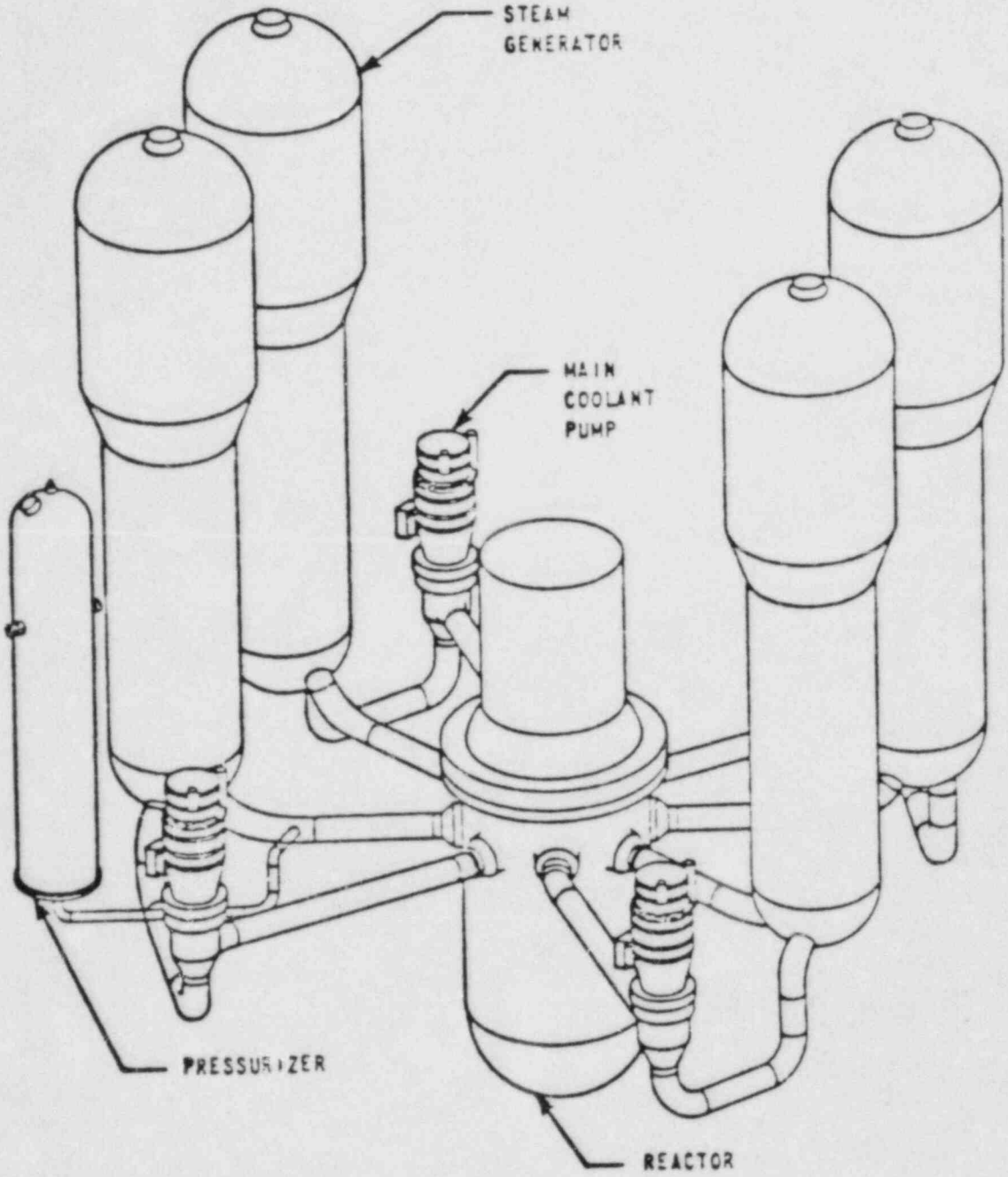

Figure 2.2.2-1. Westinghouse 4-Loop Reactor Coolant System

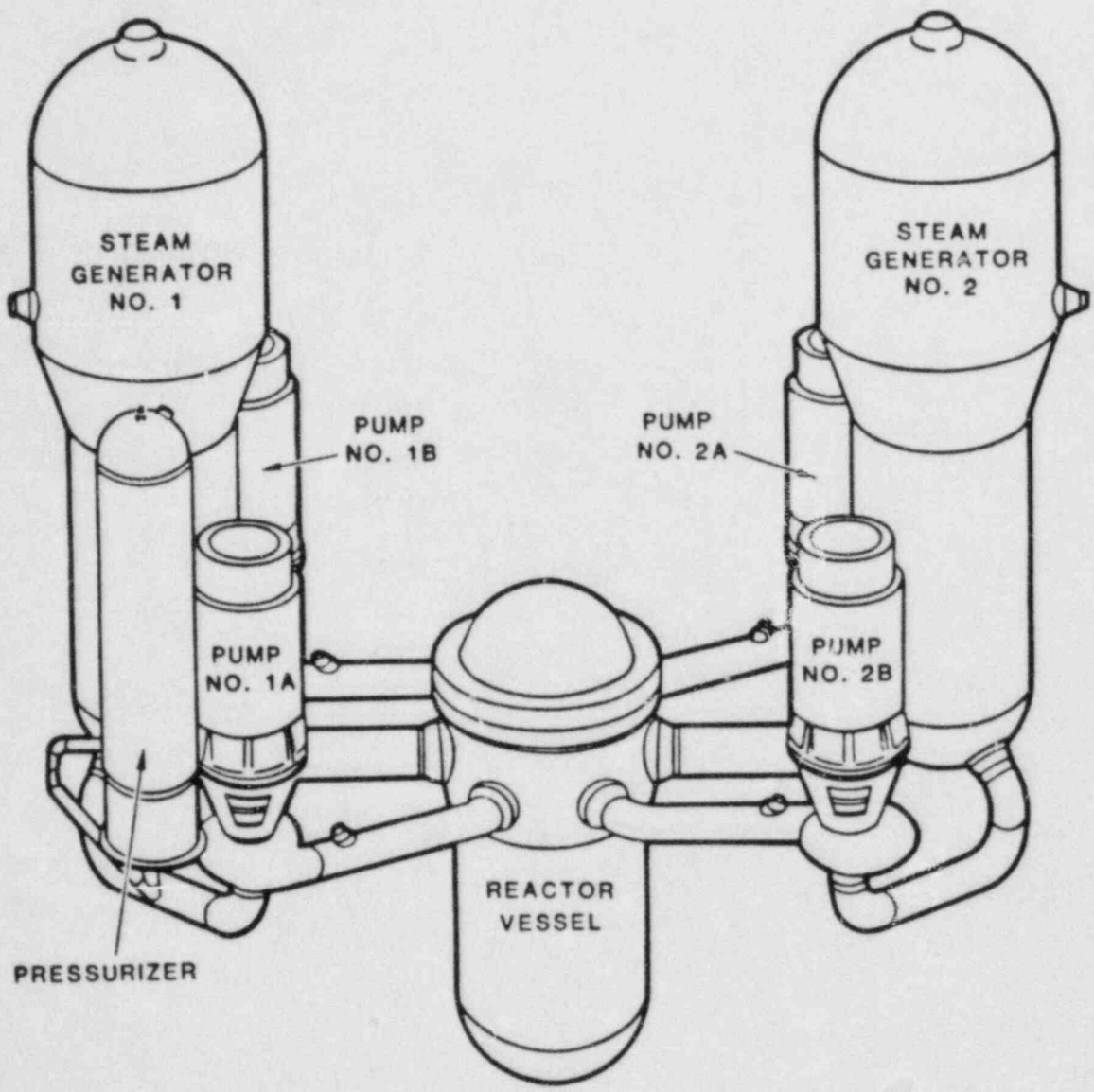

Figure 2.2.2-2. Combustion Engineering 2-Loop Reactor Coolant System

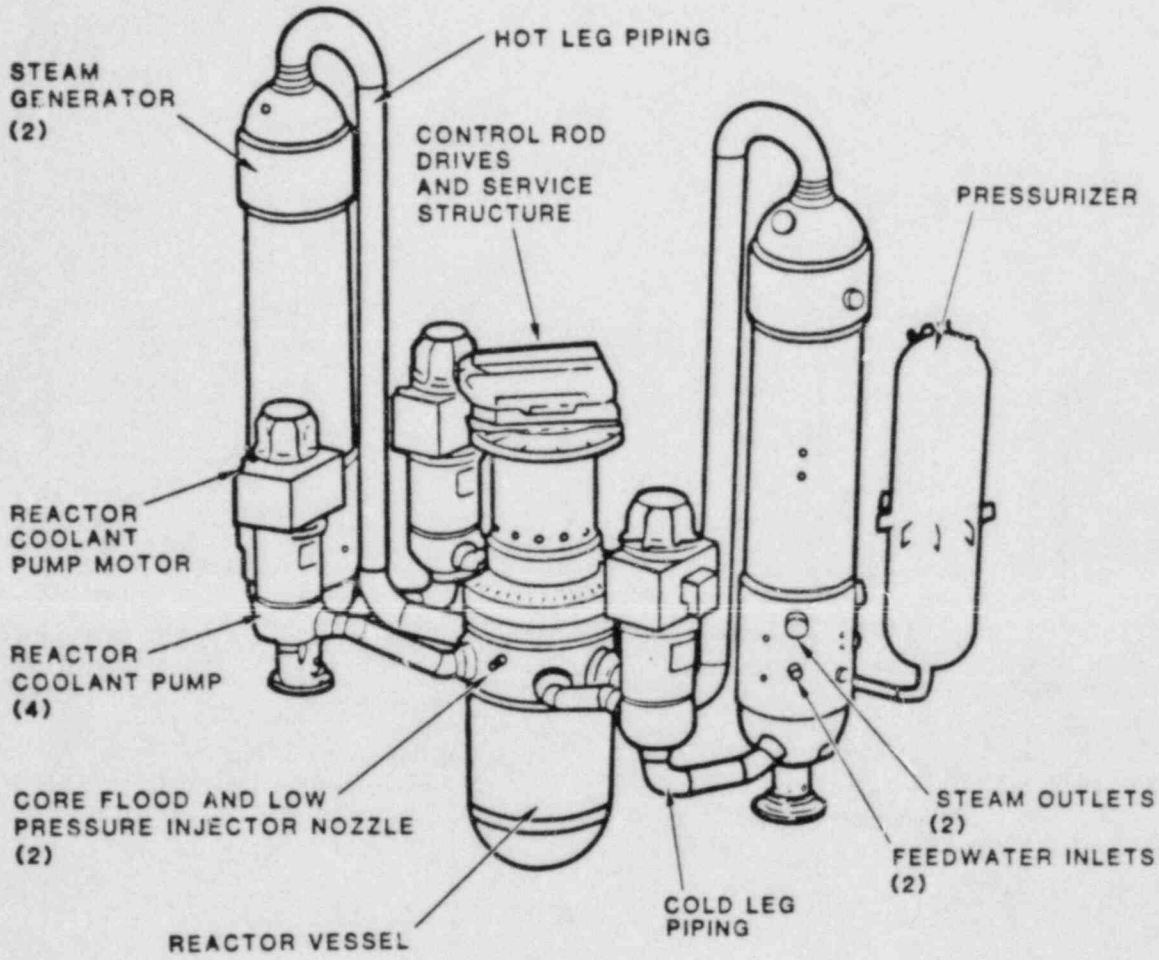

Figure 2.2.2-3. Babcock and Wilcox 2-Loop Reactor Coolant System

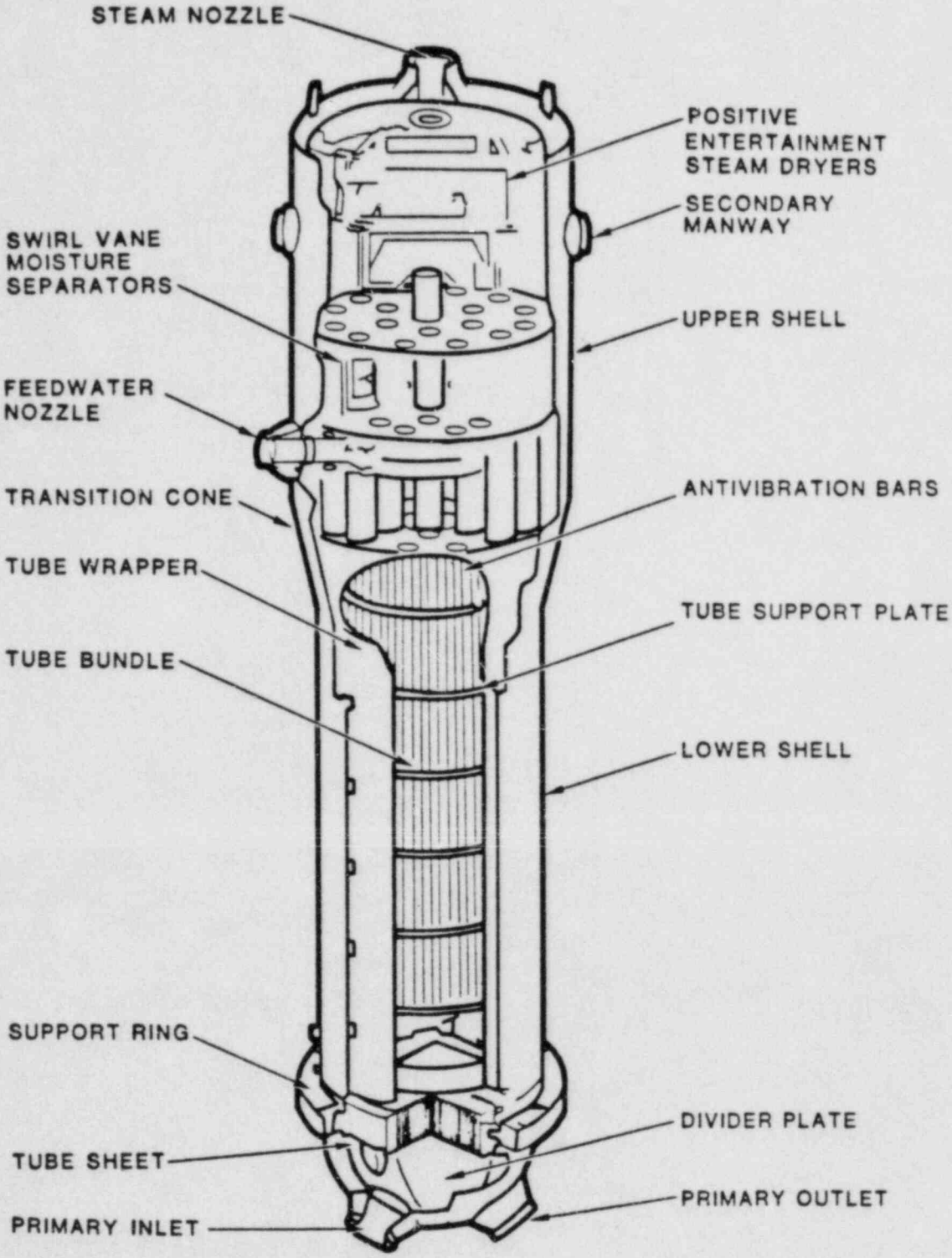

Figure 2.2.2-4. Westinghouse Steam Generator

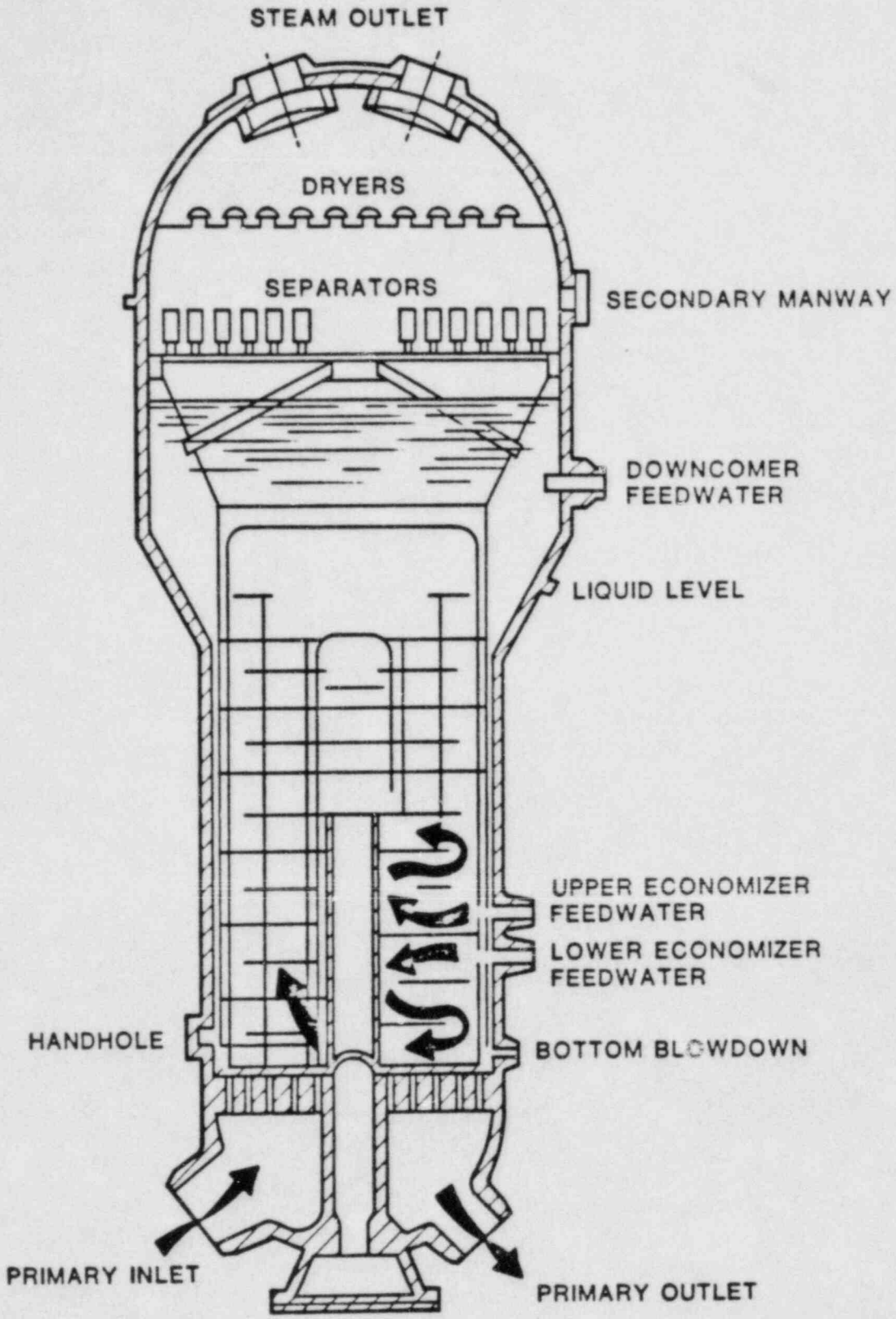

Figure 2.2.2-5. Combustion Engineering Steam Generator

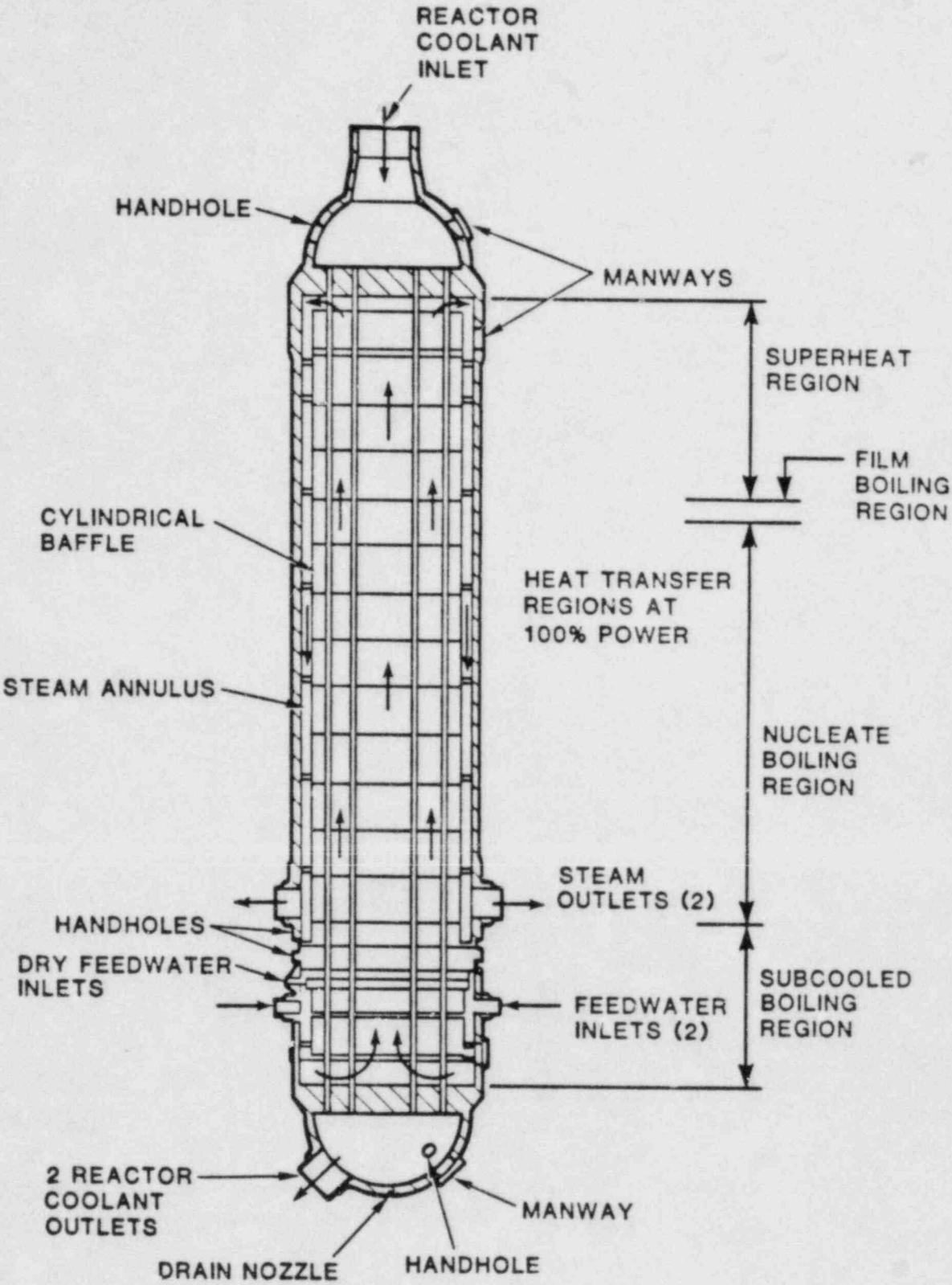

Figure 2.2.2-6. Babcock and Wilcox Once-Through Steam Generator

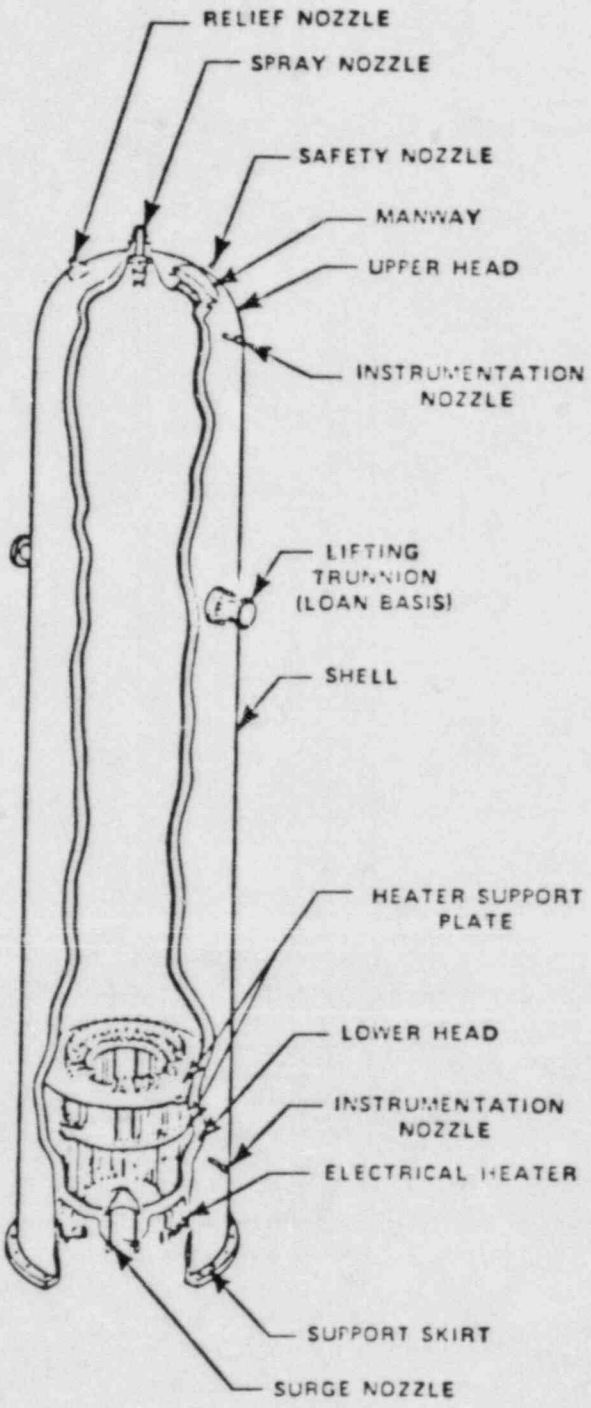

Figure 2.2.2-7. Cutaway of a Typical Pressurizer

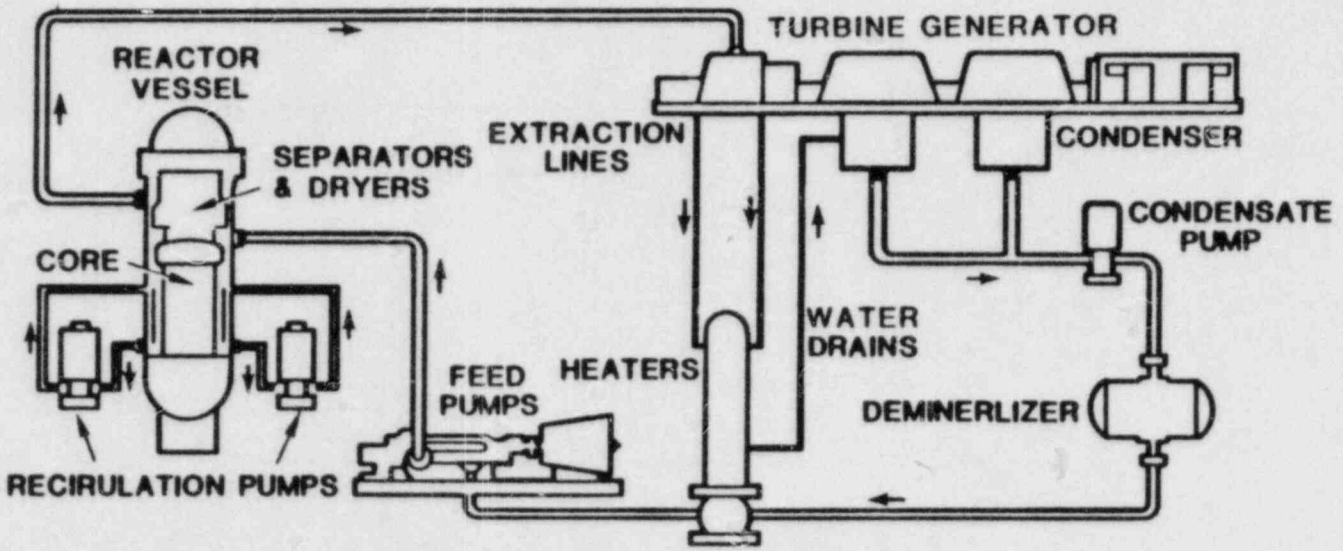

Figure 2.2.2-8. BWR Single-Cycle Power Loop

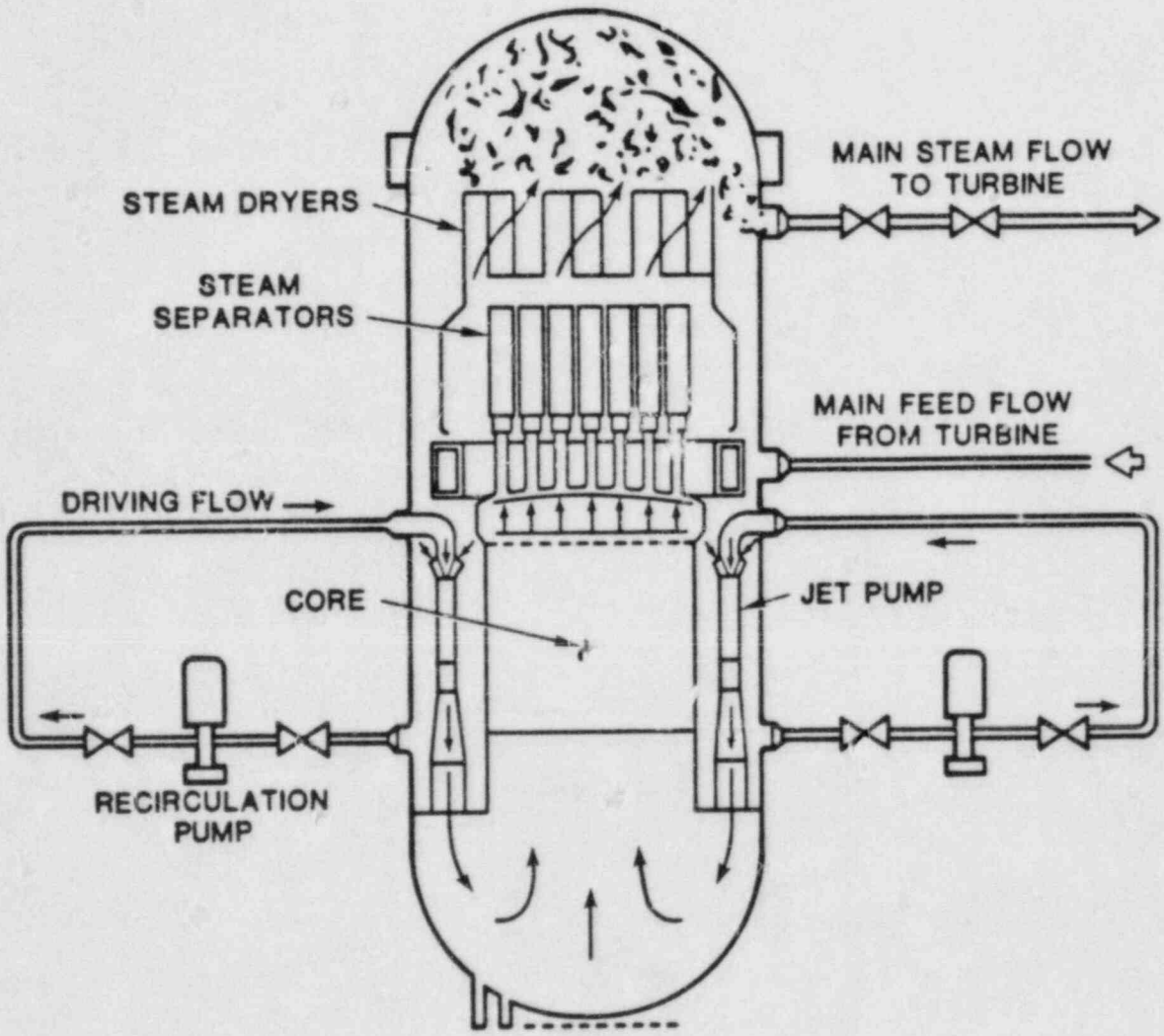

Figure 2.2.2-9. BWR Jet Pump System

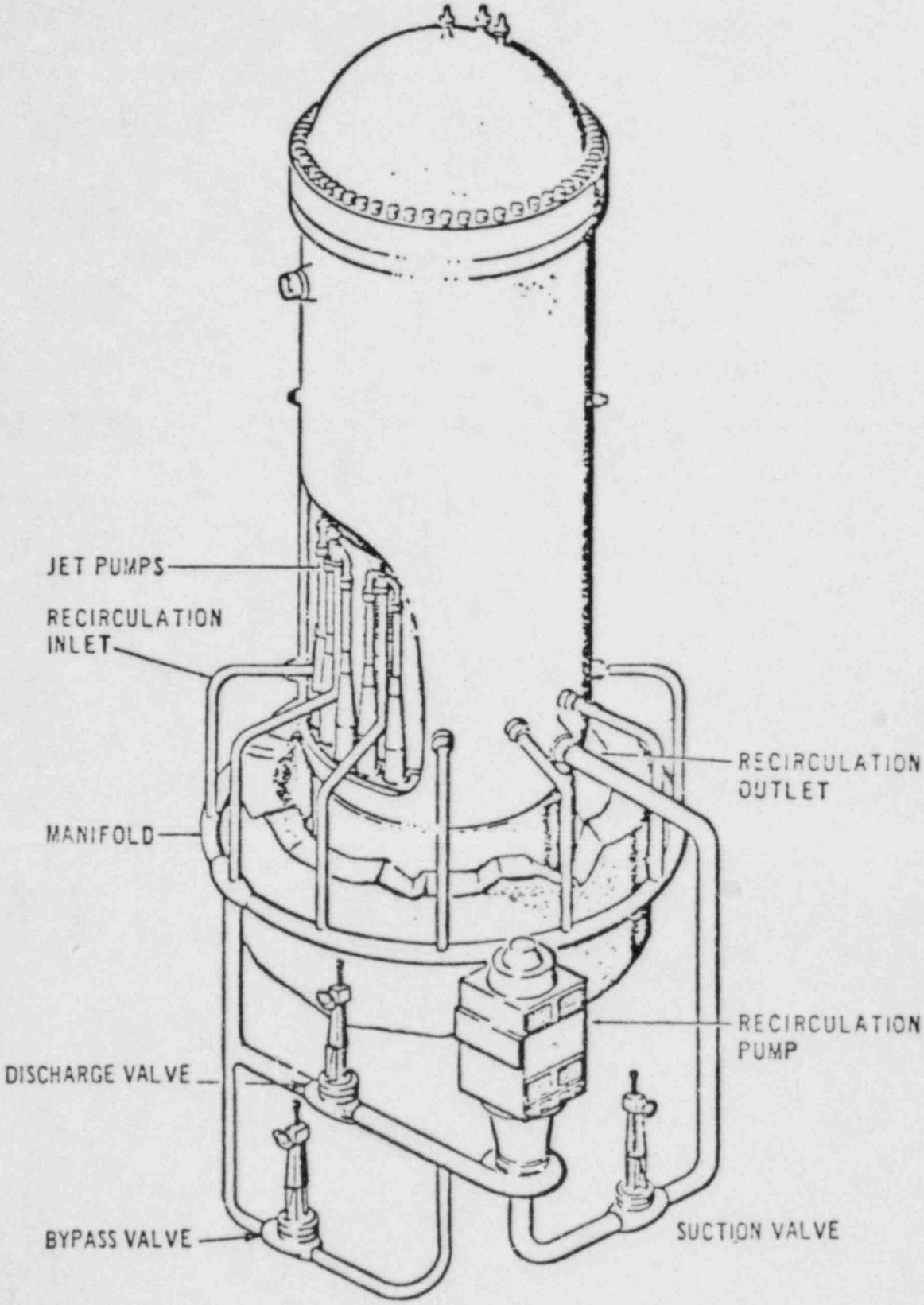

Figure 2.2.2-10. Schematic of BWR Reactor Coolant System

Steam exists from the vessel several feet below the reactor vessel flange through four nozzles to which the steam lines are welded. The steam lines, or hot legs, run parallel to the vertical axis of the vessel, downward to the elevation at which they emerge from the containment.

Two air-operated isolation valves are installed on each steam line, one inboard and one outboard of the primary containment penetration. A flow-restricting nozzle is included in each steam line as an additional safeguard to protect against rapid uncovering of the core in case of a break of a main steam line.

The safety-relief valves, which are dual-function valves that discharge directly to the pressure suppression pool, are flange-connected to the main steam line. The safety function includes protection against overpressurization of the reactor coolant system, and the relief function provides actuated opening of the valves to depressurize the reactor coolant system. For the pressure relief function, the valves are power-actuated manually from the control room or power-actuated automatically by high pressure.

2.2.3 MACROPHENOMENA

Fission products can be transported throughout the coolant system by flowing steam, water, and noncondensible gases. The transport processes will depend upon conditions such as flow rates, flow velocities, interphase mass transfer (condensation and evaporation), flow regimes (e.g., two phase, laminar or turbulent flow), fluid and wall temperatures, and the chemical and physical states of the fission products themselves.

The deposition of fission products at various locations within the coolant system can depend upon a number of complex processes in addition to those mentioned above. These processes include the transfer of fission products among the liquid and gaseous components of the fluid, aerosol deposition and resuspension, and the transfer (adsorption and desorption) of fission products at the boundary between the wall and flowing fluid.

This section will discuss the RCS system pressure, the RCS component flow rates and flow regimes, and the RCS component heat transfer.

2.2.3.1 RCS System Pressure

The effects of high-coolant system pressure in both PWR and BWR accident sequences are significant. In LOCA sequences, high pressures in the reactor coolant systems may engender critical break-flow phenomena. In transient sequences, pressure spikes, generated for example by in-vessel steam explosions, can cause breaks and rapid fission-product transport. More generally, the effects of high-coolant system pressure will be manifested in thermohydraulic properties (in particular, the latent heat of vaporization of water), the steam void fraction, and the mechanism of reactor vessel rupture.

2.2.3.1.1 PWR

The RCS system pressure for a series of PWR accident sequences is shown in Figure 2.2.3-1 for four degraded core events as a function of event time. This data was obtained for the ZION PWR using the MARCH code. The degraded core events shown include (1) the time of core uncovering, (2) the metal-water reaction ignition time (i.e., the time at which the rate becomes very rapid which coincides approximately with the first 2000° F fuel temperature), (3) the time at which first core melt occurs, and (4) the time of first significant melt-water interaction (i.e., the MARCH code slump time). The sequences shown include small

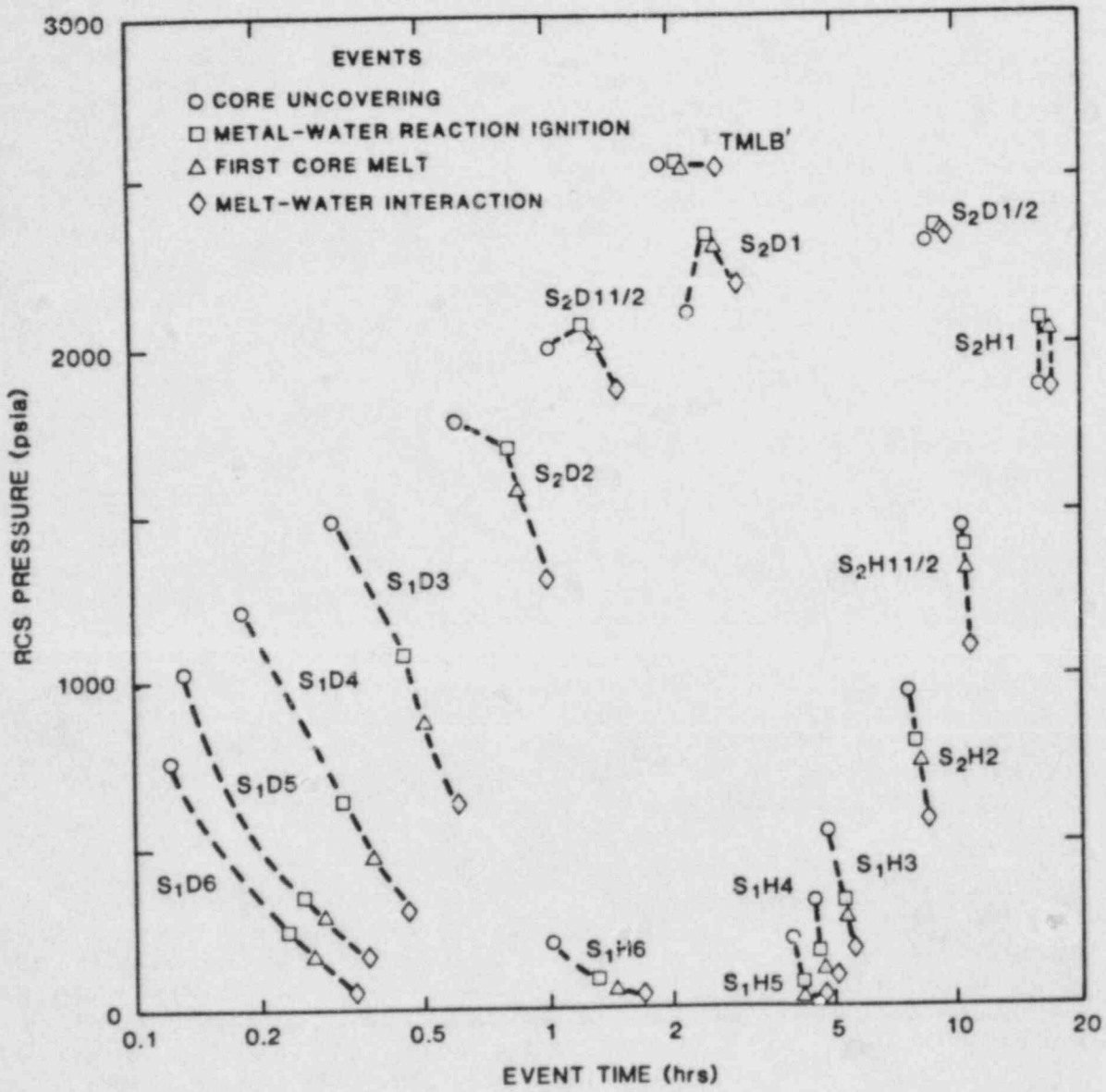

Figure 2.2.3-1. PWR RCS System Pressure

and intermediate break sizes (S_1 and S_2) of 1/2, 1, 1 1/2, 2, 3, 4, 5, and 6 inches in diameter for the total failure of ECC injection (D) and the failure of ECC recirculation after injection (H). A TMLB' is also shown.

In Figure 2.2.3-1, the RCS pressure is shown as a function of the ECC failure mode, the LOCA break size, and the core degradation process for each accident sequence. The pressure is shown lower for the larger breaks and decreases throughout the core degradation process from the core uncovering time to the melt-water interaction time. The pressure is shown higher for the smaller breaks and in some of the smaller break sizes the pressure increases through the boil down period and then decreases again. The large break sequences, AD and AH (greater than 6 inches diameter), are not shown but would be located in the lower left corner of the figure. Transient accident sequences other than the TMLB' would appear on same pressure line as the TMLB' except those with the failure to close the system relief valves after opening, Q, (TMLQB', TMQU, TMQH, and TKQ) which will appear at lower pressures along with small break, S_2 sequences.

2.2.3.1.2 BWR

The boiling water reactors which generates steam directly within the reactor core operate at a lower system pressure than the pressurized water reactors. For example, Dresden 1 Station of the Commonwealth Edison Company generates primary steam at 1000 psia.

The BWR RCS system pressures during a severe accident differs considerably from the PWR RCS pressures. The BWR automatic depressurization system (ADS) which employs pressure relief valves for steam discharge to the pressure suppression pool is used to reduce the RCS pressure so that flow from the low-pressure ECC systems can operate successfully. When the ADS functions successfully the RCS pressure during the core-degradation period is relatively low (< 300 psia).

A high RCS pressure transient accident sequence (such as TQUX) is possible should the ADS system fail. The safety relief valves will operate for pressure relief and will open when the RCS pressure exceeds 70 to 90 psi above the rated operating pressure and close when the pressure falls to a preset pressure of 35 to 55 psi below the pressure switch setpoint. Intermediate RCS pressure accident sequences are possible when the ADS fails for sequences involving a small break (S_1QUX and S_2QUX) or a stuck open relief valve (TPQUX).

2.2.3.2 RCS Fluid Flow

2.2.3.2.1 RCS Fluid Flow Rates

The RCS fluid flow rates during the course of a severe accident will vary from high to low and include single-phase liquid, single-phase gas and two-phase flows. The flow rates can be broken down into six specific time periods as follows for easier examination.

1. From accident initiation to the time of core uncovering.

2. From the time of core uncovering to the metal-water reaction ignition time.

3. From the metal-water reaction ignition time to the time of the first significant melt-water interaction.

4. From the time of the first significant melt-water interaction to the time of relatively slow transient lower plenum boiling rates.

5. From the time of relatively slow transient lower plenum boiling rates to the time of vessel rupture.

6. From the time of vessel rupture to the time of complete depressurization.

2.2.3.2.1.1 Time Period 1

Time period 1 includes the time from the accident initiation to the time of core uncovering. During this period the RCS flow rates can be very high and all single and two-phase flow regimes are possible. Flow modeling through this period of time is very complex and accurate calculations require computer programs like TRAC and RELAP. The flow calculations during this period should use TRAC/RELAP results as input to MELCOR. Period 1 is important mainly to initialize the code for period 2. The important fission product release processes do not begin until after the core begins to uncover.

2.2.3.2.1.2 Time Periods 2 and 3

These periods include the time from the core uncovering to the time of significant melt-water interaction. These periods can be characterized as relatively easy to model in terms of the RCS flow rates and important in terms of fission product release to the containment. In contrast, period 4 will be relatively difficult to model even though it is important in terms of fission product release also.

2.2.3.2.1.2.1 PWR

The RCS flow rate during periods 2 and 3 can be characterized by the break flow rates as determined by the MARCH code. These break flow rates are shown in Figures 2.2.3-2 and 2.2.3-3 for a series of small and intermediate break (S_1 and S_2) LOCA sequences with injection (D) and recirculation (H) failures, respectively. Figures 2.2.3-2 and 2.2.3-3 show higher break flow rates for period 2 than period 3, higher flow rate ranges for the larger break accidents, and the injection failure sequences have higher flow rates than the recirculation failure sequences. For 1/2 and 1 inch small break-injection failure accident sequences, the RCS pressure was high enough to involve pressure relief by means of the safety relief valves. In these sequences, the totals of the relief valve and break flow rates are shown as dashed curves in the left side of the Figure 2.2.3-2. The RCS flow rates for the TMLB' accident sequence calculated by MARCH are 750 to 3000 and 550 to 750 lbm/min for periods 2 and 3, respectively.

Transient and possibly even LOCA sequences containing the letter K (TKQ, TKMU, TKML, S_1K, and S_2K) involve the total failure or the partial failure and belated response of the reactor's protection systems. These sequences can entail a critical and partially uncovered core operating at power during the critical time interval. Some risk assessments estimate that this power is about 30 percent of normal core power (F. T. Harper et al. 1982). This power level can produce steam in the range of 100,000 to 160,000 lbm/min. which must exit the RCS system through either a break or a relief valve.

Steam condensation in the steam generators due to either the main or auxiliary feedwater or water tapped in the secondary side of the steam generators can be an important heat removal mechanism for the RCS. This condensation which will flow back towards the reactor vessel in both the hot and cold legs of the RCS due to gravity can create two-phase flow regimes both cocurrent and countercurrent which can greatly effect fission product release to the containment. The possible two-phase flow regimes which can exist depends upon the amount of condensation occurring, the total break steam flow rate and the distribution of the break flow through the broken and intact loops.

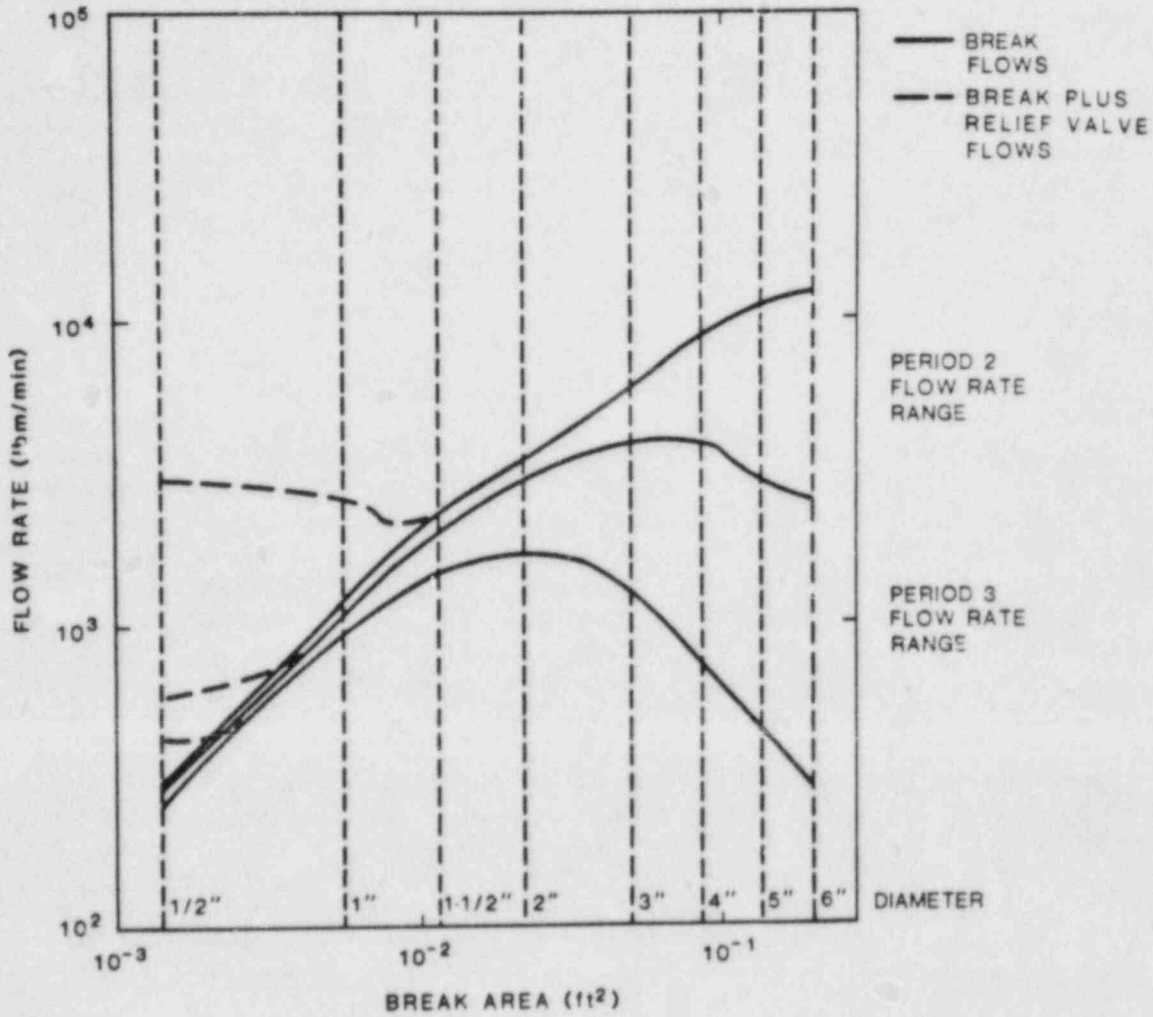

Figure 2.2.3-2. RCS Periods 2 and 3 Fluid Loss Rates for Injection (D) Failure Small and Intermediate Break-Accident Sequences

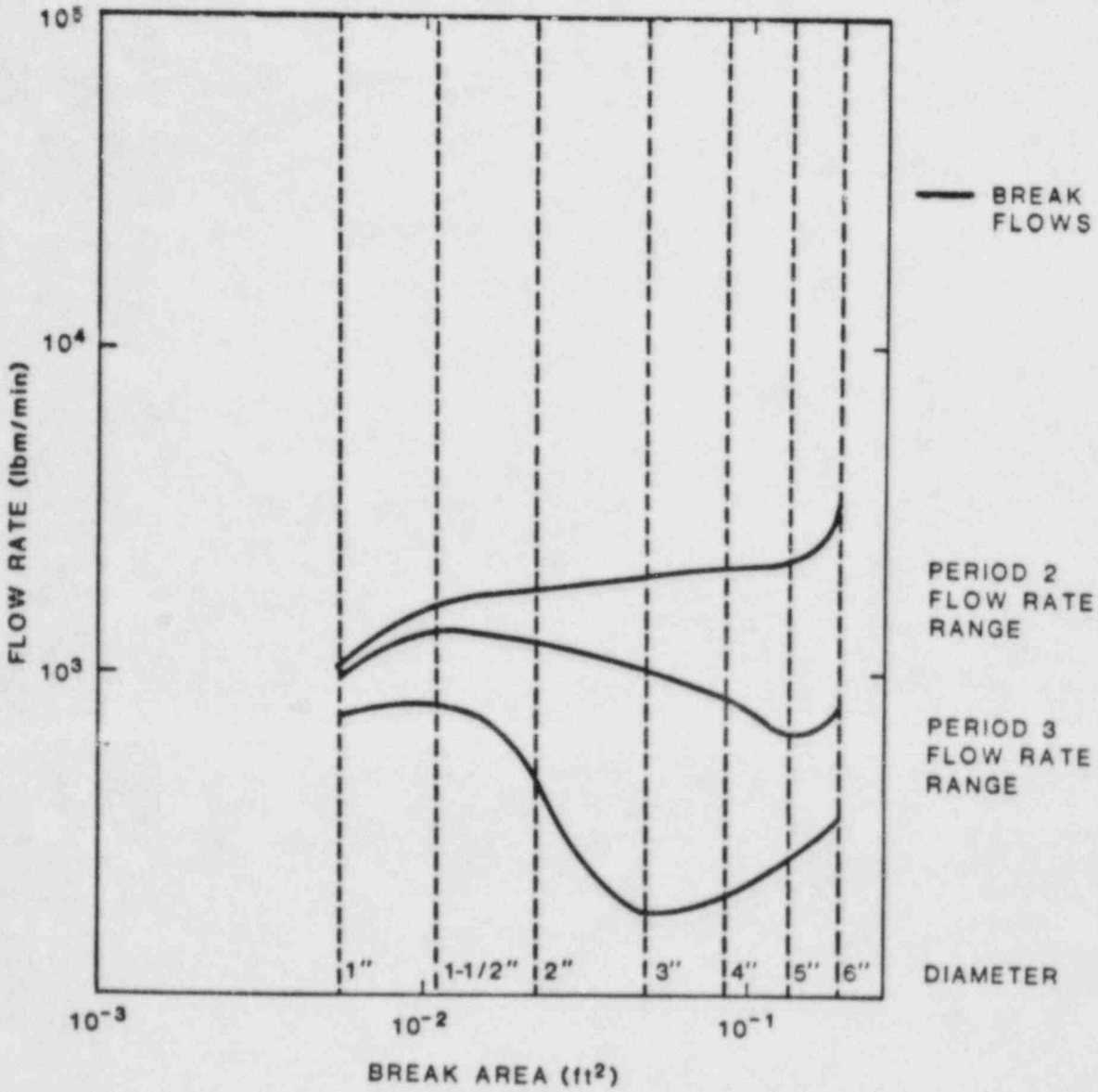

Figure 2.2.3-3. RCS Periods 2 and 3 Fluid Loss Rates for Recirculation Failure (H) Small and Intermediate Break-Accident Sequences

The distribution of the break flow through the broken and intact RCS loops during periods 2 and 3 depends upon the break location and the amount and location of liquid water in the loops from the steam generator condensation. The flow distribution as a function of break location is shown in Figure 2.2.3-4 and Table 2.2.3-1. Seven possible break locations are shown in Figure 2.2.3-4 as follows:

B1. Hot leg break close to the reactor vessel.

B2. Hot leg break close to the steam generator.

B3. Steam generator tube rupture at the tubes midpoint.

B4. Cold leg break close to the steam generators.

B5. Cold leg break at the midpoint between the main circulation pump and the steam generator (lowest elevation in the loop).

B6. Cold leg break close to the main circulation pump between the reactor vessel and the pump.

B7. Cold leg break close to the reactor vessel.

During a LOCA, steam formed by blow down and boil off will leave the upper head of the reactor vessel through the hot leg piping of the broken loop and exit the RCS directly at the break. Also, a portion of the steam can leave the upper head of the reactor vessel through the remaining intact loop and could eventually reach the break by a less direct route. After passing through the intact loops, steam will reenter the reactor vessel and the downcomer and flow on to the break via the cold leg and steam generator of the broken loop. These indirect paths to the break can offer greater flow resistance than the direct path depending upon the break location in the RCS loop. The portion of the break steam flow flowing through the intact loops depends upon the break location and the amount and location of liquid water in the loops. The steam flow distribution for a case of no liquid water in any of the loops (implies that the steam generators are not condensing steam) is shown in Table 2.2.3-1. Table 2.2.3-1 shows the approximate ratios of the steam flowing in the intact loops to the steam flowing in the broken loop as measured in the hot leg piping where the steam exits the reactor vessel. The ratios are listed for the three PWR plant designs, i.e., Westinghouse, Combustion Engineering, and Babcock and Wilcox. The Westinghouse design has four RCS loops which lets the ratio be greater than one for cold leg breaks close to the reactor vessel. The Combustion Engineering and Babcock and Wilcox designs each have two RCS loops which limit the ratio to a maximum of one.

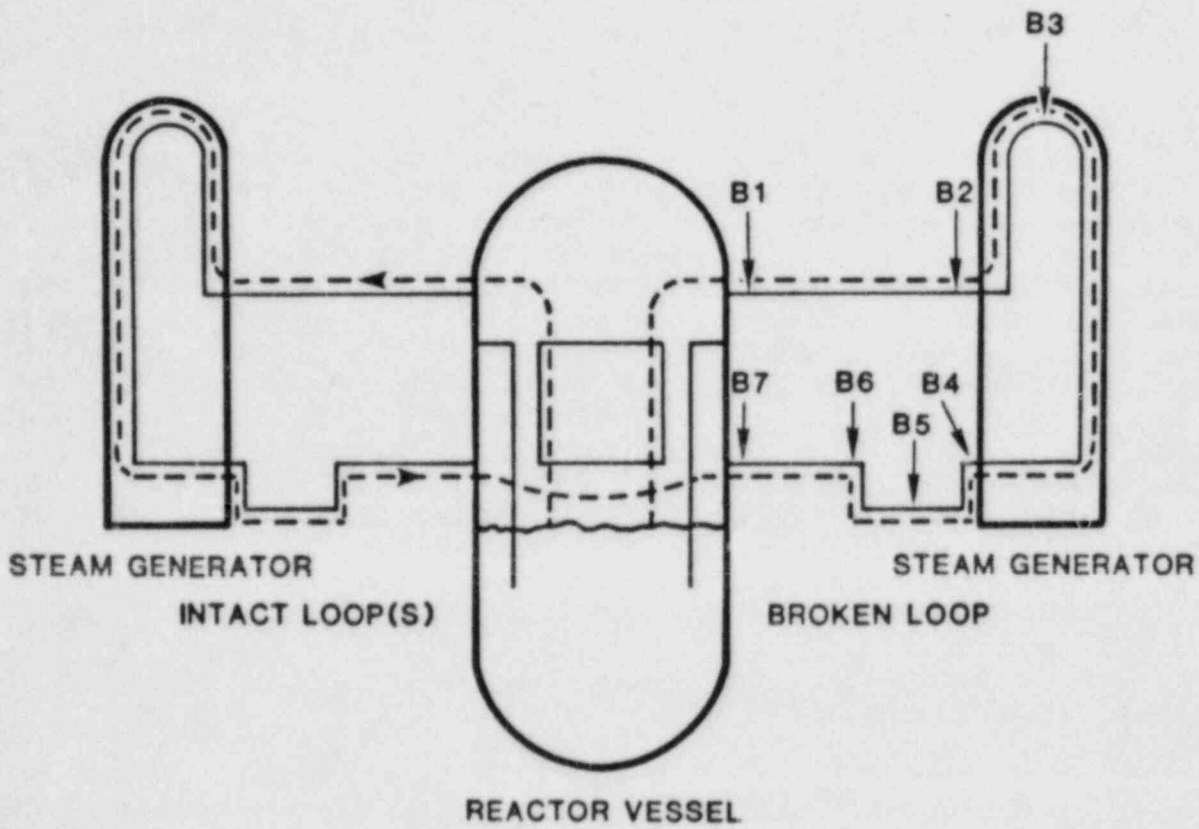

Figure 2.2.3-4. Designated Break Locations

Table 2.2.3-1

Approximate Intact-To-Break Loop Steam Flow Ratios

	Break Location						
RCS Design	B1	B2	B3	B4	B5	B6	B7
Westinghouse	1/3	1/2	3/5	2/3	1	1 2/5	2
Combustion Engineering	1/5	1/3	3/8	2/5	2/3	9/10	1
Babcock & Wilcox	1/5	1/2	3/5	2/3	3/4	9/10	1

Liquid water in the RCS loops can greatly alter the flow resistance. The water can be present in the loops either by condensation of steam in the steam generator or by ECC injection into either the hot or cold piping. Steam generator condensate could fill the cold leg pipes between the main circulation pumps and the steam generators. These pipes have the lowest elevation in the loops. During periods 2 and 3, the RCS loop steam flow rates might not be high enough to pass through this liquid region. In this case the intact loop flow rates will be small relative to the broken loop flow. In this case, a significant amount of steam can still convect to the steam generators of the intact loops by means of natural convection. After hydrogen gas has accumulated in the intact loops during period 3, a diffusion of steam through hydrogen gas in the intact loops will be established.

2.2.3.2.1.2.2 BWR

The BWR period 2 and 3 break flow rates will be somewhat lower than the PWR rates due to the lower RCS pressures. If the ADS operates successfully, then the break flow will be driven by a relatively low pressure differential and if the ADS fails as in the transient sequence TQUX, the relief valve operating pressure will maintain a pressure considerably lower than the PWR transient pressure. The highest steam flow rates will occur when the core is operating at some level of fission power, i.e., in sequences (S_1CH and TCH) that entail failure of the reactor protection system.

Formation of condensate, as a result of natural convection of the steam to the condensers, can occur if the steam

line isolation valves fail on at least one steam line. However, the condensate will remain in the condensers because of the geometry of the hot leg piping and the condensers. As a consequence, the only significant liquid flow rates during periods 2 and 3 will depend upon feedwater flow or flow in the recirculation loops that may be possible for sequences such as S_1CH and TCH.

Possible BW[illegible]eak locations include the hot leg pipes from the react[illegible]essel to the steam turbine, the cold leg pipes from the [illegible]denser to the reactor vessels, and the recirculation loop piping. If the hot and cold leg isolation valves function successfully then the accident will be limited and contained within the containment building which will exclude the turbine/condenser unit.

The RCS flow will be primarily limited to the piping which contains the break. The exceptions will be sequences S_1CH and TCH which will have a hot leg steam flow to the turbines and a feedwater flow in the cold leg and sequences which include the failure to isolate one or more of the hot leg pipes. If the hot legs are not isolated, a natural convection flow to the condenser might be established.

2.2.3.2.1.3 Time Period 4

Time period 4 includes the time from the time of the first significant melt-water interaction to the time of relatively slow transient lower plenum boiling rates. During core degradation, structural collapse will allow some or all of the high temperature core material to enter the lower vessel head. The melt-water geometry in the lower head which determines the interfacial area available for both heat transfer and for metal-water oxidation reactions strongly influences the subsequent events. The initial events during period 4 will be highly transient if not explosive.

The RCS steam flow rates during the highly transient and possibly explosive events will be very high and can carry water and solid particles from the lower plenum into the RCS loops. Fission fragments already deposited into the RCS loops could be picked up by the flows and transported elsewhere. In the case of a steam explosion, new RCS ruptures or breaks are possible.

The time to evaporate the interstitial water between the fragmented debris particles can be used to get a handle on the possible flow rates. As discussed in reference [NUREG/CR-1988, December 1981], the interstitial water will be boiled away in seconds or fractions of seconds producing very high steam flow rates. The interstitial water for a TMLB' accident sequence was calculated to vary from 4645 to 11,443 lbm depending upon the system pressure and a fluid

volume fraction of 35 to 40 percent. The time to evaporate this water depends on the particle size (or diameter) and is listed in the above reference (page A-26, Table A.3.2-2). Table 2.2.3-2 lists the flow rates calculated from this data. Table 2.2.3-3 lists the MARCH calculated lower plenum water masses at the beginning of period 4 for several accident sequences.

The flow rates in Table 2.2.3-2 vary from 20 to 2300 times as large as the largest flow shown in Figures 2.2.3-2 and 2.2.3-3 for time periods 2 and 3. The transient flows will be relatively difficult to model in the RCS loops but can be quite important.

2.2.3.2.1.4 Time Period 5

Time period 5 includes the time from the time of relatively slow transient lower plenum boiling rates to the time of vessel rupture. If the core debris can essentially quench without boiling away all of the lower plenum water, then RCS flows could become relatively stable again before vessel rupture.

For example, the TMLB' sequence decay heat power at beginning of time period 4 is about 1.3×10^8 Btu/hr and will produce steam at the rate of 6200 lbm/min.

2.2.3.2.1.5 Time Period 6

This time period includes the time from vessel rupture to the time of complete RCS depressurization. This time period will be characterized by an RCS depressurization through the vessel rupture in the lower plenum as well as the original break. In the case of a transient accident sequence, the depressurization will be through the vessel rupture alone and the RCS loops will depressurize back into the reactor vessel.

The RCS loop flows will be directly related to the RCS pressure which will range from the pressure at the time of vessel rupture to the pressure of the containment. The RCS pressure at the beginning of period 6 will range from a low pressure associated with a large-break sequence to the high pressure of a transient sequence. The pressure at the vessel rupture, even in a large-break sequence, will have been increased by the rapid boil off of lower plenum water during periods 4 and 5 and there could still be water remaining in the lower plenum during period 6 to boil off and contribute to the system pressure.

The depressurization of the RCS through the vessel rupture will be complicated by the presence of water and core debris which will also exit the vessel through the rupture.

Table 2.2.3-2

Interstitial Water Evaporation Rates, LBM/MIN

Water Mass, lbm	Particle Diameter			
	1mm	5mm	25mm	50mm
11,443	1.4×10^7	2.6×10^6	5.2×10^5	2.6×10^5
4,645	2.8×10^7	5.6×10^6	1.1×10^6	5.7×10^5

Table 2.2.3-3

Lower Plenum Water Remaining at Beginning of Period 4
(Calculated By March)

	Sequence	L.P. Water Mass, lbm
S_2D	1/2 inch break	62,680
S_2D	1 inch break	63,200
S_2D	1 1/2 inch break	65,930
S_2D	2 inch break	67,230
S_1D	3 inch break	68,890
S_1D	4 inch break	68,240
S_1D	5 inch break	66,950
S_1D	6 inch break	69,520
S_2H	1 inch break	67,720
S_2H	1 1/2 inch break	74,360
S_2H	2 inch break	82,550
S_1H	3 inch break	89,540
S_1H	4 inch break	90,990
S_1H	5 inch break	90,930
S_1H	6 inch break	89,670
TMLB'		58,230

This flow will be dependent upon the location, type, and size of vessel rupture and geometry of the core debris.

The flow rates through the RCS loops during period 6 can be as high as the flow rates of periods 2 and 3 but not as high as the transients rates of period 4. The RCS loop flow distribution will be similar to the distribution discussed for periods 2 and 3 with the exceptions of when the vessel rupture leak rate is considerably higher than the break leak rate (transient or small break sizes) and the RCS loops depressurize back into the reactor vessel and when the lower plenum water level is below the down comer exit so that the steam flow may go up the down comer to the cold legs as well as up the core region.

2.2.3.2.2 RCS Fluid Flow Regimes

RCS fluid flow regimes include single and two-phase flow, horizontal and vertical flow, counter and cocurrent flow, critical and noncritical flow, forced and natural flow, laminar and turbulent flow, and steam diffusion flow through noncondensible gas. Two-phase flow regimes could include stratified, annular, wavy, dispersed droplet, churn, slug, plug, and bubbly regimes. Gas flow (whether single or two phase) can be a mixture of steam and noncondensible gases (in particular, hydrogen gas) and can transport solid particles. This section will examine these flow regimes for each of the six time periods.

2.2.3.2.2.1 Time Period 1

During time period 1, the possible flow regimes in the RCS components could include the full range possible from single-phase liquid flow to single-phase gas flow. Accidents involving intermediate or large breaks will be highly transient and difficult to model.

2.2.3.2.2.2 Time Periods 2 and 3

2.2.3.2.2.2.1 PWR

During time periods 2 and 3, the possible flow regimes in the PWR-RCS components will include most of the possible single and two-phase flow regimes. Only the low void fraction regimes, (i.e., plug, bubbly, single-phase liquid) will normally be missing. However, sequences involving partial ECC success could include these as well.

Single-phase gas flow through the RCS loops will occur during periods 2 and 3 if the steam generators become completely ineffective in regards to condensing steam. The

primary system water level during these time periods is already below the top of the core which means the RCS loops are essentially dry with the possible exception of the circulation pump well between the pump and the steam generator on the cold leg. Therefore, without steam generator condensate, the RCS loop flows are single phase (primarily steam and hydrogen) and the loop flow distributions are as shown in Table 2.2.3-1 of Section 2.2.3.2.1.2.1. The single-phase flow will be predominantly turbulent but could be laminar in the steam generator tubes at low flow rates or in a RCS loop convecting by natural circulation. The gas flows could carry particulates including fission products into the RCS components particularly at the higher flow rates.

The two-phase flow regimes can involve either cocurrent or countercurrent flows and either horizontal or vertical directions. The horizontal two-phase flow will occur primarily in the hot leg piping of the W and CE plant designs where steam generator condensate will flow from the steam generator back to the reactor vessel. The hot leg two-phase flow will usually be countercurrent. Horizontal cocurrent flow can occur in the cold leg pipes when flow through the intact loops is possible or when the break is in the cold leg between the vessel and the pump. In the BW design, all condensate will flow by gravitational force to the cold leg piping leaving the hot leg pipe in a single-phase flow condition. The vertical two-phase flow in both cocurrent and countercurrent flows will occur in the steam generators. For example, with the W design and a cold leg break, countercurrent flow will occur in the hot leg side of the U-tubes and cocurrent flow in the cold leg side.

Both forced and natural two-phase flows can occur in the RCS loops. Forced flow occurs anytime there is a direct flow path between the reactor vessel and the break. Natural flow can occur in a RCS loop when the cold leg of that loop has been effectively plugged by condensate from the steam generators. In these loops, steam will flow to the steam generators due to the differential pressure between the reactor vessel and the steam generator caused by the condensation. During period 3, the hydrogen gas produced by the metal-water reactions in the core will flow into the RCS loops and act to restrict the natural convection flow. As the hydrogen gas flows into the loops, a diffusion process of steam diffusing through hydrogen could be established.

During time periods 2 and 3, the break flows (or relief value flows) will be in a critical flow condition except possibly in the large-break sequences. The critical break flow could be either single or two-phase flows.

The possible two-phase flow regimes which could occur in the RCS loops given the small and intermediate break sequence (SD and SH) flow rates of Section 2.2.3.2.1.2 are shown with flow pattern maps for horizontal flow in Figures 2.2.3-5 and 2.2.3-6 and for vertical flow in Figures 2.2.3-7 and 2.2.3-8 for periods 2 and 3, respectively. The maximum flow parameters, gas and liquid, were calculated assuming that the total break flow was flowing through a RCS component as a gas and as a liquid. The minimum gas flows were based upon the break flow and the possible RCS distributions, the minimum liquid flows were considered zero, i.e., the range of steam generator condensate can go from zero to the total gas flow. The large cross hashed area in Figures 2.2.3-5 through 2.2.3-8 were calculated assuming flow in a one foot diameter pipe and the dotted area in the lower corner of Figures 2.2.3-7 and 2.2.3-8 were calculated for a typical Westinghouse steam generator.

The possible horizontal flow regimes shown in Figures 2.2.3-5 and 2.2.3-6 include stratified, wavy, annular, slug, and dispersed droplet. The possible vertical flow regimes shown in Figures 2.2.3-7 and 2.2.3-8 include annular and churn for the RCS piping and churn for the steam generators. The bubbly and plug flow regimes could still be possible in the pump cavity of the cold legs when those cavities become full of steam generator condensate.

The high flow rates associated with the failure of the reactor protection systems sequences, K, will result in either annular or annular-dispersed droplet flow regimes. The flow regimes for the transient sequences (TMLB') are the same as the regimes in Figures 2.2.3-5 through 2.2.3-8 for the SD and SH sequences.

A void fraction correlation for turbulent gas and turbulent liquid annular flow was used to calculate a minimum void fraction in a one foot diameter pipe for period 2 and 3. The results and the correlation are shown in Table 2.2.3-4 as a function of the accident sequence. The minimum void fractions calculated were 0.87 and 0.91 for periods 2 and 3, respectively.

2.2.3.2.2.2.2 BWR

The BWR flow regimes for flow rates discussed in Section 2.2.3.2.1.2.2 will be predominately single-phase gas flows with either turbulent or laminar flow regimes possible. The only significant liquid or two-phase flow regimes during periods 2 and 3 will depend upon feedwater flow or flow in the recirculation loops that may be possible for sequences such as S_1CH and TCH.

Table 2.2.3-4

Minimum Void Fraction*

Sequence	Break Diameter, in.	Time Period 2	Time Period 3
S_2D	1/2	0.88	0.91
S_2D	1	0.88	0.92
S_2D	1 1/2	0.89	0.92
S_2D	2	0.90	0.93
S_1D	3	0.91	0.95
S_1D	4	0.92	0.96
S_1D	5	0.92	0.97
S_1D	6	0.93	0.97
S_2H	1	0.89	0.92
S_2H	1 1/2	0.91	0.94
S_2H	2	0.92	0.95
S_1H	3	0.94	0.97
S_1H	4	0.95	0.98
S_1H	5	0.96	0.98
S_1H	6	0.96	0.96
TMLB'	-	0.87	0.91

* $\frac{(1-\alpha)^2 [1+75 (1-\alpha)]}{\alpha^{5/2}} = \frac{\rho_f j_f^2}{\rho_g j_g^2}$

(Reference: G. B. Wallis, "One-Dimensional Two-Phase Flow," McGraw-Hill, 1969, Page 325.)

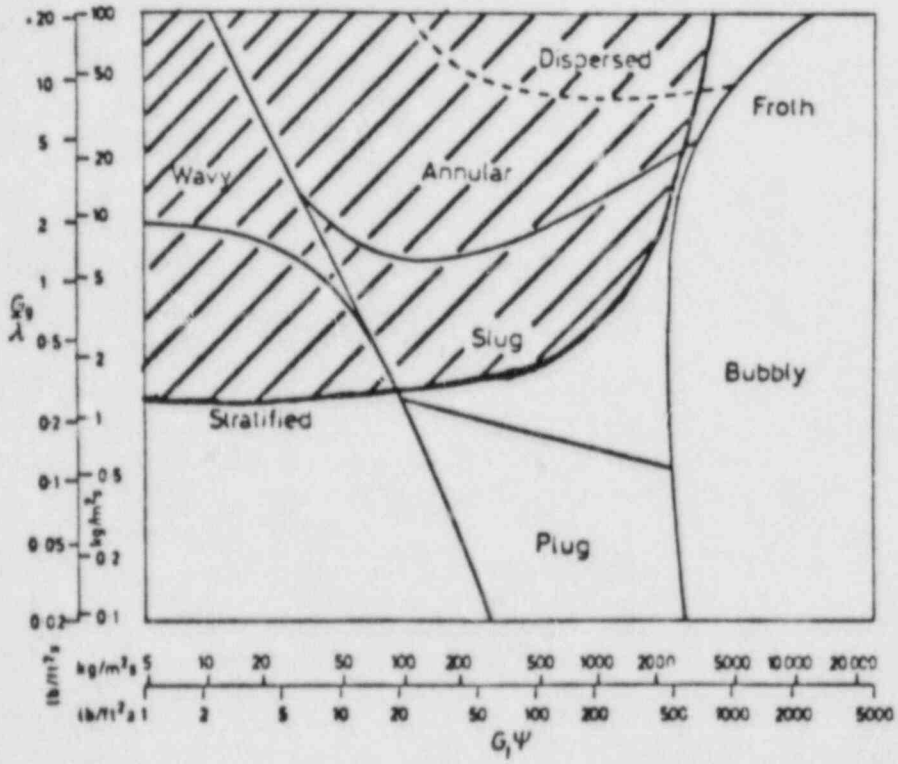

Figure 2.2.3-5. Flow Pattern Map for Horizontal Flow (Baker) for Period 2

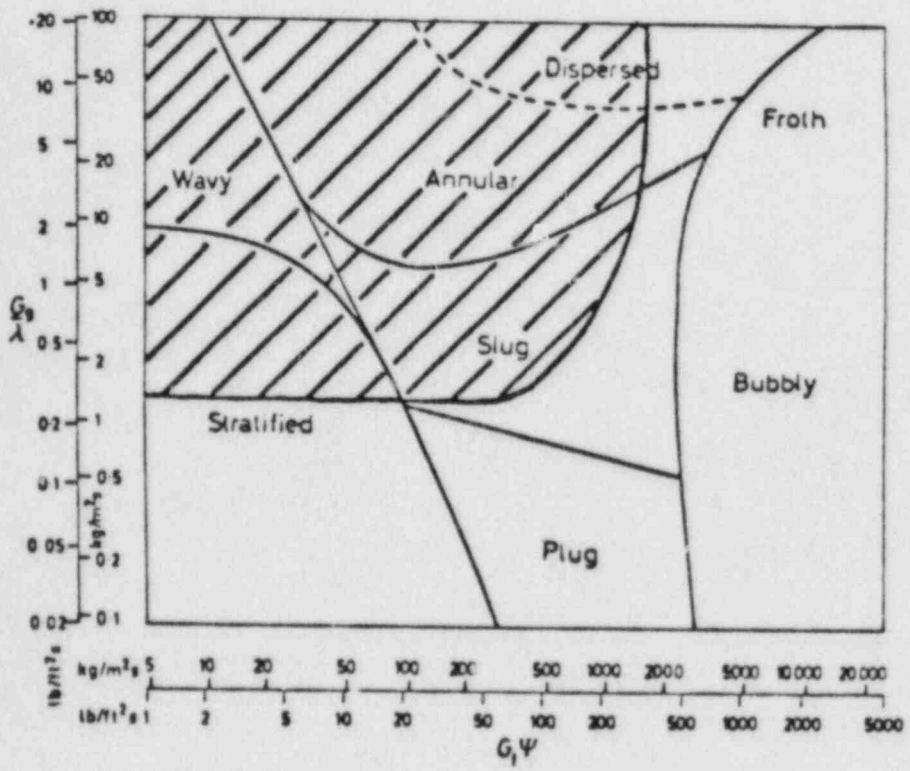

Figure 2.2.3-6. Flow Pattern Map for Horizontal Flow (Baker) for Period 3

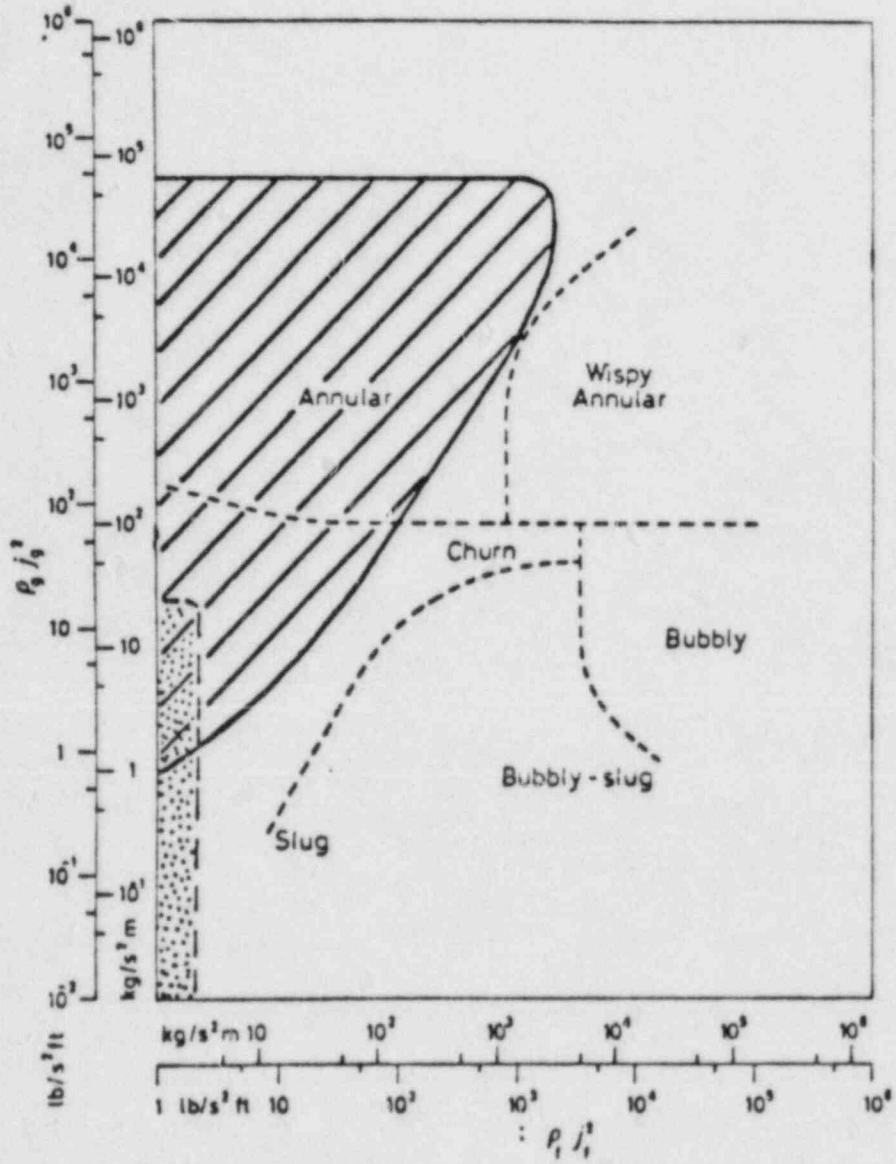

Figure 2.2.3-7. Flow Pattern Map for Vertical Flow (Hewitt and Roberts) for Period 2

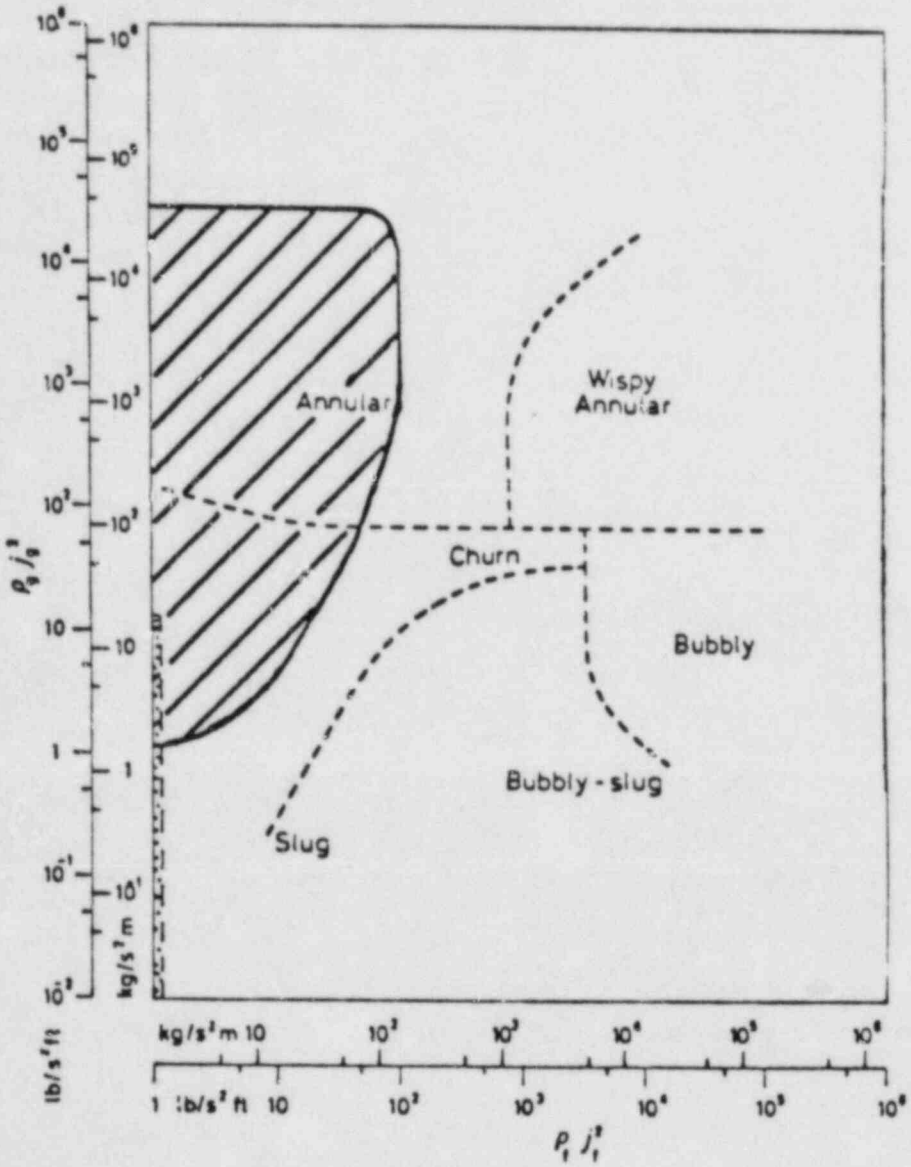

Figure 2.2.3-8. Flow Pattern Map for Vertical Flow (Hewitt and Roberts) for Period 3

2.2.3.2.2.3 Time Period 4

The flow rates during time period 4 will be highly transient if not explosive. If flow regimes were predicted based upon the flow rates of Table 2.2.3-2 and the flow pattern map in Figure 2.2.3-5 through 2.2.3-8, the regimes would be either annular or annular-dispersed droplet. However, the transient nature of the period 4 steam flows could carry water and solid particles from the lower plenum to the RCS loops. More understanding of period 4 phenomena will be needed before the flow regimes can be accurately defined.

2.2.3.2.2.4 Time Period 5

The flow regimes of period 5 will be similar to the flow regimes of period 2. The regimes will probably be annular with stratified a possibility.

2.2.3.2.2.5 Time Period 6

The flow regimes of period 6 will be similar to the flow regimes of periods 2 and 3. Towards the end of the depressurization as the flow rates go to zero, the flow regimes will probably be either single-phase gas or horizontal-stratified and vertical churn.

2.2.3.2.3 RCS Heat Transfer

2.2.3.2.3.1 Component Surface Heat Transfer

Surface heat transfer by conduction will occur throughout the RCS loops. Wall surface temperatures will initially be at the operating temperature of the component and will cool as the system depressurizes. The temperature will increase again for components subject to the hot upper plenum gases during core meltdown. The heat transfer rates and surface temperatures can effect the RCS flow regimes and fission product processes.

2.2.3.2.3.2 Convective Heat Transfer Coefficients

The convective heat transfer coefficients will be a function of the system pressure, fluid temperatures, and flow regimes present in each RCS components. The system pressure and flow regimes have already been discussed. The liquid fluid temperatures will be close to saturation except for ECC flows. The gas fluid temperatures will range from saturation to the highly superheated steam/hydrogen gases of the upper plenum during core meltdown.

2.2.3.2.3.3 Fluid Component to Fluid Component Two-Phase Heat Transfer

Heat transfer from one fluid component to another will occur whenever the components are not at the same temperature. For example, at the hot leg vessel exit, high temperature upper plenum gases could be flowing countercurrent to water at the saturation temperature. In this situation, the fluid component heat transfer is quite important and will result in a surface evaporation of the water component. Fluid component phase change is also an important phenomena.

2.2.4 RCS MODELS

2.2.4.1 Component Models

2.2.4.1.1 PWR

2.2.4.1.1.1 Primary System Flow Models

Fluid flow models for the PWR-RCS loop flows will need to include virtually all the possible single and two-phase flow regimes. The single-phase flows include both gas and liquid flows. Two-phase flows occur during time period 1 as the RCS loops void from fluid loss, during time period 4 when water could be expelled from the vessel, and during the other time periods from condensation occurring in the loops. Steam condensation in the loops is caused in the steam generator by heat transfer to the secondary system and in the other loop components by heat transfer to the component surfaces. Steam generator condensation, when occurring, is dominant over the surface condensation.

When two-phase flow exists, both cocurrent and countercurrent flow configurations are possible. The predominant component two-phase flow configurations for the three PWR plant designs are shown in Table 2.2.4-1 for each of major RCS loop components. Countercurrent flow configurations are shown for the hot leg piping and the steam generators of the Westinghouse and Combustion Engineering designs. The countercurrent flow consists of vapor flow through the hot leg pipes to the steam generators and condensate flow in the hot leg pipes by gravitational force from the steam generators back to the reactor vessel. In the Babcock and Wilcox design, the hog leg pipes enter the steam generators at the top so that all the steam generator condensate must flow downward to the cold leg pipes.

The RCS loop components involve both horizontal and vertical flows depending upon the specific component and plant design. The horizontal and vertical flow geometries are shown in Table 2.2.4-2. The hot leg piping is horizontal except for the vertical section in the BW design. The cold legs all contain vertical sections in the pump cavity wells between the pumps and the steam generators. The steam generators are vertical except for the top of the U-tubes. The pumps act as an elbow and a flow resistance in the cold leg.

The possible two-phase flow regimes are shown in Table 2.2.4-3 as a function of the RCS loop component, the accident time period, and the plant design. Figures 2.2.4-1 and 2.2.4-2 illustrate vertical and horizontal flow regimes.

Table 2.2.4-1

Predominant Component Two-Phase Flow Configurations

Plant Design	Time Period	Loop Component: Hot Leg Pipe	Cold Leg Pipe	Steam Generator	Pump
Westinghouse and Combustion Engineering	1	Co	Co	Co	Co
	2	Counter	Co	Co/Counter	Co
	3	Counter	Co	Co/Counter	Co
	4	Co	Co	Co	Co
	5	Counter	Co	Co/Counter	Co
	6	Co/Counter	Co	Co/Counter	Co
Babcock and Wilcox	1	Co	Co	Co	Co
	2	-	Co	Co	Co
	3	-	Co	Co	Co
	4	Co	Co	Co	Co
	5	-	Co	Co	Co
	6	-	Co	Co	Co

Co - Cocurrent Flow

Counter-Countercurrent Flow

Table 2.2.4-2

Loop Component Flow Geometry

Plant Design	Hot Leg Pipe	Cold Leg Pipe	Steam Generator	Pump
Westinghouse	Horizontal	Horizontal & Vertical (3)*	Vertical (3)	Horizontal & Vertical (1)
Combustion Engineering	Horizontal	Horizontal & Vertical (3)	Vertical (3)	Horizontal & Vertical (1)
Babcock & Wilcox	Horizontal & Vertical (3)	Horizontal & Vertical (3)	Vertical (3)	Horizontal & Vertical (1)

* The number of flow direction changes

Table 2.2.4-3

Loop Component Two-Phase Flow Regimes

Plant Design	Time Period	Loop Component: Hot Leg Pipe	Cold Leg Pipe	Steam Generator	Pump
Westinghouse and Combustion Engineering	1	All	All	All	All
	2,3	Stratified Wavy Slug Annular Dispersed	All	Churn	All
	4		Annular Explosive Fast Transient Particulate		
	5,6	Stratified Wavy Slug Annular Dispersed	All	Churn	All
Babcock and Wilcox	1	All	All	All	All
	2,3	-	All	Churn	All
	4		Annular Explosive Fast Transient Particulate		
	5,6	-	All	Churn	All

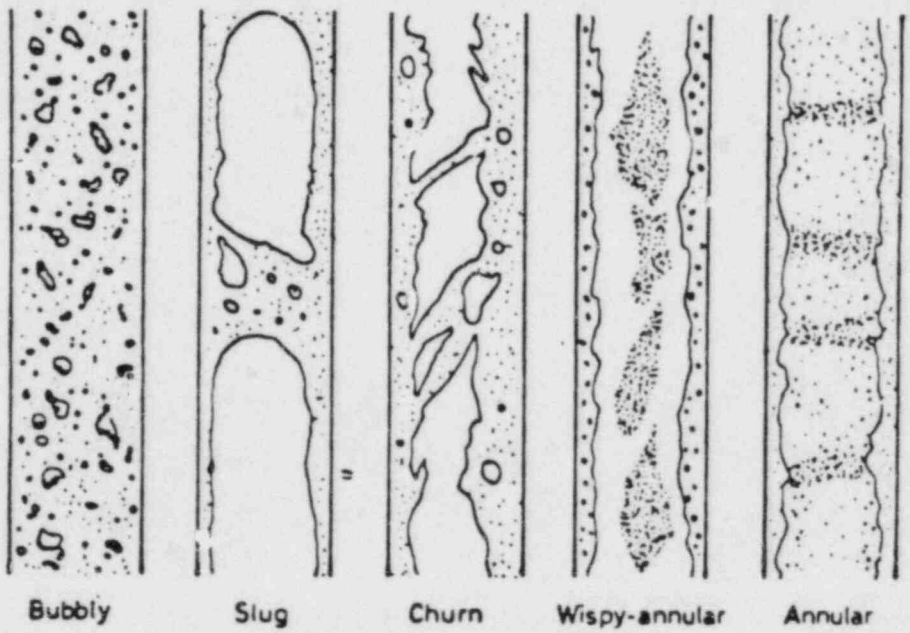

Figure 2.2.4-1. Vertical Flow Patterns

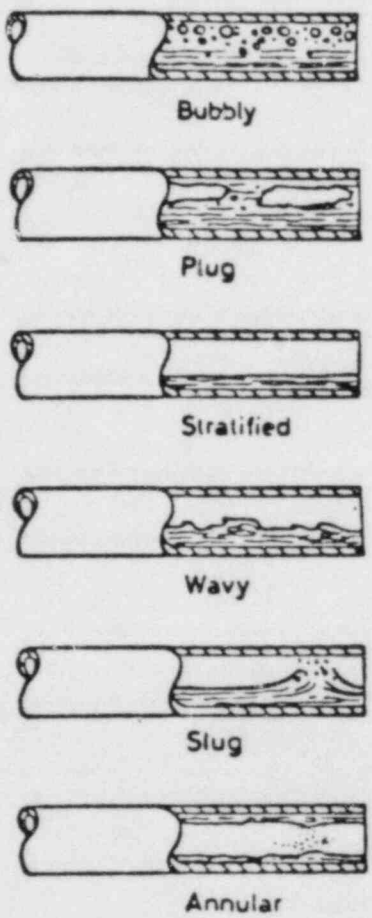

Figure 2.2.4-2. Horizontal Flow Patterns

During time period 1, all two-phase flow regimes are possible from single-phase liquid to single-phase gas. Flow models through this time period are very complex and accurate calculations require computer programs like TRAC and RELAP.

During periods 2, 3, 5, and 6, the hot leg pipe flow regimes will involve the high void fraction horizontal regimes (plug and bubbly flows require relatively low void fractions). In the BW design, the hot leg pipe flow is basically simple phase gas. The cold leg pipes involve both horizontal and vertical flow and will involve high void fraction regimes at locations of high elevation and can involve low void fraction regimes (or even single-phase liquid) in the pump cavity well. The steam generator flows will be in the vertical-churn regime as shown in Figures 2.2.3-6 and 2.2.3-7. The pump flow regimes will basically be the same as the cold leg regimes.

The flow regimes during time period 4 are highly transient, if not explosive, and will be difficult to model. To accurately calculate the flow during this time will require a complex program similar to TRAC or RELAP. There may be some possibility of using TRAC or RELAP to develop models for time period 4.

The steam flows can carry water and solid particles from the lower plenum into the RCS loops. If the time period 4 flow rates are nonexplosive such that the RCS flow regimes are definable, then the regimes would be of the annular or dispersed annular type.

The RCS loops flows will be forced except when a loop is blocked by water in the pump cavity well. When a loop is blocked, a natural convection flow to the steam generator can be established. A natural convection flow can involve steam diffusion through hydrogen.

Turbulent flows will be predominant throughout the RCS loops. However, laminar flows could occur in forced flow through a steam generator at low rates (due to high cross-sectional flow areas), in a natural convection flow, or possibly in a liquid film flow.

Critical flows could involve either single or two-phase flows. The break flow will be critical except possibly the low flows associated with large-break sequences during time period 2, and 3, or the low flows toward the end of time period 6. During period 4, critical flows could be established throughout the RCS loops under the possible explosive conditions.

2.2.4.1.1.2 Relief Line and Quench Tank

Gas escaping to the relief line experiences a large pressure drop on passage through the relief valve. The pressure drop is from the primary system pressure (~2550 psia) to quench tank pressure (< 150 psia) for a pressure differential of the order of 2300 to 2400 psi. The adiabatic expansion cooling will produce steam condensation in the relief line except possibly during time periods 3 and 4 when the relief valve flow gas temperature can be higher than 1500°F.

For example, a gas at 1500°F and 2500 psia will have an entropy of 1.7116 Btu/lbm/°R and will have to expand isentropically down to 31 psia for condensation to begin. For nonisentropic expansion, the tank pressure will have to be even lower. The quench tank pressure can very likely be higher than this during period 3 implying that superheated flow is possible.

The relief line and quench tank condensation will wet the surfaces affording good possibilities of fission product trapping on the surfaces. In addition, scrubbing of the exit gases in the quench tank can further attenuate fission product release to the containment.

2 2.4.1.1.3 Surface Heat Transfer

Conduction heat transfer occurs throughout the RCS loop components. Surface heat transfer and surface temperatures can be important to the fluid flow regimes and fission product processes. Lumped parameter or finite difference models can be used to model the conductive heat transfer.

The lumped heat capacity model, for example, models systems which can be considered uniform in temperature. In general, the smaller the physical size of the body, the more realistic the assumption of a uniform temperature throughout the body and also when the outside convection heat transfer resistance is dominant over the body conduction resistance. Another example of a lumped parameter model is a model that uses an analytical solution for a steady state temperature distribution and treats the time-dependent solution as a perturbation.

A finite difference model (one or more dimensions) divides the region to be modeled into a finite mesh. Although the accuracy of the treatment is a function of both the mesh size and the temperature gradient, finite difference models can be used to treat a wide variety of boundary conditions and rapid transients. These models can also be formulated implicitly in space and time.

The level of treatment of the two models varies from low to high. The lumped-parameter model provides a low to medium level depending on the geometric detail treated. The finite difference model provides a level of treatme t that varies from low to high depending upon the dimensions represented and the calculational mesh size.

A one-dimensional finite difference model should be adequate for RCS loop components with relatively uniform geometry such as a pipe, steam generator tube or a vessel wall. A component such as a circulation pump rotor which has a considerable more complex geometry would probably do well with a lumped parameter, time-dependent model.

2.2.4.1.1.4 Secondary System

A secondary system model will be needed to establish the steam generator heat transfer rates and to determine fission product transport in the secondary system in the case of a steam generator tube rupture. Initially relatively simple models will suffice.

The steam generator heat transfer model will require the fluid condition of the secondary side to determine the heat transfer coefficient. The conditions needed are the water level, water and steam temperature, secondary system pressure, and flow velocities. If the steam generator is isolated from the remainder of secondary system, the flow velocities will be zero.

2.2.4.1.2 BWR

The BWR RCS loop component models will, in general, be, simpler than the PWR models. The fluid flows during time periods 2, 3, 5 and 6 will be predominantly single-phase gas flows with either turbulent or laminar flow regimes possible. The fluid flows during periods 2 and 4 will be similar to the corresponding PWR flows. Wall heat transfer and surface condensations models will also be similar to the corresponding PWR models. The flow paths will be primarily from the reactor vessel to the break (or relief valve) location and the piping not involved in the flow path will function as a steam volume.

2.2.4.2 System Models

2.2.4.2.1 System Flow Models

A separated two-phase flow model will be needed to model the variety of flow conditions in the RCS components. The homogeneous model, for instance, will not model the countercurrent flow situations. The separate flow model

should include the conservation of mass, momentum, and energy. The available separate flow models include the drift-flux model and the multifield model.

The drift-flux model is characterized by a single momentum conservation equation, but slip ratios are used to account for velocity differences between fluid components. In theory, a drift-flux model can be used to treat a variety of flow regimes including annular flow and countercurrent flow. In practice, however, it is difficult to calculate slip ratios for rapidly changing conditions.

The multifield model is characterized by separate mass, momentum, and energy equations for each major fluid component. The equations are coupled to one another through interface equations which describe mass, momentum, and energy exchanges between the components and the containing wall. For example, the phase change between the liquid and gas, the convection heat transfer between components and the friction drag between components. This model explicitly calculates individual component velocities and is applicable to a wide variety of flow regimes and flow conditions including annular flow, countercurrent flow, quenching and flashing. In fact, the multifield model can model more than two components at a time, for example, dispersed annular flow with its three flowing components, liquid film, gas, and dispersed droplets.

2.2.4.2.2 System Nodalization

The nodalization system divides the RCS into several volumes, each of which may contain a mixture of liquid and vapor (or single-phase liquid or vapor) and each having a temperature and pressure of its own. Each volume conserves mass, momentum, and energy. The TRAC and RELAP nodalization experience may be useful in defining the MELCOR nodalization system. In fact, the nodalization system for time period 1 should be a TRAC or RELAP system and for time period 4 should be similar.

The nodalization controlling phenomena will be different during time periods 2, 3, 5, and 6 than during periods 1 and 4 and optimum nodalization system may be different. The MELCOR nodalization system during time periods 2, 3, 5, and 6 should include sufficient nodes to model the following controlling phenomena.

1. Hot leg pipe heat transfer between fluid components and between a fluid component and the pipe surface is important because of the large fluid component temperature differential possible. Liquid-to-vapor phase change may be quite important also. More than one hot leg node may be needed.

2. The steam generator should have sufficient nodes to model both sides of a U-tube design, a steam generator tube rupture, and variations in the heat transfer rates. In the case of a variable secondary water level, a variable steam generator node may be considered.

3. The cold leg pipe node model should include a node for each of four sections of the pipe and a pump node. The cold leg pipe between the pump and a steam generator will probably need three nodes to model water blockage. Each of the three individual sections may have a different flow regimes. From the steam generator, the first vertical section may be a high-void fraction regime, the next section may then be a low-void fraction regime in horizontal flow, and the third section may be a low-void fraction regime in vertical flow.

4. Other loop considerations will need to consider major flow resistances, the break location, and ECC injection locations.

5. For transient or very small break accident sequences, a node system for the pressurizer, relief valve, relief line, and quench tank will be needed. The controlling phenomena for this node system will be fission product processes.

3.0 CONTAINMENT SYSTEMS

3.1 CONTAINMENT

INTRODUCTION, OVERVIEW,

AND

FLOW AND THERMODYNAMICS

M. J. Clauser
Advanced Reactor
Safety Analysis Division, 9424

CONTENTS

LIST OF TABLES

Acknowledgment

The author wishes to express his gratitude to K. D. Bergeron, A. L. Camp, R. K. Cole, and S. E. Dingman for their valuable comments and consultation during the course of preparing this section.

3.1.1 INTRODUCTION AND OVERVIEW

A variety of reactor containment structures, discussed in earlier sections of this document, are currently in use, and MELCOR can be expected to be used to model a wide variety of accident sequences in these containments. Rather than provide specialized versions of the code for different situations, a flexible structure and a general purpose set of models are recommended which can be selected and tailored through the code input to meet the needs of a particular task. A containment system can be divided into a number of pieces for analysis, with the number of pieces determined by the degree of detail or accuracy desired in the analysis. In general, each of these pieces is different, however, several generic building blocks or main components can be identified out of which the containment systems model can be built up: Cells, Flow paths, Structures, a Reactor Cavity, and Engineered Safety Features. Each of these components consists of a set of phenomenological models which can be tailored to suit various situations. Some of the main components can be further subdivided into several pieces.

3.1.1.1 Cells

Reactor containment systems consist of one or more physically distinct rooms, chambers, or compartments. Most codes which deal with containment phenomena allow the containment to be modeled as a set of separate computational cells, each of which has its own temperature, pressure, etc. Depending on the problem, several physical compartments can be modeled as a single computational cell if their pressures, temperature, and gas compositions are all nearly equal. However, for the purpose of modeling natural convection within large compartments, codes such as RALOC, HECTR, and CONTAIN can model a single physical compartment as a set of computational cells. When convection is the only significant mechanism for transporting gases (and suspended particles and droplets) from one cell to the next, these codes currently provide an acceptable approach. However, within a compartment there are additional transport processes that can be important; intermixing of the constituents of adjacent cells due to diffusion, turbulence, or fine-scale convection loops; particle settling into lower cells; radiation transport; etc.

As a consequence, the following approach is recommended for MELCOR I. The <u>cell</u> should be the primary computational unit of the code. Within each cell the gas is assumed to be well mixed and characterizable by a single temperature, pressure, composition, etc. Since the basic code structure may be difficult to change, and since some aspects (e.g., natural convection, aerosol settling) of a multicell compartment can be readily modeled, the structure of MELCOR should be

designed to allow several computational cells within a physical compartment; however, MELCOR I may not have all the models needed for realistic modeling of multicell compartments in all cases. For example, intercell radiation transport may not be modeled until MELCOR II. In addition to providing places for the addition of the needed models, MELCOR I should provide compartment-wide auditing of mass, energy, etc.

In addition to the cells that are modeled in containment, the outside atmosphere needs to be taken into account. This can be done, as in CONTAIN by treating the outside atmosphere as a very large cell. However, this requires more storage space and computational time than may be warranted. An alternative that may be preferable is to designate cell 0 (zero) as the outside atmosphere, with composition and temperature which are specified in the input, and which may vary with time. As with any other cell, material may flow to and from the outside atmosphere through flow paths and engineered safety systems, and heat may be transferred through the structures; however, this would not change the outside atmosphere conditions. Information on the amount of material, fission products, aerosols released to the atmosphere will be available through the mass and energy accounting described in Section 3.1.2.3.

3.1.1.2 Flow Paths

A second basic building block of the code is the flow path, which provides for the transport of gases and suspended particles and droplets from one cell to another. These can vary from the simple junction or interface between two adjacent cells in the same compartment, to more complex flow paths which may contain fans, filters, etc. It may be possible to use a single generic flow path model which can be specialized to handle various cases by setting appropriate terms to zero. However, there are several basic types of flow paths, and it may be desirable to provide separate generic models for each of them. The four main types of flow-path models are: (1) parametric flow models where the rate of flow is specified in the input; (2) pressure-driven noninertial flow models; (3) pressure-driven inertial flow models; and (4) special-purpose flow models such as BWR suppression pools and ice condensers.

The flow paths can also be divided for purposes of discussion into two categories, incompartment and excompartment. The incompartment flow paths connect two cells within the same compartment and are simple interfaces between the cells. The first three types of models can be used for these flow paths. The excompartment flow paths pass outside of the compartment and may have a finite extent themselves (for example, a pipe between two compartments). A fan cooler removes

air from a compartment, and can return it to the same compartment. Since it is not a simple interface, has a finite extent, and to some extent lies outside the compartment, it would be classified as an excompartment flow path. All four types of flow models may be used for the excompartment flow paths. The excompartment flow models could include the effects of fans, or filters, and possibly heat transfer.

Most codes allow only one flow path between each pair of cells. This restriction results from the indexing scheme used for storing the flow-path characteristics. By a simple change in the indexing scheme, this restriction can be removed. With this change, an arbitrary number of flow paths can interconnect any two cells, and a flow path such as a fan cooler can have both ends connected to the same cell. This flexibility is recommended for MELCOR and is assumed in Section 3.1.2.

3.1.1.3 Structures

The third basic building block is the structure model, which deals with heat (and mass) transfer within the structures (walls, etc.) in containment, and with heat and mass transfer to and from the gas in a cell. It can also be used for heat transfer from one cell to another. The principal mechanisms for heat transfer from gas to the structures include convection, conduction, and radiation. The structure model includes steam condensation and evaporation at the structure's surface. Aerosols (particles and droplets) can be deposited on the structure surface (by the aerosol model), and, once deposited, can provide an insulating layer and/or a source of heat (if they contain fission products). The aerosols can be removed when condensed steam runs or drips off the structure surface. In addition, if the structure is concrete, the water inside it can migrate to the surface and be released when the concrete is heated.

3.1.1.4 Reactor Cavity

A fourth building block is the reactor cavity model which deals with core debris release from the reactor vessel, steam explosions, debris bed behavior, core-concrete interactions, and related phenomena. The reactor cavity model is intended to be used principally in the reactor cavity cell.

3.1.1.5 ESFs

The Engineered Safety Features (ESFs) are a set of building blocks consisting of containment sprays, fan coolers, ice condensers, cell sumps, suppression pools, filtered vents, etc. and the interconnecting fluid transfer system. In addition to dealing with the fluid transfer between parts of ESFs, the fluid transfer system should also handle run-off

from walls, overflowing of sumps, etc. A given ESF can be connected with more than one cell. For example, the spray ESF can remove water from the sump in one cell and spray it into another. Some of the ESFs such as the suppression pool may also be classified as special-purpose flow paths since they provide paths for the flow of gases between cells. The ice condenser may be modeled as one or more cells, and the ice condenser doors as special-purpose flow paths.

3.1.2 FLOW AND THERMODYNAMICS

This section discusses the equations governing the thermodynamics of the cell atmosphere. These equations are very similar, except as noted, to the equations used in the CONTAIN and HECTR codes (and are generally similar to equations used in RELAP, CONTEMPT, and other control volume codes). The equations used in both codes are nearly equivalent, except that HECTR does not treat aerosol behavior nor does it allow for a two-phase mixture of liquid and vapor in the atmosphere. Most codes use the pressure drop between cells to calculate the rate of flow from one cell to another. The correlations relating flow to pressure drop are generally similar, although some codes (e.g., CONTEMPT) include some optional correlations for special purposes. MACE, in MARCH, however, simply moves material between cells so that the pressures equilibriate each time step. CONTAIN and HECTR use somewhat different methods for numerically integrating the differential equations; these are discussed at the end of this section. The principal symbols used in this section are listed in Table 2.1; other symbols will be defined where they are used. Throughout, MKS units are used, and the unit of temperature is degrees Kelvin.

Table 3.1.2-1

Definitions of Principal Variables

Symbol	Units	Definition
A	m^2	Area
A_j	m^2	Cross-sectional area of flow path j
C_{Pk}	J/kg K	Specific heat at constant pressure of material k
C_{Vk}	J/kg K	Specific heat at constant volume of material k
C_{VAki}	J/kg K	Specific heat at constant volume of material k in the atmosphere of cell i
E_{CAki}	J	Integrated generation of heat by chemical reactions in the atmosphere of cell i
E_{DAi}	J	Integrated generation of heat from fission product decay in the atmosphere of cell i

Table 3.1.2-1 (Continued)

Symbol	Units	Definition
E_{EAi}	J	Integrated transfer of energy from ESF j to the atmosphere of cell i
E_{AFij}	J	Integrated transfer of energy from the atmosphere of cell i into flow path j
E_{IAij}	J	Integrated energy from the jth Input-specified source in the atmosphere of cell i
E_{RAi}	J	Integrated transfer of heat from the Reactor cavity to the atmosphere of cell i
E_{SAmj}	J	Integrated transfer of heat from surface j of structure m to the atmosphere
E_{VAi}	J	Integrated transfer of heat from the RCS (V for Vessel) to the atmosphere of cell i
G_k	kg/kmole	Molecular weight of material k
h	J/m^2 s K	Heat transfer coefficient
H_k	J/kg	Specific enthalpy of material k
H_{AFkij}	J/kg	Enthalpy of material k entering or leaving the atmosphere of cell i through flow path j
H_{EAkij}	J/kg	Enthalpy of material k entering or leaving the atmosphere of cell i through engineered safety feature j
H_{RAki}	J/kg	Enthalpy of material k entering or leaving the atmosphere of cell i from the Reactor cavity
H_{SAkmj}	J/kg	Enthalpy of material k entering or leaving the atmosphere from surface j of Structure m

Table 3.1.2-1 (Continued)

Symbol	Units	Definition
H_{VAki}	J/kg	Enthalpy of material k entering the atmosphere of cell i from the RCS (Vessel)
H_{IAkij}		Enthalpy of material k entering the atmosphere of cell i from Input-specified source
k	J/m s K	Thermal conductivity
L_j	m	Effective length of flow path j
m_{Ai}	kg	Total mass in atmosphere of cell i
m_{Aki}	kg	Mass of material k in atmosphere of cell i
m_{CAki}	kg	Integrated creation of mass of material k by chemical reactions in the atmosphere of cell i
m_{EAkij}	kg	Integrated transfer of mass of material k by from ESF j to the atmosphere of cell i
m_{AFkij}	kg	Integrated mass of material k that has left the atmosphere of cell i through flow path j
m_{IAkij}	kg	Integrated mass of material k from the jth Input-specified source in the atmosphere of cell i
m_{RAki}	kg	Integrated transfer of mass of material k from the Reactor cavity to the atmosphere of cell i
m_{SAkmj}	kg	Integrated transfer of mass of material k from surface j of Structure m to the atmosphere

Table 3.1.2-1 (Continued)

Symbol	Units	Definition
m_{VAki}	kg	Integrated transfer of mass of material k from the RCS (V for Vessel) to the atmosphere of cell i
N_{Aki}	kmole	Kilogram moles of material k in the atmosphere of cell i
P	N/m^2	Pressure
P_{Ai}	N/m^2	Total pressure in the atmosphere of cell i
P_{Aki}	N/m^2	Partial pressure of material k in the atmosphere of cell i
P_{bjmn}	N/m^2	Buoyancy pressure difference between cells m and n through flow path j
P_{fj}	N/m^2	Pressure difference caused by a fan in flow path j
P_{rj}	N/m^2	Pressure difference (or loss) caused by flow resistance in flow path j
Q	J/s	Energy source
Q_{CAi}	J/s	Rate of generation of heat by chemical reactions in the atmosphere of cell i
Q_{EAij}	J/s	Rate of transfer of heat from ESF j to the atmosphere of cell i
Q_{DAi}	J/s	Rate of heat generation from radioisotope decay in the atmosphere of cell i
Q_{IAij}	J/s	Energy source rate from the jth Input-specified source in the atmosphere of cell i
Q_{RAi}	J/s	Rate of transfer of heat from the Reactor cavity to the atmosphere of cell i

Table 3.1.2-1 (Continued)

Symbol	Units	Definition
Q_{SAmj}	J/s	Rate of transfer of heat from surface j of Structure m to the atmosphere
Q_{VAi}	J/s	Rate of transfer of heat from the RCS (V for Vessel) to the atmosphere of cell i
q	J/m^3 s	Energy density source
ρ_k	kg/m^3	Density or mass concentration of material k
ρ_{Aki}	kg/m^3	Mass concentration of material k in the atmosphere of cell i ($=m_{Aki}/V_{Ai}$)
s	kg/m^3 s	Mass density source
S_k	kg/s	Mass source of material k
S_{CAki}	kg/s	Rate of creation of mass of material k by chemical reactions in the atmosphere of cell i
S_{EAkij}	kg/s	Rate of transfer of mass of material k from ESF j to the atmosphere of cell i
S_{IAkij}	kg/s	Mass source rate of material k from the jth Input-specified source in the atmosphere of cell i
S_{RAki}	kg/s	Rate of transfer of mass of material k from the Reactor cavity to the atmosphere of cell i
S_{SAKmj}	kg/s	Rate of transfer of mass of material k from surface j of Structure m to the atmosphere
S_{VAki}	kg/s	Rate of transfer of mass of material k from the RCS (V for Vessel) to the atmosphere of cell i

Table 3.1.2-1 (Continued)

Symbol	Units	Definition
t	s	Time
T	K	Temperature
U_k	J/kg	Specific internal energy of material k
U_{AKi}	J/kg	Specific internal energy of material k in the atmosphere of cell i
$U_{\rho k}$	J/m^3	$= [\partial U_k(\rho_k,T)/\partial \rho_k]T$
$U_{\rho AKi}$	J/m^3	$U_{\rho k}$ in the atmosphere of cell i
v	m/s	velocity
	m^3/kg	specific volume
V	m^3	Volume
V_{Ai}	m^3	Volume of the atmosphere of cell i
W_{ij}	kg/s	Total mass flow rate from cell i into flow path j
W_{kij}	kg/s	Mass flow rate of material k from cell i into flow path j

Note that lower case subscripts i, j, k, l, m, and n are used as indices, while upper case letters qualify the symbol. The notation $\sum_i$ implies summation over all relevant values of i, and $\sum_{i \neq j}$ implies summation over all relevant values of i except i=j.

In the notation used here, fairly liberal use has been made of subscript indices. For the purpose of the discussion here some of these variables may be thought of as sparse matrices. For example, W_{ij} is zero if flow path j does not connect with cell i. In MELCOR, it is recommended that each flow path in containment be assigned a unique label of index value. For each flow path two pointers should be provided to identify the cells to which the flow path is connected.

The flow rates in and out of each end should be calculated, since some types of flow paths, such as suppression pools or filters, will not necessarily conserve mass.

3.1.2.1 Cell-Atmosphere Conservation Equations

The atmosphere in each cell consists of a mixture of gases and aerosols. As used here, the term aerosol refers collectively to small solid particles and droplets of water (smaller than a few tenths of a millimeter). Some of the constituents of the atmosphere, notably the radioisotopes and some of the constituents of the aerosols, may be present only in trace quantities. The amount and location of these trace materials need to be calculated, but their heat capacity and pressure can be neglected. Therefore, a distinction will occasionally be made between "main" materials and "trace" materials. The pressure and temperature in the atmosphere are determined by the thermodynamics of the main materials (excluding the trace materials); the trace materials affect the energy balance only through radioactive decay. The treatment here differs from the current treatment in CONTAIN in that here some of the aerosol constituents, notably the water, are included in the atmosphere mass and energy conservation equations. In CONTAIN, when the aerosol model is used, liquid water is removed from the atmosphere mass and energy inventory after it condenses on the aerosols. (In CONTAIN the aerosol mass is neglected in the atmosphere mass inventory; this is generally valid.) Here this water would remain in the atmosphere inventory, and be removed when the aerosols settle out or are deposited on surfaces. The same would be true of any other nontrace materials such as concrete or core-debris particles. The liquid water in the containment sprays should be treated separately from the other constituents of the atmosphere, since the droplets are generally not in thermal equilibrium with the atmosphere.

The main equations governing the atmosphere dynamics are the mass and energy conservation equations for each cell, and the momentum conservation equations for the flow between cells.

3.1.2.1.1 Mass Conservation

The mass conservation equation for each material in the atmosphere is

$$\frac{d\, m_{Aki}}{dt} = -\sum_j W_{kij} + \sum_j S_{EAkij} + S_{RAki} + S_{CAki} + \sum_{m,j} S_{SAkmj}\delta_{imj} + S_{VAki} + \sum_j S_{IAkij} \qquad (3.1.2.1\text{-}1)$$

where m_{Aki} is the mass of material k in the atmosphere of cell i. This form of the mass conservation applies to the main materials of the cell atmosphere; the conservation equations for radioisotopes and the trace aerosol components are similar in form, but have some additional terms. The first term on the right hand side of Equation (3.1.2.1-1) is the sum of the mass flow rates W_{kij} of material k from cell i into flow path j. The summation is only over those flow paths that are connected to cell i. The calculation of W_{kij} is discussed in Section 3.1.2.6. The second term is the sum of the rates of mass transfer S_{EAkij} of material k from engineered safety system j to the atmosphere of cell i. The engineered safety systems are discussed in Section 3.6. The third term S_{RAki} is the rate of mass transfer from the reactor cavity model (if any) in the cell to the cell atmosphere. An example is the generation of gases and aerosols from the debris-concrete interaction. The calculation of S_{RAki} is discussed in Section 3.5. The fourth term S_{CAki} is the rate of creation of material k in the atmosphere of cell i due to chemical reactions, such as hydrogen burning. Contributions to this term are discussed in Sections 3.1.2.3 and 3.4. The fifth term is the sum of the rates of mass transfer S_{SAkmj} of material k from surface j of structure m to the atmosphere of the cell in which it is located. One of the main contributions to S_{SAkmj} is steam condensation, in which case S_{SA} is negative. The notation δ_{imj} is not a rigorous use of the δ function, but it takes on the value 1 when the jth surface of the mth structure is in the atmosphere of cell i, and 0 otherwise. The next term S_{VAki} is the rate of transfer of material k from the RCS (V stands for Vessel) to the atmosphere of cell i. The last term is the sum of the rates of input S_{IAkij} of material k to the atmosphere of cell i from the jth user-specified source.

The mass of each material has been chosen as the set of principle variables characterizing the composition of the cell atmosphere because this choice results in the simplest set of conservation equation, which are least susceptible to spurious numerical effects. An alternate choice could be the moles of each material. However, this choice does not significantly simplify the chemical reaction equations and it does somewhat complicate the flow equations. Moreover, thermodynamic data and heat and mass transfer correlations are more usually formulated in terms of mass than moles. With the mass of each material in the cell atmosphere determined by Equation (3.1.2.1-1), auxiliary quantities can be calculated: the number of moles of material k,

$$N_{Aki} = m_{Aki}/G_k \qquad (3.1.2.1\text{-}2)$$

where G_k is the molecular weight of material k, the mass concentration of material k,

$$\rho_{Aki} = m_{Aki}/V_{Ai} \qquad (3.1.2.1\text{-}3)$$

where V_{Ai} is the volume of the atmosphere of cell i; and the total mass in the atmosphere of cell i

$$m_{Ai} = \sum_k m_{Aki} \qquad (3.1.2.1\text{-}4)$$

In Equation (3.1.2.1-3) ρ_{Aki} is termed the mass concentration of material k in the atmosphere rather than the density. The volume occupied by the gases is assumed to equal the cell volume; the volume occupied by suspended solids and liquids is negligible in all cases of interest. Thus, ρ_{Aki} for a gas is also equal to the gas density. For solids and liquids the density will be the solid or liquid density, which is far different from ρ_{Aki}.

3.1.2.1.2 Energy Conservation

All of the materials of the cell atmosphere are assumed to have essentially the same temperature. This temperature is determined by the energy conservation equation, which accounts for all the sources of energy which may change the temperature of the atmosphere. The general form of this equation is

$$\frac{d}{dt} \sum_k m_{Aki} U_{Aki} = \sum_{j,k} S_{jAki} H_{jAki} + \sum_m Q_{mAi} - P_{Ai} \frac{dV_{Ai}}{dt} \qquad (3.1.2.1\text{-}5)$$

where the left-hand side is the derivative of the total internal energy in the atmosphere and $U_{Aki} = U_K(\rho_{Aki}, T_{Ai})$ is the specific internal energy of material k at density ρ_{Aki} and at the temperature of the cell atmosphere T_{Ai}. The last term in Equation (3.1.2.1-5) is the work done during a change in volume of the cell such as might occur if the containment building expands due to overpressure. Intuitively, this term would seem to be generally negligible; however, informal comments have indicated that there may be situations where the expansion is significant. If so, a relation would be needed for the volume as a function of pressure, temperature, etc. The pressure P_{Ai} is the total pressure in the atmosphere of cell i, and is equal to the sum of the individual thermodynamic pressures. The first term on the

right-hand side of the equation is the sum over all external sources (positive and negative) of material, including flow paths, in the atmosphere.

$$\sum_{j,k} S_{jAki} H_{jAhi} = - \sum_{j,k} W_{kij} H_{AFkij} + \sum_{j,k} S_{EAkij} H_{EAkij} + \sum_{k} S_{RAki} H_{RAki} + \sum_{m,j,k} S_{SAkmj} H_{SAkmj} \delta_{imj} + \sum_{j,k} S_{VAki} H_{VAki} + \sum_{j,k} S_{IAkij} H_{IAkij} \quad . \tag{3.1.2.1-6}$$

Note that these source terms do not include S_{CAki}, the rate of change of mass due to chemical interactions, as this is not an external source. The enthalpy H_{jAki} is the enthalpy of the material entering or leaving the cell atmosphere. If this material is leaving, it will generally have the same composition and enthalpy as the cell atmosphere ($H_{jAki} = H_k(\rho_{Aki}, T_{Ai})$); if it is entering, it generally will not. For flow paths, this is discussed further in Section 3.1.2.5. The second term in Equation (3.1.2.1-5) is the sum over all energy sources in the atmosphere,

$$\sum_{m} Q_{mAi} = \sum_{m,j} Q_{SAmj} \delta_{imj} + \sum_{j} Q_{EAij} + Q_{RAi} + Q_{Vai} + Q_{DAi} + \sum_{j} Q_{IAij} \quad . \tag{3.1.2.1-7}$$

The first term on the right-hand side of Equation (3.1.2.1-7) is the sum of the heat transfer rates Q_{SAmj} from all the structures in the atmosphere of cell i. The δ-function notation is the same as in Equation (3.1.2.1-1). The next terms Q_{EAij}, Q_{RAi}, and Q_{VAi} are the heat transfer rates from ESF j, from the reactor cavity, and from the RCS (vessel), respectively. The next term Q_{DAi} is the rate of heat generation by radioactive decay. The last term is the sum of all the user-specified sources of energy in the atmosphere of cell i.

The form of Equation (3.1.2.1-5) is generally suitable if all the terms on the right-hand side are integrated explicitly. For implicit treatment of the temperature (or pressure) dependence in any of the terms, a different form is more suitable. By making use of the relation

$$\frac{d}{dt} m_k U_k = (U_k + \rho_k U_{\rho k}) \frac{dm_k}{dt} + m_k C_{Vk} \frac{dT}{dt} - \rho_k^2 U_{\rho k} \frac{dV}{dt} \qquad (3.1.2.1\text{-}8)$$

to expand the left-hand side of Equation (3.1.2.1-5) and rearranging terms, the energy equation becomes a temperature equation:

$$\sum_k m_{Aki} C_{VAki} \frac{dT_{Ai}}{dt} = \sum_{j,k} S_{jAki} (H_{jAki} - U_{Aki} - \rho_{Aki} U_{\rho Aki})$$

$$- \sum_k S_{CAki} (U_{Aki} + P_{Aki} U_{\rho Aki}) + \sum_m Q_{mAi}$$

$$- \sum_k (P_{Aki} + U_{\rho Aki}) \frac{dV_{Ai}}{dt} \quad . \qquad (3.1.2.1\text{-}9)$$

In these equations, U_ρ denotes the partial derivative at constant temperature

$$U_{\rho Aki} = \left[\partial U_K(\rho_{Aki}, T_{Ai}) / \partial \rho_{Aki} \right] T_{Ai} \quad . \qquad (3.1.2.1\text{-}10)$$

and C_V denotes the specific heat at constant volume (or constant concentration)

$$C_{VAki} = \left[\partial U_k(\rho_{Aki}, T_{Ai}) / \partial T_{Ai} \right] \rho_{Aki} \quad . \qquad (3.1.2.1\text{-}11)$$

For an ideal gas, U is independent of density and varies linearly with temperature; thus $U_\rho = 0$ and C_V is constant. Neither of these conditions is generally true, and is decidedly not true for a condensing vapor. Note that the sum in all the energy equations is taken over all the main (not the trace) materials.

3.1.2.2 Two-Phase Thermodynamics

In many reactor accidents, large amounts of steam will be released into the containment atmosphere from the reactor coolant system, from the reactor cavity, and from heated

concrete walls. In general the steam will be a two-phase mixture of water vapor (gas) and liquid. In most situations of interest, there will be enough particulate matter present in the atmosphere to provide nucleation sites for condensation of the steam as it cools down. Thus, to a good approximation, the steam can be assumed to be in local thermodynamic equilibrium; that is, it will not be supersaturated.

As written, the mass and energy equations will treat water as a single material. That is, the mass and energy of water that appear in Equations (3.1.2.1-1) and (3.1.2.1-5) are the totals for both the liquid and vapor present in the atmosphere. An alternative, which was tried and discarded early in the development of CONTAIN's cell atmosphere model, is to treat the liquid and vapor as separate materials. An additional source term is then needed in Equation (3.1.2.1-1) to account for evaporation and condensation.

Since the liquid and vapor are in intimate contact with each other, and since they are assumed (to first order) to flow at the same velocity through the flow paths, the single-material treatment is most appropriate. However, once the temperature and total mass of water in the cell atmosphere is determined by the solution of the mass, flow, and energy equations, the masses and pressure of liquid and vapor, individually, can be calculated from the equation of state for water. In addition to determining the cell pressure, this information is needed by the aerosol model to calculate the details of the condensation and evaporation of water on the aerosol particles or droplets. This information is also needed by the flow path model for calculation of flow characteristics.

With the single material treatment of water, the source term S_{SAkmj} in Equation (3.1.2.1-1) consists of two separate contributions: one for the condensation (or evaporation) of water on the surface of the structure, and a second for the settling or deposition of liquid water droplets on the surface. This distinction is particularly important in the energy equation, since the specific enthalpies of the two contributions are quite different. Thus, the $S_{SAkmj}H_{SAkmj}$ term for water in Equation (3.1.2.1-6) should be written as the sum of two similar terms, the first of which has the enthalpy of water vapor, and the second, of liquid water. The same will be true for the energy transfer rates from the reactor cavity and from some of the engineered safety systems such as the cell sump.

3.1.2.3 Chemical Reactions

The principal chemical reactions in the cell atmosphere are the burning of H_2 and CO. In addition, oxidation of particles from the reactor cavity may also occur. In any

case the rates of these reactions are discussed elsewhere. In this section, the general treatment of chemical thermodynamics and the connection with the conservation equations is discussed.

For the purposes of this section a general chemical reaction of the form

$$a_1R_1 + a_2R_2 + \ldots + a_nR_n \longrightarrow b_1P_1 + \ldots + b_mP_m$$

will be assumed, where $R_1 \ldots R_n$ are the reactants, $P_1 \ldots P_n$ are the products, and $a_1 \ldots a_n$, $b_1 \ldots b_n$ are the amounts of each. For example, if the reaction were

$$2H_2 + O_2 \longrightarrow 2H_2O$$

then $a_1 = 2$, $a_2 = 1$, $b_1 = 2$, $R_1 = H_2$, $R_2 = O_2$, and $P_1 = H_2O$. The rate of reaction R (kmoles/s) is defined such that a_jR kmoles/s of R_j are consumed, and b_kR kmoles/s of P_k are produced. Thus the mass source term in Equation (3.1.2.1-1) is

$$S_{CAj} = - a_jRG_j \text{ for reactants} \qquad (3.1.2.2\text{-}1)$$

$$S_{CAk} = + b_kRG_k \text{ for products} \; . \qquad (3.1.2.2\text{-}2)$$

The energy conservation equation, either in the form of Equation (3.1.2.1-5) or Equation (3.1.2.1-9) includes the effects of chemical reactions that take place within the cell atmosphere provided that the specific internal energies of the materials are properly calculated.

If the specific energies include the chemical heats of formation, then the energy released in a chemical reaction is equal to the difference in the internal energies or enthalpies of the reactants and the products. When the reaction takes place at constant volume and temperature, the rate of heat generation is

$$- \sum_m S_{CAm}U_m = \sum_j a_jRG_jU_j - \sum_k b_kRG_kU_k \qquad (3.1.2.2\text{-}3)$$

where the first sum over m includes all reactants and products, the sum over j includes all reactants, and the sum over k includes all products. If the internal energies include the chemical heats of formation, then a chemical

energy source term should not be included in Equation (3.1.2.1-6); however, it may be needed in the radiation heat transfer calculation. In the event that the internal energies do not include the heat of formation, a constant term will need to be added to each internal energy in Equation (3.1.2.3-3) and to the corresponding terms in Equations (3.1.2.1-5) and (3.1.2.1-9).

Equations (3.1.2.1-5) and (3.1.2.1-9) assume that the reactants start at, and the products end up at, the temperature of the atmosphere. A case such as the injection of hydrogen at a different temperature through a flow path, burning as it enters, should be treated as a two-step process. First, the mass and energy flow terms in Equations (3.1.2.1-1) and (3.1.2.1-7) should be treated the same as if there were no burning. Then, the hydrogen burning should be treated the same as if the burn took place entirely in the atmosphere, but with the burning rate determined by the rate of entry of hydrogen.

3.1.2.4 Cell Mass and Energy Check

In order to provide information on where the mass and energy in the cell are going and to provide for energy and mass checks, the following sources need to be integrated separately from the conservation equations:

The flow of mass and energy from cell i into flow path j,

$$m_{AFkij} = \int W_{kij}\,dt \qquad (3.1.2.4\text{-}1)$$

$$E_{AFij} = \sum_k \int W_{kij} H_{AFkij} \quad . \qquad (3.1.2.4\text{-}2)$$

The mass and energy transfer from the jth surface of structure m to the atmosphere of the cell in which it resides,

$$m_{SAkmj} = \int S_{SAkmj}\,dt \qquad (3.1.2.4\text{-}3)$$

$$E_{SAmj} = \sum_k \int S_{SAkmj} H_{SAkmj}\,dt + \int Q_{SAmj}\,dt \quad . \qquad (3.1.2.4\text{-}4)$$

The mass and energy transfer into the atmosphere from engineered safety system j,

$$m_{EAkij} = \int S_{EAkij}\,dt \qquad (3.1.2.4\text{-}5)$$

$$E_{EAij} = \sum_k \int S_{EAki} H_{EAkij}\,dt + \int Q_{EAij}\,dt \quad . \qquad (3.1.2.4\text{-}6)$$

The mass and energy transfer into the atmosphere from the RCS,

$$m_{VAki} = \int S_{VAki}\,dt \qquad (3.1.2.4\text{-}7)$$

$$E_{VAi} = \sum_k \int S_{VAki} H_{VAki}\,dt + \int Q_{VAki}\,dt \quad . \qquad (3.1.2.4\text{-}8)$$

The mass and energy transfer into the atmosphere from the reactor cavity,

$$m_{RAki} = \int S_{RAki}\,dt \qquad (3.1.2.4\text{-}9)$$

$$E_{RAi} = \sum_k \int S_{RAki} H_{VRki}\,dt + \int Q_{RAi}\,dt \quad . \qquad (3.1.2.4\text{-}10)$$

The change in mass and energy of materials in the atmosphere from chemical reactions,

$$m_{CAki} = \int S_{CAki}\,dt \qquad (3.1.2.4\text{-}11)$$

$$E_{CAi} = \sum_k \int S_{CAki} U_{Aki}\,dt \quad . \qquad (3.1.2.4\text{-}12)$$

Note that the last equation is not needed for the purpose of energy balances if the internal energies include the chemical energies of formation. Nevertheless, the chemical energy generation E_{CAi} is useful for output purposes.

The energy released into the atmosphere from radioactive decays,

$$E_{DAi} = \int Q_{DAi}\,dt \quad . \qquad (3.1.2.4\text{-}13)$$

The mass and energy transfer into the atmosphere from input-specified source j,

$$m_{IAKij} = \int S_{IAkij} dt \qquad (3.1.2.4\text{-}14)$$

$$E_{IAij} = \sum_k \int S_{IAkij} H_{IAkij} dt + \int Q_{IAij} dt \quad . \qquad (3.1.2.4\text{-}15)$$

The work done on an expanding containment volume,

$$E_{AWi} = \int P_{Ai} \frac{dV_{Ai}}{dt} dt \quad . \qquad (3.1.2.4\text{-}16)$$

These integrals can then be used to perform a mass and energy check at appropriate intervals during the calculation. The mass of each component U_{Aki} and total energy in the cell atmosphere should equal the initial mass and energy plus the sum of the sources; that is, the following equalities should be satisfied:

$$m_{Aki} = m_{Aki}(t=0) - \sum_j m_{AFkij} + \sum_j m_{SAkmj} + \sum_j m_{EAkij} + m_{VAki} + m_{RAki} + m_{CAki} + \sum_j m_{IAkij} \quad . \qquad (3.1.2.4\text{-}17)$$

$$\sum_k m_{Aki} U_{Aki} = \sum_k m_{Aki}(t=0)\, U_{Aki}(t=0) - \sum_j E_{AFij} + \sum_j E_{SAmj} - \sum_j E_{Eaij} + E_{VAi} + E_{RAi} + E_{CAi} + E_{DAi} + \sum_j E_{IAij} - E_{AWi} \quad . \qquad (3.1.2.4\text{-}18)$$

Similar mass and energy accounting should be performed for the reactor cavity, engineered safety systems, structures, and flow paths.

3.1.2.5 Flow Path Models (General)

The flow paths provide the means by which gases, aerosols, and fission products move from one cell to another.

These flow paths can range from simple interfaces between adjacent cells in the same compartment, to complex pathways such as filtered vents, suppression pools, and, perhaps ice-condenser compartments. Whereas, cells are characterized by the amount of material and energy they contain, flow paths are characterized by the rate of flow of material and energy through them. The essential characteristic, or approximation, of the flow path models is that the transit time of material through them is ignored. That is, except for losses in flow paths, equal amounts of material are assumed to enter and leave the flow path during a time step. (This does not mean, of course, that the velocity is assumed to be infinite.) Since no material "resides" in a flow path, there are no mass and energy conservation equations such as Equations (3.1.2.1-1) and (3.1.2.1-5) to be integrated for flow paths. The principle equation governing the flow path behavior is the flow equation that determines the velocity of the flow. By providing a flexible design for the flow paths, a single flow path can be used to model a complex part of containment when the transit time can be ignored. When the transit time, or resident time is significant, a series of cells and flow paths can be used.

Most codes such as HECTR and CONTAIN provide relatively simple flow path models wherein all of the mass and energy that goes in one end comes out the other. The rate of flow through these flow paths is determined by the pressure difference (including buoyant forces) between cells, the flow resistance in the flow path, and, optionally, the inertia of the material flowing through the path. A relatively simple addition to this type of flow path is a mechanism for removing aerosols such as filtration, or particle deposition on the walls. In this case less aerosol mass would leave the flow path than enters it, and the flow resistance may increase with the amount of particle deposition. Beyond this, provision can be made for heat transfer and steam condensation within the flow path to permit coolers, suppression pools, etc. to be modeled. As a consequence, the energy leaving the flow path may differ from that entering the flow path.

The rate of flow within a flow path is determined by several factors that are discussed in the following sections. For purposes of discussion, four categories of flow paths can be distinguished. In order of increasing complexity of the governing equations, they are:

1. Parametric flow, wherein the rate of flow is specified by the user in the input.

2. Pressure-driven noninertial flow, wherein the flow rate is directly related to the pressure difference between the cells, and the inertia of the material in the flow path is ignored.

3. Pressure-driven inertial flow, wherein the flow rate is determined by the pressure difference, however, the response of the flow rate to a change in pressure is delayed by the inertia of the material in the flow path.

4. Special purpose flow, wherein the flow rate is determined by a more complex model, such as BWR suppression pool.

For all of these categories the solution of the flow equations determines the total rate of flow of material from upstream cell m into flow path j. By definition this is the sum of the component flows:

$$W_{mj} = \sum_{k} W_{kmj} \quad . \qquad (3.1.2.5\text{-}1)$$

The flow rates of individual materials from the upstream cell are assumed to be proportional to their concentration in the cell atmosphere, and the enthalpies are equal to the enthalpies in the upstream cell atmosphere:

$$\frac{W_{kmj}}{W_{mj}} = \frac{m_{Akm}}{m_{Am}} \qquad (3.1.2.5\text{-}2)$$

$$H_{AFkmj} = H_{k}(\rho_{Akm}, T_{Am}) \quad . \qquad (3.1.2.5\text{-}3)$$

For gases this assumption is generally true; for aerosols, including water droplets, this assumption implies that there is no slip between the gases and the aerosols. For many flow paths there will be no loss of mass or energy in the flow path so that

$$W_{knj} = - W_{kmj} \qquad (3.1.2.5\text{-}4)$$

$$H_{AFknj} = H_{AFkmj} \qquad (3.1.2.5\text{-}5)$$

where n denotes the downstream cell. In flow paths with filters or other means of removing materials, the flow rate

of some materials leaving the flow path will be a fraction of the rate of entry.

$$W_{knj} = - f_{kj} W_{kmj} \qquad (3.1.2.5\text{-}6)$$

where the loss factor f_{kj} may depend on the material type, particle size, etc. If energy transfer takes place in the flow path, then the outgoing enthalpies may not equal the incoming enthalpies. Instead, the outgoing enthalpies will be given by

$$-\sum_k W_{knj} H_{AFknj} = \sum_k W_{kmj} H_{AFkmj} + Q_j \qquad (3.1.2.5\text{-}7)$$

where Q_j is the rate at which energy is added within the flow path by heat transfer, fans, etc. The individual enthalpies H_{AFknj} can be determined, with some effort; however, this is unnecessary, since only the sum is needed.

In the next sections the general form of the flow equations for the first three categories of flow are discussed, followed by discussions of the flow resistance, natural convection, mixing, and inertia terms in these equations. Discussions of special purpose flow paths, as well as discussions of the effects of fans, filters, etc. on the first three categories of flow paths are in the ESF section.

3.1.2.6 Flow Equations

In the following discussion the index j denotes the flow path, m denotes the upstream cell, and n denotes the downstream cell. In most cases the flow can be in either direction, and is determined by the relative pressures in the two cells. Thus the roles of upstream and downstream cells may reverse from time to time.

Parametric Flow. The simplest means of determining the flow rates is to specify them in the input to the code, generally as a function of time. Two ways of specifying the flow rate will prove generally useful: mass flow rates, and volume flow rates. In the first case the total mass flow rate from the upstream cell W_{mj} is specified directly in the input. In the second case the volume V of material to be taken from the upstream cell per second can be specified directly, or the fraction f of the upstream cell volume per second can be specified. The mass flow rates would then be

$$W_{kmj} = \dot{V}\rho_{Akm} = \frac{\dot{V}}{V_{Am}} m_{Akm} \qquad (3.1.2.6\text{-}1)$$

or

$$W_{kmj} = fV_{Am}\rho_{Akm} = fm_{Akm} \quad . \qquad (3.1.2.6\text{-}2)$$

These parametric flow rates could be used (a) to provide a simple fan model, (b) to allow the user to simulate a flow process not modeled in the code, or (c) to provide a non-mechanistic leak rate such as are used in some aerosol codes, which have no other means of determining leak rates.

Pressure-Dependent Noninertial Flow. For many flow paths the inertia of the flowing material can be ignored (see below, Section 3.1.2.9). In this case the flow rate is determined by the instantaneous value of the pressure drop, and not by the past history. The flow rate can then be determined by the solution of a relatively simple algebraic expression, not by integrating a differential equation. A general form of the equation for the flow rate is

$$P_r(W) - P_f(W) = P_{Am} - P_{An} + P_b \qquad (3.1.2.6\text{-}3)$$

where P_r is the flow-rate dependent pressure drop due to flow resistance (see Section 3.1.2.7), P_f is the pressure differential, perhaps flow-rate dependent, caused by the operation of a fan (see Section 3.6), and P_b is the buoyancy term that gives rise to natural circulation (see Section 3.1.2.8). This equation can be solved implicitly for the flow rate W in the flow path.

Pressure-Dependent Inertial Flow. When relatively long flow paths are present, the inertia of the flowing material may cause significant delays in responding to pressure changes. In this case it may be necessary to integrate a momentum conservation equation for the flow rate. A general form for this equation is

$$\frac{L_j}{A_j}\frac{dW_{mj}}{dt} = P_{Am} - P_{An} + P_{bjmn} + P_f(W_{mj}) - P_r(W_{mj}) \qquad (3.1.2.6\text{-}4)$$

where L_j is the effective length of the flow path, and A_j is its effective cross-sectional area. This equation differs from Equation (3.1.2.6-3) only by the addition of the inertia term on the left-hand side. With properly formulated difference equations, the noninertial flow case can be handled as a special case of the inertial flow simply by setting $L_j = 0$. The inertia term can take several slightly different forms, as will be discussed in Section 3.1.2.9.

3.1.2.7 Flow Resistance

Perhaps the most important characteristic of the flow in a flow path is the Reynold's number of the flow,

$$R_e = \frac{\rho v d}{\mu} \qquad (3.1.2.7\text{-}1)$$

where v is the gas velocity, d is a typical cross-sectional dimension such as the diameter of a pipe, and μ is the dynamic viscosity of the gas. For Reynold's numbers less than about 1500 the flow is generally laminar, while for Reynold's numbers greater than about 4000 the flow is turbulent. For the flow of air at 10 cm/s through a 60 cm-pipe (slow flow through a modest size pipe), the Reynold's number is 4000. Thus, most of the flow of interest in containment will be turbulent. The principle exception will be the leakage through the many small cracks that may exist in the containment building itself.

Laminar Leaks. The pressure drop P along a pipe of length L and diameter d is given by Poiseuille's formula,

$$P = \frac{128 \mu L}{\pi d^4 \rho W} \qquad (3.1.2.7\text{-}2)$$

when the flow is laminar. Generally the characteristics of the individual leaks in containment are not known, although a leak rate at a specified pressure may be known. The important feature of laminar flow is that the pressure drop is proportional to μW; thus a leak rate of the form

$$P_R = K_L \mu W / \rho \qquad (3.1.2.7\text{-}3)$$

may be most useful. The viscosity of the gas varies weakly with temperature and composition; thus it could also be lumped in with the loss coefficient. Note that the laminar

loss coefficient K_L is not dimensionless; it has dimensions of m^{-3}. The form of Equation (3.1.2.7-3) implies that the cracks do not change size with pressure (or temperature, etc.). If estimates of the scaling of crack size are available, then a different correlation can be developed from Equation (3.1.2.7-2).

Turbulent Flow. For flow through any reasonably large opening between compartments, the Reynold's number will be larger than 4000 for any velocities of interest in a severe accident, and the flow will be fully turbulent. In this case the pressure drop is related to the flow velocity through

$$P_R = \frac{1}{2} K_T \rho v^2 = \frac{1}{2} K_T W_{mj}^2 / \rho_{AM} A_j^2 \qquad (3.1.2.7\text{-}4)$$

where K_T is the dimensionless turbulent loss coefficient, which depends only on geometry of the flow path and can be estimated for most simple flow path configurations.

3.1.2.8 Natural Convection

After flow from one cell to the next has equilibrated the pressures of adjacent cells, continued circulation can take place around closed loops. This natural circulation is caused by the buoyant forces resulting from varying densities in the cells along the circulation loop. The lighter gases rise, and the heavier gases fall. The pressure difference due to gravity between two points in a gas of uniform density is ρgh where g is the acceleration of gravity, and h is the difference in elevation of the two points. When two cells are connected by a flow path, the corresponding contribution to the pressure difference between the two cells is

$$P_{bjmn} = \rho_{Am} g(z_{mj} - z_m) + \rho_j g(z_{nj} - z_{mj}) + \rho_{An} g(z_n - z_{nj}) \qquad (3.1.2.8\text{-}1)$$

where z_m and z_n are the elevations of a reference point (the center, say) in cell m and n respectively, z_{mj} and z_{nj} are the elevations of each end of flow path j, and ρ_j is the density of gas in the flow path. Since this buoyancy term is mainly important when the pressure difference between cells is small, the density inside the flow path can be assumed to be constant along the length of the flow path (unless heating occurs in the flow path) and is equal to the density in the upstream cell. The choice of

the reference point z_m in the cell is essentially arbitrary, since it drops out of the sum of the buoyancy pressure drops around any closed loop. It does have a second order effect in that the relation between pressure and density within the cell is determined at the reference point, thus something akin to the center of the cell should be chosen, perhaps the average elevation of all the flow path ends in that cell.

3.1.2.9 Flow-Path Inertia

As is well known, a finite time is required to accelerate any mass from rest to a finite velocity, or to stop it once it is moving. The noninertial flow equation, Equation (3.1.2.6-3), causes the flow rate to respond instantaneously to a change in pressure, whereas the inertial flow equation, Equation (3.1.2.6-4), causes a delayed response. The form of the inertial term used in CONTAIN is

$$\frac{L}{A}\frac{dW}{dt} = \Delta P \qquad (3.1.2.9\text{-}1)$$

where L and A are the effective length and area of the flow path. The expression used in HECTR is similar:

$$\frac{1}{2}(\rho_m+\rho_n)\ \frac{L_j}{A_j}\frac{dF}{dt} = \Delta P \qquad (3.1.2.9\text{-}2)$$

where m and n denote the upstream and downstream cells, respectively, and $F = W/\rho_m$. The CONTAIN expression appears to be valid for compressible (variable density) flow, while the HECTR expression appears to be more appropriate for incompressible (constant density flow). CONTAIN's expression uses $d(\rho v)/dt$ while HECTR's is $\rho dv/dt$. However, for the times when inertia is important (see below) it appears that $\rho dv/dt >> v d\rho/dt$, hence the two expressions are nearly equivalent.

As indicated at the beginning of this section, the inertia causes a finite delay in the response to an applied force. It can also result in an oscillation when there is no applied force. When the delay time and oscillation period are shorter than timescales of interest, then the simpler noninertial equation can be used with no loss in accuracy. When two cells at different pressures P_A and P_B are connected together the flow velocity will rise from zero to a quasi-steady state value

$$v_o = \left[2(P_A - P_B)/K_T \rho \right]^{1/2} \qquad (3.1.2.9\text{-}3)$$

with a transient time constant

$$t_T = L/2K_T\, v_o \qquad (3.1.2.9\text{-}4)$$

where turbulent flow has been assumed, and K_T and L are the turbulent loss coefficient and the effective length of the flow path, respectively. Thus, when the flow resistance is low (K_T on the order of unity) the inertial delay is on the order of the time for material to travel the length of the flow path. When the flow resistance is high ($K_T >> 1$) the resistance dominates, and the inertia may be negligible. When the velocity is high ($v_o > 10$ m/s) the transient response time will be less than 1 second, and, consequently, negligible under many circumstances of interest. It would appear that the transient response time is most significant for the low velocities found in natural circulation flow.

When there is little or no pressure difference between the two cells, the inertia of the flow can result in low amplitude oscillations which have a period of

$$t_o = 2\pi \left[\frac{V_m}{AL} \right]^{1/2} \frac{L}{c}$$

where V_m is approximately equal to the volume of the smaller of the two cells, and L/c is the time required for sound to traverse the length of the flow path. Thus the period of these oscillations will generally be rather short (< 1s) unless the length of the flow is long and its cross-sectional area is small.

It appears that inertia may have a significant effect for timescales of a few seconds, however, for many situations the inertial effects are apparently insignificant. Thus it appears to be desirable to provide the option of including inertial effects at the user's option, but not to include it routinely.

3.1.2.10 Mixing

Within a compartment, considerable movement of the atmosphere can take place, resulting in considerable intermixing.

If this mixing is complete, or nearly so, then the compartment can be modeled as a single cell. If the mixing is incomplete and is largely caused by large-scale natural convection currents, the mixing can be modeled by dividing the compartment into a few cells and calculating the convection with the buoyancy terms discussed in Section 3.1.2.8. However, in some cases the mixing may occur on a finer scale than can be modeled with a series of cells (turbulence, for example). While mechanistic models for such mixing would be desirable, the following parametric model may suffice for the first version of MELCOR.

This parametric mixing model allows the user to specify a volumetric mixing rate $\dot{V}$, which may be time dependent. In essence, equal volumes per second of material from specified pairs of cells would be interchanged. The flow rate terms for this mixing are given by

$$W_{kmj} = - W_{knj} = \dot{V}_j(\rho_{Akn}-\rho_{Akm}) \qquad (3.1.2.10\text{-}1)$$

and

$$W_{kmj}H_{Fkmj} = - W_{knj}H_{Fknj} = \dot{V}_j(\rho_{Akn}H_{Akn}-\rho_{Akm})H_{Akm} \quad . \qquad (3.1.2.10\text{-}2)$$

It should be noted that these mixing terms should be added to the flow terms that may result from pressure-driven flow.

3.1.2.11 Material Property Requirements

The equations in the flow and thermodynamics section require the following thermodynamic properties of the main (nontrace) gases, with density and temperature as the independent variables:

Pressure P
Specific enthalpy H
Specific internal energy U
Specific heat at constant volume $[\partial U/\partial T]_V$
$[\partial U/\partial \rho]_T$
Dynamic viscosity μ (this may not be needed).

The thermodynamic equations used here have not assumed that ideal gases are being used. That is, the specific heat is not assumed to be a constant. The enthalpy and the internal energy should have the chemical heats of formation included

in them, as discussed in Section 3.1.2.3. In the event that this is inconvenient, the heats of formation should be made available separately, and should be consistent with the internal energies used.

The solids and liquids suspended in the atmosphere are assumed to be at the same pressure and temperature as the gases. Thus their densities (which do not enter any of the flow or thermodynamic equations) and their internal energies and enthalpies are determined by the atmosphere temperature (and possibly pressure). For the solids and liquids in the atmosphere, then, the following properties are needed:

Specific enthalpy H
Specific internal energy U
Specific heat at constant volume or pressure.

The properties will be needed for at least the following materials:

Air
Oxygen
Nitrogen
Hydrogen
CO_2
CO
Water (liquid and gas)
Ideal gas (for test purposes).

3.2 REACTOR CAVITY PHENOMENA

by

Kenneth D. Bergeron
R. J. Lipinski
M. Pilch
M. L. Corradini

CONTENTS

CONTENTS (Continued)

LIST OF FIGURES

LIST OF FIGURES (Continued)

LIST OF TABLES

LIST OF APPENDICES

3.2.1 INTRODUCTION

In the event of vessel failure in a core-melt accident, the reactor cavity is the scene of events which strongly affect the progression of phenomena in the rest of containment. During this phase of an accident, extreme conditions and processes may be encountered which are unique to the cavity. These may include molten debris attack on concrete, melt stream breakup and quench, steam explosions, sweepout due to high pressure gas release from the vessel breach, high temperature metal-water chemistry, debris bed formation and quench, and debris bed dryout. Because conditions are so extreme and variable, there is a high level of phenomenological uncertainty associated with many of these processes.

It is natural, therefore, to deal with the reactor cavity separately from the rest of containment for this Assessment, and possibly in the MELCOR code as well. In this section, we will discuss those phenomena which are unique to the reactor cavity. Other processes, which can also occur in the rest of containment, are treated elsewhere in this report. These include heat transfer to structures, intercell flow, hydrogen combustion, aerosol behavior, and so on. The BWR pressure suppression pool is also not discussed here; since it is considered an engineered safety feature, it is analyzed in Section 3.6. Core-concrete interactions are discussed in this section mostly in the context of interactions with other processes (e.g., debris bed behavior) in the cavity. A more detailed discussion of core-concrete interactions as an isolated phenomenon can be found in Section 3.5.

In the analyses to follow, the focus of attention will be on phenomena which potentially have a high leverage with respect to consequences (i.e., risk). From the perspective of reactor cavity modeling, it is useful to consider two categories of phenomena:

1. Phenomena which may contribute directly to containment failure.

2. All other reactor cavity phenomena which might affect the radiological source term.

The first category involves processes such as basemat penetration or overpressurization due to core-concrete interactions. In these cases, the cavity models will be used to predict the likelihood of containment failure, as well as the source terms to the environment. For the second category of phenomena the emphasis in modeling should be on predicting the disposition of fission products as a function of time, so as to provide an accurate estimate of the source term for consequence calculations.

A different degree of accuracy is required for these two types of calculation because they affect risk differently. However, it is extremely difficult to quantify the required degree of accuracy for any particular phenomenon. Instead, it is currently necessary to rely heavily on the intuitive judgment of specialists in the field concerning what level of modeling is desirable or acceptable. The selection of existing, tested models for cavity phenomena following vessel melt through is extremely limited, so this reliance on specialists' judgment is even greater than for many other aspects of severe accident modeling.

In the modeling recommendations section of this report, a distinction will be made between "mechanistic models" and "parametric models." It is, to some extent, an arbitrary distinction, since every model has some degree of uncertainty. Nevertheless, it is important for the phenomenological specialist to have a way of conveying to the ultimate user of the MELCOR code which models have a reasonable degree of predictive capability, and which are more speculative. To the extent possible, the uncertainties in the parametric models will be embodied in a set of independent, boundable parameters, designated in Section 3.2.5 as "nodal parameters." This designation emphasizes the viewpoint that MELCOR should be a tool for calculating the consequences of making certain model and parameter choices, rather than an indistinguishable mix of best estimates, best guesses, and pure speculation.

This section will be organized in the following manner: First, the geometry and structure of a variety of different reactor types will be reviewed (Section 3.2.2). Then, in Section 3.2.3, the important phenomena which may occur in the cavity will be described, along with the current state of experimental and analytical knowledge. Section 3.2.4 focuses on the uncertainties inherent in the available phenomenological models. Finally, Section 3.2.6 contains specific recommendations for modeling approaches to be used in MELCOR-1, as well as some discussion of the needs of MELCOR-2. A number of technical appendices supplement the main text.

3.2.2 BRIEF SURVEY OF TYPICAL CAVITY DESIGNS AND FEATURES

There is a high degree of variability in reactor cavity designs. This is due in part to the fact that the cavity plays no significant role in design basis accidents. In particular, there is a wide range of variation in concrete composition, in geometry, in accessibility of the cavity to water overflow from the upper containment, and in degree of resistance to pressure relief through gas and liquid flow. As a consequence, cavity models must be quite flexible. In many cases, the price of this flexibility will be detail and accuracy.

The reactor cavity region of a typical PWR is shown in Figure 3.2.2-1. Both large dry PWR's and ice condenser PWR's have similar features, but the cavity geometry and the outlet paths for flow of gases, liquids or solids are highly variable. Another important variable for cavity phenomena is related to upper containment geometry: the presence or absence of sumps or curbs around access ports to the cavity region which will determine whether there is likely to be a significant amount of water in the cavity at the time of melt release.

Since all commercial BWR's are manufactured by the same vendor, there is more standardization, but there are still three distinctly different types: Mark 1, Mark 2, and Mark 3. The Mark 2 cavity region is shown in Figure 3.2.2-2. An important difference from the PWR is the height of the region below the vessel. For the Mark 2 it is about 25 m, whereas for the Zion PWR, it is less than 4 m. The increased fall height could change the nature of the initial fuel-coolant interaction significantly.

A more important difference is that in BWR's the cavity is isolated from the containment atmosphere by the pressure suppression pool. One consequence is that explosions in the cavity must be relieved through the pool, so that a large steam explosion could conceivably disrupt the pressure suppression pool to the point of loss of function for the remainder of the accident. This point will be discussed further in Section 3.2.5. On the favorable side, it is likely that much of the aerosols and fission products released in the cavity of a BWR will be removed by the pressure suppression pool rather than being released to the upper containment.

Besides these considerations, there is probably more variation within a given containment type (e.g., large dry PWR) than across category boundaries. For example, most reactor cavities have a thick concrete basemat (typically over 3 m) which serves to prevent or delay the melt through of the molten core material. But the composition of the concrete is highly variable, being determined by local material availability. As will be discussed in Section 3.5, the course of an accident can be substantially affected by the amount and species of gases evolved in the core-concrete interaction, and this is highly dependent on composition.

Similarly, the size of the flow paths from the cavity are critical in determining the amount of material which might be removed by a high pressure melt or gas release from the vessel, or following a large steam explosion. PWR's vary substantially in this respect. For example, the Zion plant has a flow area of about 10 m^2 up the instrumentation tube, while in the Byron plant this path is blocked off with a concrete plug (flow area $<<1$ m^2).

One consequence of this variability in cavity designs for MELCOR is that a high degree of generality must be built into the models used. This results, of course, in a trade-off with speed or accuracy. Another consequence is that generic studies will suffer from an additional uncertainty: not phenomenological uncertainty, and not uncertainty in physical parameters (since each individual plant is well characterized), but an uncertainty which comes from choosing a "typical" cavity design to represent a class of designs which are highly variable. This problem will be further discussed in Section 3.2.4.

One cavity feature which may be of interest for MELCOR, even though no existing LWR has it, is a retrofittable core retention device. A typical design for such a system involves a stratified bed of refractory particles below the vessel, in layers of different particle diameters. The presence of such a bed could have a profound effect on the course of events following vessel breach.

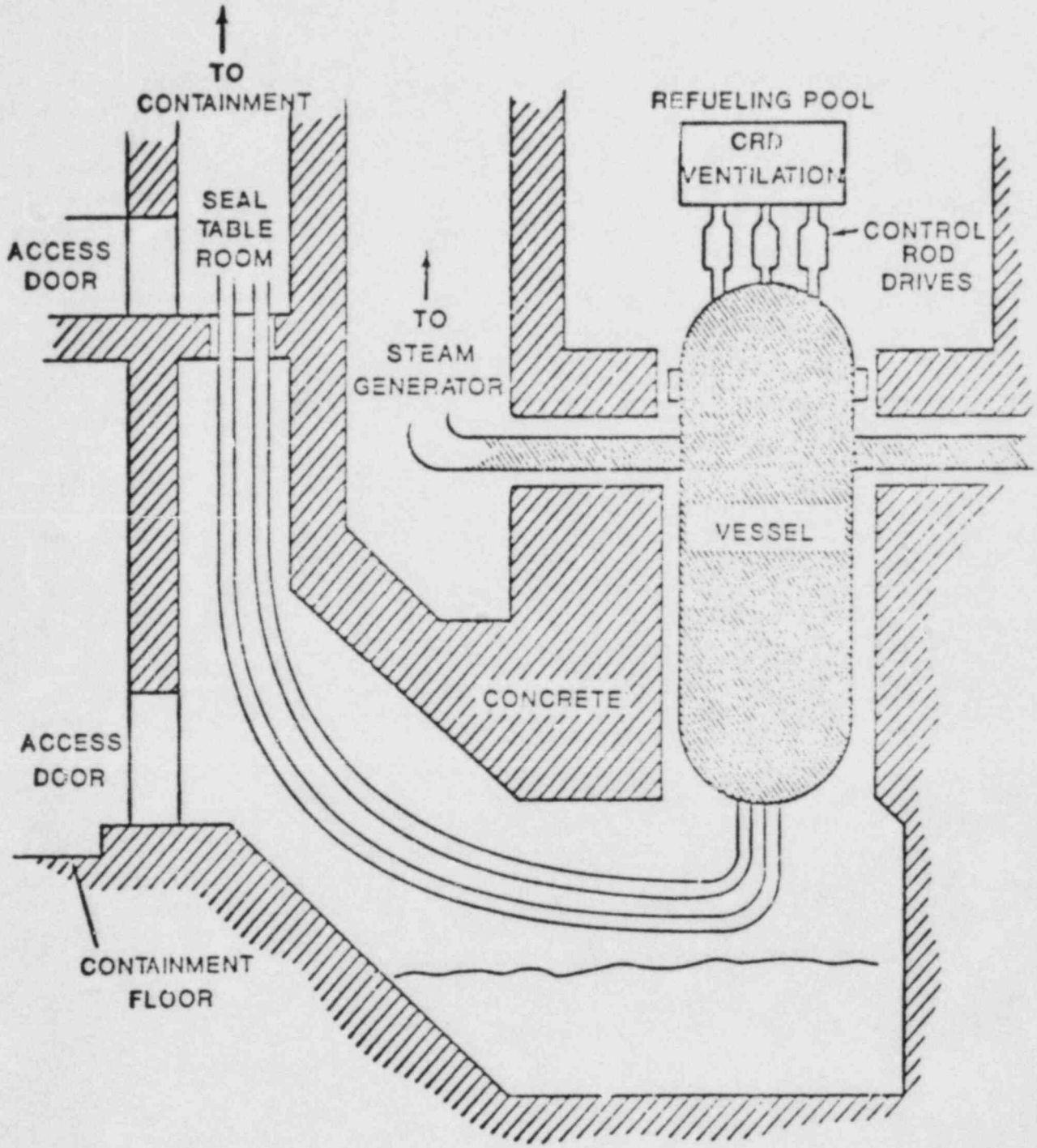

Figure 3.2.2-1. Typical PWR Cavity Region, Showing Instrumentation Tube

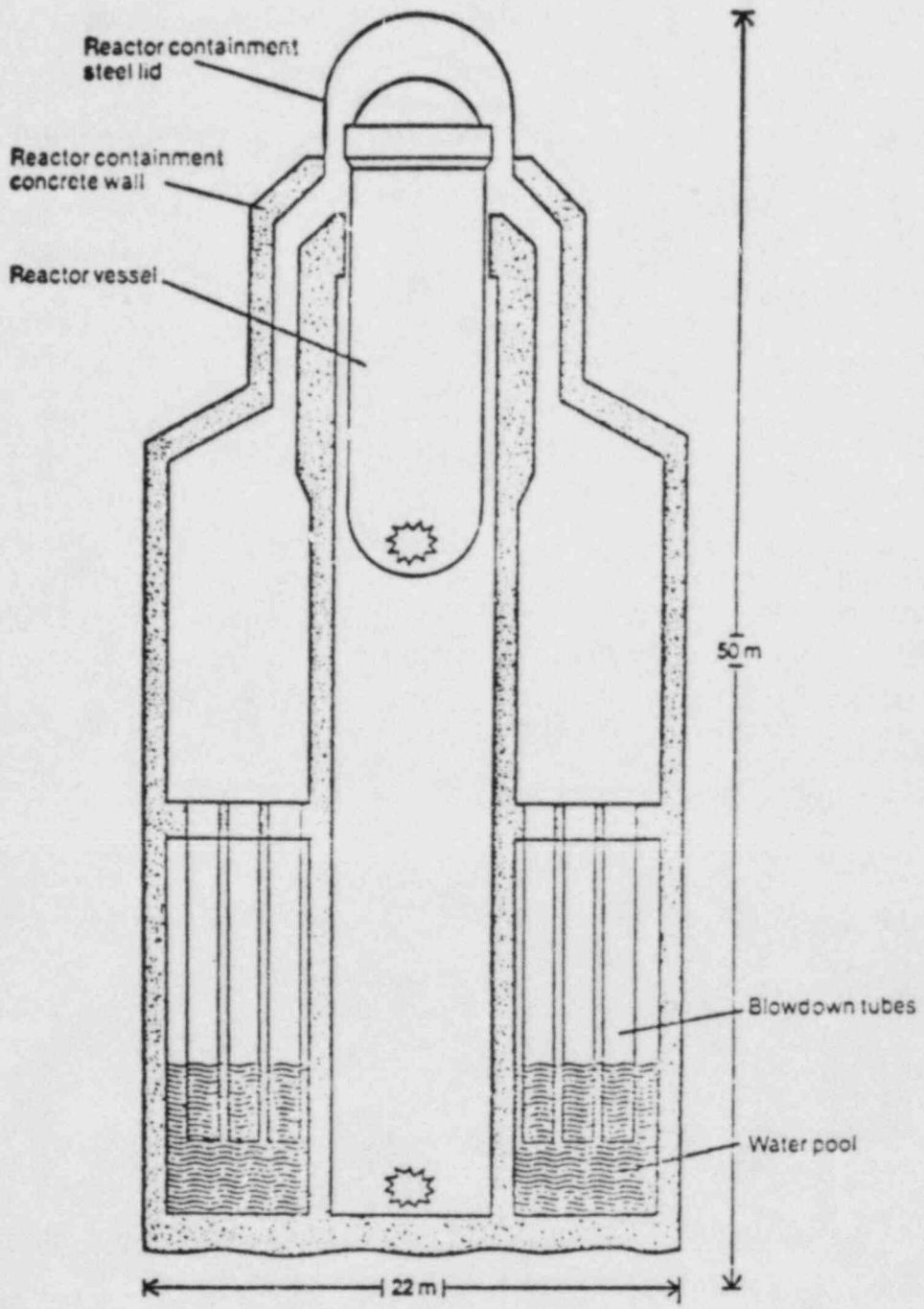

Figure 3.2.2-2. BWR Mark II Cavity Region, Showing Pressure Suppression Pool

3.2.3 PHENOMENA

It is useful to distinguish three categories of reactor cavity phenomena. In the first few minutes following vessel failure, a number of rather fast processes may take place, including jet breakup of the melt stream, sweepout from the cavity due to high pressure gas release, fuel-coolant mixing, steam explosions, and fluidization and expulsion of debris and water from the cavity. We will call these processes "Initial Interactions," and will discuss them in Section 3.2.3.2.

When and if a stabilized debris bed is formed, a longer time scale becomes appropriate. If water is present, there may be a quenching process, and core-concrete interactions may also occur. Other possible phenomena in this category include metal-water chemistry (in particular, hydrogen and carbon monoxide generation) in the hot debris zones, dryout, and remelt of debris. We identify this group of phenomena "Wet Cavity Debris Bed Behavior" and discuss them in Section 3.2.3.3.

Finally, if the cavity is dry, we have a third category, "Dry Cavity Phenomena." The main reason for isolating this as a separate category is that these phenomena are discussed separately in Section 3.5.

However, before discussing in detail these specific categories of phenomena, it is useful to bring them into perspective by considering, in a briefer narrative, some typical sequences of events which might occur in the reactor cavity following failure of the pressure vessel and release of molten core material.

3.2.3.1 Representative Severe Accident Event Sequences

The typical event sequence will be grouped into two phases. Phase 1 involves the exit of core materials from the pressure vessel, the dynamics of fuel release from the vessel and the initial interaction of melt materials with water. Phase 2 involves the long-term interaction of the core materials with cooling water and with the containment or cavity floor.

3.2.3.1.1 Phase 1: Melt Release and Initial Interactions

There are three major modes of release of core materials from the pressure vessel: (1) a pressure-driven melt jet; (2) a gravitationally driven drop of a large melt amount; and (3) a continuous dripping of core materials not involved in the initial release (which could comprise 50 percent or more of the core).

A pressure-driven jet will occur if the reactor is at high pressure (as in a small-break LOCA or transient) and the breach occurs at the bottom of the melt (e.g., the instrument penetration welds). The ejected material may blow out any water in the cavity and accumulate in the cavity as a pool. Subsequent high-velocity steam and hydrogen release from the vessel may blow the melt out of the cavity and disperse it over a wide area on the containment floor. Such a dispersal would probably assure ultimate debris coolability but would also generate a sizeable steam pressure spike in containment as the hot debris hit the water on the floor.

On the other hand, such dispersal is presently only speculation with little experimental support. The ejected melt may just collect in the cavity. In either event, some of the jet may create aerosols. These aerosols could be a sizeable airborne radiological source. In addition, the aerosols may hinder safety systems by clogging fans or filters, and by the rapid burning of the hot metal particles.

A gravitationally driven drop of a large amount of melt will occur if the reactor is at low pressure (e.g., in a large-break LOCA, or after a high-pressure vessel failure near the top of the molten pool). It may also be necessary for the breach to occur at the melt pool bottom, although a rapid downward erosion of a higher breach may allow a fairly fast release.

There are several possibilities for what happens when a large melt mass enters a pool of water in the reactor cavity. The initial part of the stream may induce a small steam explosion which blows out all the water in the cavity, and allows the remaining melt to form a large molten pool. When the water returns it may enter film boiling on top of the melt, or interact violently with it (with fragmentation or more explosions). Conversely, the melt may penetrate the water without any significant fragmentation at all and form a molten pool below the water. A third possibility is coarse fragmentation of the bulk of the melt followed by a large steam explosion with finer fragmentation. The fine fragmentation will result in quenched debris, but in the process, large amounts of pressurizing steam may be produced. If the debris is too fine, the debris bed may not be coolable, and may remelt.

A slow release of melt from the damaged vessel may follow either a pressure-driven melt release or a gravity-driven large melt release. The slow release comes from the gradual melting of the core materials not involved in the initial release. As small masses of this secondary melt release enter a pool of water, they may induce small steam explosions. These explosions may encourage more violent

interactions between the water pool and any large melt pool the water may be resting on. These events may induce fragmentation of the melt and large generation rates of steam and hydrogen.

3.2.3.1.2 Phase 2: Long-Term Melt Interactions

The net outcome of the various sequence paths of Phase 1 is either fragmented solid debris (in the reactor cavity or scattered throughout the containment building) or a molten pool of core materials (possibly submerged below a pool of boiling water).

Since the rate of energy release in quenching fragmented debris is potentially very large (much greater than the decay power level), a bed of fragmented debris will probably start out dry, even if it is below a pool of water. The hot dry debris will begin immediately to heat the concrete. This will release steam and noncondensible gases from the concrete. It is possible that the lower regions of the debris may begin to erode the concrete or remelt before the quench front reaches the bottom of the bed.

In some cases, quenching of the debris may not be possible, regardless of the timing. This is because for some conditions the decay heat will produce sufficient steam during boiling to prevent the entry of adequate replenishing water from the overlying pool. Under these conditions, even a prequenched bed will become dry because the decay power level exceeds the critical dryout power for that particular bed configuration. The unquenchable debris will then begin to melt the concrete and sink into it, and may itself begin to remelt.

Another consideration is the long-term changes in the coolability of quenched debris. Fragments from secondary melt releases into the cavity water pool will settle on debris from the initial release. This will make the debris less coolable. If the new fragments are smaller than the old ones (because of small steam explosions as the secondary melt enters the water pool) the reduction in coolability will be large and bed dryout will likely occur.

The long-term interaction of a molten pool of hot, solid debris with underlying concrete is the second realm of concern in Phase 2. The interaction with the molten pool may be affected by whether there is a pool of water overlying the melt.

The process of melt attack on the concrete without an overlying pool of water has been a subject of intense experimental and theoretical analysis over the past six years. The heat from the molten materials vaporizes free water and

releases chemically constituted water within the concrete. It also produces carbon dioxide from any carbon- ates present. Steam passing through the molten debris will oxidize the melt and generate hydrogen gas. Similarly, carbon dioxide will be reduced to carbon monoxide. Both of these gases will pressurize containment and have the potential to burn. The attack will also generate aerosols. The aerosols could add to the airborne radiological source term or they could help reduce the airborne radiological source term by agglomeration. They also might damage safety systems by clogging fans or filters. Hot solid debris could attack concrete with similar effects, but at a much slower rate.

The presence of water above a molten pool complicates the process of melt attack on the concrete. With a stable crust between the water and the melt, the water may have little or no effect on the attack process. But the water will help to remove aerosols generated by the attack. Without a stable crust, strong interactions between the water and melt may occur. Entrapment of pockets of liquid water in the melt may induce fragmentation of the melt, which may lead to small steam explosions, which could yield further fragmentation or explosions. Small steam explosions from secondary melt releases coming from the reactor vessel may also cause the melt to mix with the water and result in fragmentation or explosions. Fragmentation will greatly increase the steam and hydrogen generation rate. Fragmentation will also raise the question of quenching a particle bed again.

3.2.3.2 Initial Interactions

The early response of the reactor cavity depends greatly on the nature of the melt release from the vessel, about which there is considerable uncertainty. For some categories of accident (e.g., large-break LOCA's) it is expected that the pressure vessel will be at a pressure close to that of the containment building, and melt will be driven out of the vessel primarily by gravity. Other sequences could result in vessel failure while a moderate to high pressure persisted in the vessel, resulting in pressure-driven release of core melt material, mixed or followed by high pressure, high velocity steam and noncondensible gas.

3.2.3.2.1 <u>High Pressure Melt Release Phenomena</u>

High pressure ejection of melt from the reactor vessel following a PWR core melt accident is an area of recent concern. The following scenario, taken from the Zion Probabilistic Safety Study (ZPSS),[1] is an example of current thinking on this subject. (It is not the only scenario which could be postulated.)

Failure of the pressure vessel occurs at an instrument-tube penetration, which is initially 4 cm in diameter. Ablation increases the hole diameter to 40 cm in diameter during the period of melt ejection from the reactor vessel.

A coherent jet of molten core debris cuts through the pool of water, impacts on the floor of the reactor cavity, and triggers a small scale steam explosion that expels all the water from the reactor cavity.

A pool of molten, core debris temporarily forms in the reactor cavity. Following complete ejection of melt from the reactor vessel, high velocity steam removes melt from the reactor cavity by two processes: film sweepout and film entrainment (i.e., droplet formation). Core debris, which is removed from the reactor cavity, is distributed over a large area of containment floor forming a coolable bed of particulated debris.

The following two sections will discuss briefly the key phenomena which could occur during and following a high-pressure melt release. Substantially more technical detail can be found in Reference [41].

3.2.3.2.1.1 High Pressure Sweepout

The Zion PSS proposes four hydrodynamic phenomena which could result in core material deposition outside the reactor cavity in the event of high pressure melt ejection: (1) film sweepout, (2) film entrainment, (3) particle levitation, and (4) splashout.

Film Sweepout. A liquid film can be dragged up and out of the instrument tunnel by the high velocity gas stream which results from reactor vessel blow down; this process is called film sweepout. According to the ZPSS, film sweepout occurs when

$$\frac{\rho_g V_g^2}{9\left[g\sigma\rho_L\right]^{1/2}} \geq 1 \quad . \qquad (3.2.3\text{-}1)$$

Here, ρ_g is the gas density in the tunnel; V_g is the gas velocity in the tunnel; g is the acceleration due to gravity; σ is the liquid surface tension; and ρ_L is the density of the molten degraded core material.

Film Entrainment. Waves will form on the liquid film if the gas velocity is sufficiently large. Liquid droplet entrainment into the gas results from wave crest erosion by the high velocity gas stream. According to the ZPSS, film entrainment occurs when the following criterion is satisfied:

$$\frac{\rho_g V_g^2}{13.7\left[g\sigma\rho_L\right]^{1/2}} \geq 1 \quad . \tag{3.2.3-2}$$

Note that this differs from the film sweepout criterion only by the constant of proportionality.

An alternate criterion for film entrainment is given by Ishii and Grolmes:[2]

$$V_g = (N_\mu)^{.8} \frac{s}{\mu_L}\left[\frac{\rho_L}{\rho_g}\right]^{.5}, \quad \text{for } N_\mu < .07 \tag{3.2.3-3}$$

where μ_L is the melt viscosity, and

$$N_\mu = \left[\frac{\mu_L}{\rho_L \sigma\left[\frac{\sigma}{(\rho_L-\rho_g)g}\right]^{.5}}\right]^{.5} \quad . \tag{3.2.3-4}$$

Splashout. The ZPSS proposes that a high amplitude, small wavelength wave is accelerated down the instrument tunnel. Film mass is converted to wave mass which has an ever-increasing material velocity. Splashout occurs when the wave impacts the far tunnel wall if the wave mass has sufficient kinetic energy to overcome the gravity potential associated with lifting material up and out of the instrument tunnel. The necessary condition for removal is

$$\frac{V_L^2}{2gh} \geq 1 \quad . \tag{3.2.3-5}$$

Here, V_L is the material velocity when the wave impacts the far tunnel wall, and h is the height which material must be lifted to get it out of the instrument tunnel.

Particle Levitation. Entrained particles can be swept out of the instrument tunnel if hydrodynamic drag forces are sufficient to overcome gravity. This occurs when the following criterion is satisfied.

$$\frac{3}{4} C_d \frac{\rho_g V_g^2}{g \rho_L D} \geq 1 \quad . \qquad (3.2.3\text{-}6)$$

Here, C_d is the aerodynamic drag coefficient, and D is the entrained particle size.

Discussion. The threshold conditions for debris dispersal are exceeded for accident scenarios associated with high pressure ejection of melt. Indeed, the debris dispersal mechanisms postulated in the ZPSS and the relevant threshold conditions have been confirmed at ANL [3, 3a] using simulant fluids (water, Cerrelow, and Wood's metal) in a 1:40 linear scale model of the Zion cavity. Recently, more prototypical experiments at ANL and SNL, using thermitic melts in wet and dry cavities, also resulted in significant dispersal of debris from scaled reactor cavities.

Future experiments will determine if dispersal is affected by core debris/concrete interactions or core debris temperature. Tests on a 1:30 scale at ANL along with tests at 1:20 and 1:10 may substantially change current perceptions concerning the efficiency of debris removal.

Differences in reactor-cavity geometry can also influence mass removal. The effect of obstructions in the flow path (e.g., instrumentation tubes) is at present poorly understood, but it is likely to vary greatly with cavity design, furthermore, they will affect flows of water, gas, and debris differently. The Zion cavity has only one path for steam to exit the reactor cavity, the keyway for the instrumentation tubes. Other reactor cavities, however, have a second access passageway into the reactor cavity. This second escape route for steam means lower velocity steam as it exits the cavity. Furthermore, it may enable steam to bypass core debris that piles up under the first passageway. Preliminary reports on British experiments at Winfrith indicate very little removal via the sweepout process described above. The reason may be that the scaled cavity represented the Sizewell B reactor, which has two separate steam flow paths out of the cavity.

Sandia's recent HIPS/SPIT experiments have provided information on the dispersal process that was not considered in the ZPSS. These include:

1. The possibility that pressurized ejection of material from the reactor vessel is accompanied by intense aerosol generation.

2. The dispersed debris may directly heat the containment atmosphere.

3. The dispersed debris may chemically react with the containment atmosphere producing heat and perhaps evolving fission products and hydrogen.

4. The dispersed debris may act as a distributed ignition source for hydrogen in the containment building even in conditions which would ordinarily be considered steam inerted. Heat evolved during hydrogen recombination will add to the pressurization of containment caused by quenching of the dispersed debris and blow down of the pressure vessel.

3.2.3.2.1.2 Jet Breakup and Aerosolization

The ZPSS concluded that the high-pressure melt release scenario described in 3.2.3.2.1.1 should be relatively benign with respect to consequences. This conclusion may be premature, for there are a number of mechanisms for the generation of large amounts of core debris aerosols from this jet which were not considered in the ZPSS. The possible mechanisms include:

1. Jet breakup resulting from melt streaming through air,

2. Jet breakup by degassing, dissolved gases, or flashing,

3. Debris fragmentation on impact with the floor of the reactor cavity,

4. Atomization at the reactor vessel breach during steam discharge,

5. Film entrainment in the reactor cavity during steam discharge.

At Sandia, tests which are preliminary to the HIPS project have reinforced concern about aerosols. The tests involved 10 Kg of thermite driven through a 1-inch hole by 600 psi nitrogen gas. A cloud of aerosols immediately appears with a total spread angle of about 80°.

Most of processes listed above are discussed in some detail in Reference [41]. It is concluded there that much additional experimental and theoretical analysis is needed,

but that some of the mechanisms are likely to occur in realistic vessel failure conditions. In particular, pneumatic atomization can occur when steam in the pressure vessel breaks through the breach before the melt is fully released. This could occur when there is still a substantial amount of molten debris in the bottom of the vessel as a result of hydrodynamic surface instabilities during the melt blow down. The amount of mass atomized in this process is extremely difficult to predict, but the particle size is estimated in Reference [41] to be 5-10 μm, which would imply that they would be relatively long-lasting aerosols.

3.2.3.2.2 Low Pressure Melt Release Phenomena

If molten core material is released at lower pressure, the phenomena described in the previous section will not occur. The debris will traverse the air above the water pool, then enter the pool, possibly fragmenting as it falls to the bottom of the cavity. One of the most important concerns is whether the debris is fragmented and quenched to form a coolable debris bed. If a quenched, coolable bed is not formed, the hot debris will attack the concrete. Another concern is the possibility of steam explosions, which are a very effective quench and fragmentation mechanism, but which could threaten containment by overpressurization due to the cumulative steam and hydrogen buildup from a large number of steam explosions occurring over a relatively short period of time.

3.2.3.2.2.1 Fall Through Air

If the fuel pours into the water pool below the reactor pressure vessel it may begin to break apart and produce steam and hydrogen. The fuel will first fall through the gases in the reactor cavity before it enters the water pool. During this fall through the gas the fuel can break apart due to the pressure forces generated by the fuel relative velocity and the difference in density (this effect will also occur when the fuel enters the water). If the fuel pour rate is large (large characteristic pour diameter, D_f, or velocity, v_f) its characteristic Weber number, (ratio of destabilizing dynamic pressure forces to the stabilizing surface tension force)

$$We \equiv \frac{\rho v_f^2 D_f}{\sigma} \qquad (3.2.3\text{-}7)$$

may be greater than a critical value. Here, ρ is the gas density and σ is the surface tension of the fuel-fluid interface. When We > 12 the fuel pour stream will begin breaking up into smaller masses, generating more surface area. This increase in surface area will cause the fuel to cool faster or allow its metallic components to react more rapidly with the water vapor and to generate hydrogen. However, because the mechanism of fragmentation is hydrodynamic in nature, extensive fuel breakup would not occur before the fuel enters the water pool. Therefore, it is also not expected that significant amounts of fuel will cool down or be oxidized during its time in the gas phase.

3.2.3.2.2.2 Fall Through Water

Once the fuel enters the water pool, fuel breakup and mixing with the water can continue, but the rate of breakup would change and the complicating effect of water vaporization is added. The generic term for these processes is Fuel-Coolant Interactions (FCI's). The hot fuel will enter the water pool in film boiling and will begin to distort in shape. As it continues to fall through the pool it breaks apart into smaller pieces and mixes with the surrounding water, which is still in film boiling. These smaller pieces may subdivide further as the steam produced in film boiling (and hydrogen if the fuel is partially metallic) flows out through the top of the fuel-coolant mixture and more water flows in from the sides and bottom. Once again, one might model this fuel breakup process as purely hydrodynamic, using Weber number breakup models. However, the major difference here is that film boiling heat transfer separates the two liquids and would affect the mixing dynamics. Current experiments at Sandia using real reactor materials at intermediate scale seem to indicate that the film boiling process impairs the mixing process by slightly delaying the rate of fuel breakup. There are currently no detailed models of this dynamic process. However, simple analyses of the Sandia fuel-coolant experiments have successfully correlated the fuel-coolant mixing process in a manner analogous to hydrodynamic breakup. (See Section 3.2-A.3.2.)

The reason that such mixing between the fuel and coolant is important is that the amount of steam and hydrogen produced during this process may be substantial, and the final fuel size and temperature are important in the determination of whether a steam explosion could take place (see next section). As the fuel falls through the water and breaks apart it will transfer its internal energy to the surrounding coolant by steam production and liquid coolant heating. Hydrogen and heat will be produced by exothermic reactions between water and the metals and fuel in the debris.

In the film boiling regime energy transfer will occur primarily by radiation heat transfer from the fuel surface to the water liquid-vapor interface. Conduction through the vapor film will also transfer energy, but at molten fuel temperatures, radiation is likely to be the dominant mechanism. All the energy that is not conducted away from the water liquid-vapor interface into the bulk coolant goes into producing steam.

This steam will flow up through the fuel-coolant mixture. It can (if the velocity is quite large) fluidize the liquid (fuel or coolant) in the upper portions of the mixture and inhibit further mixing by carrying these liquids out of the mixture. The expulsion of liquid water from the interaction region was the basis for a criterion on minimum fuel diameter proposed by Fauske and Henry.[4, 5] This also imposes a limit on steam generation rate. As discussed in Appendix 3.2-A.3.2, however, the correlation they used was taken from pool boiling experiments, in which steam and water must have a counter-flow configuration. The situation of interest is distinctly different in that liquid and steam flow can have different pathways, and time dependent effects are expected to be important. Indeed, actual mixing data from FCI experiments show that the pool-boiling criterion is violated (cf. Section 3.2-A.3.1).

Another limitation on steam generation rate was discussed by Rivard, in [6]. If the steam generation rate is sufficiently high, the gas flow rate from the cavity can levitate and entrain the smaller fuel particles. This process is known as elutriation, and a quantitative criterion for the occurrence of the process for a given particle size was proposed in [6]. Removing these small particles should decrease the steam production rate substantially, but since the water is of much lower density than the fuel, it is likely that removal of water from the interaction zone (as proposed by Fauske and Henry) will impose a lower steam generation limit.

Corradini [39] has proposed two expressions for the minimum diameter for fuel fragmentation. (See Section 3.2-A.3.3.) One is based on levitating the fuel particle; the other is based on entraining the water and expelling it from the interaction zone. A limit to fragmentation also limits steam generation, and although the use of Corradini's formulas require the estimation of key parameters from experiments, there appears to be reasonable experimental corroboration of the model.

The steam produced is available for chemical reaction with any metallic debris that may be present. The rate of hydrogen generation is controlled by two mass-transfer processes, the rate of diffusion of steam through the gas

film to the fuel surface, and the rate of diffusion of oxygen to the metallic phase of the fuel in the liquid or solid fuel mass. Oxidation of zirconium is limited by diffusion through the oxide layer at the interaction surface. On the other hand, for molten iron, the oxide that is formed is soluble in the high temperature iron phase and no solid oxide crust would be formed to impede oxidation, so that the diffusion through the gas film may be limiting when the fuel temperature is high. These metal-water chemical reactions are exothermic to varying degrees and will heat up the fuel mass.

Finally, the fuel temperature will change as it falls through the water. Knowing the temperature of the fuel would allow one to decide if it has cooled sufficiently to become part of a debris bed or if it is still molten so that it will become part of a molten pool that can thermally attack the concrete. There are three aspects that must be considered when doing the fuel energy balance; energy transfer to the surrounding water, debris heating due to chemical reactions and debris heating due to fission product decay heat.

Additional technical details concerning the Fall through Water stage can be found in Appendix 3.2-A.3.2.

3.2.3.2.2.3 Steam Explosions

When molten metals are poured into water, a shock-driven rapid fragmentation and quenching process, usually called a steam explosion, can occur. These events are an important concern in the metallurgical industry, where they have occurred on both small and large scales causing, in some cases, substantial property damage, injury and death. In the past 10 years, a considerable amount of research has gone into this phenomenon, as it applies to reactor safety, and our understanding has improved significantly. However, there remains a great deal of uncertainty concerning the criteria for a steam explosion, and how to predict the key output parameters (energy released, final fragment size, and hydrogen generated).

In-vessel steam explosions have been discussed in Section 2. For that situation, the principal concern, historically, has been the threat of pressure vessel and/or containment failure due to the steam explosion. For ex-vessel situations, the emphasis is different. It is highly unlikely, for example, that a containment-threatening missile could be generated by a steam explosion in the cavity. However, multiple steam explosions could pressurize containment more rapidly than heat sinks could respond, and, in conjunction with other pressure sources (e.g., a hydrogen burn), these processes could threaten containment through

overpressurization. Another concern is that all the water in the cavity could be removed by steam explosions, so that a dry core-concrete interaction could occur.

On the positive side, it is clear that to prevent the core-concrete interaction, the molten core material must be substantially cooled to solidification by the water pool before it comes to rest on the cavity floor. As discussed in Section 3.2.3.2.2.2, the rate at which steam can be generated by normal quenching processes is limited by flooding and fluidization processes. In a steam explosion, these limits are overcome by inertial confinement: the fragmentation and liquid-liquid contact occurs so rapidly (i.e., in less than 10 ms) that the material does not have time to respond by moving away from the interaction region. Thus a steam explosion is the most effective known mechanism for quickly quenching the debris. Whether the resulting particulate debris bed is coolable or not is another question. Coolability depends greatly on particle size (see Section 3.2.3.3.1), and steam explosions can generate extremely fine particles. The most favorable outcome following a melt release into a water-filled reactor cavity is thus that a steam explosion which quenches the debris occurs, but the debris particles are not too small (e.g., 0.1-1.0 cm) and adequate water remains in the cavity to keep the debris bed cool, and to quench subsequent low-level debris release.

Because of its importance to safety in the metallurgical industry, the liquefied natural gas industry, as well as the nuclear industry much has been written concerning steam explosions. (E.g., see reviews in [7-9].) In addition, there have been extensive experimental investigations of the phenomenon, most notably the single droplet and FITS series at Sandia,[10-12] which have shown that steam explosions can occur at small (20 g) and intermediate (20 kg) scales, for iron, iron-alumina, and corium melts.

The steam explosion phenomenon can be conceptually divided into four stages: (a) fuel-coolant coarse premixing; (b) explosion triggering; (c) explosion propagation, and (d) expansion (see Figures 3.2.3-1a and 3.2.3-1b).

Fuel-Coolant Coarse Premixing. In this phase, the hot molten material (often called corium) contacts the colder, more volatile liquid coolant (water) and the fuel subdivides into smaller fragments, interpenetrating the coolant over a relatively long span of time (on the order of a few tenths to one second). This "premixing" occurs when the heat transfer between the fuel is quiescent (e.g., film boiling heat transfer). A breakup to a particle size of about 1 cm in diameter seems to be necessary for the more violent stages of the steam explosion to occur. Even in the absence

of the explosive phenomena, this stage is important for steam and hydrogen generation, and debris bed formation. It was discussed in the previous Section (3.2.3.2.2.2).

Explosion Triggering. Rapid heat transfer between the fuel and coolant is initiated or "triggered" by near liquid-liquid contact at fuel temperatures substantially above the coolant boiling point. This film boiling collapse may be initiated by contact of the falling debris with the cavity floor, or by pressure disturbances due to falling objects, or simply by the noise level of the boiling pool.

Explosion Propagation. The rapid local heat transfer initiates fuel fragmentation, which increases the heat-transfer area. This further increases the heat-transfer rate, accelerating fuel fragmentation, transferring the fuel thermal energy to coolant in the vicinity, and vaporizing it at high pressure. If the fuel coolant mixture is large, this explosive heat transfer can spatially propagate through the mixture, producing high-pressure shock waves much as in a chemical explosion. The time scale for these events is of the order of 1 ms, and fuel fragments of the order of 10^{-4} m. diameter are typically produced.

Explosion Expansion. The high pressure coolant vapor then expands and does work on the surrounding cold liquid. The conversion efficiency between the thermal energy in the hot vapor and mechanical energy in the accelerated liquid is much lower than the Carnot efficiency, however, because the low density, high-temperature vapor is accelerating a high density, low-temperature liquid. The result is a classic Rayleigh-Taylor surface instability, resulting in rapid breakup of the interface, mixing between the hot and cold fluids, and rapid recondensation of the vapor. Net efficiencies observed in the Sandia experiments (final mechanical energy divided by initial thermal energy) range from 3 percent down to less than 1 percent. However, the explosion efficiency is expected to depend on the degree of confinement, and on the size of the interaction zone (in these respects, it resembles a chemical explosion). The UKAEA PWR Degraded Core Analysis,[13] for example, proposes 4 percent as a reasonable estimate of a reactor scale ex-vessel steam explosion. (Broad uncertainty bands are also proposed in association with this estimate.)

Numerous attempts have been made to model the steam explosion process, ranging from hydrodynamic simulations to simple applications of engineering correlations taken from conventional heat transfer studies. The subject is still poorly understood, and considerable controversy exists among specialists in the field. The crucial question for our purposes is whether, and when, a steam explosion can occur.

CONCEPTUAL PICTURE OF FUEL-COOLANT MIXING

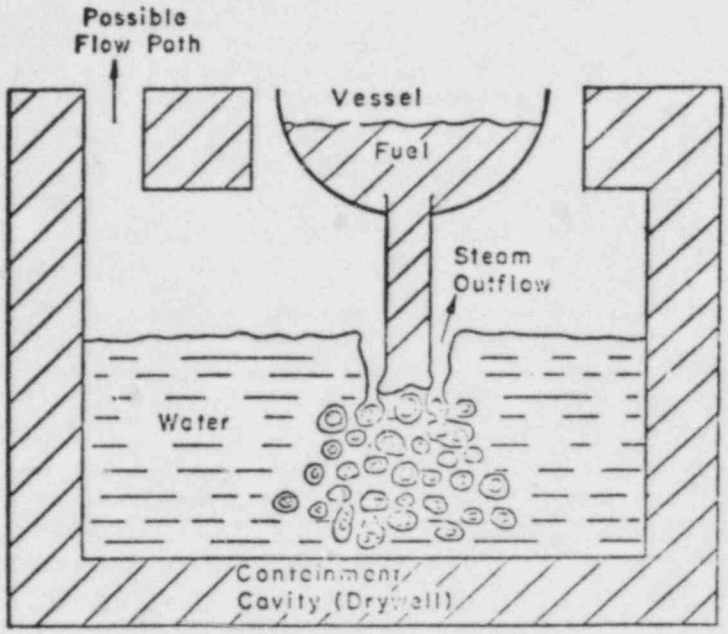

Figure 3.2.3-1 A

CONCEPTUAL PICTURE OF STEAM EXPLOSION

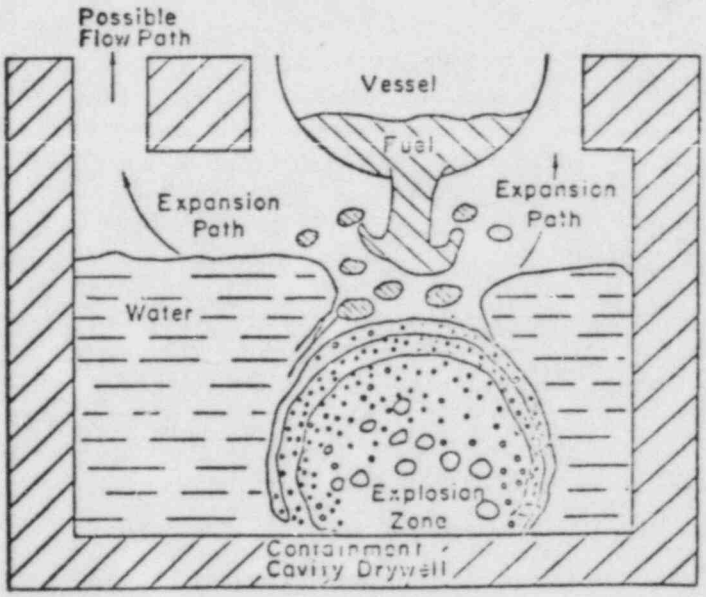

Figure 3.2.3-1 B

Figure 3.2.3-1. Conceptual Picture of Ex-Vessel Steam Explosion
a. Coarse Premixing Phase
b. Explosion propagation phase

Criteria for excluding the possibility of very large steam explosions have been proposed, based on the difficulty of achieving the initial coarse fragmentation and mixing required for the explosion to occur.[14,15] However, as pointed out in [16] and [13], it is not possible to apply these scaling arguments with any confidence to the situation of interest.

What is most important for our purposes is the knowledge from experiments [12] that intermediate scale (20 kg) drops of stainless steel and smaller (5 kg) drops of Corium into water can sometimes (but not always) result in steam explosions. In the Model Recommendation section, this phenomenon will be treated as highly uncertain, but too important to exclude from consideration. Thus a variety of options for determining whether a steam explosion will occur, what the energy might be, what the final fragment size will be, and when the event is initiated, will be proposed for inclusion into MELCOR, with actual selection of the option to be used left to the analyst.

3.2.3.2.3 MARCH-HOTDROP Features

The only current model available for FCI phenomena that occur in containment is the MARCH 1.1 computer program;[16] specifically the HOTDROP subroutine.* After the reactor vessel fails, the core debris is assumed to fall instantaneously onto the containment floor under the vessel, and to react with any water that may be present there. The core materials are assumed to be in a particulate form suspended in the water pool, such that there is no interaction between any of the fuel droplets. The initially molten droplets transfer energy to the water first raising its temperature to saturation and then vaporizing it. At the same time the fuel debris gains energy by the fission product decay heat and any metal-water reactions that may occur at its surface. HOTDROP models only consider zirconium metal oxidation. This physical picture of fuel-coolant interaction is only considered when water is present, and continues to be used until the debris is quenched to the water temperature, or the water in the cavity is completely vaporized, at which point a molten core-concrete interaction begins (this is modeled by the INTER computer program).

Since there is no interaction between fuel debris particles, the energy balance for an isolated fuel droplet is considered and multiplied by the number of droplets, N, where

*Recently, a number of new models have been developed for use in MARCH 2.0. Since this project is not complete, and documentation for the new models is not yet available, they will not be discussed in this assessment.

$$N = \frac{V_f}{\frac{4\pi}{3} R_f^3} \quad .$$

Here, V_f is the fuel volume and R_f is the user input fuel droplet radius. The energy equation for a single droplet is given by

$$\frac{4}{3} \pi R_f^3 \rho_f c_f \frac{dT_f}{dt} = Q_D + Q_{CHEM} - Q_w \qquad (3.2.3\text{-}8)$$

where T_f, ρ_f, and c_f are the fuel temperature, density and specific heat and where Q_D and Q_{CHEM} are the decay and chemical heating powers, respectively. The heat transferred from the droplet is

$$Q_w = h_{TOT} (4 \pi R_f^2) (T_f - T_w) \qquad (3.2.3\text{-}9)$$

where the heat transfer coefficient is a combination of the thermal resistance in the fuel droplet (assumed to be given by a steady state production model $^{5}k_f/R_f$) and that due to surface boiling, h_b

$$h_{TOT} = \frac{1}{\frac{R_f}{5k_f} + h_b^{-1}} \quad .$$

The value, h_b, is given by a correlation for transition boiling and nucleate boiling from a cylindrical wire (the film boiling regime is neglected). Q_D is given by a decay power curve correlation, while Q_{CHEM}, due to the zirconium-water reaction, is determined by the rate of diffusion of oxygen to the zirconium metal. The fuel droplet is an homogeneous mixture of uranium dioxide, iron, zirconium and zirconium dioxide. The oxidation rate and exothermic chemical energy release rate equations are based on a solid state diffusion correlation (either Baker-Just or Cathcart-Powell) computed for diffusion through the spherical shell.

There are a number of shortcomings to the HOTDROP model.

1. Instantaneous fuel discharge is assumed and transient mixing phenomena between the fuel and coolant are neglected;

2. Steam explosions are not considered;

3. Iron and chromium oxidation is neglected;

4. Fuel debris dispersal during debris quenching is neglected;

5. Interaction between debris particles is neglected;

6. A molten core-concrete interaction can only occur in the absence of water or if the user of the program skips the HOTDROP model (IHOT = 2 or 3).

Additional discussion of this model and its limitations can be found in [6]. Such a model, although simple and easily understood, is inadequate for MELCOR, particularly in regard to the hydrogen and steam source terms and fuel debris dispersal.

3.2.3.3 Wet Cavity Debris Bed Behavior

The presence or absence of water in the reactor cavity following the initial interactions is a fundamental branch point in the analysis of event sequences. If water is present, there is a second major branch point: either the debris is primarily in the form of a porous, boiling rubble bed, or there is a substantial consolidated layer of core material (mostly molten) at the bottom of the cavity (possibly in addition to an overlying rubble bed). In either case, the presence of the overlying water layer probably has a profound effect on the radiological source term, and on the course of thermal-hydraulic phenomena.

The discussion to follow is based on the conceptual picture of multiple layers in the reactor cavity shown in Figure 3.2.3-2. Not all layers will be present in all situations. The key issues are steam and noncondensible gas generation, debris coolability, and concrete erosion.

3.2.3.3.1 Debris-Water Interactions

Melt release from the reactor vessel can result in either a bed of hot particulate debris or a molten pool of core materials. The hot particulate debris will attack the concrete or remelt if it is not quenched by water. The molten pool may undergo severe structural changes if water

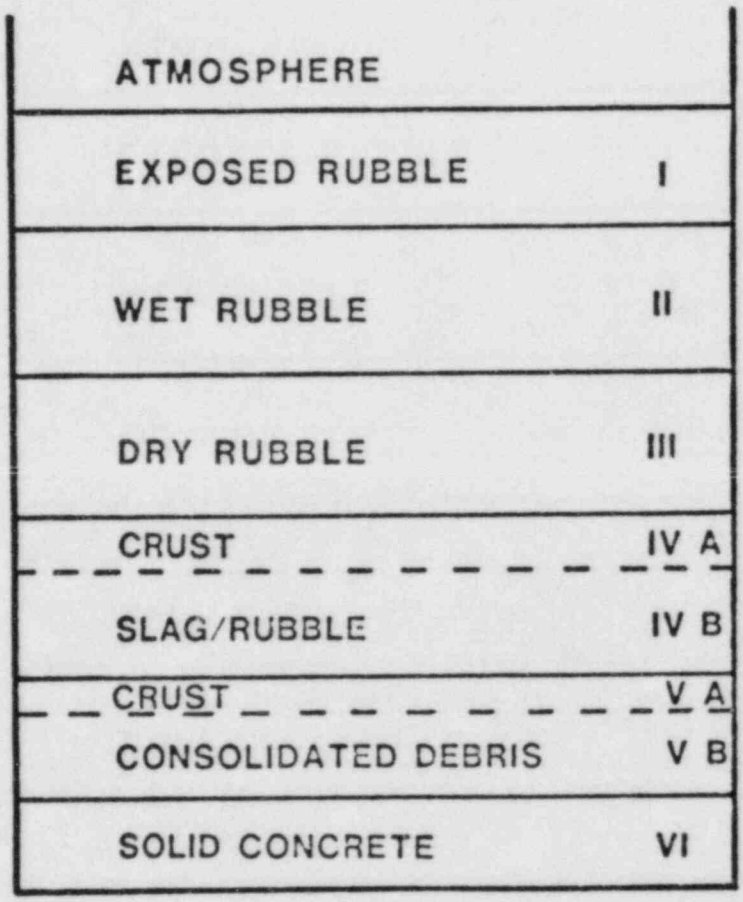

Figure 3.2.3-2. Schematic Diagram of Layered Structure of Wet Cavity

is introduced onto it. This section discusses the interactions of water with particulate debris and with a molten pool.

3.2.3.3.1.1 Determination of the Incipient Dryout Power

Figure 3.2.3-3 depicts boiling and dryout in a volume-heated particle bed submerged in a pool of water and resting on an impermeable support. The liquid must enter the bed from an overlying pool against the resistance of upward-flowing vapor. For simplicity, all the liquid is assumed to be at the boiling point so that heat is removed solely by boiling. Experiments show that channels form at the top of the bed if the particles are small (less than about 1 mm). These channels are typically small and negligible for thick LWR beds, but may be important in interpreting data from small-sized experiments. The vapor in the debris flows upward while the liquid flows downward into the bed. The vapor is driven from the bed by the pressure developed as it boils. The liquid is pulled into the bed both by gravity and by capillary force. If these two forces are sufficient to overcome the frictional forces of the upward-moving vapor, steady state boiling can occur throughout the bed. However, for high-power generation rates within the bed, the flow of liquid is retarded sufficiently that all of it vaporizes before it reaches the bed bottom. In such a case the bottom of the bed becomes dry. The bed power at which some part of the bed just becomes dry is called the dryout power. A measure of the dryout condition is the dryout heat flux, defined as the total bed power at dryout divided by the bed top (cross sectional) surface area. (Note that this is not the heat flux per unit area from the surface of an individual particle.) Often powers only moderately above the incipient dryout power will cause a large fraction of the bed to become dry. Thus, at these powers only a small fraction of the bed can be quenched. Decay heat removal capabilities from the dry portion of a debris bed is much reduced relative to the boiling zone. Because of the low thermal conductivity of dry debris, the low efficiency of radiation at low temperatures, and the low vapor flow rates expected, high temperatures can be achieved over short distances, and initially much of the dry zone can heat at near adiabatic rates. Thus dryout marks a sharp change in the coolability of debris and indicates the potential for prolonged thermal attack on the concrete. Many experiments have attempted to simulate dryout in reactor debris (see Appendix 3.2-B). In most of these, inductive heating of single-sized metal spheres has been used to simulate the nearly uniform volumetric power of decay heat. These experiments (and some theoretical considerations) have shown that the dryout heat flux generally increases with increasing particle diameter, bed porosity, ambient pressure, and

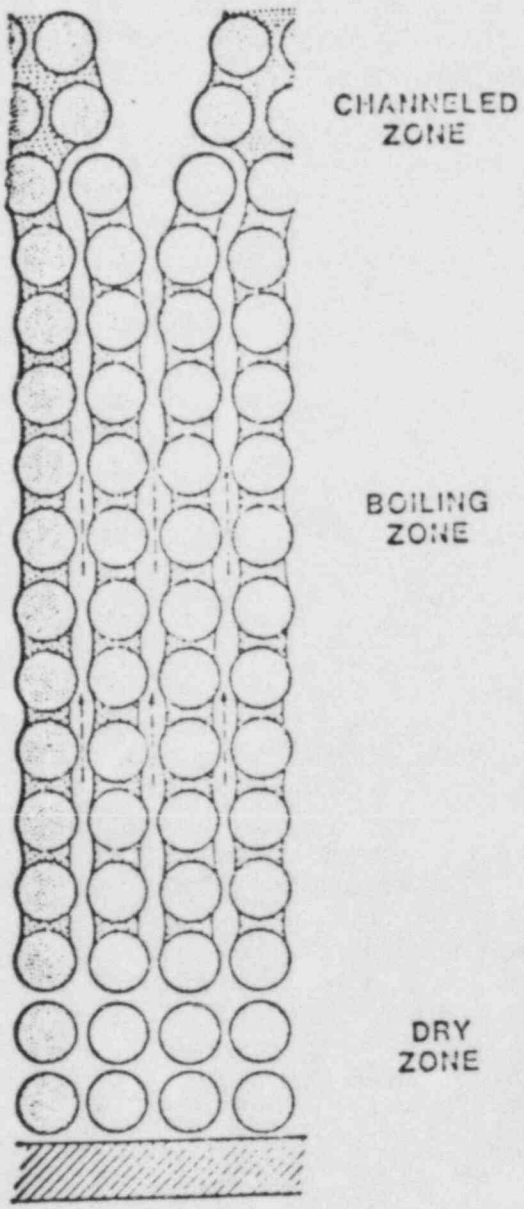

Figure 3.2.3-3. Volumetrically Heated Rubble Bed on Impermeable Support

liquid mass flux entering the bottom of the debris (as might occur if the bed were on a porous support). The dryout flux is essentially independent of bed thickness for deep debris, but starts to increase as the debris becomes shallow. Debris stratification (in which the average particle diameter varies with elevation) can strongly decrease the dryout flux if the small particles are at the top of the bed.

The debris in the reactor cavity or on the reactor floor may consist of particles ranging from less than 0.1 mm to tens of millimeters or more, with a debris thickness of as much as 1 to 2 meters, porosity from 30 percent to 60 percent or more, and ambient pressures from 1 to 10 bars. The debris may be mixed or stratified, with or without gas or liquid entry from below. The flow regimes and important phenonema are different at the different ends of the parameter ranges described. A good debris cooling model must be able to handle all the regimes and be able to identify where changes in behavior occur.

3.2.3.3.1.2 Debris Bed Dryout Models

Since the start of dryout marks the division between benign coolable debris and debris which can heat, remelt, and attack concrete or steel, considerable research has gone into developing dryout models (see Appendix 3.2-B). The simplest models are based on "flooding" correlations developed in the chemical industry. Flooding occurs in a rubble bed when liquid enters the top of the bed, gas enters the bottom, and the gas flow is just sufficient to cause some of the liquid to overflow the container. All flooding correlations have been based on beds with large particles, and so all dryout models derived from them are restricted to large particles (i.e., the turbulent flow regime). These models usually fail for particles smaller than 1 mm. Dryout models for small particles (laminar flow regime) have been developed for Liquid Metal Fast Breeder Reactor (LMFBR) accident debris. These models have been based on first principals and have combined conservation laws for mass, momentum, and energy to obtain dryout criteria. The primary challenge is to include all the important phenonema and choose the proper relations in describing those phenonema. For small particles and moderately shallow beds, capillary force can draw liquid toward a dry zone even more strongly than gravity, and this effect must be included in the modeling. Channels where the vapor has pushed back the particles and opened a wide flow path occur at the top of the bed and are important in shallow beds. These small-particle models usually fail for particles larger than 1 mm.

Advanced models have been developed which combine laminar and turbulent flow in the conservation formalism of the LMFBR small-particle models. Some are one-dimensional and give a detailed description of the liquid fraction within the bed as a function of elevation, predict the thickness of a steady state dry zone when the power is above the incipient dryout power, and allow for liquid flow entry into the base of the bed. A one-dimensional model is needed to determine the effect of stratification on dryout.

A comparison of the dryout predictions of various models with experimental data is made in Appendix 3.2-B. The best model can predict nearly all of the measured dryout fluxes within a factor of two and most of it within 50 percent.

3.2.3.3.1.3 Quenching of Hot Particulate Debris

The quenching of hot particulate debris by water is a dynamic process involving the counter flow of liquid and vapor, as well as the heating of the dry particles by decay heat and the heating of the concrete below the debris. Since the rubble bed is expected to be relatively flat (numerous settling processes ensure this [17]) and the initial boiling rate should be much higher than the dryout flux, we expect the bed to be initially dry. A quench front then moves down through the bed from the overlying pool.

Steady state dryout models describe the maximum amount of heat or vapor flow which can be removed from a particle bed while still allowing liquid to enter the bed (cf. (3.2.3.3.1.2)). Thus they can predict whether or not debris can eventually be quenched, assuming no bed alterations occur during the quenching process. The dryout models also provide a good first estimate of the rate at which a quench front will progress downward. The average heat removed from the bed during quenching is probably related to the dryout flux since the liquid entering the bed is restricted by the vapor leaving it in the quench process just as it is near incipient dryout. However, initially most of the vapor is produced at the bottom of the quenched zone. This is more like a bottom-heated bed than a volume-heated bed. Experiments have shown [18, 19] that the dryout flux for a bottom heated bed is half that of a volume-heated bed for large particles. As the quench progresses, boiling from decay heat in the quenched zone slows down the quenching rate, the volumetrically-produced vapor becomes more important, and the bed would tend toward a volume-heated bed.

An important phenonemon noted in recent quench experiments by Cho et al.[20] at Argonne, and by Ginsberg et al.[21] at Brookhaven is the rapid quenching of a central column of the debris by a finger of liquid while the

surrounding annulus remains hot. After the central finger reaches the bed bottom, the water quenches the annulus from the bottom upward. The time to quench the entire bed is close to the sensible heat in the bed divided by the dryout flux times the bed area. However, the central quench occurs in about one third of the total quench time. The central quench time is important since it would halt the heatup of the dry debris and the concrete.

Another feature of the two-stage quench process is that while the fingering quench is occurring, steam is passing superheated debris (which is being kept hot by decay heat). If the temperatures are high enough, metal in the debris will be oxidized during this process. This will add heat and hydrogen to the system (as during the in-vessel core degradation process) and will reduce the quenching rate.

During the quench process the debris is being heated by decay heat. If there is no steam source below the dry region, heat transfer in that region will be primarily by conduction and radiation. Initially conduction dominates, but at higher temperatures radiation between the particles increases the effective conductivity several times. Because of the low thermal conductivity of dry particulate debris (many times lower than oxide alone), much of the dry zone will heat adiabatically. The quench rate will slow considerably as it enters levels with hotter particles. (This feature has not been seen in quenching experiments [20, 21] because they have not been volumetrically heated during the quench.)

A dynamic "sharp quench front" model has been developed for the MEDICI code which includes all the processes discussed in this section. (Quench front progression, decay heating of dry zone, hydrogen generation, quench front fingering.) Results from a representative calculation with the sharp quench front model are shown in Figure 3.2.3-4.

Note that the curvature in the first part of the front motion is due to decay heating of the dry zone, which slows the front. A complete description of the model and the parameter choices for Figure 3.2.3-4 is given in Appendix 3.2-C. Ginsberg et al.,[21] have developed a similar model for interpreting their quenching experiments, though decay heating is not considered.

The sharp quench front assumption is probably a reasonable approximation insofar as it affects steam generation and debris bed temperature. However, it is inadequate for modeling hydrogen generation since the oxidation of metal requires the simultaneous conditions of high surface temperature and presence of steam. An approach for estimating hydrogen generation at the quench front will be discussed in 3.2.3.3.2.

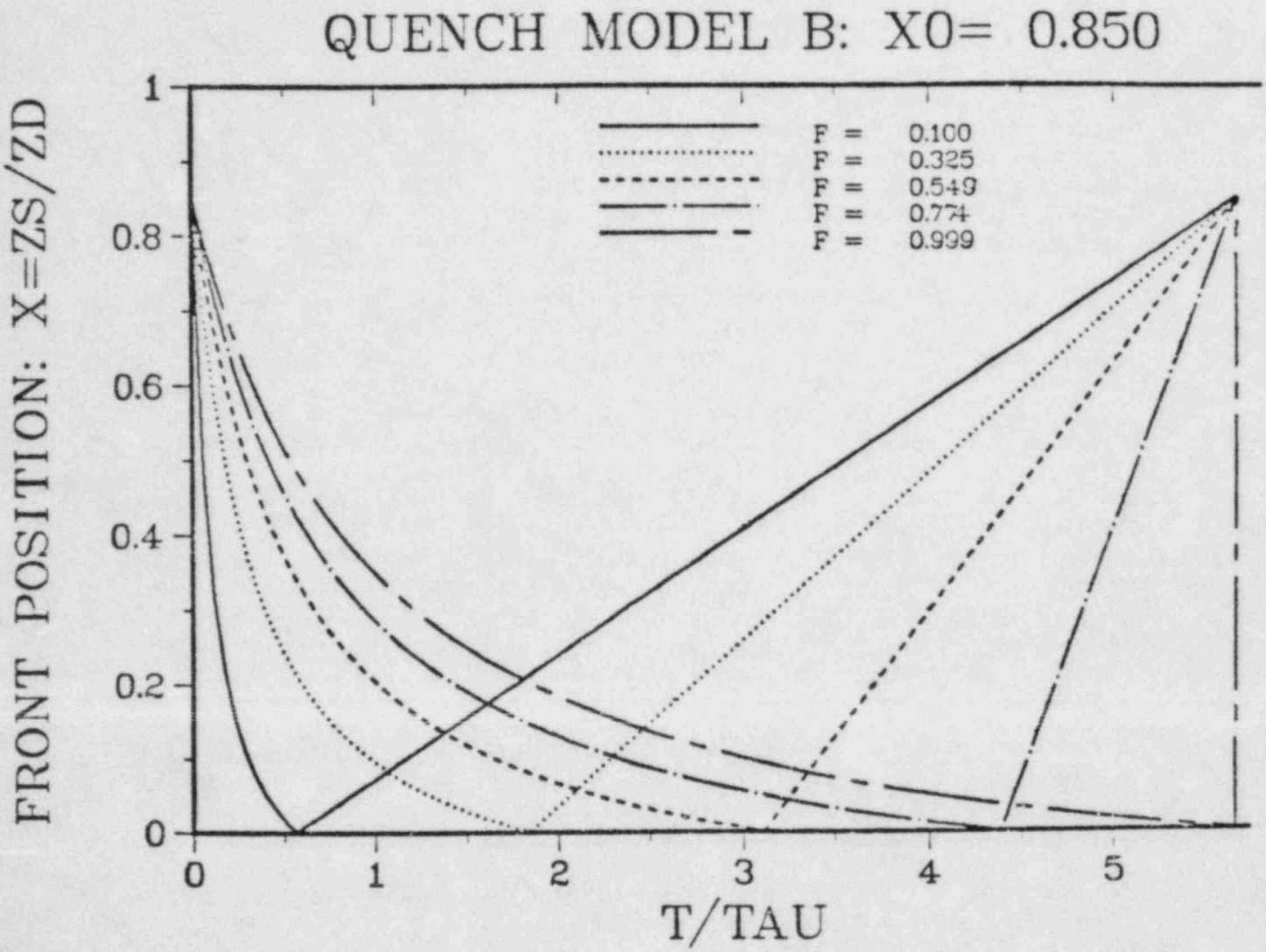

Figure 3.2.3-4. Motion of quench front predicted by sharp quench front model described in Appendix 3.2-C. The second front moving upward quenches the channels between the initial quench front fingers. Z_S is the quench front height, Z_D is the dryout height, XO is the initial value of X, T is time, Tau is the characteristic quench time, and F is the fraction of the initial enthalpy quench to the total.

3.2.3.3.1.4 Postquench Considerations

A final concern of quenching particulate debris is keeping it cool after it is quenched. As long as a water supply is maintained and the bed structure is not changed, a fully quenched bed should remained cool, and attack of the concrete will be avoided. However, if the coolable debris bed is formed from the initial melt release from the reactor vessel, debris formed from the secondary (continuous) release of residual core materials may cause the debris to dry out and attack the concrete. The slow secondary release may comprise on the order of 10,000 kg of melt over a period of hours. If the release comes in one thousand 10-kg drops, there may be as many as 1000 small steam explosions (depending on the ambient pressure and void fraction in the pool). Assuming the explosions are small enough to allow the water to remain in the reactor cavity, each event will create fine debris which will settle on top of the coolable debris, creating a stratified bed.

Models and experiments for stratified beds indicate that they are not easily cooled. In deep beds, the dryout criterion is established by the top layer of particles, which in this case is composed of small particles. If the debris is essentially one-dimensional, the top layer will inhibit the downward flow of water sufficiently to cause nearly the entire debris bed to dry out, even though it had previously been cooled. However, in a two-dimensional bed there may be regions where the liquid can bypass the small-particle layer, travel horizontally, and help cool the debris below the layer. A model which allows liquid flow from below is a start for describing this situation, but a two-dimensional model is really needed. At present, no such capability exists.

3.2.3.3.1.5 Quenching a Molten Pool with Water

Quenching a large molten pool with water is another poorly understood phenomenon. Important considerations are the stability of a fuel crust between the water and the melt, the size of the water and melt pools, and possible external perturbations, such as small steam explosions from secondary melt releases coming from the reactor vessel.

That a molten pool-water interface might be naturally unstable to progressive mixing, fragmentation and quenching is suggested by experiments using simulant materials; e.g., the experiments by Theofanous.[43] The role of a sparging nitrogen gas flow through both the "melt" (water) and the "coolant" (liquid nitrogen) was found to be of critical importance in causing the surface disruption process to proceed to full quenching of the "melt."

On the other hand, when prototypical, rather than simulant materials are used for such experiments, the interface is found to be stable. In the Transient Water Test Series, Tarbell, et al.[22] introduced water on top of a 20-kg iron-alumina melt at 2700°K. Initially the water seemed to boil fairly slowly as in film boiling. As the system cooled, a more active nucleate boiling regime was entered, which also slowed with time. But the gas generation rates and the rate of melt penetration of the concrete were not affected by the addition of water. Similar results were observed in experiments at ANL by Spencer, et al.,[44] which had no gas flow from below. If such behavior is typical of large melts, the primary effect of adding water might be the trapping of aerosols generated by the melt-concrete interaction. Quenching of the melt would not occur.

Another consideration in quenching a large melt is the possibility of small "external" steam explosions in the overlying pool. On the order of 10,000 kg of core materials will probably continue to melt and fall from the reactor vessel after the initial primary release of materials. Experiments show [24] that when 10 kg of molten oxide drops through a water pool, it fragments and a small steam explosion is sometimes (but not always) triggered when the melt contacts the pool bottom. These "small" steam explosion were enough to blow the debris 10 meters into the air in the experiments, but are probably not enough to clear the cavity of water. Melt releases on the order of 10 kg are not unreasonable during the slow melting of 10,000 kg.

If these secondary melt releases caused steam explosions in the water pool above the primary melt pool, the pressure generated could push the melt down strongly at one location, causing it to rise up strongly in another. Mixing of the melt and the water might then be induced. The molten pool could be fragmented and perhaps dispersed after these events, and the question of quenching hot particulate debris may be raised again.

3.2.3.3.2 Debris-Gas Interactions

Two processes are important for Debris-Gas Interactions. They are heat transfer and the generation of flammable gases by oxidation of metallic melt constituents. The processes which occur when the pool is molten are discussed in Section 3.5. However, there is also significant potential for hydrogen generation in the rubble bed.

There are two zones (I and III in Figure 3.2.3-2) in which the debris may be hot enough and in good enough contact with a steam flow for significant hydrogen generation

to occur. If there is a dry zone above the core-concrete interaction zone, it could be extremely hot, and the steam and CO_2 from the CCI could be reduced to hydrogen and carbon monoxide. Similarly, if the water level is below the bed height, a dry zone will exist above the pool. The upper dry zone (designated the "exposed" layer in Figure 3.2.3-2) is likely to be much cooler than the lower one, but the steam flow rate is much higher, so it is necessary to calculate the gas-solid heat transfer and hydrogen generation rate in this region.

A great deal of work has been done on in-vessel analysis of metal oxidation in a steam environment, particularly for zirconium, but also for stainless steel. An excellent review is contained in Chapter 4 of Reference [25]. Furthermore, the subject is discussed in some detail for in-vessel model in Section 2. Therefore, the discussion here will be limited to a description of models to be recommended for the cavity model. Similarly, the emphasis will be on hydrogen generation, rather than CO generation; presumably similar formulations for CO_2 reduction phenomena could be formulated.

In the presence of an abundance of steam, a number of correlations for the reaction rate in solid-state diffusion-limited conditions have been deduced from experimental data. The best known of these is the Baker-Just correlation for zirconium.[26] If W is the cumulative mass gained per unit surface area, and t is time, then this correlation specifies that

$$W^2 = K_z t \qquad (3.2.3\text{-}10)$$

$$K_z = 2.643 \times 10^8 \exp(-1.905 \times 10^8/RT) \qquad (3.2.3\text{-}11)$$

where $R = 8.314 \times 10^3$ J/Kmol °K.

For stainless steel, a similar parabolic rate law has been observed at the temperatures of interest for our problem, (and for relatively high oxidation fractions) by Bittel, et al.[27] Powers [28] has formulated their rate data into a correlation of the same form as (3.10) and (3.11):

$$K_s = 2.4 \times 10^8 \exp(-3.527 \times 10^8/RT) \; . \qquad (3.2.3\text{-}12)$$

The reaction rates quoted above are based on experiments with pure metals. The debris to be expected in the rubble bed is expected to be a mixture of zircalloy, steel, and fuel, so some assumptions must be made to adapt these results to the required analysis. This will be discussed in more detail in Section 3.2.5.3.2. Also discussed there will be the effect of a limitation on the steam supply to the surface.

The previous discussion related to sustained hydrogen generation in the two dry zones. There is, in addition, the potential for significant hydrogen generation at the quench front, where both high temperature and abundant steam are present. No experimental data exist for this process, and there are no tested models available. In 3.2.6.3.3.2, a model will be proposed based on the Baker-Just correlation and a quench zone thickness which is a variable parameter.

Since hydrogen generation is very sensitive to the temperature of the interaction region, it is necessary to follow the temperature of the gas and of the debris in the two dry zones. For the lower zone, gas-rubble heat transfer is also important for the proper treatment of the concrete surface. Considerable research concerning heat transfer between a flowing gas and a packed bed for the chemical processing industry. A correlation for heat transfer which corresponds to our problem has been developed by Martin.[29] There are simpler alternatives to Martin's formulas, however, which might be acceptable. Schlunder reviews the available options for packed bed gas-solid heat transfer in Reference [40].

3.2.3.3.3 Debris-Concrete Interactions

The interaction of hot debris, either molten or solid, with the concrete basemat of the reactor cavity, is of critical importance in safety analysis. In fact, it is so important that a separate section (Section 3.5) of this report is devoted to it. For that reason, the subject will not be discussed in great detail here. However, it is important to consider those aspects of core-concrete interactions (CCI) which are closely coupled to other phenomena discussed here. Of particular importance is the simultaneous existence of core-concrete interactions and a debris bed boiling in a water pool.

3.2.3.3.3.1 Simultaneous Debris Bed-CCI Configurations

The analysis of the full multilayer configuration shown in Figure 3.2.3-2 will be extremely difficult. It is useful to consider under what circumstances, if any, it is necessary to analyze the simultaneous behavior of a rubble bed and core-concrete interactions.

A number of potential configurations are unstable, i.e., can persist for a period of time which is short compared to other CCI phenomena. Suppose, for example, that a large molten debris pool is formed, and begins to erode the concrete. A layer of molten slag (light oxides and liquified concrete) forms over the debris layer. Even though the concrete above the debris is in contact with the overlying pool, it may not be cooled below the solidus temperature (pool boiling is limited in its ability to extract heat from a lower surface, whereas there is no corresponding limit to the rate at which the underlying debris can heat the concrete-water interface). Thus any crust forming on the top of the molten slag region may be extremely thin. Now suppose some quenched particulate debris descends to the bottom of the pool. As the debris collects on the thin crust, the weight will eventually collapse the crust, and the rubble will sink into the slag zone, and descend to merge eventually with the molten debris. These processes take place at a relatively rapid rate, and it does not appear profitable to model them carefully.

However, once the solid debris has found a new floor (either a solidified crust at the top of the consolidated debris region, or at the CCI interaction interface) the rubble bed can again form, now suspended partly in the concrete slag layer and partly in the overlying pool.

A similar sequence could even occur without the initial molten debris pool. A melt stream may be fragmented and solidified (via a steam explosion or by a less violent interaction), and the resulting debris bed may be coolable, in a technical sense, but to be assured of ultimate coolability, we must analyze the process by which full quench to the water temperature is achieved. Initially, the rubble bed will expel the liquid water, and the bed will be dry. The quench process is expected to occur by means of a quench front progressing from the top of the bed to the bottom. To determine if it is important to analyze the simultaneous motion of the quench front into the rubble, and the descent of the rubble into the CCI slag layer, some bounding estimates of the appropriate velocities can be used. We assume the rubble bed descends at the same rate as the concrete ablation front, and that the debris attacking the concrete has cooled to the quasi-steady state value associated with the decay heat. The key heat-transfer parameter is then the ratio of upward to downward heat transfer. We define

$$\beta = \frac{\text{heat transferred downward}}{\text{heat transferred upward}} \qquad (3.2.3\text{-}13)$$

For a one-dimensional layer of debris which is d thick, with decay power density of q w/kg, the steady state erosion velocity is given by:

$$V_a = \frac{\rho_d q\ d\ \beta}{\rho_m H_{ab}(1+\beta)} \qquad (3.2.3\text{-}14)$$

where $\rho_{d,c}$ are the densities of the debris and concrete, respectively, and H_{ab} is the heat of ablation of the concrete (which includes sensible heat). For a representative calculation, we assume the concrete is fully melted; we therefore take $H_{ab} = 4.0 \times 10_6$, $\rho_d/\rho_c = 1.4$, $d = 0.5$, and, for simplicity, $\beta = 1$. For decay heat we take a relatively high value, $q = 200$ w/kg. The result is $v_a = 1.76 \times 10^{-5}$ m/s. This value is, in fact, typical of ablation velocities seen in CCI experiments.

For quench front velocity, we use the sharp front model of Appendix 3.2-C. The dryout height is

$$z_d = \frac{\phi_d}{q\ \rho_{eff}} \qquad (3.2.3\text{-}15)$$

where ϕ_d is the dryout flux (w/m^2) and ρ_{eff} is the effective debris density (modified by the porosity). The quench front velocity is given by

$$v_q = \frac{\phi_d}{f\ \rho_{eff} H_d} \qquad (3.2.3\text{-}16)$$

where f is the quench fraction, typically found in experiments [21] to be about 0.3, and H_d is the enthalpy removed by quenching to the steady state (J/kg). The dryout flux is highly variable, depending principally on the diameter of the debris. Table 3.2.3.1 shows representative calculations for three particle diameters, d_ρ. (Assumptions: 0-D Lipinski model, deep bed approximation, 40 percent porosity, $H_d = 7.0 \times 10^5$, $\rho_{eff} = 5.4 \times 10^3$.)

Table 3.2.3-1

Representative Quench Velocities and Dryout Heights

d_p(m)	$\emptyset_d$(W/m^2)	z_d(m)	v_q(m/s)
0.01	5.0×10^6	4.63	4.0×10^{-3}
0.003	1.0×10^6	0.926	8.0×10^{-4}
0.0003	3.0×10^4	0.028	2.4×10^{-5}

A typical ex-vessel debris bed might be 0.5 m (e.g., see [D20], p. 291). The conclusion from this table is that if the bed is coolable, it is unlikely that significant concrete erosion can take place during the time the quench front is moving downward. We can apply a similar analysis to the rate at which partially solidified debris might remelt before the quench front arrives. A characteristic time for the quench front is obtained by dividing the dryout height by the initial quench velocity:

$$t_q = z_d/v_q = H_d\, f/q \qquad (3.2.3\text{-}17)$$

which is independent of $\emptyset_d$, and for the parameters of Table 3.2.3.1 is equal to 1155 seconds. Of course, decay heat will slow the front down, so this time might correspond to a coolable debris bed whose height is perhaps one half the dryout height. This can be compared to the characteristic time for adiabatic remelt from pure solid to pure liquid at the melting temperature:

$$t_{rm} = H_{fd}/q \qquad (3.2.3\text{-}18)$$

where H_{fd} is the heat of fusion of the debris. A representative value would be $H_{fd} = 2.8 \times 10^5$, which results in a remelt time of 1400 seconds, indicating that significant remelting could occur at the bottom of the bed before the quench front arrives. This result is independent of decay heat power and debris diameter.

$$g = t_q/t_{rm} = f\, H_d/H_{fd} \qquad (3.2.3\text{-}19)$$

is a measure of the amount that the melt fraction can change during the quench. For our parameters, it is 0.825. Thus, in the time that it takes for the quench front to penetrate to the bottom of a coolable debris bed (of approximately half the dryout height, debris at the bottom could heat up enough to change from pure solid at the melt temperature, to 82.5 percent molten, doubtless causing a collapse of the lower layer).

The conclusion is that for coolable debris beds, while significant erosion of the concrete during the quench period is unlikely, it is important to consider the simultaneous heatup and possible remelt of the lower zone. For uncoolable beds, of course all three processes must be considered simultaneously. Either the lower zone will remelt, then attack the concrete, or it will sink into the concrete first.

In either case, the rest of the dry zone will follow into the slag layer, and, as discussed earlier, even the saturated zone may be lost in the molten concrete.

As complex as this situation is, it is important to analyze, because it can persist for a long time (the entire debris bed presumably descends at the rate of the concrete ablation front) before the last of the rubble sinks into the concrete pool. One major concern is the boiling rate in the pool, because water inventory is crucial to the future course of events; i.e., it is critical to know if and when the cavity boils dry. Another reason this configuration needs to be modeled is that the rate of concrete erosion depends on how much debris collects in the concrete. Decay heat which is removed in the overlying debris bed is heat which otherwise may have contributed to the concrete attack. Thus, modeling the overlying debris bed may have the effect of substantially mitigating or terminating the core-concrete interaction below. Another difficult, but important question is whether it is possible for a strong concrete crust to form which can support the overlying rubble bed. If this is possible, and water remains in the cavity, that debris will be isolated from the core concrete interaction going on below.

The principal couplings between the CCI and debris bed behavior are (a) CCI gas flooding of the debris bed, decreasing the quench front velocity and the dryout height; (b) submergence of solid debris into the slag layer, isolating it from quench water; (c) reduction of CCI-generated steam and CO_2 by metals in the debris bed dry zone; (d) added heat to the rubble bed due to exothermic chemical reactions, also causing decreased dryout height; (e) cooling of the dry zone by CCI gases, preventing remelt; and (f) decontamination of CCI-generated aerosols by the overlying water pool. These phenomena will be discussed briefly in the following sections.

3.2.3.3.3.2 Water Migration in Concrete

If a concrete surface is exposed to a moderately intense heat flux, the first process which occurs is the release of steam from water trapped in the pores of the material. Since water boils at a lower temperature than the temperature at which concrete begins to melt, there are two distinct fronts of interest in the concrete: one is a dehydration front, where the water changes from liquid to vapor; the other is the onset of melt of the concrete. (There are actually a number of such fronts, but for the present purpose, this simple picture will suffice.) When the debris first contacts the concrete surface, these fronts are in the same location. The dehydration front, however, moves faster than the melt front because of the lower transition temperature.

As time passes, the dehydration front will slow down and eventually (assuming constant decay power level) a steady state will be achieved in which both fronts advance at the same rate. In the classification to be used in Section 3.3.3.4, this would be the "sustained" interaction regime, and the steam generation rate during this period is in the same proportion to other gas generation rates as in the original composition of the concrete. However, during the initial period, the steam generation rate is increased by the quantity of free water contained in the volume between the two separating fronts. Conversely, when the debris cools, the quantity of steam generated is less than a steady state model would predict.

A similar process occurs with respect to CO_2 release. The transition temperature for the breakdown of some of the carbonates in the concrete is significantly lower than the solidus temperature, so that generation of CO_2 can be an important process at temperatures between 600° and 1000°C. This gas can be reduced to CO, which, like hydrogen can threaten containment either by long-term pressurization, or by burning. The generation of CO has generally not been included in most models. The process is complicated by the fact that there is an oxidation-reduction reaction between hydrogen and carbon dioxide, so that modeling of these processes requires equilibrium analysis of all four gases simultaneously.

The fraction by weight of free water in typical concretes is not large (typically about 3 percent[30]), but this effect is nonetheless extremely important for consequence analysis. Accidents involving early containment failure due to hydrogen combustion contribute heavily to risk, and the core concrete interaction can be a larger source of hydrogen than in-vessel processes.[31] Experiments involving transient interactions of both simulant and real core materials with concrete have shown total hydrogen and steam production due to the dehydration effect to be often much larger than that due to steady state concrete decomposition.[30, 32]

For very high debris temperatures (i.e., high decay heat power densities) the erosion rate of concrete is high, e.g., 10^{-4} m/s. Under these circumstances, the time required for the melt front to achieve the same velocity as the dehydration front is not large. However, for intermediate temperatures (but above the debris melting point) the transition period is likely to be long enough for the enhanced hydrogen production to be important. For solid debris (as in the dry zone of a debris bed under a pool of water) the rate of steam evolution from the concrete is likely to be many times the quantity which would be predicted on the basis of the volumetric erosion of the concrete.

Physically, the water migration process is relatively well understood. The level of available modeling is quite good (compared to other cavity processes). In 1980, the DOE sponsored a code validation exercise to compare available computer codes. Reference [33] reports on the results of this exercise. All three of the water-migration codes performed reasonably well, but the USINT code was notably more accurate and also somewhat faster (30 hours of real time were run in $4.00 worth of computer time). Recently, a more robust and faster code has been developed for LMFBR analysis,[33] which uses essentially the same equations, but different solution techniques, including a moving grid. The USINT physical model is described in detail in Reference [33]. A simplified version of the USINT model has been coupled to a concrete erosion model for the CONTAIN code. This will be discussed in Section 3.2.3.3.3.5.

Another possible application for the water migration model involves wall heatup by radiational heat transfer from the hot pressure vessel. It is not clear whether this is an important source of water vapor to containment, but it may affect overall heat balance in the cavity. At any rate, if a water migration model is implemented, it should be possible to activate it for the radiational wall heatup problem as well as for core-concrete interactions. It should also be noted that in some circumstances the concrete removal mechanism is mechanical (spalling or crumbling) rather than melting. Existing MCCI models are not designed for this phenomenon.

3.2.3.3.3.3 Aerosol Generation and Removal

Copious production of aerosols has been observed in many CCI experiments.[30] Unlike the aerosols released from the primary system earlier in the accident sequence, the decay heat power density is low, since they are constituted principally of decomposed concrete materials. The total mass of aerosol generation due to CCI may exceed the mass of the aerosols released from the primary system by an order of magnitude. It is important to consider this source of aerosols for three reasons: (a) the dense, nonradioactive aerosols may wash out the radioactive aerosols by the agglomeration and deposition processes described in Section 3.8; (b) they may interfere with the functioning of some Engineered Safety Features; and (c) the CCI-generated aerosols may contain a considerable radioactive inventory possibly of different isotopic content from in-vessel aerosols, which must be tracked for the ex-plant source term.

As discussed in Section 3.2.3.3.3.1, the principal scenario of interest for this section is the simultaneous occurrence of a debris bed under water and a core-concrete interaction. Total aerosol emission for these situations

are expected to be quite small, because, first, the CCI is expected to be relatively slow, and second because the overlying pool is expected to remove all or most of the aerosols.

3.2.3.3.3.4 Classification of Interaction Regimes

When high temperature debris comes into contact with concrete, the concrete may spall some solid material. Then, as the thermal gradient decreases, the concrete will begin to melt and decompose, generating great quantities of gas (some of which are flammable) and aerosols (some of which are radioactive). When the debris is in the form of a molten pool, heat transfer to the solid concrete and through the melt layer is high and the interaction is vigorous, generating copious aerosols (possibly more than from the primary system, though far less radioactive). If the debris is solid, the reaction is slower, but must still be considered both as a source of pressurizing gas, flammable gas, and ultimate basemat penetration. The physical and chemical processes involved are highly complex, and highly variable, depending on the composition of the debris and of the concrete, and on the temperature or decay power.

Figure 3.2.3-5 shows the temperatures at which important transitions occur in the materials involved in the CCI. The melting point of pure UO_2 is around 2800°C, but the eutectic temperature is more relevant in describing the solidification of core materials in the cavity. Because of decay heating occurring both before and after melt release, temperatures of the core materials in the cavity could exceed 2500°C.

A range of temperatures is shown for representative concretes. Since these are composite materials, there is a continuous increase in melt fraction as the temperature increases from the solidus (lower temperature of the range) to the liquidus (upper temperature). Fuel materials (e.g., UO_2) are heavier than the metals (such as steel) which are expected among the debris. The mode of interaction of the descending CCI region is thus determined by the fuel temperature. Figure 3.2.3-5 illustrates that one must consider interaction of the fully molten concrete with both liquid and solid core material, interactions between solid core material and partially liquified concrete, and interactions between solid concrete and solid debris.

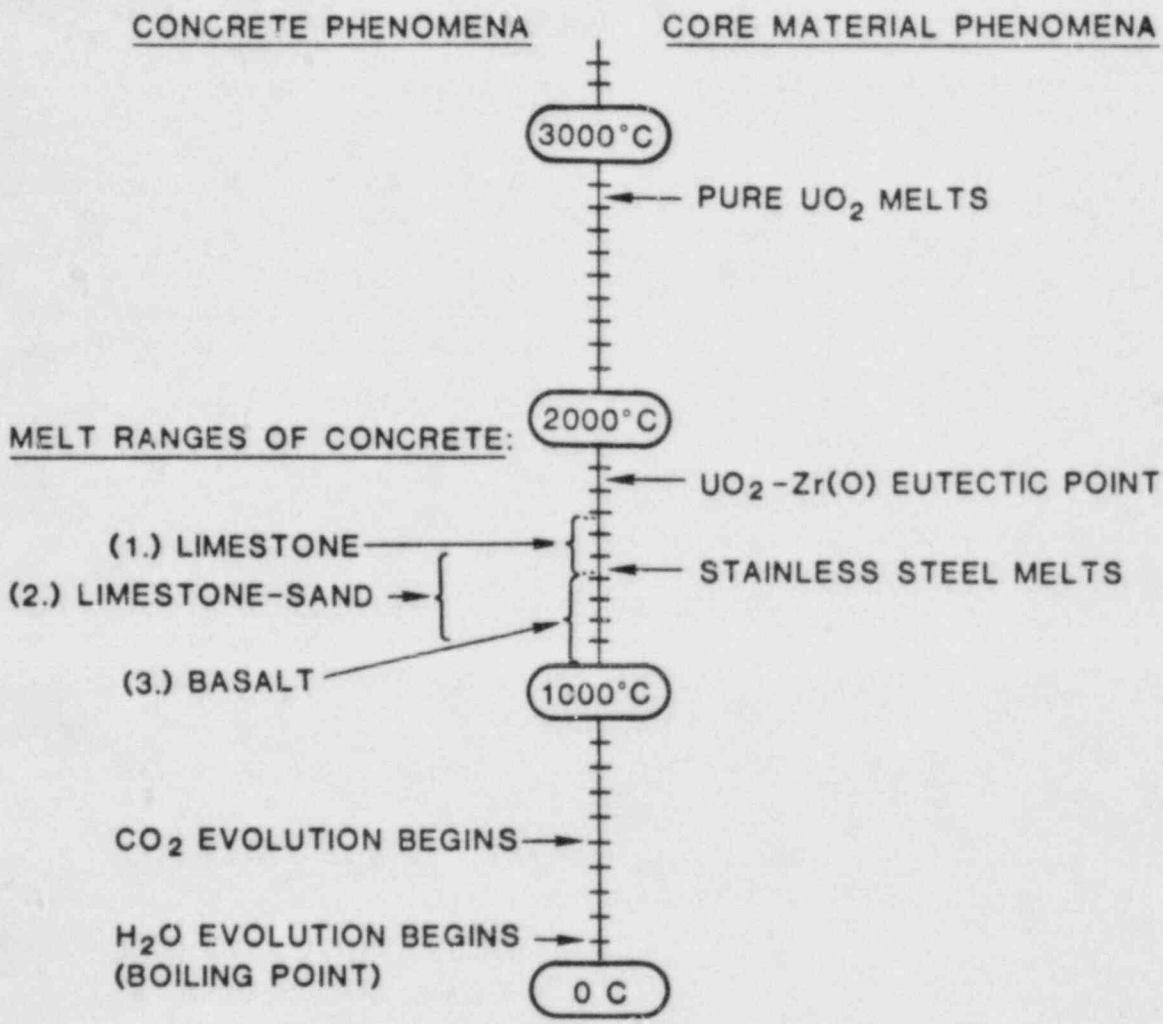

Figure 3.2.3-5. Transition Temperatures for Core-Concrete Interactions

To systematize the evaluation of models for CCI, we consider a number of parameter regimes for analysis.

Interaction Regimes

Regime 1: Initial attack, molten debris
Regime 2: Initial attack, solid debris
Regime 3: Sustained attack, molten debris
Regime 4: Sustained attack, solid debris.

Different threats are important for different interaction regimes, and different levels of modeling may be desirable. A tentative breakdown of the requirements in the different regimes is shown in Table 3.2.3-2.

For example, in regime 3, two-dimensional effects may be important, because there has been sufficient time for substantial erosion of the concrete floor to have taken place, but no enhanced steam generation is expected. On the other hand, in regime 1, a one-dimensional treatment may be acceptable, but it is not acceptable to ignore transient water migration effects.

Aerosol generation is important in regime 1, and also (to a lesser extent) in regime 3. It is of little importance late in time in regime 3, or in regime 4 because of the formation of a porous, solidified layer of slag over the interaction zone. In regime 2 the scenario is partly quenched solid debris under a water pool. The rate of attack is low, so copious aerosol generation is not expected, and furthermore, significant aerosol removal can be expected in the water pool.

In regime 4, the principal concern is basemat penetration. Flammable gas generation should be at a low rate because of the oxide barrier to steam and CO_2 diffusion at the debris surface. Noncondensible gas is expected to percolate up through the molten and porous-solid overlying layers, but the production rate should be low, and in many cases pressure should be dropping in containment because heat sinks are overcoming heat sources. (In a few cases, this may not be true, however.) Thus the principal concern in regime 4 is penetration velocity, though some attention should also be paid to total gas production rate.

It will be seen in the next section that no existing model can treat all of the required phenomena. The conclusion to be drawn from Table 3.2.3-2 is that it is possible to achieve a better coverage of the important phenomena by using different models in different regimes. In particular,

Table 3.2.3-2

Modeling Requirements in Different
CCI Interaction Regimes

REGIME	(1)	(2)	(3)	(4)
Aerosol Generation	yes	yes	yes	?
Flammable Gas Generation	yes	yes	yes	no
Non-Condensible Gas Generation	yes	yes	yes	yes
Water migration	yes	yes	no	yes
2-D Ablation	no	no	yes	no

we note that two-dimensional effects are important only in regime 3, which does not require a water migration model. This situation will be exploited in Section 5 on model recommendations.

3.2.3.3.3.5 CCI Models

A wide variety of computational models exist for the case of a molten debris pool interacting with concrete in a dry cavity. The first code to receive widespread use was the INTER code,[37] which has been the basis for numerous more detailed treatments. These include WECHSL, KAVERN, IMM, and CORCON-MOD1. In addition, the GROWS and GROWS-II have been developed independently. Most of these models are capable of treating the growth of the eroded region as a two-dimensional process. For basemat penetration considerations, two-dimensional effects are of critical importance, though total volumetric erosion rate is relatively insensitive to two-dimensional effects.[36] The most advanced of the U.S. codes is the CORCON code, which is discussed in substantial detail in Section VI.

However, no existing CCI code has the capability to do two-dimensional analysis including water migration in concrete. The models used in CONTAIN, on the other hand, include the water migration effect, but are only one-dimensional. The model used [38, 42] is based on the INTER model for concrete attack, and the USINT model for water migration.

As discussed in the previous section, the two-dimensional capability is probably unnecessary for situations in which water migration is important, e.g., before significant erosion has taken place. For these situations, the models implemented in CONTAIN would appear appropriate. For more vigorous attack, or when a quasi-steady state has been achieved, the more sophisticated two-dimensional models may be needed. Finally, there are regimes in which no existing model is appropriate. An example is the rubble bed descending through the concrete slag zone which has been created by a molten debris pool below. Some provision must be made in MELCOR to handle these cases, and Section 3.2.5 proposes an approach which at least has the virtue of allowing a systematic analysis of the phenomenological uncertainties.

3.2.4 UNCERTAINTIES IN PREDICTING THE OUTCOME OF CAVITY INTERACTIONS

The uncertainty in predicting the outcome of debris interactions in the reactor cavity can come from several sources. These sources include:

1. Uncertainties in initial or boundary conditions because of uncertainties in the prediction of preceding activities. These may be called inherited uncertainties.

2. Inaccuracies in modeling known processes (i.e., where the best model still fails to agree with all the data). These may be called modeling uncertainties.

3. The failure to foresee an accident path. These may be called path-ignorance uncertainties.

An example of an inherited uncertainty for reactor cavity processes is the location of the reactor vessel breach and the amount of melt at the time of breach. An example of a modeling uncertainty is the amount of fragmentation when a large melt mass drops into a pool of water. An example of a path-ignorance uncertainty is the assumption that introducing water into a reactor vessel will cause temperatures to decrease, when actually it will cause the opposite in some cases because it supplies steam for oxidation in steam-starved situations. Path-ignorance uncertainties can only be identified in retrospect, but they may reside in out-of-date or simplified analyses.

The combination of these uncertainties becomes the inherited uncertainty for the next process in the sequence, although, in practice, the path-ignorance uncertainties are often omitted. There are other uncertainties such as uncertainties in material properties, ignorance of certain construction details, and the stochastic spread in the outcome of supposedly identical events, but these are all small compared to the three uncertainty groups just described.

3.2.4.1 Inherited Uncertainties

Inherited uncertainties are the primary responsibility of the analyses preceding the one under consideration. However, the range of their impact can be determined by parametrically varying the initial and boundary conditions over the range that the previous analyses conclude is reasonable. A clear definition of what are the important input parameters for a given process will help to limit the number of inherited uncertainties that need be considered.

Important input parameters for debris interactions in the reactor cavity are:

1. Amount, flow rate, composition, oxidation state, and temperature of molten core materials at the time of reactor vessel breach.

2. Steam and gas flow from the vessel as a function of time.

3. Amount of liquid water in the reactor cavity at the time of the initial melt release, and subsequent influx from outside the cavity.

4. Amount and release rate of core materials melting after the initial melt release.

Obviously, the reactor cavity geometries are also important inputs, but they are, at least in principle, not subject to much uncertainty.

Items 1 through 2 above are important for determining how the melt is released from the vessel and they strongly impact aerosol formation, debris dispersal, and the subsequent contact mode of the melt with water. Item 3 influences the potential for steam explosions and the ultimate coolability of the debris. Item 4 affects particulate debris coolability and may strongly alter the configuration of a water pool on a molten pool.

The above items refer to inherited uncertainties relevant to the reactor cavity interactions as a whole. In a similar manner, each of the reactor cavity processes is subject to inheriting uncertainties from a previous reactor cavity uncertainty. Thus it is important to identify the most influential input parameters for each reactor cavity process. Table 3.2.4-1 lists the most influential input parameters for each of the major cavity processes.

Table 3.2.4-1

Primary Influential Input Parameters
for the Major Cavity Processes

Process	Input Parameter
Pressure-Driven Melt Initial Release	Initial Pressure
	Liquid Inventory and Temperature in Vessel
	Breach Size
	Mass, Temperature, and Composition of the Melt Ejected
	Cavity Geometry
Melt Sweepout from Reactor Cavity	Melt Mass
	Steam Flow Velocity and Duration
	Cavity Geometry
Interactions from a Large-Melt Entry into a Water Pool	Melt Mass, Temperature, and Composition
	Water Depth
	Water Pool Area
Particulate Debris Quenching and Steady-State Coolability	Debris Configuration
	Particle sizes and stratification
	Debris thickness and power
	Initial Debris Temperature
	Ambient Pressure
	Bottom Boundary Condition
Large Molten Pool Quenching	Melt Mass, Temperature, and Composition
	Water Mass
	Water Entry Mode
	System Perturbations (e.g. small steam explosions)

3.2.4.2 Modeling Uncertainties

The amount of modeling uncertainty present in a process is a function of both the complexity of the process and the amount of effort that has been put into the modeling. Unfortunately, debris interactions in the reactor cavity are fraught with both complex processes and poorly studied ones. Steam explosions have been extensively studied, but they are so complex that considerable uncertainty still surrounds their modeling. The removal of molten core materials from the reactor cavity by high-velocity steam is not as complex, but only superficial modeling has been performed and there is still much uncertainty as to how much material might be removed.

The impact of modeling uncertainties can be estimated by using simple models which bound the best estimate or preferred model. This only need be done where the preferred model fails to produce reasonable agreement with most of the data, or where very little data exists to support the model. Table 3.2.4-2 lists the cavity processes for which the best-estimate model is not very accurate. The bounding models for these processes are discussed in Section 3.5.

3.2.4.3 Path Ignorance Uncertainties

Path-ignorance uncertainties stem from accident paths which are either ignored in a particular code for simplicity or which are not present because of ignorance of their existence. A good accident code should be able to accommodate new phenomena and processes easily in order to keep current as new accident paths are discovered by experiments or deeper analyses.

Initial versions of MEDICI will have some path-ignorance uncertainties for simplicity. (One example already discussed is the interaction of secondary melt releases.) However, the modular and well-organized structure of MEDICI will allow easy inclusion of these accident paths in later versions, as well as the inclusion of accident paths which may be revealed by future research.

Table 3.2.4-2

Cavity Processes with Inaccurate Models

Pressure-Driven Melt Initial Release
Melt Sweepout from Reactor Cavity
Interactions from a Large-Melt Entry into a Water Pool
Debris Dispersal Following Steam Explosion
Solid Debris-Concrete Interactions
Aerosol Generation in CCI and Removal in Water Pool
Large Molten Pool Quenching

3.2.5 MODEL RECOMMENDATIONS

The selection of appropriate models for MELCOR-1 and MELCOR-2 requires the evaluation of a number of difficult tradeoffs. It is desirable to use existing, fully tested models, but there is general recognition that it is essential to treat the problem with a higher degree of realism than that of the MARCH code. In the case of reactor cavity phenomena, the situation is particularly difficult, because experimental programs have recently provided an improved data base for many of the key processes, but there is still a severe shortage of tested models.

It was because of this quandary that the MEDICI project was initiated somewhat in advance of the rest of MELCOR. The goal is to provide a stand-alone code which will be a test bed for new models and for new combination of old models. At the time of writing, most of the models for the first version of MEDICI have been developed or selected, and implementation into an integrated code structure is underway. It is expected that development, testing and review of the MEDICI code will be accomplished early enough to be evaluated for implementation in MELCOR-1. In many respects, then, the recommendations and rationales presented below will be reflected in the forthcoming MEDICI code.

An assessment of the dominant pathways to significant radiological release leads to the conclusion that MELCOR-1 should have the following general features:

-- The option of generating aerosols at the vessel breach.

-- Reasonably realistic quench of molten debris as a function of time as it enters the pool, including limitation due to fluidization of debris.

-- The ability to allow (but not require) steam explosions, including material removal, quenching, and fragmentation.

-- A debris bed quench model including hydrogen generation and simultaneous core-concrete interactions.

-- A model for the long term behavior of both coolable and uncoolable debris beds.

-- A model for water migration during early core-concrete interactions.

-- The ability to calculate penetration velocity of solid core melting through concrete.

-- The ability to remove liquid water by entrainment in a high velocity gas release from the vessel.

Each of these features represents a substantial increase in the level of modeling detail compared to codes previously used in PRA's (cf. [6]), and it is unlikely that such a task could be accomplished in the time available if all the models are required to be highly mechanistic and complex. In fact, it is neither desirable nor possible to provide a high level of complexity for all of these features. In many cases, simple models have been found which can be shown to model the physics adequately. In others, more mechanistic models are needed, but are simply not available.

3.2.5.1 Mechanistic Models, Parametric Models, and Nodal Parameters

The approach used in developing the recommendations below is to choose mechanistic models when available, feasible, and suitable, and to propose parametric models otherwise. Furthermore, it is essential to distinguish as clearly as possible between these two categories, so that the PRA analyst can exercise the code over a reasonable range of the phenomenological parameters. In the recommendations to follow, we will emphasize this distinction by designating the highly uncertain parameters in the parametric models as "nodal parameters." This designation emphasizes the view of MELCOR as a tool for evaluating the consequences of a particular set of model or parameter choices, rather than as an all-knowing computer code (in which modeling and parameter assumptions are buried in the coding). While it is true that the judgment of experts will be important in establishing best estimates and reasonable bounds for the nodal parameters, it is also important that the user of MELCOR is aware of which models are considered well founded, and which are not.

The explicit identification of parametric models contrasts with another tempting, but unwise approach: neglecting a phenomenon because there are no "adequate" models available. Realistically, it will always be necessary to set aside certain event pathways as being beyond the scope of the code. These situations will have to be treated with the traditional type of highly conservative hand calculations in any study which purports to be comprehensive. However, every effort should be made to incorporate a high level of comprehensiveness into MELCOR, even if parts of some sequence are treated with simplistic or bounding models.

For any given phenomenon, there will a variety of ways that parametric models might be constructed. Because it is to be expected that phenomenological uncertainties will be dealt with by assuming a statistical distribution of parameters, it is important to take some care in choosing the set of nodal parameters which will embody the uncertainties. The model developer should, even though complete physical understanding of a phenomenon is lacking, try to break it up into component subprocesses, each of which can be characterized by a single parameter for which realistic bounds can be identified. Furthermore, every attempt should be made to ensure that the nodal parameters are statistically independent--i.e., not strongly correlated with each other. Otherwise, two unfortunate consequences may occur: (1) probabilistic risk calculations will include portions of the parameter space which are physically unrealistic; (2) calculations of uncertainty will be grossly overestimated.

In the following sections, the recommendations for models to be used in MELCOR-1 are given, following the organizational structure of Figures 3.2-D-1-5. Following this, there is a brief discussion of desirable additional features for MELCOR-2. These are summary descriptions only; additional technical detail can be found in the indicated Appendices 3.2-A-D.

3.2.5.2 Initial Interactions

3.2.5.2.1 High Pressure Melt Release Phenomena

The state of knowledge and model development for many of the phenomena described in Section 3.2.3.2.1 are limited. The sweepout entrainment criterion of Equations (3.2.3-1) and (3.2.3-2) are, however, a reasonable estimate for activating a parametric model of water removal. Since the two criteria differ only by a constant, the lower velocity criterion (3.2.3-1) is the operative threshold. The rate of sweepout is, however, highly uncertain, and highly dependent on cavity geometry. A parametric model is desirable here, therefore. One choice of nodal parameter is mass fraction of liquid in the two-phase mixture exiting the cavity. This fraction would flow out as long as the film sweepout criterion (3.2.3-1) was satisfied. It is presumed that a general containment water level calculation will make it possible for some or all of the water to return to the cavity.

For molten debris sweepout, the situation is more complex. Experiments have shown that debris removal can occur quite efficiently, and it is clear that some kind of

parametric model is desirable for this process. Similarly, aerosol generation at the vessel breach, and fragmentation at the outlet of the flowpath into the upper containment have been shown to be operative in scaled experiments. However, considerable additional uncertainty remains regarding the mechanisms involved. It is therefore recommended that even more control of the debris sweepout process be given to the user than for water sweepout. In particular, the entrainment velocity should be under user control. This might be accomplished by inserting a multiplicative factor into the entrainment criteria of Equations (3.2.3-1) and (3.2.3-2). In addition, it is necessary to specify the degree of fragmentation of the fuel leaving the cavity. For the purpose of aerosol behavior modeling, the particle size distribution needs to be specified. It is probably adequate to assume a lognormal distribution with user-specified mean particle size and standard deviation.

However, this is still not enough information for containment response analysis, since direct heating of the atmosphere must also be modeled. There are two sources of this heating: (1) gas-quenching of the sensible heat of the debris, and (2) chemical heating sue to oxidation of the metal. Typically, the total potential for atmosphere heating due to these two effects is about equal, but a different fraction will be realized, since the mechanisms are different. It is recommended that the user be able to specify the two fractions of available heat actually transferred to the atmosphere before the debris contacts structure or water.

This treatment of high-pressure melt release phenomena depends on an unusually large number of user-input parameters. This is unfortunate, but at present it is unavoidable. Presumably, a much better understanding of these phenomena will emerge from analysis of experiments which have been recently completed or which are now being planned. This may provide us with empirically-based parameter choices, or even with mechanistic models for use in future versions of MELCOR.

3.2.5.2.2 Low Pressure Melt Release Phenomena

The following models are based on a simple one-dimensional, time-dependent treatment of the atmosphere and pool. The principal calculations are heat and mass transfer between the debris, water, and atmosphere, and the disposition of the debris into the molten layer and the debris bed.

3.2.5.2.2.1 Fall Through Air

Melt which is not aerosolized is assumed to fall through the air at a velocity and cone angle which are determined by the melt release model. In each time step a new "parcel" of melt is added to the atmosphere, and the position of each parcel released in earlier time steps is updated by a simple accelerated fall model. Parcels do not interact with each other, though they can overtake each other spatially.

The initial particle size is also specified by the melt release model. A particle size distribution is not recommended for MELCOR-1. Heat transfer and hydrogen generation for the melt particles should be neglected, since the rates are low.

In the absence of water in the cavity, this mass should be added to the molten layer and the core concrete interaction model activated.

When water is present, the water level is calculated and updated each time step to determine the time of contact with the pool. The water level calculation includes pool swelling effects due to voids in the boiling debris bed and the dry zone. It also includes the displacement due to the debris. Note that the principal function of keeping track of how much debris is in the air, water, debris bed, and molten layers is to determine what quantity of debris can be interacting with water at a given time--particularly for the steam explosion.

3.2.5.2.2.2 Fall Through Water

This is the key Initial Interaction model, determining steam and hydrogen generation in the fall phase, and calculating the degree of quenching of the melt. In each time step, the debris in those parcels which are falling in the water zone interacts with the water to form steam according to the analysis of Appendix 3.2-A. Coarse mixing (particle size reduction) and spreading occurs according to the correlations given in Section 3.2-A.3.2. A constant velocity advances the parcel downward. A parcel which reaches the debris bed level is added to the debris bed, or the molten layer if not enough heat transfer has occurred. The boiling heat transfer model is given by Equation (3.2-A-22). Hydrogen generation is neglected in this phase (see Equation (3.2-A-23) and discussion following).

Note that since not all of the melt is suspended in the water at any given time, this approach should give significantly smaller steam generation rates than HOTDROP does. However, excessive rates are still possible. An upper limit

is needed. As discussed in Section 3.2.3.2.2.2, and in Appendix 3.2-A, a pool boiling criterion is too low. The fragmentation limit developed in Equations (3.2-A-17) and (3.2-A-21) serve the required purpose. With this limit imposed, it is probably unnecessary to consider the elutriation process discussed in [6], which would be difficult in any case for a model which does not include a distribution of particle sizes.

3.2.5.2.2.3 Steam Explosions

Several physical criteria for steam explosions are examined at each time step, including particle size and water/fuel mass ratio in the interaction zone (see Appendix 3.2-A). Most important, the occurrence of a steam explosion is controlled by user options, which can be based on the time of contact with the floor, or an arbitrary time, or spontaneously, as soon as the physical criteria are satisfied. The user can also specify that no steam explosion occurs.

The model for the steam explosion itself is semimechanistic. A steam explosion efficiency determines mechanical work available as a fraction of the available thermal energy in the interaction zone. This efficiency is discussed in Section 3.2-A.4.4, and will be a suitable nodal parameter for uncertainty analysis. A nominal value of 4 percent is suggested. The extent of fragmentation appears, however, to be strongly correlated with this efficiency, so it will be modeled according to a correlation based on Figure 3.2-A-7 (see Section 3.2-A.4.5). The resultant fragmented debris should be assumed fully quenched.

The amount of melt which can participate in the explosion is limited to the suspended, molten material. This determines the thermal energy available corresponding to the steam explosion efficiency. The amount of water is determined by the volume of the interaction zone. It should be noted, however, that multiple steam explosions might disrupt a molten layer, allowing it to participate in a steam explosion. Alternative models which include this effect should be given serious consideration for future versions of MELCOR.

Because of the assumed strength of the reactor cavity, shocks in the water and atmosphere will not be modeled, but the final pressure increase due to the heat transferred will be calculated in the thermodynamics module. (Note: the possibility of failure of a BWR drywell wall due to a steam explosion has not been analyzed for this report.) Hydrogen generation during the steam explosion can be significant (up to 25 percent of the metal was oxidized in some FITS tests). However, the oxidation process appears to be too

complex at present to model mechanistically for the first version of MELCOR. It is recommended that a fraction of metal oxidized be specified as a nodal parameter, and that the oxide be assumed distributed uniformly in the particle. It is expected that models to predict this fraction will become available soon.

One of the largest uncertainties in the analysis of steam explosions concerns the expulsion of material from the cavity following the explosion. The process is highly complex, and there are no adequate models and no experimental data relevant to typical cavity geometries. A parametric model is suggested. An energy criterion, based on the energy required to lift all of the water in the cavity to the outlet level, should be calculated. For steam explosion energies much less than this quantity, no removal should occur. For energies far in excess of it, total fluidization can be assumed, and an arbitrary fraction of the water and rubble (but not the molten layer) can be ejected into the upper containment areas. The intermediate energy region can be treated with a continous fit between these limits. Efforts are currently underway to model this process less crudely, but the variability of cavity geometry (particularly of the outlet flow paths) for different reactors will probably continue to make this problem analytically difficult.

Since water level in the cavity is critical to many aspects of fuel-coolant interactions, it is important that pathways for intercell transport of water be adequately modeled. This requires models for overflow of sumps and for pipes and drains. Provision should also be made for a user-specified steam explosion following the return of water to the reactor cavity from the upper containment.

3.2.5.2.2.4 Debris Bed Formation

The mass and enthalpy in debris parcels which reach the bottom of the water layer are added either to the rubble layer or the consolidated debris layer, depending on their enthalpy. A solid fraction criterion (based on specific enthalpy) determines which layer is chosen. In the simplified treatment proposed for the first version of this model, all of the melt is released in a short period of time. It is assumed that debris bed phenomena do not substantially influence the processes described above as Initial Interactions, so that debris bed heat and mass transfer can be postponed until all of the debris has settled out. This allows the debris bed model to start with a well-defined initial condition. Late melt entry should be allowed, but it must be treated in much the same way as the initial melt, so that such phenomena as stratified beds cannot be treated.

3.2.5.3 Wet Cavity Debris Bed Behavior

The layered model depicted in Figure 3.2.3-2 is the basis of this discussion. The treatment is one-dimensional, in that the two dry rubble zones are allowed to have a temperature which is a function of height. All other zones, however, are assumed to be well mixed and at a uniform temperature. The cumulative mass of oxidized metal per unit surface area (cf. Equation (3.2.3-10)) must be stored for all zones as a function of height.

Many simplifying assumptions are made for the model. For example, coupled fluid flow and heat transfer equations are not, in general attempted. There are simply too many materials, too many phases, and too many layers for such a treatment to be implemented with algorithms which are of acceptable speed and stability.

The critical calculations for this model is the growth, diminishment, and disappearance of the various zones shown in Figure 3.2.3-2, and the generation of steam, hydrogen, and other noncondensible gases.

3.2.5.3.1 Debris-Pool Interactions

The initial condition for the debris bed is that it is completely dry. (The debris is assumed to be so hot that quenching floods all the liquid water from the bed.) The validity of this initial picture is not essential to the model, since a more realistic situation will evolve in the model after a very short period of time (a few seconds). A "sharp quench front" model has recently been developed for the MEDICI code which assumes perfect solid-liquid heat transfer and zero solid-gas or liquid-gas heat transfer. Furthermore, it is assumed that there is a limited rate at which steam can pass through the top of the bed (see Section 3.2.3.3.1). This limiting steam flux is calculated by means of a well-established dryout heat flux model with corrections for gas flow from below due to core-concrete interactions. Appendix 3.2-C contains a complete description of the model.

The descending quench, however, is not necessarily complete. Allowance is made for steam channels to form which are not fully quenched. Since the steam generation rate results from a combination of the decay heat in the saturated zone and the quench heat swept out as the front moves downward, the front velocity is increased when such steam channels form. As discussed in Section 3.2.3.3.1, formation of steam channels has been observed in debris bed quenching experiments, and there is some experimental basis for the quench fraction parameter used in this model.

Arbitrarily rapid quench front penetration should not be allowed, however. A simple expression for the limiting penetration velocity, based on fluid flow through a cold porous medium, is imposed, which will result in an increase in the quench fraction parameter, or if that is unity, a reduction in the steam generation rate below the dryout flux.

The lower dry zone (Zone III) heats up adiabatically before the quench front arrives, or until the debris remelts, or until the rising slag layer consumes it and isolates the debris from the coolant. Figure 3.2.3-4 shows the predictions of this model for quench front position. An alternative to the adiabatic treatment would be to use a packed bed Nussell number [40] to calculate heat transfer to CCI-generated gas. This effect could prevent remelting.

3.2.5.3.2 Debris-Gas Interactions

There are two rubble zones (I and III) exposed to steam flow. Both are potential sources of large amounts of hydrogen. Diffusion of steam through the oxide layer must be modeled to treat this problem. The Baker-Just correlation will be used for the zirconium oxidation (cf., Equation (3.2.3-11)). The geometry assumed will be that of a sphere whose radius specified by the debris bed formation model. The surface area available will be reduced in proportion to the volume fraction of each zirconium in the debris composition. This also results in a release of heat to the debris, which will be added to the enthalpy of the debris layer. (Note that these two layers are treated as single nodes; i.e., one-dimensional effects are not treated.) Oxidation of stainless steel will be modeled in a similar way, except that the reaction rate will follow Equation (3.2.3-12).

In the exposed zone (Zone I) a heat transfer correlation appropriate for gas flow through a packed bed [34, 40] is used to determine the temperature of the exposed zone for the hydrogen generation calculation. As long as there is water in the cavity, the temperature in the exposed zone is expected to be sufficiently low that radiational heat transfer need not be considered.

Hydrogen generation at the quench front needs to be modeled because it may be the earliest hydrogen generated in the cavity. Baker-Just correlations can be applied, but it is necessary to define the thickness of the zone in which there is sufficient steam and hot enough debris. This process has not been studied extensively, and it is suggested that the zone thickness be subject to parametric variation and sensitivity analysis. If d_q is the quench zone thickness, then we define

$$K_q = d_q/d_p \qquad (3.2.5\text{-}1)$$

where d_p is the debris particle diameter. Thus, k_q is suggested as the nodal parameter for sensitivity and uncertainty analysis. We assume the temperature drops linearly across the quench zone (which is centered on the quench front calculated by the sharp quench front model) and that an abundance of steam exists in this region, but not below it. We can then obtain the total hydrogen production by integrating (3.2.3-10), (3.2.3-11), and (3.2.3-12) across this zone. Note that W in Equation (3.2.3-10) is a function of height, depending on the history of the debris bed, so a closed form solution is not possible.

There is a high degree of uncertainty in the total hydrogen generation rate from metals in the reactor cavity. One must know the locations, temperatures, exposed surface areas, and local steam concentrations for all significant masses of unoxidized metal. These might include aerosolized debris as well as the larger particles in the debris bed. In view of this uncertainty, an alternative modeling strategy would be to take the conservative view that as long as there is water in the cavity, there is abundant steam available to all debris. Solid debris oxidation would then proceed at the rate specified by the Baker-Just correlation until all the metal is oxidized.

3.2.5.3.3 Debris-Concrete Interactions

There is a wide variety of possible configurations for the debris, concrete, and water which may require a CCI model. In some configurations, the phenomena are reasonably well understood, and there are tested models available. In other cases, there are high levels of phenomenological uncertainty, and no suitable models. Furthermore, conditions can evolve from one of these situations to the other in any given accident sequence.

In view of this, the first requirement of models intended for MELCOR is that there be a systematic structure for the analysis, which is relatively comprehensive with respect to possible configurations. Those configurations for which suitable models are lacking should be treated with simple parametric models with clearly identified nodal parameters.

The movement of the boundaries between the zones illustrated in Figure 3.2.3-2 are of critical importance to the

behavior of the debris bed. For example, the descent of the rubble bed into the slag layer determines how thick the boiling debris bed is, which determines how much steam is generated, which strongly affects cavity water inventory and containment pressure. The consumption of the rubble bed by the consolidated layer determines its thickness, which determines the ablation rate (see Equation (3.2.3-14)). The volumetric concrete ablation rate (determined in our one-dimensional model by the ablation velocity) determines the noncondensible gas generation rate, which is of great importance with regard to containment pressurization.

Thus, the first level of quantitative description for simultaneous CCI and debris bed behavior should focus on four front velocities:

1. Quench front velocity;
2. Rubble bed descent velocity;
3. Effective concrete ablation velocity;
4. Concrete dehydration front velocity.

In some cases, acceptable models exist to predict these velocities; in others, parametric models should be substituted until more mechanistic treatments become available.

As discussed in 3.2.3.3.3.4, a two-dimensional concrete ablation model is probably unnecessary, and probably impractical for situations in which a debris bed in a water pool exists simultaneously with the CCI. What is needed is a model for migration of water in concrete, at least until the dehydration front becomes relatively stationary with respect to the erosion front. The equations used in the USINT model appear to be the best choice for this process. These should be coupled efficiently with the heat conduction model for structures. The numerical treatment used in [33] should be seriously considered for implementation, because it is considerably faster than other water migration models, and it focuses explicitly on front motion. An alternative to a full implemenation of these equations would be to develop a correlation for water migration based on the controlling parameters, and established by a stand-alone water migration.

A one-dimensional concrete erosion model is needed which is applicable to a molten debris pool as well as hot, solid rubble. No existing model has these capabilities. Nonetheless, it is essential to estimate the noncondensible gas generation rate and the rate of descent of the rubble bed into the molten pool. The erosion rate at the CCI interface depends on the thickness of the consolidated zone and on the heat transfer rates upward and downward from the consolidated zone. In cases where a suitable mechanistic CCI model is available, as with molten pool-concrete interactions, it

should be used. The treatment used in CONTAIN, for example, shows that it is possible to model water migration and molten pool concrete interaction simultaneously. In cases where suitable models are not available, it is recommended that ß, (defined in (3.2.3-13) as the ratio of heat transfer rates upward and downward) be the nodal parameter. (Note that "upward" in this one-dimensional model should also take into account "sideward" losses in real geometries.) With this ratio defined, we can use the total volumetric heat production in the debris to calculate total downward heat flux, which is directly related to the erosion rate (see Equation (3.2.3-14)).

Having calculated the erosion rate, the noncondensible gas generation rate for steady state processes can be calculated on the basis of stoichiometric composition. To this, we can add excess steam due to water migration (water in the volume swept out by the diverging ablation and dehydration fronts).

The rubble bed descent velocity is, in general, difficult to model. However, it is easy to define some bounding values, and some easily characterized configurations. The maximum value is equal to the ablation front velocity plus a relative velocity which would result from the adiabatic remelt of the submerged debris. The minimum velocity is zero, which occurs when either the concrete freezes or a stable debris crust forms which adheres to the solid concrete at the boundary of the interaction zone. (This could probably only occur for low rubble bed decay heat power, since concrete is a poor heat conductor.) A third easily characterized configuration would be a rubble bed kept solid by heat transfer to the molten slag, bubbling gas, and molten steel, and resting on a crust at the top of the consolidated zone, so that the rubble descent velocity equals the actual downward velocity of the ablation front. (This velocity could be less than the effective one-dimensional velocity used to characterize the volumetric erosion rate because some of the erosion might be radial.) It is recommended that some simple models be available at the user's option which correspond to these simple configurations. Alternatively, the unknown descent velocity can be characterized as a bounded nodal parameter and subject to sensitivity and uncertainty analysis.

3.2.5.4 Model Development Recommendations for MELCOR-2

The recommendations offered in the previous section have been severely constrained by the timetable established for MELCOR-1. Many of the treatments, though improvements over earlier system level models, are still unsatisfactory for

the final version of MELCOR. Hopefully, new model development can proceed in the interval between the two code versions. In addition, several important experiments will be completed in the near future which will have important bearing on reactor cavity modeling. These include high pressure melt release experiments at Sandia, core retention device tests at Sandia, melt-water interactions in scale model reactor-cavities at Argonne, cavity sweepout experiments at Winfreth, England, solid debris-concrete interaction experiments at Sandia, and many others.

As a consequence of the insights obtained from these experiments and continuing analysis and model development, improvements should be anticipated for MELCOR-2 in the following areas:

1. Aerosolization of molten debris at the vessel breach,
2. High-pressure sweepout of water and debris,
3. Improved predictive criteria for steam explosions,
4. Debris expulsion following steam explosions,
5. Hydrogen generation at the quench front of a particle bed,
6. Particle size distribution effects for the fall phase and for debris bed behavior,
7. Core retention device behavior (particularly the retrofit particle bed concept),
8. Postquench molten debris impingement,
9. Solid debris-concrete interactions, and
10. Aerosol generation in the CCI and removal in the overlying pool.

3.2.6 REFERENCES

1. Zion Probabilistic Safety Study, (Chicago, IL: Commonwealth Edison, 1982).

2. Ishii, M. and Grolmes, M., "Inception Criteria for Droplet Entrainment Film Flow," AIChE J., Vol 21 (1975).

3. Spencer, B. W. and Bengis, M., "Molten Core Entrainment and Sweepout in Reactor Cavity Interactions," Trans. ANS, Vol 38, pp 551-553 (1982).

4. Henry, R. E. and Fauske, H. K., "Core Melt Progression and the Attainment of a Permanently Coolable State," Proc. of Ther. Reac. Fuels Mtg., Sun Valley, ID (1981).

5. Henry, R. E. and Fauske, H. K., "Required Initial Conditions for Energetic Steam Explosions," Fuel-Coolant Interactions, ASME HTD-V19, Washington, DC (1981).

6. Rivard, J. B., ed., Interim Technical Assessment of the MARCH Code, NUREG/CR-2285, SAND81-1672.R3, Sandia National Laboratories, Albuquerque, NM, November 1981.

7. Cronenberg, A. W. and Benz, R., "Vapor Explosion Phenomena with Respect to Nuclear Reactor Safety Assessment," in Advances in Nuclear Science and Technology, Vol 12, (1980).

8. Bankoff, S. G., "Vapor Explosions", in Nuclear Reactor Safety Heat Transfer (1981).

9. Corradini, M. L., "A Critical Review of Vapor Explosion Research," to be published.

10. Mitchell, D. E., Corradini, M. L. and Tarbell, W. W., Intermediate Scale Steam Explosion Phenomena: Experiments and Analysis, SAND81-0124, NUREG/CR-2145, Sandia National Laboratories, Albuquerque, NM, September 1981.

11. Buxton, L. D., Benedek, W. B., and Corradini, M. L., Steam Explosion Efficiency Studies: Part II Corium Experiments, SAND80-1324, Sandia National Laboratories, Albuquerque, NM, October 1980.

12. Berman, M., Light Water Reactor Safety Research Program Semi-Annual Report, April-September 1981, SAND82-0006, February 1982.

13. Gittus, J. H., chairman, PWR Degraded Core Analysis, ND-R-610(S), UKAEA, April 1982.

14. Cho, D. E., Fauske, H. K., and Grolmes, M. A., "Some Aspects of Mixing in Large Mass, Energetic Fuel-Coolant Interactions," Proc. Int. Mtg. on Fast Reactor Safety and Related Physics, Chicago, IL, CONF-761001, Vol 4, p 1852 (October 1976).

15. "Steam Explosions in Light Water Reactors," Report of the Swedish Government Committee on Steam Explosions, DsI 1981:3 (Stockholm: Liber Forlag, 1981).

16. C.1

17. Alvarez, D. and Amblard, M., "Fuel Leveling," Proceedings of Fifth Post Accident Heat Removal Information Exchange Meeting, 1982, Karlsruhe, Germany (Braun, G., Karlsruhe, 1982).

18. Barleon, L. and Werle, H., "Dependence of Dryout Heat Flux on Particle Diameter for Volume and Bottom-Heated Beds," KfK-3138, KfK, Karlsruhe, W. Germany (1981).

19. Gabor, J. D., Cassulo, J. C., Jones, S. W., and Pedersen, D. R., "Studies on Heat Removal from Fuel Debris," Trans. ANS, Vol 39, p 642 (1981).

20. Cho, D. H., Armstrong, D. R., Bova, L., Chan, S. H., and Thomas, G. R., "Experiments on Quenching of a Hot Debris Bed," Post Accident Debris Cooling, Proc. of the Fifth Post Accident Heat Removal Info. Exchange Mtg., July 28-30 1982, Karlsruhe, W. Germany, p 145.

21. Ginsberg, T., Klein, J., Klages, J., Schwarz, C. E., and Chen, J. C., "Phenomenology of Transient Debris Bed Heat Removal," ibid. 3, p 151; also, LWR Steam Spike Phenomenology: Debris Bed Quenching Experiments, NUREG/CR-2857 (June 1982).

22. Advanced Reactor Safety Research Quarterly Report, April-June 1982, SAND82-0904 (2 of 4), Sandia National Laboratories, Albuquerque, NM.

23. Gorham-Bergeron, E., "A Debris Bed Model to Predict the Effect of Gas Influx from Below on the Dryout Heat Flux," Proc. Int'l. Mtg. on Thermal Nuclear Reactor Safety, Chicago, IL (August 27, 1982).

24. Mitchell, D. E., and Evans, N. A., Proc. of the Thermal Reactor Safety Mtg., Chicago, IL, (August 29 - September 2, 1982).

25. Powers, D. A., Chapter 4 of Core Meltdown Experimental Review, SAND74-0382(Revised) Sandia National Laboratories, Albuquerque, NM (March 1977).

26. Baker, L., Jr. and Just, L. C., Studies of Metal-Water Reactions at High Temperatures III, ANL-6548, Argonne National Laboratory, Argonne, IL (1962).

27. Bittel, J., Sjodahl, L. H., and White, J. F., Corrosion-NACE, Vol 25, p 7 (1969).

28. Powers, D. A., "A Review of Steam Oxidation of Steels; The Forgotten Source of Hydrogen," Hydrogen Workshop, October 1982, Sandia National Laboratories, Albuquerque, NM.

29. Beck, J. V. and Knight, R. L., User's Manual for USINT, SAND79-1694, Sandia National Laboratories, Albuquerque, NM (1980).

30. Powers, D. A. and Arellano, F. A., Large-Scale, Transient Tests of the Interaction of Molten Steel with Concrete, NUREG/CR-2282, SAND81-1753, Sandia National Laboratories, Albuquerque, NM (January 1982).

31. Levine, H., "Noncondensible Gas Evolution," Ch. 9 in Core Meltdown Experimental Review, SAND74-0382 (Revised), Sandia National Laboratories, Albuquerque, NM.

32. Powers, D. A., "Direct Observation of Melt Behavior During High Temperature Melt/Concrete Interactions."

33. Chen, K. H., Gluekler, E. L., Lam, S. T., and Shippey, V. S., Comparison of Mechanistic Codes for Predicting Water Release from Heated Concrete, General Electric Company, Sunnyvale, CA, GEFR-00521 (1980).

34. Martin, Chem. Eng. Sci., 1980 or 1981. Quoted in Schlundler (1980).

35. Murfin, W. B., Report of the Zion/Indian Point Study-v.1, SAND80-0617/1, Sandia National Laboratories, Albuquerque, NM (1980).

36. MARCH Code Description and User's Manual, NUREG/CR-1711, BMI-2064, Battelle Columbus Laboratories (October 1980).

37. Murfin, W. B., A Preliminary Model for Core-Concrete Interactions, SAND77-0370, Sandia National Laboratories, Albuquerque, NM (October 1977).

38. Sengaub, M. E., The Corium/Concrete Interaction Model of CONTAIN, RS 4450/82/50, Sandia National Laboratories, Albuquerque, NM (July 1982).

39. Corradini, M. L., "Hydrogen Generation During Molten Fuel-Coolant Mixing," Hydrogen Workshop, Sandia National Laboratories, Albuquerque, NM (October 1982).

40. Schlunder, E. U., "Transport Phenomena in Packed Bed Reactors," in Chemical Reaction Engineering--Houston, Luff, D., and Weekman, V., Eds., Am. Chem. Soc. (1978).

41. Pilch, M., "Molten Debris Jet Breakup Analysis," to be published.

42. Senglaub, M. E., et al., CONTAIN, A Computer Code for the Analysis of Containment Response to Reactor Accidents-Version 1A, NUREG/CR-2224, SAND81-1495, Sandia National Laboratories, Albuquerque, NM, draft (June 1981).

43. Theofanous, T. G., and Saito, M., "An Assessment of Class-9 (Core-Melt) Accidents for PWR Dry Containment Systems," Nuc. Eng. and Design, Vol 66, p 301 (1981).

44. Powers, D., private communication.

45. Tarbell, W. W. and Bradley, D., Sustained Concrete Attack by Low-Temperature Fragmented Core Debris, NUREG/CR-3024, SAND82-2476, Sandia National Laboratories, Albuquerque, NM (1983).

APPENDIX 3.2-A

MOLTEN FUEL-COOLANT INTERACTIONS: RECENT EXPERIMENTS AND ANALYSIS

M. L. Corradini,+, D. E. Mitchell,* N. A. Evans*

3.2-A.1 SUMMARY

If a complete failure of normal and emergency coolant flow occurs in a light water reactor, fission product decay would eventually cause melting of the reactor fuel, and eventual contact with water. An energetic fuel-coolant interaction (steam explosion) may result. Experiments were performed in which approximately 20 kg of molten fuel simulant was delivered into water in which the water mass was 1.5 to 50 times greater than the fuel. Experiments in subcooled water showed that spontaneous explosions occurred over the range of water/fuel mass ratio and that, in certain experiments, multiple explosions occurred. With multiple explosions, the first explosions enhanced fuel-coolant mixing for the subsequent explosion. The kinetic energy conversion ratio was limited to less than 2 percent. However, the total energy transferred to the coolant was much larger; e.g., 1-8 percent of the fuel energy eventually resulted in air pressurization of the chamber. A model is proposed to describe the fuel-coolant mixing process. The model is compared to the intermediate scale experiments. Additional data analyses indicate that the steam explosion is affected by the mixing process.

+Nuclear Engineering Department, University of Wisconsin, Madison, WI 53706

*Reactor Safety Studies Division, Sandia National Laboratories, Albuquerque, NM 87185

Table 3.2-A-1

Nomenclature

A - area
C_D - drag coefficient for sphere
D_o - diffusion coefficient between H_2 and H_2O
D - diameter
E_m - mixing energy
g - gravitational acceleration
h - heat transfer coefficient
H_C - depth of the water pool
i_{fg} - latent heat of vaporization
m'' - max flux (kg/m^2s)
N - number of moles
ΔP - steam partial pressure difference between the ambient and at the fuel surface
q'' - heat flux
R_o - universal gas constant
T - temperature
T_V - $(T_{sat}+T_f)/2$
v - velocity
V - volume
W_{Hw} - mass flux of H_2 generation
a - void fraction
δ - vapor film thickness
ρ - density

Subscripts

b - breakup
c - coolant
d - displaced
FR - fuel fragment
f - fuel
H_2 - hydrogen
M - mixture
v - vapor
sat - saturated

3.2-A.2 INTRODUCTION

Given the absence of adequate cooling water to the core of a light-water reactor (LWR), the fission product decay heat would eventually cause the reactor fuel and cladding to melt. This could lead to slumping of the molten core materials into the lower plenum of the reactor vessel, possibly followed by failure of the vessel wall and pouring of the molten materials into the reactor cavity. Recent analyses [1-5] have indicated that residual water is likely to be present both in the lower plenum and in the reactor cavity. Therefore, when the molten core materials enter either region, there is a strong probability of molten core contacting water. The physical process by which the molten core ("fuel") contacts and mixes with the water ("coolant") is important for three reasons--(1) because of its potential for rapid steam generation from a fuel-coolant interaction either energetic (steam explosion) or nonenergetic (steam spike), (2) because it is a source of combustible hydrogen from the oxidation of the metallic components of the molten core (e.g., iron, chromium, zirconium), and (3) because it will affect the size of the fuel debris.

In this Appendix we focus on recent fuel-coolant interaction (FCI) experiments (designated Fully Instrumented Test Series-FITS) conducted at Sandia National Laboratories. In many of these FCI experiments, steam explosions were observed, which occurred in a series of stages:

1. Fuel mixing with the coolant in a drop mode of contact,

2. Triggering of the explosion at or near base contact,

3. Propagation of the explosion through the fuel-coolant mixture producing high pressure coolant vapor,

4. Expansion of the explosion products producing mechanical work.

First the experimental apparatus is described. Then data from the fuel-coolant mixing phase are analyzed and criteria are proposed for limits for fuel-coolant mixing. Finally, the explosion data are presented and analyzed relative to the explosion conversion ratio and the debris generated.

3.2-A.3 FITS EXPERIMENTS

The FITS experiments were conducted both outside and in a containment chamber. The earlier tests outside the chamber were performed to perfect instrumentation and melt delivery techniques (MD and MDC series), while mixing behavior was observed; the in-chamber experiments allowed more detailed measurements of the explosion conversion ratio and the collection of the explosion debris.

The water interaction chambers used were designed such that water volumes were in the form of rectangular parallelepipeds, with square cross-sectional area and open tops. These were fabricated from clear 6.3 mm thick plexiglas stock in sizes calculated to result in initial water-to-fuel mass ratios of 1.5:1 to 50:1.

The in-chamber experiments were instrumented with pressure transducers: in the water chamber base and side walls to measure water phase pressure; in the FITS chamber upper head to study debris slug characteristics; and in the FITS chamber side wall ports to measure the gas phase pressure. Melt delivery was initiated automatically through the use of probes in the crucible that sensed when the thermite reaction was complete. Melt entry time was measured by photodiodes 2.5 cm above the water surface; shape and velocity of the melt at water impact and during mixing were recorded by high-speed cameras. Debris recovered from the experiments was characterized by sieving using sieve sizes ranging from 38 μm to 25 mm.

The fuel used in these experiments was prepared by a metallothermic (thermite) chemical reaction. The resulting fuel melt consisted of either iron-alumina ($55^{w}/o$-iron, $45^{w}/o$-alumina) or corium (CORIUM-A+R: UO_2-ZrO_2-$70^{w}/o$, Stainless Steel-$30^{w}/o$) at a theoretical maximum temperature of 3100 K. This corresponds to an internal energy content of 3.3 MJ/kg for iron-alumina and 1.8 MJ/kg for the Corium. Calorimetry tests indicated that the actual fuel internal energy was about 90 percent of this value. This suggests a fuel melt entry temperature into the water pool of about 2800 K; this value is in agreement with optical pyrometer measurements made in a few tests. The iron-alumina was used more extensively in these tests because it is an inexpensive high-temperature simulant for the actual fuel melt (corium).

Water from the local water supply was used as the coolant. No special treatment, such as degassing or deionizing, was done. Water temperature was not controlled for the majority of the experiments and was between 309 and 319 K. Two experiments were done with saturated water at 368 K.

3.2-A.4 FUEL-COOLANT MIXING

3.2-A.4.1 Mixing Criteria

Past research into fuel-coolant mixing (sometimes called "premixing") has been directed at predicting the physical limits for which mixing could or could not occur. Fauske [6, 7] originally proposed that the fuel-coolant interface temperature upon liquid-liquid contact must exceed the spontaneous nucleation temperature (approximately the homogeneous nucleation temperature) to allow premixing for an energetic FCI; the homogeneous nucleation temperature for water is 583 K. The physical picture was that stable film boiling is established above this limit for a liquid-liquid system and this allows the fuel time to penetrate and mix with the coolant. For the LWR system, the fuel (UO_2, ZrO_2 steel) and coolant (water) easily satisfy this first criterion (interface temperature calculated to be well in excess of the water critical temperature, 647 K). This criterion could be considered necessary but not sufficient.

Cho, et al. [8] proposed that beyond this criterion, consideration must be given to the energy used in fuel-coolant mixing that creates more surface area and overcomes frictional effects. He concludes that frictional effects dominate the mixing process and developed a simple model to estimate the minimum required energy, E_m, for progressive mixing of the fuel and coolant.

$$E_m = 1.81\ \rho_m\ V_f \left[\frac{V_f^{2/3}}{t_b^{\,2}}\right]\left[1 - \frac{D_{FR}^2}{4V_f^{2/3}}\right] \ln\left[\frac{2V_f^{1/3}}{D_{FR}}\right] . \qquad (3.2\text{-A-1})$$

Using this approximate model the energy required for fuel-coolant mixing can be calculated and compared to that available as thermal energy in the fuel, E_{fth}. If E_m is substantially less than E_{fth}, then it indicates that mixing is possible from an energy standpoint.

Recently, Fauske and Henry [9, 10] have proposed a simple model to predict the minimum fuel on the physical concept that the fuel can break up and premix with the water to a uniform size no smaller than that which would prevent liquid from entering the mixture zone; i.e., the fuel surface area increases (diameter decreases) to such a degree that steam generation stops liquid water inflow. To determine this minimum diameter, D_{MIN}, they equated the energy transferred from fuel to coolant in the mixture to the critical heat flux in pool boiling (q_{CHF}) multiplied by

the cross-sectional area of the coolant. The critical heat flux was viewed as an approximate hydrodynamic limit for steam outflow and water inflow (one-dimensional, counter-flow, steady state). The minimum diameter is given by

$$D_{MIN} = \frac{6 m_f q''_{DROP}}{\rho_f A_c q''_{CHF}} \qquad (3.2\text{-A-}2)$$

where

$$q''_{DROP} = \sigma_r (T_f^4 - T_c^4) + h_{film} (T_f - T_C) \qquad (3.2\text{-A-}3)$$

where σ is the Stefan-Boltzmann constant and h_{film} is the film boiling heat transfer coefficient.

Again, this model can be viewed as an approximate physical limit. This physical model is geometrically approximate in two important respects: it assumes that the critical limit is reached in a planar surface neglecting transient effects, and it assumes that a counterflow of water and steam occurs neglecting the possibility of steam outflow from one surface and water inflow from another surface (multidimensional effects). These omissions cause the model to neglect two possibly important effects: (1) time is not considered relative to that allowed due to geometry characteristics; such as coolant depth or width, (2) mixing is not a static process occurring regardless of time, rather it is a dynamic process always occurring to some degree, allowing the fuel to fragment to smaller and smaller sizes. These omissions might prompt one to seek strict limits to mixing which are time independent; rather the physics seem to suggest such limits are highly time dependent.

During the FCI, the rate of fragmentation and the final debris size is empirically known from small intermediate scale experiments.[11] These experiments indicate that the fuel fragments quickly (100-300 μsec) to small sizes (from 1-10 mm to 50-150 μm mass average). Knowing the empirical debris size distribution one can calculate the available surface area. The surface area combined with chemical kinetics on hydrogen production (e.g., References 12-15) can then be used to calculate hydrogen generation rates.

3.2-A.4.2 Correlations for Recent Mixing Data

During a severe accident, fuel-coolant contact may occur in one of two ways; the fuel may pour into a water-filled cavity by gravity (or under pressure), or the water may reflood a cavity containing molten fuel. In the former case the fuel falls through the coolant and mixes with it. In the latter case the fuel is stratified with the coolant on top, and a slow quenching is the most probable result. In regard to fuel-coolant mixing, the former contact mode is of more concern, because of the possibility of a steam explosion during the mixing process.

This drop (pouring) contact mode was used extensively in FCI tests at Sandia.[16-19] In these tests, the hot fuel enters the water pool in film boiling and begins to distort in shape. As it continues to fall through the pool, it breaks apart into smaller pieces and mixes with the surrounding water while still in film boiling. These smaller pieces may subdivide further as the steam produced in film boiling flows out through the top of the fuel-coolant mixture and escapes the pool as water flows in from the sides. This mixture grows radially as the fuel, now mixed with water and steam, continues to fall through the pool finally reaching the chamber base. Usually before base contact two possible events can occur: an energetic FCI (steam explosion) is triggered, or the "premixed" molten fuel settles on the chamber base and eventually quenches. During this transient fall phase of the fuel through the water pool one reason for fuel breakup is inertial forces generated by the fuel initial relative velocity, v_f, and differences in density (ρ to ρ_c). If the fuel mass is large (characteristic diameter, D_f, large) or its relative velocity high, its characteristic Weber number, We, (ratio of destabilizing hydrodynamic force, $\rho_c v_f^2 D_f^2$, to stabilizing surface tension force, σD_f) will be greater than a critical value (we_{crit} = 7-12 for relatively inviscid fluids).[20] The fuel will begin to distort and break apart.

One could develop an empirical model for this mixing phenomena, if the assumption is made that hydrodynamic forces are the major cause of fuel-coolant mixing as in the case of isothermal experiments.[21-25] The major difference in these FCI experiments is that film boiling separates the two liquids; one might presume that the film acts like a low impedance fluid which delays the fuel breakup relative to the isothermal case. The dependent variables would be the depth of the fuel-coolant mixture, H_m, the lateral dispersion diameter of the fuel-coolant mixtures, D_m, the mixture volume, V_m, the displaced water volume, V_D (i.e., the fuel and steam volume in the mixture at a given time),

and the average fuel diameter during mixing, D_{FR}. The independent variables are the fuel mass, m_f, its diameter, D_f, initial entry velocity, v_f, coolant mass, m_c, its depth, H_c and width, W_c, properties and time, t.

To nondimensionalize the dependent variables one can choose the fuel diameter, similar to hydrodynamic analyses;[21-23] the resultant groups are H_m/D_f, D_m/D_f, V_m/V_f, V_D/V_f, where V_f is the initial fuel volume ($V_f = \pi/6 D_f^3$). The independent variable, time, can be nondimensionalized by a characteristic time for hydrodynamic breakup, τ_β. This time, τ_β, can be derived if one postulates the mechanism for mixing. Consistent with past analyses of hydrodynamic breakup,[24] we consider fuel breakup during this phase of the FCI to be controlled by Rayleigh-Taylor instabilities. In particular, τ_β is given by

$$\tau_\beta \sim D_f/v_b \qquad (3.2\text{-A-4})$$

where v_b is the velocity of the Rayleigh-Taylor instability as it penetrates the fuel and subdivides it into smaller masses. Experiments in Rayleigh-Taylor instabilities [26] have indicated that, shortly after the instability begins, it reaches a constant velocity given by

$$v_\beta \sim \sqrt{aD} + \sqrt{a\lambda_m} \qquad (3.2\text{-A-5})$$

where D is the length scale of the system (D_f in this case), λ_m is the fastest growing Taylor wavelength given by

$$\lambda_m = 2\pi \left[\frac{3\sigma_f}{a(\rho_f - \rho_c)} \right]^{1/2} \qquad (3.2\text{-A-6})$$

and where a is the acceleration. In this case, the acceleration is induced by the relative velocity between the fuel and the coolant

$$a \sim \frac{3}{8} \frac{C_D}{D_f} \frac{\rho_c}{\rho_f} v_f^2 \quad . \qquad (3.2\text{-A-7})$$

This penetration velocity appears to be composed of two parts; one due to the overall system length scale, D_f, causing large wavelength instabilities to grow, and another due to the smaller fastest growing wavelength, λ_m. For the phenomena considered here it is not clear which component of the velocity is dominant.

To estimate τ_β and arrive at a dimensionless time let us consider each component of v_B separately. If $v_{bI} \sim \sqrt{aD_f}$ then τ_β becomes

$$\tau_{B_I} = \frac{D_f}{v_f}\left[\frac{3}{8} C_D \frac{\rho_c}{\rho_f}\right]^{-1/2} \qquad (3.2\text{-A-8})$$

where we have substituted for the acceleration from Equation (3.2-A-7). The dimensionless time, t/τ_{BI}, then becomes

$$\frac{t}{\tau_{B_I}} = \frac{t v_f}{D_f}\left[\frac{\rho_c}{\rho_f}\right]^{1/2} \qquad (3.2\text{-A-9})$$

where $(3/8\ C_D)$ is approximately one for liquid droplets. If $v_{BII} \sim \sqrt{a\lambda_m}$, then $t/\tau_{B_{II}}$ is given by

$$\frac{t}{\tau_{B_{II}}} = \frac{t v^*}{D_f}\left[\frac{\rho_c}{\rho_f}\right]^{1/4} \qquad (3.2\text{-A-10})$$

where

$$v^* = \left[\frac{v_f^{\,2}\,\sigma_f}{D_f(\rho_f-\rho_c)}\right]^{1/4} . \qquad (3.2\text{-A-11})$$

It is interesting to notice that t/τ_{BI} is the same dimensionless time, T^+, used in empirical correlations for hydrodynamic droplet breakup.

In the FITS experiments, a wide range of conditions was investigated using molten iron-alumina and corium as the fuel. The experiments analyzed for their mixing behavior

are listed in Table 3.2.A.1; the dimensionless time ranged from $0 < T^+ < 5$, with characteristic Weber numbers of $1000 < We < 10{,}000$. In all of the experiments performed the width of the water chamber was large compared to the fuel diameter; subsequent FITS tests will investigate this parameter.

The mixing data from some of the FITS experiments are plotted as a function of t/τ_{BI} (T^+ in Figures 3.2-A-1 - 3.2-A-3). Mixture properties are used for the metal-oxide fuel in these calculations. First, note that the data follow similar trends for the range of experiments performed to date ($1 < m_f < 20$ kg). If one plots the same data as a function of the other dimensionless time, t/τ_{BII}, the same trends are observed (Figures 3.2-A-4 and 3.2-A-5); actually the data correlates better using this dimensionless time. Subsequent experiments might be performed at larger scales to determine if these dimensionless groups can still successfully correlate the data, or if other groupings are appropriate. In particular, the fuel fragment diameter, the mixture volume, and displaced water volume are important since they determine the fuel surface area and the average volume fraction of fuel and steam. Knowing these quantities will aid in predicting hydrogen generation. Second, no effect of the fuel Weber number was observed. This may be partially due to the small range over which it varied. Finally, if one compares the trends of H_m/D_f and D_m/D_f for this FITS data with previous data from isothermal tests, one finds that the rate of growth of the fuel coolant mixture in FITS is slower for a given time than for isothermal tests. This seems to confirm the notion that the steam generated in these tests adds compliance to the fuel-coolant system and slows fuel-coolant mixing for a given time span.

The data for the observed fuel fragment size, D_{FR}/D_f, are not plotted, but tabulated in Table 3.2-A-1. This is because the visual data could only be obtained at the end of the test near base contact when the fuel-coolant mixture was large and the fuel droplets could be individually measured. It is recognized that visual measurement of fragment sizes is prone to error. The diameter measured may be larger than the actual diameter due to the luminous image the drop creates on the film; the posttest debris data bear this observation out for two other FITS experiments (FITS-1A and 4A).

The previous correlation of test data applies as the fuel falls through the coolant. If the coolant chamber is narrow or its depth shallow mixing during the fall phase would be impeded or stopped. Mixing on the chamber bottom would probably not be very efficient.

Current FITS data indicate in the absence of an explosion that the melt falls to the base and reagglomerates as it quenches. There is no definitive data to indicate how effective the fuel-coolant mixing is on the chamber base.

3.2-A.4.3 Limits to Fuel-Coolant Mixing

If the steam generation rate becomes too large as the fuel and coolant mix the fuel (or coolant) could be rapidly carried out (fluidized) of the mixture and mixing would be impeded. It is important that one identifies these physical limits to mixing because they represent the bounds that would be set on this dynamic process.

The effect of the physical boundaries is qualitatively obvious, although not quantitatively know. Base contact could trigger an energetic FCI (steam explosion) as the FITS data indicate. If not, the fuel would settle on the chamber base, and slowly quench. However, in the accident, the decay heat power combined with the fuel molten state might cause prolonged thermal attack of the concrete basemat.

Limits on fuel-coolant mixing due to steam generation could cause the fuel (or coolant) to be carried away with the steam flow. One would expect the mixing process to be self-limiting; i.e., given sufficient time, the fuel would mix and break up to an average size no smaller than that which would cause the liquids to be fluidized and swept away. The fuel droplet distribution and the average diameter, D_{FR}, may be larger than this limit if time is short (due to a small water depth or a triggered explosion). In addition, because the fuel enters the water in a pouring mode of contact, the mass first to reach the coolant chamber bottom would be better mixed than fuel at the top of the water pool. Therefore, if one were to identify this limit on mixing it would represent the minimum average fuel diameter to which all the fuel falling through the coolant could fragment before the mixture would begin to be fluidized.

To find this minimum fuel diameter, D_{FR}, for the case of fluidization of the fuel droplets, the velocity needed to fluidize a particle, v_{FL}, is equated to the steam velocity, v_v, at any location in the fuel-coolant mixture caused by fuel-coolant heat transfer. Based on a steady state momentum balance the fluidization velocity for a single droplet is given by

$$v_{FL} = \left[\frac{4}{3} \frac{D_{FR_I} g}{C_D} \left[\rho_f / \rho_v \right] \right]^{1/2} \qquad (3.2\text{-A-12})$$

where ρ_v is the steam density, g is the gravitational acceleration, and C_D is the drag coefficient, corrected for the effect of an array of droplets [27, 28] ($C_D \sim 1$). Now the steam velocity cannot exceed this value or else the fuel droplets will be swept away. This would first occur at the top of the mixture where all the steam from the mixing zone exists to maintain equal pressure with the ambient. Let us consider the steam velocity at the top of the mixture, realizing that the fuel droplet diameter determined from this simple analysis would signal the beginning of the fuel sweepout. Actually, the average fuel diameter in a test would fall slightly below this limit before a majority of the fuel begins to be swept away. The steam velocity at the top of the pool is found by an energy balance to be

$$v_{v_{TOP}} = \frac{m_{v_{TOP}}}{\rho_v A_m \alpha_v} \qquad (3.2\text{-A-13})$$

$$m_{v_{TOP}} = \frac{6\alpha_f V_m q''_{drop}}{D_{FR_I} i_{fg}} \qquad (3.2\text{-A-14})$$

$$q''_{DROP} = \sigma_r(T_f^4 - T_{sat_c}^4) + h_{film}(T_f - T_{sat_c}) \quad . \qquad (3.2\text{-A-15})$$

Notice that all the energy transferred from the fuel to the coolant was assumed to go into producing steam primarily by black body radiation. These assumptions neglect subcooling of the coolant, the reduction of the radiation view factor, and radiation to other fuel particles. Although one may consider these second order effects both would reduce the predicted minimum mixing diameter (i.e., allow more mixing). When all of these terms are substituted back into Equation (3.2-A-13) the result is

$$v_{v_{TOP}} = \left[\frac{\alpha_f}{\alpha_v}\right]\left[\frac{q''_{DROP}}{\rho_v i_{fg}}\right]\left[\frac{H_m}{D_{FR_I}}\right] \qquad (3.2\text{-A-16})$$

where H_m is the mixture height. When the two velocities are equated, one gets for the average minimum mixing diameter (3.2-A-12) and (3.2-A-16).

$$D_{FR_I} = 3\left[\frac{C_D}{\rho_f \rho_v g}\left[\frac{\alpha_f q''_{DROP} II_m}{\alpha_v i_{fg}}\right]^2\right]^{1/3} \qquad (3.2\text{-A-17})$$

Remember that all the assumptions used to derive this simplified mixing diameter limit predict the threshold for fuel sweep out from the top of the mixture. The average fuel size could fall slightly below this limit before a major fraction of the fuel would begin to be fluidized. For example, if one equated these velocities near the bottom of the mixture (e.g., the lower third of V_m) to assure that a majority of the fuel would be swept out the predicted D_{FR_I} would decrease by a factor of two. Also realize that this is a quasisteady limit and applied only insofar as one knows the mixing zone conditions (i.e., volume fractions in mixing zone - Figure 3.2-A-1 and 3.2-A-2) at any point in time. The empirical correlations developed from FITS tests that were just presented would give one the initial conditions needed to use this model.

Notice that this physical limit is different from the model proposed by Henry.[9, 10] In the model considered here, the physical picture is that the steam flows out the top of the fuel-coolant mixture, water flows in from the bottom and sides, and the fuel falls and disperses radially. This picture is more in line with the debris bed sweepout concepts put forth by Rivard and Lipinski.[29] (Actually, the counterflow hydrodynamic criteria of Henry does seem reasonable if one applies it to the mixture surface area rather than the coolant surface area; in this case the area of interest grows with time.)

To find the minimum fuel diameter for the case of fluidization of the coolant which enters the mixing zone, $D_{FR_{II}}$ one would perform the same analysis as before except the fluidization velocity is based on the coolant length scale, D_c.

$$v_{FL} = \frac{3}{4}\frac{D_c g}{C_D}\left[\rho_{c/\rho_v}\right]^{1/2} \qquad (3.2\text{-A-18})$$

Let a unit volume of the mixing region contain N_f fuel droplets of diameter $D_{FR_{II}}$ with each surrounded by a layer of vapor and an outer layer of coolant. Now, when coolant

fluidization occurs, assume that the coolant around each fuel drop leaves as a coolant drop of diameter D_c, with the number of coolant drops produced per unit volume being $N_c = N_f$.

$$\frac{D_c^3}{D_{FR_{II}}^3} = \frac{\alpha_c V_M}{\alpha_f V_M} \qquad (3.2\text{-A-19})$$

where α_c is the coolant volume fraction in the mixture. This gives a relation between D_c and $D_{FR_{II}}$.

$$D_c = D_{FR_{II}} \left[\alpha_c/\alpha_f\right]^{1/3} \qquad (3.2\text{-A-20})$$

The result in combination with Equations 3.2-A-9 and 3.2-A-13 gives an estimate of $D_{FR_{II}}$.

$$D_{FR_{II}} = \left[\frac{3C_D}{4\rho_v \rho_c g} \left[\frac{\alpha_f}{\alpha_c}\right]^{1/3} \left[\frac{\alpha_f \, q''_{DROP^{II}_m}}{\alpha_v \, i_{fg}}\right]^2\right]^{1/3} . \qquad (3.2\text{-A-21})$$

The same comments concerning D_{FR_I} are applicable here; the volume fractions of fuel and steam are needed from the experiments or separate analysis to employ this model.

A prediction of the minimum fuel mixing diameter due to fluidization can be made using Equations (3.2-A-17) and (3.2-A-21). These calculations can then be compared to the actual data of D_{FR} (Table 3.2-A-1) to determine if the model is in agreement with the observed data. The results of the calculations are presented in Table 3.2-A-2, and the agreement between the model and the data is good. The agreement also suggests that the fall time was sufficiently long enough ($2.5 < T^+ < 5$) to allow the fuel to break apart to a small diameter. One could use this criterion of dimensionless time to predict the mixing time and minimum diameter for larger scale FCI events.

Note that in all the tests the fuel mass was a mixture of an oxidic phase (UO_2-ZrO_2 or Al_2O_3) and a metallic phase (stainless steel or iron). In the calculation, it

was assumed that the heterogeneous mixture behaved as a homogeneous fuel with average mixture properties. This is a reasonable first approximation based on the data [16] indicating that posttest debris was compositionally homogeneous for any diameter range. Also note that the minimum energy required for mixing, E_M (Equation 3.2-A-1), is very small, of the order of 5-10 J; this is less than 0.1 percent of the fuel thermal energy.

3.2-A.4.4 Steam/Hydrogen Generation During Mixing

Assuming that one can now estimate the minimum fuel diameter during mixing, and therefore, calculate the maximum fuel surface area, then the steam and hydrogen generation rates could be determined. The rate of steam generation is found by multiplying the heat flux from one drop, q''_{DROP} (Equation 3.2-A-15) by the heat transfer area and dividing by the energy necessary to vaporize the water

$$(i''_{fg} = i_f + c_{Pc}(T_{sat}-T_c));$$

the result is

$$m_v = \left[\frac{6\ m_f}{D_{FR}}\right] \frac{q''_{DROP}}{i''_{fg}} \quad . \qquad (3.2\text{-A-}22)$$

If one uses the minimum mixing diameter the resulting steam generation rate is a maximum. Numerical results are presented in Table 3.2-A-2 for the FITS tests.

The kinetic rate of metal oxidation and hydrogen generation is a function of three important variables; the temperature of the fuel surface at which oxidation is occurring, the rate of diffusion of the vapor to the fuel surface, and the rate of diffusion of the oxygen into the fuel liquid phase. Currently there is no experimental data available to determine the rate of reaction of water with molten metallic reactor materials (zirconium or stainless steel). It is expected that this reaction rate would also be controlled by mass transfer in the liquid fuel phase given an abundance of steam. In his zirconium-water experiments, Baker [12] approximated the molten reaction rate in calculations by assuming mass transfer in the gaseous phase (steam diffusion) was the limiting process. If one uses this assumption, the metallic fuel droplet can be modeled to be in a quasisteady oxidation process. The governing mass

transfer Equation [30] can be written in spherical coordinates and integrated to give the molar hydrogen generation rate for the droplet

$$\dot{N}_{H_2} = \frac{4\pi D_o P_{H_2}}{R_o T_o} \left[\frac{1}{R_{FR}} - \frac{1}{R_C} \right]^{-1} \qquad (3.2\text{-A-}23)$$

where R_C is the radius of vapor-liquid coolant interface. Based upon small scale FCI tests [11] the vapor film thickness is on the order of 1 mm when hydrogen is present. The total generation rate is found by multiplying the rate per droplet by the total number of droplets (the total metallic fuel mass divided by the mass of a droplet).

Using the minimum mixing diameters, the maximum hydrogen generation rate was calculated and is given in Table 3.2-A-2. Notice that the rate of hydrogen production is approximately 50 times smaller than that for steam. In fact if one uses this maximum generation rate with the mixing time in the FITS experiments, only a few gmole of hydrogen are predicted to be produced. This corresponds to about 5 percent of the total metallic mass.

3.2-A.5 STEAM EXPLOSIONS

3.2-A.5.1 Triggering and Propagation

In References 16 and 31, we described the steam explosion process and divided into four separate phases: mixing, triggering, propagation and expansion. The recent FITSB experiments, which we discuss here, showed that these phases were still distinct, but that triggering and propagation are more complicated than was first reported in Reference 16.

As opposed to the more common base triggering phenomena observed in those experiments that only used 2-5 kg of melt, we observed triggers that occurred randomly: at or near the water surface; at or near the water chamber base or side walls; on occasion at all these locations. Some of these triggers escalated into a propagating wave through the melt-water mixture, while the remainder decayed locally with no continuing observable effect. When recorded by the cameras, triggers appeared as rather complicated wave-like phenomena in the water surrounding the melt-water mixture. Propagation had a similar appearance, but occurred in the melt-water mixture and resulted in significant extinction of melt luminosity.

3.2-A.5.2 Single Explosions

Table 3.2-A-3 describes the nine experiments conducted in the FITSB series and a description of some of the important features is discussed below. The table also includes data from the first in-chamber tests (FITSA).

Experiments 2B, 3B, 7B, and 9B all resulted in single explosions triggered either at the water surface or water chamber base. The sequence of events leading to these explosions was similar to the earlier 2-5 kg experiments. Immediately after contact with the water, the melt was observed to fragment into droplets estimated to be between 10 and 20 mm in diameter. The fragmentation and mixing continued until the time of explosion trigger. Chamber air-pressure records for these single explosions showed three characteristic features which depended on initial conditions such as water depth and mass ratio. These characteristics were: a short rise time to the pressure peak; a relaxation in approximately 20 ms to a quasistatic plateau; and late time chamber repressurization due to steam generation with possible augmentation by hydrogen production.

3.2-A.5.3 Multiple Explosions

Three of the experiments (FITS 1B, 4B, and 8B, see Table 3.2-A-3) having mass ratios of 12, 12, and 15 and water depths of 61, 61, and 76 cm respectively, resulted in double explosions; i.e., there were two explosive interactions separated by approximately 120 to 140 ms in each experiment.

The first explosion in FITS1B occurred 142 ms after melt entry and was similar to the single explosions described above. We estimated that 14 kg of the total of 18.7 kg of melt was coarsely mixed in the water prior to triggering of the explosion at the melt-water interface on or near the water surface. The explosion was triggered before the submerged leading edge of the melt had contacted the water chamber base, and the direction of propagation was downward at approximately 300 m/s. Pieces of water chamber and residual water and melt impacted the camera ports before the second explosion which was not immediately observed; this explosion only became apparent when active pressure data became available. Comparison of active data and visual observations showed that there was a second explosion 133 ms after the first.

Chamber air pressure data showed two peaks due to the steam explosions and two corresponding pressure plateaus, followed by a small late time repressurization.

FITS4B and 8B were attempted to reproduce the FITS1B double explosion result and to determine if entry velocity and/or water depth were important initial conditions for a

double explosion; the results, however, were quantitatively different from FITS1B. Only a small quantity of melt was in the water prior to a surface-triggered first explosion (1.7 kg in FITS4B and 1.9 kg in FITS8B). These explosions, although not recorded by the water phase transducers (60 cm from the explosion site), were observed visually and were sufficiently energetic to cause the water chambers to fail; i.e., the walls and water began to move radially outward toward the camera ports.

Melt fragmentation and mixing in the residual water was enhanced by the first explosion. We observed that the melt was fragmented more thoroughly: there were more droplets, and they were typically in the 5-10 mm diameter range. In addition, the melt was more dispersed, and its velocity as it fell through the residual water was approximately twice that observed when no explosion occurred. The second explosion occurred at approximately the time the melt-water mixture contacted the water chamber base. Due to the severe geometry distortion caused by the first explosion, a propagating wave was not visually observed in either of these second explosions. Late time pressurization following the peak from this explosion was smaller than any others observed, indicating a more efficient explosive utilization of the melt thermal energy. Similar results were obtained from FITS4B.

3.2-A.5.4 Energetics of the Explosion

In a steam explosion, some fraction of the internal energy of the fuel is transferred to the coolant and increases its internal energy during the triggering and propagation phase. The coolant then, having a large vapor pressure, expands against its inertial constraints and transforms some of its internal energy into kinetic and potential energy of the constituents involved in the explosion (fuel, water, air). If the explosion occurs in the open environment then the explosion products expand down to one atmosphere. In the FITS experiments, in the containment chamber, some of the fuel internal energy eventually goes into compressing the chamber atmosphere. Therefore at any time after the steam explosion trigger in the FITS tests the fuel internal energy appears principally in two forms; internal or kinetic energy of the constituents. The sum of these two quantities at any point in time (assuming adiabatic chamber walls) is a measure of the energy derived from the explosion; i.e., analogous to a heat of detonation from a chemical reaction. Different geometries and degrees of confinement can alter the partition of the energy between fuel and coolant, kinetic and internal.

By measuring the dynamic pressure in the water phase, the impulse delivered to the base, and the velocity of the chamber walls during the early expansion phase, the peak

kinetic energy of the explosion was calculated. Because of the difficulties in obtaining some of the data these calculations are subject to errors of 10-30 percent. One ratio of interest then is this kinetic energy relative to the original fuel internal energy sometimes called the explosion conversion ratio, η_{KE}. The internal energy of the constituents at any point in time is a much more difficult quantity to measure. An estimate of it can be obtained by measuring the rise in the internal energy of the air phase in the FITS containment chamber. The internal energy rise in an ideal gas if fixed volume V_c and known specific heat ratio is given by

$$\Delta Q_A = \frac{\Delta P V_c}{\gamma - 1} \qquad (3.2\text{-A-}24)$$

where ΔP is the pressure rise in the air measured before and after the explosion; i.e., from ambient to the quasi-static pressure plateaus recorded by the chamber gas phase pressure transducers. This expression applies to the gas species (air) initially present in the chamber, and does not take into account the (unknown) volumes of product gases such as steam and hydrogen generated by the explosion. This energy can also be expressed as a conversion ratio of internal energy of the air to the original fuel melt internal energy, η_D. Conversion ratios (η_{KE} and η_D) were calculated assuming that the total mass delivered was involved in the explosion; this assumption is reasonable because the resulting debris distributions from the explosion showed no evidence of only part of the fuel participating. The values of η_{KE} and η_D are given in Table 3.2-A-4.

3.2-A.5.5 Conversion Ratio and Debris Data

The mixing that occurs before the explosion is triggered should have an effect on the subsequent explosion. If ample time is given for the fuel to break up into smaller diameter droplets and disperse in the liquid coolant pool more of the fuel mass will be able to rapidly fragment during the explosion into fine debris; this in turn will probably increase the explosion conversion ratio (ratio of the measured kinetic energy to the initial fuel thermal energy). This is empirically demonstrated for the FITS test if one plots the explosion conversion ratio, η_{KE}, and the fuel debris diameter as a function of the initial coolant to fuel mass ratio (Figure 3.2-A-6). In these tests the fuel is dropped into the water as a coherent mass; therefore to a first approximation the coolant to fuel mass ratio is a measure of the mixing that could take place before the explosion. Notice that the conversion ratio rises to almost a constant value (1-2 percent) after the fuel to coolant mass ratio increases above 3

to 1. In contrast the average fuel debris diameter continues to decrease in magnitude until the mass ratio becomes very large (20 to 1).

The same effect can be better observed in one plots the debris diameter and the conversion ratio as a function of the ratio of the fuel-coolant mixture volumes at the time of explosion to the original fuel volume, V_m/V_f. The reasoning here is that as the mixture to fuel volume ratio increases the fuel has more time to disperse in the coolant, breakup into smaller sizes and produce a more efficient explosion. Figure 3.2-A-7 indicates even more clearly the strong correlation of the explosion fuel debris size to initial mixing behavior. Again one notes how the conversion ratio quickly rises to nearly constant values.

It is interesting to note that even when the fuel debris seems relatively coarse (1 mm as in the FITSB Series) the conversion ratio is still large 1-2 percent. This suggests that the percentage of fuel "participating" in the explosion cannot be arbitrarily taken to be small (e.g., based on a thermal equilibration time during the explosion 200 μm). Rather, even the "coarse" fuel debris probably "participates" in the explosion to the extent that it can transfer the thermal energy of its outer surface quickly, and therefore, can affect the explosion conversion ratio. These data suggest one must be careful when trying to distinguish between what fuel "mixed" with water and what fuel "participated" in the explosion.

3.2-A.6 CURRENT OBSERVATIONS AND CONCLUSIONS

The current FCI experiments conducted at Sandia were analyzed to determine the fuel-coolant mixing behavior and the effect of mixing on the explosion energy and debris. Data were well correlated in terms of dimensionless groups derived from the concept that fuel mixing was governed by hydrodynamic breakup (i.e., Taylor instabilities). Physical limits to mixing were proposed which indicate that the minimum mixing diameter is limited by fuel or liquid coolant fluidization. Equations (3.2-A-17) and (3.2-A-21). Using experimental values for steam volume fraction allowed us to predict with good agreement the fuel diameter after mixing had taken place. This mixing model was used to calculate the rate of hydrogen and steam generation in the FITS tests. Finally, the explosion data (η_{KE} and debris size) was noticeably affected by the fuel-coolant mixing process.

The steam explosion experiments show that the conversion ratio η_{KE} did not vary significantly with either mass ratio or water geometry with the exception of the extremely lean mass ratio (FITS7B). The values calculated from chamber pressure data for η_D show a dependence on these two

parameters. Although the test matrix was rather sparse, this result suggests that, as the water/melt mass ratio increased, better mixing was possible and the associated tamping increased the total utilization of the converted thermal energy. Then, since the kinetic energy held roughly constant, it would follow that the stored energy conversion ratio would increase. It is finally important to point out that multiple explosions occurred (100 ms apart) when $12 < m_c/m_f < 15$; also with these multiple events, it appeared that the first explosion enhanced the coarse mixing for the subsequent explosion.

Table 3.2-A.1

Fuel Fragment Size Data During Mixing for FITS Experiments

FITS TEST	MOLTEN FUEL* COMPOSITION	MOLTEN FUEL* MASS (kg)	ENTRY VELOCITY (m/s)	COOLANT DEPTH (m)	TIME TO BASE CONTACT t(msec)	MASS ANG. FUEL FRAGMENT SIZE-BASE CONTACT VISUAL (mm)	MASS ANG. FUEL FRAGMENT SIZE-BASE CONTACT POSTTEST+ (mm)
MD-8	Iron-Alumina	4.7	6.4	0.71	180	8	explosion
MD-11	Iron-Alumina	4.7	4.2	0.71	162	8	explosion
MD-15	Iron-Alumina	1.88	4.6	0.43	121	7	explosion
MD-16	Iron-Alumina	1.85	5.4	0.43	121	7	explosion
MD-19	Iron-Alumina	5.1	5.9	0.61	172	7	explosion
MDC-2	Corium	4.1	6.0	0.53	150	11	explosion
MDC-16	Corium	8.5	6.0	0.53	140	12	explosion
FITS-1A	Iron-Alumina	1.95	6.2	0.43	115	7	2 (partial interaction
FITS-4A	Iron-Alumina	4.3	7.0	0.61	140	7	4

* Fuel was either Iron-alumina (Fe-55 w/o, Al_2O_3-45 w/o) or Corium (UO_2-53 w/o, ZrO_2-17 w/o, Stain. Steel-30 w/0)

\+ Visual data based on camera speed of 2000-9000 fsp and posttestmixing debris is not obtained when there is an explosion

Table 3.2-A.2

Prediction of FITS Mixing Behavior

FITS TESTS	TIME TO BASE CONTACT T*	MINIMUM MIXING DIAMETER		MAXIMUM STEAM GENERATION RATE		MAXIMUM HYDROGEN GENERATION RATE	
		D_{FRI} (mm)	D_{FRII} (mm)	for D_{FRI} (gmoles/sec)	for D_{FRII} (gmoles/sec)	for D_{FRI} (gmoles/sec)	for D_{FRII} (gmoles/sec)
MD-8	8.66	6.5	8.3	101	79	2.2	1.7
MD-11	5.23	8.3	10.4	79	63	1.7	1.3
MD-15	5.57	6.3	8.2	33	26	0.88	0.66
MD-16	5.07	6.3	3.2	33	25	0.88	0.66
MD-19	7.45	7.0	8.9	81	64	2.2	1.7
MDC-2	8.60	6.0	12.1	76	38	2.0	1.0
MDC-16	6.88	6.0	12.1	156	78	4.2	2.1
FITS-1A	7.13	5.8	7.3	47	37	0.98	0.77
FITS-4A	7.13	7.3	9.3	82	65	1.8	1.4

* Calculations are based on volume fractions from FITS data and measured fuel temperatures of ~2700 K

Table 3.2-A.3

FITS Initial Conditions and Observations

EXPT	MELT			WATER			INITIAL RATIO WATER/MELT		SPONTANEOUS EXPLOSION		OTHER OBSERVATIONS
	MASS (kg)	Entry Vol (m/a)	Avg. dia. at (a) Entry (cm)	Geometry (cm) sq. x deep	Mass (kg)	Temp. (°C)	MASS	VOL.(b)	Location	Time After Melt Entry (ms)	
1A	1.94	6.2	3.5	.46 x .43	90	10	46	178	n.o.	0.115	Mild Interaction
2A	2.87	4.6	3.6	.53 x .53	152	13	53	203	Surface	0.075	Surface Explosion
3A	5.3	5.0	3.3	.61 x .61	226	24	43	163	Below Surface	0.150	Single Explosion
4A	4.3	7	3.5	.61 x .61	226	25	53	201	n.o.	-	No spontaneous explosion at 1.1 MPa
5A	5.4	5.3	3.2	.61 x .61	226	24	43	163	Base Trig-gered	0.150	Triggered explosion at 1.1 MPa
1B	18.7	5.4	4.1	61 x 61	226	25	12.0	46.0	Surface Unknown	142 275	First Explosion Second Explosion
2B	18.6	6.0	6.0	61 x 30	113	25	6.0	23.0	Surface	84	Single Explosion
3B	18.6	6.0	24.0	43 x 30	57	22	3.0	11.5	Base	77	Single Explosion weak interaction at 70 ms after entry that did not propagate
4B	18.7	6.8	5.8	61 x 61	226	26	12.0	46.0	Surface Base	16 134	First Explosion Second Explosion
6B	18.7	7.2	6.5	46 x 30	63.4	94	3.4	12.9	None	-	Multiple Inter-actions at 40, 57, 82 and 153 ms after melt entry, no prop-agation or steam explosion
7B	18.7	7.4	n.o.	43 x 15.2	28.1	18	1.5	5.7	n.o.(c)	80	No camera data, time estimated from water phase gages
8B	18.7	6.5	29.0	61 x 76	283.5	15	15.0	57.4	Surface Base	27	First Explosion Second Explosion
9B	18.7	7.0	5.6	61 x 45.7	170.0	16	9.0	34.6	Base	98	Single Explosion

(a) Optical measurement (b) Melt density 3.8 gm/cm^3 (c) n.o.= not observed

Table 3.2-A.4

FITS Steam Explosion Results

EXPT	INITIAL MASS RATIO M_c/M_f	MELT[a] ENERGY Q_m (MJ)	MELT MASS AVERAGED PARTICLE SIZE (μm)	SAUTER MEAN DIAMETER (μm)	CONVERSION RATIO (PERCENT) η_{KE}	η_D	$\eta_{KE}+\eta_d$	COMMENTS
1A	46	5.43	2000	2400	0.0	-	-	
2A	53	8.04	260	176	<<1.	-	-	
3A	43	14.8	155	90	1.5	6	7.5	
4A	53	12.04	3800	4740	-	-	-	
5A	43	13.1	155	92	1.5	5.5	7.0	Explosion at 1.1 MPa
1B	16	39.2		188	1.1	2.6	3.7	First Explosion η_{KE} not available
	12	52.4	200		-	5.1	-	
2B	6	52.0	1400	565	1.6	2.8	4.4	
3B	3	52.0	1100	330	1.3	4.0	5.3	
4B	12	52.4		215	1.3	5.7	7.0	
			250		1.3	8.6	9.9	
7B	1.5	33.6	7000	1190	0.3	0.2	0.5	
8B	15	52.4	145	100	1.5	5.9	7.4	
					1.5	7.7	9.2	
9B	9	52.4	900	326	1.1	4.4	5.5	

(a) Based on 2.8 MJ/kg
(b) Melt mass estimated from posttest debris. Only fragmented melt quantity used.

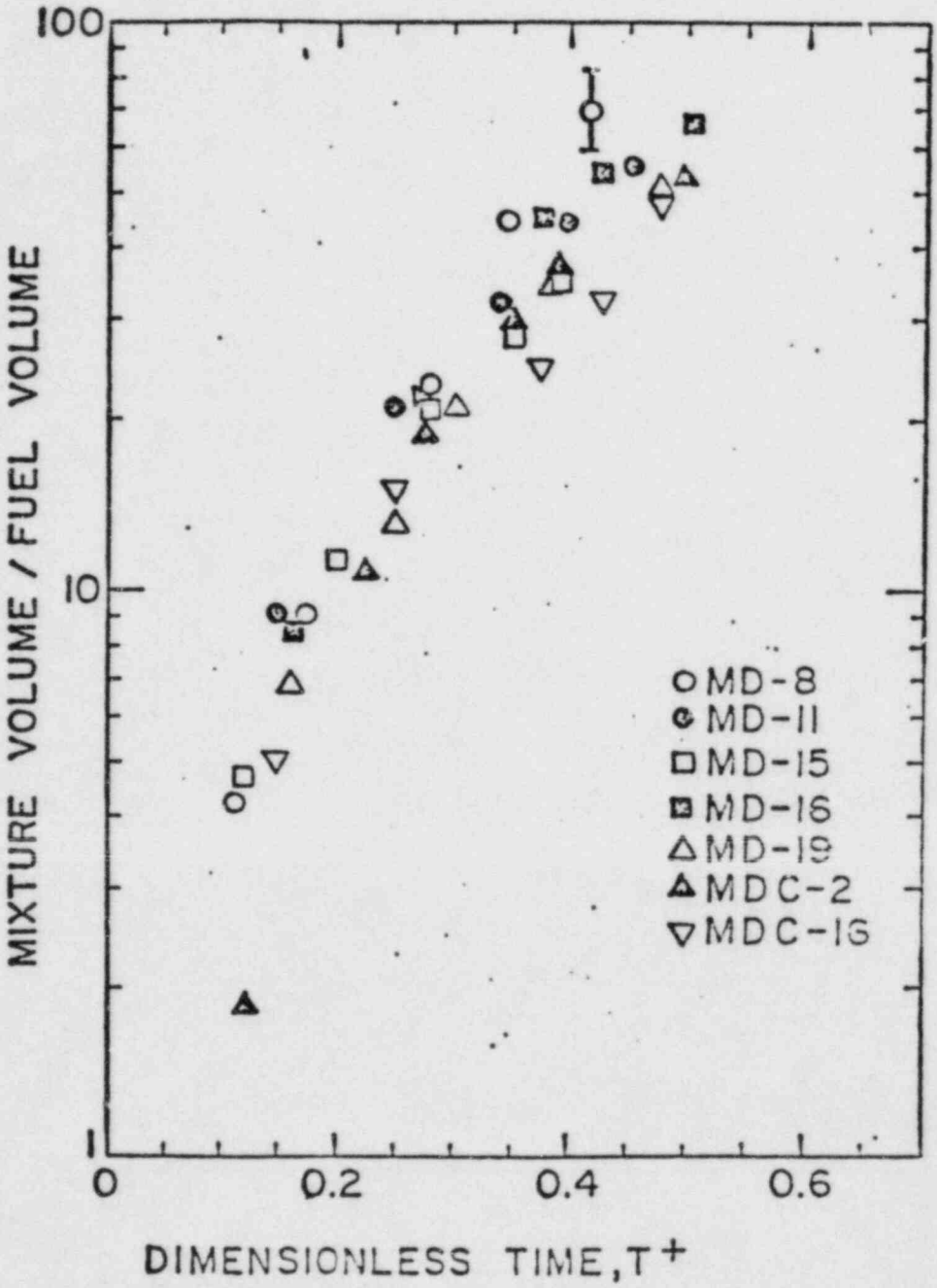

Figure 3.2-A-1. FCI Experiment Results: Mixture-Fuel Volume Ratio vs. Dimensionless Time

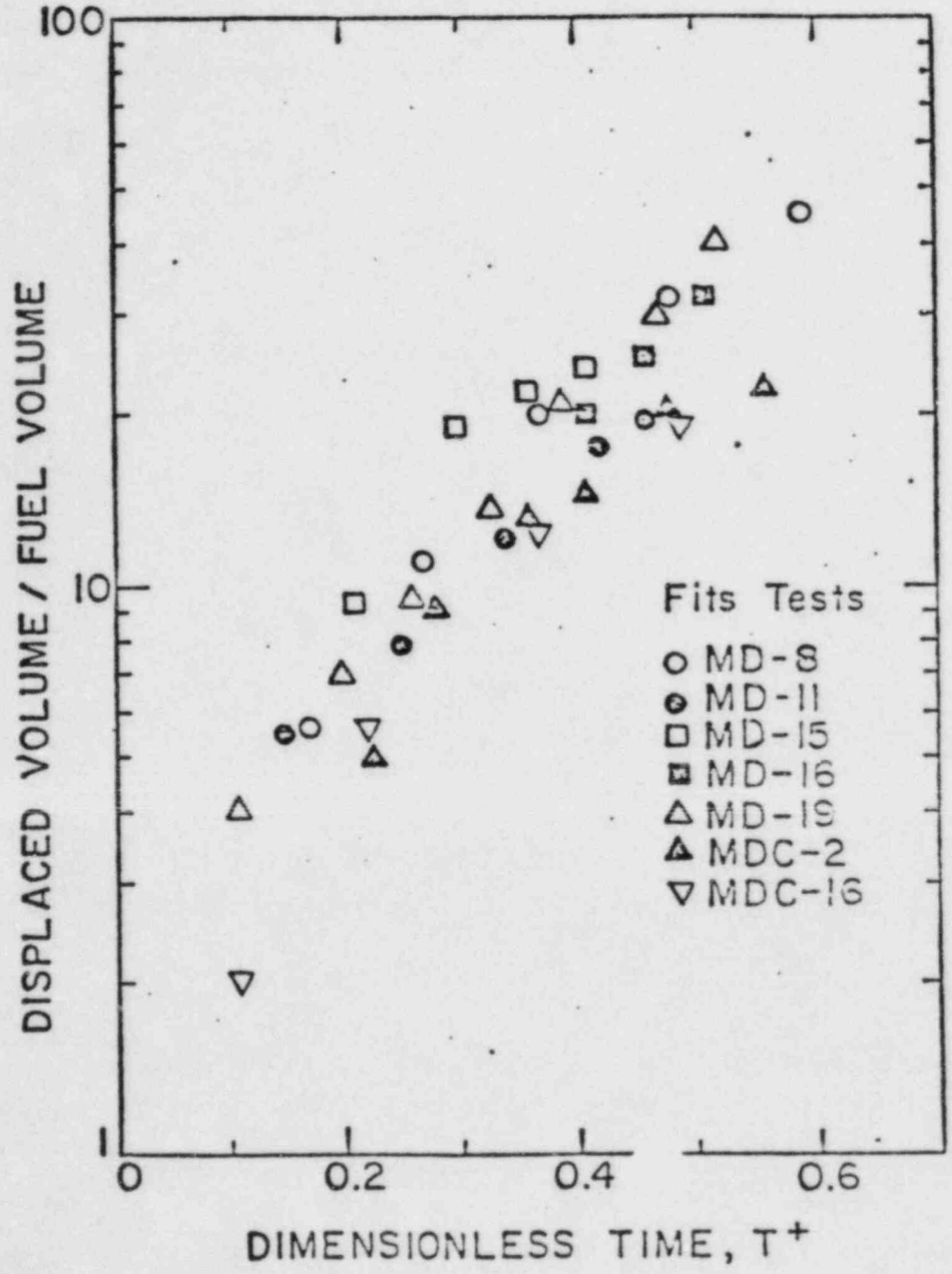

Figure 3.2-A-2. FCI Experiment Results: Displaced Volume-Fuel Volume Ratio vs. Dimensionless Time, T^+

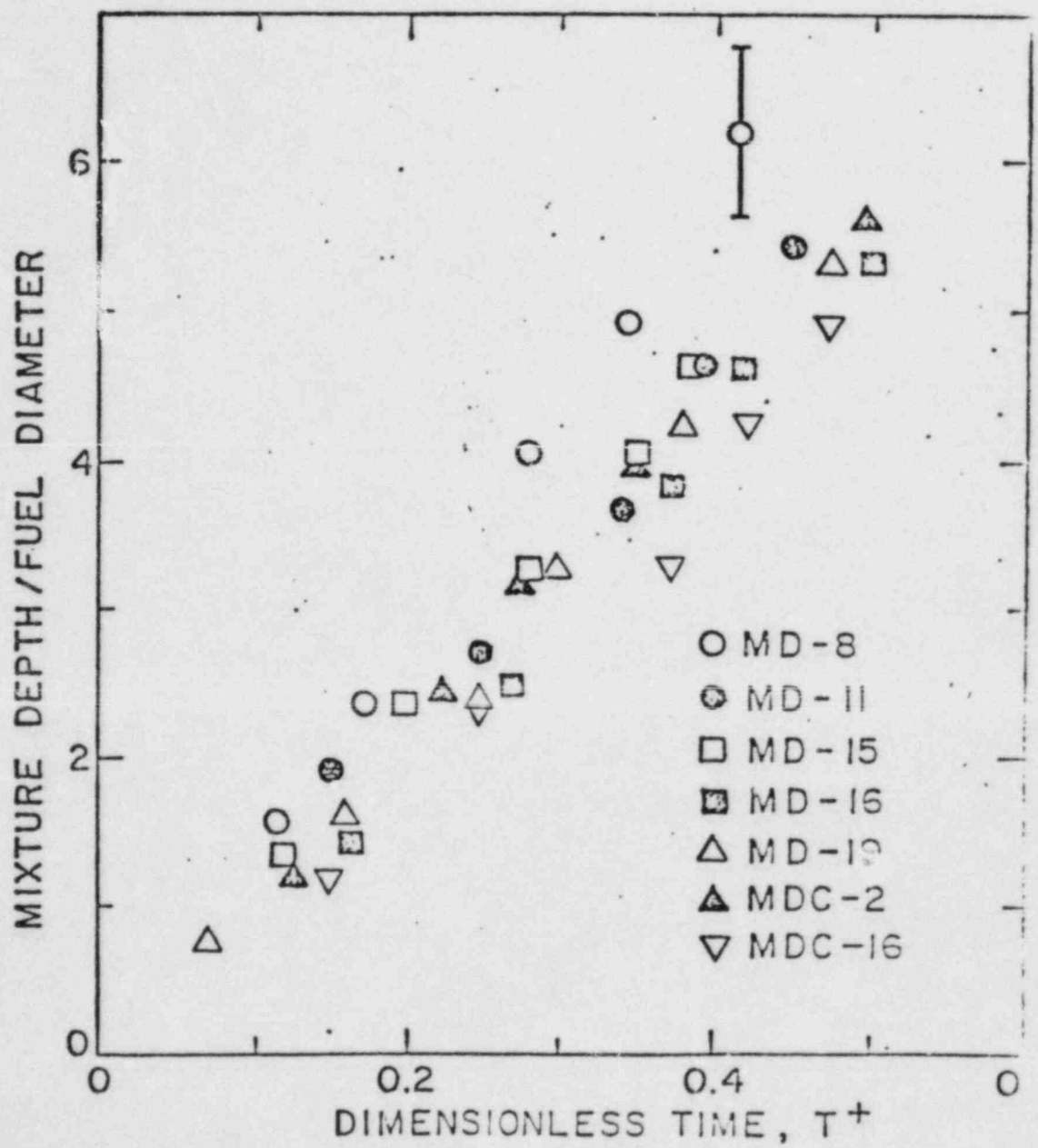

Figure 3.2-A-3. FCI Experiment Results: Mixture Depth-Article Diameter Ratio vs. Dimensionless Time

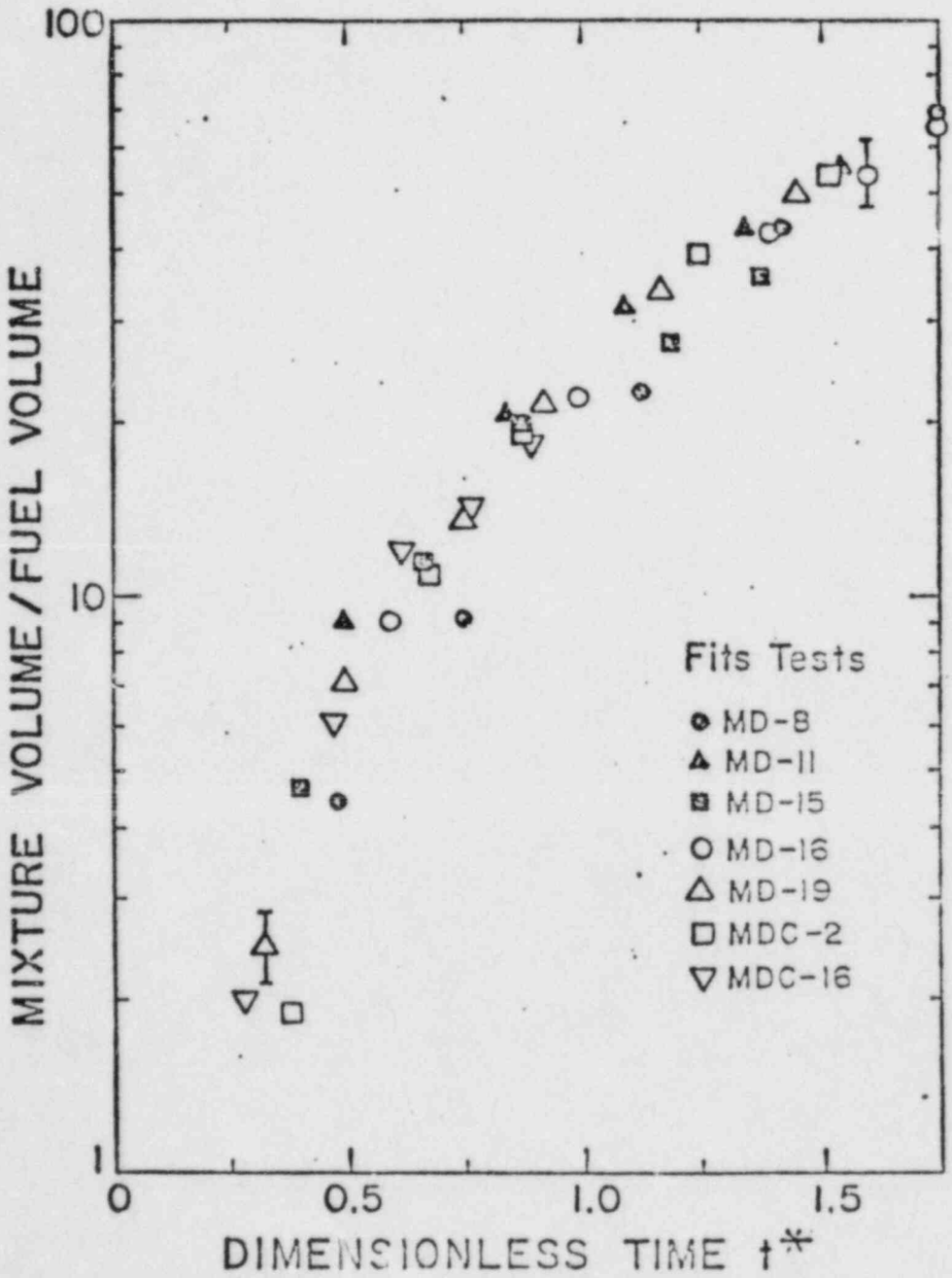

Figure 3.2-A-4. FCI Experiment Results: Mixture-Fuel Volume Ratio vs. Dimensionless Time, t*

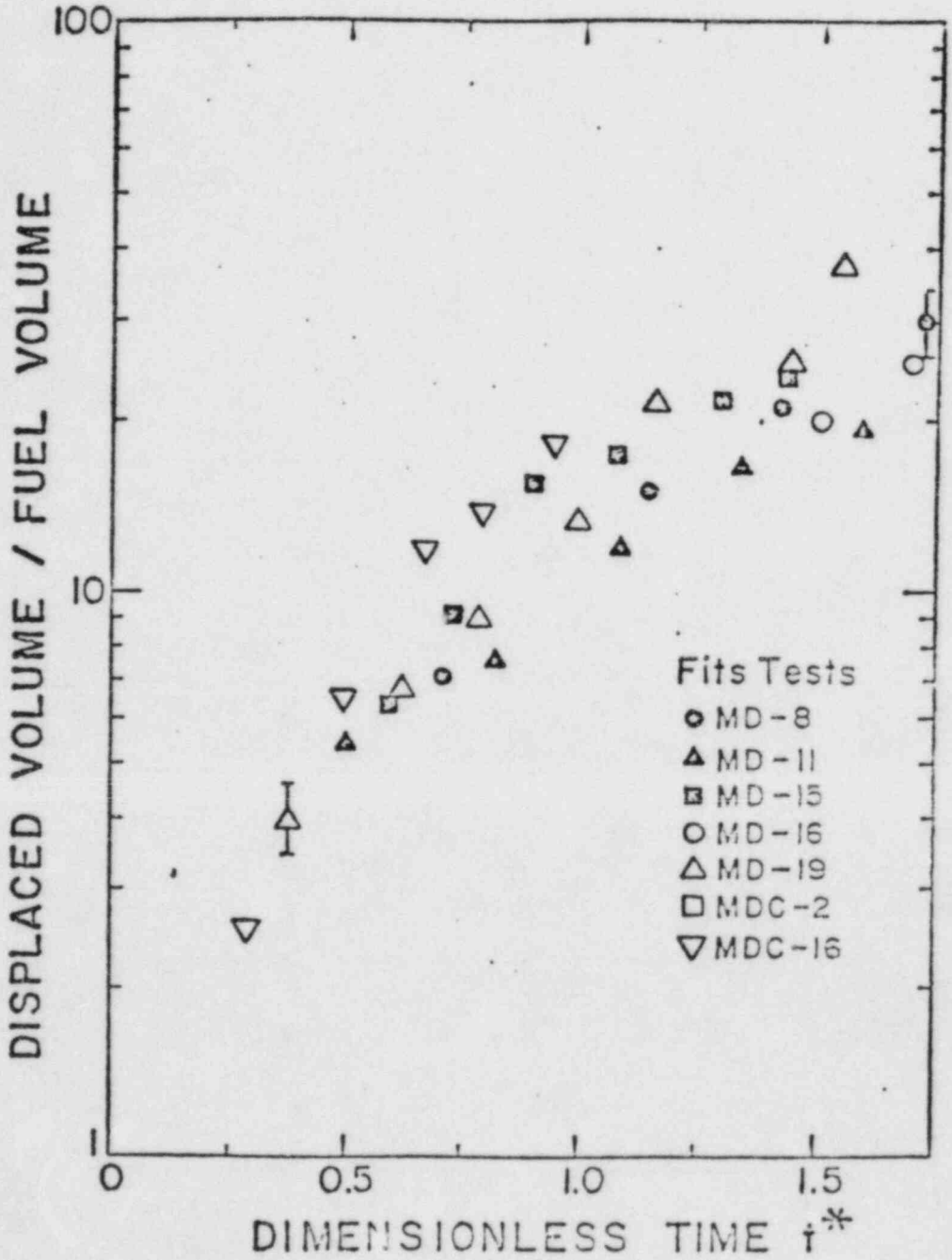

Figure 3.2-A-5. FCI Experiment Results: Displaced Volume-Fuel Volume Ratio vs. Dimensionless Time, t*

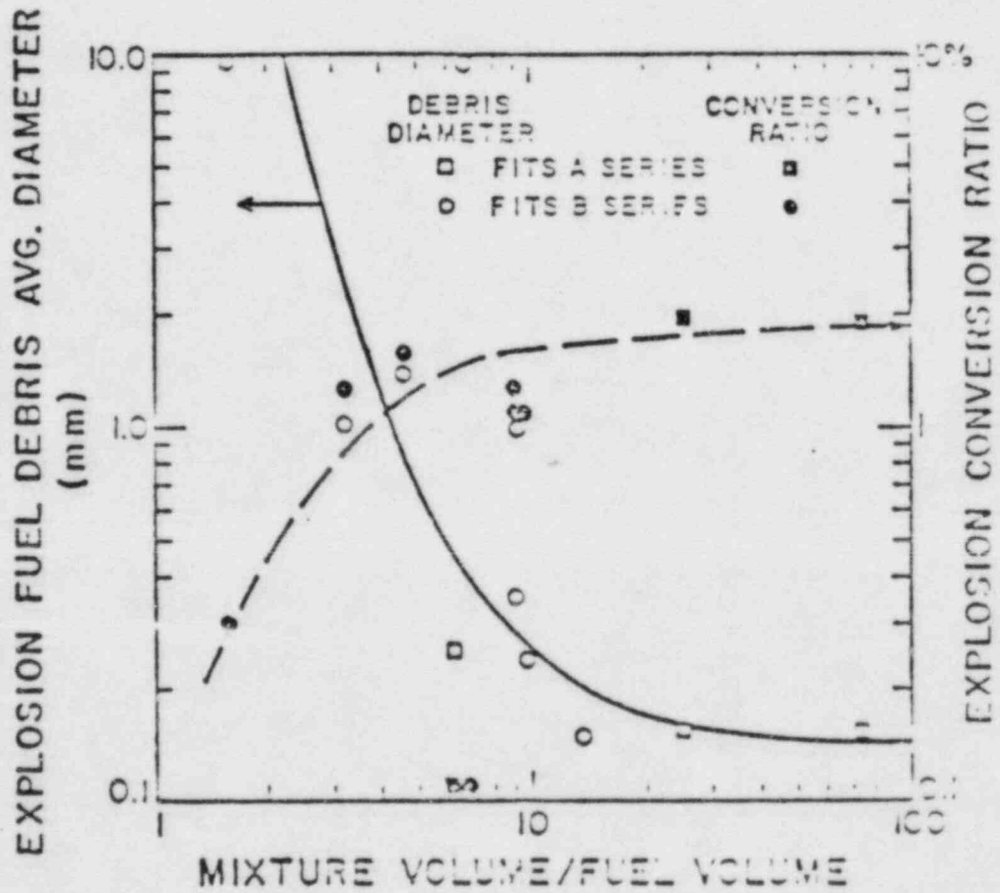

Figure 3.2-A-6. FCI Experiment Results: Poststeam Explosion Debris Size and Energy Conversion Ratio *vs.* Volume Ratio

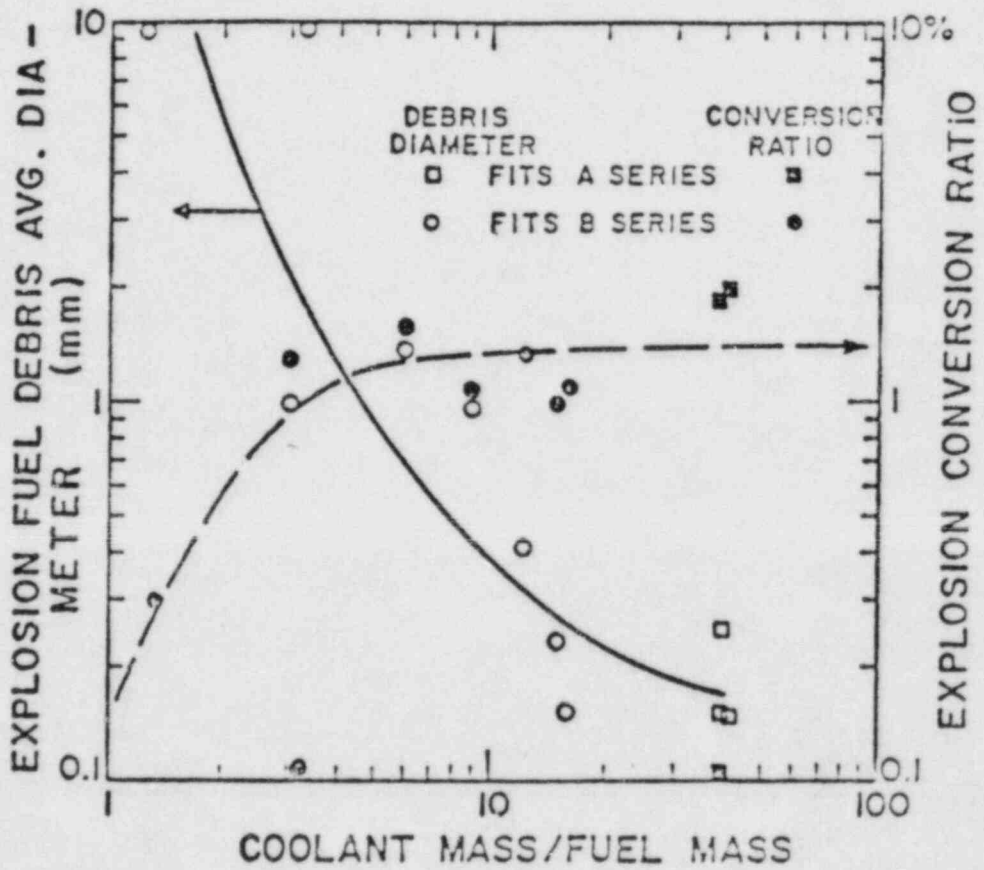

Figure 3.2-A-7. FCI Experiment Results: Debris Size and Conversion Ratio vs. Mass Ratio

3.2-A REFERENCES

1. Buxton, L. D., Molten Core-Water Contact Analysis, SAND77-1842, Sandia National Laboratories, Albuquerque, NM (1979).

2. Murfin, W. B., Editor, Report of the Zion/Indian Point Study: Volume 1, SAND80-0617/1, NUREG/CR-1410, Sandia National Laboratories, Albuquerque, NM (1980).

3. Meyer, J. F., et al., Preliminary Assessment of Core Melt Accidents at the Zion and Indian Point Nuclear Power Plants and Strategies for Mitigating Their Effects, NUREG-0850, Vol 1, USNRC Report (1981).

4. Klopp, G., et al., Zion Probabilistic Safety Study, (Chicago, IL: Commonwealth Edison, 1981).

5. Henry, R. E., et al., "Establishment of a Permanently Coolable State," Trans. ANS, Vol 39, p 368 (1981).

6. Fauske, H. K., "Some Aspects of Liquid-Liquid Heat Transfer and Explosive Boiling," Proc. Fast Reac. Safety Mtg., Beverly Hills, CA (1974).

7. Henry, R. E., and Fauske, H. K., "Nucleation Characteristics in Physical Explosions," Proc. of Third Spec. Mtg. on Sod. Fuel Int. in Fast Reac., Tokyo, Japan (1976).

8. Cho, D. H., et al., "Mixing Considerations for Large-Mass, Energetic Fuel-Coolant Interactions," Proc. ANS/ENS Fast Reac. Safety Mtg., Chicago, IL (1976) CONF-761001.

9. Henry, R. E., and Fauske, H. K., "Core Melt Progression and the Attainment of a Permanently Coolable State," Proc. of Ther. Reac. Fuels Mtg., Sun Valley, ID (1981).

10. Henry, R. E., and Fauske, H. K., "Required Initial Conditions for Energetic Steam Explosions," Fuel-Coolant Interactions, ASME HTD-V19, Wash., DC (1981).

11. Berman, M., Light Water Reactor Safety Quarterly, SAND80-1304, Sandia National Laboratories, Albuquerque, NM, January-March, 1 of 4 (1980), April-June, 2 of 4 (1980), July-September, 3 of 4 (1981), October-December, 4 of 4 (1981).

12. Baker, L., and Just, L. C., Studies of Metal-Water Reactions at High Temperatures, III Experimental and Theoretical Studies of the Zirconium-Water Reaction, ANL-6548, Argonne National Laboratory (May 1962).

13. Cathcart, J. V., et al., Zirconium Metal-Water Oxidation Kinetics IV. Reaction Rate Studies, ORNL/NUREG-17, Oak Ridge National Laboratory (August 1977).

14. Lien, G. F., Superheater Alloys in High Temperature High Pressure Steam, ASME, New York (1968).

15. Bittle, J. T., et al., "Oxidation of 304L Stainless Steel by Steam and by Air," Corrosion NACE, 25, No. 1 (January 1969).

16. Mitchell, D. E., Corradini, M. L., and Tarbell, W. W., Intermediate Scale Steam Explosion Phenomena: Experiments and Analysis, SAND81-0124, Sandia National Laboratories (1981).

17. Buxton, L. D., and Benedick, W. B., Steam Explosion Efficiency Studies, SAND69-1399, NUREG/CR-0947, Sandia National Laboratories, Albuquerque, NM.

18. Buxton, L. D., Benedick, W. B., Corradini, M. L., Steam Explosion Efficiency Studies: PartII--Corium Experiments, SAND80-1324, NUREG/CR-1756, Sandia National Laboratories, Albuquerque, NM (October 1980).

19. Berman, M., Light Water Reactor Safety Research Program Semiannual Report, October 1981 - March 1982, SAND82-1572, NUREG/CR2841, forthcoming.

20. Hinze, J. O., "Fundamentals of the Hydrodynamic Mechanisms of Splitting in Dispersion Processes," AIChE Jnl., Vol 1, No. 3 (1981).

21. Benz, R., et al., "Hydrodynamic Analysis of Shock-Wave Induced Fragmentation in Liquid-Liquid Systems (Part I)," 4th CSNI Specialist Meeting on Fuel-Coolant Interactions in Nuclear Reactor Safety, Bournemouth, England (April 1979).

22. Baines, M., and Buttery, N. E., CEGB Report RD/B/N3497, Berkeley Nuclear Lab. (1975).

23. Theofanous, T. G., "Fuel-Coolant Interactions and Hydrodynamic Fragmentation," Proceedings of the Fast Reactor Safety Meeting, Seattle, WA (August 1979).

24. Pilch, M., Acceleration Induced Fragmentation of Liquid Drops, Doctoral Thesis, Univ. of Virginia (1981).

25. Pilch, M. and Erdman, C. A., "Consideration of Liquid Fragmentation in Safety Analysis," Trans. ANS. Vol 38, p 403 (1981).

26. Corradini, M. L., Heat Transfer and Fluid Flow Aspects of Fuel-Coolant Interactions, Doctoral Thesis, MIT (1978).

27. Collier, J., Convective Boiling and Condensation, 2nd ed. (New York, NY. McGraw-Hill, 1981).

28. Wallis, G., One-Dimensional Two-Phase Flow, 2nd ed., (New York, NY: McGraw-Hill, 1981).

29. Rivard, J. B., Chapter 5, Report of the Zion/Indian Point Study: Volume I, SAND80-0617/1, NUREG/CR-1410, Sandia National Laboratories, Albuquerque, NM (1980).

30. Bird, R. B., et al., Transport Phenomena (New Jersey: Wiley, 1960).

31. Corradini, M. L., "Analysis and Modeling of Large-Scale Steam Explosion Experiments," Nuclear Science and Engineering, (December 1982).

APPENDIX 3.2-B. DEBRIS BED DRYOUT

B. Lipinski

3.2-B-1 COMPARISON OF DRYOUT MODELS FOR VOLUME HEATED PARTICULATE DEBRIS

Volume-heated particulate debris submerged in water may produce boiling so strong that portions of the debris may become dry even though the pool of water overlying the debris is maintained. The dry regions will heat rapidly and attack the structures supporting the debris (e.g., concrete). For this reason, the conditions needed to cause debris dryout have been studied extensively.

Figure 3.2-B-1 depicts boiling and dryout in a volume-heated particle bed submerged in a pool of water and resting on an impermeable support. The liquid must enter the bed from an overlying pool against the upward-flowing vapor. For simplicity all the liquid is assumed to be at the boiling point so that heat is removed solely by boiling. Channels form at the top of the bed if the particles are small (less than about 1 mm). Theses channels are typically small and negligible for thick LWR beds, but may be important in interpreting data from small-sized experiments.

The vapor in the debris flows upward while the liquid flows downward into the bed. The vapor is driven from the bed by the pressure developed as it boils. The liquid is pulled into the bed both by gravity and by capillary force. If these two forces are sufficient to overcome the frictional forces of the upward-moving vapor, steady state boiling can occur throughout the bed. However, for high-power generation rates within the bed, the flow of liquid is retarded sufficiently so that all of it vaporizes before it reaches the bed bottom. In such a case the bottom of the bed becomes dry. The bed power at which some part of the bed just becomes dry is called the dryout power. An historical measure of the dryout condition is the dryout heat flux, defined as the total bed power at dryout divided by the bed top (cross sectional) surface area. (Note that this is not the heat flux per unit area from the surface of an individual particle.)

Many experiments have attempted to simulate dryout in reactor debris.[1-9] In most of these, inductive heating of single-sized metal spheres has been used to simulate the nearly uniform volumetric power of decay heat. These experiments (and some theoretical considerations) have shown that the dryout heat flux generally increases with increasing particle diameter, bed porosity, ambient pressure, and liquid mass flux entering the bottom of the debris (as might occur if the bed were on a porous support). The dryout flux is essentially independent of bed thickness for deep debris, but starts to increase as the debris becomes shallow. Debris stratification (in which the average particle diameter varies with elevation) can strongly decrease the dryout flux if the small particles are at the top of the bed.

The debris in the reactor cavity or on the reactor floor may consist of particles ranging from less than 0.1 mm to tens of millimeters or more, with a debris thickness of as much as 1 to 2 meters, porosity from 30 percent to 60 percent or more, and ambient pressures from 1 to 10 bars (depending on the containment failure pressure). The debris may be mixed or stratified, with zero or some liquid entry from below. The flow regimes and important phenomena are different at the different ends of the parameter ranges described. A good debris cooling model must be able to handle all the regimes and be able to identify where changes in behavior occur.

3.2-B.1.1 Debris Dryout Models

Since the start of dryout marks the division between benign coolable debris and debris which can heat, remelt, attack concrete, and generate combustible gases, considerable research has gone into developing dryout models.[9-26] A variety of driving forces, flow resistances, and dryout criteria have been used in the derivation of these models. The Dhir-Catton [9], Hardee-Nilson [11], Shires-Stevens [12], and Jones, et al. [14] models are all based on laminar flow only and are applicable to small particles only. The Sowa, et al. [10], Theofanous-Saito [16], Henry-Fauske [17], Ostensen-Lipinski [18], Squarer [20], and Dhir-Barleon [25] models are all based on flooding correlations and applicable to turbulent flow and large particles only. The Lipinski [13,15,22], Gabor, et al., [19], Reed [21], Henry, et al. [23], Turland-Moore [24], and Gorham-Bergeron [26] models all include both laminar and turbulent flow. Only the Shires-Stevens, Lipinski, Reed, and Turland-Moore models include capillary force. The Turland-Moore and Gorham-Bergeron models include time dependence, but the dryout heat flux criteria are similar to simplified cases of the Lipinski [22] model.

Squarer, et al.,[2], Appendix 3.4.5 of the Zion Probabalistic Safety Study [27], and the Gittus report on PWR Degraded Core Analysis [28] each compare the Lipinski (1980) model [13] to various other models and conclude it is the best (of those compared) in matching the available dryout data. (They also note that it tends to overpredict the dryout flux for large particles.) The Lipinski (1980) model was extended in 1981 to one dimension [15] so as to be applicable to stratified beds as well as mixed beds, and to describe postdryout behavior. The Lipinski (1981) model was extended in 1982 [22] to include channels at the top of the debris, and to allow for liquid flow entry at the bottom of the bed. Recently (1983) Lipinski [29] has suggested a minor improvement for large particles which reduces the predicted dryout powers by about 40 percent.

The Lipinski 1982 model [22] is very broad, but results in a first order differential equation which must be solved numerically. Fortunately, for many LWR applications, the differential equation simplifies to an algebraic equation. One regime is for zero liquid flow entry from below the bed and negligible channels (nonshallow debris on an impermeable support). The first requirement is met for debris resting on concrete. The second is met for moderately thick debris.

3.2-B.1.2 Nonshallow Debris on an Impermeable Support

The thickness requirement for nonshallow debris is that the debris thickness exceed three channel lengths:

$$H > \frac{18\ \sigma\ \cos\theta}{\varepsilon d\ (\rho_p - \rho_l)\ g} \qquad (3.2\text{-B-}1)$$

where σ is surface tension, θ is contact angle between the liquid and particle, ε is bed porosity, d is average particle diameter, ρ_p and ρ_l are particle and liquid densities, and g is gravitational acceleration. For example, for 0.5 mm UO_2 particles in water, the bed thickness must exceed 0.06 m. (This criterion uses the channel length model of Jones, et al.,[30]). Most LWR debris of interest will meet this requirement.

Under these conditions, the Lipinski (1983) model dryout criterion reduces to

$$q_d = \left[\frac{q_t^4}{4q_l^2} + q_t^2\right]^{1/2} - \frac{q_t^2}{2q_l} \qquad (3.2\text{-B-}2)$$

where

$$q_l = \frac{(\rho_l-\rho_v)\ g\ d^2\ \varepsilon^3\ h_{lv}\left[1 + \frac{6\ \sigma\ \cos\theta\ (1-\varepsilon)}{\varepsilon d(\rho_l-\rho_v)gH}\right]}{150\ (1-\varepsilon)^2\ (\nu^{1/4}+l^{1/4})^4} \quad (3.2\text{-B-3})$$

and

$$q_t = h_{lv}\frac{\rho_v\ \rho_l\ (\rho_l-\rho_v)\ g\ d\ \varepsilon^3\left[1 + \frac{6\ \sigma\ \cos\theta\ (1-\varepsilon)}{\varepsilon d(\rho_l-\rho_v)gH}\right]}{1.75\ (1-\varepsilon)\ (\rho_v^{1/6}+\rho_l^{1/6})^6} \quad (3.2\text{-B-4})$$

where q_d is the dryout flux, h_{lv} is latent heat of vaporization, H is bed thickness, ν and l are vapor and liquid kinematic viscosities, and ρ_v is vapor density. Note that q_l and q_t are also the dryout fluxes in the laminar and turbulent limits respectively.

The parameter which most influences the dryout flux is the diameter of the particles which comprise the bed. Figure 3.2-B-2 shows dryout data from various References [1-6] for beds of single-sized spheres in water. Only data from beds near 200 mm thick are shown, except for large particles where the deep bed limit is reached before 200 mm. The models of various researchers are also shown in the figure. (The model by Henry, et al.[23] contains a jump because of an assumed increase in dryout flux when bubbles form within the liquid film on the particles.) The transition from laminar (small-particle) to turbulent (large-particle) behavior can be seen to occur at about 1.5 mm. The Lipinski 1983 model agrees with nearly all the data within a factor of two.

Similar plots for Freon-113 and acetone are shown in Figures 3.2-B-3 and 3.2-B-4. These figures show the effect of changing material properties, such as would occur with saturated water as the pressure in the containment building or reactor vessel changed. The Lipinski model agrees with most of the data within about 50 percent.

3.2-B.1.3 Deep Debris on a Permeable Support

The full one-dimensional Lipinski model may also be reduced to an algebraic equation for debris resting on a permeable support (i.e., where liquid may enter the debris from below). However, the simplification can only be made if the debris is thick enough that capillary forces are negligible. This requirement is approximately

$$H > \frac{18\ \sigma\ \cos\theta\ (1-\varepsilon)}{\varepsilon\ d\ (\rho_l-\rho_v)\ g} \quad . \tag{3.2-B-5}$$

For 0.5 mm diameter particles in water, the debris thickness must exceed about 0.1 m.

In this case the dryout flux may be determined from

$$\frac{1.75\ (1-\varepsilon)\ q^2}{\varepsilon^3\ d\ h_{lv}} \left[\frac{1}{\rho_v(1-s)^5} + \frac{1}{\rho_l s^5}\right]$$

$$+ \frac{150\ (1-\varepsilon)^2\ q}{\varepsilon^3\ d^2\ h_{lv}} \left[\frac{1}{(1-s)^3} + \frac{1}{s^3} - \frac{3.5\ d\ w}{150\ \rho_l\ (1-\varepsilon)s^5}\right]$$

$$+ \frac{(1-\varepsilon)\ w}{\varepsilon^3\ d\ \rho_l} \left[\frac{1.75\ w}{s^5} - \frac{150\ (1-\varepsilon)\ \mu_l}{d\ s^3}\right] - (\rho_l-\rho_v)\ g = 0 \tag{3.2-B-6}$$

where w is the inlet liquid mass flux, μ_l is the liquid dynamic viscosity, and s is the saturation at the top of the debris and must be varied between 0 and 1 until q is maximized. The maximized q is then the dryout heat flux. If the inlet mass flux is zero, then the result of the maximization process is approximated (within about 5 percent) by Equation (3.2-B-2).

If the inlet liquid is subcooled, the dryout flux is increased by the amount of heat required to raise the incoming liquid to the boiling temperature:

$$q_d = a_0 + w\, C_p\, \Delta T \qquad (3.2\text{-B-}7)$$

where q_0 is determined by Equation (3.2-B-6), C_p is specific heat of the liquid, and ΔT is the amount of subcooling.

Figure 3.2-B-5 compares the calculated dryout flux from Equation (3.2-B-7) with the measured dryout flux from Tsai, et al,[7] for debris in Freon-113 with liquid flow entry at the base of the debris at 25°C. The calculated dryout flux as the inlet mass flux is increased agrees with the data within about 20 percent.

3.2-B.1.4 Stratified Debris

If the debris bed is formed in several stages by different processes, or if the debris settles through a thick layer of water, the bed may be stratified (i.e., the particle diameter may be a function of elevation in the debris). For nondeep debris, a full one-dimensional model (Reference) must be used. However, for deep debris, the one-dimensional Lipinski (1982) model may again be simplified to an algebraic equation. The criterion for dryout is that each layer in the bed must be able to pass all the vapor generated below it without unduly restricting the liquid flow at that layer. Specifically, Equation (3.2-B-6) is applied at each level using the particle diameter at that level. If the heat flux from heat generated below that level exceeds the Equation (3.2-B-6) dryout flux, then dryout will occur.

If the debris is completely stratified with particle diameter monotonically decreasing with elevation, the dryout flux can be very low and even shallow debris might dry out at typical LWR decay powers. With completely stratified debris, dryout is dictated by the upper layers where the particles are smallest. However, channels will penetrate the upper layers, so Equation (3.2-B-6) must be applied to the layer at the base of the channels. The channel length is determined by finding the highest layer which satisfies

$$L_c = \frac{6\,\sigma\,\cos\theta}{\varepsilon\, d\, (\rho_p - \rho_l)} \qquad (3.2\text{-B-}8)$$

where L_c is the channel length and d and ϵ are the values at the level L_c below the top of the bed.

3.2-B.1.5 Three-Dimensional Effects

All of the above considerations are for one-dimensional debris in which the scale of horizontal variations in the debris is much larger than the debris thickness. Simple models are not presently available for two or three dimensional beds (e.g., steep conical piles). Horizontal liquid and vapor flow will alter the dryout criterion in a manner not yet modeled. However, The dryout equations described above may be used on the thickest portions of the bed (or regions with the smallest particles) to obtain a conservative criterion for dryout.

3.2-B.1.6 Postdryout Behavior

If the debris has liquid flow entry at the base and the heat flux from the debris exceeds the dryout flux predicted by Equation (3.2-B-6), the temperature at the top of the debris can be fairly well approximated by calculating the enthalpy rise in the coolant assuming all the heat generated in the debris goes into the liquid entering the debris base. The enthalpy is then converted to temperature. If the resulting temperature exceeds metal oxidation thresholds, then temperature excursions will occur until the metals are oxidized.

If the debris is resting on an impermeable support such as concrete, then the postdryout behavior will become very time dependent. Experiments by Hofmann [4] suggest that dryout will begin somewhere within the debris (depending on the amount the power is above the incipient dryout power). The dry zone will then grow downward to the debris base. A transient model by Gorham-Bergeron [26] can give an estimate of how long this process will take. The dry zone will then begin to expand upward. Simultaneously, the dry base of the debris will begin to heat itself and the supporting concrete. Gases and water vapor generated within the concrete will further increase the thickness of the dry zone and alter the heatup rate of the debris. Experiments by Tarbell, et al.,[31] show that the debris can melt the concrete and sink into it before the debris itself melts. The experiments also indicate that this process will seal this debris from the cooling effects of any overlying water. With thick beds, the dry debris above the molten concrete might also begin to melt and form a molten pool. At present, there is no model which can follow the heatup, possible melting, and concrete penetration of debris cooled by overlying water.

IMAGE EVALUATION TEST TARGET (MT-3)

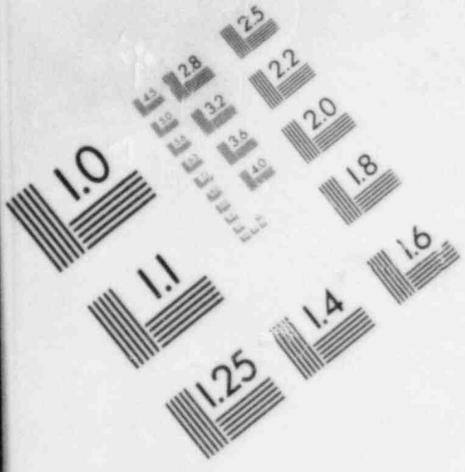

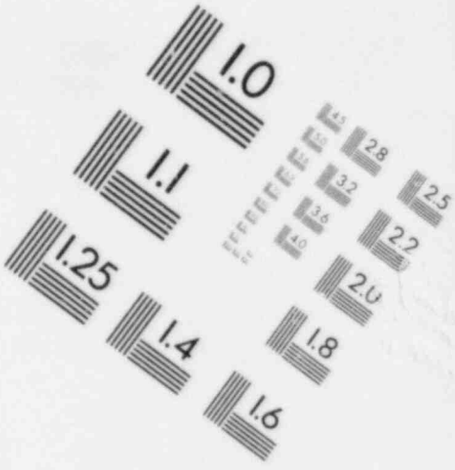

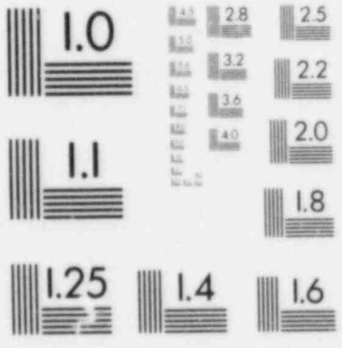

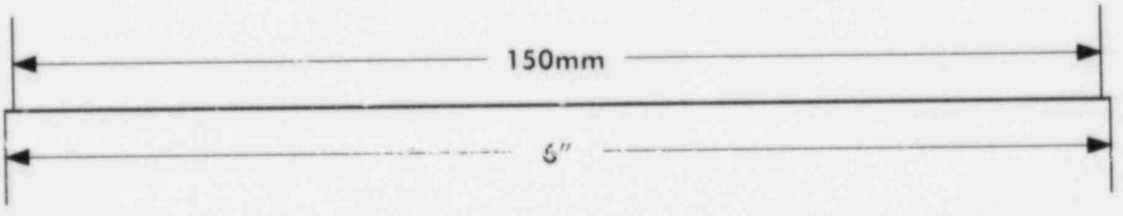

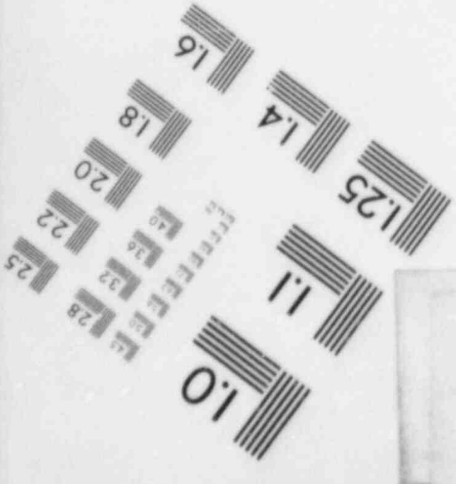

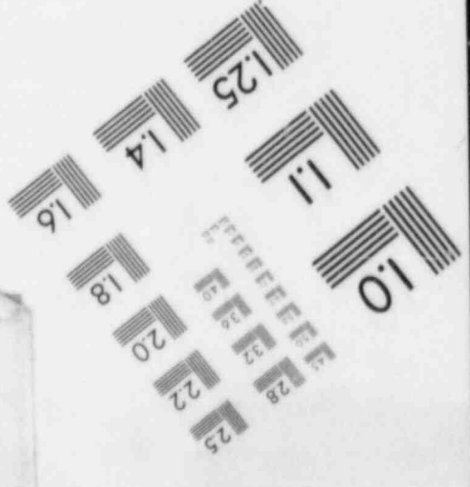

IMAGE EVALUATION
TEST TARGET (MT-3)

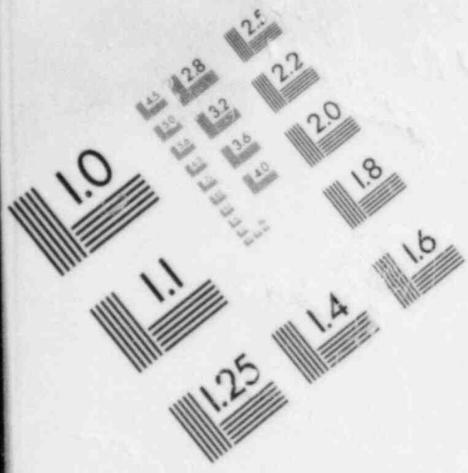

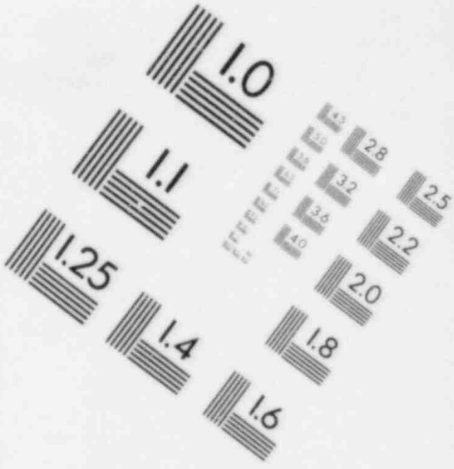

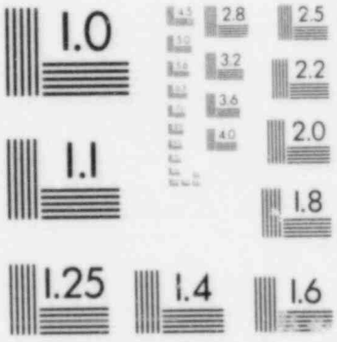

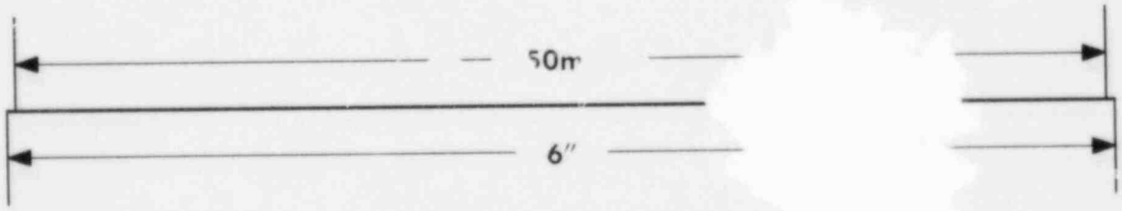

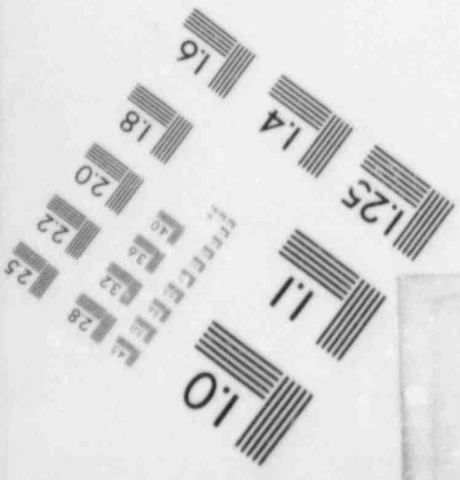

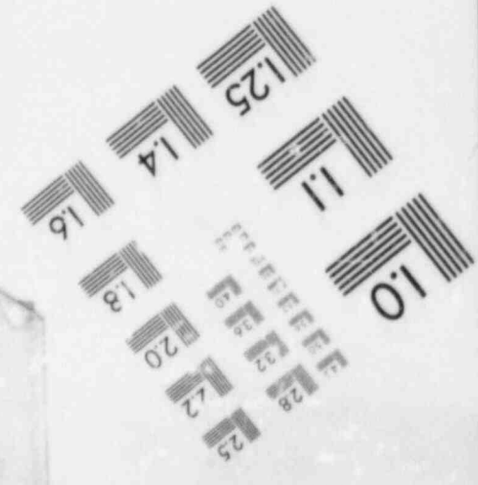

3.2-B.2 CONCLUSIONS

Particulate core debris submerged in water is not necessarily coolable. If the particles are small enough, flow resistance within the debris will not allow liquid water to penetrate all regions of the debris and parts of the debris will boil dry (even with a continuous overlying pool of liquid). Fairly accurate models for the conditions required to initiate dryout are available. Debris which does not dry out will remain below the boiling temperature of water. Debris which does dry out will heat and attack the supporting concrete. The dynamic process of dry particulate debris heatup and concrete attack in the presence of overlying water is not yet well modeled.

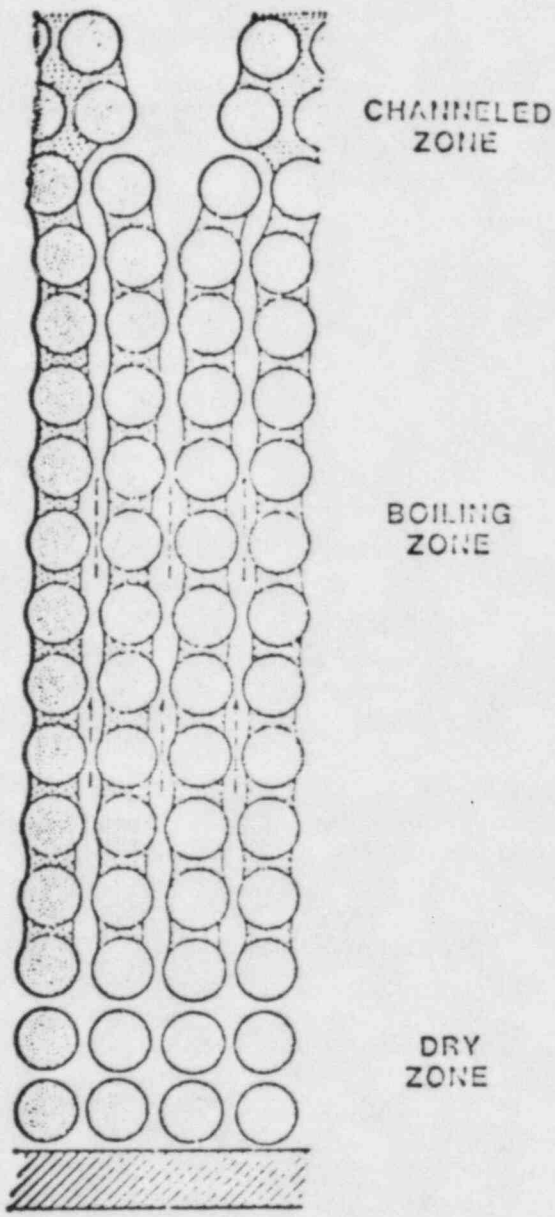

Figure 3.2-B-1. Debris Bed Zones

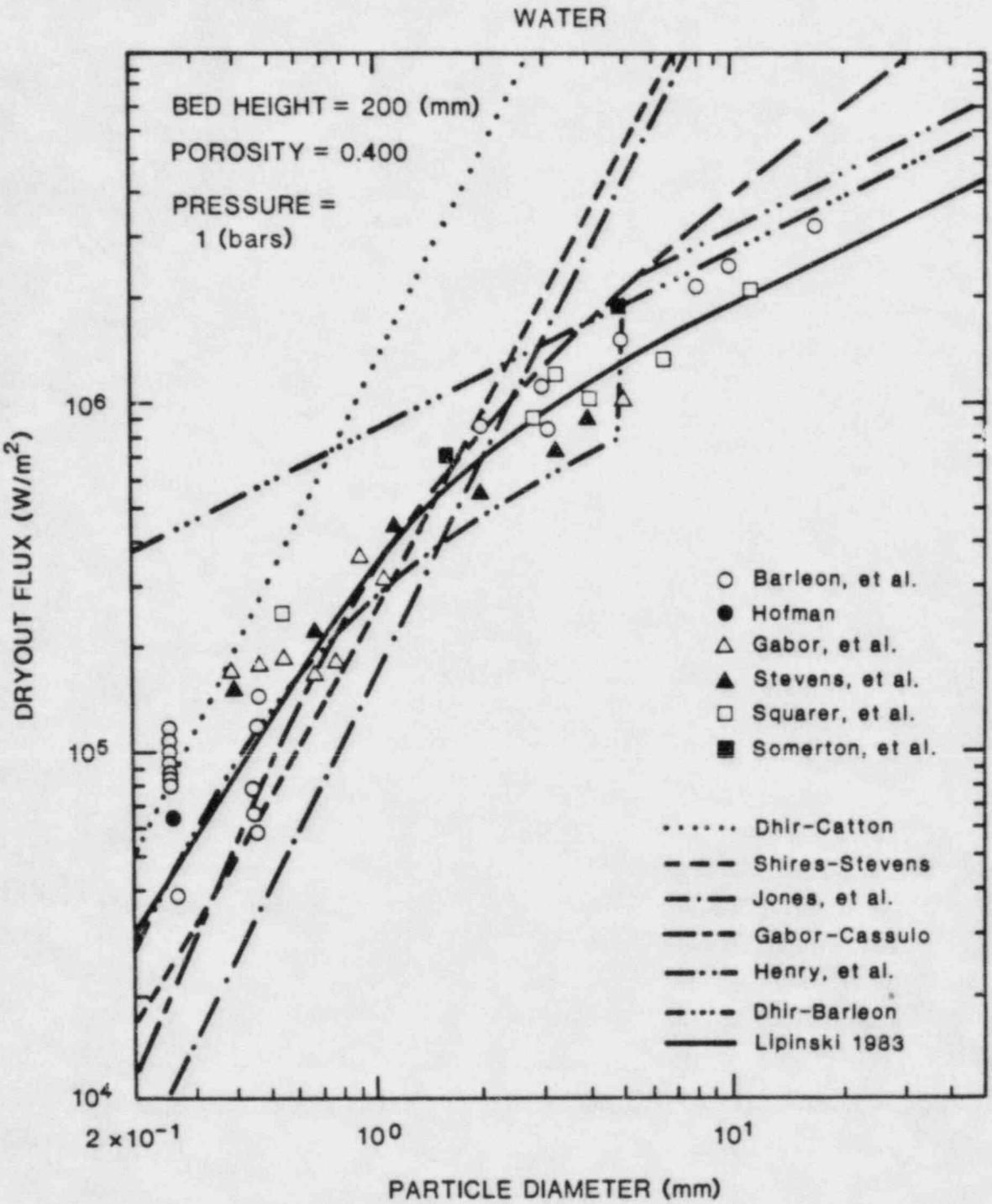

Figure 3.2-B-2. Bed Dryout Flux vs. Particle Diameter for Water

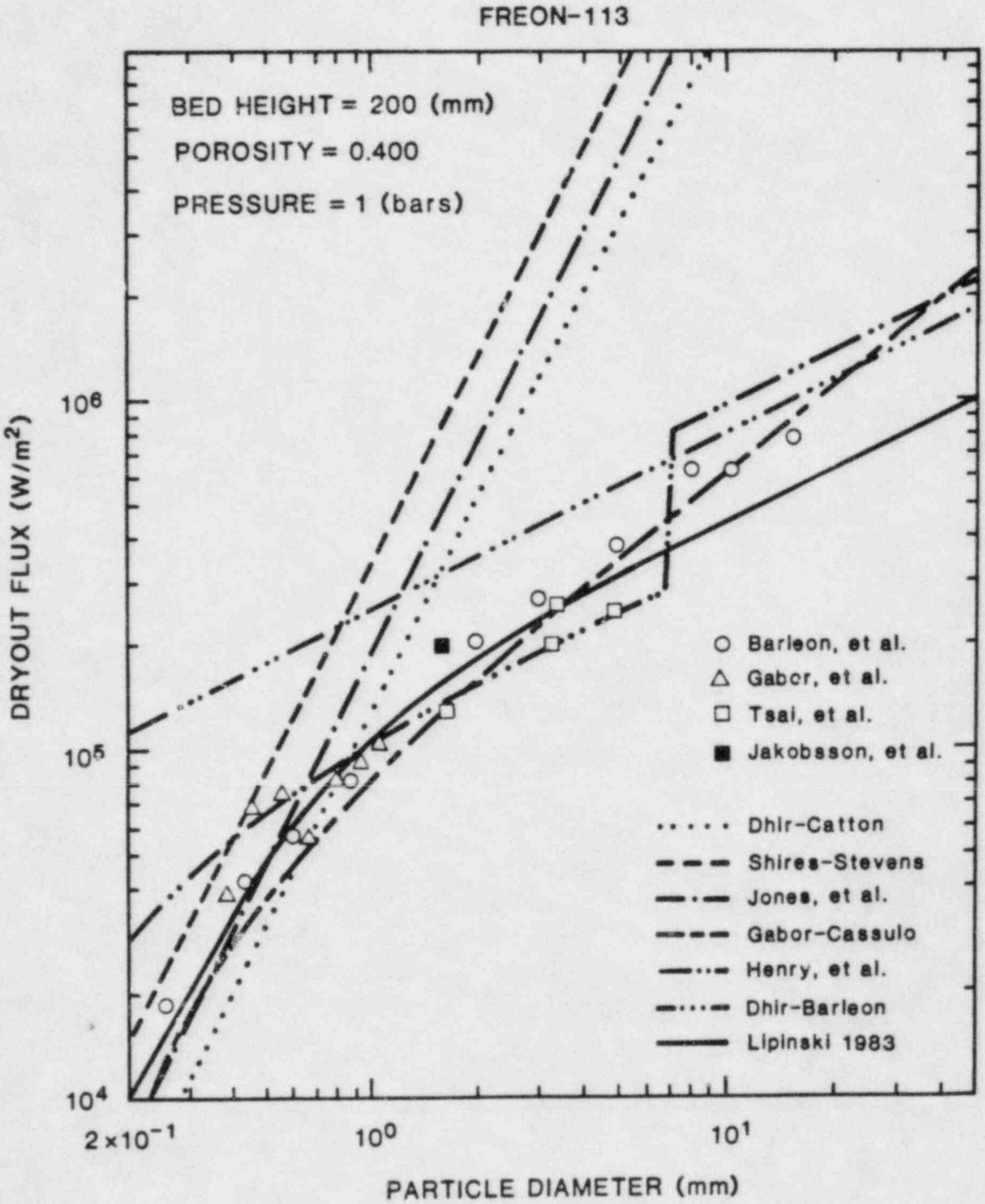

Figure 3.2-B-3. Bed Dryout Flux vs. Particle Diameter for Freon-113

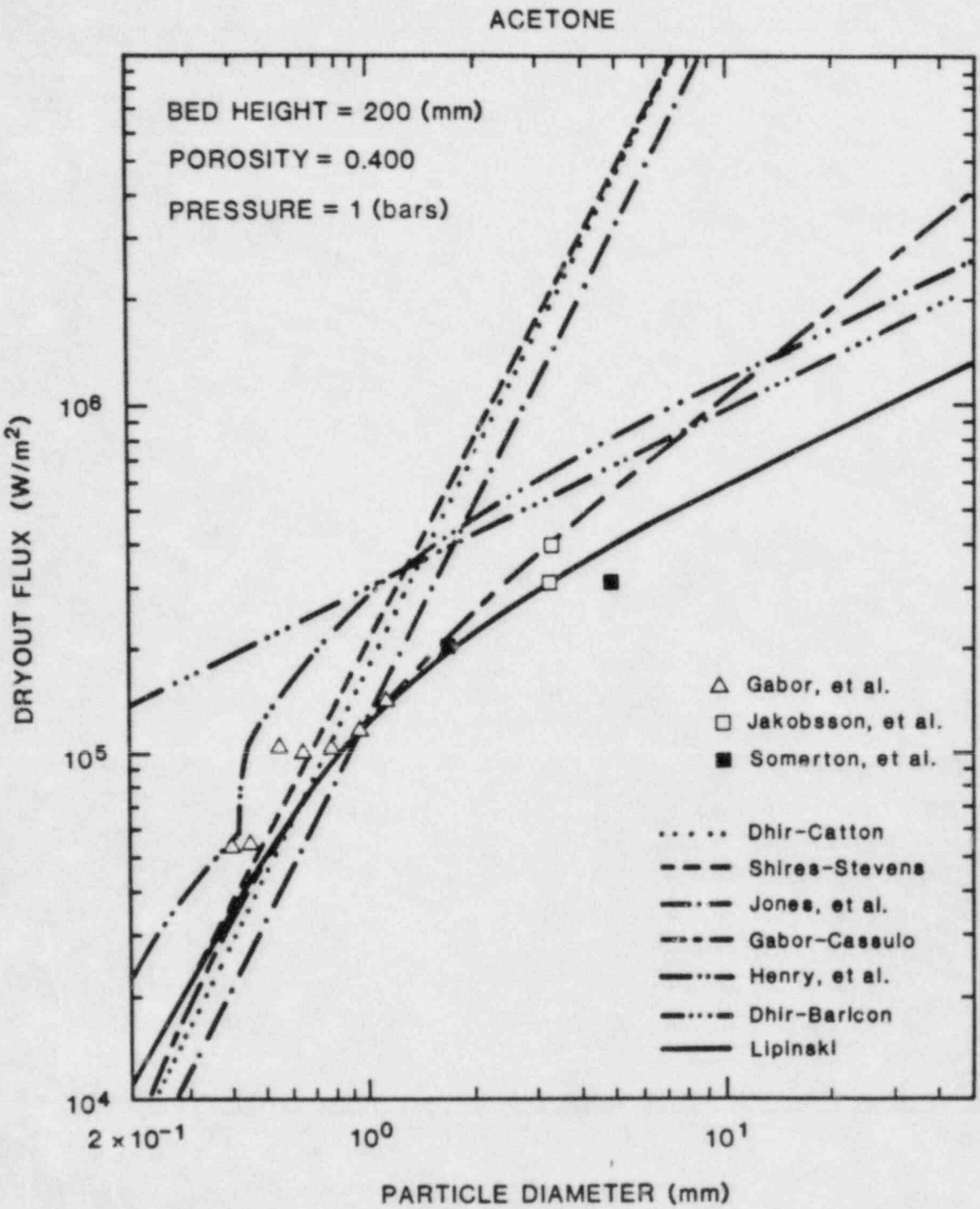

Figure 3.2-B-4. Bed Dryout Flux vs. Particle Diameter for Acetone

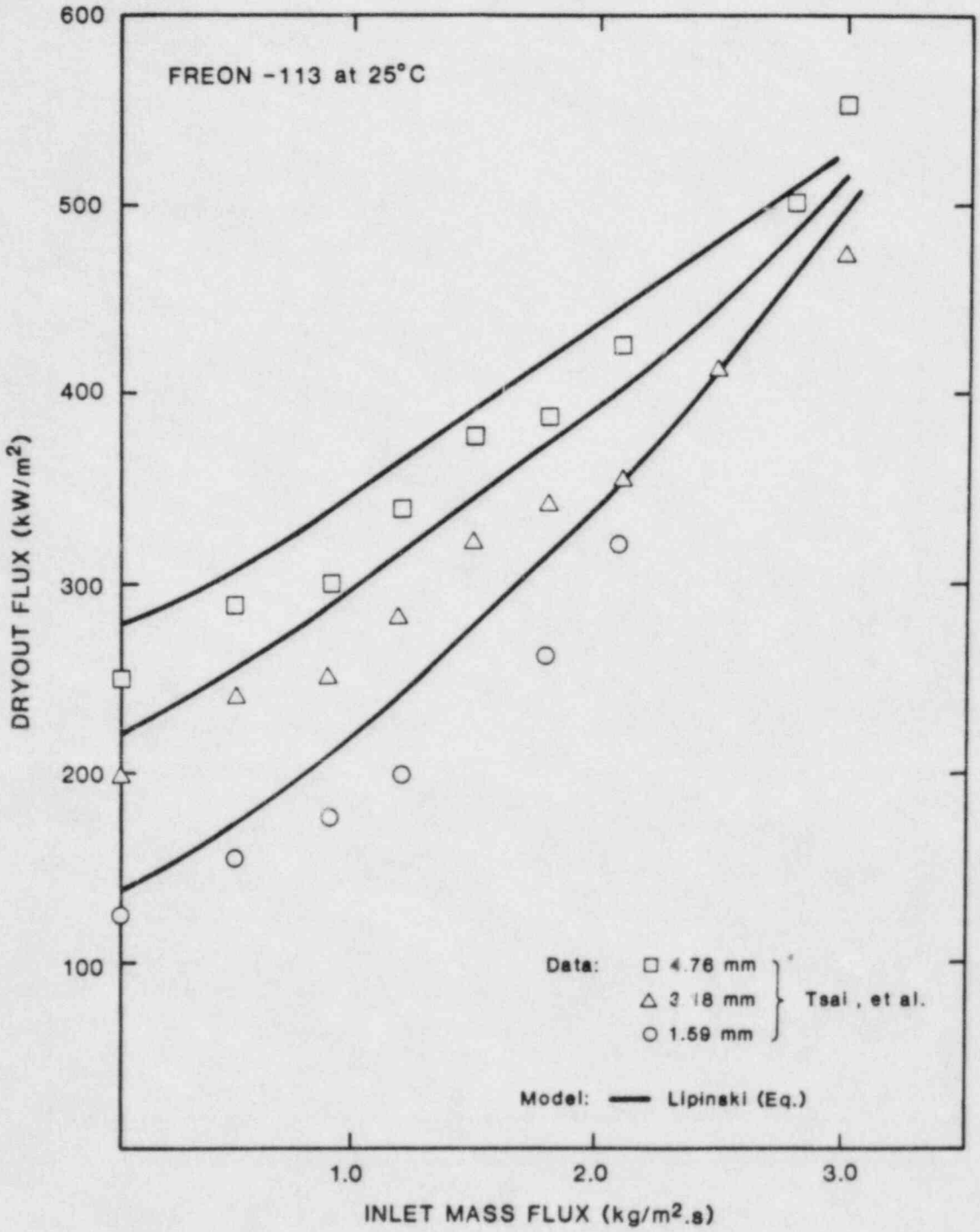

Figure 3.2-B-5. Bed Dryout Flux vs. Inlet Mass Flux for Freon-113

3.2-B.2 REFERENCES

1. Somerton, C., Catton, I., and Thompson, L., "An Experimental Investigation in Deep Debris Beds," LWR Safety Information Exchange, Gaithersburg, MD, October 26-31, 1981 (October 1981).

2. Squarer, D., Pieczynski, A. T., and Hochreiter, L. E., "Effect of Debris Bed Pressure, Particle Size, and Distribution on Degraded Nuclear Reactor Core Coolability," Nucl. Sci. and Eng., Vol 80, (1982).

3. Barleon, L., Thomauske, K., and Werle, H., "Dependence of Dryout Heat Flux on Particle Diameter and Bed Height and Effects of Stratification and Bed Reconfiguration," Post Accident Debris Cooling, Proc. of the Fifth Post Accident Heat Removal Information Exchange Mtg., Karlsruhe, Germany (July 28-30, 1982).

4. Hofmann, G., "On The Location and Mechanisms of Dryout in Top-Fed and Bottom-Fed Particulate Beds," ibid. 3.

5. Stevens, G. F. and Trenberth, R., "Experimental Studies of Boiling Heat Transfer and Dryout in Heat Generating Particulate Beds in Water at 1 Bar," ibid. 3.

6. Baker,Jr., L., Pedersen, D. R., Gabor, J. D., Jones, S. W., Bingle, J. D., "Correlations of Particulate Debris Bed Coolability Data," ibid. 3.

7. Tsai, F. P., Jakobsson, J., Catton, I., Dhir, V. K., "Dryout Heat Flux in a Debris Bed With Flow From Below," ibid. 3.

8. Jakobsson, J., Catton, I., and Squarer, D., "The Effect of Pressure on Dryout Heat Flux in a Volume Heated Porous Bed," to be published, somewhere, eventually.

9. Catton, I., Dhir, V. K., "Prediction of Dryout Heat Fluxes in Beds of Volumetrically Heated Particles," Proc. of Int. Mtg. On Fast Reactor Safety and Related Physics, Chicago, Ill, October 508, 1976, CONF-761001, pp 2036-2044 (October 1976).

10. Sowa, E. S., Hesson, J. C., Gebner, R. H., and Goldfuss, G. T., "Heat Transfer Experiments Through Beds of UO_2 in Boiling Sodium," Trans. ANS, Vol 14, No. 2, p 725 (November 1971).

11. Hardee, J. C., and Nilson, R. H., "Natural Convection in Porous Media With Heat Generation," Nuc. Sci. and Eng., Vol 63, pp 119-132 (1977).

12. Shires, G. L., and Stevens, G. F., Dryout During Boiling in Heated Particulate Beds, AEEW-M1779, UKAEA, Winfrith, UK (April 1980).

13. Lipinski, R. J., "A Particle Bed Dryout Model with Upward and Downward Boiling," Trans. ANS, Vol 35, pp 358-360 (November 1980).

14. Jones, S. W., Epstein, M., Gabor, J. D., Cassulo, J. C., and Bankoff, S. G., "Investigation of Limiting Boiling Heat Fluxes From Debris Beds," Trans. ANS, Vol 35, pp 361-363 (November 1980).

15. Lipinski, R. J., "A One-Dimensional Particle Bed Dryout Model," Trans. ANS, Vol 38, pp 386-387 (June 1981).

16. Theofanous, T. G., and Saito, M., An Assessment of Class 9 (Core-Melt) Accidents for PWR Dry-Containment Systems, PNE-81-148, Purdue University, West Lafayette, IN (June 1981).

17. Henry, R. E., and Fauske, H. K., "Core Melt Progression and the Attainment of a Permanently Coolable State," Mtg. on Light Water Reactor Fuel Behavior, Sun Valley, ID (August 1981).

18. Ostensen, R. W., and Lipinski, R. J., "A Particle Bed Dryout Model Based on Flooding," Nuc. Sci. and Eng., Vol 79, pp 110-112 (September 1981).

19. Gabor, J. D., Cassulo, J. C., Jones, S. W., and Pedersen, D. R., "Studies on Heat Removal from Fuel Debris," Trans. ANS, Vol 39, pp 643-644 (November 1981).

20. Squarer, D., "The Limiting Dryout Flux in a Large Particle Heat Generating Debris Bed," ibid. 19.

21. Reed, A. W., The Effect of Channeling on the Dryout of Heated Particulate Beds Immersed in a Liquid Pool, Ph.D. Thesis, MIT, Cambridge, MA (February 1982).

22. Lipinski, R. J., A Model for Boiling and Dryout in Particle Beds, SAND82-0765, NUREG/CR-2646 Sandia National Laboratories, Albuquerque, NM (June 1982), or R. J. Lipinski, "Boiling Heat Removal in a Particle Bed," Proc. of LMFBR Safety Topical Mtg., Lyon, France, July 19-23, 1982, III-399 (1982).

23. Henry, R. E., Epstein, M., and Fauske, H. K., "Cooling of Debris Beds - Methods of Analysis for LWR Safety Assessments," Presented at the International Meeting on Thermal Nuclear Reactor Safety, Chicago, IL (September 1982).

24. Turland, B. D., and Moore, K. A., "One-Dimensional Models of Boiling and Dryout," ibid 3.

25. Dhir, V. K., and Barleon, L., "On Counter Current Flooding in Porous Layers," submitted to Letters in Heat and Mass Trans.

26. Gorham-Bergeron, E. D., "A One-Dimensional Time-Dependent Debris Bed Model," to be presented at the ASME/JSME Thermal Engineering Joint Conference, March 20-24, 1983, Honolulu, HI.

27. Zion Probabalistic Safety Study, (Chicago, IL: Commonwealth Edison, 1982).

28. Gittus, J. H., chairman, PWR Degraded Core Analysis: A Report by a Committee Chaired by Dr. J. H. Gittus, NDR-610(S), Springfields Nuclear Power Development Labs, Salwick, Preston, UK, 1982.

29. Lipinski, R. J., to be published.

30. Jones, S. W., Baker, Jr., L., Bankoff, S. G., and Epstein, M., "A Theory for Prediction of Channel Depth in Boiling Particulate Beds," to be published.

31. Tarbell, W. W. and Bradley, D., Sustained Concrete Attack by Low-Temperature Fragmented Core Debris, NUREG/CR-3024, SAND82-2476, Sandia National Laboratories, Albuquerque, NM, 1983.

APPENDIX 3.2-C

PARTICLE BED QUENCH MODEL

K. D. Bergeron

3.2-C.1 SUMMARY

This analysis focuses on heat transfer and steam generation in a rubble bed which starts at a temperature which is high, but in which the debris is solid. The model can be extended to include remelt and hydrogen generation, but these features will not be discussed here. The bed is assumed to start dry, with an overlying pool of water, which immediately begins to descend through the one-dimensional bed. Because of the steam-water counterflow restriction at the top of the bed, the leading edge of the wet zone can move downward at a limited rate. There are two limitations considered. First, friction between the water and the rubble limits the descent velocity in the same way as if here were no heat transfer. We specify an arbitrary "trickle velocity" as the upper limit of quench front velocity. Correlations based on flow through porous media experiments can be used to calculate an upper limit for this velocity. This calculation will not be further discussed here.

More important is the counterflow limit imposed on the steam flux emanating from the top of the bed. This is the normal limiting mechanism for hot debris. A key simplifying step is to assume that this steam flux limit is the steady state dryout flux. (E. Gorham-Bergeron [1] has developed a more complicated model which does not make this assumption.) Another simplification is that there is perfect heat transfer between the debris and the water, so that all the debris in the wet zone is at the same specific enthalpy. Zero heat transfer is assumed between the debris and gases in the lower, dry zone. The result is a sharp quench front which sweeps out heat from the rubble as it moves downward.

The quench is not necessarily complete, since the front may leave behind steam "chimneys" which are not fully quenched. Such phenomena have been observed in experiments by Ginsberg, et al., [2] and by Cho, et al. [3], and are also commonly observed in analogous processes in the chemical and oil industries. In our model, these zones are assumed to be brought to a stable, but high, temperature by the steam flowing through them. When the quench front reaches the bottom of the debris bed, there is now a liquid flow path which allows the chimney regions to be filled from below. This two-front behavior was also a feature of the model of Ginsberg, et al.[2]

In the zone above the first quench front, decay heat contributes to the steam flux (which is treated as an energy flux). It may seem somewhat inconsistent to treat the decay heat in the steam chimney as contributing directly to the dryout flux, but any better treatment requires one- or two-dimensional analysis of the chimney, and uncertainties about the chimney area for reactor scale debris beds would seem to overwhelm the modeling uncertainties in this case. The dry zone below the first quench front is adiabatic, so decay heating simply increases the specific enthalpy of the debris. The dry zone is treated as one dimensional, though the model described below does not have features which would cause temperature gradients to occur in an initially uniform bed.

TABLE 3.2-C-1

Notation

$\emptyset$ = Heat flux of steam at top of bed (W/m^2)
$\emptyset_d$ = Dryout limit of $\emptyset$ (W/m^2)
T_s = Saturation temperature of water (° K)
ρ_s = Solid debris density (kg/m^3)
ϵ = Porosity of debris bed
z_s = Saturation (or quench) front height from bottom of bed (m)
z_o = Height of bed (to top of saturated zones) (m)
c_s = Debris heat capacity (j/kg-° K)
ω = 1 for $v_s > 0$, = 0 for $v_s < 0$
v_1 = First quench front velocity (positive downward)
v_2 = Second quench front velocity (positive upward)
γ = Steam chimney area fraction of total bed area
$H_{d_o}(z,t)$ = Debris specific enthalpy
H_d = Initial value of H_d
H_q = Enthalpy at full quench (function of T_s)
H_r = Residual excess enthalpy in chimney in first quench
H_1 = Average enthalpy above first quench ($H_q+\gamma H_r$)
H_{d1} = H_d-H_1
F = Decay heat rate (W/kg)
F_1 = Decay heat plus chemical heating in dry zone (W/kg)

$$\tilde{F} = F - c_p \frac{dT_s}{dt}$$

$$\tilde{F} = F_1 - c_p \frac{dT_s}{dt} \quad .$$

3.2-C.2 MODEL EQUATIONS

Phase 1. Initial quench front

We presume T_s is specified as a function of time, t. If the saturation front motion is not limited by flow resistance, the steam generation rate is limited to the dryout flux:

$$\emptyset = \emptyset_d(T_s) \quad . \tag{3.2-C-1}$$

Presumably, we can use a well-established steady state model to calculate $\emptyset_d$ (e.g., Lipinski zero-dimensional model). The steam generation rate is given by the decay heat behind the front plus the quench rate at the front:

$$\emptyset = \rho_s(1-\varepsilon)(z_o-z_s)(F-c_p \frac{dT_s}{dt} + u_o v_l H_{dl}) \quad . \tag{3.2-C-2}$$

This can be rewritten

$$R = \tilde{G}(z_o-z_s) + u_o v_l \tag{3.2-C-3}$$

where

$$R = \frac{\emptyset_o}{\rho_s(1-\varepsilon)H_{dl}} \tag{3.2-C-4}$$

$$\tilde{G} = \tilde{F}/H_{dl}(z_s) \quad . \tag{3.2-C-5}$$

The heatup of the dry zone is described by

$$\frac{dH_{dl}}{dt} = F_l - c_p \frac{dT_s}{dt} \quad (z < z_s) \quad . \tag{3.2-C-6}$$

Defining $z_1 = z_o - z_s$, the final Phase 1 equations are Equation (3.2-C-6) and flux-limited case:

$$v_1 = \tilde{R} - z_1\tilde{G} \quad (v_o > v_1 > 0) \qquad (3.2\text{-C-7a})$$

$$z_1 = R/\tilde{G} \quad (v_1 < 0) \qquad (3.2\text{-C-7b})$$

$$\emptyset = \emptyset_o \quad (v_1 < v_o) \quad . \qquad (3.2\text{-C-7c})$$

The flow limited case is defined by

$$R-z_1\tilde{G}) > v_o \qquad (3.2\text{-C-8})$$

In this case v_1 is set equal to v_o. The flux can still be made equal to $\emptyset_d$ by decreasing the channel fraction, λ, i.e., increasing H_1. If this would require H_1 to be greater than H_q (the fully quenched value), there are no steam chimneys, H_1 is set equal to H_q, and the flux is reduced to

$$\emptyset + \rho_s(1-\varepsilon)\tilde{F} + v_o H_{dq} \quad . \qquad (3.2\text{-C-9})$$

Phase 2: Since the decay heat in the chimneys is carried away by the steam, there is no heatup, and the velocity is constant:

$$v_2 = \frac{(\emptyset_d - \emptyset_1)}{\gamma H_t} \qquad (3.2\text{-C-10})$$

where

$$\emptyset_1 = \rho_s(1-\varepsilon)\tilde{F}(z_o - z_m) \quad . \qquad (3.2\text{-C-11})$$

We do not impose a flow limit to this upward velocity, because the timing of the arrival of the upward quench front is not particularly important.

3.2-C.3 REFERENCES

1. Gorham-Bergeron, E., "A One-Dimensional Time-Dependent Debris Bed Model," presented at the ASME/JSME Thermal Engineering Joint Conference, March 20-24, 1983, Honolulu, HI.

2. Cho, D. H., Armstrong, D. R., Bova, L., Chan, S. H., and Thomas, G. R., "Experiments on Quenching of a Hot Debris Bed," Post Accident Debris Cooling, Proc. of the Fifth Post Accident Heat Removal Info. Exchange Mtg., July 28-30, 1982, Karlsruhe, W. Germany, p. 145.

3. Ginsberg, T., Klein, J., Klages, J., Schwarz, C. E., and Chen, J. C., "Phenomenology of Transient Debris Bed Heat Removal," ibid p. 151, also, LWR Steam Spike Phenomenology: Debris Bed Quenching Experiments, NUREG/CR-2857 (June 1982).

APPENDIX 3.2-D

THE MEDICI REACTOR CAVITY MODEL

K. D. Bergeron

3.2-D.1 SUMMARY

In the past several years, considerable effort has been devoted to improving our understanding of reactor cavity phenomena during core-melt accidents. In particular, experimental programs on core-concrete interactions and steam explosions have provided a great deal of critical information. A parallel development of analytical tools has also occurred, most notably the CORCON code for molten core-concrete interactions. However, there remains a substantial gap between what is needed for system-level analysis of cavity events and what is available as a tested, workable code. The same can be said, of course, for all aspects of reactor safety modeling, but for the cavity, the disparity between existing models and analysis requirements is extreme.

The need for improved system-level models for severe accident cavity phenomena has been recognized for some time throughout the reactor safety analysis community. In particular, acceptable models of events following the release of core melt into a pool of water in the cavity were not available. The limitations of the MARCH-HOTDROP model have been been pointed out in several critiques, most notably the MARCH assessment (see Section 3.2.3.4.2). In recognition of this problem, a model development effort was initiated in the summer of 1982. The project was designated MEDICI, and the goal was to develop, implement and test models for reactor cavity phenomena which would be suitable for both the MELCOR and CONTAIN codes.

At the time of writing, the MEDICI model is not yet complete. However, the basic structure has been defined, and the major features of the component models have been specified for the first version of the code. In the following sections, the MEDICI structure will be described, though not all calculational details can be provided at present. It is expected that in most ways, the MEDICI code will incorporate the modeling recommendations of this Assessment.

3.2-D.2 DEVELOPMENT APPROACH

As a stand-alone code, MEDICI is intended to be a test-bed for recently developed models. It is also intended to be integrated into larger system models (CONTAIN and/or MELCOR), when the initial period of review and evaluation is complete. Because of these multiple applications, and because of the high degree of phenomenological uncertainty involved, a strong emphasis has been placed on developing MEDICI with a systematic, top-down design. This means that the overall structure of the code has been laid out clearly prior to the development of the details of all the models. Furthermore, the structure is highly modular, with well-defined interfaces between the distinct physical models.

This systematic development technique is based on methods which have emerged primarily from the nonscientific software development industry over the past several years. Structured Program Development is one of the terms applied to this type of approach. Although the requirements of scientific simulation codes are different in many respects from more conventional programming applications, it is clear that Structured Program Development methods can accomplish many of the same goals in both fields: improve quality control, facilitate team efforts, reduce debugging and testing time, ensure adaptability and flexibility of the code for future development, and ensure more effective management and control of the code development project.

For PRA codes, there are additional benefits to this approach. It will always be necessary to distinguish between models which are considered satisfactory best estimate calculations, and those which are simple bounding estimates which are used because satisfactory models have not yet been developed. In fact, there is a continuous spectrum of reliability of models between these two limits. A careful PRA requires that the analyst have a reasonable understanding of the strengths and weaknesses of the component models in his system model, without being an expert in all of the relevant fields. A structured, modular, well-documented code design can facilitate this understanding, allowing reasonable estimates to be made for the ranges of parametric variations to be applied in the PRA.

3.2-D.3 MEDICI STRUCTURE

The structure of the MEDICI code is specified by a series of flow charts shown in Figures 3.2-D-1 through 3.2-D-5. The description is provided at several levels of detail, starting with a statement of the basic purpose of the model (Level 0), and progressing with successively more detailed levels of description. The lowest level of diagrammatic description is Level 3 (Figures 3.2-D-4 and 3.2-D-5),

which indicates the actual sequence of calculations, though there are still some subroutines which require flow charting at lower levels. The series of charts is supplemented by a textual description of the functions of each module at each level in a number of documents which are organized (via the module indices) to correspond exactly with the diagrams.

MEDICI - LEVEL 0 DESCRIPTION

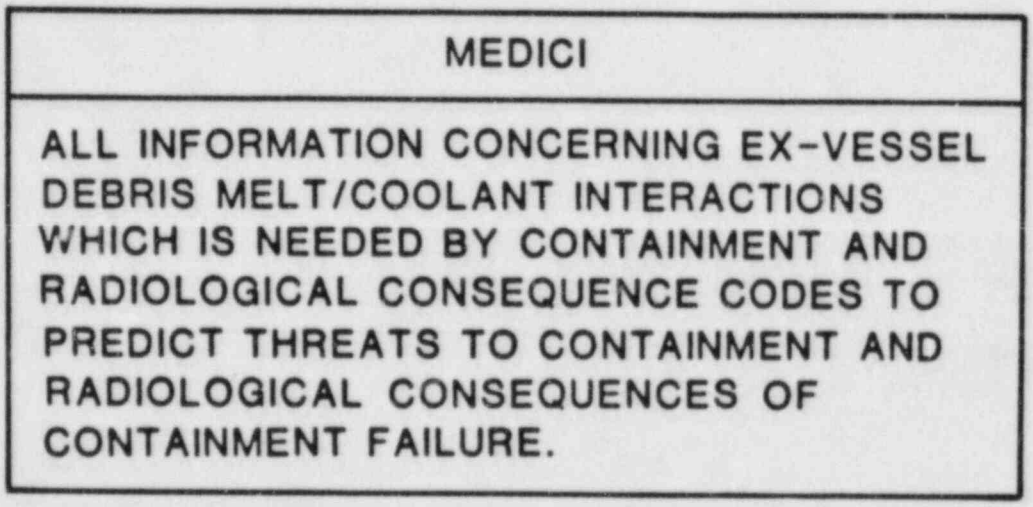

Figure 3.2-D-1. MEDICI Structure Diagram: Level 0

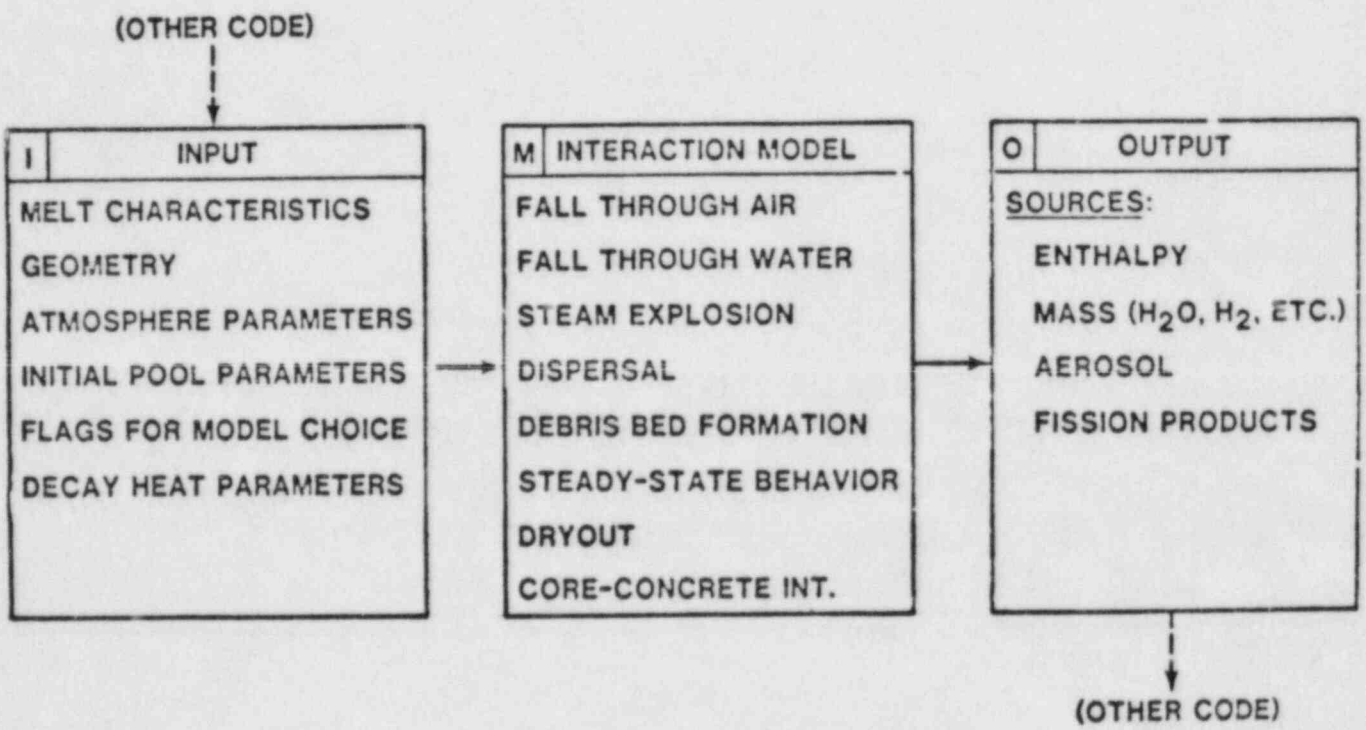

Figure 3.2-D-2. MEDICI Structure Diagram: Level 1

MEDICI - LEVEL 2 DESCRIPTION

INTERACTION MODEL - M

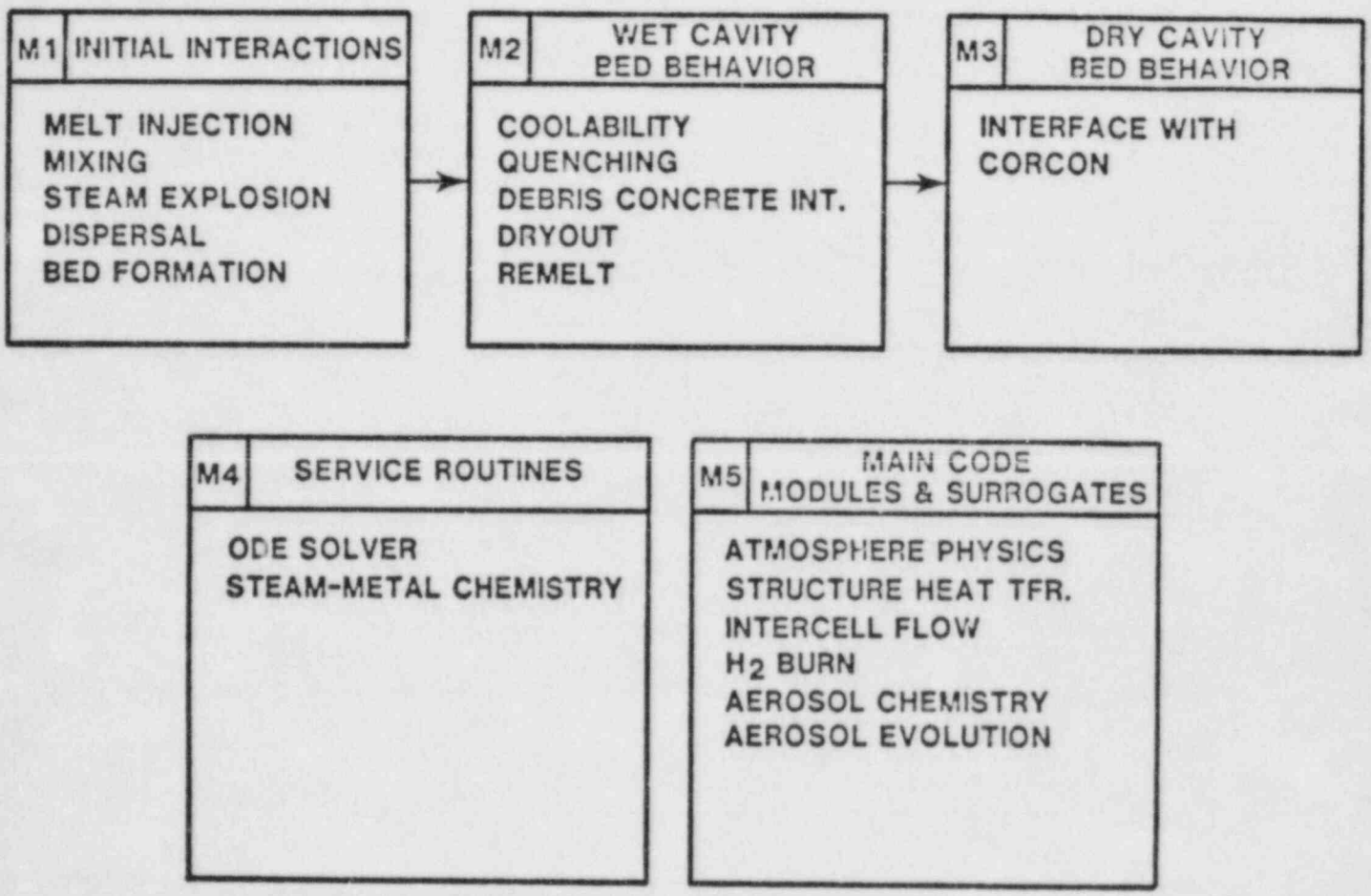

Figure 3.2-D-3. MEDICI Structure Diagram: Level 2; Models

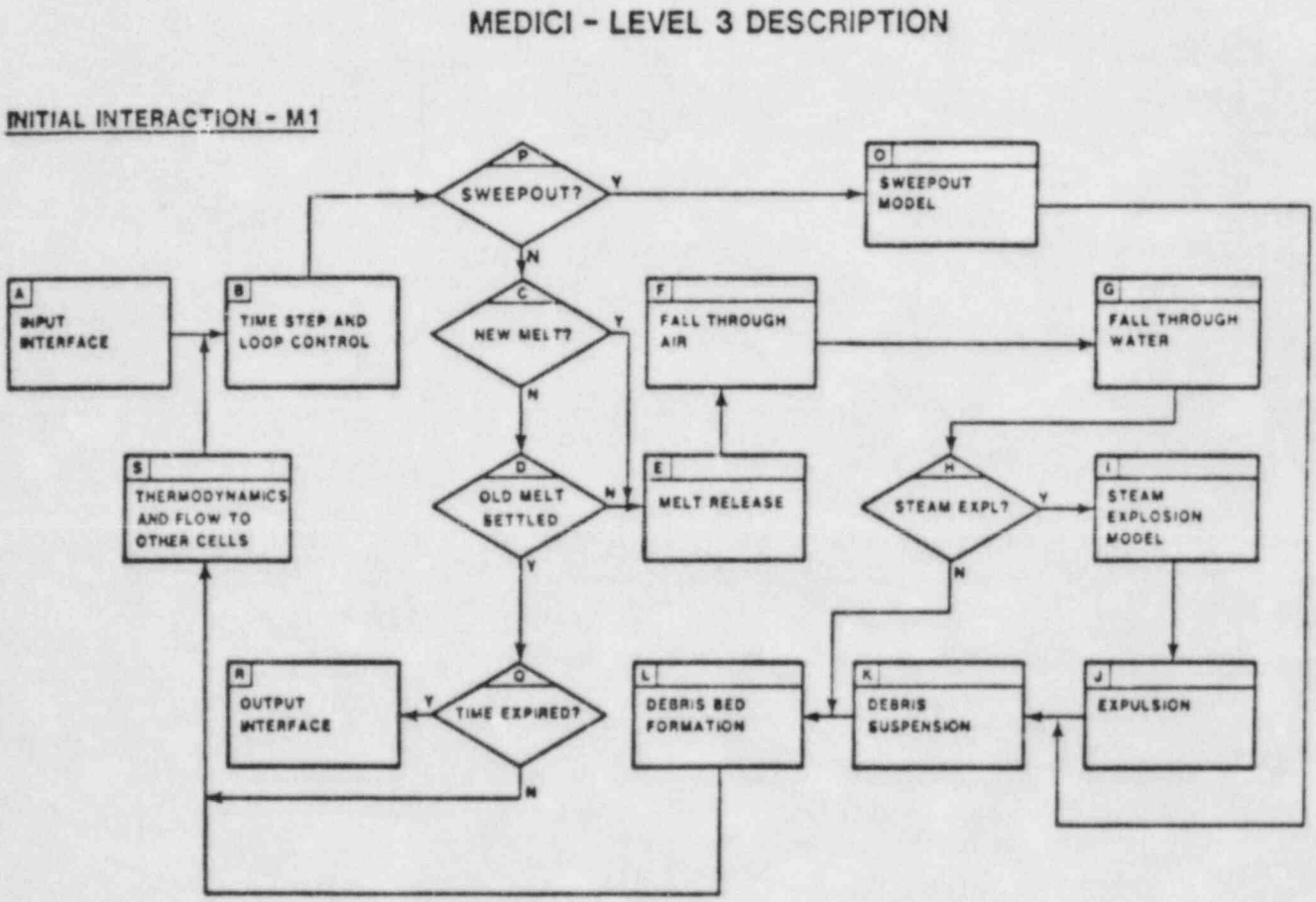

Figure 3.2-D-4. MEDICI Structure Diagram: Level 3; Initial Interactions

MEDICI - LEVEL 3 DESCRIPTION

WET CAVITY DEBRIS BED MODEL - M2

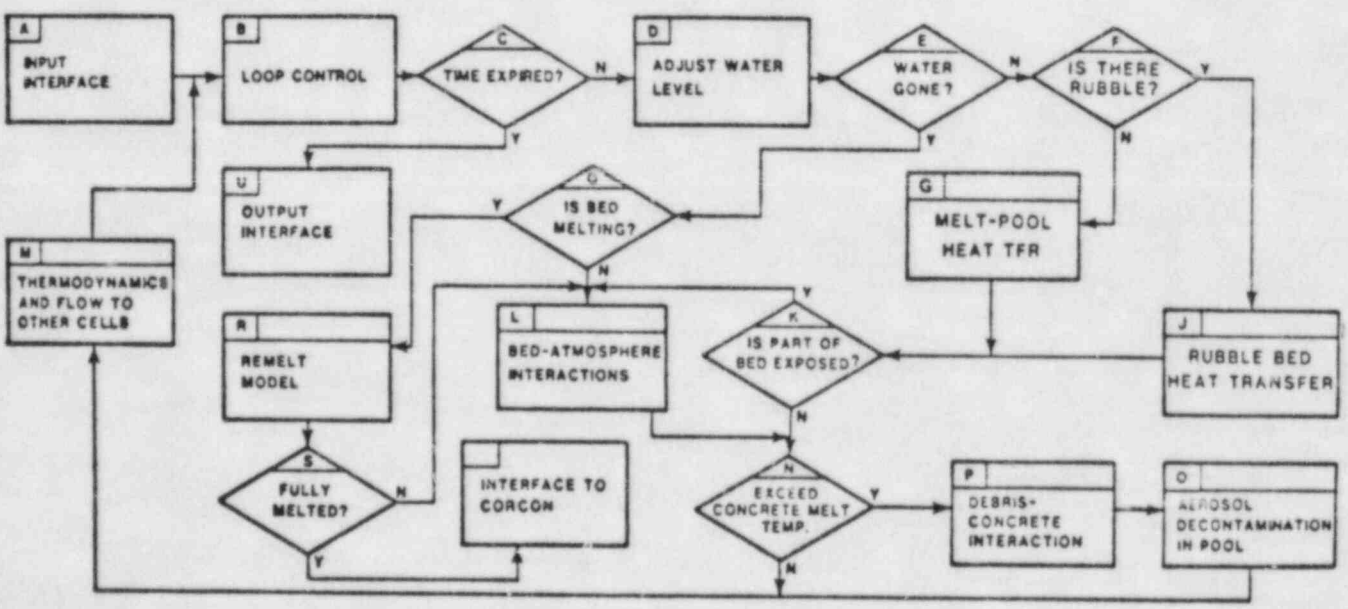

Figure 3.2-D-5. MEDICI Structure Diagram: Level 3; Wet Cavity Debris Bed

The principal division in the model is the distinction between three distinct time frames and cavity conditions. One of these is the long-term response of the cavity to molten debris when there is no water in the cavity. These are the conditions for which CORCON was designed, and it is not intended that new modeling will be required for this regime. Thus, the principal concern is phenomena involving water in the cavity, and a major separation is made between the relatively fast processes which occur shortly following vessel breach, and the longer term response after the debris has settled to the floor. In both regimes, the code will calculate the following:

- heat transfer among the water, debris, atmosphere, and structures;
- flammable gas generation (H_2 and CO);
- other noncondensible gas generation;
- transport out of the cavity of water, debris, and gas.

All of these quantities will be calculated as functions of time. In fact, one of the principal goals of the MEDICI code is to predict the timing of the various events which can occur in the cavity more realistically than previous models.

As seen in Figure 3.2-D-3, the calculational sequence from Initial Interactions to Wet Cavity Debris Bed Behavior is one-way, not a loop. This implies the assumption that all of the melt will be released in a single short period. This may be true for some accident sequences, but it is also possible to imagine scenarios in which the melt release occurs intermittently, or over a sustained period of time. Later versions of MEDICI will be able to treat this problem, but a number of phenomena involving the impingement of molten debris on quenched debris beds would have to be considered. Since similar considerations would apply to this case as to the pebble bed core-catcher concept, it would be desirable to include such a capability in any case. However, for simplicity (and for lack of adequate models) this capability will not be included in the first version MEDICI.

The following sections provide a brief description of the key models to be used in MEDICI. Additional details can be found in Section 5, since it is anticipated that in most respects the recommendations made for MELCOR-1 will be incorporated in MEDICI.

3.2-D.4 MODEL SUMMARY: INITIAL INTERACTIONS

This module treats all phenomena which occur on the short time scale (20 seconds, typically) during and immediately following RPV breach. These include the transit of the melt through the atmosphere and into the pool, possible steam explosion and subsequent dispersal, and formation of a debris bed. Both water and debris are in motion during this phase. Numerous slow processes are neglected to simplify calculations (e.g., heat transfer to the walls, some chemical reactions, etc.).

The principal models implemented here are the Fuel-Coolant Interaction models described in Appendix 3.2-A. They describe fuel breakup and mixing during the fall, along with steam generation and debris quenching, and they also allow for a steam explosion if a number of criteria are satisfied (this option will be at the control of the user). The models are primarily based on analyses done by Corradini of FCI experiments done at Sandia over the past several years.

Core-concrete interactions are probably not important on the time scale we are considering here, and so will not be included in the first version of MEDICI. (These processes will be treated in Section 3.5, however.)

Another feature which is likely to be missing from the first version is a mechanistic model for high pressure sweepout of core debris. The reason for this neglect is that the level of understanding of the processes is not high, and, as discussed in Section 3.2.3.2.1, the application of purely hydrodynamic criteria is probably not appropriate. It is, however, desirable that model development proceed for this phenomenon as rapidly as possible, for possible incorporation into later version of MEDICI, and, possibly, MELCOR-2.

3.2-D.5 MODEL SUMMARY: WET CAVITY DEBRIS BED MODEL

After the debris bed has settled into a relatively stable configuration (no new melt, no violent disruptions possible) then it is necessary to consider the slower processes which were neglected or treated crudely in the initial interactions phase. The important processes are: (a) heat transfer from the debris to the water, atmosphere, and structures, (b) core-concrete attack, with associated combustible gas and aerosol generation, and (c) hydrogen generation from melt-water chemical reactions.

The basic model used in this module divides the debris into a number of layers, some of which may be of zero thickness, (Figure 3.2.3-2). The top layer is exposed to the atmosphere. The next two layers are solid debris under water (nonzero porosity rubble bed). The upper one of these is saturated and quenched (substantially at the saturation temperature) while the lower one is dry, and presumably much hotter. Next, there are two molten layers, each of which may have a solid crust. The upper one is concrete slag, with some light metal oxides interspersed and possibly some rubble suspended or drifting downward through it. Finally, there is the molten debris layer, which is penetrating the solid concrete.

3.3 CONTAINMENT HEAT TRANSFER

by

A. L. Camp
K. D. Bergeron
R. Knight
A. C. Ratzel
S. N. Kempka

CONTENTS

LIST OF FIGURES

LIST OF TABLES

3.3.1 CONVECTION AND CONDENSATION HEAT TRANSFER

3.3.1.1 Introduction

Condensation heat transfer is generally the dominant passive mechanism for removing heat from containment atmospheres. It is clearly essential to have a model for this process which is applicable over the wide range of conditions which can occur during a severe accident. There are several features to be desired in a condensation/evaporation model. In addition to accuracy, the formulation should be as transparent as possible; it should also be flexible--capable of handling a variety of flow conditions and parameter regimes; it should also be verified against experimental data; it should, if possible, be presented so as to make maximum contact with standard treatments of heat and mass transfer; finally, it should be no more complicated or detailed than necessary, in light of uncertainties in the correlations and other parameters which are to be used for the calculation.

Generally, convective heat transfer will take place between the bulk gas and a surface, through the resistance of a gas boundary layer and a liquid condensate layer. Both mass diffusion and sensible convective heat transfer occur in the gas boundary layer, and conduction occurs in the liquid layer. In most cases the resistance in the gas boundary layer is the dominant one; however, the liquid layer cannot always be neglected.

3.3.1.2 Review of Literature

There are, basically, two approaches to condensation heat transfer being used in the light water reactor safety literature. One is to use correlations for heat transfer coefficients developed by Uchida [1] and/or Tagami [2]. The other is to use a relatively mechanistic model involving something like Couette flow in the gas boundary layer in order to model the diffusion of condensible vapor through the noncondensible gas. All of the approaches of the latter type are based on treatments similar to that of Collier [3], but there are variations among them involving the choices of mass and heat transfer correlations in the gas boundary layer. It appears that the condensation heat transfer model in MARCH is based on the Uchida data.

The Uchida and Tagami correlations are based on small-scale experiments, and involve very few parameters. There is practically no evidence for the absence of dependence on other parameters. Nevertheless, these correlations were widely used in the industry for many years. Then, in 1970, the first steam blowdown experiment on a containment building scale was conducted. This was the Carolinas-Virginia Tube Reactor (CVTR) experiment, which showed that Uchida-

Tagami heat transfer coefficients were too low by a factor of 2 or 3 during the blowdown phase, though the agreement in the more quiescent post-blowdown phase was much better.[6]

These findings prompted numerous researchers to develop more mechanistic models.[7]-[11] Good examples are [7] and [9], both of which compared their predictions with the CVTR results. Both came to the conclusion that the high-heat transfer coefficients observed in CVTR can be predicted by the mechanistic models if forced convection correlations corresponding to gas velocities in the range 2-7 m/s are used. Both also concluded (in their own ways) that the mechanistic models agreed with Uchida-Tagami models if natural convection is assumed, and that the latter is probably acceptable for the post-blowdown phase. However, for reasons which will be discussed below, none of the models identified is completely adequate, though the one to be proposed (which has been recently implemented in CONTAIN and HECTR) is similar in many respects to that in [9] and that developed recently be Corradini in [18].

The most recent validation experiment is the HDR series of steam blowdowns in a decommissioned power reactor near Frankfurt, Germany. Blind predictions of pressures, temperatures, and heat transfer coefficients are being made by a number of reactor safety codes, including CONTAIN. Results of the experiments and the code validation exercise should be available in early 1983. Preliminary results from the CONTAIN analysis indicate that it is important to allow evaporation as well as condensation, and that it is also important to include the resistance of the liquid film during the blowdown phase.

3.3.1.3 Gas Boundary Layer Model

We consider a gas boundary layer in series with a liquid film of a specified depth. As in conventional lumped parameter treatments, the effect of the film can be included after the resistance of the boundary layer is calculated. Therefore, for the first part of the analysis, we set the interface temperature equal to the wall temperature, T_w, and separate the heat flux from the surface into two components, convective and condensing mass flow:

$$q = q_c + q_m \qquad (3.3.1\text{-}1)$$

$$q_c = h_b(T_w - T_o) \qquad (3.3.1\text{-}2)$$

$$q_m = M_g J_g i_{fg} \qquad (3.3.1\text{-}3)$$

where T_o is the bulk temperature, M_g is the vapor molecular weight and i_{fg} is the latent heat of vaporization. The molar flux, J_g, is given by a mass transfer correlation:

$$J_g = K_g(P_{g1}-P_{g2}) \qquad (3.3.1\text{-}4)$$

$$P_{g1} = P_{sat}(T_w) \qquad (3.3.1\text{-}5)$$

where p_{g1} is the partial pressure of steam at the interface, p_{g2} is the partial pressure of steam in the bulk gas, and K_g is the mass transfer coefficient. Note that there are many different conventions for the driving force of Equation (3.3.1-4), and correspondingly different definitions of the mass transfer coefficient. A review of the fundamental literature concerning what the natural differential equations are can be enlightening. If the liquid-vapor boundary is to be analyzed in detail, the proper thermodynamic potential is chemical potential. If, as in our approach, only the gas layer is of interest and thermal diffusion can be neglected, the diffusion equation is properly expressed in terms of partial pressure, or mole fraction (cf. [12], p 244., [13], p 336).

The key feature of the formulation proposed here is that the fundamental quantity determining both heat and mass transport is the Nusselt number, which comes from user-selected correlations. This determines, first, the heat transfer coefficient:

$$h_b = Nu\ k_t/L \qquad (3.3.1\text{-}6)$$

where k_t is the thermal conductivity of the gas-vapor mixture, and L is a characteristic length. The mass transfer coefficient is obtained from Nu via a mass transfer-heat transfer analogy. The most general one is:[16]

$$Sh = Nu(Pr/Sc)^{2/3} \qquad (3.3.1\text{-}7)$$

where Pr and Sc are the Prandtl and Schmidt numbers, respectively, of the mixture and the Sherwood number, Sh, is the dimensionless mass transfer coefficient, from which we obtain K_g.[16]

$$K_g = \frac{Sh\ p\ D_v}{RT\ p_{am} L} \qquad (3.3.1\text{-}8)$$

$$p_{am} = \frac{p_{a1} - p_{a2}}{\ln(P_{a1}/p_{a2})} \qquad (3.3.1\text{-}9)$$

where $p_{a1,2}$ are the partial noncondensible pressures at the wall and in the bulk, respectively, P is the total pressure, and D_v is the mass diffusivity of the vapor in the noncondensible. It should be pointed out that the previous three equations are given in References [5], [9], [16], and [18], and that the bulk flow correction derived in [3], [4], [5], and [16] is included in the p_{am} term. (This term is also the reason for the use of ln(1+B) in [7].)

Equation (3.3.1-7) differs from the corresponding equation in Reference [16] by a factor of (Pr/Sc). This factor (the Lewis number, Le) is probably approximately equal to 1.0 for the gasses of interest. The reason for this difference is that there are two competing mass-transfer/heat-transfer analogies. One is based on the Colburn j factors (used here) and the other makes a direct substitution of Sc for Pr and Sh for Nu in explicit correlations.

For high mass transfer rates the convective term, q_c, is influenced by the mass flow, because of the sensible heat and momentum carried by the diffusing vapor. The correction factors available in the literature appear to be derived for cases other than those of interest to us. For that reason, we propose only minor changes for the first version of MELCOR, with reasonable modifications to be made as they become available. For now, we propose to replace i_{fg} in Equation (3.3.1-3) with

$$i_{fg} = i_g - i_f \qquad (3.3.1\text{-}10)$$

where i_g and i_f are the enthalpies of the vapor in the bulk gas and liquid water at the interface, respectively. All that remains is to select an appropriate value of Nu. A wide variety of choices of Nu are available as discussed below. After this is specified, the calculation is straightforward: K_g is then calculated, then J_g, q_c, and q_m.

3.3.1.4 Choice of Nusselt Number Correlations

The convective heat transfer coefficient is often correlated in terms of the Nusselt number with parameters such as

the Rayleigh number, Ra, for free convection and the Reynolds number for forced convection. These correlations are derived from experimental measurements of heat transfer rates in which the characteristic length to be used in the correlation parameters is an appropriate dimension of the experimental apparatus. Fluid properties in free convection parameters are typically evaluated at the arithmetic mean of the wall and fluid temperature; fluid properties in forced convection parameters are usually evaluated at the temperature of the fluid. The correlations are, in general, valid only for steady state heat transfer under specified conditions of the convecting fluid; a quiescent medium for free convection and a uniform free-stream for forced convection. The heat transfer rates result from boundary layer transport mechanisms for the specified flows.

Empirical correlations are valid only for the parameter ranges investigated during the original experiments (e.g., $10^9 < Ra < 10^{12}$). Similitude, however, is not guaranteed simply by satisfying the parameter range constraints. Length scales and wall-fluid temperature ratios must also be similar to those of the experiment. For example, studies have shown that turbulent free convection is not correlated by the Rayleigh number if wall-fluid temperature ratios (absolute temperatures) are greater than 1.1. Likewise, a correlation may not be accurate for length scales greater than that of the experimental data base.

Application of widely accepted convection correlations to containment geometries may not be appropriate for several reasons. First, the heat transfer phenomena during and immediately after blowdown or combustion are highly transient. The use of steady state heat transfer correlations in this situation is clearly incorrect. Steady state treatment of transient heat transfer processes will, in general, underpredict heat transfer rates. Second, correlation parameters may not provide similitude for reactor accident phenomena because containment-length scales and the large wall-fluid temperature differences exceed those of the experimental data base. Third, the atmospheric environment during an accident cannot be well characterized by a quiescent or uniform free stream flow during the critical periods of blowdown, combustion, and immediate post-combustion cooldown. The transport phenomena result from fluid-wall interactions that are different from those modeled in correlations.

In summary, the use of generally accepted convective heat transfer correlations to model reactor accident phenomenology may result in inaccurate predictions. Correlations verified for containment geometries are not presently available. Use of unverified correlations as "engineering approximations" may result in nonconservative predictions of

accident phenomena, especially during and immediately following any combustion in containment.

Noting the uncertainties mentioned above, we are still faced with selecting correlations for use. As examples of choices of Nu, the following are proposed (cf [20] p 4-67):

1. Forced Turbulent Convection $0.037Re^{.8}Pr^{.33}$ (3.3.1-11)

2. Turbulent Natural Convection $0.13(GrPr)^{.33}$ (3.3.1-12)
   (vertical walls and cold roof)

3. Laminar Natural Convection $0.27(GrPr)^{.25}$ (3.3.1-13)
   (cold floor)

where Re, Pr, and Gr are the Reynolds, Prandtl, and Grashof numbers, respectively.

If a new application arises with special flow characteristics (e.g., a jet impingement problem on a cylindrical heat sink) the model can be easily adapted by inserting a new correlation for the Nusselt number.

The model proposed here is very similar to that used in [9], which was developed for a version of the CONTEMPT code. One difference is an additional factor of (Sc/Pr) in Equation (3.3.1-7), i.e., they use Collier's formula. But as discussed above, this is not expected to make much difference, since Sc = Pr for our case. It has been tested against Tagami [2] and Uchida [1] correlations, and has done well. As with most attempts to compare against CVTR data, a forced convection velocity around 3.0-5.0 m/s was required to obtain rough agreement with the observed heat transfer coefficients during the blowdown. The forced convection velocity for MELCOR could either be user-specified or estimated based on intercompartment-flow velocities.

3.3.1.5 Liquid Layer Model

The principal thermal resistance in the typical condensation heat transfer problem for containment analysis is the gas boundary layer adjacent to the structure. The coolant vapor must diffuse through a region of enhanced noncondensible concentration. This resistance is in series with the condensate film layer, and also, possibly, with a layer of paint or other coating which one might want to include in this analysis (rather than in the heat conduction model). A liquid layer model should account for the quantity of steam

removed as condensate and simulate the thermal resistance of the layer. Neglect of the liquid layer thermal resistance can result in overprediction of heat transfer.

Structure condensation calculations taken from the standard heat and mass transfer literature typically use an iterative calculation approach,[7] since the interface temperature, T_i, is unknown, and heat transfer through both the gas boundary layer and the liquid film depend on T_i nonlinearly. For heat-exchanger applications, this is necessary. However, for reactor containment response calculations, the need is less clear. Furthermore, it is almost certainly incorrect to use the same type of formulation for film resistance as are used in heat exchanger models (i.e., steady state Nusselt film analysis). A highly detailed model of steady state film flow on smooth surfaces would be inappropriate under these circumstances, particularly if an iterative technique is required to solve for the surface temperature of the film.

For these reasons, it is recommended that the film be modeled as a layer of water of a specified depth (which is user-input and can be varied for sensitivity studies). The Nusselt models may give some insight concerning a good choice for the film depth, but it should be realized that the surfaces encountered in reactor containment buildings are far rougher than the assumptions of the Nusselt model would allow. A film depth of 0.001 m seems a reasonable starting point.

It is also useful to consider treating the growth of the film up to the specified limiting depth during the early phases of condensation. The reasons are first, it is a very simple calculation; second, peak temperatures on thin sheet metal may be affected by this process; third, it allows us to keep track of the inventory of water collected on surfaces, and to delay depositing that water into sumps, pools or overflow pathways (such delays may be important in establishing realistic timing of some important containment phenomena); and fourth, the amount of water which can be evaporated from the walls is limited to a physically reasonable value.

The resistance of the liquid film is known if the effective film depth, d_f, is known. We presume that this depth is calculated by allowing condensation to build up, so that the depth is the accumulated condensate volume divided by the structure area, as long as this does not exceed the specified limiting (or "overflow") depth. Condensate which accumulates beyond this depth is assumed to flow into a sump or pool. When evaporating conditions occur, the amount which is available for evaporation from the wall is limited by the film depth.

Since the film depth is known at all times, its effect on heat and mass transfer is easy to account for. We assume that heat transfer in both layers behaves as if there were an effective heat transfer coefficient associated with the temperature difference between the wall and the saturation temperature in the atmosphere. The film heat transfer coefficient is

$$h_f = k_f/d_f \qquad (3.3.1\text{-}14)$$

to which we can add the resistance of a paint or oxide layer, h_p, if desired. (Paint or oxide layers could also be included in the wall conduction model if that turns out to be more appropriate.)

$$h_{eff} = \frac{h_f h_p}{h_f + h_p} \quad . \qquad (3.3.1\text{-}15)$$

Then we modify both the convective and condensing parts of the heat transfer. The condensation heat flux, Φ, is modified to become

$$\Phi = \frac{\Phi h_{eff}(T_w - T_o)}{\Phi + h_{eff}(T_w - T_o)} \quad . \qquad (3.3.1\text{-}16)$$

And the convective heat transfer coefficient becomes:

$$h_c = \frac{h_c h_{eff}}{h_c + h_{eff}} \quad . \qquad (3.3.1\text{-}17)$$

To illustrate the effect of treating the surface resistances, a number of calculations have been run on the CONTAIN code using the model described above. The problem was a realistic large-break LOCA in a large dry PWR (modeled after the H. B. Robinson NPP). Internal heat sinks included a substantial amount of steel over 6 cm. thick, so one might expect the condensate film and paint layer resistances to play a role when heat transfer coefficients are very high. To obtain high heat transfer coefficients, the forced convection option was used with a surface velocity of 20 m/s. A more realistic 5 m/s case was also considered. The paint-layer heat transfer coefficient was 2×10^3 $w/m^{2-o}K$, and the film overflow depth was 0.001 m.

Table 3.3.1-1

Effect of Surface Layers on Peak Pressure
in a Blowdown Problem

Water Film	Paint Layer	(v=5.0) P_{max}	(v=20.0) P_{max}
No	No	2.01e5	1.61e5
No	Yes	2.07e5	1.72e5
Yes	Yes	2.08e5	1.75e5

3.3.1.6 Interface With Other Parts of MELCOR

Interfacing the condensation/evaporation model with the rest of MELCOR is relatively straightforward, as long as control volumes are properly defined and sign conventions are consistent.

The principal reason for the film layer is to provide a thermal resistance, and to track mass balance of the water. However, the treatment of film enthalpy is somewhat problematic. Ideally, we would treat it as a variable thickness node in the conduction model, but such an approach will increase the computational cost and is probably not warranted for the first version of MELCOR. We then have two alternatives for the enthalpy of the liquid film. We can track it as a separate quantity, not allowing transfer to the wall, or we can add it all to the first node of the wall. The latter approach appears to be more meaningful physically, and to pose fewer numerical problems, so we will adopt it here. The various energy transfers then involve only the bulk atmosphere, the first node of the structure, and the film overflow. The change in enthalpy of the bulk gas is

$$E_B = q_C - M_g J_g i_g \qquad (3.3.1\text{-}19)$$

which is valid for either evaporation or condensation. The enthalpy which flows with the overflow water (to a sump or pool) is related to the mass flow rate, f_O, of the film overflow by

$$E_O = -E_B + E_O \qquad (3.3.1\text{-}20)$$

(which is zero except when water is condensing and the film is at its overflow thickness). Finally, the heat transferred to the first node of the conduction model is the difference between these:

$$E_S = -E_B + E_O \qquad (3.3.1\text{-}21)$$

a formulation which explicitly guarantees energy conservation.

For a condensing situation the atmosphere loses water mass at the rate

$$W_O = M_g J_g \quad . \qquad (3.3.1\text{-}22)$$

This is added to the condensate film mass until the upper limit on film mass is reached. This is just the total structure surface area times the overflow thickness divided by the water density. After this upper limit is reached, the overflow water does not add to the film thickness. Presumably it can be added to a sump or pool model.

For the evaporating case, the evaporation water must come from the film mass. When the film thickness reaches zero, no more water can be evaporated.

In order to evaluate the heat and mass transfer rates, a variety of properties are required. For all gas species, thermal conductivities, viscosities, and specific heats are required. Additionally, for water, liquid and vapor enthalpies are necessary.

3.3.1.7 Conclusions

The recommended model has the following desirable features:

1. It uses the driving force ($P_{g1} - P_{g2}$) which is natural to the problem.

2. It allows the vapor sensible heat correction.

3. It has good contact with standard treatments.

4. The formulation is transparent.

5. It is a flexible treatment, allowing many geometries, flow regimes, and parameter regimes to be treated, with

the user specifying only the Nusselt number correlation, which is better understood and more widely measured than any other transport coefficient.

6. The model has been verified to some extent by comparison with experiment.

7. An iterative treatment is unnecessary. The film is treated in a simple way which limits evaporation and which treats the delay in overflow of condensate to the sump, floor, or pool in a physically reasonable way.

3.3.1.8 References

1. Uchida, H., et al., Proc of the Int Conf. of the Peaceful Uses of Atomic Energy, (a/CONF.28/P436).

2. Tagami, T., unpublished (1965) cited in [6].

3. Collier, J. M., Convective Boiling and Condensation, McGraw-Hill, NY, 1972.

4. Bird, R., Stewart, W., and Lightfoot, E., Transport Phenomena, Wiley, NY, 1960.

5. Roshenow, R. and Choi, Heat, Mass and Momentum Transfer, Prentice Hall, 1961.

6. Slaughterbeck, D. C., "Review of Heat Transfer Coefficients for Condensing Steam in a Containment Building Following a Loss of Coolant Accident" (1970), Idaho Nuclear Corporation, IN-1388.

7. Whitley, R. H., "Condensation Heat Transfer in a Pressurized. . ." Master's Thesis, UCLA, 1976. R. H. Whitley, et al., Ann. Nucl. Energy, 3, 515 (1976).

8. Ayyaswamy, P. S., et al., Nucl. Technology, 33, 243 (1977).

9. Krotiuk, W. J. and Rubin, M. B., "Condensing Heat Transfer Following a Loss of Coolant Accident," Nucl. Tech., 37, 118, (1978).

10. Marshall, J., Nucl. Eng. and Design, 51, 409 (1979).

11. Almenas, K. and Marchello, J., "The Physical State of Post-Loss of Coolant Accident Containment Atmospheres," Nucl. Techn. 44, 411 (1979).

12. Chapman and Cowling, The Mathematical Theory of Non-Uniform Gasses, Cambridge Univ. Press, Cambridge, 1960.

13. Hanley, H. J. M., Transport Phenomena in Fluids, Marcel Dekker, NY, 1969.

14. Suo-Antilla, A. J., "Simplified Multicomponent Phase Transition Model," Los Alamos Scientific Laboratory, LA-7557-MS (January, 1979).

15. Kreith, F., Heat Transfer, International, Scranton, PA, 1958.

16. Eckert and Drake, Analysis of Heat and Mass Transfer, McGraw-Hill, NY, 1972 and 1959.

17. Parker, Boggs, and Blick, Introduction to Fluid Mechanics and Heat Transfer, Addison Wasley, NY, 1970.

18. Corradini, M. L., "Turbulent Condensation on a Cold Wall in the Presence of a Noncondensible Gas," to be published.

19. Baumeister, T. B., ed., Marks' Standard Handbook for Mechanical Engineers (8th ed.), McGraw-Hill, NY, 1978.

3.3.2 RADIATION

3.3.2.1 Introduction

Radiant heat transfer is important during and following combustion events in containment, steam spikes following vessel failure and melt ejection, and to a lesser extent, following blowdown, if relatively high temperatures and steam partial pressures exist. Both containment pressures and surface temperatures can be significantly affected. Radiant heat transfer is not treated in MARCH. Most of the radiant heat transfer will come from steam, although carbon dioxide and carbon monoxide may play an important role during core-melt accidents, if core-concrete interactions occur. Generally, the air in containment can be treated as inert with respect to radiation for the temperature regimes considered to be likely. Reflection of radiation by the containment surfaces is important, as is emission from the walls if their temperatures are elevated during the accident. In the sections that follow, emittance models for steam are discussed, the governing equations describing radiant exchange in containment are presented, and models to include carbon dioxide and carbon monoxide are discussed. Subjects not addressed here are the interaction of radiation with containment sprays and aerosols and radiation in the reactor cavity. Radiation heat transfer in the reactor cavity is different than radiation heat transfer in the rest of containment due to the high aerosol loadings in the reactor cavity. A diffusion approach may be more suitable to this problem.

3.3.2.2 Emittance Calculations for Steam

A gas emittance model which has been widely used is the exponential wide-band formulation of Edwards and co-workers which has been summarized in the monograph entitled "Molecular Gas Band Radiation."[1] This model is based upon statistical models of gas absorption in discrete wavelength bands and was developed utilizing measured spectral absorption data obtained with total gas pressures near atmospheric and in chambers such that only moderate radiation path lengths (usually less than 1.0 m) were considered. The model is well thought of in the "radiation community" and is excellent for performing band-by-band radiative calculations. Unfortunately, radiation band calculations are computationally expensive, especially if there are several gas species which are thermal radiators. Further, extensive band-by-band computations may not be warranted if the geometry (i.e., path lengths), pressures, and temperatures are significantly different from those conditions for which the exponential wide-band correlations were developed. Instead, single equivalent band radiative calculations may be appropriate, and total emittance models can be utilized.

Steam is generally the most important gas radiator in thermal analyses undertaken for reactor containment studies. Steam emittance data are typically obtained from Hottel emittance charts,[2] from emittance charts compiled by Ludwig, et al.[3] or from the Edwards exponential wide-band correlations [1] described previously. In the latter case, the individual band data from the Edwards model are summed using a black body weighting function to compute the total emittance as given in Equation (3.3.2-1) (variables are defined in the nomenclature).

$$\varepsilon_g = \sum_{j=1}^{J \text{ bands}} \bar{\alpha}_j \, F \, \Delta\lambda_{jT} \quad . \qquad (3.3.2\text{-}1)$$

Note that in these computations Kirchhoff's Law ($\alpha_i = \varepsilon_i$) is assumed to hold. The more recent evaluations of the measured spectral data by Ludwig et al.[3] have resulted in emittance charts for steam which compare well with Hottel results at low pressures and temperatures but which may differ significantly at high temperatures (>1000 K) and for the larger steam pressure-path length values.

Using data from the emittance charts in computer models is difficult and until recently, most codes have incorporated the exponential wide-band formulation. An alternative emittance model has been suggested by Cess and Lian [4] for mixtures of steam and air (air being mixtures of nitrogen, oxygen, and inerts), in which the Hottel data have been fit to an exponential form as shown in Equation (3.3.2-2):

$$\varepsilon_{H_2O} = a_0[1-\exp(-a_1\sqrt{X})] \qquad (3.3.2\text{-}2)$$

where

$$X = P_{H_2O} L_e \left(\frac{300\ P}{T}\right)\left[\frac{1 + x_{H_2O}\ 5\sqrt{\frac{300}{T}-1}}{(101325)^2}\right] \qquad (3.3.2\text{-}3)$$

and a_0 and a_1 are given as functions of temperature in Table 3.3.2-1.

Table 3.3.2-1

Coefficients of Cess-Lian Correlation

T, K	a_o	a_1, $m^{-1/2}$ atm^{-1}
300	0.683	1.17
600	0.674	1.32
900	0.700	1.27
1200	0.673	1.21
1500	0.624	1.15

Note that pressure broadening effects are included in this formulation (through X) and also that the relation reduces to the well-known square-root dependence for the limit of nonoverlapping strong absorption lines. The temperature limits specified above coincide with the range of experimental data used in the Hottel charts and omit the emittance data extrapolated by Hottel for the higher temperatures. As would be anticipated, the value of such a correlation is that it is computationally inexpensive.

Gas emittance values as a function of temperature and steam pressure-path length are presented in Figures 3.3.2-1 and 3.3.2-2 comparing results from the Cess-Lian parameterization correlation with the exponential wide-band model and with data obtained from emittance charts. Figure 3.3.2-1 results are obtained from a total gas pressure of 1.0 atm in the limit of the steam partial pressure approaching zero. The agreement between the three emittance calculations is rather good, which is not surprising since the data from which these correlations were developed were primarily measured under atmospheric pressure conditions. From Figure 3.3.2-1, it is apparent that results from the Cess-Lian correlation match the Hottel results for the conditions considered, and thus in Figure 3.3.2-2, Cess-Lian results are only compared with the estimates of Ludwig [3] and with the exponential wide-band results. The emittance results of Figure 3.3.2-2 are given for three different total pressure conditions (1.0, 3.0, and 5.0 atm) and for three different steam pressure-path lengths (0.1, 1.0, and 10.0 atm-m). While the trends are similar for the three methods for the two lowest values of steam pressure-path length, the discrepancies may be as great as 20 to 30 percent at the lower temperatures. At the largest pressure-path length considered, the Ludwig model results increase with temperature while the other model results decrease. This difference is

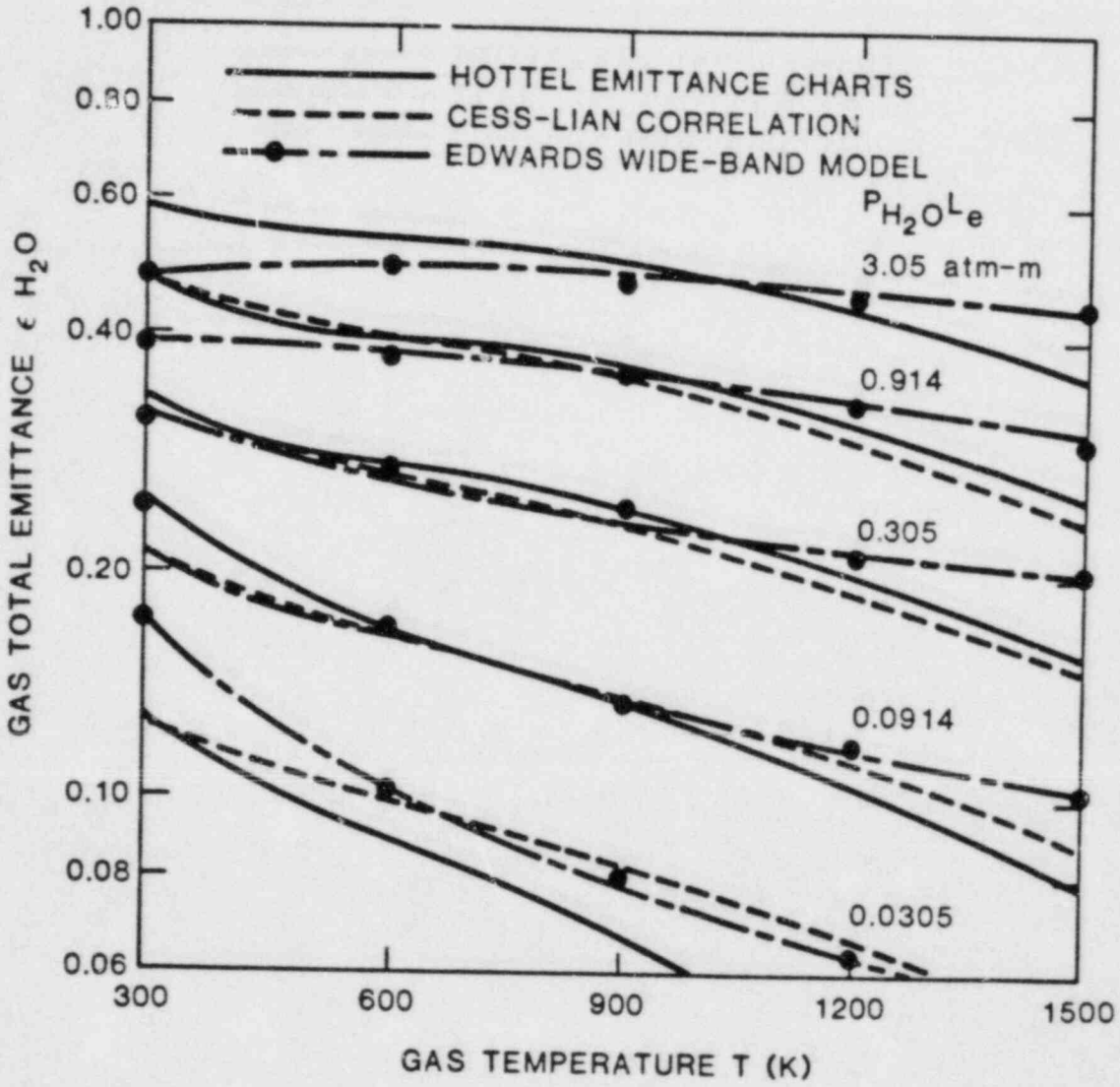

Figure 3.3.2-1. Comparative total steam emittance calculations for 1 atm total pressure in the limit as P_{H_2O} approaches zero

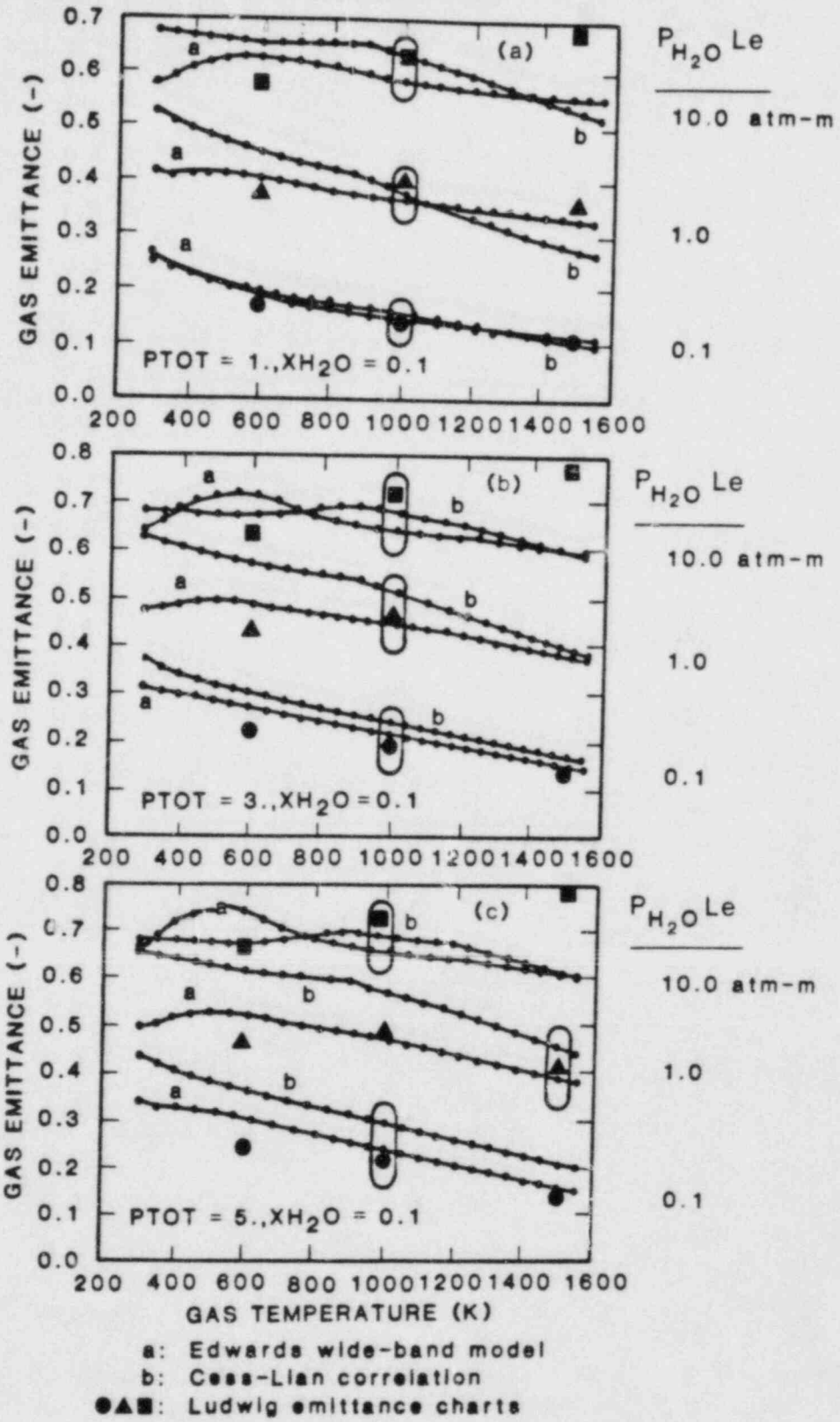

Figure 3.3.2-2. Comparative total steam emittance calculations for different pressure and path length conditions

significant, and suggests that the limitations of the models must be considered when the temperatures, pressures, and path lengths are outside of the ranges for which the emittance data were correlated.

In summary, it has been indicated that the computed steam emittance values may vary significantly between the different calculational methods, particularly if the total gas pressure and the radiative path lengths are large. This is particularly important in nuclear reactor geometries since hydrogen-air deflagrations could occur in regions where characteristic path lengths are > 20 m and total pressures and steam mole fractions could exceed 3 atm and 20 percent, respectively. Further, it is not apparent that the exponential wide-band model is superior to the Cess-Lian correlation for the conditions considered. Therefore utilization of either model for computing single equivalent band emittances should be acceptable in simulation models such as MELCOR.

3.3.2.3 Radiation Exchange Calculations

The radiative exchange package can be formulated assuming that the wall temperatures and gas environment are fixed during each time step. The model will compute the net energy transfer for each band (including transparent regions) and sum the contributions to obtain the total net radiative heat flux. These governing relations are summarized below.

$$\frac{k_{TH} \text{ surface, } j_{th} \text{ band}}{\sum_{i=1}^{N\ SURF} \left(\frac{\delta ki}{ei} - F_{k-i} \frac{1 - \epsilon i}{\epsilon_i} \tau_{k-i} \right) \Delta q_{ij}} =$$

$$\sum_{\epsilon i=1}^{N\ SURF} \left(\delta ki - F_{k-i} \tau_{k-i} \right) e_{bij} - F_{k-1} (1 - \tau_{k-i}) e_{bgj} \qquad (3.3.2\text{-}4)$$

and

$$qi = \sum_{j=1}^{J\ BANDS} \Delta q_{ij} \ . \qquad (3.3.2\text{-}5)$$

A single equivalent band model formulation for gaseous and surface radiative exchange can also be incorporated by applying Equation (3.3.2-4) for one band and using the total emittance data from any of the previously described methods (i.e., chart data, Cess-Lian, or exponential wide-band).

Although this method is a gray-gas formulation and omits some of the important band detail, the emittance data remains the critical input, and as shown previously, may be suspect anyway for elevated pressures, temperatures, steam partial pressures, and path lengths as would be encountered in nuclear reactors. These uncertainties would similarly be encountered in band-by-band computations using the exponential wide-band results for each wavelength band. For an enclosure comprised of many surfaces, the advantage of using a single equivalent band model would be computational, since the N-surface simultaneous equations would only need to be solved once per time step instead of once for each band. Further, the Cess-Lian correlation is applicable for a single-band model and this model is significantly less expensive (computationally) than is the exponential wide-band total emittance correlation.

3.3.2.4 Carbon Dioxide and Carbon Monoxide Emittance Models

Including carbon dioxide and carbon monoxide gas species in an environment which contains steam complicates the radiative interchange problem since the different radiating bands of each gas may overlap. The number of radiating bands also will increase significantly, and thus multiple band radiative computations will become even more time consuming than has been previously shown for the steam radiation calculations. In a typical wide-band formulation, for example, a seven-band model is incorporated, in which two bands are transparent. If carbon monoxide and carbon dioxide gas species are also present in the steam environment, there could be between 15 to 25 bands (many transparent) which would need to be considered depending upon gas makeup, temperature, and pressure. Such band-by-band computations would be cost-wise prohibitive, especially given the emittance value uncertainties in nuclear reactor configurations.

As with steam, overall emittance data for carbon monoxide and carbon dioxide can be obtained from Hottel emittance charts or from the Edwards exponential wide-band formulation. Because the three gaseous radiators may have overlapping absorbing bands (see Table 3.3.2-2), additional Hottel charts or other correction techniques are required to account for band overlap ($\Delta\varepsilon$) according to a relation similar to that given by Equation (3.3.2-6).

$$\varepsilon_g = \varepsilon_{H_2O} + \varepsilon_{CO_2} + \varepsilon_{CO} - \Delta\varepsilon \quad . \qquad (3.3.2\text{-}6)$$

Such corrections are functions not only of the gas make-up, but will also depend on the gas temperature and pressure. The difficulty in programming such effects necessitates using the exponential wide-band models. Edwards recommends

that each radiating species be treated as an independent gas in an otherwise inert medium. Once the different gas band characteristics (i.e., band minima, maxima, and absorptance) are obtained for each gas, they are ordered in terms of increasing wavelength, and the bands which overlap are broken into different absorbing parts such that the absorptance for each region is obtained from Equation (3.3.2-7).

$$\bar{\alpha}_{BAND} = 1 - \prod_{i=1}^{M \text{ gases}} (1-\bar{\alpha}_i) \qquad (3.3.2\text{-}7)$$

where α_i is the absorptance of gas species i over the overlapped region.

Table 3.3.2-2

Absorption Band Centers for Radiating Gases

Gas	No. of Radiating Bands	Band Centers
Steam	5	1.38, 1.87, 2.7, 6.3 μm and rotational band
Carbon Monoxide	2	2.35 and 4.7 μm
Carbon Dioxide	6	2.0, 2.7, 4.3, 9.4, 10.4, and 15.0 μm

Exponential wide-band models for carbon dioxide and carbon monoxide have been coded for a version of HECTR. In addition, a subroutine package to order the band intervals has been developed (but it has not been optimized for fast running). These models have been compared with sample calculations provided in Reference [1] and with Hottel emittance data for steam-carbon dioxide mixtures. The agreement between the Edwards and Hottel emittance predictions is better at the lower pressure but is still acceptable at the higher pressure-path length condition. Overall, the computation times will increase when carbon dioxide and carbon monoxide are included, but these increases should not be too great so long as the single equivalent band model is used for radiative exchange calculations.

3.3.2.5 Interface with Other Parts of MELCOR

Interfacing the radiation package with the rest of MELCOR is straightforward. The heat flux from Equation (3.3.2-5) defines the rate of energy transfer between the surfaces and the bulk gas. In order to perform the calculations, one needs only the gas composition and thermodynamic state, and the emissivities of the surfaces. Note that the surface emissivity may be altered if there is a liquid layer present on the surface.

3.3.2.6 Summary and Recommendations

Several different types of radiation models are available that could be used in MELCOR. Uncertainties exist for all of these models in the regions of interest for reactor containments. Given these uncertainties and the desire to minimize computation time, relatively simple approaches should be used. The Cess-Lian correlation is appropriate for most of the conditions that will be encountered. For calculations where the Cess-lian correlation is not appropriate (temperatures above 1500 K) it may be reasonable to switch to the wide band model. Including carbon dioxide and carbon monoxide clearly complicates the problem, probably making multiple band calculations necessary. However, code logic should be such that carbon dioxide and carbon monoxide are ignored whenever they are either not present or the temperature, partial pressures, and beam lengths ae such that their effects are negligible. In any case, if multiple band calculations are necessary, it may still be possible to use a total emittance and only solve the equations for radiant exchange once per time step.

Finally, we should point out that the discussions above have only considered radiant exchange within a single compartment. For this case, configuration factors and path lengths need only be defined for surfaces within the same compartment (even this can be a difficult job). Radiant exchange between compartments is extremely difficult to model in any manner that is computationally fast enough for a code like MELCOR. This problem is being addressed in the HECTR program, but no solutions appear imminent. As it appears that the first version of MELCOR will consider a minimum number of compartments, with those compartments representing physically defined volumes, this may not be a major problem. However, future versions of the code will certainly have to address the problem.

3.3.2.7 Nomenclature

a_o, a_1	coefficients given in Table 1
e_{bij}	black body emissive power of surface i for band interval j
e_{bgj}	black body emissive power of gas for band interval j
F_{i-j}	radiation configuration factor for surface i to surface j
$F\Delta_{iT}$	Planck black body fraction for wavelength band interval i
J	number of band intervals
L_e	characteristic path length
N	number of surfaces comprising the enclosure
P	total gas pressure
$P_{H\ O}$	steam partial pressure
q_i	total heat flux to (from) surface i
Δq_{ij}	heat flux to (from) surface i for band interval j
T	gas temperature
X	pressure broadening term given by Equation (3)
x_{HO}	steam mole fraction
x_{CO2}	carbon dioxide mole fraction

Greek

$\bar{\alpha}$	gas absorptance = $1-\bar{\tau}$
δig	Kronecker delta
ϵg	gas total emittance
ϵi	emissivity of surface i
ϵCO	carbon dioxide gas emittance
ϵCO	carbon monoxide gas emittance
ϵH_2O	steam emittance
	emittance correction for band overlap
$\pi i\Delta-\epsilon$	gas transmittance for path length between surfaces i and j.

3.3.2.8 References

1. Edwards, D. K., "Molecular Gas Band Radiation," Advances in Heat Transfer, 12, Irvine, T. F. and Hartnett, J. P., ed., Academic Press, NY, 1976.

2. Siegel, R. and Howell, J. R., Thermal Radiation Heat Transfer, Second Edition, McGraw Hill Book Co., NY, 1981.

3. Ludwig, C. B., Malkmus, W., Reardon, J. E. and Thomson, J. A. L., Handbook of Infrared Radiation from Combustion Gases, NASA SP-3080, Goulard, R. and Thomson, J. A. L., ed., 1973.

4. Cess, R. D. and Lian, M. S., "A Simple Parameterization for Water Vapor Emissivity," Trans, ASME Journal of Heat Transfer, Vol. 98, No. 4, pp. 676-678, 1976.

3.3.3 HEAT TRANSFER IN SOLID STRUCTURES

3.3.3.1 Introduction

Conduction heat transfer plays a vital roll both in the normal operation and in the sequence of events in an accident scenario of a modern power reactor. Heat flows by conduction from the fuel rods through the cladding and finally to the coolant. At the fuel rods, the conduction equation contains an energy source term to account for the nuclear power generated. Transfer of energy from the primary to the secondary systems of PWR reactors is also by conduction.

Important considerations in a containment code such as MELCOR are mass and energy conservation. These together with some thermodynamic considerations lead to knowledge of the containment pressure. Heat conduction contributes to both the phasic mass and energy inventories. The mass is affected in two general ways. First, evaporation or condensation may occur at the surface of a heat slab depending on the temperature. Second, in a scenario in which a molten core pours onto a concrete containment floor, heat is conducted into the concrete with consequent release of water and carbon dioxide. These materials flow through the concrete to the pool, react chemically with the molten materials in the pool, and finally contribute to mass inventories of both the pool and the cell atmosphere.

The energy inventory in the containment building is affected in a variety of ways by heat conduction in solids. (1) Heat is lost by conduction to the containment walls, the atmosphere and ground (2) Heat is transferred between adjoining cells by conduction through a common wall. (3) Heat is trasnferred to and from major heat structures (e.g., overhead cranes, etc.) within the containment. (4) Heat is conducted to and from the reactor coolant as mentioned above.

In Section 3.3.3.2 the transient heat conduction equation and its finite difference solution are discussed. The Crank-Nicolson algorithm is suggested since it is implicit, stable, and is of second order accuracy. An analytic transformation has been performed on the differential equation to allow rezoning. Thus, in regions where the temperature gradient is small, large grid spacing may be used. This will save both computer time and storage space. The steady state heat conduction equation has two applications. First, it is used to initialize transient heat conduction problems and second, it can be used to do heat conduction portion of the containment problem in regions of time in which a quasi-static solution is appropriate. The steady state solution is discussed in Section 3.3.3.3. Boundary conditions for

both the transient and steady state problems are treated in Section 3.3.3.5.

Perhaps the most difficult part of the heat conduction problem is that of providing accurate heat transfer correlations at the various boundaries. Heat transfer from a solid to an atmosphere can depend on whether forced or free convection exists, whether or not the atmosphere contains a condensing vapor, and whether the vapor contains noncondensible gases. Heat transfer from a solid to a two-phase fluid depends on the flow regime of the fluid which in turn depends on variables such as flow rate and fluid quality.

3.3.3.2 Heat Conduction Equation

The equation for conduction of heat in solid materials is

$$\frac{\partial}{\partial t}(\rho c_p T) = \nabla \cdot (k \nabla T) + \sum_m \dot{Q}_m \qquad (3.3.3\text{-}1)$$

where T, ρ, c_p, k and Q_m are respectively: temperature, density, heat capacity at constant pressure, thermal conductivity and heat source of type m. Equation (3.3.3-1) will be written in generalized orthogonal coordinates. For this purpose note that

$$\nabla T = \sum_i \frac{1}{h_i} \frac{\partial T}{\partial x_i} \hat{e}_i \qquad (3.3.3\text{-}2)$$

and for any vector,

$$\nabla f = \frac{1}{h_i h_j h_k} \sum_i \frac{\partial (h_j h_k f_i)}{\partial x_i} \quad i,j,k \text{ cyclic} \qquad (3.3.3\text{-}3)$$

then,

$$\nabla \cdot (k \nabla T) = \frac{1}{h_i h_j h_k} \sum_i \left[\frac{\partial}{\partial x_i} \left(\frac{h_j h_k}{h_i} k \frac{\partial T}{\partial x_i} \right) \right] \quad i,j,k \text{ cyclic} \quad . \qquad (3.3.3\text{-}4)$$

For one dimensional problems in the first coordinate, Equation (3.3.3-4) becomes,

$$\nabla \cdot (k\nabla T) \rightarrow \frac{1}{h_1 h_2 h_3} \frac{\partial}{\partial x_1}\left(k \frac{h_2 h_3}{h_1} \frac{\partial T}{\partial x_1}\right). \qquad (3.3.3\text{-}5)$$

Include analytic rezoning by transforming the differential equation according to,

$$\frac{\partial}{\partial x_1} = \Psi \frac{\partial}{\partial u_1} \quad . \qquad (3.3.3\text{-}6)$$

The transformation is used to provide uniform zones in the u-space and corresponding nonuniform zones in the x-space. The finite difference equations are evaluated in the uniform space. The nonuniform space corresponds to the physical problem. This provides an accurate method of rezoning without the usual errors introduced by evaluating the finite difference equations in a nonuniform grid.

Rezoning is important because it allows proper resolution of the physical processes in regions of high gradient and in addition conserves computer time and storage by using larger zones in regions where the gradients are small.

Equation (3.3.3-1) becomes

$$\frac{\partial(\rho c_p T)}{\partial t} = \frac{\Psi}{h_1 h_2 h_3} \frac{\partial}{\partial u_1}\left(K\Psi \frac{h_2 h_3}{h_1} \frac{\partial T}{\partial u_1}\right) + \sum_m \dot{Q}_m \quad . \qquad (3.3.3\text{-}7)$$

Define

$$G_1 = \frac{\Psi}{h_1 h_2 h_3} \qquad (3.3.3\text{-}8)$$

$$G_2 = \Psi \frac{h_2 h_3}{h_1} \quad . \qquad (3.3.3\text{-}9)$$

Equation (3.3.3-7) becomes

$$\frac{\partial}{\partial t} (\rho c_p T) = G_1 \frac{\partial}{\partial u_1} \left(G_2 \, k \frac{\partial T}{\partial u_1}\right) + \sum_m \dot{Q}_m \quad . \qquad (3.3.3\text{-}10)$$

The capability to treat heat structures composed of different materials will be implemented. The treatment will be similar to the composite material treatment described in Reference [15]. By utilizing such methods, the air gap between the steel lines and concrete in a containment structure and other significant discontinuities in thermal conductivity can be handled.

For most applications, the useful coordinate systems are Cartesian, cylindrical and spherical. The metric terms and and vector operators will be given for the one dimensional problems in these cases.

Cartesian coordinates:

$$h_1 = 1,\ h_2 = 1,\ h_3 = 1$$

$$\nabla\ (k\nabla T) \longrightarrow \frac{\partial}{\partial x}\ \left(K\frac{\partial T}{\partial x}\right) \qquad (3.3.3\text{-}11)$$

Cylindrical coordinates:

$$h_R = 1,\ h_d = R,\ h_z = 1$$

$$\nabla \cdot (k\nabla T) \quad \frac{1}{R}\frac{\partial}{\partial R}\left(k\ R\ \frac{\partial T}{\partial r}\right) . \qquad (3.3.3\text{-}12)$$

Spherical coordinates:

$$h_r = 1,\ h_\theta = r,\ h_\phi = r\ \sin\theta$$

$$\nabla \cdot (k\nabla T) \quad \frac{1}{r^2}\frac{\partial}{\partial r}\left(kr^2\ \frac{\partial T}{\partial r}\right) . \qquad (3.3.3\text{-}13)$$

The finite difference approximation of Equation (3.3.3-10) is,

$$\frac{1}{\Delta t}\ (\rho c_p)_i^{n+1}\left(T_i^{n+1}-T_i^n\right) = \frac{G_i^1 G_{i+1/2}^1}{\Delta u_1^{\ 2}}\ k_{i+1/2}^{n+n}\ *$$

$$\left[\eta\left(T_{i+1}^{n+1}-T_i^{n+1}\right) + (1-\eta)\left(T_{i+1}^n-T_i^n\right)\right]$$

$$- \frac{G_i^1 G_{i-1/2}^2}{\Delta u_1^2} k_{i-1/2}^{n+n} *$$

$$\left[\eta \left(T_i^{n+1} - T_{i-1}^{n+1} \right) + (1-\eta) \left(T_i^n - T_{i-1}^n \right) \right] + \sum_m \dot{Q}_m \quad . \qquad (3.3.3\text{-}14)$$

This equation is tridiagonal in the temperature at time (n+1) · dt. It can be written in the as,

$$-A_i \, T_{i+1}^{n+1} + B_i T_i^{n+1} - C_i \, T_{i-1}^{n+1} = D_i \quad . \qquad (3.3.3\text{-}15)$$

A solution exists of the form

$$T_i^{n+1} = E_i \, T_{i+1}^{n+1} + F_i \qquad (3.3.3\text{-}16)$$

where

$$E_i = \frac{A_i}{B_i - C_i \, F_{i-1}} \qquad (3.3.3\text{-}17)$$

and

$$F_i = \frac{D_i + C_i \, F_{i-1}}{B_i - C_i \, E_{i-1}} \quad . \qquad (3.3.3\text{-}18)$$

E and F must satisfy appropriate boundry conditions. These depend on the form of the boundary conditions for the heat conduction problem.

3.3.3.3 Steady State Heat Conduction

3.3.3.3.1 Applications

Two major applications of the steady state heat conduction are (1) Initialization of transient problems and (2) Calculation of conduction heat flow in quasi-static problems. Each application will be discussed below.

Specification of a transient heat conduction problem requires, among other things, boundary conditions at all

conductor boundaries at all time and initial conditions i.e., specification of all relevant parameters at all space points at time t=0. Two types of initial conditions will be treated. First, cases in which the entire problem space is initially at thermal equilibrium require that at time, t=0, all conductors have a single uniform temperature, the equilibrium temperature. In this case, all heat fluxes are zero.

The second type of initial condition considered arises from the assumption that previous to t=0, the state of the system was changing slowly, local thermodynamic equilibrium existed in individual compartments, and that the steady state solution adequately described the conduction heat transfer. For this case, the steady state conduction equation is solved at t=0 with appropriate boundary conditions. This solution determines temperature profiles and heat fluxes to be used as initial conditions in the transient problem.

The second application for the steady state heat conduction equation is to use it for the solution of the time dependent problem in regions where a quasi-static solution is appropriate. At late time after sharp transients have passed and the state of the system is changing slowly, one can assume that at any time step a steady state solution of the heat conduction equation is adequate to obtain heat fluxes that are necessary to update energy inventories in the problem cells. Cell to cell fluid flow is calculated. The cell thermodyanmics is then reevaluated and new equilibrium cell temperatures are obtained. From these, new steady state heat conduction problems are defined at the new time step. This process is repeated to obtain the time dependent solution.

3.3.3.3.2 Differential Equation and Solution

Set $\frac{\partial}{\partial t} = 0$, then the heat conduction equation becomes,

$$\nabla \cdot (k\nabla T) + \sum_m \dot{Q}_m = 0 \qquad (3.3.3\text{-}19)$$

where k is the thermal conductivity, T is the temperature and Q is a heat source. Following the method used for transient heat conduction, one writes the equation in generalized coordinates, transforms to a uniform mesh using Equation (3.3.3-6) and employs the definitions (3.3.3-8) and (3.3.3-9). The Crank-Nicholson form of the finite difference equation is then,

$$G_i^1 G_{i+1/2}^2 \; k_{i+1/2}^{n+n} \left[\eta\left(T_{i+1}^{n+1} - T_i^{n+1}\right) + (1-\eta)\left(T_{i+1}^{n} - T_i^{n}\right)\right]$$

$$- G_i^1 G_{i-1/2}^2 \; k_{i-1/2}^{n+n} \left[\eta \left(T_i^{n+1} - T_{i-1}^{n+1} \right) + (1-\eta) \left(T_i^n - T_{i-1}^n \right) \right]$$

$$+ \Delta U_1^2 \sum_m \dot{Q}_m = 0 \quad . \qquad (3.3.3\text{-}20)$$

This equation is tridiagonal in the spacial coordinate and is of the same form as Equation (3.3.3-15). Thus the solution is given by Equations (3.3.3-16) through (3.3.3-18).

Equation (3.3.3-20) must be solved subject to proper boundary conditions. They are the same as the boundary conditions for the time dependent problem discussed in Section 3.3.3.5.

3.3.3.4 Material Properties

The quantities, ρ, c_p, k, and Q may be temperature dependent. Since the heat flow equation is solved implicitly, the temperature and therefore the temperature dependent properties are now known at the new time step until after the implicit equations are solved. Thus one uses properties at the old time, n dt, to obtain temperatures at time, (n+1) dt. If the temperature dependence of the thermal properties is weak, this is sufficient. However, if necessary, an iterative technique can be used to obtain a more accurate solution. Thus T(n+1) is calculated using properties at t(n). Next, properties are calculated at time, (n+1) · dt, using T(n+1). These new properties are then used to recalculate T(n+1). This procedure is repeated until the solution has converged to the desired accuracy.

3.3.3.5 Boundary Conditions

A number of boundary conditions for the heat conduction equation are required, depending on the physical problem to be treated. The following ones should be incorporated into MELCOR:

1. Dirichlet boundary conditions. The temperature is specified at the surface of the heat conductor, i.e.,

$$T\big|_S = T_0 \qquad (3.3.3\text{-}21)$$

where s indicates the surface of the heat structure. This boundary condition is appropriate for cases where the temperature of the surface is a known function. Examples are: When thermodynamic equilibrium is assumed in a cell, an approximation that has been used is to set the surfaces of the conductors to this equilibrium temperature. If contact

resistance is neglected, two conductors in contact may be assumed to be at the same temperature. In problems involving conductors of great thickness, the temperature at the surface away from heat sources or fluxes may be assumed to be at a known ambient temperature. An example of this is conduction of heat from the reactor containment into the surrounding ground.

2. Neumann boundary conditions. The normal derivative of the temperature is specified at the surface of the heat conductor, Thus

$$\left.\frac{\partial T}{\partial n}\right|_s = g_o \quad . \tag{3.3.3-22}$$

There are three important applications of this boundary condition to the containment problem. First, if the heat structure is bounded by a good insulator, then

$$\left.\frac{\partial T}{\partial n}\right|_s = 0 \quad . \tag{3.3.3-23}$$

Second, a symmetrical heat structure may be modeled using a mesh that represents only half of the structure by applying a symmetry condition at the center. This condition is also given by Equation (3.3.3-23). Third, the heat flux at the surface is a known function. Then,

$$-k \left.\frac{\partial T}{\partial N}\right|_s = f_o \quad . \tag{3.3.3-24}$$

3. Heat flux correlations. This is a special case whose application employs a combination of the Dirichlet and Neumann conditions. Assume that the surface heat flux is related to a heat transfer coefficient, H, by

$$-k \frac{\partial T}{\partial n} = H(T-T_o) \tag{3.3.3-25}$$

where k and T are the thermal conductivity and temperature of the heat structure and T_o is the temperature of a fluid adjoining the heat structure. The fluid, for example, may be a cell atmosphere. In this equation, H is assumed to be determined by a correlation function that depends on the state of the fluid. When written in finite difference form,

Equation (3.3.3-25) provides the appropriate boundary condition necessary to calculate the temperature profile in the heat structure.

3.3.3.6 References

1. Collier, J. G., "Convective Boiling and Condensation," McGraw-Hill, 1981.

2. Delhaye, J. M., Giot, M., and Riethmuller, M. L., "Thermodynamics of Two-Phase Systems for Industrial Design and Nuclear Engineering," McGraw-Hill, 1981.

3. Dittus, F. W. and Boelter, L. M. K., "Heat Transfer in Automobile Radiators of the Turbular Type," University of California Publications, 2, 1930.

4. Gido, R. G., et al., "COMPARE-MOD 1: A Code for the Transient Analysis of Volumes with Heat Sinks, Flowing Vents, and Doors," LA-7199-MS, Los Alamos Scientific Laboratory, 1978.

5. Hestroni, G., "Handbook of Multiphase Systems," Hemisphere Publishing Corp., 1982.

6. Katsma, K. R., et al, "RELAP4/MOD5, A Computer Program for Transient Thermal-Hydraulic Analysis of Nuclear and Related Systems User's Manual, Vol.1," ANCR-NUREG-B35, Idaho National Engineering.

7. Lawton, R. G., "The AYER Heat Conduction Program," LA-5613-MS, Los Alamos Scientific Laboratory, 1974.

8. Mandel, D. A., et al., "TRAC-PD2 An Advanced Best-Estimate Computer Program for Pressurized Water Reactor Loss of Coolant Accident Analysis," LA-8709-MS, Los Alamos National Laboratory, 1981.

9. Ransom, V. H., et al., "RELAP5/MOD1 Code Manual, Vol. 1," NUREG/CR-1826 EG&G Idaho, Inc., 1981.

10. Richtmyer, R. D. and Morton, K. W., "Difference Methods for Initial-Value Problems," Interscience Publishers, 1967.

11. Senglaub, M. E., et al., "CONTAIN A COMPUTER Code for the Analysis of Nuclear Reactors and Related Systems Users Manual," Vol.1, ANCRD-NUREG-B35, Idaho National Engineering Laboratory, 1976.

12. Tagami, T., "Interim Report on Safety Assessments and Facilities Establishment Project in Japan for Period Ending June 1965 (No. 1)," Unpublished Report, 1966.

13. Uchida, H., Ogama, A., and Togo, Y. "Evaluation of Post Incident Cooling Systems of Light-Water Power Reactors," Proceedings of the Third International Conference on the Peaceful Uses of Atomic Energy, Geneva, Switzerland, Vol. 13, pp. 93-104, 1964.

14. Wagner, R. J., "HEAT1 A One-Dimensional Time-Dependent or Steady State Heat Conduction Code for the IBM-650," IDO-1445, 1963.

15. Ransom, V. H., et al., RELAP5/MOD1 Code Manual Volume 1: System Model and Numerical Methods; Volume 2: User Guide and Input Requirements, NUREG/CR-1826, EGG-2070, Idaho National Engineering Laboratory, March 1982.

3.4 COMBUSTIBLE GAS TREATMENT

by

F. E. Haskin

A. J. Camp

CONTENTS

LIST OF FIGURES

LIST OF TABLES

3.4.1 INTRODUCTION

Since the accident at Three Mile Island (TMI), there has been a great deal of interest regarding hydrogen production and combustion in light water reactors (LWRs). During the TMI accident the core was uncovered for a time and significant quantities of hydrogen were produced and released into containment. This hydrogen eventually ignited and produced about a 192 KPag (28 psig) pressure rise in containment. While this combustion event did not result in a loss of the containment integrity, there is concern that static or dynamic pressure loads from combustion events in other accidents could result in direct loss of containment integrity or damage safety-related equipment due to either high pressure or temperature. In order to assess the possible threats, it is necessary to model how hydrogen and other combustible gases are produced, transported, and mixed within containment, and how they combust.

The major mechanism for hydrogen production are the zirconium-steam reaction, the steel-steam reaction, core-concrete interactions, radiolysis of water, and corrosion of zinc and aluminum. Core-concrete interactions can also produce significant amounts of carbon monoxide which is also combustible. Other combustible gases, such as methane, are produced during core-concrete interactions and radiolytic decomposition of organic materials; however, their amounts are generally felt to be small compared to the amounts of hydrogen and carbon monoxide produced during severe accidents. A discussion of the sources of combustible gases is presented in Section 3.4.2.

Gas transport and mixing determine where and when combustible mixtures are likely to be present. Thus, one must consider hydrogen transport out of the primary system and away from ex-vessel debris into the containment atmosphere (accounting for hydrogen which remains dissolved in water). Hydrogen solubility and transport and mixing are discussed in Section 3.4.3.

Combustion can occur if the mixture meets certain flammability criteria and an ignition source is present. The presence of steam, carbon dioxide, or other diluting gases can have a significant effect upon combustion. Sections 3.4.4, 3.4.5, and 3.4.6 discuss the conditions required for three types of combustion: deflagrations, detonations, and diffusion flames.

3.4.2 COMBUSTIBLE GAS GENERATION

There are five sources of hydrogen which could be significant during a severe accident:

1. Zirconium-steam reaction
2. Steel-steam reaction
3. Core-concrete interactions
4. Radiolysis, and
5. Corrosion.

The zirconium-steam and steel-steam reactions arise when steam passes through an uncovered core region or when hot metallic debris interacts with liquid water either in-vessel or ex-vessel. If the core debris penetrates the reactor vessel and the resulting ex-vessel debris configuration is not coolable, core-concrete interactions can produce substantial quantities of hydrogen and carbon monoxide. Radiolysis and corrosion can produce significant quantities of hydrogen over long time periods (many hours to several days). Each of the major sources is discussed in more detail below.

3.4.2.1 Zirconium-Steam Reaction

Zirconium can react with steam to produce hydrogen when the zirconium is heated to a sufficiently high temperature and an adequate supply of steam is present. Typically, a zirconium temperature in excess of 1000°C (1832°F) is required to produce a significant reaction rate,[1] so the zirconium-steam reaction is only important when the reactor core is partially or completely uncovered or when hot debris contacts liquid water either in-vessel or ex-vessel.

The chemical formula for the reaction of zirconium with steam is:

$$Zr + 2H_2O \rightarrow ZrO_2 + 2H_2 + \text{Energy (Heat)} \quad . \qquad (3.4.2\text{-}1)$$

For every mole of zirconium oxidized, two moles of hydrogen are produced (or 0.044 kg of H_2 per kg of Zr oxidized). The reaction is exothermic, releasing 140 kcal per mole (2765 Btu per lb). By assuming that all of the available zirconium reacts, one can estimate the maximum amount of hydrogen that can be released from this reaction. Note that some zirconium may react with the uranium dioxide fuel, and thus not be available to react with steam. Representative amounts of hydrogen from oxidation of all zirconium are 1000 kg (2200 lb) for a PWR and 2000 kg (4400 lb) for a BWR.[1]

The actual amount of hydrogen from oxidation of all zirconium will vary depending on the size and manufacturer of the reactor.

The rate at which hydrogen is produced from the zirconium-steam reaction depends on the zirconium temperature, the exposed surface area, the oxide thickness over the unreacted zirconium, and the availability of steam. All of these factors change as the accident progresses. Assuming that steam is present in sufficient quantities, that restrictions to steam diffusion in the hot gas are negligible, and that the cladding surface does not crack open, the amount of zirconium reacted as a function of time and temperature can be calculated from the expression:[2]

$$\frac{dW^2_{Zr}}{dt} = K(T) \qquad (3.4.2\text{-}2)$$

where

W_{Zr} = the mass of metal reacted per unit surface area, kg/m^2 (lb/ft^2).
$K(T)$ = an experimentally-determined parabolic rate constant, $kg^2/m^4/s$ ($lb^2/ft^4/s$).
T = zirconium temperature, K(°R).
t = time, s.

Alternative expressions for K(T) are discussed elsewhere [4.1]. K(T) usually takes the form

$$K(T) = A \exp[-B/RT] \qquad (3.4.2\text{-}3)$$

where A is a constant, B is the activation energy, and R is the universal gas constant. For example, using the Cathcart-Pawel[3] formulation, Figure 3.4.2-1 shows the hydrogen production rate per unit area for four different temperatures. Figure 3.4.2-2 shows the corresponding quantities of hydrogen as a function of time for a representative PWR clad surface area (4900 m^2 for TMI). These figures are presented here to illustrate that the relative rate of hydrogen production due to zirconium-steam reaction is rapid compared to that due to other processes. None of the curves represent an actual accident. Neither the temperature nor the exposed surface area would be constant in an actual accident. For temperatures above approximately 1000°C, the energy released from the zirconium oxidation can dominate decay heating. Cladding failure and subsequent melting and slumping processes can drastically change the surface area

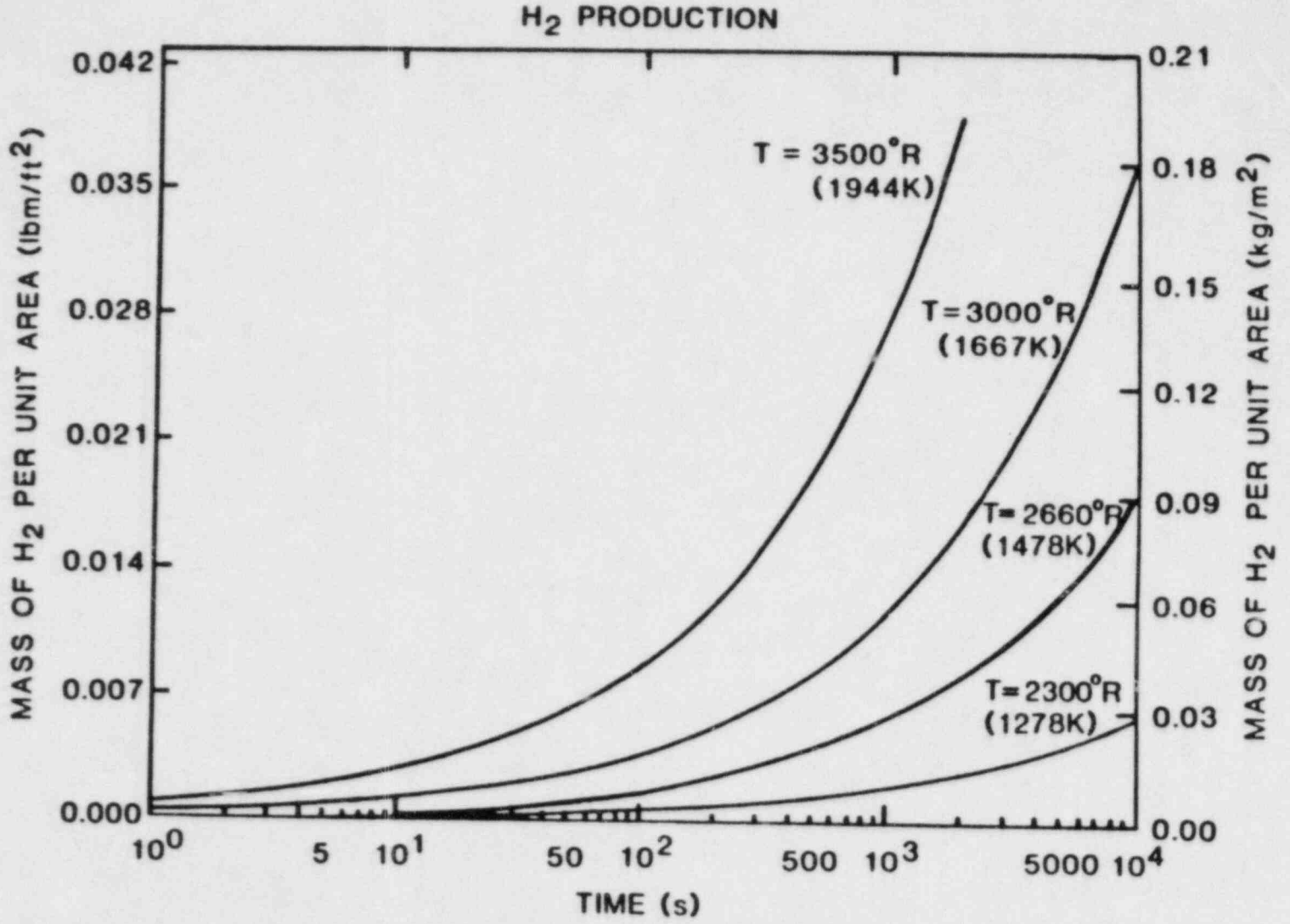

Figure 3.4.2-1. H_2 Production Per Unit Area from the Zr:H_2O Reaction

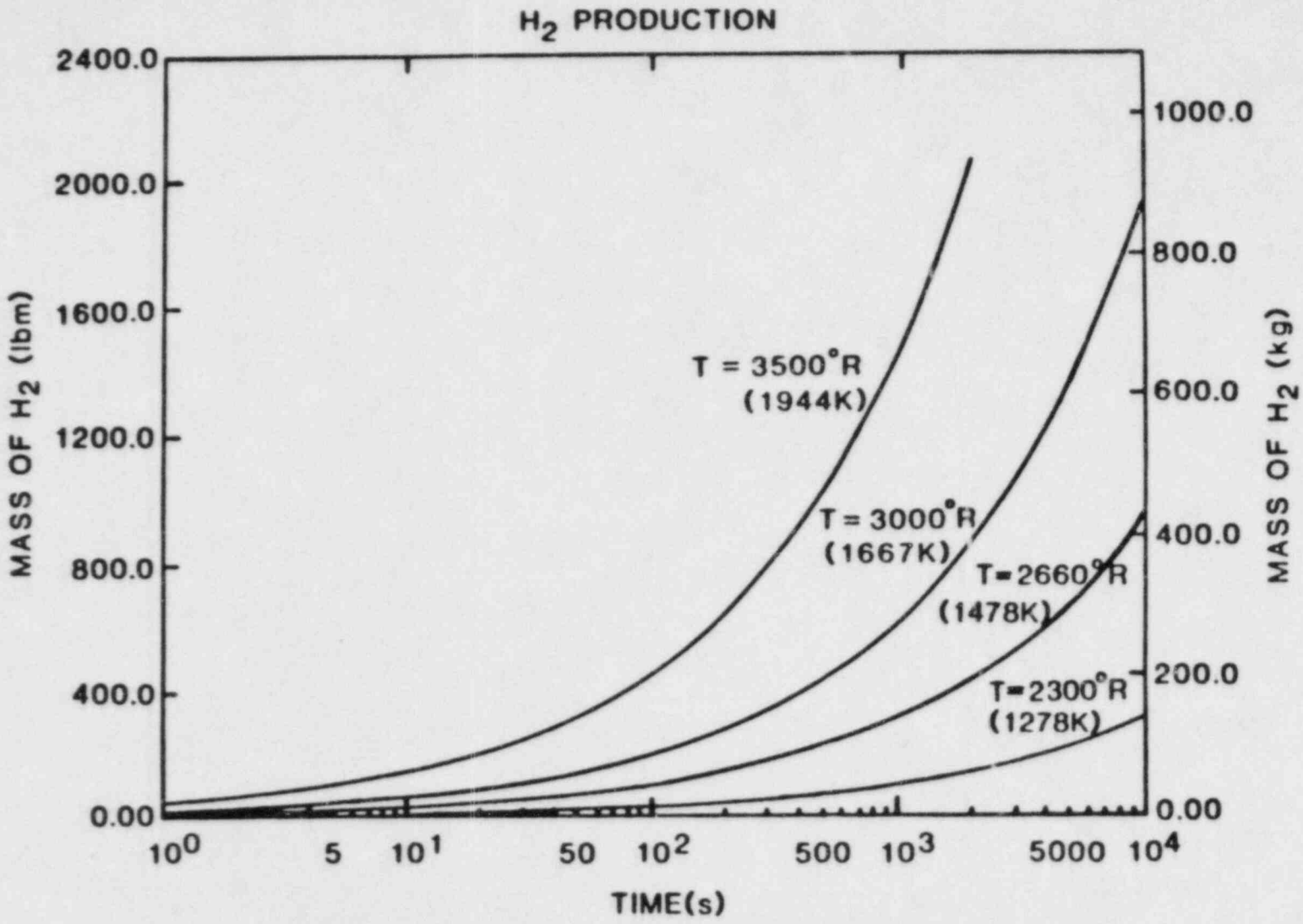

Figure 3.4.2-2. Total H_2 Production from the Zr:H_2O Reaction

available for oxidation. In-vessel and ex-vessel zirconium oxidation are discussed more extensively elsewhere [2.1, 3.2].

3.4.2.2 Steel-Steam Reaction

Steel heated to high temperatures and exposed to steam will oxidize to produce hydrogen. Large quantities of steel are present in the core support structures and elsewhere within the reactor pressure vessel. In addition, some steel from the in-vessel support structures and the bottom head of the vessel could become part of the hot ex-vessel debris in many postulated accidents. Oxidation of steel by high-temperature steam is highly complex, and several different oxide forms are possible. Fe_3O_4 is a major product; however, other oxides involving Fe, Cr, and Ni are also possible.[4] These oxidation reactions are less exothermic than the oxidation of zirconium; for example, approximately 8.6 kcal/mol (277.6 Btu/lb) of steel oxidized.

The oxidation of steel does not appear to be important below temperatures of about 1200°C (2192°F), and prolonged core uncovery would probably be required to achieve such high temperatures. However, as the melting point of steel is approached at 1370-1500°C (2498-2732°F), the oxidation rate of steel can become much larger than that of zirconium.

Investigations into the oxidation kinetics of steel indicate that two stages of oxidation exist.[5] The oxidation is characterized initially (5 to 30 minutes) by linear kinetics:

$$\Delta W_{steel} = \left|1.1 \times 10^{3} \exp(-4.44 \times 10^{4}/RT)\right| t \text{ kg/m}^2 \qquad (3.4.2\text{-}4)$$

where

ΔW = mass gained per unit of steel surface
R = gas constant, 1.98583 cal/mol/K
T = temperature, K
t = time, s.

The second stage of steel oxidation is characterized by parabolic kinetics:

$$\Delta W_{steel} = \left|2.4 \times 10^{8} \exp(-8.43 \times 10^{4}/RT)\right| 1/2t1/2 \text{ kg/m}^2. \qquad (3.4.2\text{-}5)$$

The mass of hydrogen generated can be determined from:

$$W_{H_2} = 2 M_{H_2} \Delta W_{Steel} / M_{O_2} \qquad (3.4.2\text{-}6)$$

where

W_{H_2} = the mass of hydrogen produced per unit of steel surface

M_{H_2} = the molecular weight of hydrogen, 2.002

M_{O_2} = the molecular weight of oxygen, 31.998.

Figure 3.4.2-3 shows a plot of hydrogen production versus time for four different temperatures. Figure 3.4.2-3 assumes that linear kinetics governs the production rate.

In order to calculate the hydrogen production from the steel-steam reaction for a particular accident, it is necessary to know the surface area of steel which could reach the necessary temperature and be exposed to steam. In-vessel, such steel surfaces as control-rod cladding, core barrels, control-rod guide tubes, and core support plates should be considered. If core slump occurs, then the bottom head of the reactor vessel and nearby structures should be considered. Hydrogen production due to steel oxidation in debris-water interactions is discussed elsewhere [2.1, 3.2].

3.4.2.3 Core-Concrete Interactions

In accident scenarios in which core debris penetrates the reactor pressure vessel and cannot be cooled by water in containment, decay heating can maintain the debris at temperatures which can result in thermal decomposition of adjacent concrete. Such decomposition of concrete produces large volumes of water vapor and carbon dioxide which, if they come into contact with molten metals, can be reduced to hydrogen and carbon monoxide.

Paper 3.5 discusses the modeling of core-concrete interactions for MELCOR. Quantitative predictions of hydrogen and carbon monoxide releases due to core-concrete interactions in general require detailed modeling. However, it has been established that significant quantities of both hydrogen and carbon monoxide could be produced (several hundred moles of each). Cole and Kelly[6] have demonstrated, based on analyses with the CORCON1 computer code that the amounts of hydrogen and carbon monoxide released increases with the decay heat level, the area of core-concrete contact, and the carbonate content of the concrete.

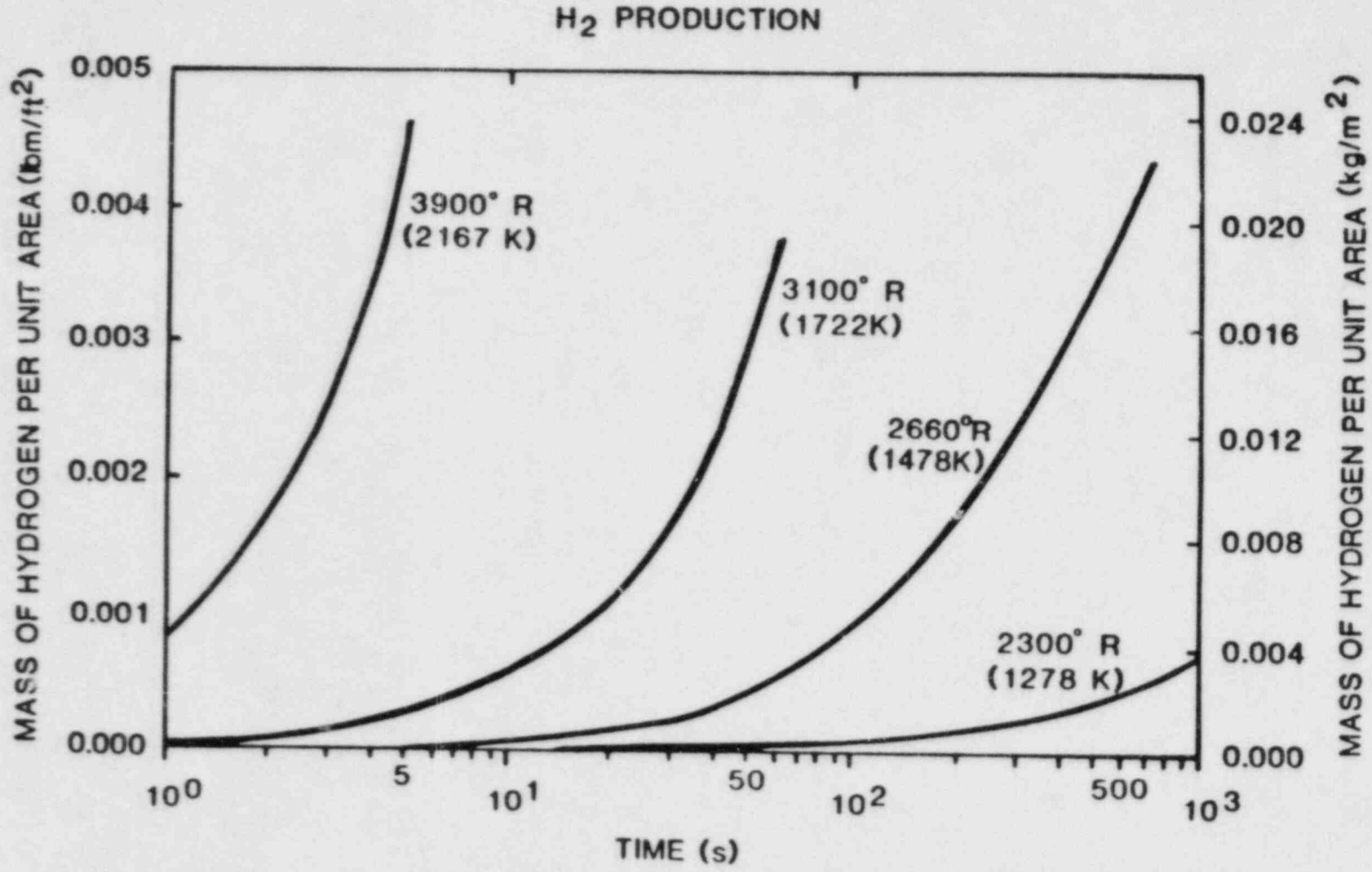

Figure 3.4.2-3. H_2 Production Per Unit Area From the Steel: H_2O Reaction

3.4.2.4 Radiolysis of Water

Radiolysis of water occurs during both normal operation and accidents. Radiolysis involves the decomposition of water molecules by radiation (α, β, γ, or n). Radiolysis of water (H_2O) can produce OH, H, HO_2, H_2, and H_2O_2.[8] These products can subsequently react with either themselves or other chemicals present in the water to produce a variety of products. An important point to be noted is that H_2 and O_2 can be produced by radiolysis.[9] Radiolysis can occur in the core, or elsewhere in the primary system, or in containment (if fission products are transported to those areas).

The rate of hydrogen and oxygen generation is controlled by three factors: (1) the decay energy, (2) the fraction of this energy that is absorbed by the water, and (3) the effective rate of hydrogen and oxygen production per unit of energy absorbed by the water. The yield of a product species due to the radiolysis of water is generally expressed as that product's "G" value (molecules of product formed per 100 eV of energy absorbed). Distinction must be made between the primary or direct radiolytic yield of a species and the net yield of the same species. The direct or primary yield is usually expressed as a subscript to G while the net or actual yield is written as a parenthetical notation. Thus, G_{H_2} is the hydrogen formed directly from the water by radiation, while $G(H_2)$ is the net hydrogen formed directly by radiation and indirectly by all subsequent chemical reactions. The G(x) value can be larger or smaller than G_x due to secondary reactions taking place between the various radiolytic species and the solutes. Typical values[10] of G_{H_2} in pure water are 0.44 for $\beta + \alpha$ radiation, 1.12 for reactor fast neutrons, and 1.70 for the recoil nuclei from the reaction $^{10}B(n,\alpha)^{7}Li$. Since molecular oxygen is not produced directly by radiolysis, $G_{O_2} = 0$; however, $G(O_2)$ is not necessarily zero.

A closed water/gas system will eventually attain equilibrium with respect to radiolytic decomposition of the water. The concentration of gaseous products at equilibrium will be a function of the reactor power density, the water pH and temperature, and the impurity (solute) type and concentration. Once equilibrium is attained, $G(H_2) = G(O_2) = 0$ (although the concentrations of H_2 and O_2 may not be zero). It is well established that small quantities of hydrogen (less than 10^{-3} moles/liter) dissolved in pure water or boric acid solutions will effectively limit the equilibrium condition to one in which negligible O_2 is generated. This technique is employed routinely in PWRs.

An open water/gas system will not attain an equilibrium condition because the product species are being continuously removed. A typical BWR power plant operates in such a manner. If the water is boiling vigorously, H_2 and O_2 will be produced in stoichiometric portions and $G(O_2) = 1/2\ G(H_2) = 1/2\ G_{H_2}$. For pure water exposed to $\beta + \alpha$ radiation, this would result in the production of ~22 molecules of O_2 and ~44 molecules of H_2 for each 10^4 eV of radiation energy.

The rate of radiolytic decomposition of pure water increases linearly with the reactor decay power but the equilibrium concentrations of product species in a closed system increase as the square root of the power. Variations in pH have little effect on α-irradiated water, but not much is known about the effect of pH variations with other forms of radiation. It has been speculated that pH variation may have a significant effect when combined with solutes.[10] Increasing temperature will tend to decrease equilibrium concentrations of product species in <u>pure</u> water, but it has been suggested that increasing temperature will enhance solute effects due to increased reaction rates between solute molecules and radiolytically produced radicals.[10]

The effect of the many possible solutes are not well understood. The impurities can react with the radiolytically produced radicals and upset the chemical balance. Only very small quantities of impurities are necessary to upset this balance.[9]

The specific accident scenario can have a major effect on the relative importance of radiolytic production of H_2 and O_2. In order to realistically estimate the effects of radiolysis, it is necessary to know the extent and distribution of fission-product release, the water temperature and pH, the degree of bubbling and turbulence of the water, and the types and quantities of impurities dissolved in the water. Presently we cannot assess the effect of simultaneous variations in several of these parameters. We can state, however, that the <u>rate</u> of production of combustibles from radiolysis is slow compared to that from the high-temperature Zr-steam and steel-steam reactions when the latter reactions are occurring.

In view of the complexities mentioned above, a simple parametric model of radiolytic decomposition seems most appropriate for MELCOR. Initially a two-parameter model should suffice, the two key parameters would be the net G-value of hydrogen, $G(H_2)$, and the fraction of the core fission and decay power absorbed directly by water, f. The parameter f could be treated as a constant, or estimated for the predicted core-water or debris-water geometries. Unless all core debris were somehow dissolved in liquid water, f

and hence $fG(H_2)$, would be much less than unity due to self shielding of radiation emitted within the debris particles of fuel. Provisions could be made to treat $G(H_2)$ as a function of water temperature, pH, and dissolved solute and hydrogen concentrations; however, initially $G(H_2)$ could be treated as a constant. Table 3.4.2-1 illustrates that even with $G(H_2)$ conservatively set equal to unity, radiolytic decomposition of water would not become a significant source of hydrogen until late in an accident ($t \geq 10^4$ s).

Table 3.4.2-1

Conservative Calculation of Radiolysis Yield and Rate for a 3300 MW(t) Reactor with $fG(H_2) = 1.0$

Time After Shutdown (s)	Integrated Decay Energy MJ/MW (Ref. 9)	Radiolysis Yield and Rate With $fG(H_2) = 1.0$ for 3300 MW Reactor			
		Total Yield (lbm)	(kg)	Average Rate (lbm/s)	(kg/s)
10^2	6	8.8	4	.0881	.0400
10^3	25	37.4	17	.0322	.0146
10^4	160	242.3	110	.0229	.0104
10^5	800	1207.0	548	.0106	.0048
10^6	3500	5286.3	2400	.0044	.0020

3.4.2.5 Other Sources

Other materials are present within containment that can react to form hydrogen. Zinc-based paint, galvanizing, and aluminum surfaces can react with water to produce hydrogen. Additionally, radiolysis of organic material may also lead to hydrogen production.

Corrosion of zinc-based paint and galvanizing is a function of temperature, composition, surface area, and pH of the spray solution. A detailed examination of the effects of these parameters can be found in Reference 11. However, for example purposes it is reasonable to assume that the reactions proceed according to:[12]

$$W_{H_2} = C\, e^{-B/RT}\, \text{Area}\, t \qquad (3.4.2\text{-}7)$$

where

W_{H_2} = mass of H_2 produced, kg

C = constant = 1.292×10^4 kg/m^2/hr
B = activation energy = 14500 cal/mole
R = gas constant = 1.98583 cal/mole/K
T = absolute temperature, K
Area = surface area, m^2
t = time, hours.

This equation agrees well with the data presented in Reference 11.

A typical PWR contains about 1.39×10^4 m^2 (1.5×10^5 ft^2) of zinc-based paint and about 2.8×10^3 m^2 (3×10^4 ft^2) of galvanized steel.[13,14] Figures 3.4.2-4 and 3.4.2-5 show the quantity of hydrogen produced as a function of time for these reactions, assuming the above surface area. Note that the total quantities produced are about 106 kg (233 lbm) of H_2 from corrosion of paint and about 52 kg (115 lbm) of H_2 from corrosion of galvanized steel. While in some reactors these numbers may be higher, this is still significantly less hydrogen than can be produced from other reactions discussed previously in this section.

The surface area of aluminum has been estimated to be 44 m^2 (475 ft^2) in a typical containment.[14] The corresponding mass of aluminum is about 568 kg (1250 lbm). Under severe-accident conditions of 149°C (300°F), a maximum of about 63 kg (139 lbm) of hydrogen could be produced over a seven day period, assuming the surface area and mass identified above and a production rate of 0.4 kg/hr (0.88 lbm/hr). Other estimates of the mass of aluminum in containment have been as high as 1800 kg (4000 lbm).

Organic materials such as cable insulation, epoxy paints, lubricating solutions, and gasket seals may produce combustible gases (primarily hydrogen or methane) due to radiolysis and corrosion. For most nuclear plants, the quantity of combustible gas that could be produced from organic materials inside containment is relatively small.

An example of hydrogen generation from radiolysis of cable insulation (polyethylene) follows. The yield of hydrogen $G(H_2)$, for polyethylene is 5 molecules for 100 eV of absorbed radiation.[15] If we take 200 Mrad as a 30-day radiation dose for the cable insulation, then the dose per pound is roughly 6×10^{24} eV (1.3×10^{25} eV/kg). A typical containment might have 4.5×10^4 kg (10^5 lbms) of cable insulation. Therefore, roughly 100 kg of hydrogen could be generated from radiolysis of cable insulation over a period of 30 days.

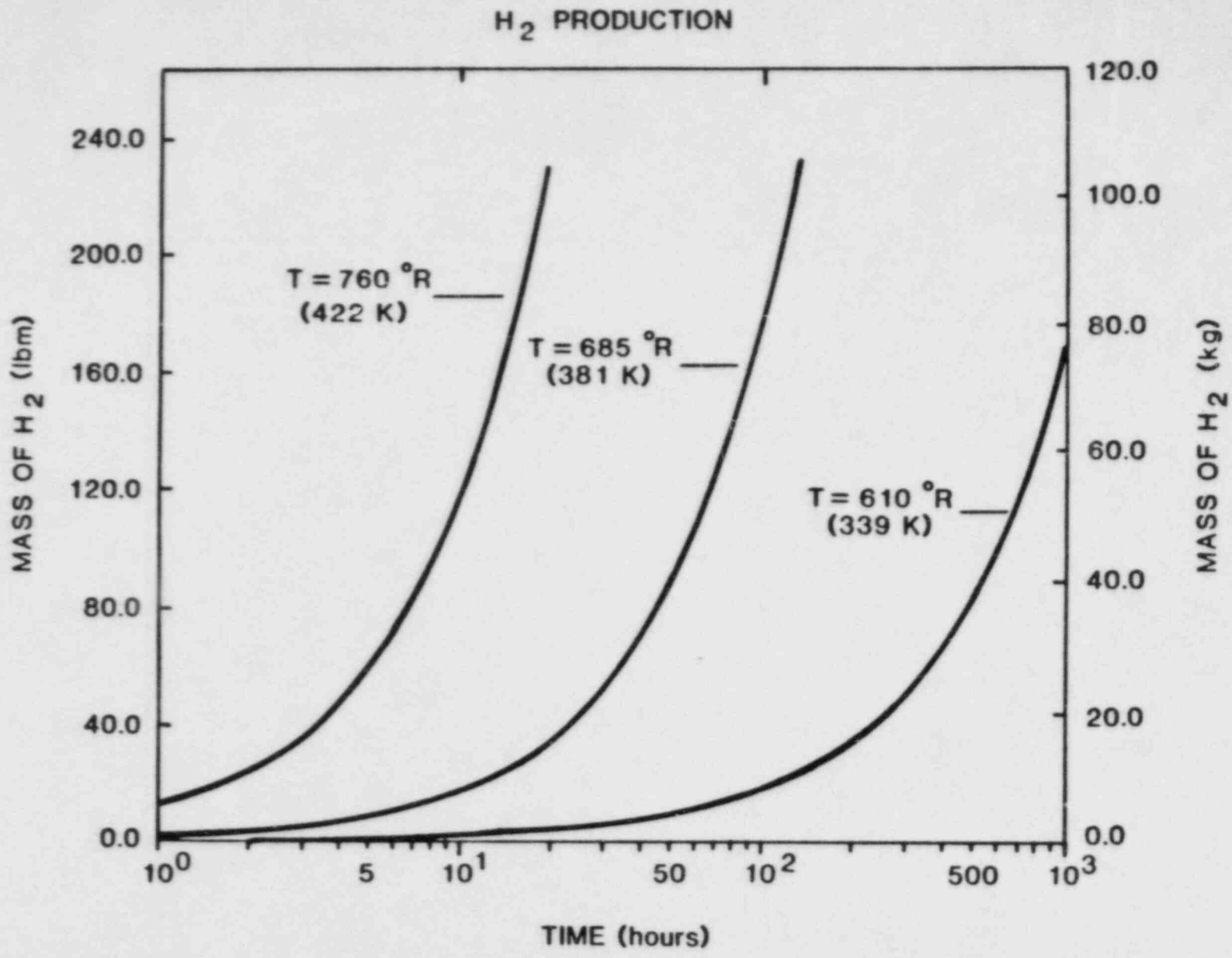

Figure 3.4.2-4. H_2 Production from Zinc-Based Paint

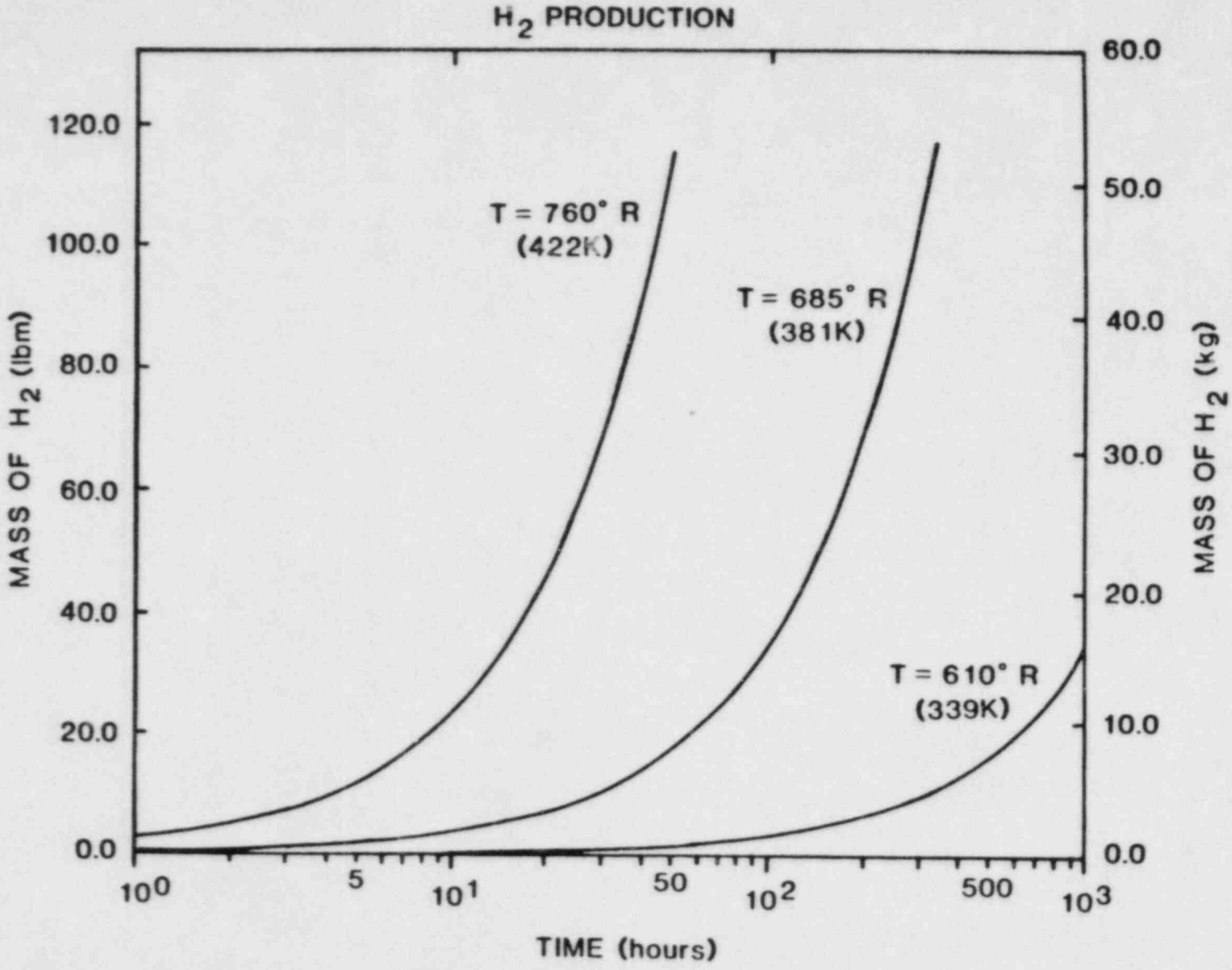

Figure 3.4.2-5. H_2 Production From Galvanized Steel

3.4.2.6 Time Sequence of Hydrogen Production

Of the sources of hydrogen discussed in this chapter, the most important one is the zirconium-steam reaction. This reaction requires temperatures above 1000°C (1832°F) which typically occur within the first few hours of a severe accident (after core uncovery). Large amounts of hydrogen can also be produced from steel-steam reactions. These reactions are initiated after the zirconium-steam reaction due to the higher temperatures required; however, they are still initiated during the first few hours of the accident and can be concurrent with the zirconium-steam reaction.

Core-concrete interactions do not occur until the core has fallen through the reactor vessel. Once the interactions start, vigorous gas generation results. Corrosion of paint and other surfaces within containment can begin once hot steam is released into containment or the containment sprays are activated. However, these reactions are slow, taking many hours to produce relatively small quantities of hydrogen.

Radiolysis is always present in a reactor. The rate of radiolysis can increase during the accident as fission products are released from the fuel. However, radiolysis is still a long-term concern relative to the zirconium-steam reaction. Using the information presented earlier in this chapter and making certain assumptions, we can estimate the relative quantities and timing of hydrogen production for the various reactions (see Figure 3.4.2-6). Figure 3.4.2-6 should be treated as qualitative in nature, as actual numbers depend upon the specific reactor and accident sequence.

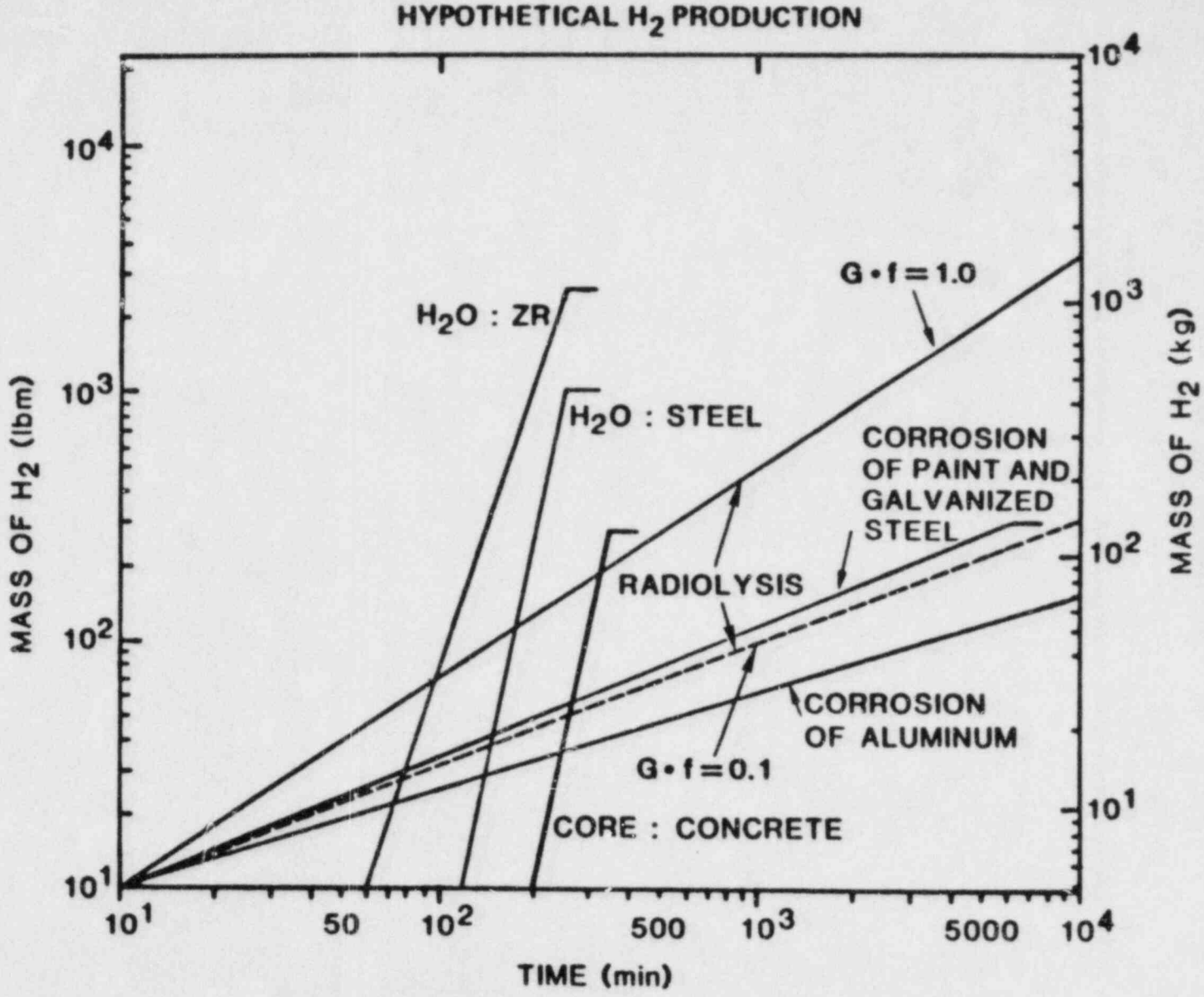

Figure 3.4.2-6. Qualitative H_2 Production for Various Reactions

3.4.3 HYDROGEN SOLUBILITY, TRANSPORT, AND MIXING

The transport and mixing of hydrogen determine when and where combustion is likely to occur. Some hydrogen will remain dissolved in water, with actual amounts depending upon the temperature, pressure, and composition. Hydrogen that does enter the containment atmosphere will mix with the steam and air due to pressure-driven motion, convective motion, and diffusion. The rate at which mixing will occur depends upon the particular mixing mechanisms at work. The following sections discuss solubility and mixing and what may be expected to occur under actual accident conditions. Detailed analysis of hydrogen transport generally requires sophisticated computer modeling; consequently, many of the discussions that follow are qualitative in nature.

3.4.3.1 Solubility of Hydrogen in Water

The solubility of hydrogen is a measure of how much hydrogen will remain dissolved in water under various conditions. Solubility of hydrogen in water can be treated fairly well by assuming that both the gas and the liquid solution are ideal. We can then assume that Henry's law is obeyed:

$$P_{H_2} = H(T)X_{H_2} \qquad (3.4.3\text{-}1)$$

where

P_{H_2} = partial pressure of hydrogen in the gas,
$H(T)$ = Henry constant (This constant is also a weak function of pressure, but that effect is ignored here),
X_{H_2} = mole fraction of hydrogen in the liquid.

$$X_{H_2} = P_{H_2}/H(T) \quad . \qquad (3.4.3\text{-}2)$$

H(T) has been experimentally determined over a wide temperature range and is plotted in Figure 3.4.3-1.[16] Detailed expressions for H(T) can be found in Reference 15. Using appropriate values for H(T), we can determine the amount of hydrogen dissolved, and Figures 3.4.3-2 and 3.4.3-3 show some results for various conditions in which the gas above the liquid consists of steam and hydrogen--as in a reactor coolant system.

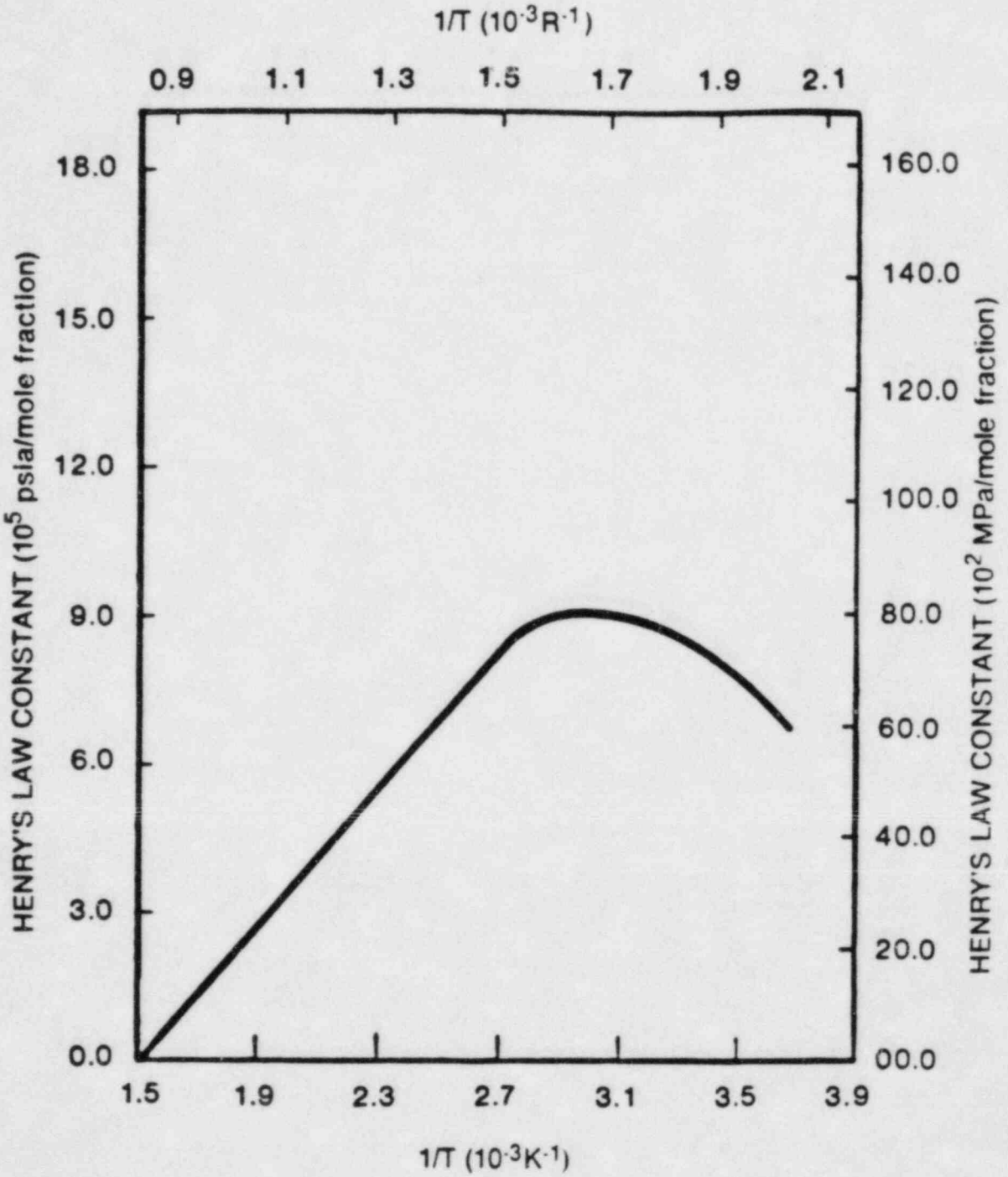

Figure 3.4.3-1. Henry's Law Constant for Hydrogen in Water

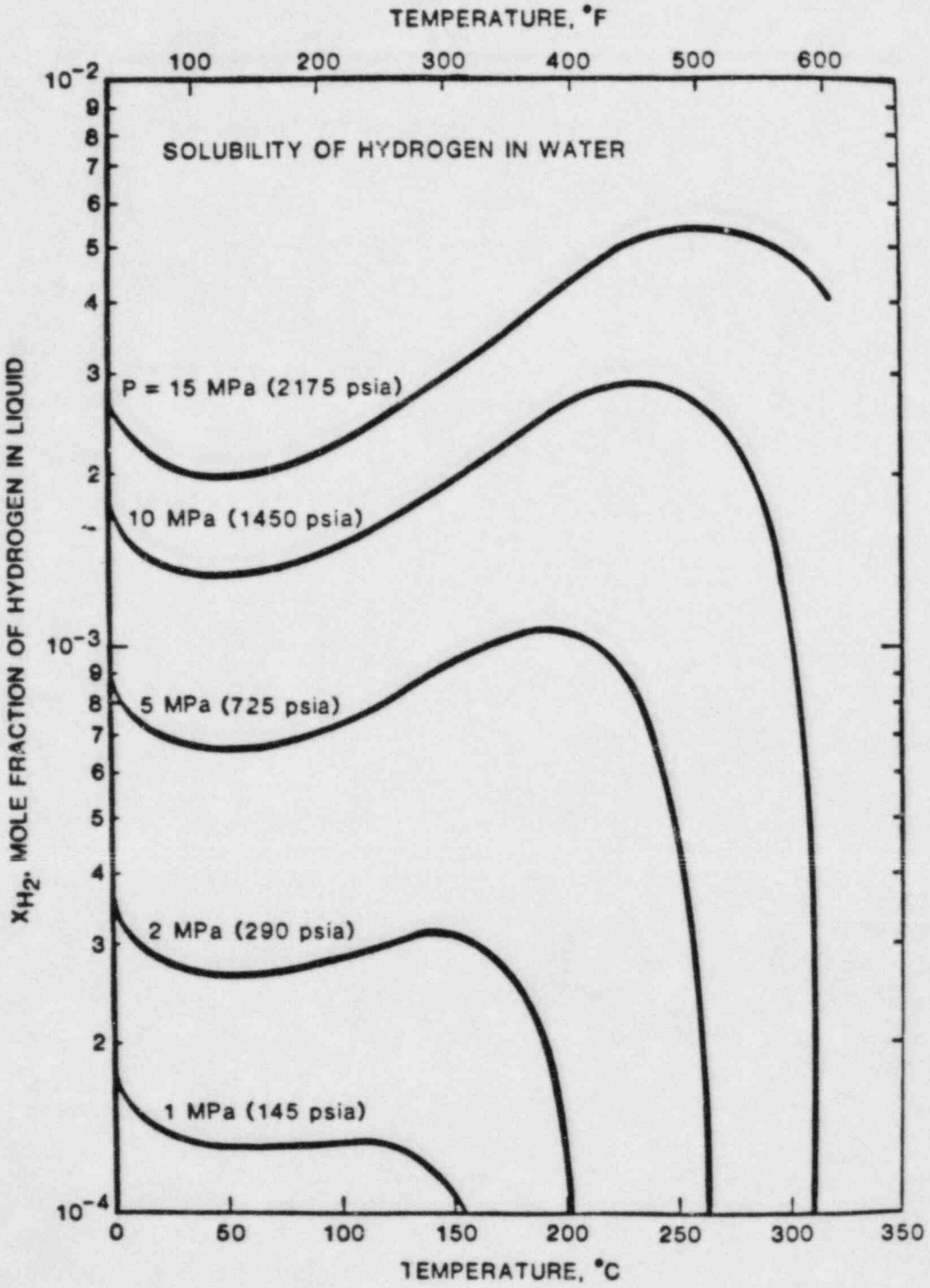

Figure 3.4.3-2. Mole Fraction of Dissolved Hydrogen Under Various Conditions

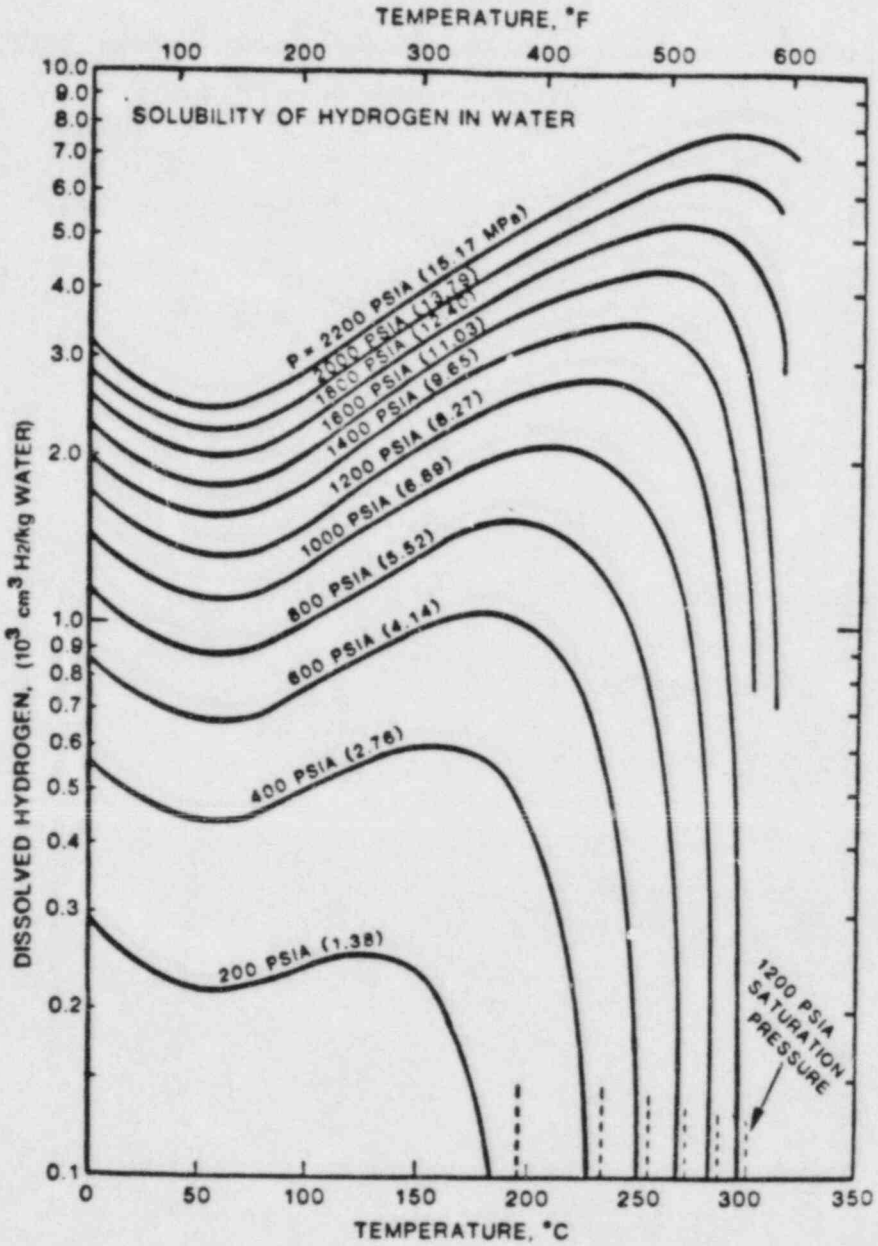

Figure 3.4.3-3. Hydrogen Concentration in Water Under Various Conditions

The effect of boric acid or other chemicals present in the water is generally to reduce the amount of hydrogen dissolved. However, it appears that, in most cases, the effects are small.

The discussions above have dealt with closed systems at equilibrium. Little is known about the dynamics of hydrogen solubility (i.e., how fast equilibrium will be attained during a transient event). It is widely believed that turbulent effects will cause a rapid approach to equilibrium, but the details are not well known.[17]

Dissolved hydrogen may be released whenever a change in the temperature and pressure occur. Figures 3.4.3-2 and 3.4.3-3 clearly show that a decrease in pressure (such as when a relief valve opens) will reduce the amount of hydrogen in solution. The effects of temperature changes are more complex, depending upon the particular temperature and pressure region.

3.4.3.2 Transport and Mixing Within Containment

The transport and mixing of gases determines when and where combustion will occur, if at all. Rapid mixing could result in burns that are global in nature, while slow mixing may lead to localized burning. Mass is normally transported around containment due to natural or forced convection and diffusion.

Phenomena

If significant pressure differences exist within containment, there will be bulk gas motion from the high pressure to the low-pressure region. This motion occurs very rapidly, with the time required to equalize pressure depending on the pressure difference, and the resistance to flow. Mass transfer due to pressure differences will dominate other forms of mass transfer whenever significant pressure differences exist.

Natural convection occurs due to density differences (buoyant effects) within the containment atmosphere. Convective motions tend to form loops with lighter gases rising up one side and heavier gases falling down the other. The convective gas velocity will increase with increasing values of the density gradient in the vertical direction. Note that the addition of hydrogen reduces the average molecular weight. Therefore, if hydrogen is introduced low in the containment, the drop in molecular weight and the possible higher temperature of this mixture will give it a lower density than the atmosphere in the top of the containment. This can lead to rapid natural convective motions and mixing of the containment atmosphere. The condensation of steam on

containment surfaces can also produce composition and temperature gradients and thus lead to substantial natural convection.

Forced convection can occur due to the presence of fans or jets from a pipe break or open valve. The degree of mixing from forced convection depends, of course, upon the flow rates and velocities associated with the particular fan or jet. One can get a feel for the mixing times by comparing the volumetric flow rate with the volume of a particular containment compartment. Significant mixing will occur in a time frame on the order of the time required to turn over the entire compartment volume. Usually, forced convection involves higher gas velocities than natural convection. These higher velocities tend to induce more turbulence, and thus enhance mixing.

Forced convection may also occur due to operation of the containment sprays. Current analytical capability does not allow us to model mixing due to sprays in any detail. However, observation of sprays in operation and intuition tell us that mixing due to sprays may be quite rapid. The sprays entrain air, inducing bulk gas motion, and create both large and small-scale turbulence. Complete mixing should occur within a few minutes.

Diffusion occurs due to concentration gradients. Gases will tend to diffuse from regions of high concentration to regions of low concentration according to Fick's Law:

$$J_A = -D_{AB} \nabla C_A \qquad (3.4.3\text{-}3)$$

where J_A is a vector describing the molar fluxes of component A relative to the bulk gas velocity, D_{AB} is the diffusion coefficient for component A diffusing through component B, and ∇C_A is the concentration gradient for component A.

The most important thing to note about diffusion is that its effect falls off very rapidly as the size of the volume increases. The time to mix a volume is proportional to the square of the length scale. Normally, we can expect that diffusion alone would take days in order to mix the containment atmosphere. Thus early versions of MELCOR should neglect diffusion and concentrate on forced and natural convection.

MELCOR Approach

Because MELCOR will be a lumped-volume code, it must be assumed that mixing within a compartment is perfect (i.e., gases are homogeneous at all times). However, mixing between compartments can be controlled, and is very important in determining the results. In general, the mixing will be controlled by the compartmentalization, by the choice of a momentum equation to be applied at the junctions, and by the selected flow resistances.

The choice of compartment and flow junction locations determines the flow paths. At least three compartments are required to set up any type of natural convection loop. Selecting a proper compartment arrangement is more an art than a science. Typically, one needs to try several different arrangements to get a feel for the problem and its sensitivities. Another lumped-volume code, RALOC,[18] generally uses somewhere between 8 and 30 compartments within containment.

The rate of flow between compartments will be determined by the momentum equation that is applied at the flow junctions. This equation will be a simplified form of the Navier-Stokes momentum equation. For example, the junction equation used in HECTR[19] is:

$$\frac{dF_\ell}{dt} = \frac{1}{\frac{(\rho_i+\rho_k)}{2}\frac{L}{A_\ell}} \left[(P_i-P_k) + \frac{(\rho_i+\rho_k)}{2} g(z_i-z_k) - \frac{K_\ell(\rho_i+\rho_k)\, F_\ell|F_\ell|}{4A_\ell^2} \right] \quad (3.4.3\text{-}4)$$

where

F_ℓ = volumetric flow rate at junction
t = time
ρ_i = density of compartment i
ρ_k = density of compartment k
L/A_ℓ = inertial length divided by the flow area for junction ℓ
P_i = pressure in compartment i
P_k = pressure in compartment k
g = gravitational constant
z_i = elevation of compartment i
z_k = elevation of compartment k
K_ℓ = flow coefficient of junction ℓ.

Other forms of this equation are possible; however, each of the terms presented in the above equation has importance if mixing is to be properly modeled. In particular, the time derivative of flow (inertial term) helps determine the duration of convective loops that may form. Therefore, while the steady state form of the momentum equation may have application (e.g., in cases where a forces convection mechanism sets up steady state flows), the capability for including inertial effects is important.

Another important issue is the choice of flow coefficients, particularly in cases that include parallel flow paths. The flow coefficients will determine the preferential direction of flow. Normally, the flow coefficients are of order one. Mechanical engineering handbooks can provide some guidance regarding the selection of flow coefficients; however, the geometries encountered in a containment are nonstandard, and some judgment is usually required. Since MELCOR results could be sensitive to the flow coefficients, some guidelines on selection of flow coefficients should be provided in the code documentation.

From the above discussion, it should be clear that there is much uncertainty in the treatment of mixing within containment. For this reason it will probably be desirable to use other, more sophisticated, codes for calibration purposes when developing the MELCOR containment model. These two and three-dimensional codes are very expensive to run, but a minimum number of calibration runs would be required. Available codes include, but are not limited to, COBRA-TF,[20] TEMPEST,[21] and HMS.[22]

3.4.4 DEFLAGRATIONS

Deflagrations are combustion waves in which unburned gases are heated by thermal conduction to temperatures high enough for chemical reactions to occur. Deflagrations normally travel subsonically and result in quasi-static (nearly steady state) loads on containment.

3.4.4.1 Adiabatic, Constant-Volume Approximation

The reactions for combustion of hydrogen carbon monoxide are:

$$H_2 + \frac{1}{2} O_2 \rightarrow H_2O \quad \Delta H = -57.798 \text{ kcal/mol} \qquad (3.4.4\text{-}1)$$

$$CO + \frac{1}{2} O_2 \rightarrow CO_2, \quad \Delta H = -67.637 \text{ kcal/mol} \quad . \qquad (3.4.4\text{-}2)$$

The enthalpies listed on the right-hand side of the above equations are the standard heats of combustion; that is, the thermal energies released per mole in a process in which both reactants and products are at 1 atm and 25°C (298.15 K). Complete deflagration in containment is more closely approximated by an adiabatic, constant-volume process in which, by the first law of thermodynamics, the change in internal energy is zero:

$$\Delta U = \sum n_{i2} u_{12} - \sum n_{i1} u_{i1} = 0 \qquad (3.4.4\text{-}3)$$

where

n_{i1} = number of moles of species i before constant-volume adiabatic process,
n_{i2} = number of moles of species i after constant-volume adiabatic process,
u_{i1} = internal energy per mole of gas species i at preburn pressure and temperature,
u_{12} = internal energy per mole of gas species i at final pressure and temperature.

Figures 3.4.4-1 and 3.4.4-2 depict the adiabatic, constant-volume (final) pressures and temperatures required to satisfy Equation (3.4.4-3) for a variety of initial conditions and gas compositions. Computer codes such as that of Gordon and McBride[23] are available to perform the thermochemical calculations required to solve Equation (3.4.4-3)

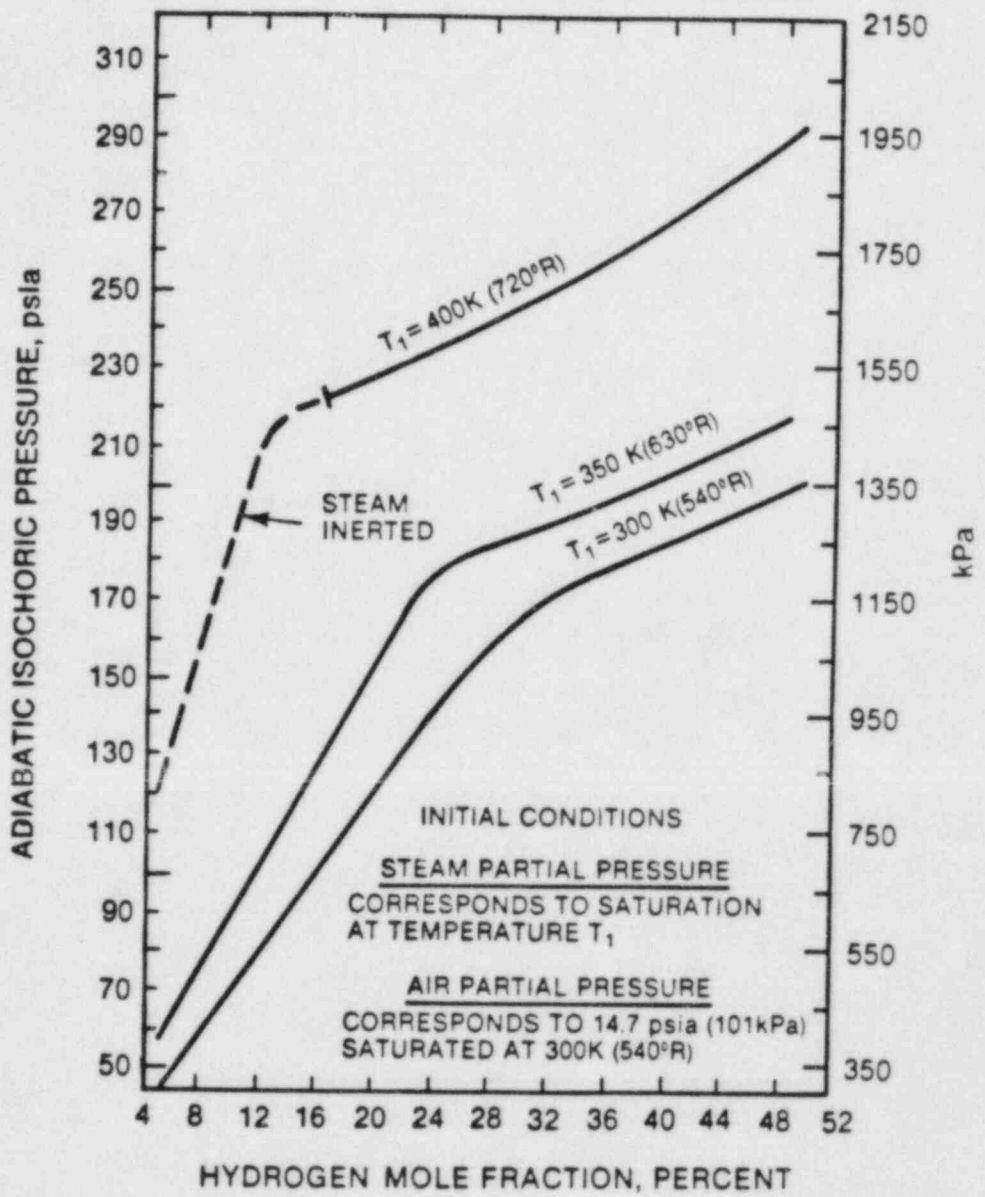

Figure 3.4.4-1. Adiabatic, Constant-Volume Combustion Pressure for Various Containment Initial Conditions

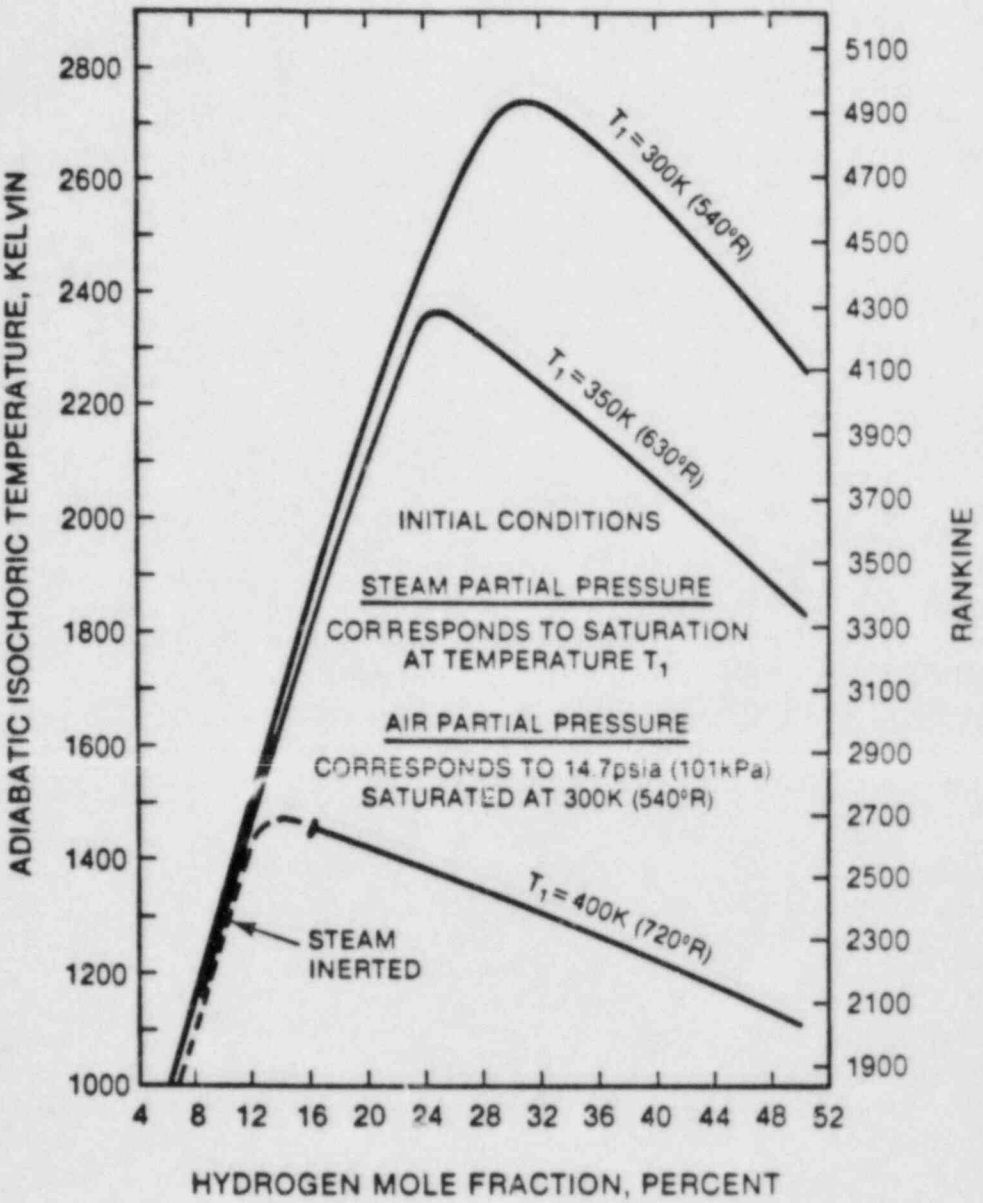

Figure 3.4.4-2. Adiabatic, Constant-Volume Combustion Temperature for Various Containment Initial Conditions

and generate Figures 3.4.4-1 and 3.4.4-2. One significant observation regarding such calculations is that the pressure ratio, P_2/P_1, is relatively insensitive to the initial pressure and to small changes in the initial temperature.

3.4.4.2 Conditions Necessary for Combustion

For substantial combustion to take place, the gaseous mixture must be flammable, and an ignition source must be present. For a mixture of flammable gases such as hydrogen and air, the flammability limits are defined as the limiting concentrations of fuel, at a given temperature and pressure, in which a flame can be propagated indefinitely. Limits for upward propagation of flames are wider than those for downward propagation. Limits for horizontal propagation are between those for upward and downward propagation.

There is some doubt concerning the applicability of flammability limits, as defined above, to accident conditions. There may be scale effects due to the large size of reactor containments, and variations in flammability due to the ignition source strength. It is known that flames can propagate for short distances in mixtures which are outside the standard flammability limits. Flammability limits are useful guidelines and are not expected to vary substantially, but do not appear to be fundamental quantities.

The lower flammability limit is the minimum concentration of hydrogen required to propagate a flame, while the upper limit is the maximum concentration. At the lower limit, the hydrogen is in short supply and the oxygen is present in excess. At the upper limit of flammability for hydrogen in air, the oxygen is in short supply, about five percent oxygen by volume. The behavior of the upper limit of flammability of hydrogen with various mixtures such as air:steam is more easily understood if one considers it as the lower flammability limit of oxygen.

In most large containments we are usually interested in the lower limit of flammability of hydrogen, there being large amounts of oxygen present. In the smaller containments, particularly the inerted containments, we may be interested in the upper flammability limit of hydrogen.

For hydrogen:air mixtures, the flammability limits of Coward and Jones[23] are still accepted. Values for hydrogen flammability in air saturated with water vapor at room temperature and pressure are given in Table 3.4.4-1.

Table 3.4.4-1

Hydrogen Flammability Limits In Steam-Saturated Air[24]

	Lower Limit. Vol%	Upper Limit. Vol%
Upward Propagation	4.1	74
Horizontal Propagation	6.0	74
Downward Propagation	9.0	74

In reactor accidents, the conditions inside containment prior to hydrogen combustion may include elevated temperature, elevated pressure, and the presence of steam. Figure 3.4.4-3 illustrates that the flammability limits widen with increasing temperature. At 212°F (100°C) the lower limit for downward propagation is approximately 8.8 percent. In the temperature range of interest, the widening of the downward propagation limits is small. No data for the widening of the upward or horizontal propagation limits were found.

If the containment atmosphere is altered by the addition of carbon dioxide, steam, nitrogen, or other diluent, the lower flammability limit will increase slowly with additional diluent, while the upper flammability limit will drop more rapidly. With continued increase in diluent concentration, the two limits approach one another until they meet and the atmosphere is inerted. A flame cannot be propagated a significant distance for any fuel:air ratio in an inerted atmosphere. Figure 3.4.4-4 shows the flammability limits with the addition of excess nitrogen or carbon dioxide. Note that for 75 percent additional nitrogen, the atmosphere is inert.[24,25] This corresponds to 5 percent oxygen at the limit of the flammable region, a value very close to that of the upper limit for hydrogen:air combustion. Roughly speaking, hydrogen:oxygen:nitrogen mixtures will be flammable if the hydrogen concentration is above 4 percent and the oxygen concentration is above 5 percent. For carbon dioxide, the atmosphere is inerted when the carbon dioxide concentration is 60 percent or above, corresponding to 8 percent oxygen or less. The larger specific heat of the carbon dioxide reduces the flame temperature and flame velocity, hence carbon dioxide suppresses flammability more than nitrogen. It requires about 60 percent steam to inert hydrogen:air:steam mixtures. The triangular diagram of Shapiro and Moffette[26] indicates regions of flammability and detonability of hydrogen:air:steam mixtures. It has been widely reproduced and appears as Figure 3.4.4-5.

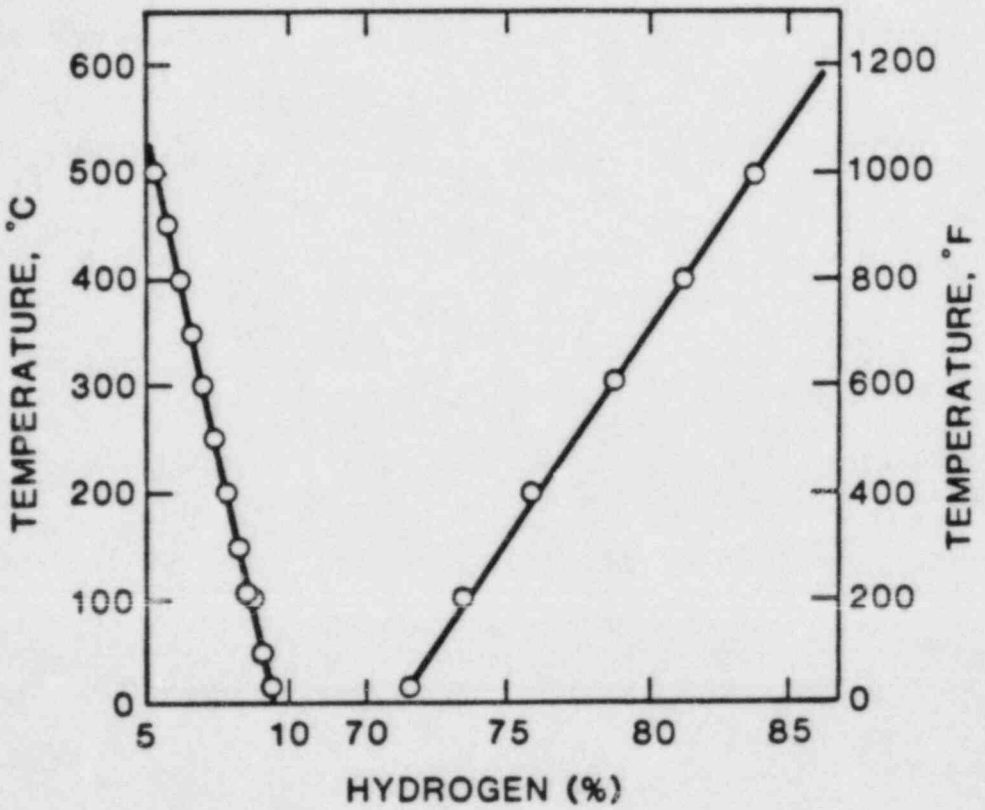

Figure 3.4.4-3. Effect of Initial Temperature on Downward Propagating Flammability Limits In Hydrogen:Air Mixtures, Reference 24

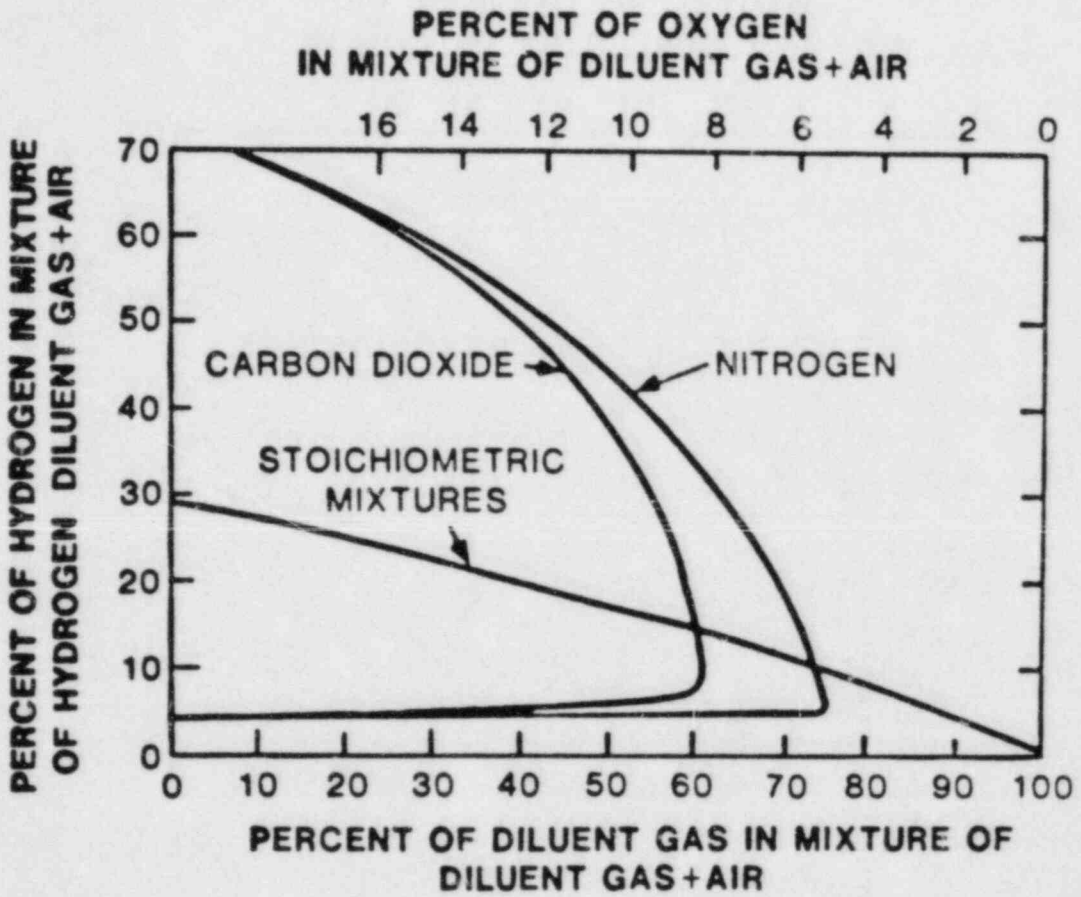

Figure 3.4.4-4. Flammability Limits of Hydrogen in Air Diluted with CO_2 and N_2

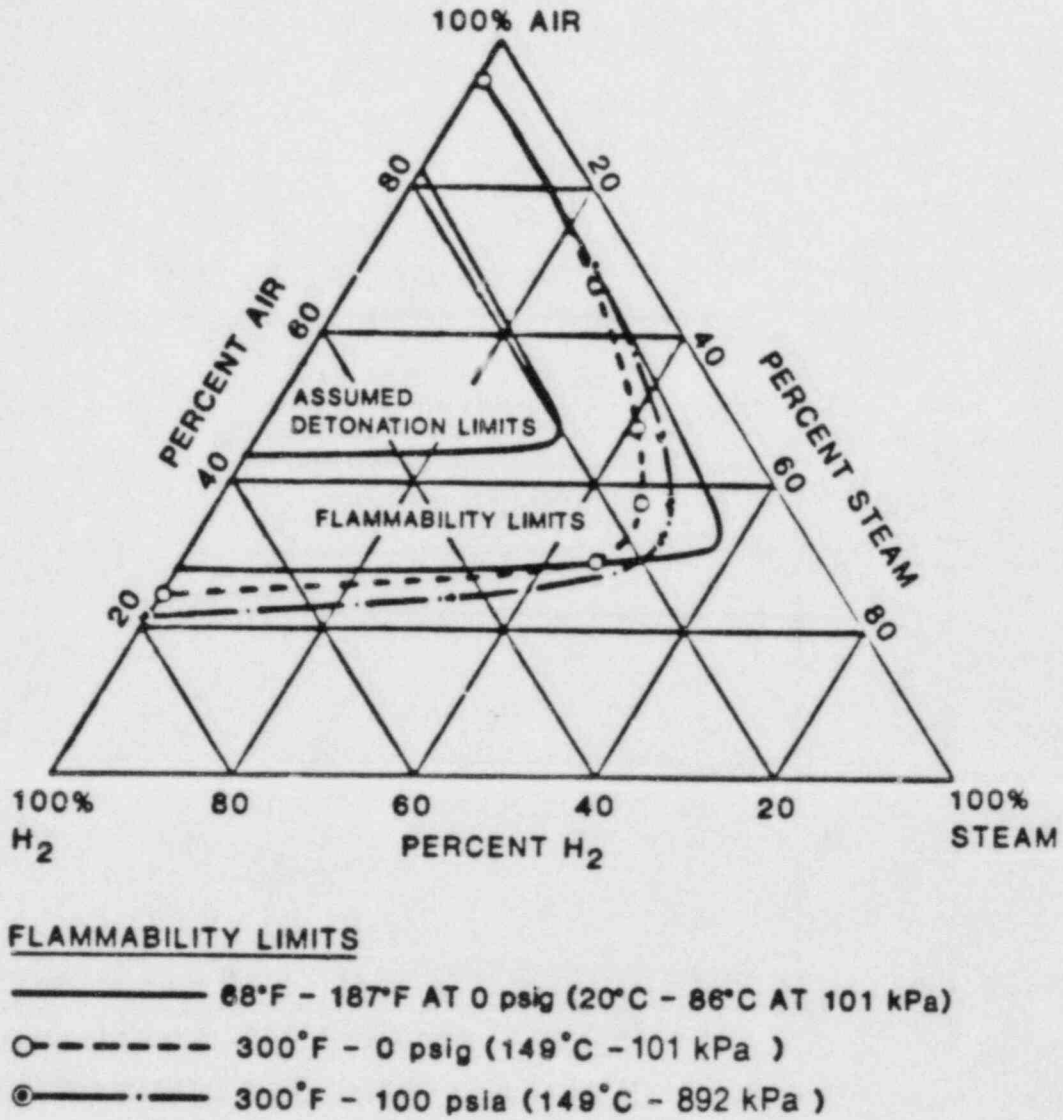

Figure 3.4.4-5. Flammability and Detonation Limits of Hydrogen:Air:Steam Mixtures

In addition to diluents such as steam or carbon dioxide which have a large thermal effect on a flame, certain substances react chemically to impact hydrogen combustion. For example, Halons (halogenated hydrocarbons) appear to cause quenching by interacting with free radicals such as H, O, and OH. Figure 15[27] shows the flammability limits for a mixture of H_2:air:CF_3Br (Halon-1301).

Ignition of dry hydrogen:air mixtures, particularly when the mixtures are well within the flammability limits, can occur with a very small input of energy.[26] Common sources of ignition are sparks from electrical equipment and from the discharge of small static electric charges. The minimum energy required from a spark for ignition of a quiescent hydrogen:air mixture is of the order of tenths of a millijoule. The ignition energy required as a function of hydrogen concentration is shown in Figure 16.[28] For a flammable mixture, the required ignition energy increases as the hydrogen concentration approaches the flammability limits. The addition of a diluent, such as steam, will increase the required ignition energy substantially. As mentioned previously, high-energy ignition sources can cause mixtures outside the flammability limits to burn for some distance.

To our knowledge, a purely mechanistic correlation expressing flammability as a function of gas composition, temperature, and pressure does not exist. For this reason, and because of the limited variation in flammability limits with temperature, pressure, and gas composition, we recommend that ignition, propagation, and inerting criteria for hydrogen burning in MELCOR be based on constant hydrogen, oxygen, and noncombustible gas mole fractions. Proposed default values are summarized in Table 3.4.4-2.[29]

The effect of having carbon monoxide as well as hydrogen is to alter the effective flammability limits and this needs to be accounted for in MELCOR. Unfortunately, information regarding the simultaneous combustion of carbon monoxide and hydrogen in geometrics approximating containment volumes is scarce. A simple formula proposed by LeChatelier has been shown to predict the lower limits of flammability for air:hydrogen:carbon monoxide mixtures to within 0.4 percent.[30] Haskin and Trebilcock[29] have used the following form of LeChatelier's formulas to characterize thresholds for many important combustion events:

$$x_{H_2} + \frac{L_{H_2}}{L_{CO}} x_{CO} \geq L_{H_2} \quad . \qquad (3.4.4\text{-}4)$$

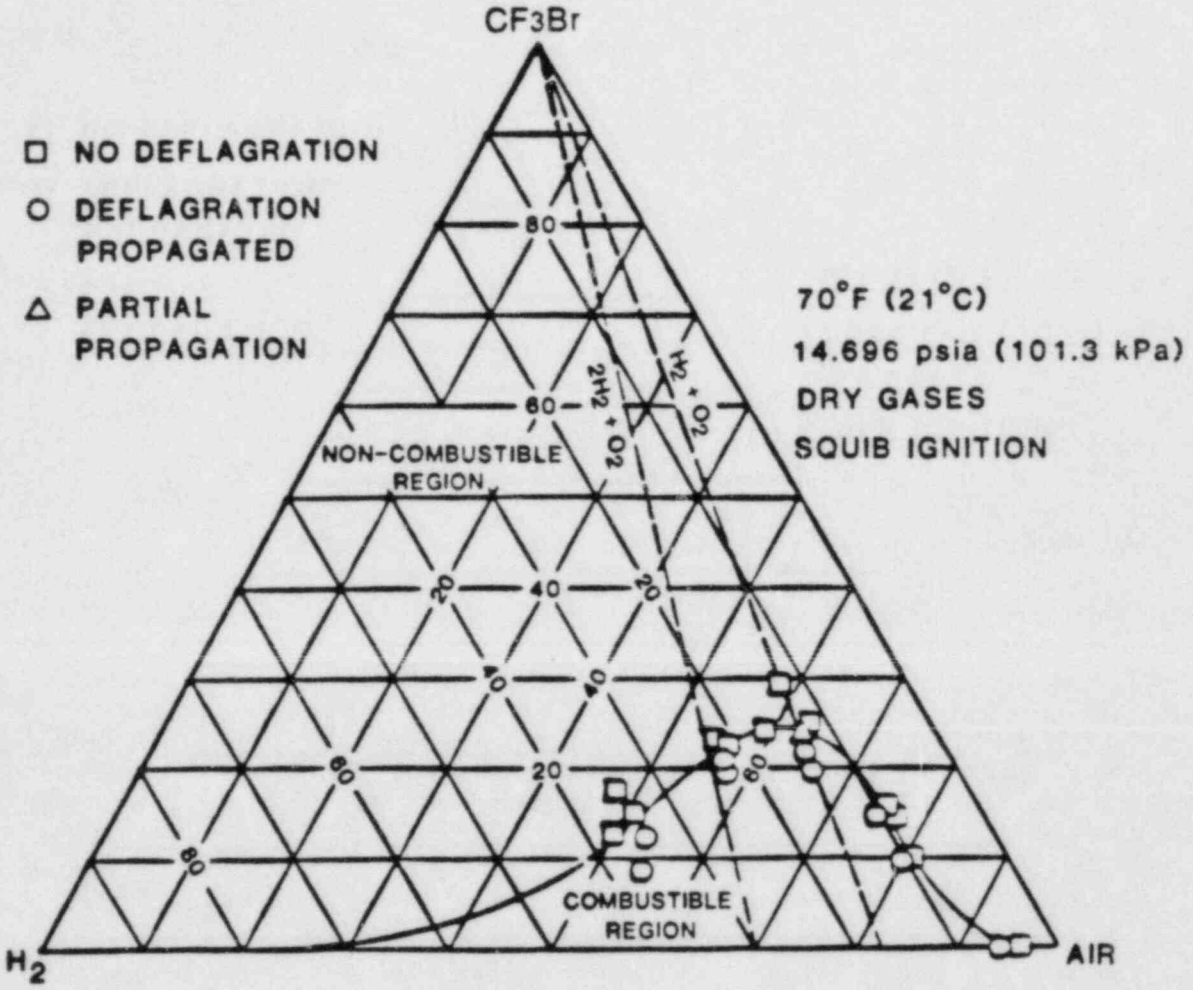

Figure 3.4.4-6. Deflagration Limits, H_2:Air:CF_3Br (Halon 1301), Reference 26

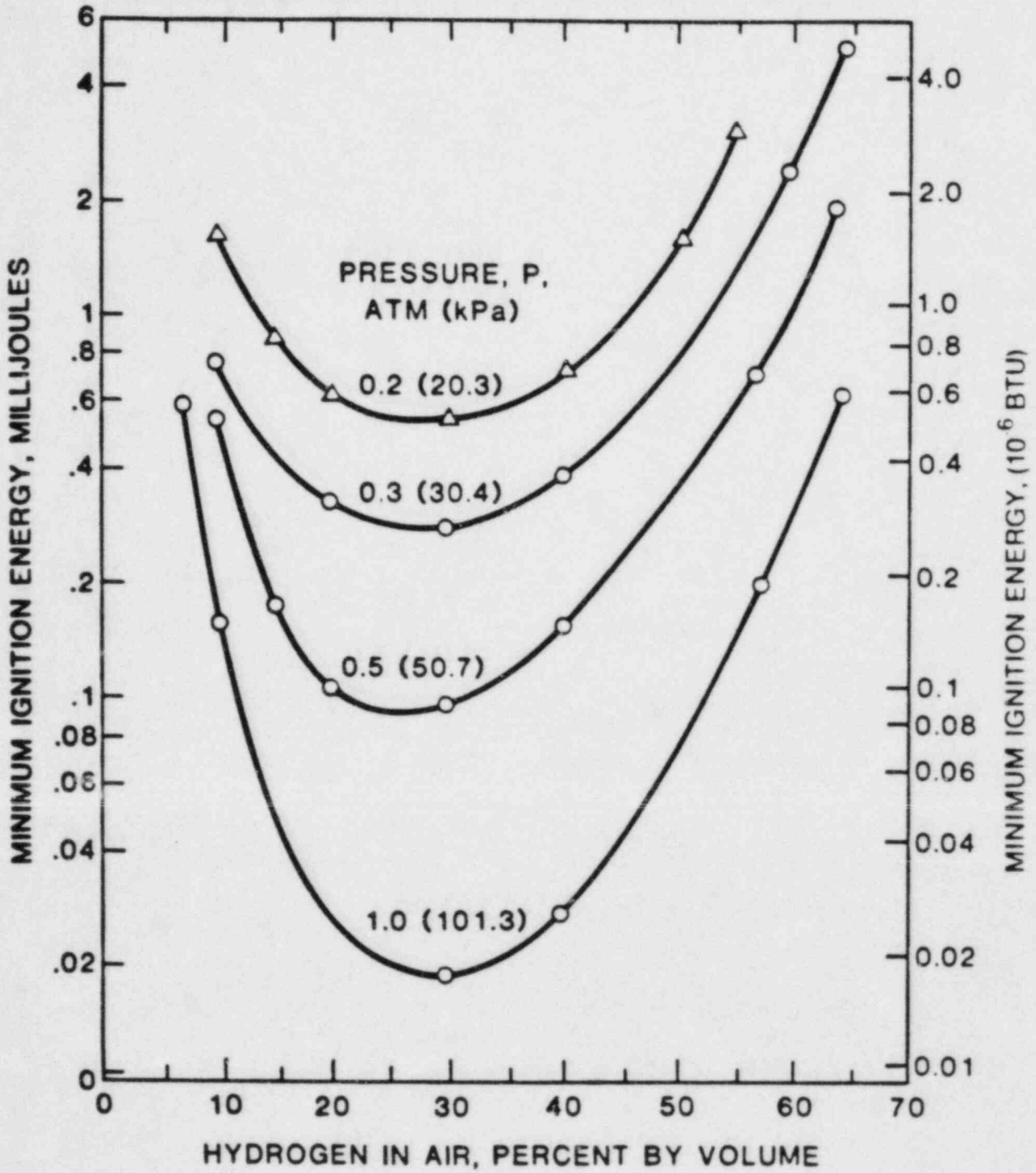

Figure 3.4.4-7. Spark Ignition Energies for Dry Hydrogen:Air Mixtures, Reference 27.

Here the x's denote the mole fractions of hydrogen and carbon monoxide in the gas mixture. The Ls denote the threshold mole fractions for the combustion event being considered, in gas mixtures containing only one (the subscripted) combustible gas. LeChatelier's formula can be applied in tests for ignition, propagation, and completeness.[29] The default limiting mole fractions used for the various combustion events are summarized in Table 3.4.4-2.

Table 3.4.4-2

Proposed Default Limiting Mole Fractions
For Deflagration Tests Using
LeChatelier's Formula, Reference 29

Combustion "Event"	L_{H_2}	L_{CO}	L_{H_2}/L_{CO}
Upward Propagation	0.041	0.125	0.328
Horizontal Propagation	0.06	0.138	0.435
Ignition With Igniters	0.08	0.148	0.541
Complete Combustion	0.08	0.148	0.541
Downward Propagation	0.09	0.150	0.600
Ignition Without Igniters	0.12	0.167	0.600

Later, in discussing completeness and rate of combustion, we will make use of the variable y, based on the left-hand side of LeChatelier's formula:

$$y = x_{H_2} + \frac{L^*_{H_2}}{L^*_{CO}} x_{CO} \qquad (3.4.4\text{-}5)$$

Here the L*s denote combustible mole fractions above which burning is likely to be complete in mixtures containing only one (the subscripted) combustible gas (L^*_{H2} = 0.08 and L^*_{CO} = 0.148 see Table 3.3.4-2). In the absence of carbon monoxide, y is equal to the hydrogen mole fraction, x_{H_2}.

Ignition

For ignition in MELCOR, the mole fractions of hydrogen and carbon monoxide should satisfy LeChatelier's formula. The limits, as indicated in Table 3.4.4-2, would depend on whether the user wants to approximate ignition with or without igniters. In addition to sufficient combustible gases, ignition requires sufficient oxygen.

$$x_{O_2} \geq 0.05 \text{ (default)} \quad . \qquad (3.4.4\text{-}6)$$

Also, the mole fractions of steam and carbon dioxide must be sufficiently low to preclude inerting:

$$x_{H_2O} + x_{CO_2} \leq 0.55 \text{ (default)} \quad . \qquad (3.4.4\text{-}7)$$

Inerting due to the presence of large amounts of nitrogen, although not explicitly modeled by Equation (3.4.4-7), is implicitly modeled by Equation (3.4.4-6) because the presence of sufficient nitrogen to cause inerting usually implies an oxygen mole fraction less than 0.05.

Propagation

The ignition tests should be applied to each nonburning compartment at the beginning of each time step. After ignition in any compartment, burn propagation to a connected compartment should be precluded if the atmosphere in that compartment is inerted per Equation (3.4.4-6) or Equation (3.4.4-7). MELCOR should test the combustible mole fractions in noninert, connected compartments using Equation (3.4.4-4) (with the appropriate values of L_{H_2} and L_{CO}--see Table 3.4.4-2) to determine if burn propagation is possible.

The ignition and propagation criteria set forth in Equations (3.4.4-4) through (3.4.4-7) and Table 3.4.4-2 are admittedly simplistic. No single set of thresholds could be used with these equations to cover the entire spectrum of gas composition and flow regimes. However, the expressions are capable of modeling a wide range of experimentally observed conditions, they provide a good parametric analysis capability, and they are consistent with the level of modeling sought for MELCOR.

3.4.4.3 Extent of Combustion

It has been found in several small- and medium-scale laboratory experiments when hydrogen:air mixtures with hydrogen concentrations in the range 4-8 percent were ignited with a spark, much of the hydrogen was not burned.[31-34] The resultant pressure rise was below that predicted for complete combustion, as shown in Figure 3.4.4-8.[36] Experimental results with a spark ignition source indicate that the completeness of combustion in quiescent mixtures increases with increasing hydrogen concentration, and is nearly complete at about 8-10 percent hydrogen. The range of incomplete combustion corresponds to the range in which the mixture is above the flammability limit for upward propagation, but below the flammability limit for downward propagation. In upward propagation of lean hydrogen:air flames, "separated globules" of flame have been observed.[36] Even when ignition occurs at the bottom of a chamber, the upward propagating flame fails to burn some of the hydrogen. The fraction of unburned hydrogen increases with the cross-sectional area of the chamber because more gases can remain outside of the upwardly expanding burn front. As shown in Figure 3.4.4-8 for the "fans on" case, turbulence and rapid mixing of the gases will significantly increase the completeness of combustion.

The phenomenon of incomplete burning of lean hydrogen:air mixtures may be of great importance in reactor safety. Combustion of lean mixtures, below 8 percent hydrogen, appears to be a method of partly eliminating hydrogen without significant pressure rise. MELCOR should permit the extent of combustion in a given compartment to be user specified or calculated as a function of the initial and transient conditions in the compartment. Once combustion is started in a given compartment, it would continue until y, as defined by Equation (3.4.4-6), decreases to a user specified or code-computed level, y_{min}.

As one possible function, y_{min} could be calculated as a function of y_{max} to approximate a linear variation in the extent of reaction from zero percent at $y_{max} = 0$ to 100 percent at $y_{max} = L^*_{H_2}$.[29]

$$y_{min} = \max \left[0,\ y_{max} \left(1 - y_{max}/L^*_{H_2}\right) \right] . \qquad (3.4.4\text{-}8)$$

It may be possible to develop functions which fit the experimental data better than Equation (3.4.4-8), possibly including effects of high steam or carbon dioxide concentrations which tend to reduce the extent of combustion.

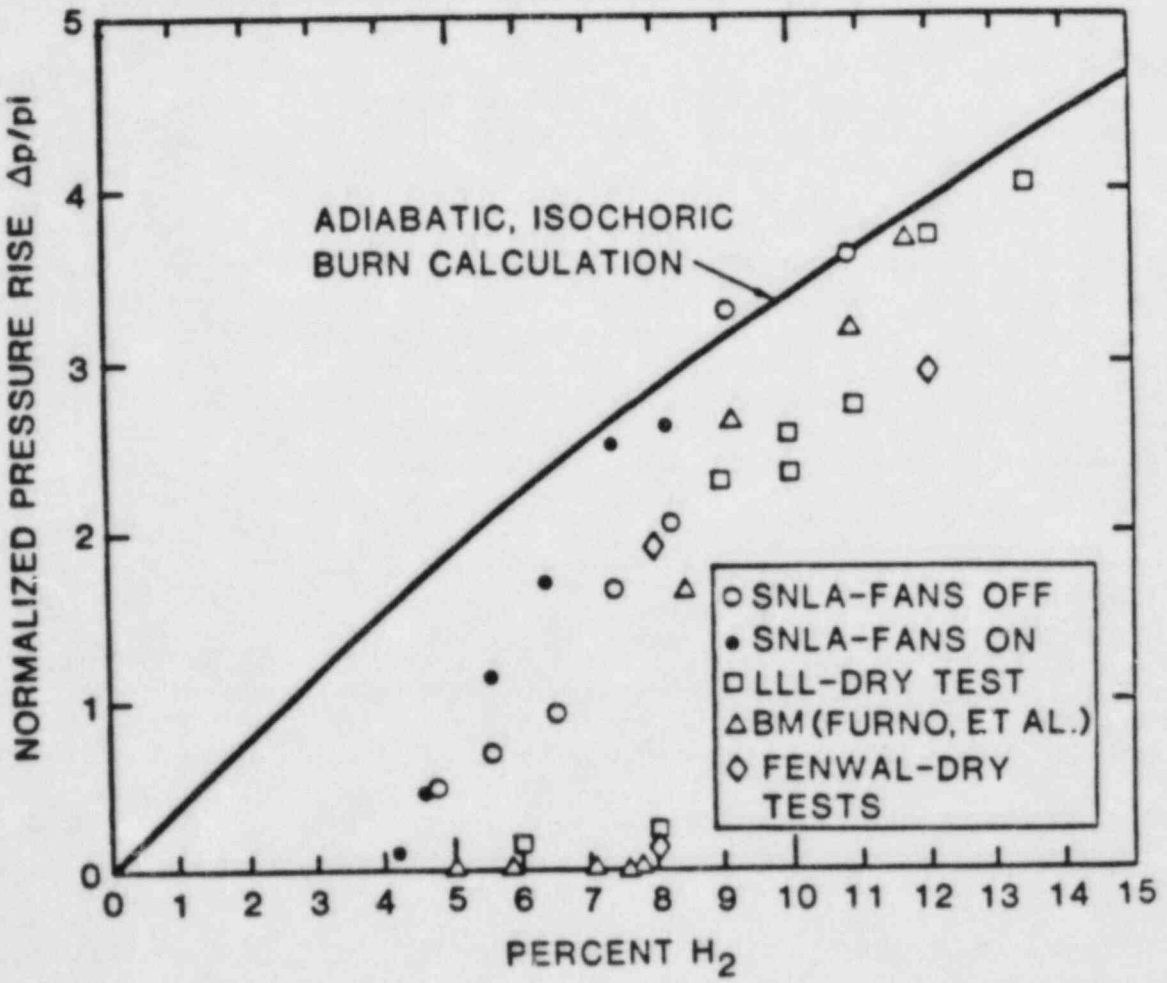

Figure 3.4.4-8. Normalized Pressure Rise Versus Hydrogen Concentration

3.4.4.4 Combustion Rate

Another important parameter when studying deflagrations is the combustion rate or flame speed. The flame speed determines how much time is available for heat transfer during a burn. Heat transfer results in pressures and temperatures below those predicted in Figures 3.4.4-1 and 3.4.4-2. The predominant heat transfer mechanisms are containment sprays, radiation, and convection. Some reactors also contain fan coolers. Normally, if the sprays are on, they will dominate the heat transfer process. Radiation heat transfer can also be important due to the high gas temperatures expected during a hydrogen burn. Convective heat transfer during a burn may also be significant.

The presence of sprays may significantly increase the flame speed due to the increased turbulence induced by the sprays. Typically, pressure rises above 80 percent of the adiabatic pressure rises are predicted for reasonable values of the flame speed, assuming complete combustion.

Warnitz[37] computed the laminar burning velocity* for hydrogen:air mixtures and compared his results with those of several other workers. The results are shown in Figure 3.4.4-9. The maximum laminar burning velocity of hydrogen:air mixtures is about 3 m/s (9.8 fps) near a concentration of about 42 percent hydrogen. The burning velocity becomes much smaller as the flammability limits are approached. The effect of diluents such as nitrogen is to reduce burning velocity by reducing flame temperature. Steam also reduces burning velocity, but by less than the amount expected from equilibrium flame temperature considerations.

The laminar burning velocity will be changed only slightly by moderate changes in ambient temperature and pressure. For a 50°C (90°F) temperature rise above room temperature, the increase in laminar burning velocity is less than 0.2 m/s (0.7 ft/s). The variation of hydrogen:air burning velocity with pressure is very small for pressure changes in the range of interest for reactor containments.

The plane or spherically expanding laminar flame front has been shown to be unstable. Freely propagating laminar flame fronts, if they do not become turbulent, have complex cellular structure. Hydrogen-lean flames tend to form

---

* The laminar burning velocity (in a Lagrangian sense) denotes the speed of gases at a steady burner. Propagating laminar flames have flame speeds (in a Eulerian sense) which are 5-7 times faster due to volumetric expansion of the burned gases.

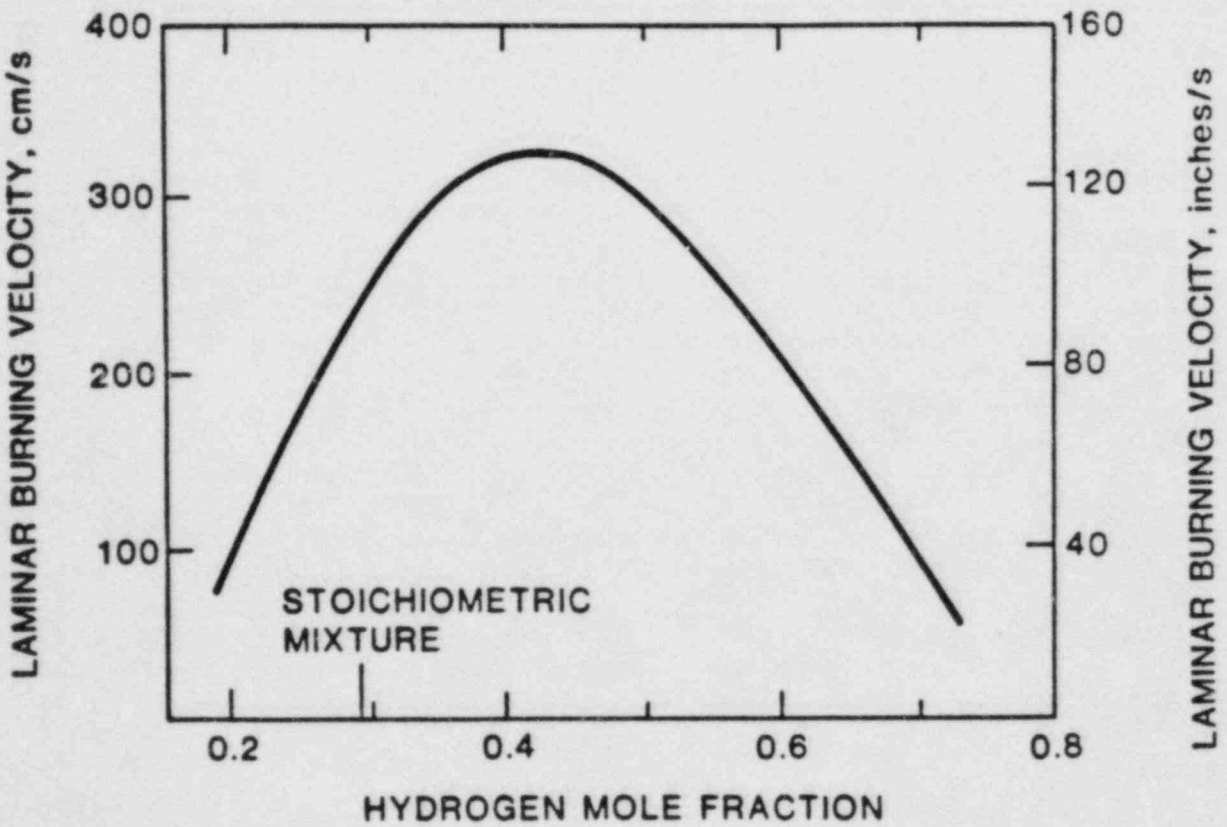

Figure 3.4.4-9. Laminar Burning Velocity of Hydrogen:Air Mixtures

nonsteady cellular structures, and will eventually become turbulent. For hydrogen-rich flames, one expects "wide-spaced wrinkled irregular steady surfaces."[38]

As noted above, it is likely that a laminar deflagration in containment will become turbulent. Many turbulent flames have mean speeds in the range 2 to 5 times the laminar flame speed. If the turbulent flames speed becomes greater than about one-tenth of the sound speed (the sound speed is approximately 1150 fps (350 m/s) in containment air), shock waves will be formed ahead of the flame front. Dynamic loads in addition to static loads would then be created at the containment structure.

Once acceleration mechanism under active study is the action of obstacles in the path of flames.[39] The flame front is stretched and turbulence is promoted due to the presence of the obstacles. Dramatic increases in flame speed have been observed when a flame front passes through a field of obstacles. Many obstacles, such as pipes, pressure vessels, etc. are present in the lower sections of most containments. However, much of the upper portion of such containments is fairly open. There have been few experiments to study flame speed behavior when the flame front leaves an obstacle field and enters an open region. Several researchers suggest that the flame speed will decrease after leaving the obstacle field. Very fast burns may also occur due to the presence of a very intense ignition source. As was suggested earlier, this could be a jet of hot combustion products formed subsequent to ignition in some adjoining semiconfined volume.

The subject of fast deflagrations and quasi-detonations is one of active current research. It is not well understood. Further work will be needed to determine its importance to hydrogen combustion in reactor containments.

For MELCOR we recommend the use of a simple function to correlate the flame speed to the initial combustible gas concentration, for example, the expression

$$v = v(y_{max}) = 1.8 + 59\ y_{max}\ (m/s) \quad . \qquad (3.4.4\text{-}9)$$

This expression is derived from upward, turbulent, hydrogen-flame experiments performed at Sandia and is applicable for hydrogen mole fractions below about 10 percent. The application of Equation (3.4.4-9) to gases containing both hydrogen and carbon monoxide is a modeling hypothesis which has not been tested experimentally. As more experimental data is

collected, flame speed expressions, which consider direction (upward, horizontal, or downward), gas composition, and transverse area may be developed.

Given a flame speed v, the molar combustion rates of hydrogen and carbon monoxide in compartment are

$$\dot{n}_{H_2} = n_T \dot{y} x_{H_2}/y \qquad (3.4.4\text{-}10)$$

$$\dot{n}_{CO} = n_T \dot{y} x_{CO}/y \qquad (3.4.4\text{-}11)$$

where

n_T = moles of gas in compartment

$$\dot{y} = y_{max} v/D, \qquad (3.4.4\text{-}12)$$

y_{max} = maximum value of y, as defined in Equation (3.4.4-6), since beginning of the burn.

D = effective linear burn distance for compartment.

3.4.4.5 Multicomponent Deflagration Model for MELCOR

A deflagration is a highly transient, three-dimensional fluid dynamic process. Proper modeling of such a process is very difficult, even with two- and three-dimensional hydro-dynamics codes. The problem is clearly not well suited to a lumped-volume code such as MELCOR. Unfortunately, detailed fluid dynamic calculations are computationally prohibitive and not consistent with the level of modeling planned for MELCOR. What is suggested for the first version of MELCOR is a relatively simple model that assumes the burning is uniform within a compartment and the burned and unburned gases are perfectly mixed.

Using a flame speed model one can calculate the burn time, and hence the combustion rate. During combustion, the amounts of H_2, O_2, H_2O, CO, and CO_2 will change. Assuming that the model calculates the rates of change of H_2 and CO due to the combustion, the rate of change of the other species due to combustion can be found from:

$$\dot{N}_{H_2O,comb} = -\dot{N}_{H_2,comb} \qquad (3.4.4\text{-}13)$$

$$\dot{N}_{CO_2,comb} = -\dot{N}_{CO,comb} \qquad (3.4.4\text{-}14)$$

$$\dot{N}_{O_2,comb} = -\left[\dot{N}_{H_2,comb} + \dot{N}_{CO,comb}\right]/2 \quad . \qquad (3.4.4\text{-}15)$$

The internal energy, U, within a compartment is not changed due to combustion alone. However, since $U = \sum N_i u_i$, the temperature will increase according to the expression.

$$\frac{dT}{dt} = \frac{\frac{dU}{dt} - \sum \dot{N}_{i,\,total}\, u_i}{\sum N_i C_{V_i}} \qquad (3.4.4\text{-}16)$$

Thus, the combustion process is properly treated by applying proper mass conservation equations including the $\dot{N}_{i,comb}$ terms.

The major shortcomings of the lumped-volume approach described above are that the heat transfer cannot be properly accounted for, and the wrong gas composition may be used in intercompartment flow equations. The heat transfer may be incorrect for several reasons. Because the real process involves hot and cold gas regions and radiative heat transfer increases as T^4, using a mixture temperature will tend to cause an underestimation of the radiative heat transfer. The convective heat transfer may be incorrect due to uncertain gas motions that are induced by the combustion process. Using a mixture composition in the intercompartment flow equations may be totally incorrect, as the actual composition will depend on the position of the flame front relative to the flow junction. It may be possible to formulate a simple one-dimensional burn front model that would delineate between reacted and unreacted species within a volume. In this manner, mass flow out of junctions on either side of the burn front could be identified unambiguously.

Addressing any of the above problems is difficult in a lumped-volume code. Some relatively simple improvements are being considered for incorporation in HECTR; however, these

improvements will probably not be available for use in MELCOR in the near term.

3.4.5 DETONATIONS

A detonation is a combustion wave that travels at supersonic speeds relative to the unburned gas in front of it. The compression of the unburned gas by shock waves raises the gas temperature high enough to cause rapid combustion. It is not appropriate to model shock wave phenomena in a code like MELCOR. The detailed physics and fine meshing necessary are computationally prohibitive. What might be appropriate for MELCOR is to include logic in the code that will notify the user that a potentially dangerous situation exists. The user may then wish to use data from MELCOR as input to a more sophisticated fluid dynamics code, such as CSQ, and examine the likelihood and consequences of detonations in detail. The following logic, from HECTR, could be used in MELCOR to define the detonable region:

$$x_{H_2} > 0.14, \text{ default} \qquad (3.4.5\text{-}1)$$

$$x_{O_2} > 0.09, \text{ default} \qquad (3.4.5\text{-}2)$$

$$x_{H_2O} < 0.30, \text{ default.} \qquad (3.4.5\text{-}3)$$

These numbers are far from fixed, as detonability depends on many factors. While the effects of CO and CO_2 are not included in the above logic, they could be included if appropriate data become available.

3.4.6 DIFFUSION FLAMES

If hydrogen is injected into containment in the form of a steam:hydrogen jet or plume, it is possible that hydrogen may start to burn as a turbulent diffusion flame. A diffusion flame is one in which the burning rate is controlled by the rate of mixing of oxygen and fuel. For the jet or plume to burn, it is necessary that at some locations the hydrogen:air:steam mixture be within flammability limits.

Combustion can begin either because of an outside ignition source, or because the mixture temperature is above the spontaneous ignition temperature. Shapiro and Moffette[26] have presented data showing the spontaneous ignition temperature to be in the range of 515-580°C for some particular cases. A stable flame will occur at a distance from the injection point such that the turbulent burning velocity is equal to the gas flow velocity.

Clearly, treating a localized, three-dimensional phenomenon in a lumped-volume code such as MELCOR would be very difficult. It is probably advisable to ignore the phenomenon entirely in the first version of the code. One rather crude approach that might be tried is to simply burn all the hydrogen in a selected compartment as it enters, assuming certain criteria are met. This would allow a consistent treatment of mass and energy balances, although the heat transfer and fluid dynamic phenomena would be clearly wrong. In any case, one should note that it is very difficult to predict whether or not a diffusion flame can exist, given the current state of knowledge.

3.4.7 REFERENCES

1. Sherman, M. P. et al., The Behavior of Hydrogen During Accidents in Light Water Reactors, NUREG/CR-1561 SAND80-1495, Sandia National Laboratories, Albuquerque, NM (August 1980).

2. Pawel, R. E., J. Electro Chem. Soc. 126. 1111-1118 (1979).

3. Cathcart, J. V. et al., "Zirconium Metal-Water Oxidation Kinetics IV, Reaction Rate Studies," ORNL/NUREG-17, Oak Ridge National Laboratory, Oak Ridge, TN (August 1977).

4. Wilson, R. E. et al., Isothermal Studies of the Stainless Steel Steam Reaction, pp. 150-153 in Chem. Eng. Div. Semiannual Progress Report, July December 1965, USAEC Rept. ANL-7125, Argonne National Laboratory (May 1966).

5. Bittle, J. T., et al., "Oxidation of 304L Stainless Steel by Steam and Air," Corrosion NACE, Vol. 25 No. 1 (January 1969).

6. Cole, R. K. and Kelly, D. P., "Combustible Gas Generation From Molten Fuel-Concrete Interactions," Proceedings of the Second International Workshop on the Impact of Hydrogen on Water Reactor Safety, Albuquerque, NM (October 1982).

7. Muir, J. F., et al., "CORCON-MOD1: An Improved Model for Molten-Core/Concrete Interactions," SAND-2415, NUREG/CR-2142, 1981.

8. Row, T. H., et al., "Design Considerations of Reactor Containment Spray Systems." Part 1, ORNL-TM-2412, Oak Ridge National Laboratory (April 1969).

9. Turner, S. E., "Radiolytic Decomposition of Water in Water-Moderated Reactors Under Accident Conditions," Reactor and Fuel-Processing Technology, 12(1), 6679 (Winter 1968-69).

10. Cohen, P., Water Coolant Technology of Power Reactors, Chapter 4, Gordon and Breach, New York (1969).

11. Loyola, V. M. and Womelsduff, J. E., "The Relative Importance of Temperature, pH, and Boric Acid Concentration on Rates of H_2 Production from Galvanized Steel Corrosion." Sandia National Laboratories, Draft (April 1982).

12. Van Rooyen, D., Memorandum, Brookhaven National Laboratory (April 7, 1978).

13. Zittel, H. E., "Radiation and Thermal Stability of Spray Solutions in ORNL Nuclear Safety Research and Development Program Bimonthly Report for September-October 1970," ORNL-TM-3212, Oak Ridge National Laboratory.

14. Lopata, J. R., "Control of Containment H_2 Levels Evolved from Zinc Primers During a LOCA." Power Engineering, 48-51 (November 1974).

15. The Radiation Chemistry of Macromolecules, Vol. 1, Ed. by Dole, Malcom , Academic Press, New York (1972).

16. Himmelblau, D. M., "Solubilities of Inert Gases in Water," J. Chem. Eng. Data, 5:10-15 (1960).

17. EPRI Meeting on Hydrogen Hazards in Nuclear Reactors, EPRI Hdq., Palo Alto (March 1980).

18. Jahn, H. L., "Hydrogen Distribution After a Loss of Coolant Accident in the Subdivided Containment of Light Water Reactors--Translation," NUREG/CR-1831, SAND80-6031, Sandia National Laboratories (November 1980).

19. Camp, A. L., et al., "HECTR: A Computer Program for Modeling the Response to Hydrogen Burns in Containment," Proceedings of the Second International Workshop on the Impact of Hydrogen on Water Reactor Safety, Albuquerque, NM (October 1982).

20. Thurgood, M. J., "Application of COBRA-NC to Hydrogen Transport," Proceedings of the Second International Workshop on the Impact of Hydrogen on Water Reactor Safety, Albuquerque, NM (October, 1982).

21. Trent, D. S. and Eyler, L. L., "Applications of the TEMPEST Computer Code for Simulating Hydrogen Distribution in Model Containment Structures," Proceedings of the Second International Workshop on the Impact of Hydrogen on Water Reactor Safety, Albuquerque, NM (October 1982).

22. Travis, J. R., "HMS: A Model for Hydrogen Migration Studies in LWR Containments," LA-UR-82-2702, Proceedings of the Second International Workshop on the Impact of Hydrogen on Water Reactor Safety, Albuquerque, NM (October 1982).

23. Gordon, S. and McBride, B. J., "Computer Program for Calculations of Complex Chemical Equilibrium Compositions, Rocket Performance, Incident and Reflected Shocks and Chapman-Jouquet Detonations," NASA SP-273 (1971).

24. Coward, E. F. and Jones, G. W., Limits of Flammability of Gases and Vapors, Bulletin 503, Bureau of Mines, U.S. Department of Interior (1952).

25. Bregeon, B., et al., "Near-Limit Downward Propagation of Hydrogen and Methane Flames in Oxygen-Nitrogen Mixtures," Comb. & Flame, 33:33-45 (1978).

26. Shapiro, Z. M. and Moffette, T. R., Hydrogen Flammability Data and Application to PWR Loss of Coolant Accident, WAPD-SC-545, Bettis Plant, (September 1957).

27. McHale, E. T., Hydrogen Suppression Study and Testing of Halon 1301: Phases I and II, Atlantic Research Corp. Report No. ARC 47-5647; Maritime Administration, U.S. Department of Commerce, Contract RT-3900, (December 1976).

28. Drell, I. L. and Belles, F. E., Survey of Hydrogen Combustion Properties, NACA R 1383, National Advisory Committee for Aeronautics (1958).

29. Haskin, F. E. and Trebilcock, W. R., "Combustion Modeling in MARCH, Developments and Limitations," Proceedings of the Second International Workshop on the Impact of Hydrogen on Water Reactor Safety, Albuquerque, NM (October 1982).

30. Coward, H. F., Carpenter, C. W., and Payman, W., Journal of Chemical Society, 115, 27, 1919.

31. Furno, A. L., Cook, E. B., Kuchta, J. M., and Burgess, D. S., "Some Observations on Near-Limit Flames," 13 Sym. on Comb., Pittsburg, Comb. Inst., 593-599 (1971).

32. Slifer, B. C. and Peterson, T. G., "Hydrogen Flammability and Burning Characteristics in BWR Containments," NEDO-10812, 73NED49, General Electric (April 1973).

33. Paulson, M. P. and Bradfute, J. O., "Pressure and Temperature Transients Resulting from Postulated Hydrogen Fires in Mark III Containments," EI 75-4, Energy Inc.

34. Berman, M., "Light Water Reactor Safety Research Program Quarterly Report," January-March, 1981," NUREG/CR-2163/1of4, SAND81-12116/1of4, Sandia National Laboratories, Albuquerque, NM (July 1981).

35. Lowry, W. E., et al., "Final Results of the Hydrogen Igniter Experimental Program," NUREG/CR-2486, UCRL-53036 Lawrence Livermore National Laboratory (February 1982).

36. Keilholtz, G. W., Hydrogen Considerations in Light-Water Power Reactors, ORNL-NSIC-12, Oak Ridge National Laboratory (February 1976).

37. Warnitz, J., "Calculation of the Structure of Laminar Flat Flames II: Flame Velocity and Structure of Freely Propagating Hydrogen-Oxygen and Hydrogen-Air Flames," Ber Bunsenges Phys Chem, 82:643-649 (1978).

38. Shivashinsky, G. I., "On Self-Turbulization of a Laminar Flame," Acta Astron, 5:566-591 (1978).

39. Berman, M., "Light Water Reactor Safety Research Program Semiannual Report, April-September 1981," NUREG/CR-2481, SAND82-0006, Sandia National Laboratories (February 1982).

40. Byers, R. K., "CSQ Calculations of H_2 Detonations in Zion and Seqmoyah," Proceedings of the Workshop on the Impact of Hydrogen in Water Reactor Safety, Albuquerque, NM (January 1981).

3.5 MOLTEN-CORE/CONCRETE INTERACTIONS

by

Randall K. Cole, Jr.

3.5 MOLTEN-CORE/CONCRETE INTERACTIONS

by

Randall K. Cole, Jr.

This report describes the phenomena involved in the interactions between molten reactor core materials and concrete in a hypothetical core-melt accident, the interrelations of these phenomena, and current practice in modeling them for computer calculations. Recommendations are made for the models to be included in the Probabilistic Risk Analysis (PRA) code MELCOR, which is being developed at Sandia National Laboratories for the Nuclear Regulatory Commission to replace the MARCH/MATADOR/CRAC family of codes.

CONTENTS

LIST OF FIGURES

LIST OF TABLES

3.5.1 INTRODUCTION AND SIGNIFICANCE FOR REACTOR SAFETY

There is a class of hypothetical accident sequences in nuclear power plants where loss of normal and emergency cooling systems leads to melting of the core, failure of the pressure vessel, and deposition of molten core and structural materials onto the concrete floor of the containment building. This can result in a molten pool of debris which is maintained at elevated temperatures by the tens of Megawatts of decay heat from nonvolatile fission products retained in the melt. The temperatures and heat fluxes involved are sufficient to decompose and ablate concrete.

In addition to the possibility of containment failure by melt-through, the decomposition of concrete produces large volumes of water vapor and carbon dioxide which, if they come into contact with molten metals, can be reduced to hydrogen and carbon monoxide. (Very small quantities of hydrocarbons and other species are also formed.) All four major gases contribute to the risk of eventual overpressurization of containment; hydrogen and carbon monoxide are also combustible, presenting an additional risk of sudden overpressurization if they are ignited.

While not strictly part of the core/concrete interaction process, the debris pool is also a source of direct heat and of volatile species and aerosols to the rest of containment. Fission products are present among the volatile species and in the aerosols. The heat may degrade above-pool structures, the aerosols may affect fans and filters, and the fission products are the ultimate determinants of accident consequences.

3.5.2 GROSS PHENOMENOLOGY

A great deal may be understood about core/concrete interactions from a very simple picture. The attack of core debris on concrete is largely thermal in a light-water reactor. Decay heat (and some heat from chemical reactions) is generated in the pool and may be lost either through its top surface or to concrete. The situation rapidly approaches a quasi-steady state where these losses balance the internal sources. The partition of internally generated heat between concrete and surface is determined by the ratio of the thermal resistances of the corresponding paths. In this simple view, pool behavior is dominated by conservation of energy, with heat-transfer relations providing the most important constitutive relations.

The heat flux to concrete is sufficient to decompose it, releasing water vapor (adsorbed and from hydroxides) and carbon dioxide (from carbonates), and to melt the residual oxides. The surface of the concrete is ablated at a rate which is typically several centimeters per hour. The molten oxides, and molten steel from reinforcing bar in the concrete, are added to the pool. The gases are strongly oxidizing at pool temperatures and will be reduced, primarily to hydrogen and carbon monoxide, on contact with metals in the pool. Ultimately the reacted and unreacted gases enter the atmosphere above the pool. These gases may or may not burn immediately, depending on their temperature at the time that they reach a region which is not already depleted of oxygen.

Gas released at the bottom of the pool rises through it as bubbles, while that released at the sides may form a rising gas film between the melt and the concrete (this is not directly observable, and is not universally accepted). The presence of gas bubbles in the pool swells it, increasing its depth and its interfacial area with concrete. These rising gas bubbles also result in the production of aerosols containing fission products stripped from the fuel debris. The source may be large from the point of view of consequences; in terms of reducing pool inventories, however, it is a relatively minor effect, although a few fission-product species may be completely depleted.

Because of decomposition in depth, the thermal response of the concrete is complex. The released gases produce internal pressures which drive flows of carbon dioxide, steam, and liquid water through the pores of the concrete. Experiments [Muir, 1977] performed at heat fluxes sufficient to ablate concrete, together with an analytic model [Beck and Knight, 1979] suggest that the major effect of all this is the creation of a "wet zone" in the concrete at about 400 K, with pores partially filled with liquid water. Here,

adsorbed water has been freed but not vaporized, and is being driven away from the heated surface by the internal pressure. At greater temperature rises, however, the temperature profile has been shown [Chu, 1978] to be consistent with pseudo-steady ablation of an effectively homogeneous material.

Experimental evidence [LWRSRP, 1976], [Powers et al., 1978] shows that the various oxidic species in the melt are highly miscible, as are the metallic species, but that the two groups are mutually immiscible. Buoyancy forces are sufficient to separate the molten debris into two phases, even in the presence of vigorous mixing by gases from the decomposition of concrete. If the oxidic phase is initially denser than the metallic phase, and settles to the bottom, a second oxidic layer will form above the metal, composed of concrete oxides ablated by the metal (lighter than and not miscible in the metal) and steel oxides produced by chemical reaction with the concrete-decomposition gases. This configuration, oxide/metal/oxide, does not last long if it occurs at all: the fuel oxides become diluted by concrete oxides until the mixture is less dense than the metal and the pool "rolls over" into a configuration with all oxides in a single layer above the metal. Of course, this does not happen instantaneously; during the period when the difference in density is small, the separation is probably incomplete with substantial heterogeneous mixing. CORCON [Muir et al., 1981] calculations suggest that the three-layer configuration cannot last more than about one hour.

If water is present, it will form an additional layer at the top of the pool. It is often suggested that this layer does not react violently with the molten material underneath it, but merely serves as an enhanced heat sink. This is likely to cool the top of the melt below the solidification temperature, resulting in a thin solid crust on the surface. Experiments [ARSRP, 1982a] have shown that the presence of water over simulated debris does not significantly alter the attack on concrete by the debris. Another possibility has been suggested [Theofanous and Saito, 1981]: that gas stirring would be sufficient to break up crusts as they form with the result that the molten pool is rather quickly converted to a (coolable) debris bed. This is supported in the referenced paper by evidence from simulant experiments using liquid nitrogen and water or Freon-11. A third possibility is the occurrence of a steam explosion. Violent interactions have been observed when water was poured onto molten bismuth or lead. [Greene, 1983] The later two possibilities lead to phenomena considered in other sections of this study.

As time progresses, the pool grows, its surface area increases, and decay heating decreases. Therefore, pool

temperatures and heat fluxes decrease, and the possibility of refreezing arises. Substantial freezing of the metallic phase may occur. However, the large internal heating and small thermal conductivity of the oxidic phase prevent the existence of steady crusts more than a few centimeters thick. The bulk of this phase will remain liquid, probably for weeks.[LWRSRP, 1982] The question of the permeability of these crusts and solids to gases is unresolved.

Coupling between the molten pool and the rest of containment is rather one-sided: the pool serves as a source of mass and energy to containment while being only weakly influenced by conditions there. (Of course, if material is falling into the pool, there is another coupling, but it is one-sided in the other direction.) Containment pressure affects the properties of gases in the pool and of any water over the molten debris. However, the effects--on gas-related heat-transfer coefficients, on equilibrium gas compositions, and on the temperature and latent heat of the water--are relatively small. Heat loss from the top of the molten debris is dominated by radiation . . . to containment structures or to the overlying water. Because of the fourth-power dependence of the radiative flux on temperature, this loss is rather insensitive to containment temperatures (unless they are very high). In the absence of a water layer, the optical properties of the atmosphere may become significant. Molecular absorption by atmospheric gases is a relatively small effect, [LWRSRP, 1982] but aerosol concentrations may be great enough that the atmosphere is optically thick. [LWRSRP, 1983] In this case, the opacity and (probably) the above-pool geometry must be considered in evaluating the heat loss from the pool surface. For the purposes of this report, it will be assumed that these above-pool models are to be included in the containment modules of MELCOR and need not be discussed here.

3.5.3 MODELING

Treatment of molten-fuel/concrete interactions requires definition of the system components, modeling of various physical processes, and availability of various material properties. Each may be done with several levels of detail and complexity: here we will consider them in the light of suitability for a PRA code such as MELCOR. The models described will be taken primarily from INTER, [Murfin, 1977] CORCON, [Muir et al., 1981] and WECHSL. [Reimann and Murfin, 1981] Reference will be made to several other codes including GROWS II, which is a cavity-growth code developed in the breeder reactor area and has only piecemeal documentation. [Baker, 1983] The current MARCH code [Wooton and Avci, 1980] uses the INTER code [Murfin, 1977] almost intact. Therefore, for the purposes of comparing MARCH modeling with current state of the art and with recommendations for MELCOR, one may read "MARCH" for "INTER" every place the latter occurs.

3.5.3.1 System Components

The essential components which must be represented are the concrete cavity and the debris pool (including water if present). Stand-alone codes for calculation of core/concrete interactions must have models for the above-pool atmosphere and surroundings. However, in a code such as MELCOR the pool surface provides a natural boundary with the rest of containment because, as described in Section 3.5.2, the coupling across this surface is nearly one-sided. Therefore, only the concrete and the pool (including any overlying water) need be considered here. Above-pool conditions are assumed to be treated in the containment modules of MELCOR. The boundary conditions at the pool surface must, of course, be consistent in above and below-surface modules.

3.5.3.1.1 Concrete Cavity

The size and shape of the cavity must be recalculated as concrete is ablated and its surface recedes. Existing models assume that the cavity is axisymmetric, which is probably adequate. At one extreme, a simple shape may be assumed and advanced in time by calculating the recession of a few points and refitting the assumed shape. This is done in INTER, [Murfin, 1977] which assumes a hemispherical segment, possibly intersected by a cylinder, Figure 3.5.3-1, and in GROWS II, [Baker et al., 1978] which assumes a flat bottom and toroidal sidewalls, Figure 3.5.3-2. The other extreme is to define a general cavity shape which is advanced in time by point-wise recession at a large number of boundary points. Many representations and coordinate systems are possible; several were considered by Kwong, et al. [Kwong et al., 1979] Both CORCON [Muir, 1981] and WECHSL [Reimann

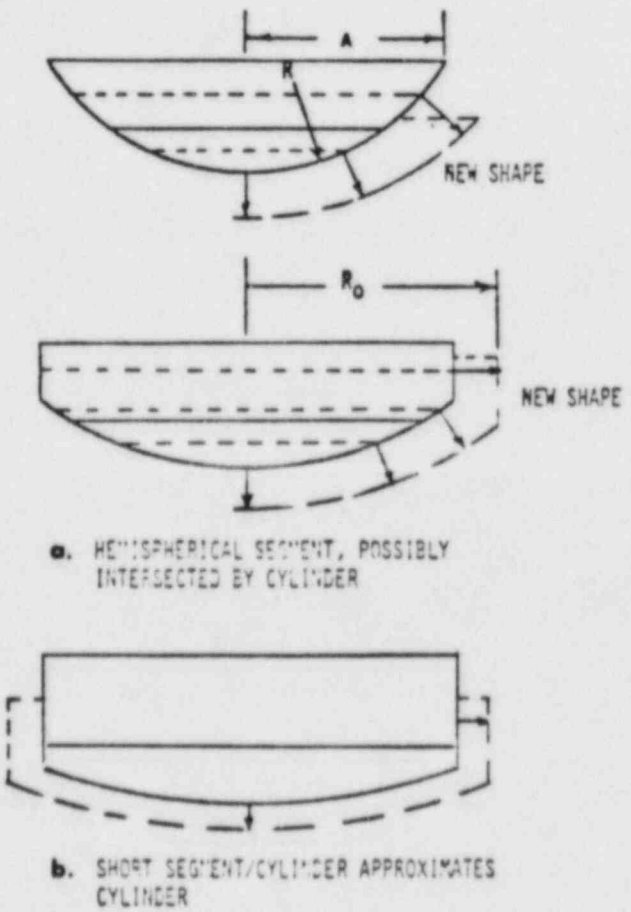

Figure 3.5.3-1. Cavity Model in INTER

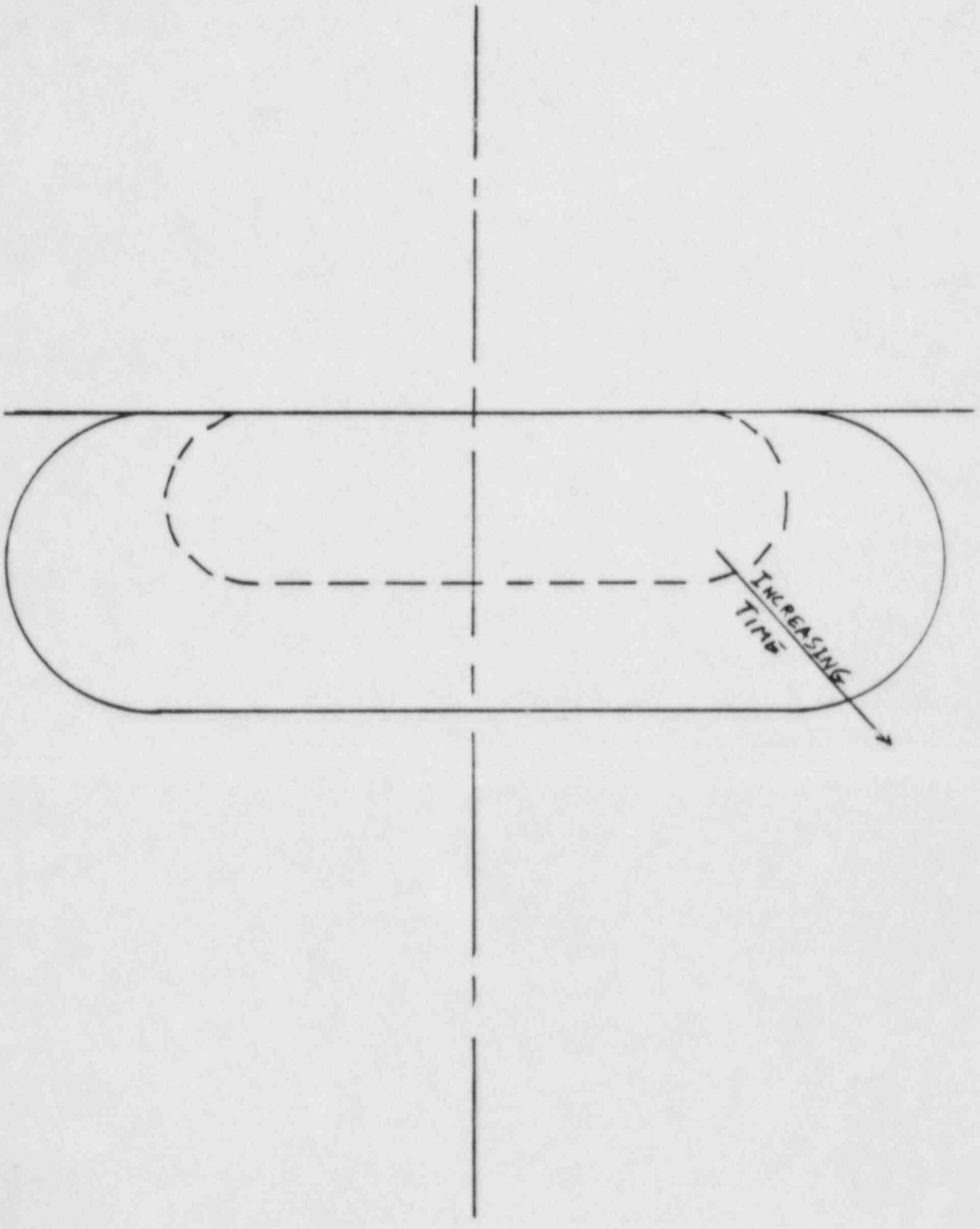

Figure 3.5.3-2. Cavity Model in GROWS II

and Murfin, 1981] employ this method, with each boundary point advanced at a locally calculated rate along the local normal to the surface. CORCON then projects these points onto a fixed ray coordinate system, Figure 3.5.3-3, while WECHSL redistributes them with equal spacing along the curve they define. Both procedures are smoothing operations, designed to prevent the development of pathological geometries.

Cavity shapes predicted by CORCON and WECHSL are more complicated than those allowed by INTER or GROWS II, largely resulting from more rapid erosion of concrete adjacent to metal compared to that adjacent to oxide. This occurs because higher thermal conductivity and lower viscosity in the metal lead to higher heat-transfer coefficients there. There is also a lesser effect caused by point-to-point variation in the thermal resistance of the pool/concrete interface.

We believe that an improvement over the fixed-cavity shape of INTER or GROWS II is appropriate. However, the full detail of CORCON or WECHSL, involving on the order of 100 points and a significant fraction of the total computing time, is probably not appropriate for PRA purposes. Given a reasonable approximation to surface areas, conservation of energy should guarantee sufficiently accurate results for concrete recession and gas generation. Reduction of the number of points, to perhaps 10, is an attractive possibility. Since both codes rely on fine zoning to avoid discrepancies between the ablated mass (evaluated as a surface integral of the ablation rate) and the change in cavity volume, some modifications would be required in the smoothing procedure and/or the calculation of ablated mass. We suggest a model below.

An axisymmetric cavity may be defined by a small number of (r,z) coordinate pairs, including one at bottom center, one at each layer interface including the pool surface, and one at the outer radius of the flat bottom (if any). The last-mentioned point is referred to in CORCON as the "tangent point." This geometry is illustrated in Figure 3.5.3-4. The volume of the cavity is the sum of the volumes of the conical frusta thus defined, each being

$$\Delta V = \frac{1}{3}\pi(r_2^2+r_2r_1+r_1^2)(z_2-z_1) \quad . \qquad (3.5.3\text{-}1)$$

During a time-step Δt, each point I is moved outward a distance Δn_r along the local normal. The normal is taken as the bisector of the angle formed by lines to the

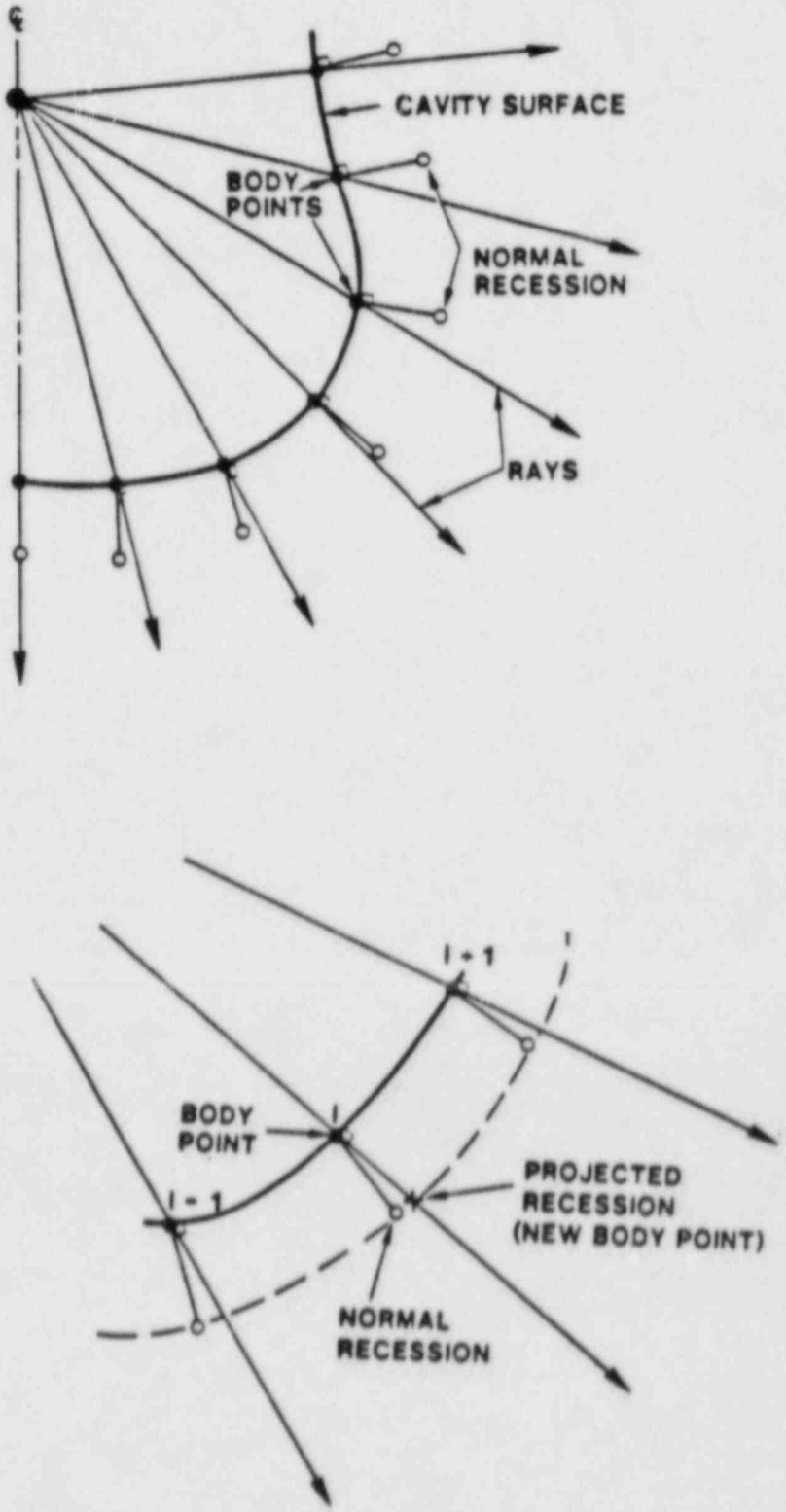

Figure 3.5.3-3. Cavity Model and Projection Scheme in CORCON

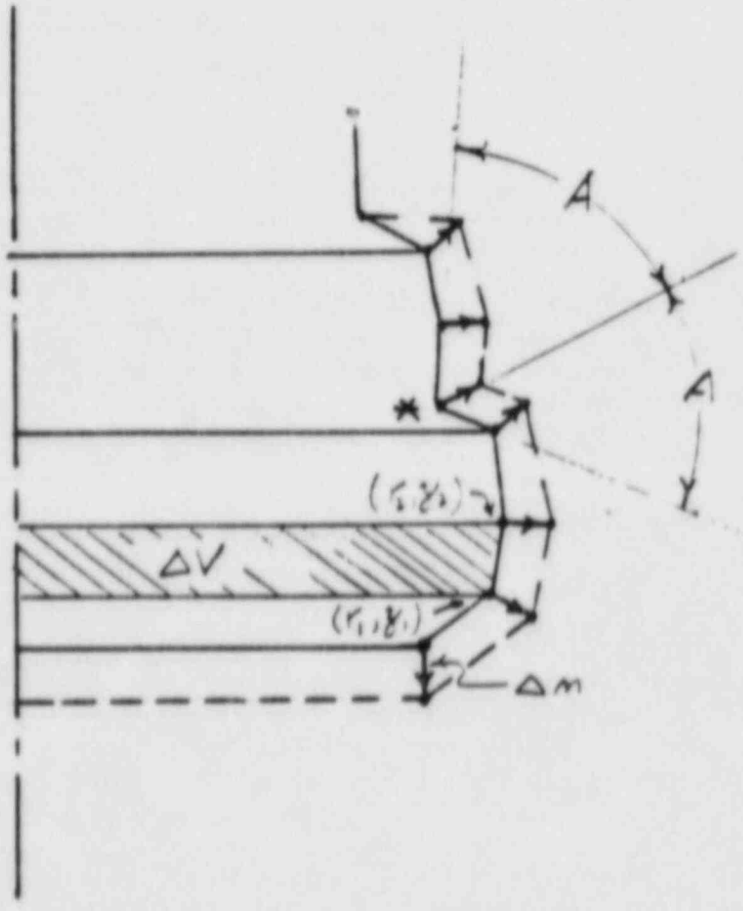

Figure 3.5.3-4. Proposed Cavity and Model

two neighboring points except at the tangent point where it is taken as vertically downward. The new points define the volume of the cavity as a function of z, allowing interface positions to be defined from known layer volumes (including gas swelling). Concrete ablation may be determined from volume changes rather than from a surface integral of ablation rate, eliminating any mass discrepancy. The "rezone," necessary to eliminate the convergence and divergence of points seen in Figure 3.5.3-4, can now be accomplished while maintaining the cavity volume as a function of z.

In most cases the recession, Δn, may be taken as the local normal ablation rate times Δt. However, CORCON experience [Cole and Kelly, 1983] has shown that this will sharpen inside corners such as "*" in Figure 3.5.3-4. The proposed correction is to multiply the recession by cosec(A), with A as shown in the figure for all such points. This is exactly the correction needed to eliminate corner sharpening as shown in Figure 3.5.3-5.

3.5.3.1.2 Debris Pool

The existing codes model the debris pool as a number of layers in the concrete cavity. INTER allows one metallic layer and one oxidic layer, with the less dense one on top. No second oxidic "slag" layer is considered when the metal is on top. WECHSL also considers only two layers, and assumes that the oxide is always on top. CORCON allows the three-layer structure described in Section 3.5.2. In fact, CORCON's structure allows a more general layering with the possibility of forming "heterogeneous mixture" layers containing both metals and oxides at the interfaces between pure phases. In the present coding, however, these layers cannot be formed because no model is available to determine their formation.

We feel that the possibility of a three-layer pool should be allowed for in the structure of MELCOR. As in the existing codes, each layer need be treated primarily as a control volume with no internal structure for the purposes of conservation of mass and of energy. Each is characterized by a mass and an energy content, which together imply an average temperature. This is quite accurate when the pool is primarily liquid, and gases maintain each layer nearly homogeneous and isothermal. At later times, when crust formation and freezing become important, it seems reasonable to treat the resulting temperatures as layer averages. An internal temperature distribution may be considered for the purpose of evaluating heat fluxes only. Layer volumes, including the swelling effects of gas bubbles, determine the elevations of layer interfaces and of the pool surface.

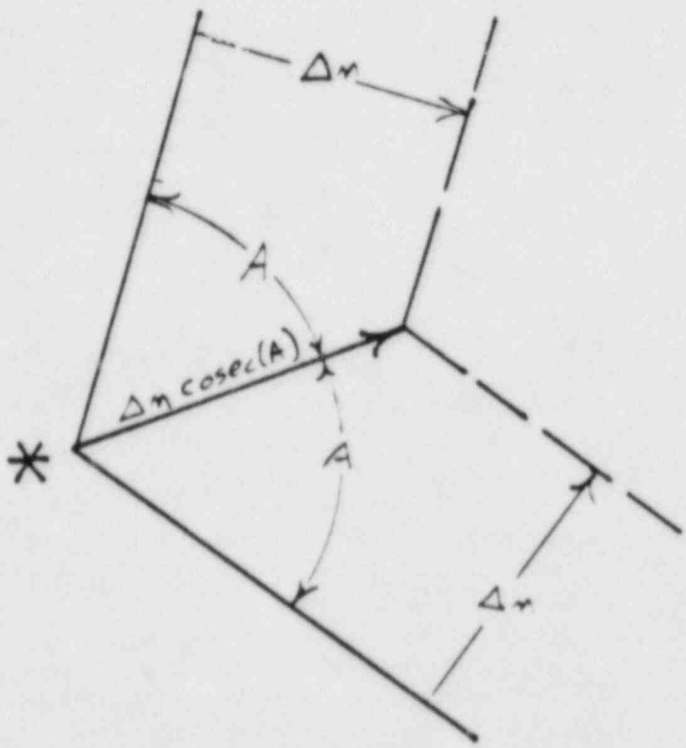

Figure 3.5.3-5. Treatment of Inside Corners

The composition of each layer must be specified in order to determine its thermophysical and transport properties. Both INTER and WECHSL consider Zr and Fe, Cr, Ni (steel) in the metallic phase and UO_2, ZrO_2 (fuel oxides), FeO, Cr_2O_3, NiO (steel oxides), and CaO, SiO_2, Al_2O_3 (the dominant concrete oxides) in the oxidic phase. This list of species is substantially enlarged in CORCON; the additional detail does not seem justified for PRA purposes as the effects of minor species can be handled in simpler ways. For example, while the alkali oxides have a significant effect on the melting temperature of concrete, this temperature will certainly be input (or default) rather than computed. Fission product inventories, for evaluation of decay heat and aerosol sources, may be kept without including the effects of these species on thermophysical properties. In addition, most of the aerosol sources are so small compared to inventories that depletion effects could be ignored as described in Section 3.5.3.2.11.

Violent interactions are not part of the core/concrete interaction problem. If they occur, they will be modeled in other modules of MELCOR such as the steam explosion module. For the purposes of core/concrete interactions, any water which is initially present or added later may be treated in the same manner as the oxides and metals. It simply forms an additional layer above the core-melt layers.

3.5.3.1.3 Pool Surface

The pool surface forms a boundary between the debris pool and the rest of containment. In the version of CORCON which will become MOD2, it is treated as a mutual boundary condition for these regions. That is, (1) material passes through it from one region to the other and (2) it is characterized by an average temperature such that the pool-to-surface and surface-to-surroundings heat flows are equal. This is a natural division of the problem; we recommend it for MELCOR.

3.5.3.2 Physical Processes

A variety of physical processes must be considered in the modeling of molten-fuel/concrete interactions. These include internal energy generation, mass and heat transfer, chemical reactions, concrete response, and bubble phenomena. In several cases, one or more phenomena are tightly coupled and must be considered simultaneously: for example, concrete response determines gas generation, which affects heat transfer and the heat flux to concrete, which in turn determines concrete response. We will try to note such interactions in the discussion which follows.

3.5.3.2.1 Energy Generation

The entire fuel/concrete interaction process is driven by decay heat generated in the pool, including actinides, decay products, and irradiated structural materials. Use of the ANS Standard decay curve is not appropriate because (at least) the more volatile fission products have been lost from the fuel before the pool is formed. A multiplier for the standard is probably not sufficient because it cannot account for variations in the decay-product inventory of the pool under differing in-vessel assumptions and scenarios.

The decay heating could be calculated using detailed decay chains. This procedure, as used in CONTAIN, is described in the CONTAIN report, [Senglaub et al., 1981] and is certainly satisfactory. However, if it is not needed for fission-product tracking--and it may not be because the major heat-generators are not the major nuclides in terms of biological consequences--the simpler model used in CORCON [Muir et al., 1981] is suggested. This model is described below.

A SANDIA-ORIGEN [Bennett, 1979] calculation was performed for a reference core representative of a large PWR core at equilibrium burnup (3320 MWt and 33000 MWD/MTU). From the results of this calculation, 27 elements (excluding noble gases) were identified which accounted for essentially all the heat production in the reference core in the 1-hour to 10-day time frame. The elements, their assumed chemical forms [Powers, 1980] and concentrations in the core, and the fraction of each expected to be retained in the melt [WASH-1400] are given in Table 3.5.3-1. In the context of MELCOR, modules which determine behavior before pool formation would determine the amounts of UO_2, Zr, and ZrO_2 in the pool, and could modify the default retention fractions for fission products if appropriate.

The decay power associated with each element, also taken from the reference SANDIA-ORIGEN calculation, were fit in the form

$$P(t) = m_e C_e e^{-\lambda t} \qquad (3.5.3\text{-}2)$$

where $P(t)$ is the decay power (W)
t is the time from SCRAM (days)
m_e is the elemental mass (gram-atoms)
and C (W/gram-atom)
λ . (day^{-1})

are the fit coefficients.

Table 3.5.3-1

Elements and Parameters in Decay Heat Model

Element	Concentration (g-atom/MWt)	Retention (-)	0.0 d < t < 0.1 d C (W/g-atom)	0.0 d < t < 0.1 d λ (1/day)	0.1 d < t < 0.6 d C (W/g-atom)	0.1 d < t < 0.6 d λ (1/day)	0.6 d < t < 2.2 d C (W/g-atom)	0.6 d < t < 2.2 d λ (1/day)	2.2 d < t < 20 d C (W/g-atom)	2.2 d < t < 20 d λ (1/day)
Metals										
MO	6.053E-01	9.700E-01	3.290E+03	2.375E+01	2.840E+02	2.590E-01	2.826E+02	2.510E-01	2.843E+02	2.530E-01
TC	1.545E-01	9.700E-01	1.560E+04	3.925E+01	2.950E+02	5.490E-01	2.560E+02	2.390E-01	2.623E+02	2.520E-01
RU	3.885E-01	9.700E-01	1.430E+03	7.820E+00	7.039E+02	1.110E+00	3.770E+02	9.400E-02	3.264E+02	1.700E-02
RH	6.900E-02	9.700E-01	9.650E+03	1.525E+01	2.116E+03	3.990E-01	1.757E+03	6.400E-02	1.495E+03	1.000E-02
SB	2.440E-03	8.500E-01	7.620E+05	2.786E+01	5.380E+04	2.980E+00	1.150E+04	4.940E-01	5.310E+03	1.330E-01
TE	6.270E-02	8.500E-01	3.400E+04	2.190E+01	3.670E+03	1.331E+00	2.110E+03	2.880E-01	1.270E+03	1.330E-01
Monoxides										
SR	2.155E-01	9.000E-01	1.640E+04	1.857E+01	2.930E+03	1.844E+00	1.180E+03	4.310E-01	4.930E+02	1.420E-02
BA	1.915E-01	9.000E-01	1.430E+04	2.345E+01	1.330E-01	9.330E-01	8.460E+02	5.200E-02	8.380E+02	4.910E-02
Dioxides										
ZR	7.352E-01	9.900E-01	3.320E+03	1.680E+01	6.430E+02	4.390E-01	5.543E+02	2.350E-01	3.290E+02	1.510E-02
CE	3.870E-01	9.900E-01	2.770E+03	1.390E+01	7.130E+02	3.350E-01	6.843E+02	2.810E-01	3.375E+02	4.500E-02
NP	4.220E-02	9.990E-01	1.920E+04	2.100E-01	1.920E+04	2.340E-01	1.940E+04	2.430E-01	2.210E+04	2.890E-01
CM	2.040E-03	9.900E-01	8.180E+03	1.220E-02	8.170E+03	1.900E-03	8.590E+03	2.800E-02	8.216E+02	2.900E-01
NB	1.139E-02	9.900E-01	4.520E+05	2.002E+01	6.360E+04	6.300E-01	5.340E+04	3.950E-01	2.080E+04	1.000E-02
PU	7.921E-01	9.900E-01	1.270E+01	2.660E+00	1.143E+01	1.950E+00	3.780E+00	2.700E-01	2.260E+00	2.000E-04
AM	5.930E-03	9.900E-01	2.560E+03	2.300E+01	2.690E+02	1.340E+00	2.120E+02	9.000E-01	1.790E+01	5.550E-02
Sesquioxides										
Y	1.099E-01	9.900E-01	4.880E+04	1.828E+01	9.315E+03	1.740E+00	3.960E+03	5.430E-01	1.314E+03	1.340E-02
LA	1.662E-01	9.900E-01	2.790E+04	1.178E+01	8.650E+03	9.400E-01	5.300E+03	4.290E-02	5.520E+03	5.200E-02
PR	1.446E-01	9.900E-01	1.030E+04	1.260E+01	2.990E+03	4.830E-01	2.300E+03	5.850E-02	2.100E+03	1.300E-02
ND	4.638E-01	9.900E-01	3.910E+02	9.920E+00	1.446E+02	6.700E-01	1.048E+02	6.680E-02	1.048E+02	6.600E-02
SM	5.396E-02	9.900E-01	5.580E+02	4.080E+00	3.860E+02	4.220E-01	3.740E+02	3.700E-01	3.540E+02	3.510E-01
EU	1.705E-02	9.900E-01	2.700E+03	7.300E-01	2.520E+03	1.000E-01	2.540E+03	5.100E-02	2.390E+03	4.200E-02
Alkali Metals										
RB	8.190E-02	1.900E-01	5.510E+04	2.938E+01	5.260E+03	5.930E+00	6.076E+02	3.160E+00	8.540E-01	3.180E-02
CS	3.776E-01	1.900E-01	1.210E+04	5.748E+01	3.185E+02	1.452E+00	1.564E+02	2.000E-02	1.531E+02	1.100E-02
Halogens										
BR	5.300E-03	1.000E-01	3.990E+05	5.113E+01	2.500E+03	4.260E+00	3.170E+02	5.220E-01	5.460E+02	6.550E-01
I	3.200E-02	1.000E-01	1.540E+05	9.610E+00	6.120E+04	1.170E+00	3.180E+04	3.670E-01	2.300E+04	1.700E-01
Fuel										
U (as UO2)			1.240E+01	3.690E+01	2.560E-01	1.470E+00	1.260E-01	6.900E-02	1.340E-01	1.060E-01
ZR (as Zr and ZrO2)			5.630E-02	1.000E-02	5.630E-02	1.000E-02	5.630E-02	1.000E-02	5.630E-02	1.000E-02

Four time intervals were used with breaks at 0, 0.1, 0.6, 2.2, and 20 days; the fit coefficients are given in Table 3.5.3-1. The different fit coefficients for each time period reflect the changing isotopic compositions of the elements.

3.5.3.2.2 Pool Layer Heat Transfer

Heat is removed at the boundaries of the pool, which are its top surface and its interface with concrete. As discussed in Section 3.5.2, the internal temperature of the pool adjusts rather quickly so that these heat losses balance the internal heat generation. The heat transfer is then almost steady state. For the multi-layered pool model of Section 3.5.3.1.2, it is reasonable to consider the problem one layer at a time. At early times the pool is entirely molten, while at later times it may develop solid crusts or freeze in some depth. Here, we will address heat transfer in a liquid layer, or the liquid portion of a partially-solidified layer. The modifications necessary to account for crusting or freezing will be described in the next section.

The problem is greatly complicated by gas stirring. There are a number of competing models and a limited amount of data. It is not surprising, therefore, that the treatments in INTER, [Murfin, 1977] CORCON, [Muir et al., 1981] and WECHSL [Reimann and Murfin, 1981] differ widely.

The model in INTER is the simplest, and is used for liquid and solid layers alike (a layer is considered to be all liquid or all solid, depending on its temperature). A thermal boundary layer is assumed to exist at the surfaces of each layer. Its thickness, δ, the same on all surfaces, satisfies a conduction-inspired growth equation

$$\frac{d\delta}{dt} = 0.72\,\kappa/\delta \qquad (3.5.3\text{-}3)$$

where κ is the thermal diffusivity of the layer. This growth is subject to certain ad hoc constraints. According to the code documentation [Murfin, 1977] these are: in a liquid layer, δ must be at least 5 mm but cannot exceed 2.5 percent of the layer thickness; if the gas flow is large (superficial velocity greater than some critical value), and the rest of the pool is also liquid, this upper limit is reduced to 0.5 percent. In the code, it appears that the lower limit on thickness is 2.54 centimeters, and a more general transition is applied at the critical gas flux (which is .001 in some units). If the layer is solid, the equation is applied "without constraint," although some

upper bound must be applied in the coding. The heat transfer coefficient from interior to surface is then calculated as

$$h = k/\delta \qquad (3.5.3\text{-}4)$$

where k is the thermal conductivity of the layer. Note that h is the same for all surfaces, which does not seem realistic (nor is it in agreement with most of the other models). This has implications for the partition of pool heat between concrete and top surface, as discussed in Section 3.5.2. This model has little justification, and does not seem appropriate for MELCOR. One must remember that it was only applied "for want of a better relationship." [Murfin, 1977]

A number of more-or-less mechanistic models have been proposed for heat transfer in the presence of bubble agitation or injection. Blottner describes several of them in a report [Blottner, 1979] which was used as the basis for selecting models for CORCON. He recommended use of a modification of the Konsetov model in the form

$$h = k(Pr\ g/\nu^2)^{1/3}(A\alpha^n + B\beta|\Delta T|)^{1/3} \qquad (3.5.3\text{-}5)$$

where Pr is the Prandtl number of the liquid
ν is its kinematic viscosity
β is its thermal expansivity
g is the acceleration of gravity
ΔT is the temperature difference
and α is the void fraction evaluated from

$$\alpha = V_S/(V_S + 1.53\sqrt{ga}) \quad . \qquad (3.5.3\text{-}6)$$

Here V_S is the superficial velocity of the gas and a is the Laplace constant

$$a = [\sigma/g(\rho_\ell - \rho_g)]^{1/2} \qquad (3.5.3\text{-}7)$$

where σ is the surface tension and ρ is density with ℓ and g referring to liquid and gas. The power n in Equation (3.5.3-5), which may be 1 or 2, is Blottner's modification; the original equation had n = 1. Equation (3.5.3-7) reduces to the familiar (turbulent) natural convection result if V_S is zero. In fact, it may be thought of as adding a bubble buoyancy term, $A\alpha^n$, to the thermal-expansion buoyancy term, $B\beta\Delta T$.

In CORCON, this form is used at the sides of the pool with n = 1, A = 0.05, and B = 0.00274, and on the bottom with n = 2, A = 0.4, and B = 0.00030. At liquid/liquid interfaces, the code uses n = 2, A = 0.4 (despite Blottner's recommendation of A = 50), and B = 0.00274. These expressions are based, in effect, on the idea that the effect of bubbles is to enhance convection while maintaining an essential similarity to thermal convection.

In WECHSL, completely different models are employed. The one used at the sides of the pool is based on the idea of a boundary layer in the pool in response to shear forces exerted by the flow of gas in the film between the pool and the concrete. The ratio of the thicknesses of the shear boundary layers in the gas and the liquid is calculated following a proposal of Lock's.[Lock, 1951] This is converted to a ratio of thermal boundary-layer thicknesses using standard methods. The result is

$$\frac{\delta_\ell}{\delta_g} = 1.236\ Pr_\ell^{-1/2} \left(\frac{\mu_\ell}{\mu_g}\right)^{2/3} \left(\frac{\rho_g}{\rho_\ell}\right)^{1/3} \qquad (3.5.3\text{-}8)$$

where δ is the thermal boundary-layer thickness
μ is the viscosity
ρ is the density
and ℓ,g refer to liquid and gas, respectively.

The thickness of the gas film is calculated from the models described in Section 3.5.3.2.4. The heat-transfer coefficient is then given by

$$h = k/\delta_\ell \quad . \qquad (3.5.3\text{-}9)$$

The same equations are employed at the bottom of the pool if Taylor-instability bubbling is occurring there, even though the model from which they were derived is not valid. The justification given is that the bottom layer is always (in WECHSL) the metallic phase, which has large thermal conductivity and small viscosity. This leads to large heat-transfer coefficients and small temperature differences which need not be accurately calculated. If the gas injection rate has fallen below that necessary to maintain a stable film (or if forced by an input flag), a "discrete bubble model" is used, with the assumption that pool and concrete are in intimate contact, except for bubbling sites. The entire thermal resistance is in the liquid, determined by microconvection cells formed between bubble sites. The heat-transfer coefficient is given by

$$h = 0.8613C(\theta)k(\rho_{water}V_s/\mu_g a)^{1/2} \qquad (3.5.3\text{-}10)$$

where

$$C(\theta) = 1.65 + 7.47\theta - 8.77\theta^2 + 3.65\theta^3 \qquad (3.5.3\text{-}11)$$

is a function which accounts for the inclination, θ, of the surface.

In the WECHSL model for an interface between layers, the heat-transfer coefficients for turbulent natural convection from each layer to the surface

$$h = 0.1348kPr^{0.417}(g\beta|\Delta T|/\nu^2)^{1/3} \qquad (3.5.3\text{-}12)$$

are first combined to get a net coefficient for natural convection

$$h_{net} = (1/h_1 + 1/h_2)^{-1} \qquad (3.5.3\text{-}13)$$

This is then multiplied by a factor

$$\Upsilon = 1.0 + 608.(V_s/u_b)[\rho_</(\rho_>-\rho_<)]^{4/3} \qquad (3.6.3\text{-}14)$$

where u_b is the bubble rise velocity and ρ is the density, with > and < referring to the more dense and less dense phases, respectively.

This factor was determined by fitting Werle's data.[Werle, 1979]

An alternative model for liquid/liquid interfaces considered by Blottner, but not originally recommended for MELCOR, is a modification of the Szekely [Szekely, 1963] model in the form

$$h = 1.69k(V_s/Kr_e)^{1/2} \qquad (3.5.3\text{-}15)$$

where r_e is the equivalent bubble radius based on volume. This may be derived from the idea that heat is transferred by transient conduction with bubbles periodically disrupting

the developing thermal gradients. It is therefore referred to as a "surface renewal" model. Since the release of CORCON-MOD1, Ginsberg and Greene [Ginsberg and Greene, 1983] have compared the Konsetov and the Szekely models with simulant data, Greene's and that of Werle.[Werle, 1978, 1981] They conclude that the Konsetov form "seriously underpredict[s] . . . the data," and that the Szekely form is preferable. They also noted that entrainment effects became significant at rather modest gas superficial velocities on the order of 1 cm/s, and suggest a combined heat expression of the form

$$1.69k(V_s/\kappa r_e)^{1/2} + CV_s\rho_\ell c_p \qquad (3.5.3\text{-}16)$$

where ρ_ℓ is the density of the entrained (lower) phase
c_p is its specific heat
and C is a coefficient in the range $0.3 < C < 1.0$.

The GROWS II code uses [Baker et al., 1978] [Baker, 1983] pool heat transfer coefficients based on correlations derived by Kulacki and others for heat transfer to the top and bottom surfaces of internally heated pools (without bubbling). These take the form

$$Nu = A\ Ra'^{m} \qquad (3.5.3\text{-}17)$$

where

$$Nu \equiv hL/k \qquad (3.5.3\text{-}18)$$

is the Nusselt number

$$Ra' \equiv g\beta HL^5/2\nu K \qquad (3.5.3\text{-}19)$$

is the internal Rayleigh number

L is the depth of the pool
H is the volumetric heating,
and A, m are the correlation coefficients.

For equal top and bottom temperatures, the values are

$$A = 0.388,\ m = 0.236 \quad \text{(upward)}$$
$$A = 1.524,\ m = 0.094 \quad \text{(downward)} \qquad (3.5.3\text{-}20)$$

for $1.86 \times 10^4 < Ra' < 1.21 \times 10^7$.[Kulacki and Goldstein, 1972] For an insulated bottom, the coefficients are

$$A = 0.305, \quad m = 0.239 \qquad \text{(upward)} \qquad (3.5.3\text{-}21)$$

for $1.5 \times 10^4 < Ra' < 2.6 \times 10^9$, [Kulacki and Nagle, 1975] or

$$A = 0.403, \quad m = 0.226 \qquad \text{(upward)} \qquad (3.5.3\text{-}22)$$

for $1.05 \times 10^4 < Ra' < 2.17 \times 10^{12}$.[Kulacki and Emara, 1975]

These correlations differ in form from the conventional Nusselt-Rayleigh expressions for natural convection, [McAdams, 1954]

$$Nu = 0.54\ Ra^{1/4} \qquad Ra < 1.1 \times 10^7 \qquad (3.5.3\text{-}23)$$

$$Nu = 0.14\ Ra^{1/3} \qquad 1.1 \times 10^7 < Ra \qquad (3.5.3\text{-}24)$$

where

$$Ra = g\beta\Delta TL^3/\nu K \qquad (3.5.3\text{-}25)$$

is the external Rayleigh number, in that the temperature difference, ΔT, has been eliminated in favor of the internal heating, H. For these experiments, which were one dimensional and steadystate, the two are uniquely related; in the case of a two-dimensional pool this is not the case because of radial heat flows. The temperature difference, which is characteristic of temperature gradients, seems the more fundamental variable. In [LWRSRP, 1981 (a)] it was shown that the conventional relations, Equations (3.5.3-23) and (3.5.3-24), combined with conservation of energy, could be used to reproduce the various internal-Rayleigh-number correlations with a maximum error of 30 percent and an average error closer to 10 percent. This work showed that the upward Nusselt number, Nu_1, may be calculated directly from Equations (3.5.3-23) and (3.5.3-24), and the downward Nusselt number, Nu_o, taken as

$$Nu_o = 1 + [1 + 2Nu_1\ \Delta T_1\ /\Delta T_o]^{1/2} \qquad (3.5.3\text{-}26)$$

in the case where the pool is cooled (or at least not heated) from below. If the pool (or layer) were heated from below as well, Equations (3.5.3-23) and (3.5.3-24) would also be used for the bottom surface. Here, of course, the ΔTs are measured between the surfaces of the pool and its interior. Because these results are based on temperatures rather than heat sources, and agree quite well with the results of the one-dimensional experiments, we feel that they are more appropriate for application to a two-dimensional pool than the correlations based on internal Rayleigh numbers.

In the Kulacki-Goldstein experiments, the unstable temperature gradient at the top of the layer produced convective flows which steepened the stable temperature gradient at the bottom, thereby increasing the heat flow for a given temperature difference. Equation (3.5.3-26) may be viewed as describing this effect of an unstable temperature gradient on a stable one. It seems reasonable to assume that the same results would apply (with "top" and "bottom" reversed) if the pool were being heated from both above and below. The natural convection limits applied to bubble-enhanced convective heat transfer in the version of CORCON which will become MOD2 use these results; in fact, it is assumed that Equation (3.5.3-26) may be applied even when Nu_1 is evaluated for bubble-enhanced convection.

Because of the lack of consensus and absence of validation, we can make no specific recommendations for bubble-enhanced convection models for MELCOR. For natural convection, however, we feel that the use of conventional heat-transfer correlations, combined with Equation (3.5.3-26), is preferable to use of correlations based on the internal Rayleigh number.

3.5.3.2.3 Crust Formation and Freezing

After some period of interaction, pool temperatures will have fallen to the point where solidification begins. In the early stages, crusts will form at one or more interfaces with the layer core remaining liquid. Crust formation has several implications for core/concrete interactions, the most obvious being that it changes the mode of heat transfer within the pool. For a given liquid temperature, it limits convective heat transfer because the boundary temperature of the liquid cannot fall below the solidification temperature. In addition, the crust provides an additional thermal resistance between the interior of the pool and its boundary. The effect is to reduce heat losses and slow internal cooling rates. At later times, considerable freezing may occur. If a layer becomes largely or completely frozen, heat can be removed from it by conduction only, which is

ordinarily far less effective than convection. Solids forming on the bottom and sides of the pool may be expected to form relatively compact crusts. Those forming on the top surface may be inflated by concrete-decomposition gases resulting in large gas pockets or even multiple crusts which would serve as radiative insulation. Such effects were seen in the pre-Beta tests at KfK, but no models exist to describe them.

Because of internal heating and the fact that cooling cannot continue unless heat losses exceed sources, freezing is largely self-limiting. Substantial freezing of the metallic layer may occur, but in the layer containing fuel oxides the volumetric heating is much greater and the thermal conductivity much lower so that only thin crusts can form. This may be seen from the steadystate relation

$$2k\Delta T/\delta \geq q \geq S\delta \qquad (3.5.3\text{-}27)$$

where k is the thermal conductivity
ΔT is the temperature across the crust
δ is the crust thickness
q is the heat flux at the outer surface of the crust
and S is the volumetric heating.

The factor of 2 arises from the quadratic temperature profile associated with steady conduction. Using typical values of these parameters, [Blottner, 1979] one finds that δ must be less than a few centimeters for the oxide, but can be on the order of a meter for the metal.

A complete formulation of the problem involves transient, two-dimensional heat transfer with conduction, convection, and freezing. Solution of such a problem would be very difficult if not impossible, particularly if centimeter-thick crusts must be resolved on layers with dimensions of meters. Its "accuracy" would also be questionable because of the many specific assumptions required as to the spatial variation of surface temperature and volumetric heating, the temperature dependence of material properties, and so on. In many cases, these would be little more than guesses, and one would have at best an "accurate" solution to the "wrong" problem.

A simpler pseudo-steady state model has been developed for inclusion in CORCON-MOD2. It uses two one-dimensional solutions, one axial and one radial, for each layer. These may be thought of as the radial and axial averages, respectively, of the full two-dimensional problem. The one-dimensional problems are formulated in terms of the average temperature of the layer, which is known from its mass and

energy content. The essential concept of the model is to develop a pseudo-steady solution to the heat-transfer equations with the correct average and boundary temperatures, and use the resulting heat fluxes. The basic assumption is that the total axial and radial heat flows are coupled only through their influence on the average temperature of the layer.

This is a familiar and reasonable approximation for convective heat transfer in an almost isothermal liquid layer with thin thermal boundary layers. It might be expected to be least accurate in the limit of conduction in a completely frozen layer. Therefore, we have compared its predictions with the "exact" solution for steady conduction in a right-circular cylinder with uniform volumetric heating and specified surface temperatures. The quantities to be compared are the resulting average temperature of the layer and the partition of internally generated heat among upward, downward, and radial heat flows. The agreement is remarkably good: the partition of heat and the effect of boundary temperatures on the average temperature are within 10 percent, while the temperature rise due to internal heating is within 20 percent. This is true for any reasonable height-to-diameter ratio of the cylinder.

Within a one-dimensional calculation, a layer may be entirely liquid, entirely solid, or liquid with a solid crust. For the axial case, the crust may be on the top, on the bottom, or both. In liquid regions, heat transfer is by convection (natural or bubble-enhanced) with a conduction limit. In solid regions, it is by conduction. The all-liquid case is handled as in the previous section, while the all-solid case uses the analytic results for steadystate conduction with a constant volumetric source which follow from

$$q_z = -k dT/dz \qquad (3.5.3\text{-}28)$$

$$dq_z/dz = S_z \qquad (3.5.3\text{-}29)$$

$$q_r = -k dT/dr \qquad (3.5.3\text{-}30)$$

$$d(rq_r)/dr = rS_r \qquad (3.5.3\text{-}31)$$

where q is the heat flux, positive upward or outward
T is the temperature
and S is the volumetric heat source.

These relations lead to familiar quadratic temperature profiles. In terms of boundary and average temperatures, the heat fluxes are

$$q_B = k(-4T_B+6\bar{T}-2T_T)/L \qquad (3.5.3\text{-}32)$$

$$q_T = k(-2T_B+6\bar{T}-4T_T)/L \qquad (3.5.3\text{-}33)$$

$$q_R = 4k(\bar{T}-T_R)/R \qquad (3.5.3\text{-}34)$$

with B, T, and R referring to the bottom, top, and radial surfaces.

Here $\bar{T}$ is the average temperature of the layer
L is its thickness
and R is its radius.

Note that the volumetric source does not appear in these results.

In the case of crusts, the liquid sublayer is solved first using assumed values of its average temperature and thickness or radius, T_ℓ and ℓ or R_ℓ, and appropriate boundary temperatures. The temperature of any boundary on which a crust exists is taken as the solidification temperature. Conduction in the crust is again governed by Equations (3.5.3-28) through (3.5.3-31), and the temperature profile is again quadratic in each crust. Matching the heat flux at its interface with the liquid, and setting the volumetric source equal to that in the liquid,

$$S_z = (q_T-q_B)/\ell \qquad (3.5.3\text{-}35)$$

$$Sr = 2q_r/R_\ell \qquad (3.5.3\text{-}36)$$

leads to crust thicknesses and average temperatures of

$$\delta_B = 2k(T_S-T_B)/\left(\sqrt{Q_{B\ell}^2 + 2k(T_S-T_B)S_z} - Q_{B\ell}\right) \qquad (3.5.3\text{-}37)$$

$$\delta_T = 2k(T_S-T_T)/\left(\sqrt{Q_{T\ell}^2 + 2k(T_S-T_T)S_z} + Q_{T\ell}\right) \qquad (3.5.3\text{-}38)$$

$$\delta_R = 2k(T_S-T_R)/(\sqrt{Q_{R\ell}^2 + k(T_S-T_R)S_r} + Q_{R\ell}) \qquad (3.5.3\text{-}39)$$

$$\bar{T}_B = (2T_S+T_B)/3 + Q_{B\ell}\delta_B/6k \qquad (3.5.3\text{-}40)$$

$$\bar{T}_T = (2T_S+T_T)/3 - Q_{T\ell}\delta_T/6k \qquad (3.5.3\text{-}41)$$

$$\bar{T}_R = (T_S+T_R)/2 \quad . \qquad (3.5.3\text{-}42)$$

Here T_S is the solidification temperature
T_x is the average temperature of crust x
and $Q_{x\ell}$ is the heat flux at the x surface of the liquid.

In some cases, one or more of Equations (3.5.3-37), (3.5.3-38), and (3.5.3-39) may have no real solution. For this to happen the effective source must be negative, which may occur if a layer is being heated by an adjacent layer. The solution is to repeat the calculation with the source made less negative by increasing the assumed liquid temperature and/or dimensions.

In general, neither the total layer thickness (or radius) nor the overall average temperature thus determined will be correct for the layer. This requires an iteration on the thickness and temperature of the liquid sublayer. A two-variable Newton iteration has been found effective for this, although a bound-and-bisect backup is advisable for reliability.

3.5.3.2.4. Melt/Concrete Heat Transfer

The exact nature of the interface between the melt and the concrete is unknown. This region, into which gases and molten or partially molten oxides from concrete decomposition are being injected, is too thin to be seen either visually or with x-rays.[Powers and Arellano, 1982] Therefore, models for the thermal resistance of this region are based on analysis and simulant tests.

Most such models assume that the boundary region is dominated by a gas film. On horizontal and near-horizontal surfaces the Taylor instability leads to formation of bubbles which enter the melt, while on more-steeply inclined surfaces the gas forms a flowing film. Heat transfer on horizontal surfaces is based on analogy with pool boiling. Blottner concluded [Blottner, 1979] that no gas film is possible, based on gas superficial velocities being less than a critical velocity given by Kutateladze and Malenkov. [Kutateladze and Malenkov, 1978] However, simulant experiments, [Dhir et al., 1977] [Dhir, 1980] are in good agreement with the film model. This discrepancy has been explained [LWRSRP, 1982] as involving the direction of motion on the

pseudo-boiling curve. Kutateladze's experiments start with small gas flows and move upward toward the analog of the critical-heat-flux point, while the simulant experiments (and, we believe, the core/concrete case) start with large gas flows and fall back toward the analog of the Leidenfrost point. Thus, the appropriate "critical velocity" is that for collapse of a stable film, which (for pool boiling) is two orders of magnitude smaller than that necessary for its formation, and a stable analog of film boiling cannot be ruled out. At later times, the interface may enter the analog of "patchy" boiling, with intermittent intimate contact between the melt and the concrete.

In addition to the gas-film models, Blottner [Blottner, 1979] has proposed a model in which the film is slag rather than gas. Benjamin [Benjamin, 1980] has proposed a model in which there is intimate contact except at bubbling sites, and the total thermal resistance is determined by the thermal boundary layer of an assumed cellular stagnation flow in the pool surrounding bubble sites. He also describes a slag-film model for the metal/concrete interface. These models are not used in existing codes, for strictly historical reasons: the gas-film models were implemented first, the alternate models do not give answers which are greatly different, and there is no convincing experimental evidence to confirm or reject any of the models.

Both CORCON [Muir et al., 1981] and WECHSL [Reimann and Murfin, 1981] also consider radiation across the gas film, using the form for a transparent gas between parallel gray walls

$$q_{rad} = \frac{\sigma_B (T_p^4 - T_w^4)}{(1/\epsilon_p + 1/\epsilon_w - 1)} \qquad (3.5.3\text{-}43)$$

where q_{rad} is the net radiative heat flux
σ_B is the Stefan-Boltzmann constant
T_p is the temperature of the pool side of the film
T_W is the temperature of the concrete surface
ϵ_p is the emissivity of the pool
and ϵ_W is the emissivity of the concrete.

This contribution to the total heat flux, which accounts for about one half of the total in CORCON calculations, is neglected in INTER.[Murfin, 1977]

The gas-film heat-transfer model in INTER is parametric, with the form

$$h_i = h_{ix}\, P[10.h_{ix}(P-1) + 1] \qquad (3.5.3\text{-}44)$$

where h_i is the heat-transfer coefficient across the gas film
P is the local total pressure in atmospheres
and h_{ix} is a "nominal coefficient" for phase x.

The h_{ix} are essentially user-input quantities, although that for the metal may be internally modified in ways which are not documented. When INTER was incorporated into the MARCH code, [Wooton and Avci, 1980] these parameters were given default values of 100.0 W/m^2 K.

For a gas film on a nearly horizontal surface, both CORCON and WECHSL use a mechanistic model based on momentum balance in a Taylor-instability bubbling cell.[Alsmeyer and Reimann, 1977] The result may be cast in the form of a Nusselt number based on film thickness as

$$Nu_B \equiv h_B \delta_B / k_g = 0.804 \qquad (3.5.3\text{-}45)$$

where Nu_B is the Nusselt number
h_B is the heat-transfer coefficient
δ_B is the film thickness
and k_g is the thermal conductivity of the gas.

The factor 0.804 is the fraction of the surface not occupied by bubble sites and therefore available for heat transfer. The film thickness satisfies

$$\delta_B^3 = 15.05\, Re_B L^3 \qquad (3.5.3\text{-}46)$$

(the coefficient in WECHSL may be slightly different). Here L is a material property

$$L = \left\{ \mu_g^2 \,/\, \left[g \rho_g (\rho_\ell - \rho_g) \right] \right\}^{1/3} \qquad (3.5.3\text{-}47)$$

where μ_g is the viscosity of the gas
ρ_g is its density
ρ_ℓ is the density of the liquid
g is the acceleration of gravity
and Re_B is the Reynolds number based on the Laplace constant a

$$Re_B = \rho_g V_s \, a/\mu_g \qquad (3.5.3\text{-}48)$$

$$a \equiv [\sigma/g(\rho_\ell - \rho_g)]^{1/2} \qquad (3.5.3\text{-}49)$$

where V_s is the superficial velocity with which gas enters the film and σ is the surface tension of the pool liquid.

The superficial velocity is determined by the concrete response. This, in turn, is determined by the total heat flux, which involves a balance ot pool-side heat transfer with radiation Equation (3.5.3-43) and the heat transfer characterized by h_B itself. A consistent solution has been found advisable for numerical stability. In CORCON, this is obtained through a simple iteration.

It is worth noting that if the process were really boiling, the equations would be closed through the relations

$$q = h_B \Delta T = \rho_g V_s i_{fg}' \qquad (3.5.3\text{-}50)$$

where i_{fg}' is the effective heat of vaporization. Relatively simple manipulation can then be used to reduce the present model to the form of Berenson's [Berenson, 1961] correlation for boiling on a flat plate

$$h = 0.67 \left[\frac{k_g^3 g i_{fg}' (\rho_\ell - \rho_g)\rho_g}{\mu_g \Delta T 2\pi a} \right]^{1/4} \qquad (3.5.3\text{-}51)$$

with a coefficient of 0.68 rather than 0.67.

The bubble model is used for inclinations less than 15° in CORCON and for inclinations less than 30° in WECHSL. Above 30°, both codes use a flowing-film model. In CORCON, models for a laminar film and a turbulent film are included. These are mechanistic models based on momentum balances in an inclined flowing film, with Reynolds analogy used for heat transfer in the turbulent case. The results, expressed as a Nusselt number, are

$$Nu_{LF} \equiv h_{LF}\delta_{LF}/k_g = 1.0 \qquad (3.5.3\text{-}52)$$

$$Nu_{TF} \equiv h_{TF}\delta_{TF}/k_g = 0.325 Pr^{1/3} Re_F^{3/4} \qquad (3.5.3\text{-}53)$$

where Pr is the Prandtl number for the film
and Re_F is the Reynolds number based on film thickness

$$Re_F = \rho_g \bar{u} \delta / \mu_g \qquad (3.5.3\text{-}54)$$

with $\bar{u}$ the average flow velocity in the film. The film thicknesses satisfy

$$\delta_{LF}^3 = 5.61\ Re_F L^3 / \sin\theta \qquad (3.5.3\text{-}55)$$

$$\delta_{TF}^3 = 0.0469\ Re_F^{7/4} L^3 / \sin\theta \qquad (3.5.3\text{-}56)$$

where θ is the inclination from the horizontal.

In MOD1, the transition from laminar to turbulent flow is assumed to occur at a Reynolds number of 100. The resulting discontinuity in heat-transfer coefficients is eliminated through application of a Persh transition [Persh, 1957]

$$Nu = Nu_{TF} - (Nu_{TF} - Nu_{LF})\Big|_{Re_F = 100} (Re_F/100)^2 \qquad (3.5.3\text{-}57)$$

in regions where the film is calculated to be turbulent. This transition was derived for external flows, and does not seem particularly appropriate for this use. Therefore, MOD2 will employ a much simpler "transition" which will ensure continuity of film thickness and heat-transfer coefficient with the appropriate limits:

$$\delta_F = \max(\delta_{LF}, \delta_{TF}) \qquad (3.5.3\text{-}58)$$

$$Nu_F = \max(Nu_{LF}, Nu_{TF}) \qquad (3.5.3\text{-}59)$$

$$h_F = k_g\ Nu_F / \delta_F \qquad (3.5.3\text{-}60)$$

where the various film thicknesses and Nusselt numbers have been defined above.

Note that $\rho_g \bar{u} \delta$ is the mass flow per unit width of film. In the absence of bubbling, it satisfies

$$\frac{d}{ds}(r\rho_g\bar{u}\delta) = r\rho_g V_s \qquad (3.5.3\text{-}61)$$

where r is the local radius of the cavity
and s is the path length, measured along the film.

The equations are again coupled, with heat transfer determined by film flow, which involves all upstream heat transfer. The gas-generation equation and Equation (3.5.3-57) form a coupled set of ordinary differential equations. In CORCON, they are solved by what is essentially a simple predictor-corrector method, with an inner iteration to solve the nonlinear (because of radiation) energy balance at each point. This model is matched to the bubble model at the point of 15° inclination by defining the value of $\rho_g u\delta$ there as that value which gives a continuous heat-transfer coefficient.

After the integration is performed, a "smoothing" operation is performed in a second pass by redefining heat-transfer coefficients for inclinations between 15° and 30°. These angles, which are somewhat arbitrary, were based on observation of simulant tests. A simple linear interpolation is used in MOD1. In MOD2, a deterministic transition, described in [LWRSRP, 1983] will be used. This model is again based on a momentum balance with a fraction f of injected gas going into bubbles and the rest into establishing the film. The results have the form

$$\delta^3 = \delta_F^3 + f(\sin 15°/\sin\theta)\delta_B^3 \qquad (3.5.3\text{-}62)$$

$$h = k_g\left[fNu_B + (1-f)Nu_F\right]/\delta \; . \qquad (3.5.3\text{-}63)$$

A transition is achieved by decreasing f linearly with $\sin\theta$ from 1 at 15° to 0 at 30°.

WECHSL applies a similar model above 30° inclination. If Equation (3.5.3-55) is differentiated along the film and variations of material properties and of the slope are neglected, one finds

$$\frac{d}{ds}\delta_{LF}^3 = 5.61\,\frac{\mu_g V_s}{g(\rho_\ell - \rho_g)\sin\theta} \; . \qquad (3.5.3\text{-}64)$$

This equation is integrated from the point where the inclination is 30° to the point where the Reynolds number, Equation (3.5.3-54), is 100. Above this point, a turbulent core is

assumed to form, and the differential equations for its development integrated as described in the reference. The heat-transfer coefficient is taken as

$$h = k_g/\delta \qquad (3.5.3\text{-}65)$$

where δ is the thickness of the laminar sublayer. These equations are integrated using a Runge-Kutta procedure.

WECHSL also includes a discrete bubbling model which is applied after the calculated collapse of the gas film at late times. This is assumed to occur when the superficial velocity falls below

$$V_{s\ crit} = 0.045 \left[\sigma g/(\rho_\ell - \rho_g)\right]^{1/4} . \qquad (3.5.3\text{-}66)$$

This model may optionally be applied throughout the problem. This equation differs from Berenson's result [Berenson, 1962] for boiling in that the coefficient is 0.045 rather than 0.090 and the terms involving $(\rho_\ell - \rho_g)$ are different. In this case, the entire thermal resistance is assumed to lie in the liquid. Details of the model are therefore in Section 3.5.3.2.2.

In all cases, the detailed integrations along the gas film are rather expensive. They consume nearly one half of the execution time of the latest version of CORCON, while WECHSL performs the calculation only every fifth time step "because of time limitations." This seems excessive for MELCOR, particularly if a relatively coarse cavity definition is employed. We recommend that the closed-form CORCON expressions, Equations (3.5.3-43), (3.5.3-45) through (3.5.3-49), (3.5.3-52) through (3.5.3-60), (3.5.3-62), and (3.5.3-63) be employed, but only at the points which define the cavity. In between, it should be sufficient to assume that the gas generation varies linearly. This would allow Equation (3.5.3-61), which defines the film flow, to be integrated analytically from point to point. An iteration would still be required to reconcile the film flow and the heat transfer at each point, but could be relatively simple.

3.5.3.2.5 Pool Surface Heat Transfer

In the context of MELCOR, calculation of the heat loss from the pool surface is the responsibility of above-pool modules, for which the surface temperature provides a boundary condition. It is highly desirable that these modules be as independent as possible. In particular, the need for simultaneous solution of above-surface and below-surface heat transfer relations should be avoided if possible.

A very simple method to do this is being used with complete success (and excellent agreement with results for simultaneous solution) in the version of CORCON which will become MOD2. Each half of the problem (above- and below-surface) defines an upward heat flow, Q_s, as a function of the surface temperature, T_s. An energy balance at the surface of the pool requires finding that T_s for which these heat flows are equal, which generally involves solution of a nonlinear--and perhaps very complicated--equation. There is another point of view: for each half of the problem, the boundary condition at the pool surface is the heat flow vs temperature characteristic of the other half. If that characteristic is linearized, say about the last-calculated surface temperature, an approximate solution is easily found. In the version of CORCON mentioned above, the response of the pool, linearized about its start-of-time-step value, T_s^m,

$$Q_s = Q_s^\circ\Big|_{Pool} + \left.\frac{dQ_s}{dT_s}\right|_{Pool} (T_s - T_s^n) \qquad (3.5.3\text{-}67)$$

is passed to the above-pool module. Here, it is used as a boundary condition for the full nonlinear problem involving atmosphere and surroundings, resulting in a provisional end-of-timestep surface temperature, $\tilde{T}_s^{n+1}$. This, together with the linearization of above-surface response about $\tilde{T}_s^{n+1}$,

$$Q_s = Q_s^\circ\Big|_{surr} + \left.\frac{dQ_s}{dT_s}\right|_{surr} (T_s - \tilde{T}_s^{n+1}) \qquad (3.5.3\text{-}68)$$

is passed back to the below-surface module, where it serves as a boundary condition for another nonlinear calculation which results in the final end-of-timestep value T_s^{n+1}. This procedure has advantages with respect to the energy-conservation equations, as will be discussed in Section 3.5.3.2.9.

As mentioned above, responsibility for the details of above-pool heat transfer will lie with the above-pool modules in MELCOR. We will only mention here that in work with the above-pool modules in CORCON, it has been found that heat loss from the surface is dominated by radiation. If aerosols are present in significant amounts, their radiative properties can become significant. Convection might be thought to provide additional heat transfer because of the

unstable temperature gradients involved. However, radiation provides a nonconvective energy transport mechanism, in addition to conduction, which increases thermal stability. Further discussion, together with references, may be found in [LWRSRP, 1983].

3.5.3.2.6. Concrete Decomposition and Ablation

The response of concrete exposed to high heat fluxes is complex. Concrete is an inhomogeneous material, which also undergoes changes in composition as it is heated. The most important of these are the vaporization of interstitial and adsorbed water at about 400 K, the decomposition of calcium hydroxide near 700 K, and that of calcium carbonate between about 1000 and 1100 K. These changes, of course, proceed at temperature-dependent rates, but the temperatures quoted are typical. Finally, the remaining oxide matrix melts, at a temperature which ranges from about 1500 K to perhaps 1800 K for representative concretes. Because the matrix is a mixture of compounds, the melting actually takes place over a range of temperatures and the rates of several chemical processes are also involved. In our case, the molten and semimolten materials are removed from the surface into the pool, and the surface recedes. The carbon dioxide, water vapor, and liquid water produced within the solid concrete flow through the pores of the remaining matrix in response to pressure gradients. This flow is Darcian, involving two species, two phases, and a spatially- and temporally-varying permeability. Heat is carried through the matrix, which may be porous, by conduction. Further terms appear in the energy equation from the flows of gases and of liquid water. Inward flows carry energy deeper into the concrete, while outward flows provide a transpiration cooling effect.

Most of the detailed physics outlined above is modeled by the USINT code [Beck and Knight, 1980] which solves finite-difference approximations to the resulting partial differential equations. The omissions are flow of carbon dioxide and recession of the surface. Details are contained in the reference, and some later improvements in numerical methods are documented in [Beck, 1981]. A different formulation, using essentially the same physics but with a moving coordinate system and different numerical methods, is described in [ARSRP, 1982b] for use in sodium concrete interaction codes.

No existing core/concrete interaction code employs the full USINT model. Resolution of the detailed concrete response would require a node spacing of no more than about one centimeter. The SINTER module, which is the pool model in CONTAIN, [Senglaub et al., 1981] does include the water-migration portion. However, SINTER is strictly one-dimensional, so that only a single solution is required, and

is typically run with a coarse mesh (tens of centimeters per node). Without modification to employ a moving mesh, hundreds of nodes would be required to follow recession over days of interaction and meters of concrete. Solution of the full model, involving several equations and many variables at each nodal point, at a number of points in the cavity, would involve substantial storage and execution time.

An alternate approach is used in GROWS II.[Baker et al., 1978] The code solves a transient heat conduction equation with an effective heat capacity "which takes account of the heat effects in concrete" and an effective thermal conductivity "which takes account of the heat transport effects of moisture migration." The solution technique involves a rezoning of the calculation mesh at each time step so that nodal points follow isotherms. The effective properties of concrete were determined by fitting experimental data; the range of applicability is unknown.

The physics modeled by these codes affects both heat transfer and the release rate for concrete-decomposition gases. The experiments and analysis of Muir, [Muir, 1977] and the additional analysis of Chu [Chu, 1978] suggest that the major effect is at small temperature rises, with a long, almost-isothermal plateau forming in the temperature profile at about 400 K. In particular, Chu demonstrated that, for heat fluxes sufficient to produce ablation, the temperature profile above this temperature is consistent with classical ablation of a homogeneous material. Also, the analytic transient conduction solution for constant properties was found to give temperatures in "excellent agreement" with the GROWS II numerical solution for a nonablating case, if the constant properties were suitably chosen.[Baker et al., 1978] This suggests that, for heat transfer, the classic conduction solutions for homogeneous materials with constant properties may well be adequate.

An obvious approach, which is employed in GROWS II, is to calculate the temperature response from simple conduction, and assume that the various gases are released as critical temperatures are reached. However, Muir's analysis showed that the low-temperature plateau region was still growing after several hours, at the $t^{1/2}$ rate associated with transient conduction, whether ablation was occurring or not. Comparison of these experimental results and analysis with the USINT model suggests very strongly that the temperature plateau corresponds to a "wet zone" in the concrete, where pores are partially or completely filled with liquid water. This water appears to arise primarily from adsorbed and interstitial water which has been freed from the matrix but not vaporized, and which is being driven away from the heated surface by internal pressures. There may also be a contribution from condensation of chemically bound water, released at higher temperatures nearer the surface and driven

deeper by pressure of evolving carbon dioxide, although the released USINT code cannot show this. The effect of this water migration (after the initial temperature profile is established) is then primarily to delay its release.

None of the codes INTER, [Murfin, 1977] CORCON, [Muir et al., 1981] and WECHSL [Reimann and Murfin, 1981] includes a water migration model. Of the three, only INTER appears to employ any approximation for time-dependent heat transfer. The other two codes assume a pseudo-steady temperature profile and employ a simple heat balance at the concrete surface

$$q = \rho_c \Delta H_a dX_a/dt \qquad (3.5.3\text{-}69)$$

where q is the net heat flux to the concrete
ρ_c is the density of concrete
Δh_a is the ablation enthalpy of concrete, a material property
and x_a is the position of the concrete surface.

The heat flux q must, of course, be reconciled with the melt/concrete heat transfer model of Section 3.5.3.2.4. In general, this will involve an iteration to determine the temperature of the pool side of the interfacial gas film, allowing for the fact that the thermal resistance of that film may depend on the gas generation which results from the ablation. We emphasize that tne pseudo-steady temperature profile, which is used to justify Equation (3.5.3-68), does not appear in it. The codes ignore the sensible heat and chemical energy (and changes in these quantities) associated with the temperature profile. This could be included in a relatively simple way. The pseudo-steady temperature profile is

$$T = T_o + (T_a - T_o)\exp\left(-\frac{dX_a}{dt}\,\frac{X-X_a}{\kappa}\right) \qquad (3.5.3\text{-}70)$$

where T is temperature, with subscripts o and a referring to initial temperature and ablation temperature, respectively
and κ is the thermal diffusivity of the concrete.

If the energy associated with this profile is calculated (by integration) and its rate of change included in the energy balance, Equation (3.5.3-69) is replaced by

$$q = \rho_c \Delta H_a \left[\frac{dX_a}{dt} - \kappa\,\frac{d^2X_a/dt^2}{(dX_a/dt)^2}\right] \qquad (3.5.3\text{-}71)$$

which is second order in time rather than first. This approach has never been tried, however, and MELCOR may not be an appropriate place to do so.

As mentioned previously, INTER employs a model which attempts to account for transient conduction. The energy balance, Equation (3.2.3-69), is replaced (for plane geometry) by

$$q = \rho_c \Delta H_d dX_a/dt + k_c(T_a-T_o)/\delta_c \qquad (3.5.3\text{-}72)$$

where ΔH_d is the enthalpy of decomposition (chemical and melting) of the concrete
k_c is its thermal conductivity
and δ_c is thickness of the preheated thermal layer in the concrete.

The second term models thermal conduction into the concrete. The velocity of the thermal penetration front is calculated as

$$d(X_a+\delta_c)/dt = 0.72k/\delta_c \qquad (3.5.3\text{-}73)$$

"by analogy [with] the advance of the thermal front into a slab of material, one face of which is maintained at a fixed temperature."[Murfin, 1977] Equations (3.5.3-72) and (3.5.3-73) are solved simultaneously, while matching the heat flux from the pool through the gas film. We note that at steady state, the requirement

$$d\delta_c/dt = 0 \qquad (3.5.3\text{-}74)$$

leads to

$$q = \rho_c \left[\Delta H_d + C_p(T_a-T_o)/0.72\right] dX_a/dt \quad . \qquad (3.5.3\text{-}75)$$

This is not consistent with Equation (3.5.3-69) for normal definitions of the material properties.

Both CORCON and WECHSL use the resulting pseudo-steady model for generation of decomposition gases; that is, the mass generation rate of each gas is taken as its partial density in the concrete times dX_a dt. INTER appears to do the same thing. Gas released in advance of the thermal front is thus ignored. It could be included by assigning a

(fixed) temperature for the release of each component, and finding the position of the release front from the pseudo-steady temperature profile, Equation (3.5.3-70). One would have to determine the relative magnitudes of this effect and the effects of water migration to determine if it would be worth considering.

If, at very late times, the heat fluxes were to fall below the threshold for ablation, this model would predict no gas generation unless the quasi-steady-ablation temperature profile were replaced by a transient-conduction profile (or, perhaps, an integral approximation to it as suggested in [LWRSRP, 1981 (a)]). However, it has been argued [LWRSRP, 1982] that this will not occur for many days for most accidents involving a large fraction of the reactor core.

We recommend that a pseudo-steady heat-transfer model be used in the first version of MELCOR, and advise against including a water migration model. The heat content and the decomposition of the concrete ahead of the ablation front should probably be included. In particular, the code should be structured so that the pseudo-steady approximation is not deeply "built in" through an implicit assumption that the concrete recession rate and the various gas geration rates are all proportional to the heat flux.

3.5.3.2.7 Chemical Reactions

The principal chemical reaction involved in core/concrete interactions is the oxidation of metals in the pool by the concrete-decomposition gases, water vapor, and carbon dioxide, which are themselves reduced, primarily to hydrogen and carbon monoxide. The CORCON code [Muir et al., 1981] was intended to include a second reaction, the reduction of oxides at the pool surface by the oxygen-poor atmosphere above the melt; this feature has been tested, but is not operational in released versions of the code. The INTER code [Murfin, 1977] and the WECHSL code [Reimann and Murfin, 1981] both allow for oxidation of metallic zirconium by contact with iron oxide at the metal/oxide interface, referred to as a "thermite reaction."

The simplest treatment of the metal/gas interaction is in INTER, which considers only a subset of the possible reactions, limited to

$$Zr + 2H_2O \rightarrow ZrO_2 + 2H_2 \qquad (3.5.3\text{-}76)$$

$$2Cr + 3H_2O \rightarrow Cr_2O_3 + 3H_2 \qquad (3.5.3\text{-}77)$$

$$Fe + H_2O \rightarrow FeO + H_2 \qquad (3.5.3\text{-}78)$$

$$Ni + H_2O \rightarrow NiO + H_2 \qquad (3.5.3\text{-}79)$$

$$Fe + CO_2 \rightarrow FeO + CO \quad . \qquad (3.5.3\text{-}80)$$

The water-gas reaction

$$CO_2 + H_2 \rightleftharpoons CO + H_2O \qquad (3.5.3\text{-}81)$$

is not considered. All reactions are assumed to go to completion, limited by several rather arbitrary expressions defining the "availability" of gases and metals for reaction. The order in which competing reactions occur is not completely defined in the reference. The heats of reaction are given as linear functions of temperature, cited without reference.

The WECHSL code includes the reactions

$$Zr + 2CO_2 \rightarrow ZrO_2 + 2CO \qquad (3.5.3\text{-}82)$$

$$2Cr + 3CO_2 \rightarrow Cr_2O_3 + 3CO \qquad (3.5.3\text{-}83)$$

in addition to Equations (3.5.3-76), (3.5.3-77), (3.5.3-78), and (3.5.3-80). Oxidation proceeds in the order: zirconium, chromium, iron. The neglect of nickel oxidation is seldom important because it would occur after iron and the iron is almost never depleted. All reactions are assumed to go to completion (without "availability factors") except for the oxidation of iron, as shown in Equations (3.5.3-78) and (3.5.3-80). For these, equilibrium constants are given by

$$\log_{10}\left[\frac{P(H_2)}{P(H_2O)}\right]_{Fe,FeO} = 0.04 + 301.5\ K/T \qquad (3.5.3\text{-}84)$$

$$\log_{10}\left[\frac{P(CO)}{P(CO_2)}\right]_{Fe,FeO} = 1.25 - 854.3\ K/T \qquad (3.5.3\text{-}85)$$

where P(x) denotes the partial pressure of chemical species x in the final state. If the gases are ideal, the ratio of

partial pressures is equal to the ratio of molar concentrations. The WECHSL report states that the water-gas reaction is neglected because "it is assumed that each bubble contains a single gas constituent." In fact, if the metal being oxidized is iron, it is effectively included because of the reactions

$$CO_2 + H_2 + Fe \rightleftharpoons CO + H_2 + FeO \rightleftharpoons CO + H_2O + Fe \quad . \tag{3.5.3.86}$$

If the assumption of complete reaction were dropped for the other metals, the water-gas reaction would be fully included. The form used for heats of reaction is not given in the reference.

The most detailed treatment is in CORCON, which employs an in-line chemical equilibrium routine to determine the products of the reaction which occurs during each time-step. This routine, which is fully described in [LWRSRP, 1982], performs a constrained minimization of the Gibbs function for 38 species composed of 11 elements. Because the metallic reactants and oxidic products are treated as mechanical mixtures, with entropy-of-mixing and heat-of-solution terms neglected in their chemical potentials, the metals are oxidized to depletion in the order zirconium, chromium, iron, nickel. Although the formulation in terms of the Gibbs function obviates the necessity of considering specific reactions, the reaction products calculated will be in equilibrium with respect to all of the reactions above, including the water-gas reaction. Small, probably negligible, amounts of various hydrocarbons are produced, and the occurrence of "coking" (reduction of carbon monoxide to elemental carbon) is sometimes predicted. The latter reaction is thought to be very sensitive to the chemical potentials used, and we are not sure whether it will actually occur in the real world. This treatment requires an equation of state, including entropy, on a chemical absolute basis, that is, referred to the separated elements in their standard states. This is necessary to evaluate the chemical potentials of the species. It also allows heats of reaction to be evaluated directly from the difference in enthalpy of reactants and products . . . in fact, the concept of heat of reaction need never arise in the equations. The minimization routine, which is now believed to function reliably, has in the past been responsible for a highly disproportionate share of trouble in the development of CORCON. It still consumes nearly one third of total execution time. For the purposes of PRA work, it is almost certainly overkill.

A reasonable compromise would be to consider the oxidation of the metallic elements in the order, zirconium, chromium, iron, nickel, using equilibrium constants similar to Equations (3.5.3-84) and (3.5.3-85) for all the oxidation reactions. As noted above, the water-gas reaction is then implicitly accounted for. Expressions for the various equilibrium constants are almost certainly available in the literature, values could also be generated using the chemical equilibrium package in CORCON and fits produced for use in MELCOR. The same approach could be used for heats of reaction. If, however, the thermal equations of state used in MELCOR are computed on a chemical absolute basis, referred to the separated elements in their standard states, the need for heats of reaction vanishes. This produces enough simplification in the general energy bookkeeping that it should be seriously considered for MELCOR.

The zirconium/iron thermite reaction,

$$Zr + 2FeO \longrightarrow ZrO_2 + 2Fe \qquad (3.5.3\text{-}87)$$

is considered by INTER and by WECHSL. This reaction is assumed to take place at the interface between the metallic phase and the oxidic phase, with its rate controlled by the circulation in the layers which brings reactants to the interface. INTER assumes that the reaction proceeds with a time constant of 300 seconds. The WECHSL document says merely that it is "extremely rapid" and that "metallic zirconium will be depleted within a short period of time." The question is significant only if there are scenarios which lead to significant steel oxidation with substantial cladding remaining unoxidized. In this case, the analogous zirconium/chromium thermite reaction

$$3Zr + 2Cr_2O_3 \longrightarrow 3ZrO_2 + 4Cr \qquad (3.5.3\text{-}88)$$

should probably also be considered. INTER's use of a simple time constant seems arbitrary, but may be adequate. In fact, it might be sufficient to consider these reactions as occurring during the process of formation of the pool so that either the metallic phase contains no zirconium or the oxidic phase contains no steel oxides.

The importance of the reaction between surface oxides and the atmosphere, which is included in the CORCON structure, is unknown. We suggest that it be allowed for in the structure of MELCOR, but not modeled in the first version.

3.5.3.2.8 Mass Transfer and Associated Heat Effects

The mass-transfer model used in the CORCON code [Muir et al., 1981] is typical of current codes and suitable for MELCOR. The masses and enthalpies of all pool layers are updated for mass transfer and associated heat transfer in two passes. It is extremely convenient to include chemical reactions in the same calculational structure, because these reactions affect the nature of transferred masses. The first pass, upward through the pool, follows the rising gases and rising condensed-phase materials from concrete decomposition or melt/gas reactions. The direction of motion is, of course, determined by the density relative to the local layer material. The compositions and enthalpies of these rising materials are followed and modified for chemical reactions, with any heat of reaction being added to the layer involved. The materials are thermally equilibrated with any layers they pass through, and their energy is ultimately added to the layer where they remain. This is taken as the first oxide-containing layer encountered for oxides, the first metal-containing layer for metals, and the atmosphere for gases. In the context of MELCOR, these gases pass through the pool-surface interface and become a source to above-pool modules. A second, downward, pass is similar, following any material entering the pool from above and sinking reaction and concrete ablation products.

Figures 3.5.3-6 through 3.5.3-8 show this in more explicit detail as implemented in CORCON. In these figures, Q denotes thermal equilibration, M/G refers to the metal/gas oxidation reaction, and O/A to an oxide/atmosphere reduction reaction included in the code structure but disabled in released versions. The "mixture" layers, containing heterogeneous mixtures of metals and oxides, are also present in the code structure but disabled. The total heat capacity of a layer is assumed to be much greater than that of materials passing through it so that thermal equilibration takes place at the start-of-timestep layer temperature. The associated change in layer enthalpy is simply

$$\Delta H_L = H(m_{in}, T_{in}) - H(m_{out}, T_{out}) \qquad (3.5.3\text{-}89)$$

where H is enthalpy
T is temperature
m is mass (including composition)
and the subscripts L, in, and out refer to the layer, to material entering it, and to material leaving it, respectively.

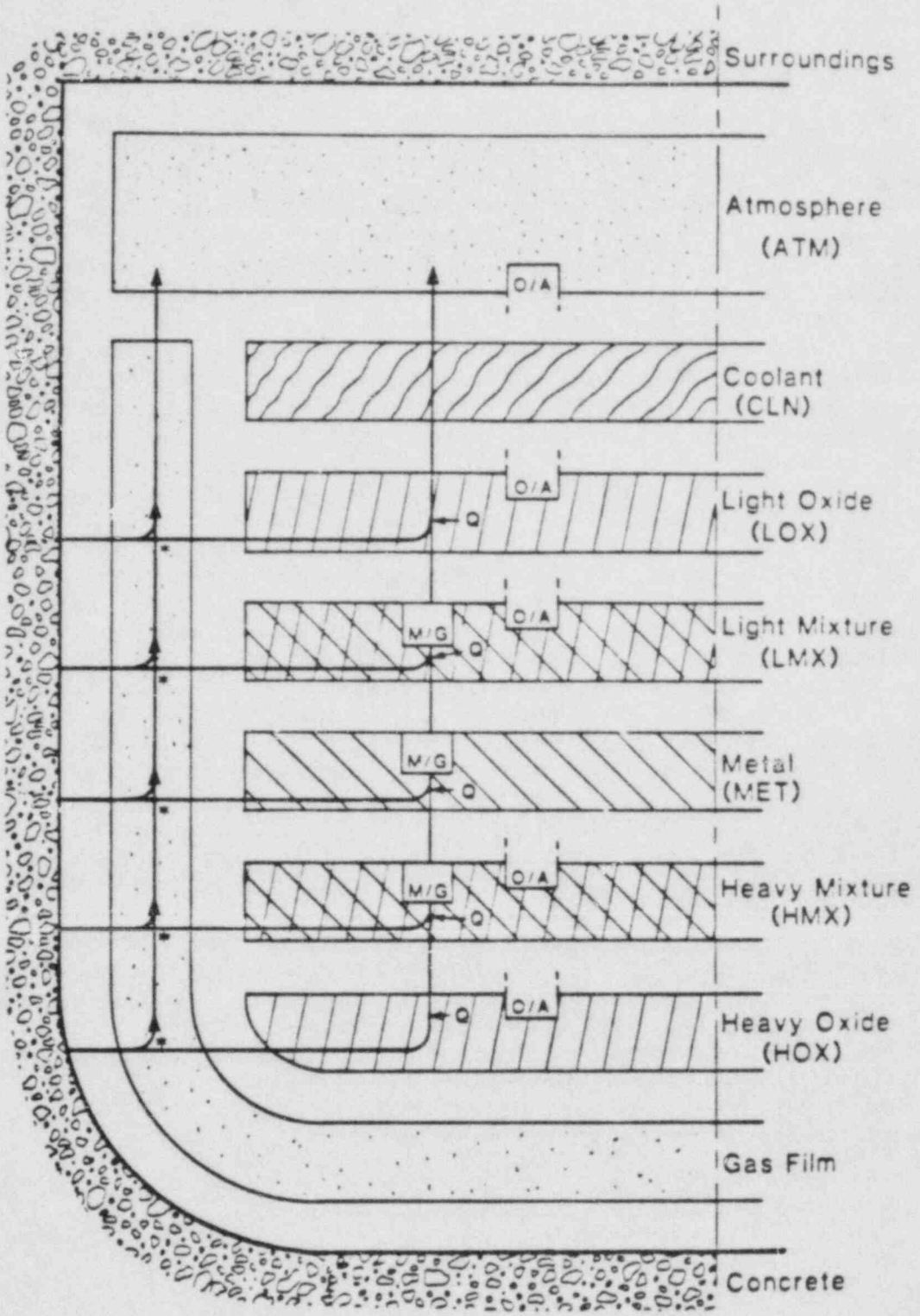

Whether gas enters the pool or rises up through the gas film at each * is determined by the local surface inclination angle. Q in the pool layers denotes thermal equilibration.

Figure 3.5.3-6. Path of Gas through Pool

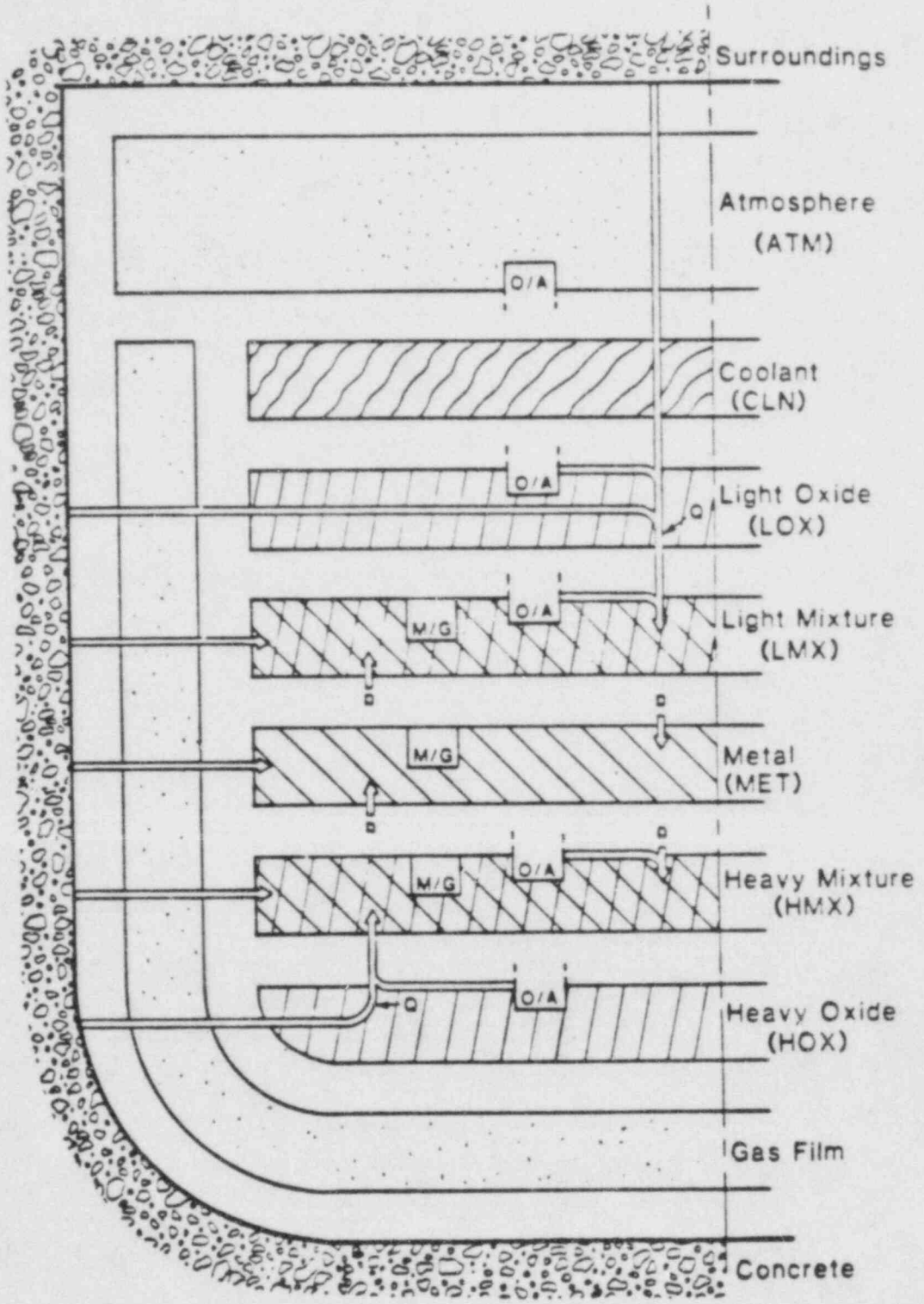

Figure 3 5.3-7. Path of Metal through Pool

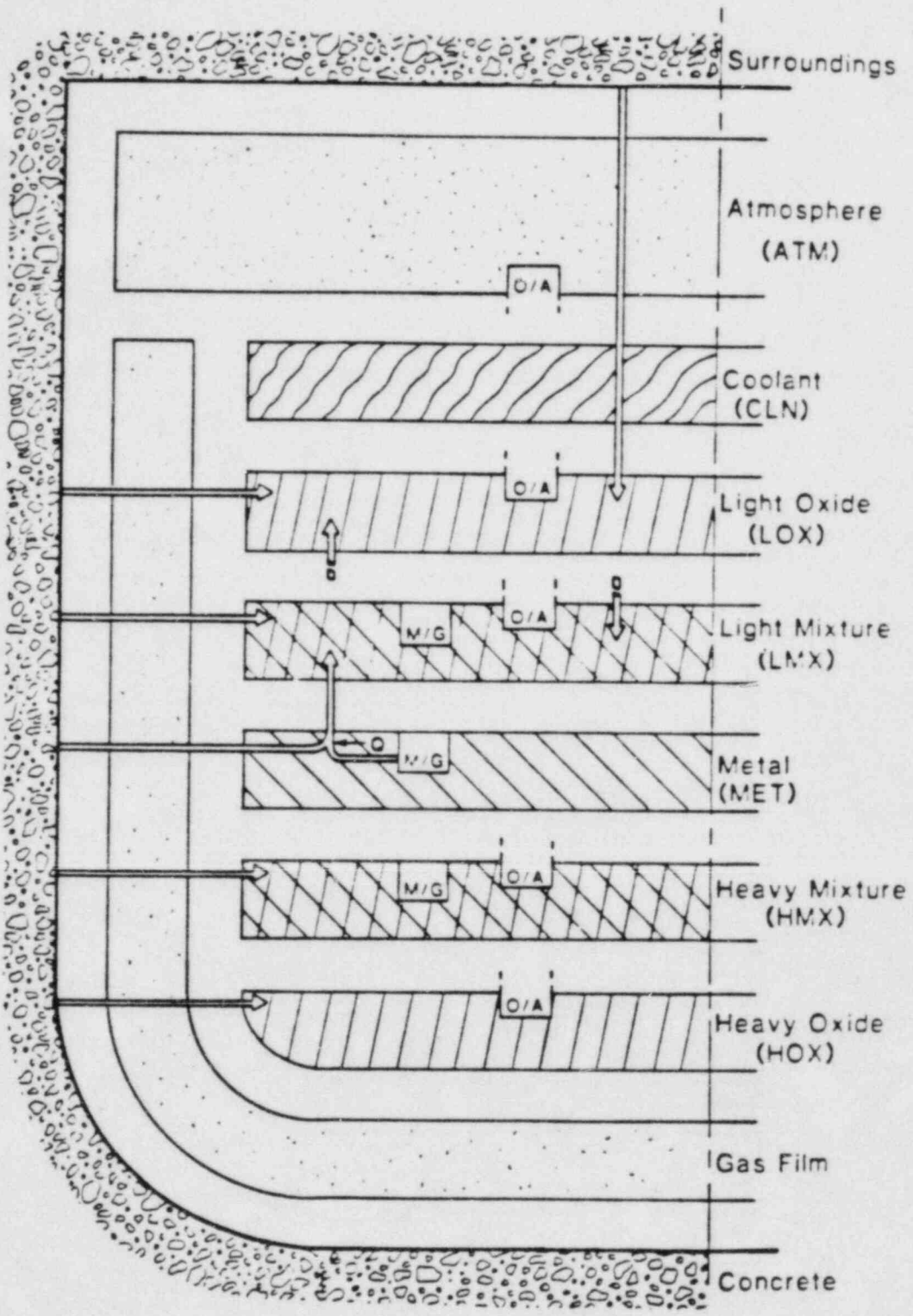

Figure 3.5.3-8. Path of Oxide through Pool

If enthalpies are on a chemical absolute basis, referred to the separated elements in their standard states, this equation will also hold including the effects of chemical reactions. If, for example, the composition of the gas which leaves the layer differs from that of the gas which entered, the the entire energy effect is accounted for through the different compositions associated with m_{out} and m_{in}.

3.5.3.2.9 Energy Conservation

The energy equation to be solved for each layer of the pool is simple, obvious, and essentially the same for all current models:

$$H_i^{n+1} = H_i^n + \Delta H_{enter\ i} - \Delta H_{leave\ i} + \Delta H_{react\ i} + \Delta H_{source\ i} - Q_{abl\ i} + Q_{Bi} - Q_{Ti} \quad . \qquad (3.5.3.90)$$

Here H_i^n is the total enthalpy of layer i at time level n

$\Delta H_{enter\ i}$ is the enthalpy of materials entering during the time-step

$\Delta H_{leave\ i}$ is the enthalpy of materials leaving during the time-step

$\Delta H_{react\ i}$ is the enthalpy gain from chemical reactions

$\Delta H_{source\ i}$ is the enthalpy gain from decay heat sources

$Q_{abl\ i}$ is the heat loss to ablate concrete

Q_{Bi} is the heat transferred from the bottom surface (zero for the bottom layer where this is part of Q_{abl})

and Q_{Ti} is the heat transferred to the top surface.

As discussed in Section 3.5.3.2.8, the second through fourth terms on the right-hand side are naturally associated, and the fourth disappears with the proper choice of reference point for enthalpies. These terms are most easily calculated as discrete changes, involving all of the material which moves during a time-step as the result of concrete ablation. None of the codes considers residence times . . . all materials which result from ablation are assumed to reach their final resting place during the same time-step.

Decay heat power changes slowly. Therefore, the corresponding term is evaluated explicitly (in the numerical methods sense) as a beginning-of-timestep power times Δt. The remaining three terms involve heat flows which are driven by temperature differences. In INTER [Murfin, 1977] and WECHSL, [Reimann and Murfin, 1981] these terms are also computed explicitly. The result is that small time steps may be required for numerical stability, particularly if a small layer is involved. In CORCON, [Muir et al., 1981] the heat loss to concrete is evaluated explicitly, but the remaining terms are treated using a linearized-implicit algorithm. These terms involve the axial heat-flows to the upper and lower surfaces of the layer (with the exception of the bottom layer for which the lower surface is adjacent to concrete), and are taken as a weighted average of the values at time n and the linearly-projected values at time n+1. This results in

$$H_i^{n+1} = H^{n+1(explicit)} + \Omega\Delta T\left[(\tilde{Q}_{Bi}^{n+1}-Q_{Bi}^{n}) - (\tilde{Q}_{Ti}^{n+1}-Q_{Ti}^{n})\right] \qquad (3.5.3.91)$$

where the tilde "~" denotes the linearized projection described below, and, of course, $H_i^{n+1(explicit)}$ includes the terms $(Q_{Bi}^{n}-Q_{Ti}^{n})\Delta t$. The implicitness factor Ω is ordinarily taken as 1.

In CORCON-MOD1, the heat fluxes are evaluated as heat-transfer coefficients times temperature differences, layer center to interface. Radiation is also included from the pool surface. Continuity of heat flux requires

$$q_{Ti} = h_{Ti}(T_i-T_I) = q_{Bi+1} = h_{Bi+1}(T_I-T_{i+1}) \qquad (3.5.3-92)$$

between layers and

$$q_{Ti} = h_{Ti}(T_i-T_I) = \sigma_B F\left(T_I^4-T_{surr}^4\right) + h_A(T_I-T_A) \qquad (3.5.3-93)$$

at the pool surface

where $q_{T(B)i}$ is the upward heat flux at the top (bottom) of layer i

$h_{kT(B)i}$ is the associated heat-transfer coefficient

T_i is the temperature of layer i

T_I is the interface temperature

σ_B is the Stefan-Boltzmann constant

F is the appropriate form factor

h_A is the heat-transfer coefficient from surface to atmosphere

T_A is the temperature of the atmosphere

and T_{surr} is the temperature of the surroundings.

These equations may be solved for the heat fluxes as functions of layer temperatures, and the terms in Equation (3.2.9-4) approximated as

$$\tilde{Q}_{Ti}^{n+1} - Q_{Ti}^{n} = A_{Ti}\left(\frac{\partial q_i}{\partial T_i}\,\Delta\tilde{T}_i + \frac{\partial q_{Ti}}{\partial T_{i+1}}\,\Delta\tilde{T}_{i+1}\right) \qquad (3.5.3\text{-}94)$$

where A_{Ti} is the interfacial area

$\Delta\tilde{T}_i$ is the linearized approximation to the change in the temperature of layer i during the time-step.

This is given by

$$\Delta\tilde{T}_i = (H_i^{n+1} - \hat{H}_i)/\hat{C}_i \qquad (3.5.3\text{-}95)$$

where $\hat{H}_i$ is the total enthalpy at temperature T_i^n of the contents of the layer at time n+1

and $\hat{C}_i$ is the corresponding heat capacity.

Equations (3.5.3-93) through (3.5.3-95) result in a set of linear equations for the layer enthalpies at time n+1, which are easily solved.

In the version of CORCON which will become MOD2, the more general heat-transfer relations resulting from crust formation and freezing are more complicated. The temperature at the lower surface of a layer, for example, may affect the heat flux at the upper surface. Furthermore, for a fixed T_{Bi}, dq_{Ti}/dT_{Ti} may not equal $-dq_{Ti}/dT_i$. An example of this occurs for a primarily molten layer with a thin crust: increasing the average temperature increases the liquid temperature and the heat flux to the crusted surface, while increasing the surface temperature merely decreases the crust thickness with little change in heat flux. While

the algebra is more complicated, the principle is the same, and we may write the energy equation in the form

$$\sum_j A_{ij}(H_j^{n+1}-H_j^n) = B_i + C_i(T_s^{n+1}-T_s^n) \qquad (3.5.3\text{-}96)$$

where T_s^n is the temperature of the pool surface at time n, which may be solved in the form

$$H_i^{n+1} = H_i^n + X_i^{(1)} + X_i^{(2)}\,(T_s^{n+1}-T_s^n) \quad . \qquad (3.5.3\text{-}97)$$

The heat flow at the top surface may also be put in the form

$$Q_s^{n+1} = Q_s^{(1)} + \frac{dQ_s}{dT_s}\,(T_s^{n+1}-T_s^n) \qquad (3.5.3\text{-}98)$$

which is the linearized pool response mentioned in Section 3.5.3.2.5. The final evaluation of layer enthalpies is left pending until after the end-of-timestep surface temperature is evaluated by the above-pool modules. This allows the implicit nature of the equations to be maintained across the pool surface even though above- and below-surface heat transfer are not evaluated simultaneously.

The stabilizing effect of the implicit algorithm makes it very attractive for use in MELCOR.

3.5.3.2.10 Bubble Phenomena

Gas which rises through the pool as bubbles influences heat transfer, as described in Section 3.5.3.2.2. In addition, the volume of the pool is inflated by the volume of the gas bubbles, a phenomena referred to as "level swell." This was not considered in INTER, [Murfin, 1977] but is treated by both CORCON [Muir et al, 1981] and WECHSL. [Reimann and Murfin, 1981] Both codes calculate a void fraction, the volume fraction of gases within the pool, which depends on the residence time of the bubble which is in turn determined by their rise velocity through the relation

$$\alpha = V_s/u_b \qquad (3.5.3\text{-}99)$$

where α is the void fraction
u_b is the bubble velocity
and V_s is the superficial velocity (volumetric flux) of gas through the pool.

In CORCON, the bubble velocity is assumed to be related to the terminal velocity of a single bubble in infinite fluid, U_T, by

$$u_b = (1-\alpha)^n U_T \qquad (3.5.3\text{-}100)$$

Wallis [Wallis, 1969] cites values of n=1 for ideal bubbly flow and n = -1 for churn-turbulent bubbly flow (note that his definition of n is different). In CORCON, the latter flow regime is assumed, resulting in

$$\alpha = V_s/(V_s + U_T) \qquad (3.5.3\text{-}101)$$

and α is limited to 0.42 as suggested by Blottner. [Blottner, 1979]

In WECHSL, Equation (3.5.3-101) is used with n taken as a function of the bubble Reynolds number,

$$Re_b = \rho_\ell r_e u_b/\mu_\ell \qquad (3.5.3\text{-}102)$$

where $\rho\ell$ is the density of the liquid
$\mu\ell$ is its viscosity
and r_e is the equivalent radius (based on volume) of the bubble.

The function used,

$$n = \begin{cases} 4.11-1.14 \log_{10}Re_b & , \quad Re_b \leq 50 \\ 3.05-0.52 \log_{10}Re_b & , \quad Re_b > 50 \end{cases} \qquad (3.5.3\text{-}103)$$

is stated to be based on a fit-to-data.[Le Clair and Hamielec, 1972] This does not permit a closed-form solution for α. We estimate that the values of n obtained from Equation (3.5.3-103) for typical bubble sizes (about a centimeter) and velocities (a few tenths of a meter per second) would range from about 3 in the metal down to about

1 in viscous slag. For $n > 0$, there is some value of V_s above which Equations (3.5.3-99) and (3.5.3-100) have no real solution. Because of this, Equation (3.5.3-100) is replaced by

$$u_b = \max\left[(1-\alpha)^n, 0.2\right] U_T \qquad (3.5.3\text{-}104)$$

and α is limited to be less than 0.55.

The terminal velocity of single bubbles is a function of their size and of fluid properties. There are several regimes. Among these, both CORCON and WECHSL consider small bubbles in Stokes flow, with terminal velocity

$$U_{T_1} = \frac{2}{9} \rho_\ell \, g r_e^{\,2} / \mu_\ell \qquad (3.5.3\text{-}105)$$

where g is the acceleration of gravity.

In WECHSL, the coefficient is 1/9, based on a higher friction factor attributed to Levich.[Levich, 1962] For larger bubbles, CORCON considers two regimes: medium sized bubbles, with terminal velocity

$$U_{T_2} = 1.53(ga)^{1/2} \qquad (3.5.3\text{-}106)$$

where a is the Laplace constant

$$a = [\sigma/g(\rho_\ell - \rho_g)]^{1/2} \quad ; \qquad (3.5.3\text{-}107)$$

and large, spherically capped bubbles for which the terminal velocity is

$$U_{T_3} = (g r_e)^{1/2} \quad . \qquad (3.5.3\text{-}108)$$

The terminal velocity is taken as

$$U_T = \min\left[U_{T_1}, \max\left(U_{T_2}, U_{T_3}\right)\right] \quad . \qquad (3.5.3\text{-}109)$$

WECHSL uses the terminal velocity

$$U_{T_4} = \left[g r_e + \sigma / \rho_\ell \, r_e \right]^{1/2} \qquad (3.5.3\text{-}110)$$

for large bubbles, which goes to U_{T_3} in the large-bubble limit. Regimes are combined as

$$U_T = \min \left(U_{T_1}, U_{T_4} \right) . \qquad (3.5.3\text{-}111)$$

Finally, both codes predict the size of bubbles entering the pool from the Taylor-instability bubbling model, which gives the form

$$r_e = Ca . \qquad (3.5.3\text{-}112)$$

Here CORCON uses C = 3.97 and WECHSL uses C = 2.74; either is probably satisfactory because, for these large bubbles, the terminal velocity is only weakly dependent on bubble size. In the development of CORCON, two other gas-velocity/bubble-size regimes were investigated: the analogs of nucleate and of patchy bubbling. They were rejected because the small bubble sizes predicted (on the order of 1 millimeter) did not agree with observation of prototypic melt/concrete experiments. In CORCON, the bubble size is recalculated at each layer interface, allowing for the effects of chemistry and the changes in temperature and pressure, but not for coalescence, and a layer average is used in the level-swell calculation.

The predictions of the two models for single-bubble terminal velocities, and comparison with experiment, is shown in Figures 3.5.3-9 and 3.5.3-10, respectively. The WECHSL form gives slightly better agreement, and is no more complicated. Its use is therefore recommended for MELCOR. When bubble interactions are included, the choice is less clear. The quite different values of n used by the two codes correspond to different assumed flow regimes. Both models are based on experimental correlations. The one in CORCON has been shown to give reasonable agreement with simulant experiments by Greene and Ginsberg [Greene and Ginsberg, 1982] as shown in Figure 3.5.3-11, and is simpler in form, not requiring solution of nonlinear equations. Therefore, we tentatively recommend its use in MELCOR.

The coding in CORCON calculates a gas flux and void fraction at many axial locations, and averages the results over

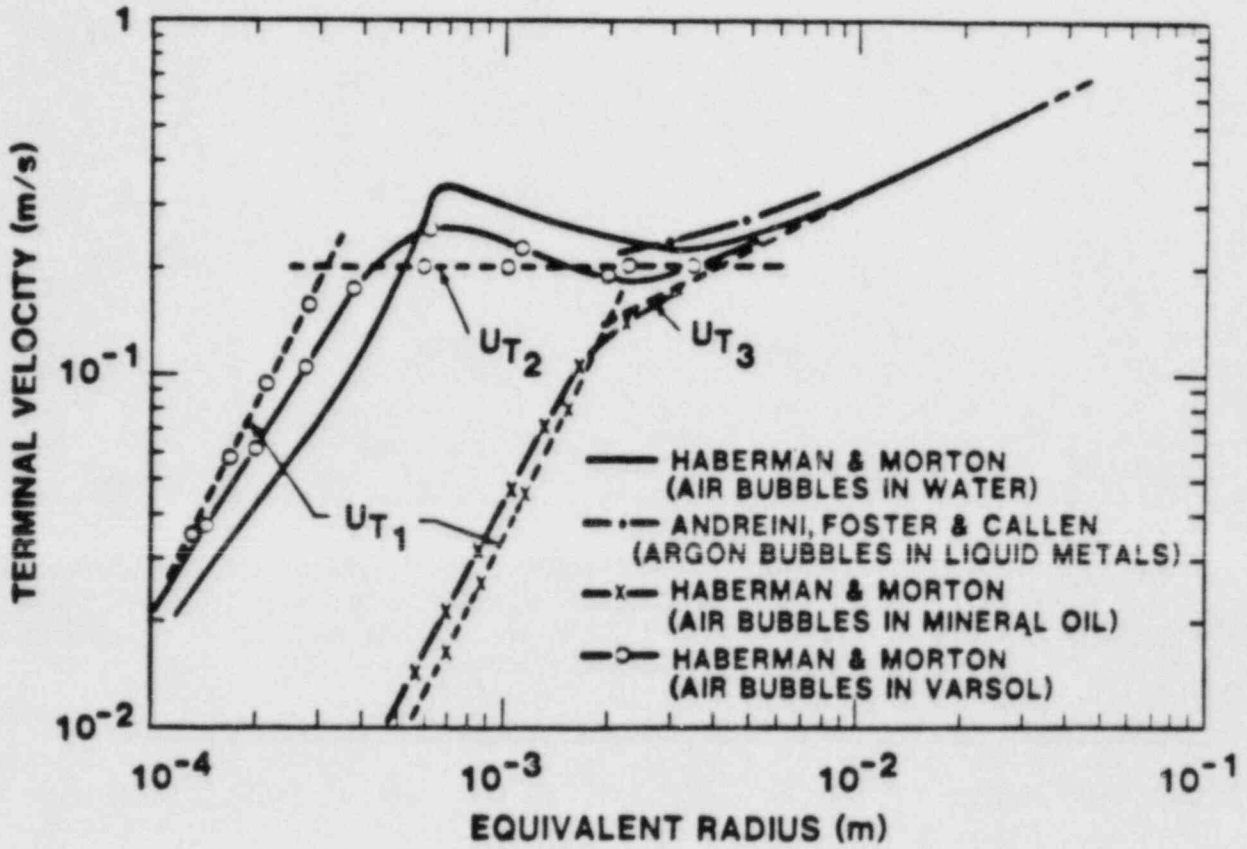

Figure 3.5.3.-9. Comparison of CORCON Bubble Velocity Model with Data

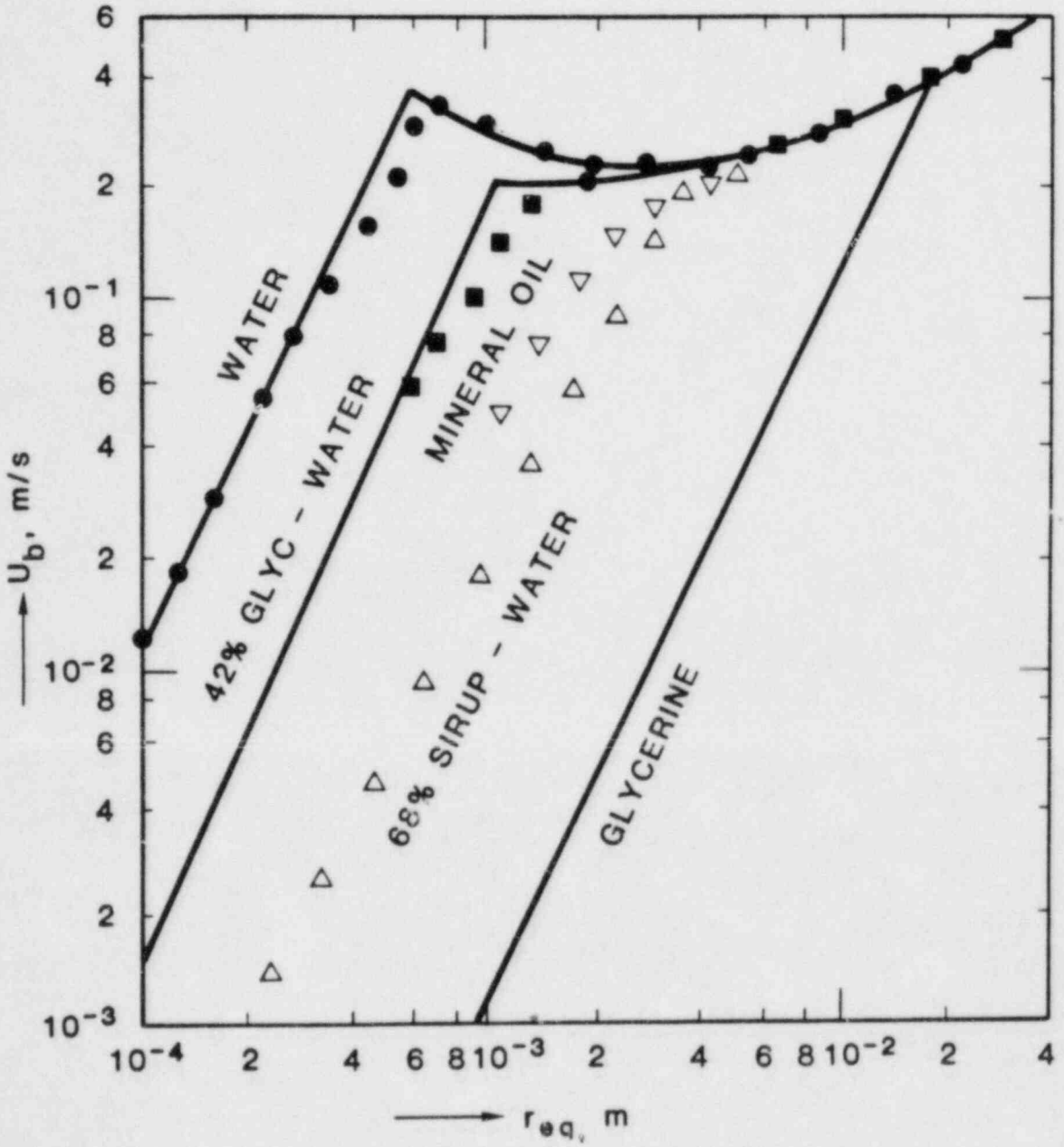

Figure 3.5.3.-10. Comparison of WECHSL Bubble Velocity Model with Data

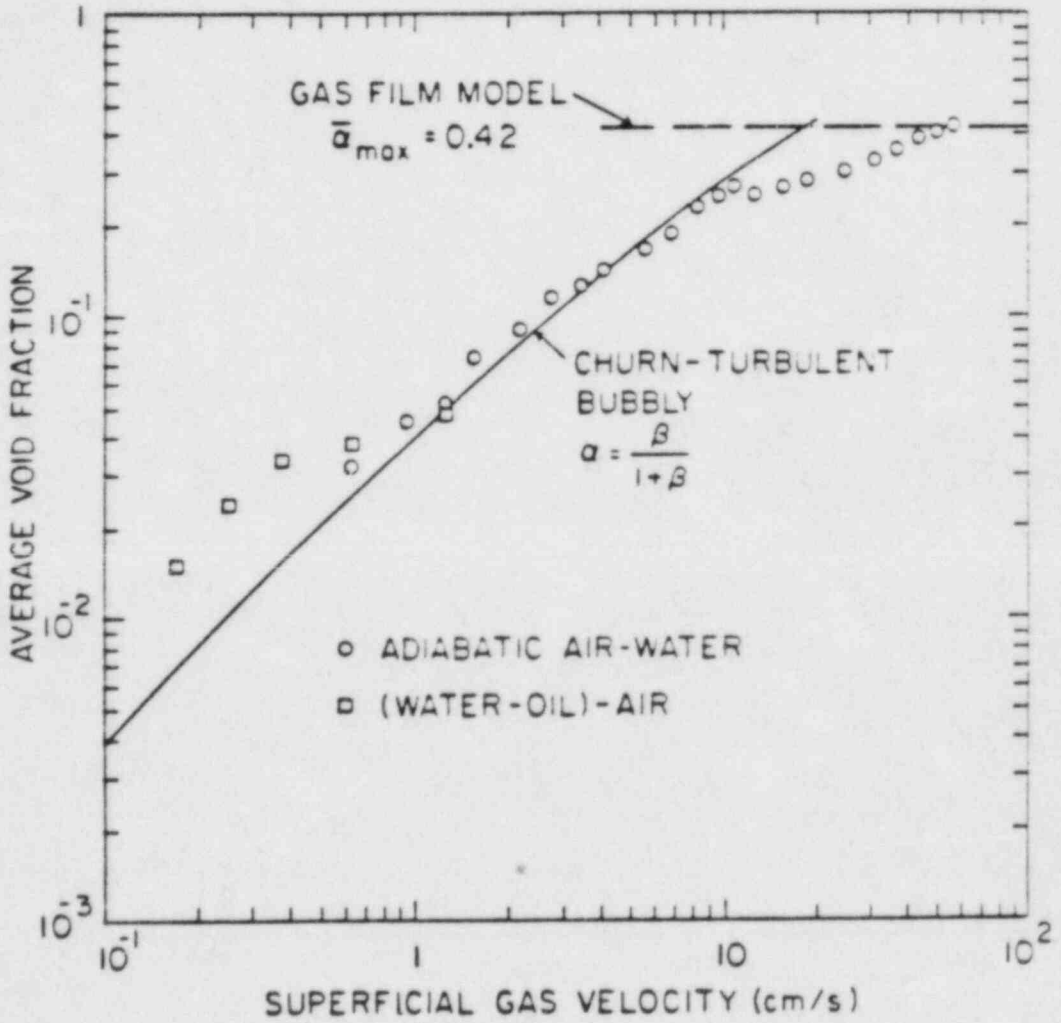

Figure 3.5.3.-11. Comparison of CORCON Void Fraction Model with Data

the pool layers. More suitable for MELCOR would be calculation of an average void fraction for each layer, based on an average volumetric gas flux. This flux could be defined as the average of the volumetric flows into and out of the layer, divided by an average cross-sectional area. The average cross-section might be taken as the layer volume divided by its height. If desired, the equations could be solved simultaneously (the layer volume depends on the void fraction), but use of start-of-timestep geometry, as is done in CORCON, would almost certainly be adequate.

3.5.3.2.11 Aerosol Generation

As gases from decomposition of concrete pass through the melt, aerosols are generated by mechanisms such as sparging and bubble bursting. The aerosols are observed in experiments, but mechanistic models of these processes are not now available, although one will be described in [Sprung et al., to be published]. None of the existing codes include aerosol generation, but their predictions of temperatures and gas flows have been used to estimate the generation through an empirical correlation [LWRSRP, 1980]

$$[A] = (33. + 240.V_s)\exp(-19000\ K/T) \quad . \qquad (3.5.3\text{-}113)$$

Where [A] is the aerosol concentration (kg/m^3 STP)
T is the melt temperature (K)
and V_s is superficial gas velocity (m^3 STP/m^2s).

It must be emphasized that, following good chemists' traditions, both the superficial velocity and the concentration in this expression have been reduced to STP (standard temperature and pressure); melt temperature affects only the exponential activation term. This is unclear in the cited reference, but has been confirmed by Powers.[Powers, 1983]

The correlation does not include effects of pool composition, nor does it predict where the material will come from in a multi-layered pool. Without this information, complete modeling is not possible. At early times, aerosol may be generated at rates of tonnes per day. Fortunately, while this is large from the point of view of the atmosphere, it will have a small effect on pool inventories for many days, and generation rates fall with time as temperatures and gas flows decrease. Therefore, the current practice of neglecting to charge aerosol masses against the pool inventory, so that they appear "from nowhere" at the pool surface, is a reasonable approximation. We suggest that the aerosol source be modeled in this way in the first version of MELCOR while maintaining, as far as possible, the option of a more complete model in later versions.

3.5.3.3 Material Properties

It is obvious that a wide range of thermophysical and transport properties must be known for calculation of the physical processes outlined in Section 3.5.3.2. In general, simple models have been used and found adequate . . . the real problem is often with availability of data. For example, assumption of a constant specific heat may well be adequate but even this much information is hard to find for some molten oxides. We do not intend to discuss material properties in great detail here. However, there are two cases where experience with CORCON may be significant in the choice of models. These are (1) calculation of the melting ranges of mixtures, and (2) calculation of the viscosity of oxidic (particularly siliceous) mixtures. These two subjects will be discussed briefly in the following subsections.

3.5.3.3.1 Melting Ranges

The situation for metallic mixtures is relatively clear. The metallic phase of the melt is mostly stainless steel. CORCON [Muir et al, 1981] uses a simple fit to the iron-chromium-nickel ternary phase diagram, given by [LWRSRP, 1981 b]

$$T^{\ell} = \min \begin{cases} 2130 - 510W_{Fe} - 1140W_{Ni}, \\ 1809 - 90W_{Cr} - 440W_{Ni}, \\ 1728 - 200W_{Cr} - 40W_{Fe}, \\ 1793 - 230W_{Cr} - 130W_{Ni} \end{cases} \qquad (3.5.3\text{-}114)$$

$$T^{s} = \min \begin{cases} 2130 - 730W_{Fe} - 3310W_{Ni}, \\ 1809 - 90W_{Cr} - 560W_{Ni}, \\ 1728 - 250W_{Cr} - 100W_{Fe}, \\ 1783 - 310W_{Cr} - 140W_{Ni}, \\ 1613 \end{cases} \qquad (3.5.3\text{-}115)$$

where T^{ℓ} is the liquidus temperature (K)
T^{s} is the solidus temperature (K)
and W_x is the weight fraction of element x.

As presently implemented, the presence of other elements is ignored, and the weight fractions of chromium, iron, and nickel are renormalized so that $W_{Cr} + W_{Fe} + W_{Ni} = 1.0$. This model was also adopted for use in WECHSL.[Reimann and Murfin, 1981] The ternary surfaces are shown in Figure 3.5.3-12. Note that although the temperatures in the equations are Kelvin, those in the figure are Centigrade.

The use of this model rather than a single melting point

or range for "stainless steel" is justified because the temperatures involved are not far from the ablation temperature of some concretes and change with time as oxidation changes the composition of the metallic phase. The neglect of zirconium is relatively unimportant because it is oxidized out of the melt in a relatively short time and at high temperatures. The effect of carbon might be significant, but is not included.

Calculation of the melting range for the oxidic mixture is far more complicated. The major constituents of concrete, CaO, SiO_2, and Al_2O_3, form a very complicated ternary system (see, e.g., [CMER, 1977]). The fuel oxides, UO_2 and ZrO_2, appear to form a relatively simple system, but it is really a single line in the far more complicated uraniumoxygen-zirconium ternary system. Consideration of the complete phase diagram for concrete oxides plus fuel oxides would give a code developer nightmares. INTER [Murfin, 1977] used a rather involved system which based on choosing the lowest solidus and the highest liquidus temperatures from (fits to) the binary phase diagrams of all pairs of constituents not deemed to be traces. While this was the best model available at the time, it has little basis in reality. Both CORCON and WECHSL use an analytic formulation for a pseudo-binary system in which the fuel oxides (and CaO in WECHSL) form one "component" with concrete (not including CaO in WECHSL) and steel oxides forming the other. The two components are assumed to form ideal solutions in both liquid and solid phases. This results in implicit equations for the liquidus and solidus temperatures in the form

$$x_1 \exp\left[-\frac{\Delta H_1}{R_o}\left(\frac{1}{T_1^{\ell}}-\frac{1}{T^{\ell}}\right)\right] + x_2 \exp\left[-\frac{\Delta H_2}{R_o}\left(\frac{1}{T_2^{\ell}}-\frac{1}{T^{\ell}}\right)\right] = 1 \quad (3.5.3\text{-}116)$$

$$x_1 \exp\left[\frac{\Delta H_1}{R_o}\left(\frac{1}{T_1^{s}}-\frac{1}{T^{s}}\right)\right] + x_2 \exp\left[\frac{\Delta H_2}{R_o}\left(\frac{1}{T_2^{s}}-\frac{1}{T^{s}}\right)\right] = 1 \quad (3.5.3\text{-}117)$$

where x_i is the mole-fraction of component i
ΔH_i is its heat of fusion
T_1^{ℓ} and T_1^{s} are its liquidus and solidus temperatures
and R_o is the universal gas constant.

An example of the resulting phase diagram is shown in Figure 3.5.3-13 by the curves labelled "Ideal Solid Solution." The model used to derive these results is inconsistent with the observation [Westrich, 1982] of very limited solubility of fuel oxides in molten concrete materials. It also causes computational problems because of

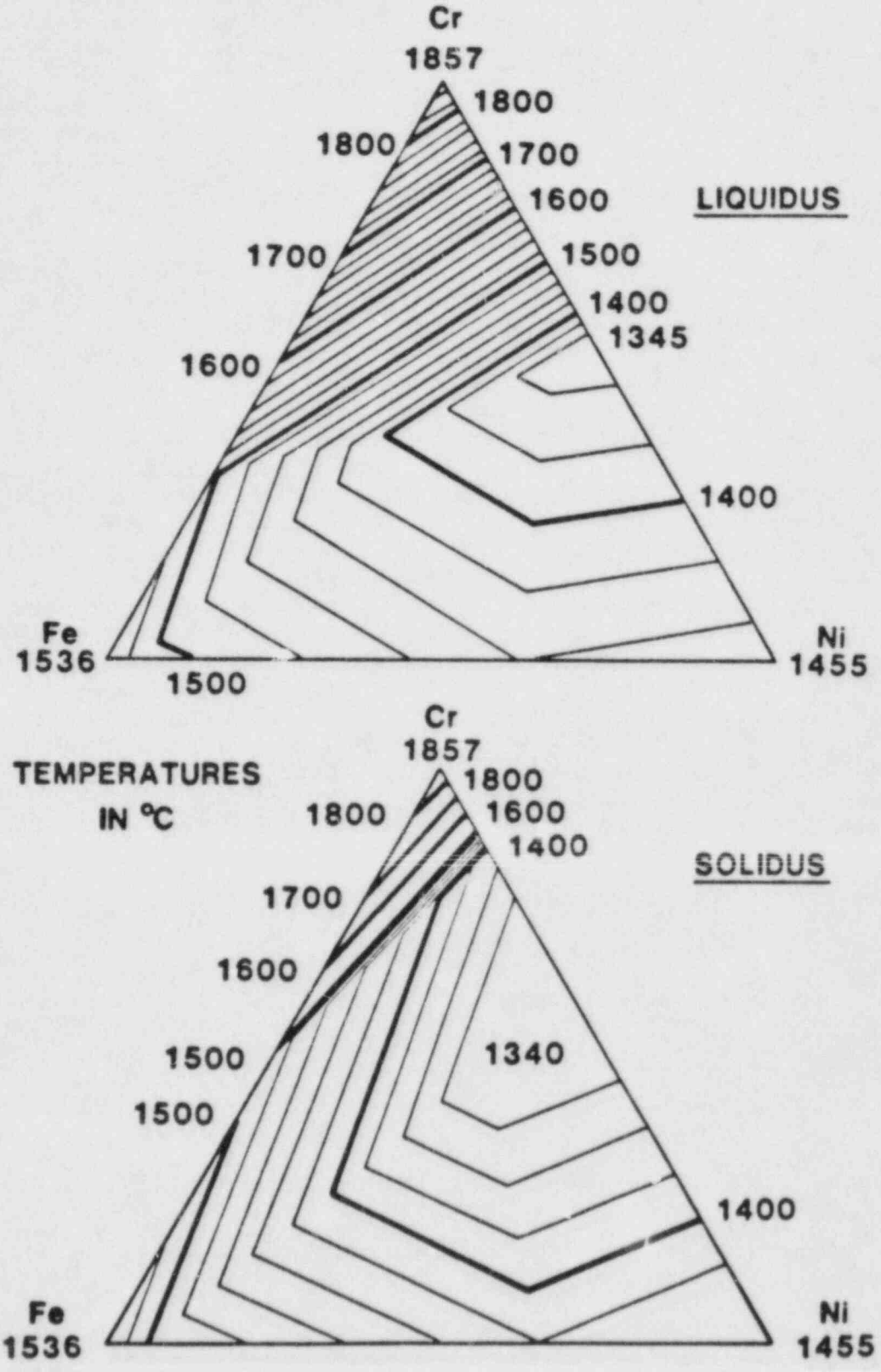

Figure 3.5.3-12. Liquidus and Solidus Temperatures for the Metallic Mixture

the high solidus temperature for almost pure fuel (in running CORCON, it has been found advisable to "salt" the initial fuel mixture with a small amount of iron oxide).

An alternative model may be derived by assuming no mutual solubility in the solid phase. This leads to the result

$$\frac{1}{T^{\ell}} = \min\left[\frac{1}{T_1^{\ell}} - \frac{R_o \ell n x_1}{\Delta H_1}, \frac{1}{T_2^{\ell}} - \frac{R_o \ell n x_2}{\Delta H_2}\right] \qquad (3.5.3\text{-}118)$$

$$T^{s} = \min\left[T_1^{s}, T_2^{s}, \min_{0 \le x \le 1} T^{\ell}\right] \qquad (3.5.3\text{-}119)$$

for which an example is shown as the curves labelled "Eutectic" in Figure 3.5.3-14. This form is not used in the existing codes, but should be considered for MELCOR. It does give "more reasonable" solidus temperatures for nearly pure fuel, but probably for the wrong reason: the initial fuel mixture is likely to be sub-stoichiometric in oxygen, which lowers its melting point.

3.5.3.3.2 Viscosity of Oxidic Mixtures

Approximately 90 percent of the decay heat generated in the pool appears in the oxidic phase, and is removed primarily by convective mechanisms. The corresponding heat-transfer coefficients are strongly influenced by the viscosity of the liquid (see Section 3.5.3.2.2). Viscosities of mixtures of refractory oxides are not well known, but values must be used in the codes. The problem is further complicated if significant amounts of silica are present because of the formation of long chains of strongly bonded SiO_4 tetrahedra, which can greatly increase the viscosity of a mixture. INTER avoided the problem; its "convective" heat-transfer relations do not involve viscosity at all. Both CORCON and WECHSL use models for siliceous mixtures which are based on the VISRHO model, [Powers and Frazier, 1977] which is in turn based on a correlation of geological data. [Bottinga and Weill, 1972] The correlation takes the form

$$\mu = 0.1 \exp[\Sigma_i x_i D_i] \qquad (3.5.3\text{-}120)$$

where x_i is the mole fraction of constituent i
and D_i is a coefficient which is tabulated as a function of temperature and silica content.

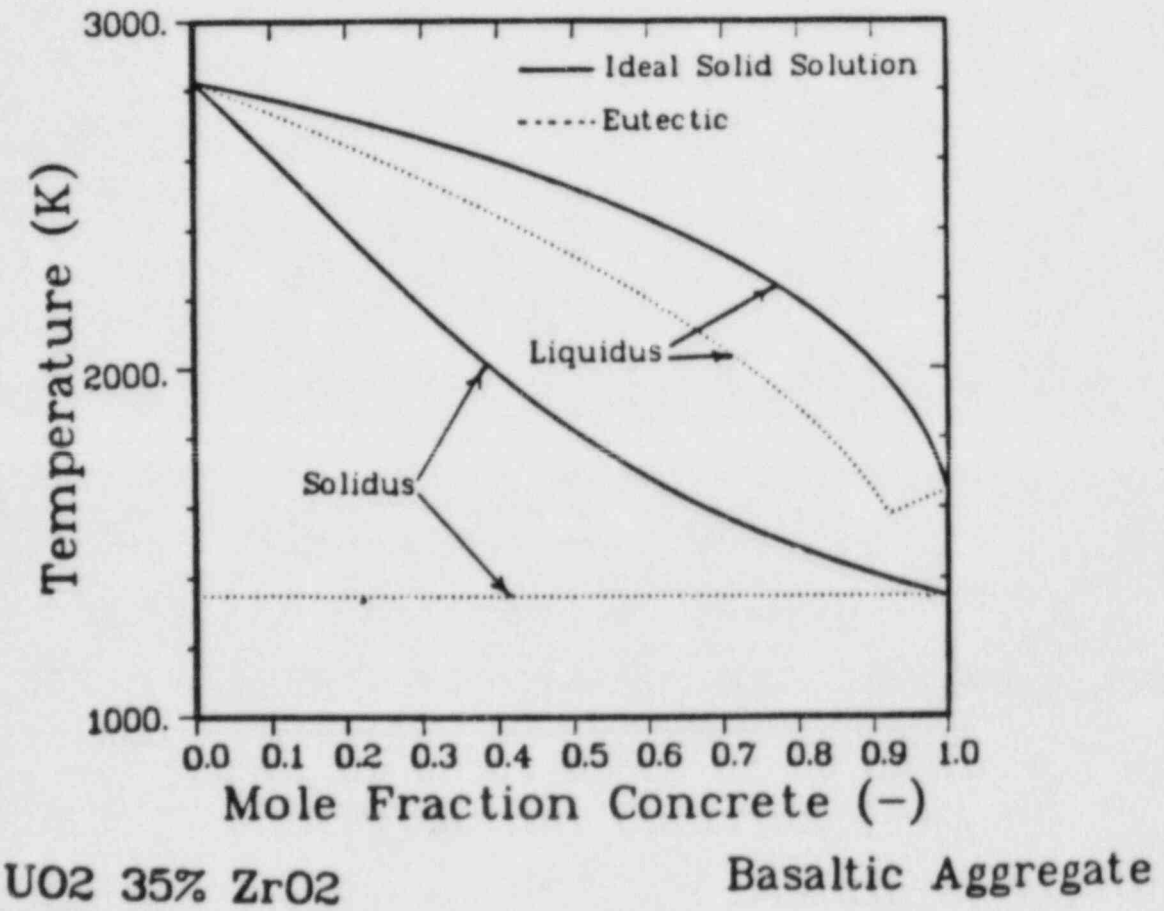

Figure 3.5.3-13. Liquidus and Solidus Temperatures for the Oxidic Mixture

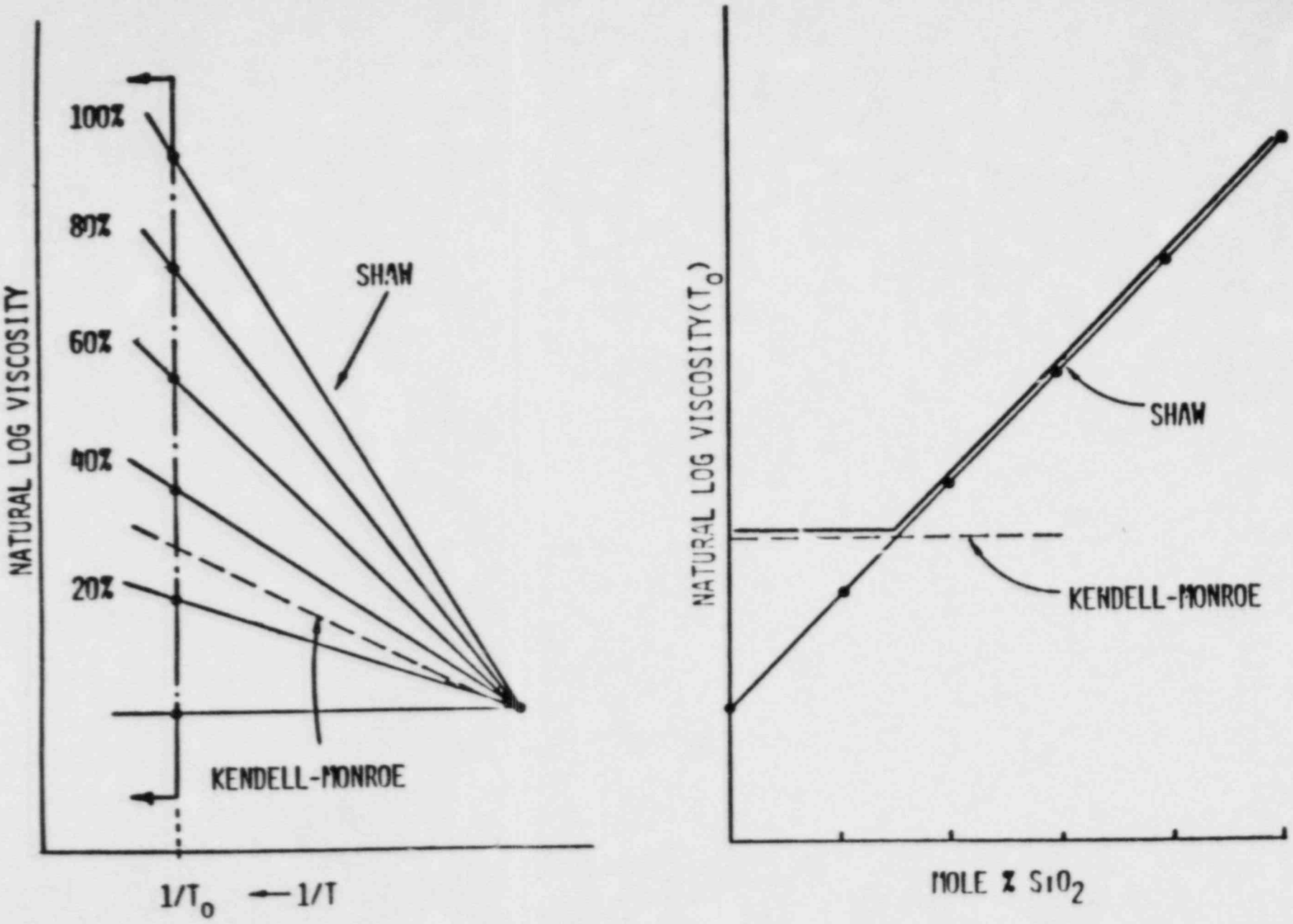

Figure 3.5.3-14. Coupling of Shaw and Kendell-Monroe Viscosity Models

In both codes, UO_2 and ZrO_2, which did not appear in the original correlation, are treated as equivalent to TiO_2. In WECHSL, each set of D_i has been fit in the form

$$D_i = A_i + B_i/T \qquad (3.5.3\text{-}121)$$

which provides interpolation and extrapolation as a function of temperature. As a function of silica content, they are interpolated within the table and extrapolated so as to match the appropriate limits. In CORCON, coefficients are interpolated as functions of temperature within the table and Equation (3.5.3-121) used for extrapolation only. No interpolation is made as a function of silica content, but an abrupt change made to a Kendell-Monroe expression [Kendell and Monroe, 1917] for mixture viscosity below 15 mole-percent silica.

$$\mu = \left[\sum_i X_i \, \mu_i^{1/3}\right]^3 \qquad (3.5.3\text{-}122)$$

where μ_i is the viscosity of pure constituent i.

In the WECHSL formulation, a two-phase slurry multiplier is applied of the Kunitz form [Kunitz, 1926] at low temperatures

$$\mu_{slurry} = \mu(1+\tfrac{1}{2}\Phi)(1-\Phi)^{-4} \qquad (3.5.3\text{-}123)$$

where Φ is the mass fraction of solids given by

$$\Phi = W_{Hi}(T^{\ell}-T)/(T^{\ell}-T^{s}) \qquad (3.5.3\text{-}124)$$

Here W_{Hi} is the weight fraction of the high melting constituents, UO_2, ZrO_2, and CaO.

As already mentioned, use of the VISRHO model for core-melt problems requires a large extrapolation from the original data base in composition. An extrapolation in temperature is often required also, because the maximum temperature for which coefficients were tabulated is 2073 K. The model was developed as a simple fit to data . . . no physics was included, and no extrapolation properties considered. This greatly reduces our confidence in the resulting estimates of viscosity. In particular, UO_2 and ZrO_2, which are major components of the melt, must be represented as

TiO_2, which is present only as a trace in geological materials. In the model, the contribution of TiO_2 to viscosity increases with increasing temperature, which may be reasonable for a trace material but is unphysical for a major component.

Therefore, the VISRHO model has been replaced in the version of CORCON which will become MOD2 by a simpler model suggested by Shaw.[Shaw, 1972] This model was generated as a fit to the Bottinga-Weill correlation, and was shown to give good agreement with it within the original data base. Its major advantage from our point of view (in addition to simplicity) is that good extrapolation properties are built in. The form is

$$\ell n\ \mu = S\left(\frac{10^4}{T} - 1.50\right) - 6.40 \quad . \qquad (3.5.3\text{-}125)$$

The constants are for viscosity in poise and temperature in Kelvin.

Here s is a function of mixture composition given by

$$s = \left(\sum n_i X_i s_i^{\,o} / \sum n_i\ X_i\right) X_{sio_2} \quad . \qquad (3.5.3\text{-}126)$$

The n_i and $s_i^{\,o}$ used in the code, including some defined by analogy with species listed by Shaw, are tabulated in Table 3.5.3-2.

As with Bottinga-Weill, this model is restricted to relatively high silica contents. In the code, it is matched to the low-silica Kendell-Monroe form by simply using the greater of the viscosities calculated from Equations (3.5.3-126) and from (3.5.3-122). This is illustrated graphically in Figure 3.5.3-14. The transition, where the two values are equal, is typically at a composition of 20 to 30 percent silica. This is suggestive of the orthosilicate point, below which silica chains are assumed to be absent.

Table 3.5.3.2

Parameters in the Shaw Viscosity Model

Species	n_i	s_i^o
TiO_2	1	4.5
FeO	1	3.4
MgO	1	3.4
CaO	1	4.5
Li_2O	1	2.8
Na_2O	1	2.8
K_2O	1	2.8
Fe_2O_3	2	3.4
Al_2O_3	2	6.7
UO_2	1	4.5
ZrO_2	1	4.5
Cr_2O_3	2	3.4

3.5.4 REFERENCES

1. Alsmeyer, H. and Reimann, M., "On the Heat and Mass Transport Processes of a Horizontal Melting or Decomposing Layer under a Molten Pool," Nuclear Reactor Safety Heat Transfer, Winter Annual Meeting ASME, Atlanta, GA, pp 47-53 (1977).

2. ARSRP, Advanced Reactor Safety Research Program Technical Highlights/Administrative Report for the NRC, Sandia National Laboratories, Albuquerque, NM, 1982a.

3. ARSRP, Advanced Reactor Safety Research Quarterly Report July-October 1981, SAND81-1529 (3 of 4), Sandia National Laboratories, Albuquerque, NM, 1982b.

4. Baker, Jr., L., et al., "Core Debris Penetration into Concrete," in Proceedings of the Third Post-Accident Heat Removal "Information Exchange," ANL-78-10, Argonne National Laboratory, Argonne, IL, 1978.

5. Baker, Jr., L., private communication, April 1983.

6. Beck, J. V., and Knight, R. L., Users Manual for USINT, SAND79-1694 Sandia National Laboratories, Albuquerque, NM, 1979.

7. Beck, J. V., Sensitivity Analysis for USINT-A Program for Calculating Heat and Mass Transfer in Concrete Subjected to High Heat Fluxes, SAND81-0026, Sandia National Laboratories, Albuquerque, NM, 1981.

8. Bennett, D. E., SANDIA-ORIGEN User's Manual, SAND79-0299, Sandia National Laboratories, Albuquerque, NM, 1979.

9. Benjamin, A. S., "Core-Concrete Molten Pool Dynamics and Interfacial Heat Transfer," in Proceedings of ANS/ASME/NRC Topical Meeting on Nuclear Reactor Thermal Hydraulics, NUREG/CP-0014, Vol 2, 1980.

10. Berenson, P. J., "Transition Boiling Heat Transfer from a Horizontal Surface," Journal of Heat Transfer, Vol 83, pp 351-358 (1961).

11. Berenson, P. J., "Experiments on Pool-Boiling Heat Transfer," International Journal of Heat and Mass Transfer, Vol 5, pp 985-999 (1962).

12. Blottner, F. G., Hydrodynamics and Heat Transfer Characteristics of Liquid Pools with Bubble Agitation, SAND79-1132, Sandia National Laboratories, Albuquerque, NM, 1979.

13. Bottinga, Y. and Weill, D. F., "The Viscosity of Magmatic Silicate Liquids: A Model for Calculation," American Journal of Science, Vol 272, pp 438-475 (1972).

14. CMER, Core-Meltdown Experimental Review, SAND74-0382 (Revised), Sandia National Laboratories, Albuquerque, NM, 1977.

15. Cole, Jr., R. K. and Kelly, D. P., to be published.

16. Chu, T. Y., Radiant Heat Evaluation of Concrete - A Study of the Erosion of Concrete due to Surface Heating, SAND77-0922, Sandia National Laboratories, Albuquerque, NM, 1978.

17. Dhir, V. K., Castle, J. N., and Catton, I. "Role of Taylor Instability on Sublimation of a Horizontal Slab of Dry Ice," Journal of Heat Transfer, Vol 99, pp 411-418 (1977).

18. Dhir, V. K., "Sublimation of a Horizontal Slab of Dry Ice: An Analog of Pool Boiling on a Flat Plate," Journal of Heat Transfer, Vol 102, pp 380-381 (1980).

19. Ginsberg, T. and Greene, G. A., "BNL Program in Support of LWR Degraded Core Accident Analysis," in Proceedings of the U. S. Nuclear Regulatory Commission Tenth Water Reactor Safety Research Information Meeting, NUREG/CP-0041 Vol 2, pp 364-395 (1983).

20. Greene, G. A., and Ginsberg, T., "BNL Program in Support of LWR Degraded Core Accident Analysis," in Proceedings of the U.S. Nuclear Regulatory Commission Ninth Water Reactor Safety Research Information Meeting, NUREG/CP-0024 Vol 3 (1982).

21. Greene, G. A., private communication, March 1983.

22. Kendell, J. and Monroe, K. P., "The Viscosity of Liquids III, Ideal Solutions of Solids in Liquids," Journal of the American Chemical Society, Vol 39, p 1802 (1917).

23. Kulacki, F. A. and Goldstein, R. J., Journal of Fluid Mech., Vol 55, p 271 (1975).

24. Kulacki, F. A. and Nagle, M. E., Journal of Heat Transfer, Vol 97, p 204 (1975).

25. Kulacki, F. A. and Emara, A. A., Trans ANS, Vol 22, p 447 (1975).

26. Kunitz, W., Journal of General Physiology, Vol 9, p 715 (1926).

27. Kutateladze, S. S. and Malenkov, I. G., "Boiling and Bubbling Heat Transfer under the Conditions of Free and Forced Convection," Sixth International Heat Transfer Conference, Toronto, Canada (1978).

28. Kwong, K. C., et al., CORCON Program Assistance, ACUREX Final Report FR-79-10/AS, ACUREX Corporation/Aerotherm Aerospace Division, Mountain View, CA, 1979.

29. Le Clair, B. P. and Hamielec, A. E., "Stromung Durch Teilchenansammelungen," in Kinetik Metallurgischer Vorgange bei der Stahlherstellung, Verlag Stahleisen, Dusseldorf (1972).

30. Levich, V. G., Physicochemical Hydrodynamics (New York, NY, 1962).

31. Lock, R. C., "The Velocity Distribution in the Laminar Boundary Layer Between Parallel Streams," Quart. Jour. Appl. Math., Vol 4, pp 42-63 (1951).

32. LWRSRP, Light Water Reactor Safety Research Program Quarterly Report, January-March 1976, SAND76-0369, Sandia National Laboratories, Albuquerque, NM, 1976.

33. LWRSRP, Light Water Reactor Safety Research Program Quarterly Report, January-March 1980, SAND80-1304/1 of 4, Sandia National Laboratories, Albuquerque, NM, 1980.

34. LWRSRP, Light Water Reactor Safety Research Program Quarterly Report, January-March 1980, SAND81-1216/1 of 4, Sandia National Laboratories, Albuquerque, NM, 1981a.

35. LWRSRP, Light Water Reactor Safety Research Program Quarterly Report, July-September 1980," SAND80-1304/3 of 4, Sandia National Laboratories, Albuquerque, NM, 1981b.

36. LWRSRP, Light Water Reactor Safety Research Program Semiannual Report, April-September 1981, SAND82-0006, Sandia National Laboratories, Albuquerque, NM, 1982.

37. LWRSRP, Light Water Reactor Safety Research Program Semiannual Report, October 1981-March 1982, SAND82-1572, Sandia National Laboratories, Albuquerque, NM, 1982.

38. McAdams, W. H., Heat Transmission (New York, NY: McGraw Hill, 1954).

39. Muir, J. F., Response of Concrete to a High Heat Flux on One Surface, SAND77-1467, Sandia National Laboratories, Albuquerque, NM, 1977.

40. Muir, J. F., et al., CORCON-MOD1: An Improved Model for Molten-Core/Concrete Interactions, SAND80-2415, Sandia National Laboratories, Albuquerque, NM, 1981.

41. Murfin, W. B., A Preliminary Model for Core/Concrete Interactions, SAND77-0370, Sandia National Laboratories, Albuquerque, NM, 1977.

42. Persh, J., A Procedure for Calculating the Boundary Layer Development in the Region of Transition from Laminar to Turbulent Flow, NAVORD Report 4438, 1957.

43. Powers, D. A. and Frazier, A. W., VISRHO: A Computer Subroutine for Estimating the Viscosity and Density of Complex Silicate Melts, SAND76-0649, Sandia National Laboratories, Albuquerque, NM, 1977.

44. Powers, D. A., et al., Exploratory Study of Molten Core Material/Concrete Interactions July 1975 - March 1977, SAND77-2042, Sandia National Laboratories, Albuquerque, NM, 1978.

45. Powers, D. A., private communication, 1980.

46. Powers, D. A., private communication, March 1983.

47. Reimann, M. and Murfin, W. B., "The WECHSL Code: A Computer Program for the Interaction of Core Melt and Concrete," KfK 2890, Kernforschungszentrum Karlsruhe, FRG, 1981.

48. Senglaub, M. E., et al., CONTAIN, A Computer Code for the Analysis of Containment Response to Reactor Accidents - Version 1A, SAND81-1495, Sandia National Laboratories, Albuquerque, NM, Draft Manuscript June 1981.

49. Shaw, H. R., "Viscosities of Magmatic Silicate Liquids: An Empirical Method of Prediction," American Journal of Science, Vol 272, pp 870-893 (1972).

50. Sprung, J. L., et al., Fission Product Behavior During Severe LWR Accidents: Phenomena Assessment, Sandia National Laboratories, Albuquerque, NM, to be published.

51. Szekely, J., "Mathematical Model for Heat for Mass Transfer at the Bubble-Stirred Interface of Two Immiscible Fluids," International Journal of Heat and Mass Transfer, Vol 6, pp 417-422 (1963).

52. Theofanous, T. G. and Saito, M. "An Assessment of Class-9 (Core-Melt) Accidents for PWR Dry-Containment Systems," Nuclear Engineering and Design, Vol 66, pp 301-332 (1981).

53. Wallis, G. B., One-Dimensional, Two-Phase Flow (New York, NY: McGraw Hill, 1969), p 55.

54. WASH-1400, Reactor Safety Study, NUREG-75-014, U.S. Nuclear Regulatory Commission, 1975.

55. Werle, H., "Modellexperimente zum Kernschmelzen," Halbjahresbericht 1978/1, PNS 4332 (1978).

56. Werle, H., "Einfluss eines Gasstroms auf den Warmeubergang zwischen zwei Flussigkeitsschichten" in PNS-Halbjahresbericht 1978/2, KfK 2750, Kernforschungszentrum Karlsruhe, FRG (1979).

57. Werle, H. "Enhancement of Heat Transfer Between Two Horizontal Liquid Layers by Gas Injection at the Bottom," KfK 3223, Kernforschungszentrum Karlsruhe, FRG (1981).

58. Westrich, H. R., "The Solubility of LWR Core Debris in Sacrificial Floor Material," Journal of Nuclear Materials, Vol 110, pp 224-332 (1982).

59. Wooton, R. O. and Avci, H. I. MARCH (Meltdown Accident Response Characteristics) Code Description and User's Manual, BMI-2064, NUREG/CR-1711, Batelle Columbus Laboratories, Columbus, OH, 1980.

3.6 CONTAINMENT ENGINEERED SAFETY FEATURES

by

P. E. Rexroth, S. E. Dingman,

and A. L. Camp

CONTENTS

LIST OF FIGURES

3.6.1 INTRODUCTION

If an LWR accident leads to rupture of the primary vessel, as will generally be the case for sequences studied with MELCOR, a variety of safety systems are potentially available to prevent or to delay and mitigate the effects of containment failure. The most common of these are designed to provide depressurization, and removal of heat and fission products from the atmosphere. Included in this category and considered in detail below are containment sprays, fan coolers, ice condensers, and pressure suppression pools. An auxiliary recirculation system is also available to provide a long-term source of cool water to the sprays. Requirements for modeling a recirculation system will be described. In addition to these depressurization systems various combinations of fans and filters may be present which provide for either removal of fission products or pressure equilibration or both. These will be treated in the next two sections. Finally, various methods for preventing or mitigating the results of hydrogen combustion have been implemented or proposed. These will be presented as a group in the last section.

3.6.2 CONTAINMENT SPRAYS

Containment sprays are a very important engineered safety system with the combined capacity to reduce the pressure rises from steam releases or hydrogen burns and to remove aerosols and soluble fission products from the containment atmosphere. Spray systems are composed of multiple nozzles mounted near the top of the main containment volume that deliver large quantities of water to the atmosphere in the form of small (0.1 to 1 mm) droplets. The initial water source is the refueling water storage tank. When this source nears exhaustion, water from the sump, having been cooled by passage through a heat exchanger, is recirculated through the nozzles. This section will deal primarily with the spray heat-transfer models, but will also include a brief discussion of gaseous fission product and aerosol washout modeling.

3.6.2.1 Phenomena

Containment sprays serve first of all to reduce the pressure rise following the injection of steam into the containment atmosphere during a loss of coolant accident (LOCA) or a main steam line break. As subcooled droplets fall through a hot, steam-rich environment, convective heat transfer and condensation on the droplets occur, removing steam and a certain amount of sensible heat from the containment atmosphere thus reducing the temperature and pressure. If a hydrogen burn or other event producing a hot, superheated, environment occurs, the sprays will again provide cooling, but different mechanisms are involved. In this case the droplets evaporate, adding steam to the atmosphere. However, because the latent heat of vaporization is taken from the atmosphere, and the resulting vapor is at a lower temperature than the containmnet gases, the net result is substantial cooling of the atmosphere and a lowering of temperatures and pressures. Because of high spray flow rates (250-1000 kg/s), containment sprays will generally dominate other heat transfer modes, typically removing 10^8 watts under LOCA conditions. Sprays are also very effective in removing elemental iodine through absorption and particulate fission products through a variety of mechanisms. As much as 99 percent of atmospheric free iodine can be removed in a matter of minutes. Similar washout rates are obtained for aerosols.

The specific spray phenomena to be considered are:

1. Droplet heatup and cool down
2. Vapor diffusion (evaporation or condensation)
3. Flashing, and
4. Droplet agglomeration.

The following sections concentrate on the first two phenomena. Reasons for the secondary importance of the latter two are given.

Droplet flashing may occur if a droplet falls into a compartment that is at a pressure lower than the saturation pressure corresponding to the droplet temperature. Such a situation may arise in a lumped-volume code if droplets are allowed to fall from one compartment to another. This is an artifact of the calculation, rather than a real effect. Generally, flashing is not a significant problem at the nozzle orifice, because the spray inlet temperature is relatively low. In any case, the effects of flashing are usually small. If it is desired to model flashing, however, it is a simple matter to instantly evaporate enough of the droplet to bring its temperature down to the saturation temperature at the compartment pressure, the vapor being added to the compartment atmosphere.

Droplet agglomeration occurs when two droplets collide and coalesce. The resultant, larger droplet will fall at a higher velocity and exhibit different heat transfer characteristics. The number of droplet collisions is enhanced by the fact that there is a droplet-size distribution (typically a log-normal distribution). Larger drops with higher velocities will overtake, collide with, and coalesce with smaller ones. Given the droplet densities expected within a cell, droplet agglomeration, while not negligible, is not a dominant effect. Calculations have indicated that for typical PWR conditions coalescence effects would reduce the total droplet surface area by no more than 10 percent [1]. This effect is relatively small compared to other uncertainties.

Sprays also have a profound effect on several other containment phenomena. In particular, they will alter the radiative heat transfer due to photon-droplet interactions, and will alter the convective heat transfer due to inpingement upon structure surfaces. These effects are difficult to model, but should be considered at this stage of planning, if not implemented in the early versions of MELCOR. The sprays will also act to remove volatile, gaseous-fission products, especially elemental iodine, and aerosols. These phenomena are relatively straightforward and should be addressed.

3.6.2.2 Droplet Heatup and Diffusion Models

In recent years most best-estimate containment codes have used similar approaches for heat and mass transfer. The heat and mass transfer rates are deduced by comparing the droplet size and temperature at the bottom of the compartment to the inlet conditions, assuming that the atmospheric conditions do not change substantially during

the fall of the drop. Total heat and mass transfer rates are calculated by multiplying the rates for one droplet by the total number of droplets of that size and summing over all droplet sizes. The obvious limitation of this approach is the implicit assumption that the containment atmosphere does not change significantly during the fall time of a drop. The alternative, however, is to keep track of layers of drops as the code proceeds. This requires a finer meshing of the containment and a significant penalty in computer storage and run time. The normal practice is to place constraints on the extent of atmospheric change allowed in a time step, though this does not totally solve the problem.

A variety of detailed models for heat transfer to droplets are available. However, if we assume that the drops are spherical and isothermal, relatively simple models can be used. These assumptions are quite valid for the droplet sizes normally produced by containment sprays (diameters on the order of 1 mm). An additional assumption that the drops come instantaneously to thermal equilibrium with the atmosphere is often made, but this can lead to significant errors in some cases (e.g., when the fall distances are small, the drops large, and heat and mass transfer rates are fairly low).

Assuming that the drops are spherical, a standard correlation for forced convection heat transfer is [2]:

$$Nu = \frac{hd}{k} = 2.0 + 0.6Re^{1/2}Pr^{1/3} \qquad (3.6.2\text{-}1)$$

where Nu, Re, and Pr are the Nusselt, Reynolds, and Prandtl numbers, respectively, h is the heat transfer coefficient, d is the droplet diameter, and k is the gas + vapor thermal conductivity. A mass transfer analogy can be used to determine the evaporation and condensation rates. A simple analogy is:

$$Nu_m = \frac{k_g d}{D_v} = 2.0 + 0.6Re^{1/2}Sc^{1/3} \qquad (3.6.2\text{-}2)$$

where Nu_m is the mass transfer Nusselt number, Sc is the Schmidt number, k_g is the mass transfer coefficient, and D_v is the diffusivity of water vapor in air. This approach is described in Reference [3]. Other mass transfer analogies may be applied in a similar manner. Instantaneous heat and mass transfer rates, dq/dt and dm/dt are obtained using the heat and mass transfer coefficients, h and k_g, from Equations (3.6.2-1) and (3.6.2-2).

$$\frac{dQ}{dt} = h*A*(Tgas-Tdrop) \qquad (3.6.2-3)$$

$$\frac{dm}{dt} = k_g*A*(Driving\ Force) \qquad (3.6.2-4)$$

where A is the droplet surface area, and the driving force in Equation (3.6.2-4) can be based upon a partial pressure, mole fraction, or mass fraction gradient, depending upon how k_g is defined.

In order to calculate the final droplet conditions at the bottom of a compartment, it is necessary to integrate equations for dm/dt, dT/dt, and dz/dt where z is the fall distance, T is the droplet temperature, and t is time. dm/dt is determined from Equation (3.6.2-4), and the other two from the relationships below.

$$\frac{dT}{dt} = \frac{\frac{dm}{dt}(h-u) + \frac{dQ}{dt}}{m * C_v} \qquad (3.6.2-5)$$

$$\frac{dz}{dt} = \frac{4\ (\rho_d-\rho_g)\ g\ d}{3\ \rho_g\ C_d}\ 1/2 \qquad (3.6.2-6)$$

where
- h = specific enthalpy of steam joining or leaving the drop
- u = specific internal energy of the drop
- C_v = constant volume specific heat of the droplet
- ρ_d = droplet density
- ρ_g = gas density
- d = droplet diameter
- C_d = drag coefficient
- g = acceleration due to gravity.

Equation (3.6.2-6) assumes that the drop is falling at terminal velocity and that there is no horizontal velocity component. These are reasonable approximations, as a transient calculations indicates that most of the droplets will be within a few percent of terminal velocity and a vertical fall after falling only a few meters. More exact treatments, requiring the evaluation of a second derivative, are more complex and costly. Equations (3.6.2-4) and (3.6.2-5) can be divided by Equation (3.6.2-6) to produce expressions for dm/dz and dT/dz, reducing the number of equations to two.

After the above equations are integrated to determine final values of m and t, m_f, and t_f respectively, (i.e.,

the conditions at the bottom of the compartment), the total heat and mass transfer rates to the containment atmosphere can be found from the following approximate relations.

$$\frac{dm}{dt_{atmos}} = \dot{m}_{vap} = n\,(m_o - m_f) \qquad (3.6.2\text{-}7)$$

$$\frac{dQ}{dt_{atmos}} = -\left(m_o n Cp_l (t_f - t_o) + \dot{m}_{vap}\left(Cp_v (T_{gas} - T_f) + h_{fg}\right)\right) \qquad (3.6.2\text{-}8)$$

where

m_o = initial droplet mass,
n = number of droplets per unit time,
Cp_v = constant pressure specific heat of vapor,
Cp_l = constant pressure specific heat of liquid, and
h_{fg} = water heat of vaporization.

As Equations (3.6.2-7) and (3.6.2-8) are written, the correct terms to be added for an energy balance on the containment atmosphere (first law analysis) would be dQ/dt_{atmos} and dm/dt_{atmos}^{*} h_s, where h_s is the enthalpy of steam at the bulk-gas conditions. If desired, Equation (3.6.2-8) can be written more precisely in terms of internal energy and enthalpy instead of specific heats and temperature differences. The differences are usually small, however, and the form of Equation (3.6.2-8) is generally more convenient.

Whenever the droplets are evaporating in a highly superheated atmosphere or are condensing in a highly steamrich atmosphere, the relations presented in Equations (3.6.2-1) and (3.6.2-2) may be in error. For these cases, corrections are needed for high-mass transfer rates. While these corrections may take various forms, a typical approach is to define h_c, where

$$h_c = \frac{h * a}{(1.0 - \exp(-a))} \qquad (3.6.2\text{-}9)$$

and

$$a = \frac{MF * Cp_v}{h} \qquad (3.6.2\text{-}10)$$

MF is the mass flux and Cp_v is the vapor-constant volume specific heat. This approach is described in more detail in Reference [3] and Section V.3 of this document.

In spite of the mass transfer corrections or other modifications, the relations presented above may be substantially in error at very high temperatures, such as might be encountered during a hydrogen burn. For this reason, a different set of correlations has been included in HECTR and should be given consideration for MELCOR. These relations have been formulated specifically for high temperature calculations, but also work well at low temperatures. This model is based upon information presented in References [4] and [5]. In this model, Equations (3.6.2-4) and (3.6.2-5) are replaced by:

$$\frac{dm}{dt} = -2\pi\rho_g d \ln(1.0+B)\left(D_f\ 1.0 + 0.25Re^{1/2}Sc^{1/3}\right) \quad (3.6.2\text{-}11)$$

and

$$\frac{dT}{dt} = \frac{1}{m\ C\rho_l}\left\{\frac{C\rho(Tdrop - Tgas)}{(1.0+B)^{1/Le} - 1.0} + h_{fg}\right\}\frac{dm}{dt} \quad (3.6.2\text{-}12)$$

where

D_f = vapor diffusion coefficient in air
Cp = gas specific heat
Cp_l = droplet specific heat
Le = Lewis number, the ratio of thermal to mass diffusivities
B = mass transfer driving force, (mfvp-mfvi)/(mfvi-1.0)
mfvp = mass fraction of vapor in bulk gas
mfvi = mass fraction of vapor at droplet surface

Once Equations (3.6.2-4) and (3.6.2-5) have been replaced by Equations (3.6.2-11) and (3.6.2-12), the calculation proceeds as described previously.

In addition to being more accurate at high temperatures, the latter formulation has been exercised extensively in HECTR and has been implemented in such a manner to minimize running time. The equations have been rewritten to increase smoothness and reduce stiffness problems. Additionally, some modifications have been made to a standard Runge-Kutta integrator to speed up the calculation.

3.6.2.4 Gaseous Fission Product and Aerosol Washout

The substantial atmospheric decontamination resulting from containment sprays should be modeled in MELCOR. Models for washout of both aerosols and elemental iodine have been

developed for the CONTAIN code and could be adapted for MELCOR.

The initial removal rate of iodine is proportional to the iodine concentration, so a rate constant, λ, is defined such that

$$\frac{dc}{dt} = -\lambda c \quad . \tag{3.6.2-13}$$

For a diffusion controlled depletion of a gas that is entering the droplet as a solute, it can be shown that the rate constant is proportional to the ratio of the volumetric spray rate to the compartment volume, [6], or

$$\lambda = \frac{FHE}{V} \tag{3.6.2-14}$$

where F is the volumetric flow rate of spray water, v is the compartment volume, H is the equilibrium-partition coefficient for the dissolved gas in the liquid, and E is a spray efficiency. The expression for E as presented in NUREG-0772 [7] is

$$E = 1.0 - \exp\left\{\frac{6\ k_g t}{d\left[H + (k_g/k_l)\right]}\right\} \quad . \tag{3.6.2-15}$$

k_g and k_l are the mass transfer coefficients of iodine in the gas and liquid respectively, and t is time. It has been observed this expression breaks down following the removal of approximately 99 percent of the elemental iodine in a compartment. Apparently after that point, back diffusion from liquid on the containment walls and floor acts to establish an equilibrium between the gas and liquid phases. It is reasonable to assume that there is no further spray induced decontamination of elemental iodine below the 1 percent level. The actual calculation of depletion of iodine will probably be performed outside of the spray model, so there needs to be an interface through which the spray model can pass the volumetric spray flow rate to the fission-product accounting model.

The aerosol washout rate is also proportional to the amount present, so a rate constant λ_{aer} is determined. For this case, the rate constant is proportional to the containment volume swept out per unit time [6]. Thus,

$$\lambda_{aer} = \frac{3FZ}{2d} E_{aer} \tag{3.6.2-16}$$

where F again is the volumetric flow rate of spray, Z is the fall height, d is the droplet diameter, and E_{aer} is the collection efficiency. Several mechanisms contribute to aerosol washout, including diffusion, diffusiophoresis, thermophoresis, impaction, and interception. The collection efficiency is the sum of the contributions from each mechanism. The contributions are functions of aerosol and droplet sizes as well as the thermo-physical conditions of the compartment. A simple graphical representation of E_{aer} is given in Reference [6] for typical containment conditions. It is recommended that the spray model provide the variables in Equation (3.6.2-16) to the aerosol model where the rate constant and the depletion is actually calculated.

3.6.3 CONTAINMENT FAN COOLERS

3.6.3.1 System Description

Fan coolers are included in dry PWR containments to augment the steam removal capabilities of the water sprays. These coolers consist of banks of finned, service-water-cooled coils through which large capacity fans pull the containment atmosphere. Each unit has several parallel coolant paths, each routing water back and forth across the path of the circulated atmosphere. The coils are horizontal, with the coolant entering at the back and leaving at the front. The geometry is, therefore, that of a cross-flow heat exchanger with counter-flow, i.e., the vapor inlet side corresponds to the coolant outlet side. The coolers usually provide cooling to the containment atmosphere under normal conditions, as well as under accident conditions. Typical emergency design temperatures are in the area of 400 to 420° K, with a saturated atmosphere, and pressures ranging between 3 and 6 atmospheres. The heat removal capability is in the range of 2 to 4 x 10^7 W. BWR and subatmospheric containments generally include fan coolers, but these are designed only for normal operating conditions. The performance of such a cooler may be important following an accident.

3.6.3.2 Model Assessment

Typical of the simplest existing fan-cooler models is that used in the CONTEMPT code [8]. In that case, the heat removal rate is input by the user as a tabular function of containment temperature. The condensation rate is calculated implicitly through the thermodynamics routine, with the condensed mass lowering the quality of the atmosphere. The amount of this water entering the sump depends on a user-specified "deintrainment rate." If the atmosphere is superheated, the condensation rate is calculated as

$$\dot{m} = \frac{\dot{Q}\, f}{(h_v - h_l)} \qquad (3.6.3\text{-}1)$$

where $\dot{Q}$ is the heat removal rate, f is a user-input parameter, h_v and h_l are the specific enthalpies of water vapor and liquid respectively. This model is attractive in its simplicity, but suffers from the supposition that the user has accurate performance data for a given cooler throughout the range of temperatures encountered in the calculation. There is also no consideration of the effect of a variable concentration of noncondensibles that might arise from metal oxidation or a core-concrete interaction.

The former drawback has been overcome in the fan-cooler model developed for the MARCH code [9]. The user input for this model includes the design conditions for the cooling capacity, inlet gas temperature, and the coolant inlet temperature and flow rate. A correlation for an effective heat-transfer coefficient, h, as a function of steam-vapor fraction has been derived from the capacity curves presented in the OCONEE Power Reactor Final Safety Analysis Report (FSAR). Using the h calculated for the design conditions, along with the input conditions, an effective heat transfer area is calculated. Using this value, the prevailing cooler operating conditions, and h, based on prevailing containment-vapor fraction, a cooling capacity can be calculated for the given conditions.

The first question one might ask regarding this model is, how appropriate is a heat-transfer coefficient, based upon one fan cooler, for the analysis of another? As it turns out, the fan coolers are very similar from plant to plant, the majority being provided by a single manufacturer. Calculations were performed using the MARCH model to construct a capacity curve for the Zion plant. The resultant curve was very similar to that published in the FSAR. Two uncertainties still exist, however. The capacity curve from which the correlation for h was derived is based upon the the assumptions that the atmosphere is saturated and that the concentration of noncondensibles is constant. Since scenarios addressed by MELCOR may present regimes of both high superheat and substantially increased concentrations of hydrogen and carbon dioxide, the validity of these assumptions has been considered.

A mechanistic fan-cooler model was developed based upon the condensation heat-transfer formulation that is used throughout the CONTAIN code. The model calculates condensation and convective heat-transfer coefficients depending upon the cell-atmospheric conditions. A user input, constant heat-transfer coefficient is used for transfer between the condensate boundary layer and the coolant. The calculation is carried out in a stepwise manner with the steam-air mixture inlet conditions known, and the coolant water exit temperature estimated. The enthalpy change across the first row is calculated, assuming a constant coolant temperature. The coolant temperature and the air-steam mixture conditions are updated prior to repeating the calculation for the next row. The process is repeated for successive rows until the water entering temperature and gas leaving conditions have been determined. The water inlet temperature is compared to the known value. If there is a substantial difference, the calculation is repeated with a revised estimate for the coolant outlet temperature. The process is continued until there is sufficient agreement between the calculated and specified coolant inlet temperatures. Since the total heat

transferred is relatively insensitive to changes in cooling water temperature, convergence is rapid.

Two input parameters that cannot be easily characterized are the effective heat transfer area and the heat transfer coefficient between the boundary layer and the coolant. For the present study, these values were chosen parametrically in order to match the capacity curves for the fan coolers given the Zion FSAR. Using these parameters, calculations were performed for superheated atmospheric conditions and saturated conditions where there was an abundance of noncondensible gas (assumed to be air). The results were then compared to those from the MARCH model. For the first case, in which the atmosphere was superheated 20° K above saturation, The MARCH predicted capacity was about 10 percent higher than that of the mechanistic model. When a saturated atmosphere with twice the nominal air content was considered, the MARCH value was 7 percent lower than the mechanistic result. Though these differences are not great, they do indicate that The MARCH model cannot account for such variations in atmospheric conditions, and the differences for more extreme conditions may be unacceptable. Another argument for employing a mechanistic model is that there will be regimes in which the coolant water boils, degrading severely the performance of the cooler. Though this is a difficult phenomenon to treat under any circumstances, it would at least be possible within the framework of a simple mechanistic model. The mechanistic model described will receive further development and testing for inclusion in CONTAIN. The model requires relatively little computer time and storage. Its level of detail seems to be consistent with that of MELCOR, and its inclusion is recommended.

3.6.3.3 Fission Product and Aerosol Removal

As a result of the relatively cool surfaces and high condensation rates provided by fan coolers, substantial amounts of elemental iodine and aerosol-fission products will be removed from the atmosphere. The same depletion mechanisms that are active on structure walls will apply to the fan cooler, but the physical and dynamic conditions will differ. A program is currently underway at Pacific Northwest Laboratories (PNL) to evaluate and/or develop models for the removal of aerosols by engineered safety systems. The results of this work may provide the basis for removal correlations to be used in MELCOR. The actual fission-product removal may be calculated elsewhere in the code, using whatever parameters are necessary from the fancooler model. Because the cooler has the potential for removing substantial quantities of aerosols from the atmosphere, the possibility that their deposition on the cooling coils may cause degradation in cooler performance should be considered.

3.6.4 ICE CONDENSERS

Ice condensers limit the maximum containment pressure during a postulated steam-releasing accident by removing energy from fluid injected into the containment rather than diluting the steam in a large volume as done in a dry PWR containment. The heat transfer and steam condensation resulting from flow through the ice beds reduces the maximum containment pressure, allowing smaller containments with lower design pressures to be used. Aerosol concentrations are also reduced by flow through the ice condenser, but this phenomena will be discussed in another section.

The ice condenser will be briefly described in the next section. The phenomena occurring in the ice condenser that need to be modeled will be discussed next. Currently available models will then be listed and a model will be recommended for MELCOR.

3.6.4.1 Ice Condenser Description

A schematic of a typical ice-condenser containment is shown in Figure 3.6.4-1. The ice is contained in an annular region along the outer containment wall in open-mesh metal baskets. During a LOCA, steam would be released into the relatively small lower compartment, then it would flow up through the ice condenser and exhaust into the large upper compartment. Most of the steam would be condensed while flowing through the ice condenser, giving a smaller pressure rise.

A schematic of the ice-condenser compartment is shown in Figure 3.6.4-2. The ice condenser can be divided into three regions: a lower plenum, an upper plenum, and the ice-bed region. The borated ice is contained in open-meshed metal frames that are stacked into long columns. The columns of ice are positioned in lattice frames in the annular ice condenser region. The inner and outer walls of the ice condenser are insulated to minimize the heat loss and the region is refrigerated under normal operating conditions.

Doors are located at the inlet to the lower plenum, between the ice-bed region and the upper plenum, and at the exit of the upper plenum. These doors isolate the ice condenser from the rest of the containment during normal operating conditions. All three sets of doors open when the lower compartment pressure exceeds the upper compartment pressure, allowing upward flow through the ice bed. When the differential pressure driving force is reduced, the lower and intermediate doors will return to a closed position. However, the upper doors are constructed such that they will not reclose after opening.

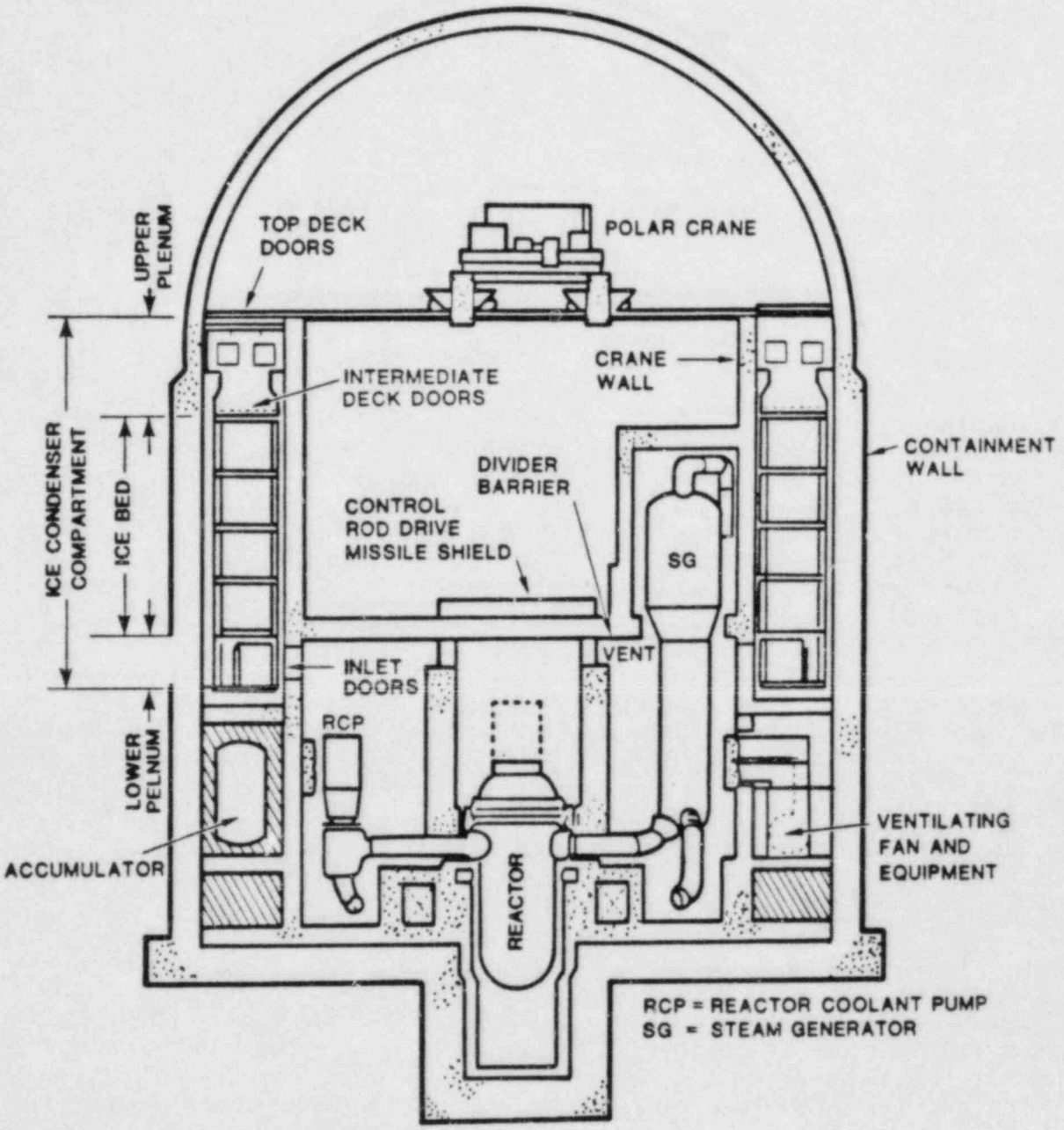

Figure 3.6.4-1. Schematic of Typical Ice Condenser Plant Containment

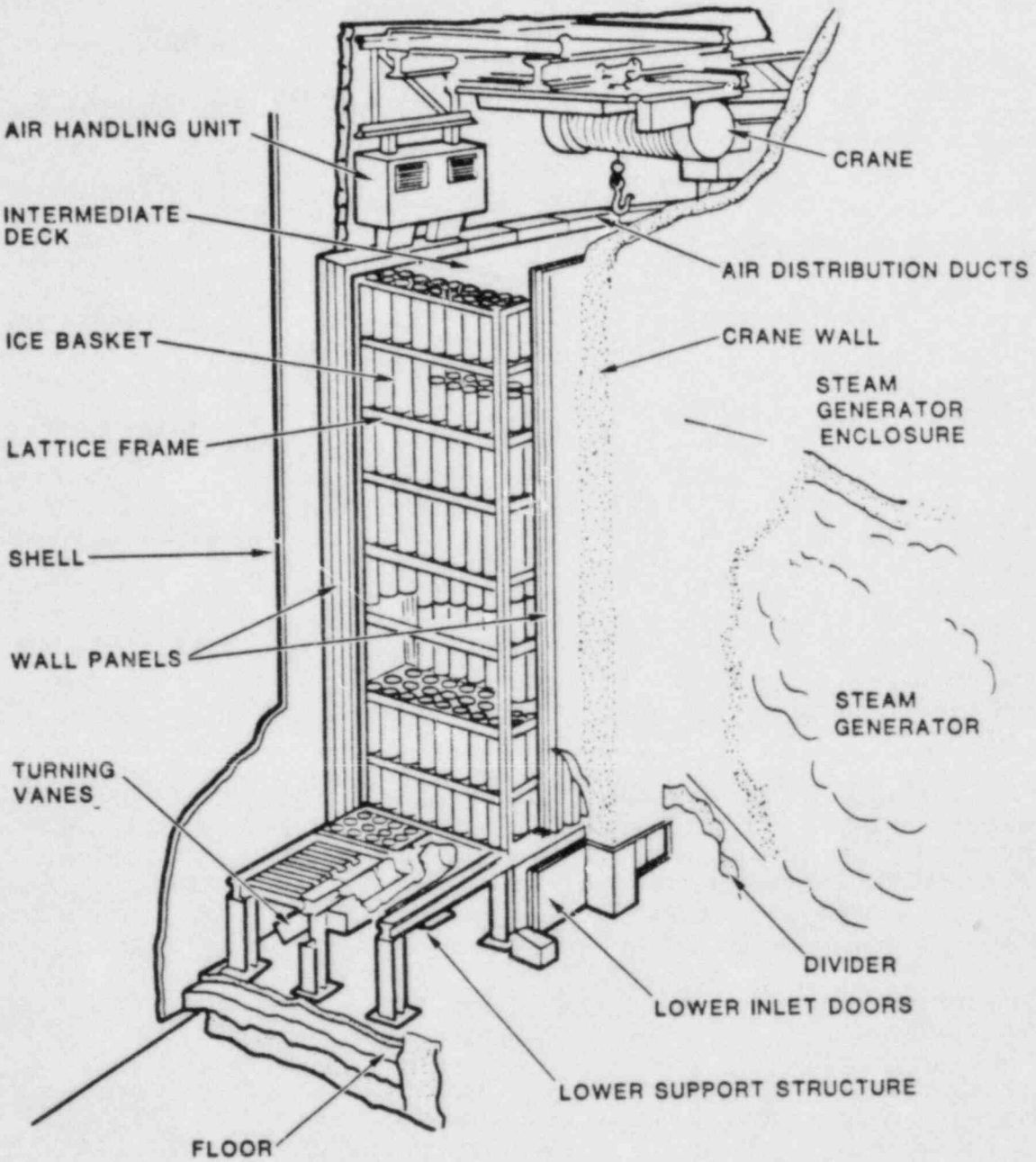

Figure 3.6.4-2. Details of Ice Compartment of an Ice Condenser Plant

3.6.4.2 Phenomena

The important phenomena that would occur in an ice condenser during an accident are described in this section. Unfortunately, most of these phenomena are difficult to model. The following section describes models currently used in computer codes to calculate ice-condenser performance.

The most important phenomena to model is the heat and mass transfer from the air-water mixture flowing up through the ice. The rates of these processes are reduced from the pure steam values by the presence of noncondensibles. The heat and mass transfer will also be affected by the turbulence created by flow past the baskets and the thickness of the film of water flowing down over the ice. Both of these effects are difficult to quantify, but they significantly affect the condensation rate, so need to be modeled in MELCOR.

The heat and mass transfer from the fluid to the ice cause the ice to melt. The change in ice geometry due to melting is difficult to calculate, since it will be simultaneously melting radially and axially. Experimental results indicate that for a large-break LOCA, the ice melts predominantly as a plane moving upward from the bottom of the ice [10].

It may be possible to form a fog as the fluid flows through the ice condenser. If a fog formed in the ice condenser, the burning of hydrogen in the upper plenum would be affected.

The fluid may also condense on and transfer heat to the walls in the ice condenser. As the ice melts, heat and mass transfer can occur with the uncovered portion of the baskets as well. As with condensation on the ice, turbulence and the presence of water films will affect the condensation rates on the walls and uncovered baskets.

Water that condenses on the ice will mix with the melted ice and will flow down through the ice chest region and fall through the lower plenum. This water could be heated either as it flows down the baskets or as it falls through the lower plenum. Data from tests performed by Westinghouse on a scale model of the ice condenser indicate that this water can heat up significantly during a large-break LOCA [10].

The water falling from the ice chest will form a pool on the floor of the lower compartment. It can flow into the lower compartment through a drain in the floor of the lower plenum. If the pool drains too slowly, the water level in the lower plenum will rise and the water will spill over into the lower plenum through the lower inlet doors. Water

flowing from the lower plenum drain will fall through the lower compartment and could provide additional cooling, acting like the sprays.

The inertia required to open the doors will be important during the first few seconds of a large-break LOCA or during a burn. It should be insignificant thereafter. The doors do need special modeling, however, to prevent backflow through them and to allow the flow area of the doors to vary with the differential pressure across them.

3.6.4.3 Available Models

Ice condenser models are used in the following computer codes: LOTIC, ICECON, RELAP4/MOD5, CONTEMPT, COMPARE, TMD, MARCH, CLASIX, and HECTR [11, 12, 13, 8, 14, 15, 9, 16, and 17 respectively]. In addition, Battelle Northwest has reviewed the TMD model and made suggestions for improvement of the model [18]. The models used in each of the codes will be described in the following paragraphs.

A very simple model is used to calculate the condensation rate in the ice condenser in MARCH, CONTEMPT, and ICECON. The codes require the user to specify the ice condenser exit temperature and the temperature of the water in the lower plenum drain. By further assuming the exit flow to be saturated, the codes calculate the heat and mass transfer rates by simple mass and energy balances for the ice-condenser control volume. Using this heat transfer rate, the ice melting rate is calculated.

RELAP4/MOD5, COMPARE, TMD, and CLASIX use a modified form of the Jakob correlation to calculate the heat transfer rate. The codes also assume the ice-condenser exit flow to be saturated. The Jakob correlation was derived for pure steam flow, so the codes use a modifier that varies with steam-mass fraction to account for the presence of air. The correlations used are:

$$h = \frac{F * (C_1 + C_2\, v)}{L^{1/3}} \quad (w/m^2 \circ K) \qquad (3.6.4\text{-}1)$$

where

h = heat-transfer coefficient
v = inlet vapor velocity
L = condensate layer length
C_1 = 1100., if saturated
1130., if superheated
C_2 = 9.9, if saturated
5.05, if superheated
F = modifier for presence of air

F is determined from:

Steam/air mass ratio	F
> 0.999	1.0
0.9	0.4
0.0	0.05

CLASIX and TMD use values for L that were found to calculate conservatively high pressures when code results were compared to experimental results from the Waltz Mill facility [10]. RELAP4 and COMPARE require a user input for L. RELAP4 and COMPARE provide two additional "dials" on the heat-transfer coefficient. The actual heat-transfer coefficient used in these two codes is:

$$h' = C_3 + C_4 * h \qquad (3.6.4\text{-}2)$$

where C_3 and C_4 are user-input values. All four codes allow the user to specify a maximum value for the heat-transfer coefficient. This is necessary because the Jakob correlation was found to predict unreasonably high heat-transfer coefficients under some conditions.

Battelle Pacific Northwest Laboratories assessed the ice-condenser model used in MD. They recommended using the Carpenter-Colburn correlation for the heat-transfer coefficient in place of the Jakob correlation because it also includes the effects of surface roughness and entrained droplets in the flow. The correlation is:

$$h = 0.065 \left[\frac{\rho_{lf}}{\rho_v^2} \frac{C_p K}{\mu} 1 \right]^{1/2} * G_m \qquad (3.6.4\text{-}3)$$

where

ρ = density
f = fanning friction factor for vapor only flow
C_p = specific heat
K = conductivity
μ = viscosity
G_m = mean mass velocity

$$= \left[\frac{G_{in}^2 + G_{in}G_{out} + G_{out}^2}{3} \right] 0.5$$

l = condensate properties
v = vapor properties.

HECTR uses a heat-mass transfer analogy to calculate the condensation rate in the ice condenser. The heat-transfer coefficient is calculated using a turbulent, forced-flow correlation with a multiplier to account for the increased heat transfer due to turbulence generated by the baskets and the water film on the ice. The heat-transfer correlations used is:

$$h = F * 0.023 * Re^{0.8} Pr^{0.3} \qquad (3.6.4\text{-}4)$$

where

F = turbulence adjusting factor
Re = Reynold's number

$$= \frac{\rho V D}{\mu}$$

Pr = Prandtl number

$$= \frac{C_p \mu}{k}$$

D = equivalent heated diameter
V = average velocity through ice condenser.

The corresponding mass transfer is calculated using the relations listed in the section describing the containment convective heat-transfer correlations (Section 3.3 of this document).

As mentioned above, the heat up of water falling through the lower plenum is included in the simplest ice-condenser model as a user-specified input. Most of the other codes do not model this heat-transfer mechanism. However, CLASIX users have attempted to approximate the phenomena by increasing the heat of fusion of the ice an appropriate amount. HECTR models the water heatup if conditions in the lower plenum are such that steam would be condensing on the water; it is ignored if the water should be evaporating in the lower plenum. The condensation is modeled by assuming enough steam is condensed to raise the water temperature to a user-specified value.

The pool on the lower plenum floor will drain into the lower compartment as gravity driven flow. Most of the codes instantaneously move the liquid from the lower plenum pool to the lower compartment sump. The draining process is modeled in LOTIC, but the model used is proprietary and not

available. ICECON also models the draining process. The drain-flow rate is calculated from:

$$W_d = A_{drain} \left[\frac{2\rho_{pool}}{K_{drain}} \frac{P_{IC} - P_{LP}}{g_c} + g*h_{pool} \right] 0.5 \qquad (3.6.4\text{-}5)$$

where

A_{drain} = sump drain-flow area
g = gravitational acceleration
h_{pool} = height of lower plenum pool above drain exit
K_{drain} = flow loss coefficient for sump drain
W_d = mass velocity through drain
ρ_{pool} = density of water in lower plenum pool.

If the water level in the pool builds up enough to allow to spill over to the lower compartment through the lower inlet doors, the ICECON flow rate is calculated using:

$$W_{weir} = 3.33[W_{dd} (h_{sump}-h_d)]^{3/2} \rho_{pool} \qquad (3.6.4\text{-}6)$$

where

W_{dd} = width of lower door
W_{weir} = flow rate
h_d = height of lower door sill above sump drain exit.

The liquid draining from the ice condenser lower plenum could absorb some heat from the lower compartment as it falls through it. In LOTIC, the heat transfer from the lower compartment fluid is calculated using:

$$q = F \dot{m} C_p (T_{LC}-T_{drain}) \qquad (3.6.4\text{-}7)$$

where

F = user-input efficiency (ability to reach lower compartment temperature)
m = flow rate of water from ice condenser
T_{LC} = lower compartment temperature
T_{drain} = temperature leaving lower plenum pool.

ICECON assumes the water acts as a "100 percent efficient spray" such that the water reaches thermal equilibrium with the lower compartment.

To adjust for melting, all of the codes model the ice as melting from the bottom up. Most of the codes treat the ice as a constant temperature surface, whose area and length vary. RELAP4 models a radial-temperature distribution in the ice, using a finite-difference formulation. The ice surface temperature must be at the freezing point, but the internal nodes may be colder. COMPARE models the ice with a finite-element formulation.

As the ice melts, the flow resistance in the ice region will change. This is modeled in ICECON using

$$k = \frac{((Z_i - z)\ K_I + z\ K_o)}{Z_I} \qquad (3.6.4\text{-}8)$$

where

K_I = loss coefficient when full of ice
K_o = loss coefficient when empty of all ice
Z_I = height of ice column
z = height melted out.

The top deck doors are assumed to remain open after opening in the codes. In CLASIX, a minimum differential pressure across the top doors is required before they will open. The simplest representation of the lower and intermediate doors is that used in HECTR, CLASIX, and ICECON. In these codes the door area is calculated as a function of the differential pressure across the door. The normal flow equations of each code are then used to calculate the flow rate through the door. Both HECTR and CLASIX prevent reverse flow through the doors. The relation for determining the door flow area used in CLASIX is:

$$\frac{\theta}{\theta_o} = \frac{\Delta P \cos\theta}{\Delta P \cos\theta_o} \qquad (3.6.4\text{-}9)$$

where

ΔP = differential pressure across door
θ = angle of opening
o = full open condition.

The corresponding door flow area is:

$$\frac{A}{A_o} = \frac{1 - \cos\theta}{1 - \cos\theta_o} \quad . \qquad (3.6.4\text{-}10)$$

A similar relation is used in HECTR, but the doors do not open until a minimum-differential pressure is exceeded (to model the weight of the door). The differential pressure used in the above expressions for the door opening angle and area is also reduced by this minimum-differential pressure. In ICECON, the relation for door area versus differential pressure is input by the user as a table. Leakage flow around the doors is modeled in CLASIX and HECTR using a user-specified flow area.

The door flow area is modeled in TMD by balancing the torques acting on the door against its angular acceleration. The angular acceleration is then integrated to determine the door position. The equations used are:

$$\text{Torque} = \Delta P\ A\ r = \frac{\ddot{\theta} I}{g} \qquad (3.6.4\text{-}11)$$

$$\dot{\theta} = \ddot{\theta}\Delta t + \dot{\theta}_{old} \qquad (3.6.4\text{-}12)$$

$$\theta = \ddot{\theta}\frac{\Delta t^2}{2} + \dot{\theta}\Delta t + \theta_{old} \qquad (3.6.4\text{-}13)$$

where

ΔP = differential pressure across the door
A = door area
r = distance from hinge to door center
$\ddot{\theta}$ = angular acceleration
I = moment of inertia
$\dot{\theta}$ = angular velocity
θ = angular position
Δt = time step length
old refers to previous time.

COMPARE uses similar equations to model the doors. However, the differential pressure used to calculate the torque on the door includes a spring force and the weight of the door. The expression used in COMPARE is:

$$\Delta P' = (\Delta P - P_S) - \frac{M_D\ g\ \cos\theta}{A} \qquad (3.6.4\text{-}14)$$

where

P_S = spring force acting to keep door closed
M = door mass.

The door inertia is calculated for COMPARE using:

$$I = H_D * W_D^3 * \frac{MA}{3} \qquad (3.6.4\text{-}15)$$

where

H_D = door height
W_D = door width
MA = door mass/area

COMPARE also allows the doors to have viscous damping. The modified equations to include this are:

$$O = O_{old} + \frac{A\Delta P}{CVD}\Delta t - \frac{2I(O_{old} - \frac{A\Delta P}{CVD})}{W_D CVD} \exp\left(\frac{W_o CVD \Delta t}{2I} - 1\right) \qquad (3.6.4\text{-}16)$$

where

CVD = viscous damping coefficient.

3.6.4.4 Recommendations

A heat-transfer coefficient similar to HECTR's seems more appropriate than the experimental correlations used in some of the codes, since conditions in the ice condenser may be significantly different than the experimental conditions. Also, the heat-transfer coefficient would then be calculated consistently with the heat coefficients used for the containment structures. To reasonably predict hydrogen burning rates, it will be necessary to subdivide the ice condenser. This is necessary because the hydrogen concentration changes significantly across the ice condenser. To calculate the amount of hydrogen burned, this variation must be modeled. Four compartments would probably be adequate. Treating the ice as isothermal and modeling the ice melt as occurring from the bottom up appears to be adequate. Since the heat up of the melted ice and condensed steam as it falls into the lower plenum is significant, it should be included in the model. Since it is not practical to model it mechanistically, a user-specified final temperature seems the best way to model this. The lower plenum pool draining phenomena are not significant for MELCOR. The water reaching the lower plenum pool can be instantaneously transferred to the lower compartment sump. Since the doors can significantly affect the transient, the model used in TMD and COMPARE seems best for MELCOR. The door model should allow for the simulation of failure of door opening or closing.

3.6.5 PRESSURE SUPPRESSION POOLS

Pressure suppression pools are used to condense the steam released from a BWR either from a break or from flow through safety/relief valves. The three basic types of suppression pool that are in common use today will be described as well as the phenomena that may expected to occur within them. The currently available models for treating pool behavior will be described, and a recommended treatment for MELCOR will be proposed.

3.6.5.1 Pressure Suppression Pool System and Phenomena Description

The three common designs that have been used for BWR pressure suppression are designated MARK I, MARK II, and MARK III. Each design embodies a region surrounding the reactor called the drywell. The drywell is separated from another region, called the wetwell, by a suppression pool. Flow between the two is channeled through the suppression pool by large vents. The vents in the MARK I and MARK II are vertically oriented while those in the MARK III are horizontal. During a LOCA, steam flows into and pressurizes the drywell. The drywell atmosphere is forced through the suppression pool where most of the steam is condensed and many aerosols and gaseous-fission products are removed. Noncondensibles and any steam that is not removed in the suppression pool is exhausted into the wetwell. Steam can also flow directly from the reactor vessel to the suppression pool through vertical vents if the safety/relief valves open. Details of the suppression pool geometry for each type of BWR containment are described in the following paragraphs.

Schematics of the MARK I and MARK II containments are shown in Figures 3.6.5-1 and 3.6.5-2, respectively. In these containments, the flow from the drywell to the suppression pool occurs through vertical vents. As shown in the figures, the geometry of the two containments are different, but in each, the drywell and wetwell are isolated from the rest of the containment building.

A schematic of the MARK III containment is shown in Figure 3.6.5-3. In this design, the drywell is a cylindrical region in the center of the containment. The suppression pool is contained in an annular region surrounding the drywell, and is enclosed on the drywell side by a weir wall. Flow from the drywell to the wetwell occurs through horizontal vents submerged in the suppression pool. The wetwell is not isolated from the rest of the reactor building in the MARK III containment.

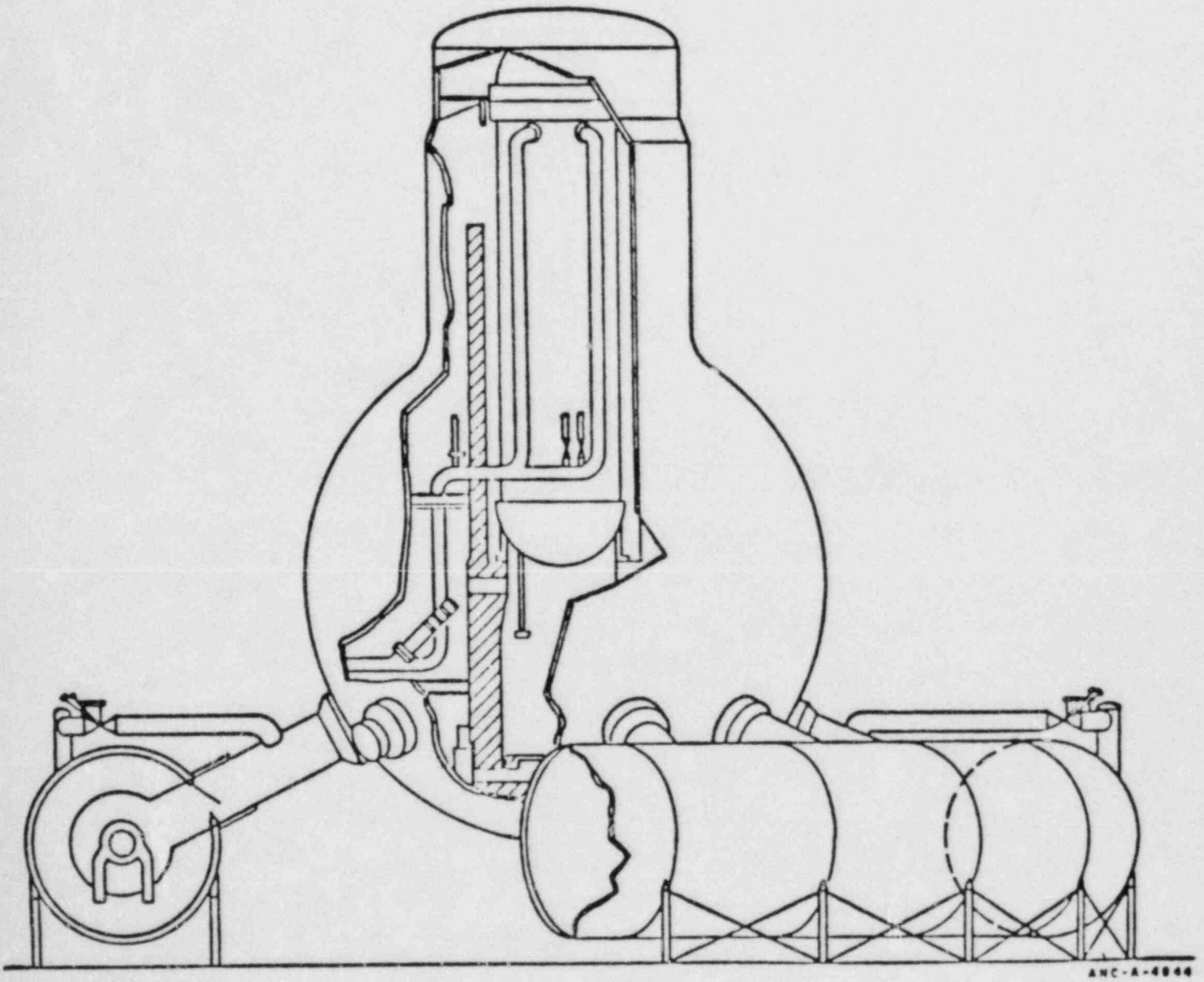

Figure 3.6.5-1. Geometry of G.E. Mark I Containment

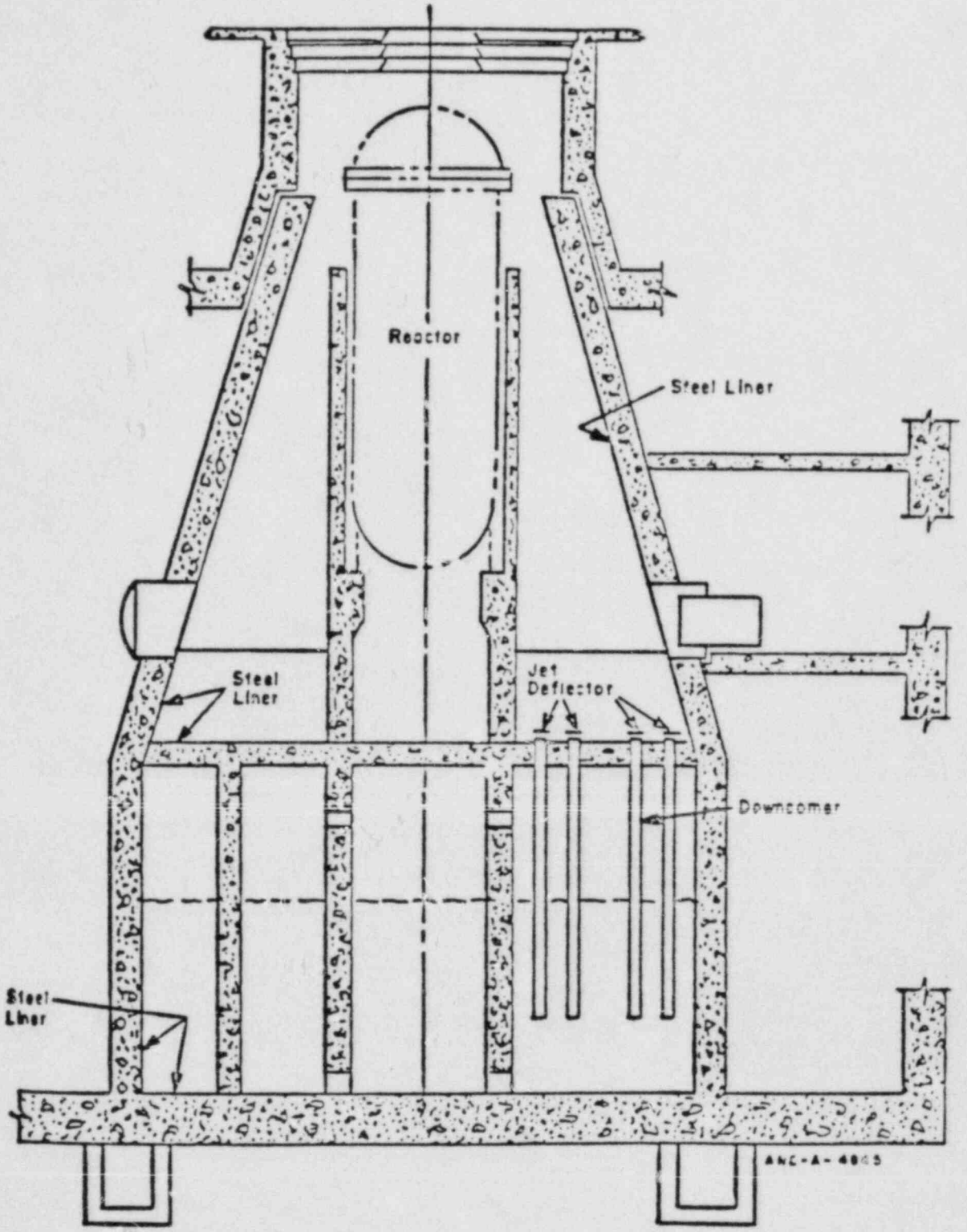

Figure 3.6.5-2. Geometry of G.E. Mark II Containment

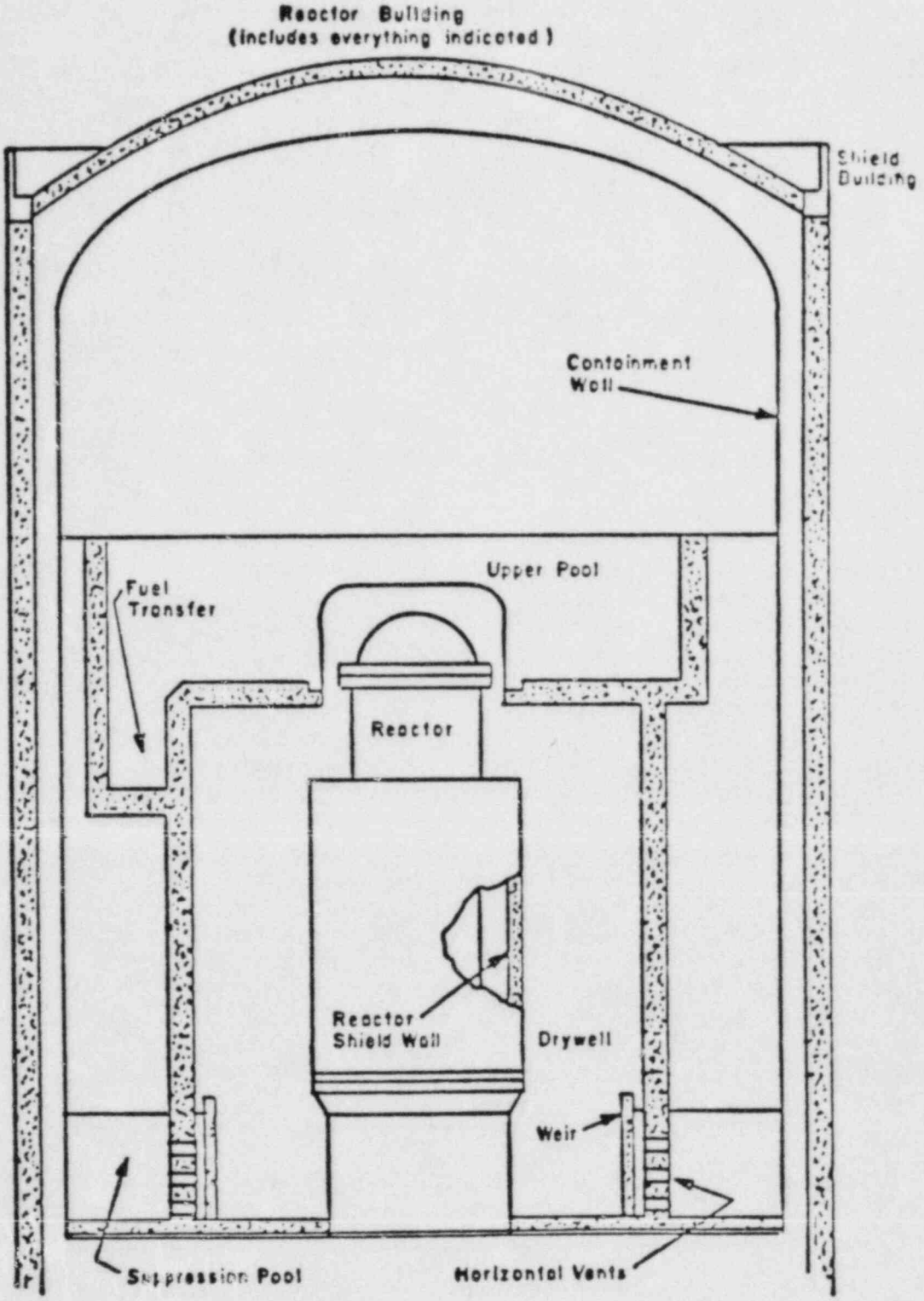

Figure 3.6.5-3. Geometry of G.E. Mark III Containment

The suppression pool phenomena that need to be modeled in MELCOR are: the dynamic motion of the pool while clearing the vents, flow of steam-air mixtures through the vents, condensation and cooling of the mixture as it flows through the pool, and the heatup of the pool, which may not be uniform circumferentially. It will also be necessary to maintain an inventory of the pool volume, since it interacts with several coolant injection systems. The chugging phenomena observed in scaled tests of suppression pools involves multidimensional fluid dynamics and is much too complex to model in MELCOR. It is more important for structural calculations than for thermal-hydraulic considerations. It may also be important to model the pool swell in a MARK III caused by the vent flow, but the models currently used to calculate it are, again multidimensional and too complex to include in MELCOR.

The pressure rise in the drywell during a LOCA will depress the water level in the vertical vents of a MARK I or MARK II containment or in the weir annulus of a MARK III containment until a path is cleared for steam flow between the drywell and wetwell. The inertia of the pool motion during this clearing process significantly affects the maximum pressure rise in the drywell. Thus, the dynamic motion of the pool must be modeled to correctly calculate the peak pressure that will occur following a rapid pressure increase in the containment. The model must be able to calculate the response of the suppression pool to pressure increases in the outer containment building of a MARK III containment, as well as pressure increases in the drywell, to correctly calculate the response to burns. The model will also need to account for flow of water between the suppression pool and the drywell (in either direction) due to flow over the weir wall.

After the vents have cleared, a steam-air mixture will flow through the suppression pool, where it will be cooled and most of the steam will be condensed. The flow rate can be calculated by a balance of momentum, but the amount of steam condensation and air cooling will probably have to be empirical. Test results indicate that essentially all of the steam is condensed when flowing through the suppression pool and that the air is cooled to the pool temperature.

The suppression pool must absorb the energy from condensing the steam. This will usually result in a fairly uniform temperature rise throughout the suppression pool. However, if the steam flow through the suppression pool is only occurring through a small portion of it (as would be the case if the flow were occurring through only one safety/relief valve), the temperature rise will not be uniform. This nonuniform heating could allow steam to escape the suppression pool if the local temperature approaches saturation.

Several systems interact with the suppression pool that will affect the water inventory during a transient. Water is drawn from the suppression pool for reactor coolant and spray injection. Water could also be added to the suppression pool by sprays. In the MARK III containment, the water inventory could be either increased or decreased by flow across the weir wall. Also in the MARK III, water can be dumped from an upper pool to the suppression pool during a transient.

3.6.5.2 Available Models

Several models have been developed to calculate the vent-clearing phenomena for both vertical and horizontal vents. Most of these use finite-difference formulations of two-dimensional flow equations to calculate the vent clearing and the subsequent bubble growth in the suppression pool. These types of formulations are much too detailed for MELCOR. There are two models available, however, that use control volume approaches with a one-dimensional representation of the flow to model the vent-clearing process. MARCH also includes a simple model for a suppression pool. These models will be described below.

General Electric [19] has developed a model to calculate the vent clearing for the horizontal vents in a MARK III using six control volumes as shown in the schematic in Figure 3.6.5-4. The conservation of mass and momentum is written for each control volume. The resulting set of equations are manipulated to a form where only the velocities are unknown. The model assumes one-dimensional, nonsteady, incompressible flow for the water and assumes friction is negligible. The turning losses for flow entering the vents from the annulus are included. In addition, an equivalent length is added to the flow length of the vents to account for the force required to accelerate the water in the suppression pool that must be moved to allow flow through the vents. When a vent clears, the air being injected into the suppression-pool forms a bubble that exerts a force on the fluid below it as it expands. This effect is included in the General Electric suppression pool model. Five sets of equations are used to model all the possible combinations of cleared/uncleared vents. The equations used are quite lengthy and can be found in Reference [19].

A separate model is used to calculate the flow rate through each vent as it uncovers. The model assures steady, one-dimensional adiabatic flow with the steam phase modeled as an ideal gas.

The General Electric suppression-pool model assumes the pool heats up uniformly. It also assumes that all steam and

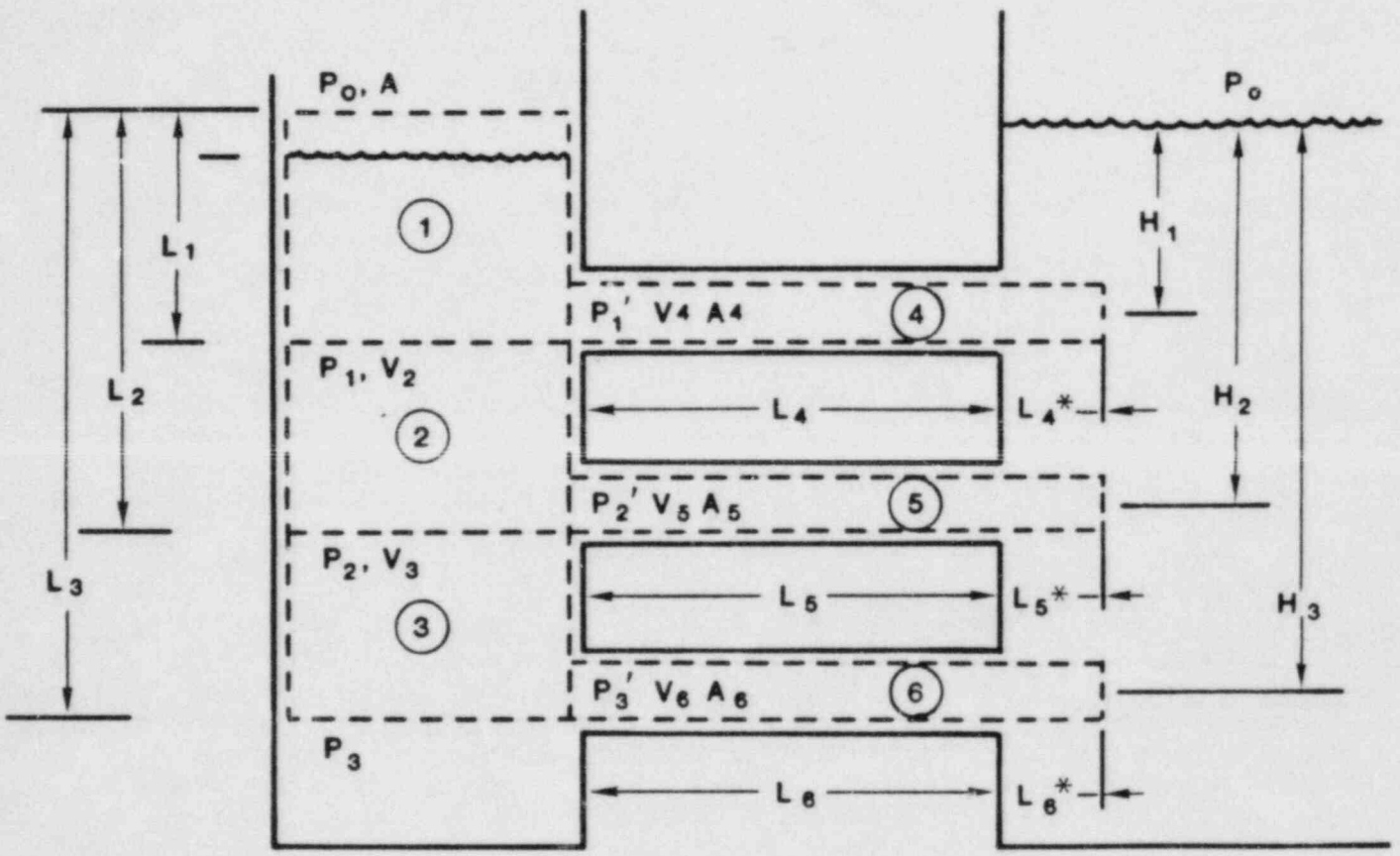

Figure 3.6.5-4. Control Volumes for Mark III Vent Clearing Model

water that enter the pool remains there and that air leaving the pool is at the pool temperature.

The CONTEMPT-LT [20] model for clearing vertical vents assumes incompressible flow of the liquid. The equation used to calculate the acceleration of the liquid in the vent is:

$$av = \frac{(p_v - p_w)}{\rho(1+\beta)\,(L-(1-\beta)Z_v)} - \frac{gZ_v}{(L-(1-\beta)Z_v)}$$

$$- \frac{f_m v_v |v_v|}{2\,D_v(1+\beta)} \frac{(L-Z_v)}{(L-(1-\beta)Z_v)}$$

$$+ \frac{v_v^2}{2\,(L-(1-\beta)Z_v)} \frac{1 - \delta(v_v) + \beta(2-2\beta^2-\beta^3)}{(1+\beta)^3} \quad (3.6.5\text{-}1)$$

where

v_v = water-surface velocity in vent
p_v, p_w = total pressure of drywell and wetwell vapor regions, respectively
Z_v = liquid displacement, respectively
L = initial vent submergence in wetwell pool
β = ratio of total vent-exit area to wetwell pool-surface area
ρ = vent and wetwell liquid density
g = acceleration due to gravity.
D_v = vent-exit diameter
f_m = Moody friction factor for vent walls.

This equation is numerically integrated to give the velocity and height of liquid in the vent. The vents are closed after the initial clearing if the differential pressure between the drywell and wetwell falls below a user-specified fraction of the hydrostatic head of water above the vents. Vent clearing is restarted if the differential pressure exceeds a second user-specified fraction of the hydrostatic head. Vent failure is also modeled, such that flow can pass directly from the drywell to the wetwell without condensing in the suppression pool.

CONTEMPT-LT uses a model that is similar to the General Electric model for the MARK III suppression pool. The CONTEMPT-LT equations are formulated for a general suppression pool with N vents, but in this discussion their equations will be reported for the specific case of three

vents. For this case, the suppression pool would be divided into seven control volumes as shown in Figure 3.6.5-5. Balances of mass and momentum are written for each control volume assuming one-dimensional, adiabatic flow, with the liquid treated as incompressible. Friction loss terms can be included using loss coefficients. CONTEMPT-LT models the wetwell side of the suppression pool as a separate control volume rather than assuming conditions at the vent exists as done in the General Electric model. This allows modeling of the vent flow in both directions, whereas the General Electric model is limited to flow from the drywell to the wetwell. The turning-loss term is modeled differently than in the General Electric model, yielding slightly different equations. The equations used are:

ANNULUS NODES

Node 2n+1 - Not Clearing

Mass balance:

$$u_{2n-1} - u_{2n+1} + \alpha_{n+1}\, u_{2n+2} \qquad (3.6.5\text{-}2)$$

Momentum Balance:

$$\dot{u}_{2n-1} = \frac{u_{2n-1}^2 - 1/2\, u_{2n+2}\, u_{2n+1} - u_{2n+1}^2}{d_n} + \frac{p_{2n-1} - p_{2n+1}}{\rho d_n}$$

$$+ g - \frac{f\left|u_{2n-1}\right| u_{2n-1}}{2R} - \frac{K_{e_{n+1}}\, \alpha_{n+1}\left|u_{2n+2}\right| u_{2n+2}}{2d_n}$$

$$n = 1, 2\ 3, \ldots, N-2 \qquad (3.6.5\text{-}3)$$

where

u = velocity
α_n = An/Sn
p = pressure
ρ = density
d_n, A_n, S_n L = See Figure 3.6.5-5
f = Fanning friction factor
R = hydraulic radius
$K_{e_{n+1}}$ = elbow loss coefficient

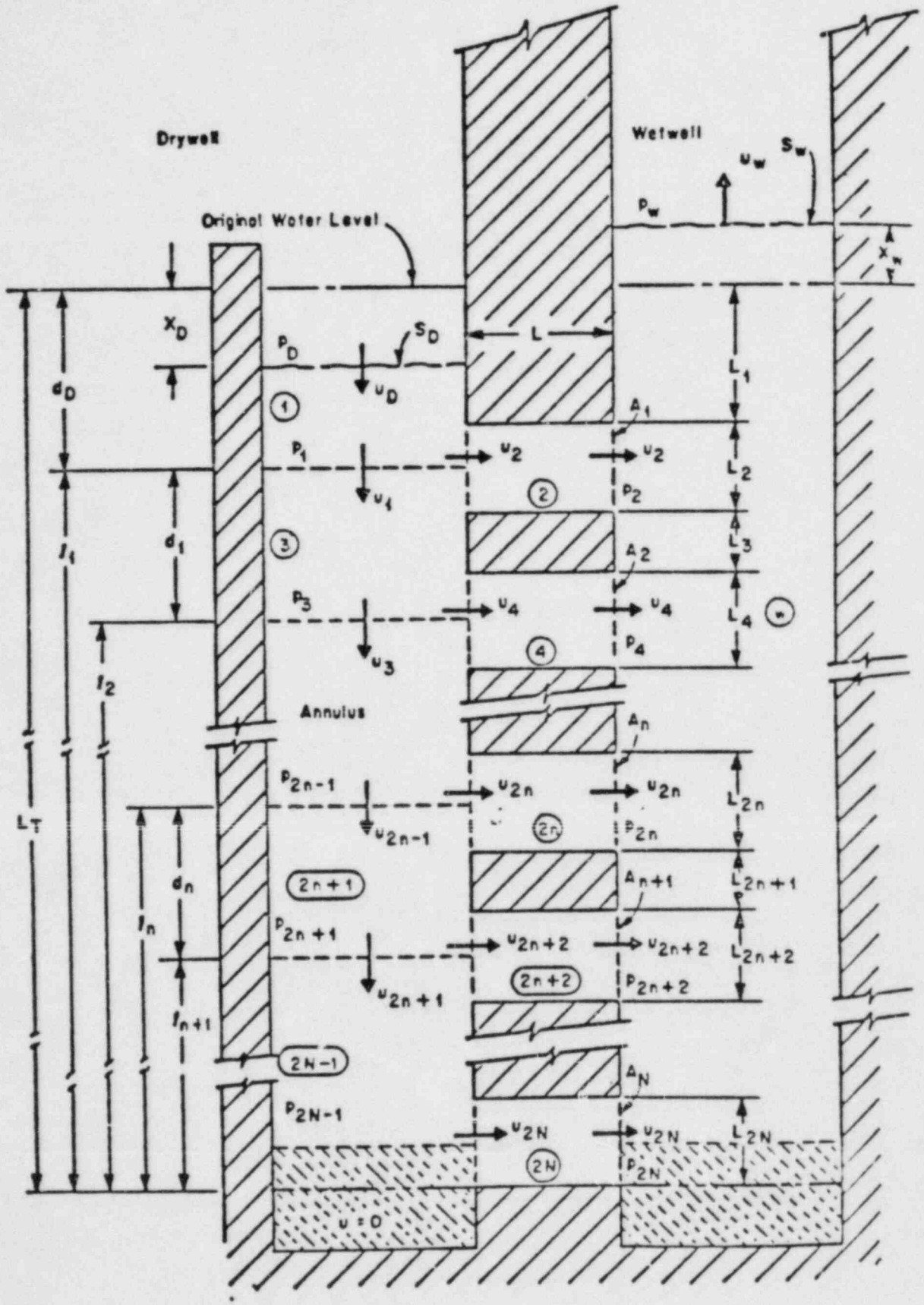

Figure 3.6.5-5. Control Volumes for Mark III Vent Flow Model

Node 2n+1 - Clearing

Use the same equations as the preceding with the following substitutions:

$$u_{2n-1} \longrightarrow u_D$$
$$P_{2n-1} \longrightarrow P_D$$
$$d_n \longrightarrow d_D$$

where

$$d_D = L_T - l_{n+1} - X_D.$$

$$L_T = \sum_{i=1}^{2N} L_i$$

$$l_n = \sum_{i=2n}^{2N} L_i - 1/2 \quad L_{2n}$$

$$d_n = L_{2n+1} + 1/2 \ (L_{2n} + L_{2n+2})$$

VENT NODES

Node 2n - Not Clearing

Mass Balance:

$$u_{2n_{in}} - u_{2n_{out}} = u_{2n} \ . \qquad (3.6.5\text{-}4)$$

Momentum Balance:

$$\dot{u}_{2n} = \frac{P_{2n-1} - P_{2n}}{\rho L} - \frac{f\left|u_{2n}\right|u_{2n}}{2R} - \frac{1}{2L} K_{sc_n} (1-\alpha_n) \left|u_{2n}\right| u_{2n}$$

$$n = 1,2,3,\ldots,N \qquad (3.6.5\text{-}5)$$

For negative u_{2n}, α_n is replaced by β_n.

where

K_{sc_n} = sudden contraction bss coefficient

$\beta = S_{D_n}/S_{w_n}$

Node 2n - Clearing

Mass Balance:

$$\frac{d}{dt} Y_n = u_{2n} \quad n = 1,2,3,\ldots,N \quad . \tag{3.6.5-6}$$

Momentum Balance:

$$\dot{u}_{2n} = \frac{P_D - P_{2n}}{\rho(L-Y_n)} - \frac{f|u_{2n}|u_{2n}}{2R} \quad n = 1,2,3,\ldots,N \tag{3.6.5-7}$$

where

Y_n = displacement of vent-water surface from entrance of vent.

WETWELL NODE

Node w

Mass Balance:

$$u_w = \sum_{n=1}^{N} \beta_n u_{2n}$$

$$= \beta u_d + \sum_{n-NC+1}^{M-1} \beta_n u_{2n} \quad . \tag{3.6.5-8}$$

Momentum Balance:

1. $n \leq M - 1$

$$\dot{u}_w^{M-1} = \frac{1}{L_{wn}} \{u_s^2 - u_w^2 + \sum_{i=NC+1}^{n-1} (d_i \sum_{j=NC+1}^{i} \beta_j \dot{u}_{2j})$$

$$+ \frac{P_{2n} - P_W}{\rho} - L_W - \frac{1}{2} \sum_{i=1}^{n} \beta_i u_{2i}^2 [K_{we_i}$$

$$+ (\beta_i - 1)^2 K_{se_i}] \quad . \qquad (3.6.5\text{-}9)$$

2. $n = m$

$$\dot{u}_w^M = \dot{u}_w^{M-1} - \frac{d_{M-1}}{L_{wn}} \beta \dot{u}_D \quad . \qquad (3.6.5\text{-}10)$$

3. $M < n \leq N$

$$\dot{u}_w^N - \dot{u}_w^M - \frac{\beta}{L_{wn}} \sum_{i=M}^{n-1} d_i \dot{u}_{2i-1} \qquad (3.6.5\text{-}11)$$

where

NC = Number of vents that have cleared
M-1 = Vent currently clearing
K_{se} = sudden-expansion loss coefficient
K_{we} = wetwell-elbow loss coefficient
$L_{wn} = L_T + X_w - l_n$.

To solve the system of equations, they are reformulated in terms of velocities, eliminating the pressures (except the drywell and wetwell pressures) from the equations. The velocities are numerically integrated to give pool level as in the General Electric model.

The flow rates through vertical and horizontal vents are both calculated assuming compressible, steady, one-dimensional, adiabatic flow. Irreversible losses are modeled using loss coefficients and choked flow limits are included. The equations solved are:

Continuity:

$$(\rho \, v \, A)_i = (\rho \, v \, A)_f - W, \text{ a constant} \quad . \qquad (3.6.5\text{-}12)$$

Energy

$$1/2\ (v_v^2 - v_i^2) + (h_f - h_i) + g(z_f - z_i) = 0 \quad . \qquad (3.6.5\text{-}13)$$

Momentum

$$p_f - p_i - \Delta p_{IR} - \rho\, g(z_f - z_i) - W\left(\frac{1}{A}\right)(v_f - v_i) \qquad (3.6.5\text{-}14)$$

where

ρ = fluid density
v = fluid velocity
A = flow area
g = acceleration due to gravity
h = fluid specific enthalpy
z = elevation being considered

ρ = average fluid density in element = $\dfrac{\rho_i + \rho_f}{2}$

$\left(\frac{1}{A}\right)$ = average-inverse-flow area = $\left(\frac{1}{A_i} + \frac{1}{A_c}\right)$

ΔP_{IR} = irreversible pressure loss due to wall friction and area or direction changes in element.

The equations require an iterative solution. Using an assumed inlet-flow rate, a solution is obtained for the remaining flow rates. Iterations are performed until the calculated pressure at the final control volume of the calculation matches its static pressure, or until the vent flow is choked.

The CONTEMPT-11 model allows flow in either direction through the vents. It also allows liquid to spill over the weir wall into a pool in the drywell.

The suppression pool is assumed to heat up uniformly. All of the steam entering the suppression pool is assumed to condense in it. Air passing through the suppression pool is assumed to leave at the suppression pool temperature.

The MARCH [9] suppression-pool model does not calculate the motion of the pool. It simply allows enough flow between the drywell and wetwell to maintain a user-specified differential pressure. If flow through a safety/relief valve is being modeled, the steam leaked from the reactor vessel can be routed directly to the suppression pool. Noncondensities are assumed to leave the pool at the pool

temperature and steam in excess of that required to keep the steam-partial pressure in the wetwell at the pool-saturation pressure is condensed. The suppression pool is assumed to heat up uniformly.

3.6.5.3 Recommendations

The CONTEMPT-LT pressure-suppression treatment is a developed, available model that treats many of the phenomena that will be of interest in MELCOR calculations. Its inclusion as a starting point for a MELCOR model is recommended. It may be desirable to modify the equations to allow non-uniform pool heatup and to include a simple pool swell model. Because MELCOR will treat severe-accident scenarios, consideration will have to be made for such phenomena as core-concrete interactions that fail the weir wall and steam explosions in the drywell. Iodine and aerosol decontamination by the suppression pool will have to be addressed. Both General Electric and the Pacific Northwest Laboratory have ongoing programs to study fission-product scrubbing by suppression pools.

3.6.6. RECIRCULATION

The initial water sources for both the emergency core-cooling system and the containment sprays are large storage tanks, typically the refueling water storage tanks. These cannot, practically, provide enough water for long-term heat removal from the core nor the containment. The water that has passed through these systems, however, is available for recirculation. A sump, located below the reactor cavity, collects this water as well as condensate that has dropped or flowed from containment walls and internal structures. As this liquid will in general, be at or near the containment-saturation temperature, it must be cooled before its reuse. Large capacity heat exchangers, using an outside source of water are used for this purpose. Another critical element of the system is the instrumentation and controls that switch the system from the primary source to recirculation. Thus, the typical recirculation system includes a sump, a recirculation pump, a heat exchanger, and the related controls.

3.6.6.1 Model Assessment

The heat-exchanger model that is used in the CONTEMPT code [8], which is based upon Reference [21], allows for the choice any one or a combination of five-heat exchanger types. Heat exchanger options include:

1. Shell and U-tube single shell pass
2. Cross flow, hot side tubes, cold side shell
3. Counter flow
4. Parallel flow
5. User-input time-dependent energy removal rate.

The important output parameter from this model is the hot-leg outlet temperature, T_{hx}. In this model it is expressed as a function of the efficiency parameter, η_{hx}, by

$$T_{hx} = T_h - \frac{C_{min}}{C}\eta_{hx}(T_h - T_c) \quad , \qquad (3.6.6\text{-}1)$$

where T_h and T_c are the inlet hotand cold-leg temperatures respectively. C, sometimes referred to as the flow capacity, is the product of the hot-leg flow rate, W_{hx}, and the cold-leg inlet, constant pressure, heat capacity, C_{pc}.

The efficiency, η_{hx}, depends upon the heat exchanger type, effective surface area, and the overall heat transfer coefficient, h_{hx}, all input parameters. Expressions for η_{hx}, are given in [8] for each of the first four

exchanger types. This formulation is simple, fast, has received extensive use and testing, and appears to be adequate for the purposes of MELCOR.

The sump may be either modeled simply as a reservoir of which the quantity and enthalpy of its contents are tracked, or the reactor-cavity pool model might serve as such. The latter is attractive in that it minimizes the total number of models that must interact. On the other hand, there may be many problems in which the detailed physical treatment afforded by the pool model are not needed. Unless the overhead of the pool model is prohibitive in these cases, I believe that the advantages of a single-integral model dominate. In any case, the net positive suction head available must be modeled to indicate onset of pump cavitation. The control function, i.e., switching to and from the recirculation, and the flow rate through the system
can be simple, user defined functions.

3.6.7 FILTERS AND FILTERED VENTS

Some early containment designs relied heavily upon high capacity, recirculating air-filter systems for aerosol and iodine removal following a postulated accident. More recently, smaller filtered vent systems have been installed in the exhaust system of plants with secondary containments. There are current considerations to provide filtered vent systems to single-containment plants in order to provide controlled release should containment integrity prove impossible to maintain. Typical of filter systems in service today are multistage units through which an exhaustside fan pulls the atmospheric mixture. The first stage is usually a mechanical moisture separator made up of horizontal louvers. Next may come a series of loosely packed fiberglass filters which remove additional moisture as well as larger dirt and debris. A heater may follow to further dry the atmosphere. Additional roughing filters may be located at this point, depending on the expected type and sources of dirt. The first actual decontamination occurs through a bank of high-efficiency particulate air (HEPA) filters. These are highly specialized and very effective aerosol filters. The HEPA filters are followed by trays of activated charcoal-filtering media. This material is extremely effective in trapping elemental iodine and only slightly less effective for methyl iodide. Following the charcoal trays is another bank of HEPA filters provided to catch any charcoal that might be released by the iodine filters.

3.6.7.1 Model Assessment

The key elements that must be addressed in the model of such filters are the effectiveness of decontamination as functions of flow rate, loading, and the characteristics of the species being filtered and flow rate as a function of loading. The HEPA filters continue to perform well as long as there is flow through them. As loading occurs, however, flow restriction increases, and the resulting pressure drop eventually results in inadequate flow. Loading of the charcoal filters has no adverse effects on flow characteristics, but results in degraded filter performance. For a recirculating filter located within a cell, each of these characteristics may specified as userinput functions. I believe that any attempt to provide hardwired functions or to calculate these parameters mechanistically would reduce flexibility and increase code complexity excessively. For filters located within flow paths, as a filtered vent would be, a flow resistance as a function of loading would have to be provided.

3.6.8 FANS

Fans, though not generally thought of as engineered safety features, play an active role in the performance in many safe systems. The containment coolers and recirculating filters require circulation fans. Icecondenser systems employ fans to equalize the pressure between the lower and upper compartments, following a blowdown. Although all fans ought, to the extent possible, be treated consistently, they should probably be treated separately within the major models in which they are active. The fan-cooler model may simply employ a user-input volumetric flow rate. The filter may require a user-specified function of volumetric flow rate versus aerosol loading. The ice-condenser vent-fan characteristics might be specified within the condenser model, but would be active within the atmospheric-flow model.

3.6.9 HYDROGEN COMBUSTION MITIGATION SYSTEMS

Following the accident at TMI-2 there has been an increased awareness of the possibility for containment damage resulting from the combustion of atmospheric hydrogen resulting from extensive zirconium-steam reaction. A variety of mitigation schemes have been proposed and a few have been installed in operating plants. Among those systems that have been considered and/or employed are;

1. Recombiners
2. Deliberate ignition
3. Inerting, and
4. Water fogs.

A brief description of each of these systems and possible modeling approaches for them is given below.

3.6.9.1 Recombiners

Several methods have been employed for recombining the small amounts of hydrogen and oxygen resulting from radiolysis of the primary coolant. Radiolytic gases are routinely vented from BWR vessels and recombined. The systems available, however have a very limited capacity. To provide enough combiners to process the gases from a substantial metal-water reaction would prohibitive. As a result there is probably no need for modeling recombiners as such in MELCOR.

3.6.9.2 Deliberate Ignition

Another method of controlling liberated hydrogen within LWR containments is deliberate ignition. This may be performed with glow plugs, spark plugs, or, perhaps pyro-fuses, with glow plugs being the most popular choice at this time. Deliberate ignition relies on multiple ignitions of low concentrations of hydrogen, producing burns that do not threaten the containment. Ignitors are currently employed in three ice-condenser PWR plants and one BWR Mark III drywell. The ignitors may be actuated automatically or manually.

The modeling of deliberate ignition in MELCOR can be fairly straightforward. For calculational purposes, an automatic actuation is probably desirable, with the criteria specified as user input. Upon actuation, the physics contained within the hydrogen burn model would provide the proper response.

3.6.9.3 Inerting

A wide variety of inerting strategies and media have been suggested and one is in common use. The idea of

inerting is to make the atmosphere chemically incompatible with a large hydrogen burn, either by decreasing the concentration of oxygen or by introducing a flame-retardant chemical. The drywells of Mark I and II BWRs currently contain an inert-nitrogen atmosphere. Continuous nitrogen inerting of larger containment volumes is impractical economically, and introduces safety problems due to the need for personnel access to the area. Continuous inerting can be treated easily in MELCOR by merely specifying the initial atmospheric chemistry. Postinerting schemes have been proposed, whereby, nitrogen, or possibly carbon dioxide is introduced to the atmosphere following an accident. This too may be simply treated in MELCOR as an atmospheric source. Another postinerting media that may be used is one of a family of halogenated hydrocarbons, known generically as halons. These have seen wide use in industry as flame-quenching agents. Treatment of such a system in MELCOR would require inclusion of the appropriate chemistry within the hydrogen-burn model. Since halon-inerting systems are not being considered for immediate use in nuclear plants, this capability might represent a lower priority item for MELCOR development.

3.6.9.4 Water Fogs

Water fogs, somewhat comparable to containment sprays with a much finer droplet size, could provide substantial pressure and temperature suppression in the event of a hydrogen burn. This involves the suspension of a large mass of liquid water, in the form of droplets, in the containment. The drops act as a large thermal capacitance, greatly reducing the temperature rise that would occur as a result of hydrogen combustion. If the droplets are sized properly, they will not interfere with the combustion itself, so that it would be logical to use the fog in conjunction with deliberate ignition.

Fogs have not been installed in plants because their development has not reached the point necessary to determine if it is practical to maintain a stable, high-density fog. A substantial amount of study will be required before such systems will see routine application. For this reason, I recommend that water-fog systems not be included in the first version of MELCOR. When and if such systems are satisfactorily defined, a model comparable to that for the containment spray might be appropriate. It is likely, however, that some aerosol physics may have to be added to treat the agglomeration of droplets.

3.6.10 REFERENCES

1. Hilliard, R. K. and Postma, A. K., "Effect of Spray Flow Rate on Washout of Gases and Particles in the Containment Systems Experiment," Battelle Pacific Northwest Laboratories Report BNWL-1591 (July 1971).

2. Ranz, W. E. and Marshall, W. R., "Evaporation from Drops," Chemical Engineering Progress, Vol. 48, No. 3 (April 1952).

3. Bird, R. B., Stewart, W. E., and Lightfoot, E. N., Transport Phenomena, John Wiley and Sons, Inc., New York (1960).

4. Williams, F. A., Combustion Theory, Addison-Wesley Publishing Company, Inc. (1965).

5. Internal memorandum from Mel Baer to Bob Kee, April 24, 1980.

6. Lewis, E. E., Nuclear Power Reactor Safety, John Wiley and Sons, Inc., New York (1977).

7. "Technical Bases for Estimating Fission Product Behavior During LWR Accidents," USNRC Report NUREG-0772.

8. Metcalfe, L. J. et al., "CONTEMPT4/MOD2 A Multicompartment Containment System Analysis Program," Idaho National Engineering Laboratory Report TREE-NUREG-1202 (February 1978).

9. Wooton, R. O. and Avci, H. I., "MARCH (Meltdown Accident Response Characteristics) Code, Description and Users Manual," Battelle Columbus Laboratories report NUREG/CR-1711 BMI-2064 R3 (October 1980).

10. Transcript of the proceedings of the United States Advisory Committee on Reactor Safeguards, Monroeville, PA (August 27, 1974).

11. Hsieh, T. and Raymund, M., "Long Term Ice Condenser Containment Code - LOTIC Code," WCAP-8355, Supplement 1, Westinghouse Electric Corporation (June 1975).

12. Exxon Nuclear Company, Inc., "ICECON: A Computer Program to Calculate Containment Backpressure for LOCA Analysis (Including Ice Condenser Plants)," XN-CC-39 Rev. 1 (December 1977).

13. Obenchain, C. F., "RELAP4/MOD5, A Computer Program for Transient Thermal-hydraulic Analysis of Nuclear Reactors and Related Systems, Users Manual, Volume 1," ANC-NUREG-1335, Aerojet Nuclear Company (September 1976).

14. Gido, R. G. et al., "COMPARE-MOD 1: A Code for the Transient Analysis of Volumes with Heat Sinks, Flowing Vents and Doors," LA-7199-MS Los Alamos Scientific Laboratory (March 1978).

15. McCurdy, M. W. et al., "Supplementary Information to WCAP-7833, Design and Performance Evaluation of the Ice Condenser Reactor Containment System," nonproprietary version, Westinghouse Electric Corporation (January 1972).

16. Fuls, G. M., "The CLASIXS Computer Program for the Analysis of Reactor Plant Containment Response to Hydrogen Release and Deflagration," OPS-36A31, nonproprietary version, Offshore Power Systems (October 1981).

17. Camp, A. L. et al., "HECTR: A Computer Program for Modeling the Response to Hydrogen Burns in Containments," SAND82-1964C, Sandia National Laboratory, Second International Workshop on the Impact of Hydrogen on Water Reactor Safety, Albuquerque, New Mexico (October 1982).

18. Batelle Pacific Northwest Laboratory, "Evaluation of Computation of Maximum Transient Pressures, Differential Pressures, and Loads for Ice Condenser Containment Systems," non-proprietary version, 211B01498/211B01499 (May 1973).

19. Bilanin, W. J., "The General Electric MARK III Pressure Suppression Containment System Analytical Mode," NEDO-20533, General Electric (June 1974).

20. Hargroves, D. W. and Metcalfe, L. J., "CONTEMPT-LT/028 - A Computer Program for Predicting Containment Pressure-Temperature Response to a Loss-of-Coolant Accident," NUREG/CR-0255, TREE-1279, EG&G Idaho, Inc. (March 1979).

21. Kays, W. M. and London, A. L. Compact Heat Exchangers, McGraw-Hill, New York, New York (1964).

3.7 CONTAINMENT LEAKAGE AND STRUCTURAL FAILURE

by

T. E. Blejwas

CONTENTS

3.7.1 INTRODUCTION

Until recently the only type of release from a containment that was considered in severe accident analyses and risk assessments was a "puff" release due to containment structural failure that left the containment vented to the atmosphere. In part because containments are leak tested at design pressure to insure that leakage is very low (on the order of 0.1 percent contained mass per day), earlier studies did not consider leakage per se. However, containment pressures and temperatures during a severe accident may cause leakage well above that allowed during operational testing. For some potential accidents, the leakage through seals, gaskets, or local penetration failures may, in fact, sufficiently relieve pressure buildup in the containment to prevent a complete containment failure. Hence, modeling of releases from the containment in MELCOR should permit the user to specify different types of containment leakage, including large release due to containment structural failure.

Although quantitative data for potential containment leakage during severe accidents is scarce, the manner in which leakage may occur has been considered and is discussed below. Significant programs are presently in place to provide a data base for leakage estimates and these programs are briefly described. A short discussion of how available and anticipated data may be used in MELCOR completes this section.

3.7.2 CONTAINMENT RESPONSE

After the beginning of an accident, the containment boundary, by design, should isolate the containment interior from the exterior. However, as summarized by Weinstein [1,2], there is a low but finite probability that paths for containment release exist at accident initiation. Assuming that preexisting paths are small or nonexistent, many accidents will cause a gradual rise in pressure and temperature in the containment. The types of leakage paths that may develop and their order is highly dependent upon the type of containment structure, the types of containment penetrations, and the particular accident scenario.

For low temperatures and pressures up to design pressure, only preexisting leak paths are likely. As pressure and temperature increase further, leakage through penetrations may occur. High temperatures cause a degradation of some sealing materials that leads directly to leakage. High pressures and aging environment due to thermal and radiation effects place additional demands on sealing devices. The behavior of operable penetrations (equipment hatches, personnel airlocks, etc.) is complicated by the structural distortion of the sealing surfaces as pressure increases. Although the leakage through an individual penetration may be small, the cumulative leakage from all penetrations may be significant.

A containment structure is designed using conservative codes or other procedures and has a pressure capacity that is generally believed to be at least twice (and in some cases four times or more) its design pressure. Although the structural "failure" pressure is important for many accident evaluations, the details of the localized behavior of the structure and penetrations may significantly affect the leakage potential leading up to structural failure. The details of the localized behavior are dependent upon the particular design details, but some generalizations with construction type are possible.

3.7.2.1 Steel Containments

Assuming that leakage does not limit pressurization, the steel-containment wall will begin to displace noticeably outward as gross membrane yielding occurs. However, the annulus between the steel containment and the concrete shield wall includes many pipes that penetrate both structures. The piping restraints may cause local failures of the piping, the penetration assemblies, the penetration sleeves, or the steel cylinder wall around the penetrations. Any of these local failures may cause increased leakage from the containment. In addition to the distortion of the containment walls, the major penetrations may undergo sufficient distortion to greatly increase the leakage around gaskets and seals.

3.7.2.2 Reinforced Concrete Containments

In reinforced concrete containments, the steel liner is attached to the concrete at close intervals. Cracks begin to form in the concrete at low pressures (often below design pressure), but the cracks are regularly spaced (because of the pattern of the reinforcing steel) and the crack widths are initially small. When yielding of the reinforcing steel occurs, the crack widths will grow rapidly. However, the liner may still provide a leak-tight boundary. Whether or not liner tearing is a probable occurrence before a structural failure occurs is a controversial question. Elaborate tests appear to be the only way to resolve the question.

Details of reinforcing around penetrations and the manner in which the penetration sleeve is attached to the concrete will also affect the potential for leakage or structural failure around penetrations. However, reinforcement/attachment related failures are improbable prior to general yielding of the containment shell.

3.7.2.3 Prestressed Concrete Containments

The concrete-cracking pattern in prestressed concrete containments is less predictable than for reinforced concrete containments. Because of the variation in prestressing direction, i.e., meridional prestressing only or meridional and hoop prestressing, and the variation in number of buttresses, general statements about the effect of concrete cracking on leakage are difficult to make. The prestressing does tend to minimize cracks perpendicular to the tendons; however, cracking around penetrations away from the buttresses may be more severe. Also, when the pressure reaches a level that causes tendon yielding, cracks perpendicular to the tendons may form at very widely spaced intervals. The large spacing will lead to large crack widths as the tendons strain plastically. Predicting steel-liner tearing in a prestressed concrete containment is very difficult.

3.7.3 PROGRAMS FOR CONTAINMENT LEAKAGE AND STRUCTURAL RESPONSE

Accurately predicting the leakage of containments at high pressures and temperatures is not possible at this time. However, as part of an NRC-sponsored program, estimates of containment leak areas with large bands of uncertainty are being made. The estimates are being used in modified versions of MARCH and other containment codes to determine the effect of containment leakage on accident analyses. Intermediate results of this work are available in draft form only [3]. It should be emphasized that the leak area estimates from this work are approximate, and the authors recognize the need for more analytical work and, more importantly, experimental data on leakage through containment boundaries.

Several programs that will provide needed data for predicting containment leakage and structural response are presently underway. The Electric Power Research Institute (EPRI) is directing a combined analytical and experimental program. Included are leakage measurements on models of concrete-containment wall sections under pressure and biaxial tension. Some of the sections will include a penetration sleeve. One of the purposes of these tests which are being conducted by the Portland Cement Association's Construction Technology Laboratories is to determine the potential for liner tearing and resulting leakage. EPRI is also sponsoring analyses at ANATECH to attempt to predict liner failure.

The NRC-sponsored Containment Safety Margins Program at Sandia National Laboratories (SNL) is a combined analytical and experimental program. The experimental effort consists primarily of tests of models of complete containment shells at 1/32, 1/8, and 1/6 sizes. The larger size models include some penetrations with closures. The models are not replicas of any containment structure and only a limited number of leakage paths are included in the models. Internal pressurization with nitrogen gas or air will be conducted up to structural failure or excessive leakage, based upon equipment limitations (probably on the order of 200 percent mass per day). Measurements from which leakage can be inferred will be conducted at a few pressure levels. Relationships for scaling leakage data have not been defined. However, one objective of the program is to qualify analytical methods for predicting containment structural response. If a relationship between deformations in penetrations and leakage around seals and gaskets can be established, the qualified analytical methods may be useful for predicting the onset of gasket/seal leakage.

Other NRC-sponsored programs include a program on Electrical Penetration Assemblies. The objective of this program is to determine the leakage potential for electrical penetration assemblies subjected to high temperature and pressure environments. Present plans call for testing of a small number of selected electrical penetration assemblies.

The NRC has also sponsored a new program on containment penetrations other than electrical. Although the precise nature of the program has not been finalized, it is expected that leakage measurements of full size personnel locks and other operable penetrations that are subjected to high temperature-pressure environments will be a part of this program.

Although experimental data for predicting containment leakage is nonexistent or not directly applicable, the potential results from existing and planned programs is promising. Some of these results will be in the form of gaseous leakage through parts of containment structures. It may be possible to inventory an actual containment and sum the leakages or leak areas for all the various penetrations and details. Because only a small number of types of containment features will be tested, many approximations/assumptions will be necessary. In any case, a better estimate of leakage as a function of pressure and temperature should be possible in the near future.

3.7.4 CONTAINMENT-LEAKAGE MODELING IN MELCOR

The containment representation in MELCOR should model at least two types of containment releases. The "puff" release, in which the containment has a predetermined "failure" pressure, must be accommodated. In addition, the leakage from the containment at pressures below the "failure" pressure must also be represented. MELCOR must be able to analyze accidents in which the containment leakage reduces the buildup of pressure so that the "failure" pressure is not reached.

The input of leakage data to the MELCOR code can be in the form of mass rate as a function of temperature and pressure, but the effective cross-sectional area of leakage holes is a preferred representation. The area should be the sum from all potential sources in the containment.

Although leak area is probably a complex function of pressure, temperature, and time (at least), the limited amount of leakage data available now or in the near future does not justify a complex representation. One possible simple representation is as follows. Assume that the leak areas due to the effects of temperature and pressure are separable. The leak area due to temperature could be a step function (due, perhaps, to groups of seals loosing their sealing abilities at specified times at specific temperatures). The leak area due to pressure could be represented by a piecewise linear function (the steps occurring when parts of the structure of some penetrations reach their yield point). As our understanding of leakage through operable penetrations improves, the number of linear segments can be increased. The total leak area would be the sum from the temperature and pressure effects.

The present programs on containment integrity are experimentally aimed at better understanding the leakage of gases or steam through the containment boundary. However, the actual containment environment during a severe accident is very complex. The leakage involves two-phase flow, aerosols, particulates, etc. Leaks may be plugged by the deposition of some components of the containment environment. As future research is conducted to better understand this complex leakage, the modeling of leakage in MELCOR will likely require changes and/or additions.

3.7.5 REFERENCES

1. Weinstein, Michael B., "Integrity Failure Experiences with Reactor Containments" Proceedings of the Workshop on Containment Integrity, June 7-9, 1982, NUREG/CP-0033, Sandia National Laboratories, Albuquerque, NM, October 1982.

2. Weinstein, Michael B., "Primary Containment Leakage Intergrity: Availability and Review of Failure Experience," Nuclear Safety, Vol. 21, No. 5, September-October 1980.

3. Containment Leak Rate Estimates, NUREG-1037 (for comment), 3rd draft, November 21, 1983.

3.8 INTERFACES BETWEEN THERMOPHYSICAL PROCESSES AND AEROSOL AND FISSION PRODUCT PROCESSES IN CONTAINMENT

by

K. K. Murata

CONTENTS

LIST OF TABLES

3.8.1 INTRODUCTION

These sections discuss the ways in which the thermophysical processes in containment can be affected by aerosol and fission product behavior. In Section 3.8.6, a summary of the main points and tentative conclusions are given.

The effects that are addressed here are of two types. There are, first of all, effects (Type I) which can significantly change the temperature and pressure threat to containment over the short term and alter aerosol and fission product behavior within containment. There are also effects which may not significantly change the temperature and pressure threat to containment over the short term, but change thermohydraulic conditions enough to alter the aerosol and fission product behavior. There are also small feedback effects which, over the long term, can change the long-term behavior within containment and the eventual course of the accident. These latter types of effects will be considered Type II. Note that an effect classified as Type I may in some circumstances degrade to Type II. These kinds of Type II effects will generally not be discussed since justification for coupling of the aerosol and fission product behavior with the thermohydraulic behavior can be established from the Type I occurrences. This approach is taken here for one reasons of economy, even though the proper description of Type II effects should be the goal of MELCOR.

For illustration of Type II effect, the decontamination rate of the containment atmosphere is apparently sensitive to the condensation rate of water vapor on aerosols: a 1 kg/sec condensation rate can have an important effect. The presence, or absence, of a small heat source to the atmosphere of 2 megawatts (corresponding to the latent heat produced) would significantly affect this amount of condensation. Two megawatts is in the range of heating expected from fission products which are provided by sources to the containment atmosphere but which can subsequently deposit out. Therefore, the fission products would have to be tracked in containment in order to know the atmosphere heating to degree required to calculate decontamination rates accurately. On the other hand, the containment heat sinks are such that this amount of heating corresponds to on the order of a 10 K difference in the atmosphere temperature, which makes little difference in the threat to containment. The effects (Type II) of aerosol and fission product behavior back on itself via thermohydraulics may therefore be significant even though the effects (Type I) on the short-term threat to containment are not.

In the approach used in the MARCH/CORRAL and MARCH/MATADOR codes, the effects of aerosol and fission product behavior on thermophysical processes were assumed to be of secondary importance and are crudely represented, if at all, in the thermohydraulics calculated by MARCH.[1] The details of the aerosol and fission product behavior are calculated separately from MARCH, given the MARCH thermohydraulic results. This methodology assumes that the feedback effects are not important. CONTAIN[2] is an integrated containment code which fully couples thermohydraulics and aerosol and fission product behavior. It is being developed for LWR calculations and can presently be used for some but not all sequences.

A systematic study of feedback effects using CONTAIN has not been conducted to date. What is known about feedback at this point comes primarily from discussions, a few sets of CONTAIN calculations, and a few hand calculations. In addition, the importance of the feedback effects depends to a great extent on the source terms used and on the timing of events within a scenario, both of which should be assigned a great deal of uncertainty. Consequently, the assessment given here of these effects should be regarded as tentative.

Even a tentative assessment is useful at this stage for providing a set of priorities for MELCOR code development. The current performance of CONTAIN demonstrates that an integrated code for containment behavior can have computational efficiencies consistent with PRA requirements. It is therefore assumed that MELCOR will be an integrated code, at least with respect to containment behavior, and that the inaccuracies in this assessment will at most effect the order of implementation of interfaces. It is with this understanding that these sections have been written. Specific, illustrative examples are given to provide the reader with a feeling for the magnitude of effects. The results of a full, systematic study are not available.

3.8.2 ATMOSPHERE THERMODYNAMICS AND INTERCELL FLOW

3.8.2.1 The Effects (Type I) on Mass Conservation

The amount of liquid water injected into or condensed in the containment atmosphere during an accident can be comparable to the water vapor and noncondensible gas masses in the atmosphere. The liquid water will be quickly removed from the atmosphere in most cases so that only a small fraction of the total amount remains. Since the liquid significantly alters the atmosphere thermodynamic properties, some attempt must be made to model the removal mechanisms.

Some of the liquid occurs as droplets which are sufficiently small to warrant description as aerosols. The water aerosol can either be due to direct injection of a high temperature water stream which subsequently flashes, entrainment of droplets in low-quality steam, or from injection of steam which subsequently condenses onto existing aerosols. In an LWR containment the only aerosol material which could contribute significantly to the atmosphere mass, thermodynamics, or intercell flow is water. (We exclude from consideration here fission products in aerosol form which have negligible mass and material properties but which will add decay heat to the atmosphere. See Section 3.8.3.1.)

The aerosol quantity of primary interest for the atmosphere thermohydraulics is the total amount of aerosolized water. To some extent the size distribution of the aerosols is expected to affect the thermodynamic response of the atmosphere during condensation and evaporation of water on aerosols through its effect on the diffusion of the vapor to and from the particles. However, diffusion is not expected to be a limiting factor except in cases where the aerosol mass concentration is sufficiently low that the effect on the atmosphere properties is negligible, or where an event, such as a hydrogen burn, occurs with a short time scale.

The aerosol mass in the containment atmosphere is controlled by various natural removal mechanisms for aerosols. For sources characteristic of an LWR containment, natural removal is expected to be efficient in limiting and then reducing the amount of water aerosol in the atmosphere. The primary removal mechanism is expected to be settling of the aerosols. The settling is generally enhanced by agglomeration and formation of large size particles which settle out rapidly. Diffusiophoresis (the drift of particles in the water vapor flux condensing on a surface) may be as effective as settling as a removal mechanism during periods of rapid condensation on structures.

The removal of water aerosol is typically a fast process at the high-mass concentration levels required for the water to be significant in the atmosphere thermohydraulics. It is therefore tempting not to model the removal accurately but to use a simplified model. MARCH[1] assumes that a certain fraction of the liquid water introduced into the atmosphere falls instantly into the containment sump, and that the rest settles out at a rate characteristic of monodisperse (one particle size) distribution. For the Zion TMLB' example given below, the MARCH modeling, or even an instantaneous removal assumption for all liquid is apparently adequate for describing Type I effects during the blowdown period. (Type II effects were not addressed in this example, but of course may be significant even if Type I effects are not.)

However, the removal of water aerosol is not always a fast process compared to other time scales of interest, and Type I effects may result. Two examples are discussed below: the case of a steam spike, or transient, and the case of a blowdown in a small cell. In these situations the water aerosol sources and removal rates should be accurately modeled. As indicated below, this would require a discrete method using a number of different particle size classes. The size distribution of the water-droplet source term to containment is required whenever water is entrained in a steam source, or a liquid water source flashes in containment. Since a discrete method would presumably be available in the aerosol and fission product module, it is recommended that the effects of a droplet source term, condensation and evaporation on aerosols, and removal rates be calculated in that module.

Table 1 gives values of the water-aerosol mass concentration calculated during the blowdown for a Zion TMLB' sequence. The blowdown source to containment is based on a MARCH calculation,[1] and the containment thermohydraulic response and aerosol behavior were calculated using CONTAIN.[2] CONTAIN uses a discrete (sectional) method to calculate aerosol behavior. The total amount of water and steam injected into containment up to the point of core slump into the lower pressure vessel head is given in units of grams per cubic meter of containment, along with the total amount of water aerosolized up to this point, the peak water-aerosol mass concentration, and the mass concentration at the point of core slump. For comparison, the amount of water condensed on structures per cubic meter of containment up to the point of core slump is also given.

The injection of liquid water into containment, as opposed to steam, occurred early in the blowdown in the calculation. A major uncertainty exists in the droplet size distribution and the subsequent settling rate when the aerosols are generated from liquid water which is injected and

subsequently flashes. A major fraction of the liquid remaining after flashing may not be aerosolized, but may fall quickly to the floor as fairly large drops or globules. (On the other hand, the size distribution of aerosols which are created by the injection of high-quality steam, which subsequently condenses onto existing aerosols, is governed by gas phase diffusion and is fairly well known.)

In order to illustrate the differences which can result from the amount aerosolized after flashing, two cases were run: in case (a) of Table 3.8.2-1 all of the blowdown water remaining after flashing was assumed aerosolized; in case (b) 70 percent of the water remaining after flashing was assumed not to aerosolize but to fall directly to the

Table 3.8.2-1

Containment Water Aerosol
Behavior for Zion TMLB'

	Case (a): 100% aerosolization (in g/m^3)	Case (b): 30% aerosolization
Total injected water	3539	3589
Total aerosolized	1420	391
Peak mass concentration	218	110
Mass concentration at core slump	31	31
Total vapor condensed on structures up to core slump	589	589

containment floor. In case (a) a somewhat greater peak mass concentration results, but this peak relaxes quickly. The mass concentration in containment at the point of core slump is essentially unchanged, because it results from continuous condensation in the atmosphere due to cooling by the containment heat sinks during the last part of the blowdown.

This example illustrates the fact that, for a simple blowdown, aerosol removal can be a fast process. The removal mechanisms reduce the peak mass concentrations to a value well below the total injected mass per cubic meter. At the

time of core slump, the mass concentration has achieved a small steady state value determined by the action of the containment heat sinks. According to Table 3.8.2-1, the amount of water removed from the atmosphere through aerosol processes up to this point is comparable to the water vapor removed from the atmosphere through condensation on structures.

At the peak mass concentration of 110 g/m^3 in case (b) the water-aerosol mass is a small component (5 percent) of the atmosphere mass. In either case, (a) or (b), the atmosphere temperature and pressure are insensitive to the presence of aerosols at the calculated mass concentrations. Essentially no difference in the temperature and pressure would result if the aerosols were assumed to settle out instantly. In part, this is due to the fact that condensing conditions were present during the blowdown period. Under evaporating conditions, such as due to hydrogen burns, mass concentrations comparable to the calculated peak values would be significant in the atmosphere thermodynamic response because of effects due to the heat of vaporization. (See Section 3.8.2.2.) This example is one in which the aerosol removal, to the degree probably required for the atmosphere thermodynamics, can be modeled very simply.

This is not always the case. For example, the source-term duration and timing of events in the vicinity of steam spikes may result in aerosolized water which contributes significantly to the atmosphere thermodynamics. As an example, operation of the ECCS during a degraded core condition may cause a steam spike with a significant amount of entrained water to be introduced into containment. Moreover, the steam spike may be quickly followed by evaporating conditions. For example, some of the steam may cause additional reaction of the zirconium cladding. The resulting hydrogen may lead to a hydrogen burn while the water aerosol mass concentration is still high. Because of the heat of vaporization, the effects of the water aerosol can be quite pronounced under these conditions. A similar situation may occur after a pressurized blowdown from the injection of accumulator water over the core debris at the point of reactor vessel failure, or from core debris entry into a reactor cavity containing water. The latter situation can result in the steam spike which can eject significant amounts of debris and water.

In the example given in Table 3.8.2-1, the blowdown was assumed to occur in a containment-sized volume. One goal within MELCOR should be to handle local conditions characteristic at the minimum of compartment volumes, if not portions of those volumes. For a compartment, the volumetric

source rate for aerosols and the mass concentration can be much higher than that expected on the average for the entire containment.

The second case in which the water aerosols cannot be neglected occurs if a steam or high-temperature water source is modeled as occurring in a compartment appreciably smaller than a typical containment volume. The volumetric source rate can obviously be high in this case. One situation is a blowdown into a small compartment which is venting into other compartments. The small compartment may ventilate so rapidly that natural removal has little effect, or it may ventilate at an intermediate rate comparable to the natural removal rate. In either case, the water aerosols can significantly affect the temperature and pressure of the small compartment and the intercell flow.

In situations where aerosols contribute significantly to the atmosphere thermohydraulics, the mass concentration will usually depend critically on the modeling of sources and natural removal mechanisms. Because of the high aerosol mass concentrations involved, agglomeration and settling will be important processes. Since these processes tend to change the shape of the particle distribution function, the aerosol behavior should be calculated using a discrete method which allows the particle size distribution to change arbitrarily with time. Experience indicates that the effects of agglomeration and settling cannot be adequately represented by a monodisperse or lognormal distribution. The mass concentrations calculated using these assumptions can be off by an order of magnitude or more. The recommendation is to model water-aerosol sources and removal in the aerosol module along with the aerosol particulates. Presumably, the discrete method will be used to model the behavior of all aerosol components.

The aerosol module must allow not only for condensation and evaporation of water on aerosols, but also for a droplet source term. The size distribution of the droplet source term should be modeled within MELCOR for use by the aerosol module. The situations in which the aerosol loadings are highest may be ones in which a significant amount of the water aerosol is entrained or created by flashing the containment. It is known that the removal rate is relatively insensitive to the size distribution of the source for small particle (less than 1 micrometer diameter) sources. For sources of larger particles, the removal rate will depend critically on the source-size distribution.

3.8.2.2 The Effects (Type 1) on Energy Conservation

The presence of water aerosol in the atmosphere can significantly affect the temperature and pressure response. The heat capacity of the liquid affects the atmosphere

thermodynamic response under either condensing or evaporating conditions. The heat capacity of the liquid is considera. / more per kilogram than that of vapor. Under evaporating conditions in containment, such as that due to injection of hot gases or to hydrogen burns, a pronounced effect is also caused by the heat of vaporization of the liquid. The heat of vaporization of water is typically 2×10^6 J/kg whereas the specific heat of water vapor under nominal saturated conditions at 422 K is about 2×10^3 J/kg-K. Therefore, if the atmosphere contains 1 percent liquid water by mass, and the atmosphere is primarily water vapor, the evaporation of that water will absorb as much heat as that required to superheat the atmosphere by 10 degrees Kelvin.

The atmosphere can be driven superheated by hydrogen burns, hot gas (reactor cavity) sources, or simply from the drying effect due to condensation on structures. To hold the error in the temperature response of the atmosphere in general to 10 degrees K, the water-aerosol mass must be known to 1 percent of the atmosphere mass. This amounts to knowing the aerosol concentration to about 25 g/m^3 under nominal conditions. During certain phases of an LWR accident, one might expect an order of magnitude more than this amount for the average mass concentration in containment.

The specific heat of the water aerosol may be important under conditions where the aerosol mass is a significant fraction of the atmosphere mass. The possibilities were discussed in Section 3.8.2.1 above.

3.8.3 HEAT TRANSFER

3.8.3.1 Localized Heating Effects (Type II) of Pools and Heat Sinks

With the exception of the noble gas fission products and perhaps methyl iodide, fission products which are released from the fuel will tend to adsorb or deposit on surfaces and deposit or wash into pools. The surfaces and pools will begin to heat locally from the deposited fission products, and because the heat transfer and water-vapor mass transfer are affected, the containment response will be different from the case where the released fission products are assumed to heat the atmosphere uniformly. It will be assumed here that a provision has been made for uniform heating of the containment atmosphere, and only possible localized heating effects will be discussed.

The retention in the RCS of fission products released from the fuel, with the exception of the noble gases, will depend on the scenario. For a pressurized blowdown, the steam and gas residence times in the RCS will be substantially longer than in the case of a LOCA with a fairly large break, and significant retention of fission products in the RCS may occur. Significant retention may also occur in the steam generators for a cold-leg break LOCA. Localized heating of the RCS structures from retained fission products should be included in the heat source to containment, along with localized heating from any fuel debris retained in the reactor vessel.

Of the fission products released to the containment atmosphere from the in-vessel or exvessel phase of the accident, those which tend to form aerosols under containment conditions will tend to relocate through various aerosol deposition mechanisms. In addition, molecular iodine, if present, will tend to adsorb on wet surfaces and react with structural steel and paint. The dominant aerosol deposition mechanisms tend to favor horizontal surfaces, including pooling areas, or good heat sinks. These mechanisms are settling, diffusiophoresis (migration in the flux of water vapor condensing on a heat sink), and thermophoresis (migration down the temperature gradient near a heat sink). The deposition of fission products on good heat sinks will tend to remove the associated fission product heating from the containment atmosphere. Barring nonlinear effects in the heat transfer, the overall effect should be to reduce the atmosphere temperature and pressure.

The magnitude of the heating associated with the relocatable fission products is expected to be a small fraction of the total available decay power. Therefore, the temperature and pressure in containment is not likely to be affected

drastically over the short term by localized heating. However, the decontamination rate is a sensitive function of the condensation rate on aerosols and may be affected significantly by localized heating effects. The long-term temperature and pressure history of containment and the course of the accident can be affected by localized heating under some conditions. The details of the localized heating effects depends on the residence times of the fission products as they move through containment. The possible consequences from eventual relocation to pooling areas or the containment sump are discussed in detail below.

The fission products deposited on heat sinks may wash off with the water which has condensed on the surface and join fission products which have settled directly into pooling areas. The pooling areas can be taken to include the containment sump. However, if the reactor cavity is not assumed dry, the decay heat from the core debris will eventually cause boiling in the reactor cavity. The resulting steam source term will effectively couple the cavity and the rest of containment and dominate the localized heating effects discussed here.

Fission products in the atmosphere provide dry heat which tends to superheat the atmosphere. However, if fission products are relocated to pools, the heating of the pools to the point of evaporation or boiling will provide a source of water vapor which will tend to keep the atmosphere saturated. The water vapor will condense either in the atmosphere or on heat sinks. The condensed water will either settle directly back into the pooling areas or drain back from other surfaces. A continuous cycling (refluxing) of the water can be set up, provided sufficient heating of the pools from deposited fission products occurs.

The reduction of fission product heating of the atmosphere in itself may enhance the condensation rate on aerosols. In addition, at the rates expected from the pools, the water vapor may also enhance decontamination. The condensation of the water vapor in the atmosphere will tend to remove the remaining aerosols through enhanced settling, and the condensation on surfaces will remove the remaining aerosols through diffusiophoresis. The net removal rate of vapor from the atmosphere will also be affected. This in itself is important, because if water vapor drives the atmosphere inert, with respect to hydrogen burns during the blowdown period, the inert period can be extended significantly.

Because the reservior of water vapor in the atmosphere is considerably larger than the reservoir of water aerosols, it is felt that significant decontamination may occur from the water vapor expected from the pools provided a reasonable

fraction condenses in the atmosphere instead of on heat sinks. A change in the condensation rate will have a geometric instead of algebraic effect on the decontamination factor. Since fission products must first deposit out to heat the pools, some decontamination of the atmosphere must occur to initiate refluxing. However, the time required to achieve decontamination between one and a few orders of magnitude could be reduced by this effect.

The conditions for condensation of water vapor in the atmosphere for the small source expected from the pools are sufficiently involved that an appraisal of the potential for decontamination cannot be given here. However, the small-scale NSPP-400 series experiments[3] have shown significant enhancement of the decontamination rate under conditions where steam was injected at a rate to maintain quasi-steady (saturated) thermohydraulic conditions in the vessel.

In addition to the decontamination effect, the water vapor from the pools may provide a source which will significantly affect the deinerting point of the atmosphere with respect to hydrogen burns. The rate of water removal from the condensation on steel-lined containment walls may, for example, be limited by the gap resistance between the liner and the concrete and by the concrete conductivity to a relatively small value. Sample calculations show that a significant change in the time required to deinert the atmosphere can result from a source of water vapor from the pools with a rate of 1 kg/sec.

The effects due to localized heating are expected to be most important for the period between the time of dry out of the reactor cavity and the time of significant heating of the cavity walls. Although the fission products remaining in the core debris will generate most of decay power, the coupling between the cavity and upper containment during this period is expected to be weak. Upward radiative transfer from the core debris is expected to be fairly efficient but most of this heat will be deposited at first in the cavity walls. Downward heating will decompose the concrete reactor cavity floor but much of the heat will go into heats of decomposition and hydration. The enthalpy carried by the evolving hot gases which escape to upper containment is therefore expected to be only a small fraction of the decay heat.

The effects of localized heating from fission products deposited in containment would presumably be largest in the case of a hot leg, large-break LOCA where the retention in the RCS is small. To give the reader an indication of the localized heating available, the decay power from noble gases and aerosols released to containment, in one such case, is given in Table 3.8.3-1. The values were obtained from an ORIGEN run[4] and the release fractions from the fuel and

from the RCS quoted in the BMI-2104 draft[5] for the Surry AB sequence for case 2. In this release iodine was assumed combined with cesium and, therefore, the iodine was assumed to be in aerosol form. Only the aerosols in this case can participate in localized heating. Table 3.8.3-1 shows that the decay power associated with the aerosols is a small fraction of the total decay power. One would not expect the temperature and pressure history of containment to be changed drastically over the short term by localized heating involving this amount of power.

Table 3.8.3-1

Fission Product Decay Heating
in Containment by Components*

	at 1 hr.**	at 2 hrs. (in watts)	at 10 hrs.
Noble Gases	1.75×10^6	1.3×10^6	5.38×10^5
Aerosols	1.00×10^7	7.33×10^6	4.11×10^6
Total ANSI Standard Decay Power***	5.24×10^7	4.26×10^7	2.77×10^7

* For Surry AB
** Time measured from shutdown
*** From ANSI/ANS-5.1-1979

However, if relocated to pools, somewhere near the maximum release of aerosols from the RCS may be sufficient to set up refluxing conditions which may help decontaminate the containment atmosphere. In addition, since the inerting or deinerting point of the atmosphere with respect to hydrogen burns can be significantly changed over the long term by the water vapor from the pools, the mode and timing of the containment failure can be affected.

3.8.3.2 Insulative Effects (Type I)

The aerosol deposits on heat sink surfaces will affect heat transfer coefficients. In dry environments these deposits tend to be very porous with a density and a thermal conductivity much lower than normal. However, in wet environments, aerosol particles tend to more compact and the deposits will tend to be much closer to full density. In addition, whatever insulative properties the deposit will have by virtue of its porous state will be mitigated by the

water deposited in the interstices. There is also the possibility that the deposits will be washed off the good heat sinks, which will condense significant amounts of water. The overall potential for insulative effects in a wet environment is small.

Insulative effects may be significant in a dry reactor cavity. In order to establish the thermohydraulic conditions and the driving terms for aerosol plating in the cavity, the convective and radiative heat transfer in the cavity must be calculated. In the presence of radiative scattering by the aerosols, this would require a multiple cell representation of the cavity and is outside the scope of MELCOR1.

3.8.3.3 Effects (Type I) on Radiative Heat Transfer

Radiative heat transfer is a major heat transfer mechanism within the reactor core structures at temperatures near core melt, but prior to significant loss of the open core geometry. It is also a major heat transfer mechanism during hydrogen burns and for upward heat transfer from core debris in the reactor cavity. The radiative heat transfer could be significantly affected by the presence of high densities of aerosols. In the core, these would be composed of fuel, control rod, and structural material. In containment these would be primarily water aerosols, and in the reactor cavity these would be core-concrete aerosols.

In the case of a hydrogen burn, the energy transfer from the burn to the containment walls may be significantly reduced by the absorption of radiation by the water aerosol. The aerosol will vaporize until the radiation can "burn through" to the walls. The effects due to vaporization of the aerosols are potentially the same order of magnitude as the effects of vaporizing the water films on the containment surfaces. In the reactor cavity, the coupling between the core debris and the reactor cavity walls and between the reactor and the rest of containment, may be affected by the change in the emissivities of the atmosphere due to the aerosols. The aerosols will allow the atmosphere to emit in bands forbidden to the gas, and significant radiation scattering may occur.

The potential for significant effects due to the aerosols has not been fully assessed. However, according to present assumptions, the multicell noding within a compartment in containment which would be required to describe the radiation effects is outside the scope of MELCOR1. The exvessel effects of aerosol scattering should therefore be included on a phenomenological level with correlations determined from separate calculations.

3.8.4 EFFECTS (TYPE I) ON THE COMBUSTION OF H_2 and CO

Fission product and aerosol behavior can affect hydrogen and CO combustion in several ways. As discussed in Section 3.1, localized heating of heat sinks and pools by deposited fission products can affect atmosphere properties. In particular, drainage relocation and direct deposition of fission products into pools can cause evaporation or boiling of the pools. This source of water vapor may significantly affect the timing of inerting or deinerting of the containment atmosphere, particularly for a dry reactor cavity. Second, as discussed in Section 3.8.3.3, absorption of radiation by the water aerosol may affect the heat transfer from the burn to the walls. Finally, the water aerosol may affect the inerting of the atmosphere and burn propagation characteristics.

3.8.5 EFFECTS (TYPE I) ON CONTAINMENT ENGINEERED SAFETY FEATURES

The possibility exists that aerosol deposition will adversely affect the operation of engineered safety features. The possible effects include clogging of values, nozzles, and filters. Degradation of performance may result from insulating effects of deposits, for example on cooling coils, and fission product heating of critical components. For the fission product heating associated with aerosols in Table 3.8.3-1 for a large break LOCA case, rapid settling of aerosols may subject an exposed settling surface to considerable heating. For a typical total settling area, at two hours after shutdown, this may be a sizable 5 kw/m^2 of surface heating.

Despite the potential for degraded performance, the effects on the performance of engineered safety systems will be bracketed by postulated complete failure of the system. A mechanistic calculation of the degradation is not recommended at the present time.

3.8.6 SUMMARY OF THE MAIN POINTS AND CONCLUSIONS

A number of Type I and Type II feedback effects from aerosol and fission product processes in containment have been discussed. Some effects are significant and bear further investigation, but have been judged too involved for mechanistic modeling within MELCOR. Nevertheless, correlations for these effects should be implemented when they become available. The most important effects which should be modeled within MELCOR involve (a) the behavior of water aerosol in the containment atmosphere (Type I), and (b) the relocation of fission products from the atmosphere and subsequent localized heating of heat sinks and pools (Type II).

(a) The natural removal of water aerosol from the containment atmosphere is generally a fast process for the sources expected in an LWR accident, and much of the time need not be modeled in detail with regard to the short-term threat to containment or the Type I consequences. However, the water aerosol in some situations may have significant Type I consequences. Two such situations were discussed. In these situations a state-of-the-art discrete or size-class method should be used for calculating the aerosol behavior. The use of a lognormal or monodisperse assumption for the particle size distribution will typically give results for the aerosol mass which can be off by an order of magnitude or more. Since such a method will presumably be available in the aerosol module, the water aerosol behavior should be calculated in that module on the same footing as the structural material and fission product aerosol behavior. Appropriate interfaces toward this end should be constructed.

(b) The retention of fission product aerosols or adsorbables in the RCS depends significantly on the accident sequence. For cases with little retention in the RCS, the relocation of these types of fission products from the containment atmosphere to pools and heat sink surfaces has a number of effects. The differences between heating of the atmosphere and localized heating of the latter may change the long-term thermohydraulic behavior of containment and the course of the accident. For example, evaporation of the pools due to heating from deposited fission products may significantly affect the water vapor deinerting point of the atmosphere with respect to hydrogen burns in the case of a dry reactor cavity. In addition, the decontamination rate of the containment atmosphere is a sensitive function of the condensation rate on aerosols. This could be enhanced significantly by reduction of fission product heating of the atmosphere, and evolution of water vapor from the pools.

3.8.8 REFERENCES

1. Wooton, R. O. and Avci, H. I., "MARCH (Meltdown Accident Response Characteristics) Description and User's Manual," NUREG/CR-1711, BMI-2064 (October 1980).

2. Senglaub, M. E., Odom, J. P., Clauser, M. J., Kelly, J. E., and Pickard, P. S., "CONTAIN, A Computer Code for Analysis of Containment Response to Reactor Accidents-Version 1A," NUREG/CR-2224, SAND81-1495, draft.

3. Kress, T. S. and Tobias, M. L., "LMFBR Aerosol Release and Transport Program Quarterly Progress Report for January-March, 1981," ORNL/TM-7946. See also the quarterly progress reports ORNL/TM-7974, -8149, -8307.

4. Bennett, D. E., "SANDIA-ORIGEN Users' Manual," SAND79-0299, NUREG/CR-0987, Sandia National Laboratories, (October 1979).

5. Battelle's Columbus Laboratory, "Radionuclide Release Under Specific Accident Conditions," Vol. I, BMI-2104, draft.

DISTRIBUTION:

Division of Technical Information & Document Control
USNRC Distribution Contractor
U. S. Nuclear Regulatory Commission
15700 Crabbs Branch Way
Rockville, MD 20850
100 copies for AN

U. S. Nuclear Regulatory Commission (7)
Office of Nuclear Regulatory Research
Washington, DC 20555

Attn: R. T. Curtis
Containment Systems Research Branch
MS 1130SS

M. A. Cunningham
Reactor Risk Branch
MS 5650NL

T. Margulies
Reactor Risk Branch
MS 5650NL

G. Marino
Fuel Systems Research Branch
MS 1130SS

R. Meyer
Fuel Systems Research Branch
MS 1130SS

M. Silberberg
Fuel Systems Research Branch
MS 1130SS

L. Soffer
Reactor Risk Branch
MS 5650NL

U. S. Nuclear Regulatory Commission (3)
Office of Nuclear Regulatory Regulation
Washington, DC 20555

Attn: J. L. Carter
Reactor Systems Branch
MS P-1132

J. E. Rosenthal
Reactor Systems Branch
MS P-1132

A. H. Spano
Reliability and Risk Assessment Branch
MS 216

Applied Physics, Inc.
8605 Camino Osito NE
Albuquerque, NM 87111
Attn: R. Knight

Battelle Columbus Laboratory (3)
505 King Avenue
Columbus, OH 43201
Attn: P. Cybulskis
R. Denning
J. Gieseke

Brookhaven National Laboratory (2)
Upton, NY 11973
Attn: G. A. Greene
T. Pratt

EG&G Idaho, Inc.
P. O. Box 1625
Idaho Falls, ID 83415
Attn: P. MacDonald

Electric Power Research Institute
3412 Hillview Avenue
Palo Alto, CA 94303
Attn: B. R. Sehgal

Fauske & Associates, Inc.
16W070 West 83rd Street
Burr Ridge, IL 60521
Attn: R. E. Henry

Future Resources Associates, Inc.
2000 Center Street, Suite 418
Berkeley, CA 94704
Attn: R. Budnitz

General Electric Company
175 Kurtner Avenue
Mail Code 766
San Jose, CA 95125
Attn: H. Careway

KfK, IRB
D-7500 Karlsruhe 1
Federal Republic of Germany
Attn: Randall K. Cole, Jr.

Oak Ridge National Laboratory (3)
Post Office Box Y
Oak Ridge, TN 37830
Attn: S. Greene
S. Hodge
T. Kress

Pickard, Lowe, and Garrick, Inc.
17840 Skypark Blvd.
Irvine, CA 92714
Attn: A. Torri

Pickard, Lowe, and Garrick, Inc.
6620 Southpoint Drive, Suite 120
Jacksonville, FL 32216
Attn: D. Walker

Prof. I. Caton
University of California
School of Eng. and Applied Science
Los Angeles, CA 90024

Prof. M. L. Corradini
University of Wisconsin
Nuclear Engineering Department
1500 Johnson Drive
Madison, WI 53706

Prof. T. G. Theofanous
School of Nuclear Engineering
Purdue University
West Lafayette, IN 47907

Risk Management Associates
5353 Wyoming
Suite 8B
Albuquerque, NM 87109
Attn: C. J. Shaffer

Science Applications, Inc.
505 Marquette NW
Albuquerque, NM 87102
Attn: P. Mast

Science Applications, Inc.
5 Palo Alto Square, Suite 200
Palo Alto, CA 94304
Attn: R. L. Ritzman

Technology for Energy Corporation (3)
One Energy Center, Pellissippi Pkwy
Knoxville, TN 37922
Attn: A. Buhl
M. Fontana
E. Fuller

S. J. Niemczyk
Union of Concerned Scientists
Connecticut Avenue NW
S.1101
Washington, DC 20036

United Kingdom Atomic Energy Authority (2)
Wigshaw Lane, Culcheth
Warrington WA3 4NE
England
Attn: M. R. Hayns
F. Abbey

Westinghouse Electric Corporation
Power Systems
Monroeville Nuclear Center
P. O. Box 355
Pittsburgh, PA 15320
Attn: R. Peak

Westinghouse Hanford Corporation
W/C-81
P. O. Box 1970
Richland, WA 99352
Attn: D. G. Nguyen

1271 M. J. Clauser
1511 G. G. Weigand
1513 S. N. Kempka
1513 A. C. Ratzel
6000 E. H. Beckner
6400 A. W. Snyder
6410 J. W. Hickman
6411 A. S. Benjamin
6411 V. L. Behr
6411 S. E. Dingman
6411 F. E. Haskin
6411 A. C. Peterson

6412 A. L. Camp
6412 G. Kolb
6415 D. C. Aldrich
6415 D. J. Alpert
6415 R. P. Burke
6415 J. M. Griesmeyer
6415 C. D. Leigh
6415 J. L. Sprung
6420 J. V. Walker
6420A J. B. Rivard
6422 D. A. Powers
6422 J. E. Brockman
6425 W. J. Camp
6425 R. J. Lipinski
6425 M. Pilch
6427 M. Berman
6440 D. A. Dahlgren
6442 W. A. von Riesemann
6442 T. E. Blejwas
6444 S. L. Thompson
6444 L. D. Buxton
6444 P. N. Demmie
6444 J. M. McGlaun
6444 R. M. Summers
6444 J. L. Orman
6444 W. H. Schmidt
6444 S. W. Webb
6449 K. D. Bergeron
6449 K. K. Murata
6449 P. E. Rexroth
7541 R. T. Reese
3141 C. M. Ostrander (5)
3151 W. L. Garner
8024 M. A. Pound

NRC FORM 335 (2.84) NRCM 1102, 3201, 3202

U.S. NUCLEAR REGULATORY COMMISSION

BIBLIOGRAPHIC DATA SHEET

SEE INSTRUCTIONS ON THE REVERSE

1 REPORT NUMBER (Assigned by TIDC add Vol. No., if any)

NUREG/CR-3986
SAND84-1219

2 TITLE AND SUBTITLE

Thermal-Hydraulic Process Modeling in Risk Analysis: An Assessment of the Relevant Systems, Structures, and Phenomena

3 LEAVE BLANK

4 DATE REPORT COMPLETED

MONTH: August | YEAR: 1984

5 AUTHOR(S)

6 DATE REPORT ISSUED

MONTH: August | YEAR: 1984

7 PERFORMING ORGANIZATION NAME AND MAILING ADDRESS (Include Zip Code)

Sandia National Laboratories
P. O. Box 5800
Albuquerque, NM 87185

8 PROJECT/TASK/WORK UNIT NUMBER

9 FIN OR GRANT NUMBER

FIN No. A1339

10 SPONSORING ORGANIZATION NAME AND MAILING ADDRESS (Include Zip Code)

Division of Risk Analysis and Operation
Office of Nuclear Regulatory Research
U. S. Nuclear Regulatory Commission
Washington, DC 20555

11a TYPE OF REPORT

Technical

b PERIOD COVERED (Inclusive dates)

12 SUPPLEMENTARY NOTES

13 ABSTRACT

The MELCOR project is developing a new generation of risk assessment computer programs for analysis of severe accidents at nuclear power plants. As a part of this project, a three-part study was conducted to identify the relevant phenomena and models required for performing these PRA studies. Evaluations were performed in (1) thermal-hydraulics, (2) fission product behavior and (3) health and environmental consequences areas. This document details the findings in the thermal-hydraulic areas for PWRs and areas common to both PWRs and BWRs. A separate BWR specific report has been published by Oak Ridge National Laboratory. Reports are being prepared for the other two topics.

The study was performed by specialists from each of the various nuclear plant design or analysis areas where thermal-hydraulics is important; these specialists conducted a review of the modeling requirements of each area and contributed a section to this report detailing their findings. The general guidance as to scope for each section provided each author was: (a) identify the systems, structures, and phenomena that must be modeled, (b) review available models, (c) assess models for uncertainties, (d) identify numerical solution strategies and (e) make recommendations for the first version of MELCOR.

The study found that the current level of thermal-hydraulic modeling that exists for performing risk assessments is typified by the modeling in the MARCH code. This level of modeling was found to be inadequate for MELCOR because of inconsistent or nonexistent modeling of important phenomena, particularly invessel phenomena, systems, and structures. Pressurized water reactor modeling was found to be more complete than modeling for boiling water reactor designs, particularly in containment. Finally, although reactor cavity modeling was considered essential for risk assessments, the lack of adequate modeling found for the cavity was identified as a serious impediment to the development of second generation risk codes.

14 DOCUMENT ANALYSIS - a KEYWORDS/DESCRIPTORS

b IDENTIFIERS/OPEN ENDED TERMS

15 AVAILABILITY STATEMENT

16 SECURITY CLASSIFICATION

(This page) U

(This report) U

17 NUMBER OF PAGES

642

18 PRICE

☆ U.S. GOVERNMENT PRINTING OFFICE: 1984—576-035 / 4393